

DISSERTATION

EFFECTS OF URBANIZATION ON THE HYDROLOGIC REGIMES AND  
GEOMORPHIC STABILITY OF SMALL STREAMS IN SOUTHERN CALIFORNIA

Submitted by

Robert J. Hawley

Department of Civil and Environmental Engineering

In partial fulfillment of the requirements

for the Degree of Doctor of Philosophy

Colorado State University

Fort Collins, Colorado

Fall 2009

COLORADO STATE UNIVERSITY

July 28, 2009

WE HEREBY RECOMMEND THAT THE DISSERTATION PREPARED UNDER OUR SUPERVISION BY ROBERT J. HAWLEY ENTITLED EFFECTS OF URBANIZATION ON THE HYDROLOGIC REGIMES AND GEOMORPHIC STABILITY OF SMALL STREAMS IN SOUTHERN CALIFORNIA BE ACCEPTED AS FULFILLING IN PART REQUIREMENTS FOR THE DEGREE OF DOCTOR OF PHILOSOPHY.

Committee on Graduate Work

---

Ellen E. Wohl

---

Chester C. Watson

---

Eric D. Stein

---

Advisor Brian P. Bledsoe

---

Department Head Luis A. Garcia

## ABSTRACT OF DISSERTATION

### EFFECTS OF URBANIZATION ON THE HYDROLOGIC REGIMES AND GEOMORPHIC STABILITY OF SMALL STREAMS IN SOUTHERN CALIFORNIA

In southern California streams, altered hydrologic and sediment regimes associated with urbanization (hydromodification) have induced significant morphologic responses such as incision, widening, and planform shifts from single-thread to braided with far-reaching effects to adjacent land and throughout drainage networks. The overarching objective of this dissertation is to improve process-based understanding of these changes such that the risk of future degradation may be mitigated through improved management. Three chapters follow from this fundamental flow of logic: changes in land cover beget changes in flow regimes, leading to increased erosive energy and sediment-transport potential, which, dependent on the relative resistance of the setting, can culminate into substantial changes in channel form.

The purpose of Chapter 1 was to understand the first step in this sequence: how urbanization affects the flow regime. Duration Density Functions (DDFs) were developed as histogram-style cumulative duration curves that represent the full range of geomorphically-significant flows as simple power functions. Using long-term data from 52 U. S. Geological Survey (USGS) gauges, empirical models were fit to both peak flows and DDF parameters (i.e., magnitude and shape) as multivariate functions of statistically-significant spatial variables including total impervious area. With little flow control at the subdivision scale to date, total impervious area became an effective hydrologic

surrogate for urbanization, demonstrating an exponential effect on peak flows, particularly the 1-, 1.5-, and 2-yr events, and increased durations of all sediment-transporting flows. For example, watersheds with ~10% imperviousness typically exhibit a ~5-fold increase in  $Q_{1.5}$  and 2 to 3 times as many days of sediment-transporting flows relative to an undeveloped setting. The models developed in Chapter 1 directly informed the hydrologic components of the subsequent chapters, where impervious area was not found to be a significant predictor of geomorphic response when considered independent of setting or sediment transport.

The focus of Chapter 2 was to understand the relative susceptibilities of regional channel types to hydromodification in the context of a ‘Screening Tool’ that is being developed to help managers assess risk across geomorphic settings. Specifically, Chapter 2 is focused on 1) the general framework of a pre-final version of the susceptibility screening tool, and 2) the development of risk-based analyses of geomorphic thresholds, a central component of key decision nodes in the screening tool. Geomorphic thresholds are real and of great concern in stream management, such that any susceptibility-assessment scheme should account for the proximity to such threshold-based responses. Logistic-regression analyses of braiding, incision, and bank stability directly and probabilistically assess proximity to geomorphic thresholds, and offer a framework for assessing risk that goes beyond expert judgment. Calibrated with local data that were collected in an extensive field campaign, the logistic models were highly significant (i.e.,  $p < 0.005$  to  $p < 0.0001$ ) and correctly classified unstable states in ~90% of the cases using simple but powerful predictor variables that can be measured at the screening/reconnaissance level. A screening tool that incorporates objective probabilistic-based components is novel relative to previous and more subjective classification

schemes, such that regionally-diverse agencies and staff can quantitatively assess channel susceptibility with less variable results.

With the objective of developing a process-based understanding of observed channel changes, Chapter 3 presents models that predict relative magnitudes, directions, and risks of channel responses as functions of cumulative sediment-transport capacity ratios ( $L_r$ ) that contrast 25-yr DDF simulations of urbanized versus undeveloped conditions.  $L_r$  was a highly significant term in quantifying channel ‘enlargement’, whereas logistic regression of  $L_r$  in combination with  $d_{50}$  suggested that fine-grained systems (i.e., especially  $d_{50} \leq 16$  mm) have little capacity to absorb any increases in sediment-transport potential. A regional Channel Evolution Model (CEM) that includes departures from the original CEM of Schumm *et al.* (1984) is also presented along with a modified dimensionless stability diagram (*sensu* Watson *et al.* (1988)) that provides a conceptual framework for assessing relative departure from equilibrium/reference form for both lateral and vertical channel responses.

The overarching conclusion of this dissertation is that urbanization markedly affects the flow regimes of streams in southern California and that the corresponding imbalances in sediment-transport capacity result in substantial geomorphic instabilities across most stream settings. Consequently, mitigation strategies should be tailored to specific stream types and incorporate process-based objectives such as maintaining sediment continuity via duration standards rather than traditional regulations focused exclusively on flow magnitude.

Robert J. Hawley  
Department of Civil and Environmental Engineering  
Colorado State University  
Fort Collins, CO 80523  
Fall 2009

## ACKNOWLEDGEMENTS

Throughout this journey I have been blessed with an invaluable support network of faculty, friends, and family. First to my advisor, Dr. Brian Bledsoe, who has been a perennial bulwark since my first bike ride out to the ERC. Through coursework and research, Skype calls from Chile, California budget crises, late registration, future plans, and family surprises, your genuine and steady guidance has been par excellence. Thank you for a first-rate project, uninterrupted funding, masterly reviews, and balanced conversations – I always leave our meetings feeling energized and could not envision a better advisor/student relationship. Cheers.

To my committee members, Drs. Eric Stein, Chester Watson, and Ellen Wohl, I cannot thank you enough for your time and care in steering this dissertation into clear waters. Eric, thank you for keeping me tied to stakeholder goals, for sharing your wealth of local knowledge, resources, and energy, and for flying out for one of our meetings. Chester, your course and pioneering research truly gave me the shoulders of a giant to stand on. Ellen, from our field trip to Pawnee Buttes to lectures, critical-thinking essays and seminars, I feel so much more complete, and at the same time completely humbled to have you on my committee.

Next to Gloria Garza, who is the eternal champion of graduate students. Despite crunched deadlines you morphed these chapters into a ‘silver singing river’ of a

manuscript. Through it all, your incredible assistance and cheerful e-mails kept the stress-meter down, and I'm still in awe of how quickly you churned out revisions. I am forever grateful. And to the staff in the CEE office, Laurie Alburn, Linda Hinshaw, and Kathy Stencel, your smiling faces and support from before I was even a student have made me feel so welcome at CSU.

To my CSU and SCCWRP colleagues, particularly Dave Dust, Becky Schaffner, Liesl Tiefenthaler, Greg Lyon, and Jeff Brown, thank you for your tireless work in the field, logistical support, GIS assistance, photography, and for making many weeks in the hot sun a quite enjoyable experience. This wouldn't have been possible without you or the detailed work of the Stillwater Science survey crew, chiefly Scott Dusterhoff and Alexander Wong. And to Dr. Derek Booth, I am very grateful to have had this indirect opportunity to collaborate with you.

In his latest book Outliers (2008), Malcolm Gladwell deduces success to the necessary combination of talent and opportunity. To advisors and mentors from my previous life, Drs. Jim Mihelcic, Kevin Hallinan, Joseph Saliba, Roddy Williams, and Art Parola, thank you for your tremendous support and collaboration that clearly helped to get me in the door.

Speaking of opportunities, I am forever indebted to my parents Jeff and Jeanie. My dad was my first role model and the man who introduced me to a love of rivers, nature, and the importance of methodically looking to the data. My mom was my first teacher, instilling in me a passion for learning, the value of hard work, and love of family. Her warm angelic presence brings tranquility to all that I do. To the rest of my family

and friends, particularly, Dan, Tiffany, David, Diane, Eric, Em, Chanda, and Lynne, thank you for your love and support.

Finally, to my wife Dr. Laura Kissel Hawley, who is my inspiration, my solace, my Dulcinea. Knowing what you had to go through during residency makes this look easy. Your grace through both life's trials and blessings gives me composure. The care and dignity you afford your patients gives me hope. Your boundless love fills me up, and I spill over. May we follow every dream and always have our time in the hammock.

DEDICATION

To Laura

## TABLE OF CONTENTS

<b>ABSTRACT OF DISSERTATION</b> .....	<b>iii</b>
<b>ACKNOWLEDGEMENTS</b> .....	<b>vi</b>
<b>DEDICATION</b> .....	<b>ix</b>
<b>LIST OF TABLES</b> .....	<b>xiv</b>
<b>LIST OF FIGURES</b> .....	<b>xviii</b>
<b>CHAPTER 1 LONG-TERM EFFECTS OF URBANIZATION ON THE FLOW REGIMES OF SMALL STREAMS IN SOUTHERN CALIFORNIA</b> .....	<b>1</b>
1.1 Introduction.....	3
1.1.1 Research foundations and justification .....	5
1.1.2 Toward cumulative durations .....	6
1.1.3 Study domain .....	9
1.2 Methods.....	11
1.2.1 Gauge-selection criteria .....	12
1.2.2 Instantaneous peak flows .....	15
1.2.3 Long-term cumulative durations.....	19
1.2.4 Measures of urbanization.....	26
1.2.5 Other physically-based parameters .....	35
1.2.6 Analytical methods and model design .....	41
1.3 Results.....	47

1.3.1	Cross-validation summaries and individual variable performance .....	48
1.3.2	Peak-flow equations.....	50
1.3.3	Duration density functions.....	56
1.4	Implications and Discussion .....	65
1.4.1	Effects of urbanization predicted by models .....	66
1.4.2	At-a-station effects of urbanization .....	71
1.5	Summary and Conclusions .....	78
1.6	Future Work .....	79
1.7	Acknowledgements.....	80
1.8	References.....	81
1.9	GIS Data Sources.....	88

**CHAPTER 2 REGIONALLY-CALIBRATED PROBABILISTIC THRESHOLDS OF GEOMORPHIC STABILITY: KEY COMPONENTS OF A SCREENING TOOL FOR ASSESSING CHANNEL SUSCEPTIBILITY TO HYDROMODIFICATION IN SOUTHERN CALIFORNIA ..... 89**

2.1	Introduction.....	90
2.1.1	The natural and anthropogenic setting.....	91
2.1.2	Hydromodification project background.....	94
2.1.3	Screening-tool development, structure, and goals .....	95
2.2	Methods.....	99
2.2.1	Site selection and channel stability.....	99
2.2.2	Field and GIS data collection.....	102
2.2.3	Hydrology, hydraulics, and sediment supply.....	106
2.2.4	Analytical and statistical methods .....	108

2.3	Results.....	116
2.3.1	Screening-tool risk types.....	116
2.3.1.1	Low .....	117
2.3.1.2	Medium.....	118
2.3.1.3	High.....	119
2.3.1.4	Very high .....	120
2.3.1.5	Alternative management .....	122
2.3.2	Screening-tool decision trees and geomorphic thresholds.....	122
2.3.3	Defining the analysis domain.....	131
2.3.4	Composite-screening rating .....	132
2.4	Preliminary Validation.....	133
2.5	Summary and Conclusions .....	137
2.6	Acknowledgements.....	139
2.7	References.....	140
2.8	GIS Data Sources .....	147

**CHAPTER 3 MODELS FOR PREDICTING LONG-TERM EFFECTS OF  
HYDROMODIFICATION IN SOUTHERN CALIFORNIA:  
MAGNITUDES AND DIRECTIONS ..... 149**

3.1	Introduction.....	150
3.1.1	The natural and anthropogenic setting.....	152
3.1.2	Channel evolution models.....	153
3.1.3	Cumulative sediment transport .....	156
3.2	Methods.....	157
3.2.1	Site selection and channel stability.....	158
3.2.2	Field and GIS data collection.....	161

3.2.3	Hydrology, hydraulics, and sediment transport .....	163
3.2.4	Channel evolution, enlargement, and representative form .....	171
3.2.5	Analytical and statistical methods .....	177
3.3	Results.....	178
3.3.1	Response direction: a CEM for southern California.....	178
3.3.2	Response magnitude: ‘enlargement’ .....	182
3.3.3	Response magnitude: departure from equilibrium.....	186
3.4	Implications.....	190
3.4.1	Mitigation implications.....	193
3.5	Summary and Conclusions .....	196
3.6	Acknowledgements.....	200
3.7	References.....	200
3.8	GIS Data Sources.....	209
	<b>APPENDIX A GAUGE DATA .....</b>	<b>210</b>
	<b>APPENDIX B CROSS-VALIDATION EQUATIONS AND FIGURES .....</b>	<b>227</b>
	<b>APPENDIX C HYDROMODIFICATION SITE CROSS-SECTIONS, BANKS, AND PHOTOGRAPHS .....</b>	<b>236</b>
	<b>APPENDIX D HYDROMODIFICATION SITE DATA .....</b>	<b>322</b>
	<b>APPENDIX E LOGISTIC-REGRESSION SUPPLEMENT: DATA, PARAMETER ESTIMATES, AND ADDITIONAL RESULTS .....</b>	<b>357</b>

## LIST OF TABLES

Table 1.1 – Selected gradients of the 52 USGS gauges used to develop models (i.e., model-application bounds).....	14
Table 1.2 – Summary of parameters tested in models with significance of variables .....	37
Table 1.3 – Summary of the 26/26 cross-validation scheme .....	48
Table 1.4 – Summary of the 40/12 cross-validation scheme .....	49
Table 1.5 – Corresponding parameters and units for Eq. (1.7).....	51
Table 1.6 – Corresponding parameters and units for Eq. (1.8).....	52
Table 1.7 – Corresponding parameters and units for Eq. (1.9).....	53
Table 1.8 – Corresponding parameters and units for Eq. (1.10).....	53
Table 1.9 – Corresponding parameters and units for Eq. (1.11).....	54
Table 1.10 – Comparison of $Q_i$ model performance with USGS rural (1977) and urban (1983) equations using $R^2$ values from arithmetic space .....	56
Table 1.11 – Summary of component (scale) equations for DDFs: $Q_{\max}$ (for Eq. (1.2)).....	57
Table 1.12 – Summary of component (magnitude and shape) equations for DDFs: d1 and d2 (for Eq. (1.5), bins 16-25).....	60
Table 1.13 – Summary of component (magnitude and shape) equations for DDFs: day1 and day2 (for Eq. (1.6), bins 12-25) .....	63

Table 1.14 – Influence of urbanization (maximum impervious extent of watershed) and Dry setting on peak-flow rates .....	67
Table 1.15 – Summary of 25-yr DDF simulation for ‘dry’, rural, and urban scenarios in an average* watershed.....	70
Table 1.16 – Comparison of flows, durations, climate, and imperviousness over the pre-urban and post-urban periods of Arroyo Simi and San Diego .....	76
Table 2.1 – Summary of key gradients across 83 morphologically-distinct sub-reaches used in screening-tool development .....	101
Table 2.2 – Corresponding ‘mobility index’ values for 50% probability of incision for cobble-bed systems .....	126
Table 2.3 – Performance measures of logistic-regression analyses of geomorphic thresholds of incision, braiding, and mass wasting .....	127
Table 2.4 – Corresponding geometries for 10% risk of mass wasting .....	128
Table 2.5 – Corresponding ‘mobility index’ values for 50% risk of braiding in gravel- and cobble-bed systems .....	128
Table 2.6 – Screening rating, estimated ‘enlargement’, and key geomorphic parameters at selected study sites .....	135
Table 3.1 – Summary of key gradients across 84 morphologically-distinct sub-reaches/project ‘sites’ used in screening-tool development .....	160
Table 3.2 – Corresponding geometries for 50% risk of mass wasting .....	174
Table 3.3 – Summary of best ‘enlargement’ models .....	185
Table 3.4 – Risk factors for response directions .....	186
Table A.1 – Primary identification .....	212

Table A.2 – Measures of urbanization past and present .....	214
Table A.3 – Measures of precipitation past and present .....	216
Table A.4 – Spatial and topographic measures .....	218
Table A.5 – Years active and return-interval flows .....	221
Table A.6 – Return-interval flows and DDF parameters .....	224
Table C.1 – Layout key .....	239
Table C.2 – Bank-stability key .....	240
Table D.1 – Location and watershed metrics .....	323
Table D.2 – USGS (1977) rural flows and Hawley-Bledsoe rural and urban flows .....	327
Table D.3 – Topographic, urbanization, and soils .....	331
Table D.4 – Rational and NRCS CN methods, valley, reach, and cross-section metrics .....	335
Table D.5 – Hydraulic geometry forms and parameters: A, R, and W, as f(d) .....	340
Table D.6 – Cross-section metrics, bed material, and critical metrics for sediment transport .....	345
Table D.7 – 10-yr hydraulic metrics, load ratio, enlargement, bank stability, and reference width .....	349
Table D.8 – Stability, planform, and channel evolution model (CEM) stage .....	353
Table E.1 – Summary of significant incising and braiding models .....	358
Table E.2 – Summary of bank stability models .....	358
Table E.3 – Incising and braiding data .....	363
Table E.4(a) – Bank data: left banks .....	369
Table E.4(b) – Bank data: right banks .....	375

Table E.4(c) – Left bank data: rationale for description of second bank height and angle .....	382
Table E.4(d) – Right bank data: rationale for description of second bank height and angle .....	387

## LIST OF FIGURES

Figure 1.1 – Locations of gauges used in equation development, overlaid by gradients of elevation and imperviousness.....	13
Figure 1.2 – Flow vs. recurrence interval of 30-yr record at USGS gauge no. 11033000, WF San Luis Rey R. near Warner Springs, California, with logarithmic, Log-Pearson Type III adjusted (Q+0.1) and (Q+100), and inverse gamma distributions .....	18
Figure 1.3 – DDFs of gauges De Luz and San Antonio fitted to centroids of logarithmically-distributed histogram bins 16-25 with selected parameters of drainage area, average annual precipitation, and record length.....	24
Figure 1.4 – 2001 imperviousness and road vectors tracked through time per USGS historic quadrangle maps and current CA-Atlas shapefiles at Arroyo Trabuco (Orange County, California, near X of I-5 and I- 405).....	29
Figure 1.5 – Imperviousness and road density through time at Arroyo Trabuco, overlaid by active gauge years and linear trendline of imperviousness (1967 - 2001).....	30
Figure 1.6 – Average linear rate of change of measured historic road density as an exponential function of measured road density in 2000 .....	32

Figure 1.7 – Exponential correlation between impervious area (2001) and road density (2000) across all sites.....	35
Figure 1.8 – Inter-annual precipitation variability recorded at Los Angeles and San Diego overlaid with number of active gauges and number greater than specified road-density levels (indicating increasing urbanization).....	38
Figure 1.9 – Integrated and estimated mean historic road density overlaid by relative difference from long-term mean in recorded precipitation at Los Angeles and San Diego during gauge records .....	39
Figure 1.10 – Main-channel length (to basin divide) vs. drainage area with southern California and Hack’s NE US relationship plotted .....	40
Figure 1.11 – Drainage density vs. area-averaged mean annual precipitation .....	41
Figure 1.12 – Comparison of performance between Eq. (1.7), USGS rural (1977), and USGS urban (1983) .....	55
Figure 1.13 – Model performance of Eqs. (1.12) and (1.13) (predicted $Q_{max}$ vs. actual) with 1:1 ‘perfect-fit’ line overlaid .....	59
Figure 1.14 – Model performance of (predicted vs. actual) with 1:1 ‘perfect-fit’ lines overlaid .....	62
Figure 1.15 – 1.5-yr flow vs. drainage area, overlaid with maximum impervious extent during record of each gauge .....	66
Figure 1.16 – DDFs of gauges Arroyo Trabuco and San Antonio fitted to centroids of logarithmically-distributed histogram bins 16-25 with	

selected parameters of drainage area, average annual precipitation, record length, and average impervious area .....	69
Figure 1.17 – DDFs of 25-yr simulations of equivalent watersheds in ‘dry’, rural, and urban settings .....	70
Figure 1.18 – Instantaneous peak flow relative to recurrence interval, with fitted gamma distributions .....	72
Figure 1.19 – Cumulative-duration histogram centroids, with fitted DDFs .....	73
Figure 1.20 – Annual peak flows overlaid with relative difference in mean annual precipitation at Los Angeles weather station .....	74
Figure 1.21 – Annual peak flows recorded at Arroyo Simi overlaid with interpolated percentage of impervious cover in the watershed as tracked via historic USGS quadrangle maps .....	75
Figure 2.1 – Overview of reaches sampled for screening-tool development .....	101
Figure 2.2 – Main channel of Cross section D at Hicks Canyon .....	104
Figure 2.3 – Watershed context .....	123
Figure 2.4 – Vertical susceptibility .....	124
Figure 2.5 – Lateral susceptibility .....	124
Figure 2.6 – Vertical supplement: logistic regression of incising channels (CEM Types II or III) vs. single-thread stable (CEM Type I) or recovered (i.e., CEM Type IV → V) systems in unconfined valleys .....	126
Figure 2.7 – Lateral supplement: logistic regression of mass wasting in moderately- and well-consolidated banks vs. stable bank geometries .....	128

Figure 2.8 – Lateral supplement: logistic regression of braided channels vs. single-thread stable (CEM Type I) or recovered (i.e., CEM Type IV → V) systems in unconfined valleys.....	128
Figure 2.9 – Cross section A at AltPerris .....	130
Figure 2.10 – Integration of vertical and lateral susceptibility ratings into a composite rating, with sediment-supply augmentation.....	133
Figure 2.11 – Photograph looking upstream at Acton_D: $d_{50} = 9.4$ mm with enlargement since development in 1990s approximated at 900% .....	135
Figure 3.1 – Dimensionless stability diagram for the CEM in incised sand-bed streams (Watson <i>et al.</i> , 2002).....	155
Figure 3.2 – Overview and locations of project stream reaches used in analysis.....	160
Figure 3.3 – DDF simulations of the past 25-yrs under developed (actual) and undeveloped regimes.....	166
Figure 3.4 – Cumulative flow durations, incremental sediment-transport rates, and cumulative bedloads across 25-yr DDF simulations under-developed regimes .....	169
Figure 3.5 – Cumulative flow durations and bedloads across 25-yr DDF simulations under-developed regimes and undeveloped regimes .....	170
Figure 3.6 – Surveyed cross sections at Borrego Canyon relative to projected 1952 form via aerial photograph and cross section at present-day drop structure.....	173

Figure 3.7 – Logistic regression of mass wasting in moderately- and well- consolidated banks with superimposed stable and unstable bank geometries .....	174
Figure 3.8 – Top width vs. flow in unconfined, unconstructed stable, braided, and incising systems with superimposed power functions fitted to stable sites .....	176
Figure 3.9 – CEM for southern California with accompanying photographs and key mechanisms/boundary conditions .....	181
Figure 3.10 – Enlargement ratio of all sites .....	183
Figure 3.11 – Modeled enlargement ratio versus estimated enlargement from best historic approximation of pre-response form of 27 most representative sites .....	184
Figure 3.12 – Dimensionless stability diagram of geotechnical bank stability ( $N_g$ ) vs. reference width ratio ( $N_w$ ) ( <i>sensu</i> Watson <i>et al.</i> (1988)) with CEM stages of single-thread/incision and braided departures .....	188
Figure 3.13 – Bedload ratio vs. median grain size of stable, unstable single- thread (CEM Types II and III), and unstable braided systems with superimposed logistic stability thresholds in the form $\ln\{\ln(L_r)\}$ vs. $\ln(d_{50})$ .....	191
Figure 3.14 – Bedload ratio vs. median grain size of stable, unstable single-thread (CEM Types II and III), and unstable braided systems with superimposed logistic thresholds developed without Escondido and Borrego_D .....	191

Figure 3.15 – Impervious area vs. median grain size of stable, unstable single-thread (CEM Types II and III), and unstable braided systems with superimposed logistic thresholds developed.....	193
Figure 3.16 – Hypothetical mitigation scenarios at Borrego_C that match the cumulative sediment transport of the pre-developed regime using various detention/retention designs. ....	195
Figure B.1 – Cross-validation for Q1: 40/12 scheme, $R^2$ clb/vld = 0.6/0.5.....	229
Figure B.2 – Cross-validation for Q1.5: 40/12 scheme, $R^2$ clb/vld = 0.6/0.7.....	229
Figure B.3 – Cross-validation for Q2: 40/12 scheme, $R^2$ clb/vld = 0.6/0.6.....	230
Figure B.4 – Cross-validation for Q5: 40/12 scheme, $R^2$ clb/vld = 0.8/0.7.....	230
Figure B.5 – Cross-validation for Q10: 40/12 scheme, $R^2$ clb/vld = 0.8/0.9.....	231
Figure B.6 – Cross-validation for Q25: 40/12 scheme, $R^2$ clb/vld = 0.8/0.8.....	231
Figure B.7 – Cross-validation for Q50: 40/12 scheme, $R^2$ clb/vld = 0.8/0.7.....	232
Figure B.8 – Cross-validation for Q100: 40/12 scheme, $R^2$ clb/vld = 0.8/0.7.....	232
Figure B.9 – Cross-validation for Qmax: 40/12 scheme, $R^2$ clb/vld = 0.7/0.8.....	233
Figure B.10 – Cross-validation for d1: 36/12 scheme, $R^2$ clb/vld = 0.7/0.7.....	233
Figure B.11 – Cross-validation for d2: 36/12 scheme, $R^2$ clb/vld = 0.9/0.9.....	234
Figure B.12 – Cross-validation for day1: 36/12 scheme, $R^2$ clb/vld = 0.8/0.8.....	234
Figure B.13 – Cross-validation for day2: 24/23 scheme, $R^2$ clb/vld = 0.9/0.8.....	235
Figure C.1 – Santiago_A.....	241
Figure C.2 – Santiago_B.....	242
Figure C.3 – Hasley1_A .....	243
Figure C.4 – Hasley1_B.....	244

Figure C.5 – Hasley1_TRIB .....	245
Figure C.6 – Hasley2_A .....	246
Figure C.7 – Hasley2_B.....	247
Figure C.8 – Hasley2_TRIB .....	248
Figure C.9 – Hicks_A .....	249
Figure C.10 – Hicks_B .....	250
Figure C.11 – Hicks_C .....	251
Figure C.12 – Hicks_D .....	252
Figure C.13 – Hicks_E.....	253
Figure C.14 – Hicks_F.....	255
Figure C.15 – Agua_Hedi_A .....	256
Figure C.16 – Agua_Hedi_B .....	257
Figure C.17 – Agua_Hedi_C .....	258
Figure C.18 – Dry_A .....	259
Figure C.19 – Dry_B.....	260
Figure C.20 – Dry_C.....	262
Figure C.21 – Hovnanian_A.....	263
Figure C.22 – Hovnanian_B .....	264
Figure C.23 – Santimeta_A (San Timetao).....	265
Figure C.24 – Santimeta_B (San Timetao).....	266
Figure C.25 – Santimeta_C (San Timetao).....	267
Figure C.26 – Ltl_Cedar_A (Little Cedar) .....	268
Figure C.27 – Ltl_Cedar_B (Little Cedar).....	269

Figure C.28 – Proctor_A.....	270
Figure C.29 – Proctor_B.....	271
Figure C.30 – Proctor_TRIB.....	272
Figure C.31 – Perris_1_A.....	273
Figure C.32 – Perris_1_B.....	274
Figure C.33 – Perris_1_C.....	275
Figure C.34 – Perris_2_A.....	276
Figure C.35 – Perris_2_B.....	277
Figure C.36 – Perris_3_A.....	278
Figure C.37 – Perris_3_B.....	279
Figure C.38 – AltPerris_A.....	280
Figure C.39 – AltPerris_B.....	281
Figure C.40 – AltPerris_C.....	282
Figure C.41 – Dulzura_A.....	283
Figure C.42 – Dulzura_B.....	284
Figure C.43 – Acton_A.....	285
Figure C.44 – Acton_B.....	286
Figure C.45 – Acton_C.....	287
Figure C.46 – Acton_D.....	288
Figure C.47 – Acton_E.....	289
Figure C.48 – Borrego_A.....	290
Figure C.49 – Borrego_B.....	291
Figure C.50 – Borrego_C.....	292

Figure C.51 – Borrego_D .....	293
Figure C.52 – Borrego_E.....	294
Figure C.53 – Topanga_A.....	295
Figure C.54 – Topanga_B.....	296
Figure C.55 – Topanga_C.....	297
Figure C.56 – Challengr_A (Challenger Park) .....	298
Figure C.57 – Challengr_B (Challenger Park) .....	299
Figure C.58 – Challengr_C (Challenger Park) .....	300
Figure C.59 – McGonigle_A .....	301
Figure C.60 – SanJuan_A .....	302
Figure C.61 – SanJuan_B .....	303
Figure C.62 – Pigeon_A (Pigeon Pass).....	304
Figure C.63 – Pigeon_B (Pigeon Pass).....	305
Figure C.64 – Pigeon_C (Pigeon Pass).....	306
Figure C.65 – Stewart_A .....	307
Figure C.66 – Santiagbd_A (Santiago at Tucker Bird Sanctuary) .....	308
Figure C.67 – Santiagbd_B (Santiago at Tucker Bird Sanctuary).....	309
Figure C.68 – Santiagnl_A (Santiago at Natural-loading site).....	310
Figure C.69 – Santiagnl_B (Santiago at natural-loading site) .....	311
Figure C.70 – Silverado_A .....	312
Figure C.71 – Silverado_B .....	313
Figure C.72 – Escondido_A.....	314
Figure C.73 – Escondido_B.....	315

Figure C.74 – SanAntoni_A (San Antonio).....	316
Figure C.75 – SanAntoni_B (San Antonio).....	317
Figure C.76 – Alt_RC2_A (unnamed headwater in Riverside County).....	318
Figure C.77 – Yucaipa_A.....	319
Figure C.78 – Yucaipa_B.....	320
Figure C.79 – OakGlenn_A.....	321
Figure E.1 – Incision logistic MI10 vs. d84.....	359
Figure E.2 – Braiding logistic MI10 vs. d84.....	359
Figure E.3 – Incision logistic MI2 vs. d50 (including confined/bedrock systems).....	360
Figure E.4 – Incision logistic MI10 vs. d50 (including confined/bedrock systems).....	360
Figure E.5 – Risk of bank failure in poorly and moderately/well-consolidated materials.....	361
Figure E.6 – Risk of bank failure in poorly and unconsolidated materials.....	361
Figure E.7 – Risk of minor mass wasting in hillslope if channel directly connected to hillslope (i.e., confined).....	362

## CHAPTER 1

### LONG-TERM EFFECTS OF URBANIZATION ON THE FLOW REGIMES OF SMALL STREAMS IN SOUTHERN CALIFORNIA

**Abstract.** Fifty-two U. S. Geological Survey gauges with records greater than ~20 yrs located in watersheds less than ~250 km<sup>2</sup> were used to empirically model the effects of urbanization on small free-flowing streams in southern California. These gauged watersheds spanned a gradient of urban development and ranged from 0 to 23% total impervious area (TIA) in 2001. With little flow control at the subdivision scale to date, most of the region's impervious area is hydrologically effective, in that it is relatively well-connected to surface-drainage networks. Consequently, TIA was a powerful hydrologic surrogate of urbanization, emerging from an expansive array of Geographic Information System derived hydrologic variables as a statistically-significant ( $p < 0.05$ ) predictor of instantaneous peak-flow rates at the 1-, 1.5-, and 2-yr recurrence intervals in all models. Urbanization proved less significant for higher flows (e.g.,  $p < 0.30$  for 5-yr flows). Most importantly with respect to geomorphic response, urbanization extent was a significant predictor of the magnitude (coefficient) and shape (exponent) of duration density functions. Duration density functions are conceptually similar to probability density functions and were fit as power functions (typical  $R^2 > 0.95$ ) to days of occurrence versus logarithmically-binned mean daily discharges greater than some nominal value, for example 1 to 10 cubic feet per second (ft<sup>3</sup>/s) (0.03 to 0.3 m<sup>3</sup>/s),

depending on watershed size. This study approach expands on drainage area or  $Q_i$  scaling procedures to produce histogram-style cumulative flow durations for ungauged sites using multiple statistically-significant physical parameters (e.g., drainage density, mean annual precipitation, and average watershed surface slope). For a particular drainage area and climatic setting, urbanization results in proportionally longer durations of all geomorphically effective flows. For example, a watershed with ~10% imperviousness could expect a ~5-fold increase in  $Q_{1.5}$  and 2 to 3 times as many days of respective sediment-transporting flows relative to the undeveloped setting (i.e., ~1% imperviousness). Basins that are susceptible to the largest increases in magnitude are those that are predisposed to flashiness, for example, spatially and topographically efficient (i.e., steep and dense networks) with high-precipitation rates. The largest increases in durations are predicted in wet, topographically efficient (steep) but spatially inefficient (low-drainage densities) settings, that is, watersheds that receive large volumes of surface water but remove it less quickly. Yet, substantial increases in flow magnitudes and durations are expected across all settings where development is left unmitigated. Increased duration of sediment-transporting flows is a primary driver of accelerated changes in channel form that are often concurrent with urbanization throughout southern California, particularly in least resilient unconfined fine-grained settings.

**Unit disclaimer:** Acknowledging the general preference of SI units among the scientific community, we felt it was beneficial to develop these equations in English units for more direct comparisons to the U. S. Geological Survey (Waananen and Crippen, 1977) equations. Without becoming overly cumbersome, we try to offer SI units in parentheses and some figures are expressed in SI units.

## 1.1 Introduction

As anyone who has ever driven in the rain can attest, impervious surfaces have an unmistakable effect on hydrologic processes. By decreasing infiltration and increasing direct runoff, impervious cover can create larger peaks, less groundwater recharge, and increased variability, especially if stormwater is routed directly to streams. These fundamental hydrologic interrelations, such as larger peaks and increased flashiness, have been demonstrated regionally (Konrad and Booth, 2002; Galster *et al.*, 2006) and on a national scale using U. S. Geological Survey (USGS) gauge data (Sauer *et al.*, 1983; Poff *et al.*, 2006).

In California, increased peak flows in developed watersheds have been documented by the USGS as early as 1963 (Waananen, 1969). Durbin (1974) reported potential increases in the 2-yr flow ( $Q_2$ ) of three- to six-fold in San Bernardino County, with little effect on higher return intervals such as the 50-yr flow. As a function of development extent and percentage of channels sewerred, Rantz (1971) developed peak factors for the San Francisco Bay area ranging from 1 to 4 for  $Q_2$ , decreasing with larger return intervals (e.g., 1 to 2.5 for  $Q_{50}$ ).

Such changes in flow, broadly associated with urbanization, are documented as having profound effects on biologic and geomorphic processes, so much so that the U.S. Environmental Protection Agency (EPA) has recently begun to mandate 'hydromodification' regulations (EPA, 2006). Channel instability and complex responses have been associated with urbanization across hydroclimatic regimes (Booth, 1990; Simon and Downs, 1995; Trimble, 1997; Bledsoe and Watson, 2001; Chin and Gregory, 2001; Chin, 2006), while altered flow and sediment regimes affect aquatic life cycles,

habitats, food webs, and facilitate colonization by invasive species, among other types of degradation (Waters, 1995; Roesner and Bledsoe, 2002; Poff *et al.*, 2006).

Field investigations seemed to indicate an increased sensitivity to hydromodification in southern California, consistent with previous studies (Coleman *et al.*, 2005) and the semiarid climate in general (Trimble, 1997). The hydrogeomorphic setting (i.e., steep topography, flashy regimes, high-sediment loads, and largely nonresistant bed material) generally compounds risk factors for far-reaching channel responses such as headcutting, bank failure, and planform shifts. As a part of a larger project focused on understanding and mitigating the physical effects of hydromodification in southern California, it was imperative to first develop an understanding of how urbanization has affected flow regimes in different regional settings. With a focus on small free-flowing streams, the ensuing investigation had the following objectives:

1. offer an updated alternative to the USGS (Waananen and Crippen, 1977) regional equations for peak flows;
2. develop a physically-based empirical method for estimating long-term cumulative duration histograms for ungauged sites; and
3. determine how urbanization affects peak flows and cumulative durations for all geomorphically important flows by including urban components (if statistically significant) in Objectives 1 and 2.

In filling these knowledge gaps, we offer the following hypotheses:

H<sub>0</sub>: urban influence on the magnitudes of peak flows will be highest at the more frequent events and lowest at the longer recurrence intervals;

- H<sub>0</sub>: the lack of representation of southern California gauges used to develop the USGS national urban equation (Sauer *et al.*, 1983) should result in better model performance from equations calibrated directly to the region; and
- H<sub>0</sub>: cumulative durations can be modeled with reasonable accuracies and will be significantly influenced by urbanization.

### **1.1.1 Research foundations and justification**

This chapter principally builds on the work and ongoing data collection of the USGS. Waananen and Crippen developed regional equations for estimating peak flows in southern California in 1977, which to this day serve as a primary method of flow estimation. Although they tested an array of variables for statistical significance, their equations became power functions of drainage area and mean annual precipitation. The equations were limited by the available data in 1977 and came with substantial standard errors. Most notably, the authors concluded that the equations were “generally applicable for streams with drainage areas greater than 10 mi<sup>2</sup>” (Waananen and Crippen, 1977). This was due to an overall lack of gauge data on “streams with drainage areas generally less than 25 mi<sup>2</sup>, and particularly less than 10 mi<sup>2</sup>.”

With over 30 more years of data, and especially more data on smaller streams, it was prudent to revisit these equations. In this chapter, I go beyond the Log-Pearson Type III distribution to a more regionally appropriate statistical distribution. With several gauges in developed watersheds, urbanization was included in the models using direct measures of total impervious area (TIA). This approach is arguably less subjective and more parsimonious than the USGS national approach to urban flow augmentation (Sauer

*et al.*, 1983), which can be time intensive and is subject to user interpretation of several metrics that are typically immeasurable with available Geographic Information System (GIS) data. Moreover, of the 199 gauges used to develop the national equations, few gauges were from semiarid settings, with only one from southern California (San Diego Creek, gauge no. 11048500). Despite largely different hydrologic behavior relative to much of the rest of the nation, the USGS national equations are currently being applied throughout the region.

### **1.1.2 Toward cumulative durations**

Peak flows alone can be useful in understanding potential erosive energy at an individual recurrence interval; however, they have less meaning when considered independent of durations. Whether a large flow lasts for minutes, hours, or days has substantial implications to the cumulative sediment transport. Moreover, all flows capable of moving sediment have the potential to influence channel form, *sensu* the concept of geomorphic *effectiveness* (Wolman and Miller, 1960).

It follows that when evaluating the potential impacts of urbanization on channel stability, researchers have begun to favor cumulative sediment-transport models based on continuous or pseudo-continuous/cumulative flows over extended periods (e.g., several years/decades). In evaluating various flow-control schemes in the Pacific Northwest, Booth and Jackson (1997) alluded to the potential benefits of ‘duration’ standards in contrast to ‘peak’ standards, particularly at flows above the threshold of sediment entrainment. Consideration of all sediment-transporting flows would seem especially important in the semiarid environment known for sporadic sediment movements (Graf,

1981, 1988), extended periods of aggradation/degradation and lagged recovery times (Wolman and Gerson, 1978), and relatively infrequent periods of equilibrium (Bull, 1997). One of the only published approaches to addressing hydromodification in California to date uses flow-duration histograms produced from long-term rainfall runoff simulations in Hydrologic Engineering Center - Hydrologic Modeling System (HEC-HMS) to compute an 'effective work index' by summing excess shear stress over cumulative flow durations of 50 yrs (Santa Clara, 2004). The corresponding mitigation goal is to design flow control such that cumulative post-developed effective shear stress matches the pre-developed regime. The Sediment Impact Analysis Method (SIAM), publicly available via the U.S. Army Corps of Engineers (USACE) in the Hydrologic Engineering Center - River Analysis System (HEC-RAS) software package, is also designed to use a histogram-style flow-duration curve and can be used to model long-term sediment transport (Mooney, 2007; USACE, 2009).

The alternative to using rainfall runoff models to develop flow-frequency curves is to base them on local gauge data. Hey (1975) proposed a drainage-area scaling approach to estimate flow-duration curves at ungauged locations based on the nearest upstream/downstream gauge. Concurrent and subsequent research proposed regionalized duration curves using a gauge from a similar watershed and scaling based on a nondimensional index such as  $Q/Q_{\text{bankfull}}$  (Emmett, 1975; Leopold, 1994) or  $Q/Q_2$  (Watson *et al.*, 1997). The advantage of the latter is that the 2-yr flow may be estimated by a USGS regional equation, whereas the bankfull flow is often difficult to define and does not have a consistent return interval across different streams (Pickup and Warner, 1976; Williams, 1978; Biedenharn *et al.*, 2000; 2001). The disadvantage of scaling based

on the 2-yr flow is that, at least in southern California, it comes with much poorer accuracies than higher recurrence intervals (Waananen and Crippen, 1977). It may also be difficult to define which gauge(s) is similar enough to the ungauged watershed for direct scaling (e.g., similar topography, basin size, precipitation etc.).

We expand on the Watson *et al.* (1997) approach by developing a statistical model to estimate and calibrate flow-duration curves for ungauged sites with all regional gauges meeting our selection criteria, such that a synthetic flow-duration histogram is predicted as a function of watershed-scale physical descriptors (e.g., drainage density, annual precipitation, and average surface slope). The resulting *conditional* probability density functions that predict cumulative durations of geomorphically effective flows in a histogram format are henceforth referred to as Duration Density Functions (DDFs). The logarithmically distributed histogram bins are represented by power functions (i.e., #days = coef \*  $Q^{\text{exp}}$ ), and scaled by the maximum daily flow of record. Given a way to predict the shape (exponent), magnitude (coefficient), and scale ( $Q_{\text{max}}$ ) based on physical parameters, one could predict long-term durations of sediment-transporting flows for any ungauged watershed. More importantly regarding hydromodification, DDFs could simulate the increases in durations of sediment-transporting flows associated with unmitigated urbanization by including a statistically-significant surrogate measure (i.e., TIA) in the model. In this light, DDFs can become a central tool in understanding, modeling, and mitigating the effects of hydromodification in southern California.

### 1.1.3 Study domain

Southern California is generally described in this study as the greater Los Angeles/San Diego area within about 100 mi of the Pacific coast. It includes portions of Ventura, Los Angeles, San Bernardino, Orange, Riverside, and San Diego Counties (moving roughly northwest to southeast, down coast) and approximately 20 to 25 million residents. Mountain ranges to the north (Transverse Ranges) and east (Peninsular Ranges) offer fairly well-defined geologic bounds, with a total relief of up to 11,500 ft (3,500 m) and short travel distances to the ocean on the order of 50 mi (~100 km). The steep slopes promote runoff and produce more hydrologically-efficient watersheds than low-relief settings.

The climate is broadly characterized as Mediterranean, but precipitation and vegetative cover vary significantly. Both tend to increase with elevation, although there are obvious differences between the west (wetter) and east (drier) slopes of the Peninsular Ranges due to an effective ‘rain shadow’ similar to our home in Fort Collins, Colorado. Regional extremes of average annual precipitation range 8 to 40 in/yr (200 to 1,000 mm/yr), while vegetation changes from sparse grasses and chaparral to dense coniferous stands at higher elevations. When rains do fall, they can be intense; the 2-yr 24-hr rainfall ranges ~2 to 6 in (50 to 160 mm) across the domain.

Semiarid climates have long been associated with flashy flow regimes (Wolman and Gerson, 1978) and southern California is no exception. Short-lived instantaneous peak flows are much larger than the corresponding daily means. For example, a 10-yr instantaneous event would typically attenuate to a daily-mean flow on the order of a 2- to 3-yr event, with the former likely 10 to 20 times the latter. Consistent with Knighton’s

(1998) generalizations for the semiarid setting, channels in southern California are predominantly ephemeral and clearly dominated by overland flow with little groundwater storage relative to humid systems. The heterogeneous lithologies have variable infiltration capacities, but differences seem to be overwhelmed during high-intensity storms, although they probably play a role in seepage losses during transmission.

Beyond seasonal patterns, large fluctuations in inter-year, decadal, and even multi-decadal precipitation result in an active fire regime. Regional fires are often newsworthy not only for home destruction and mass evacuations but indirect damage caused by post-fire landslides and flooding. Emergency response agencies, news reports, popular culture, and academic literature have and continue to document large pulses in both sediment and runoff (California Forest and Range Experiment Station (CaFS), 1951; Los Angeles County Flood Control District (LACFCD), 1959; McPhee, 1989; Booker *et al.*, 1993; Benda and Dunne, 1997a, 1997b). As early as 1947, the CaFS had recorded post-fire peaks 2 to 30 times as large as pre-fire peak flows for equivalent storms in their experimental forest, with influence decreasing with storm magnitude.

Finally, during field investigations of recently developed suburban neighborhoods, we saw little evidence of stormwater retention/detention. Developed watersheds often had lined channels (i.e., concrete or riprap) and energy dissipaters at outfalls were occasionally present. Large regional basins and dammed reservoirs do exist; however, flow controls in smaller watersheds were largely lacking. With the understanding that unmitigated urbanization largely increases flow variability, and that streams in southern California are inherently flashy, we hypothesize that the effects of urbanization may be especially pronounced.

## 1.2 Methods

Gauge data are made publicly available by the USGS, which adheres to strict quality assurance/quality control (QA/QC) procedures prior to publishing flows as accepted/approved. To ensure comparable quality in processing and analysis, we developed the following methods. Some of the methods report limited presentation and discussion of preliminary ‘results’ that informed model design and/or were less central to the overall conclusions of this research. For example, regarding peak flows, it was necessary to decide on a distribution prior to the building of statistical models. Section 1.2.2 describes how we looked at several distributions and which was selected to use in model design.

The following sub-sections summarize the process by which we methodically arrived at the final results of this research. First, I systematically selected regional gauges with sufficiently long records for these analyses. Next, peak-flow data were processed to determine recurrence-interval flows. The following step was to develop a method for processing and representing all daily-mean flows via cumulative histogram-based functions. Methods were then considered for objectively representing the extent of urbanization. Next, informed by literature and a theoretical understanding of surface-drainage network hydrology, an expansive array of spatially-based variables was populated for inclusion in the analyses. Lastly, analytical methods are presented including a multistep cross-validation process that guided final model design.

### 1.2.1 Gauge-selection criteria

The first step in this research was the systematic selection of regional gauges for inclusion in the analyses. The focus was on watersheds less than  $\sim 100$  mi<sup>2</sup> (250 km<sup>2</sup>), primarily due to the fact that most of the region's larger streams have been affected by dams and diversions. We excluded gauges that were artificially influenced by flow diversions to isolate only the effects of urbanization relative to the undeveloped, free-flowing setting. Aerial photography, GIS layers of dams/diversions, and USGS notes/site descriptions were used to verify that selected gauges were unregulated.

Additionally, attempts were made to strike a balance between selecting a large representation of sites and limiting the sample to gauges with sufficiently long records. Using gauges with short records increases the likelihood of misrepresenting the true flow regime due to the disproportional influence of extreme flows. For example, a record of only 10 yrs could have been active during a decade-long drought or, in contrast, an exceptionally wet period. Stochastic processing would treat each record as equally likely, irrespective of the wider trends.

At the same time, overly conservative record-length requirements would eliminate the bulk of gauges. For example, only 19 of the candidate gauges had records of 50 yrs or more. Yet there were 43 gauges with records of at least 25 yrs and 49 gauges with greater than 20 yrs. Identifying a set of at least 50 sites was statistically desirable due to the heuristic guideline of ca. 10 observations per predictor variable (i.e., 50 sites could result in equations with up to 5 independent variables). There was a natural break in the record lengths of the candidate gauges at ca. 15 yrs (2 gauges at 18 yrs with 1 gauge at 14 yrs and the balance less than ca. 8 yrs). With limited urban/semi-urban gauges (i.e., only

8 gauges > 2.5% imperviousness), the fact that the 14-yr record was in a partially urban watershed (imperviousness = 2.7% in 2001) supported its inclusion. This totaled 52 gauges with a spatial distribution depicted in Figure 1.1. A summary of selected gradients such as drainage area and record length is provided in Table 1.1, with a comprehensive list included in Appendix A. These gradients also serve as bounds to the applicable ranges of our models.

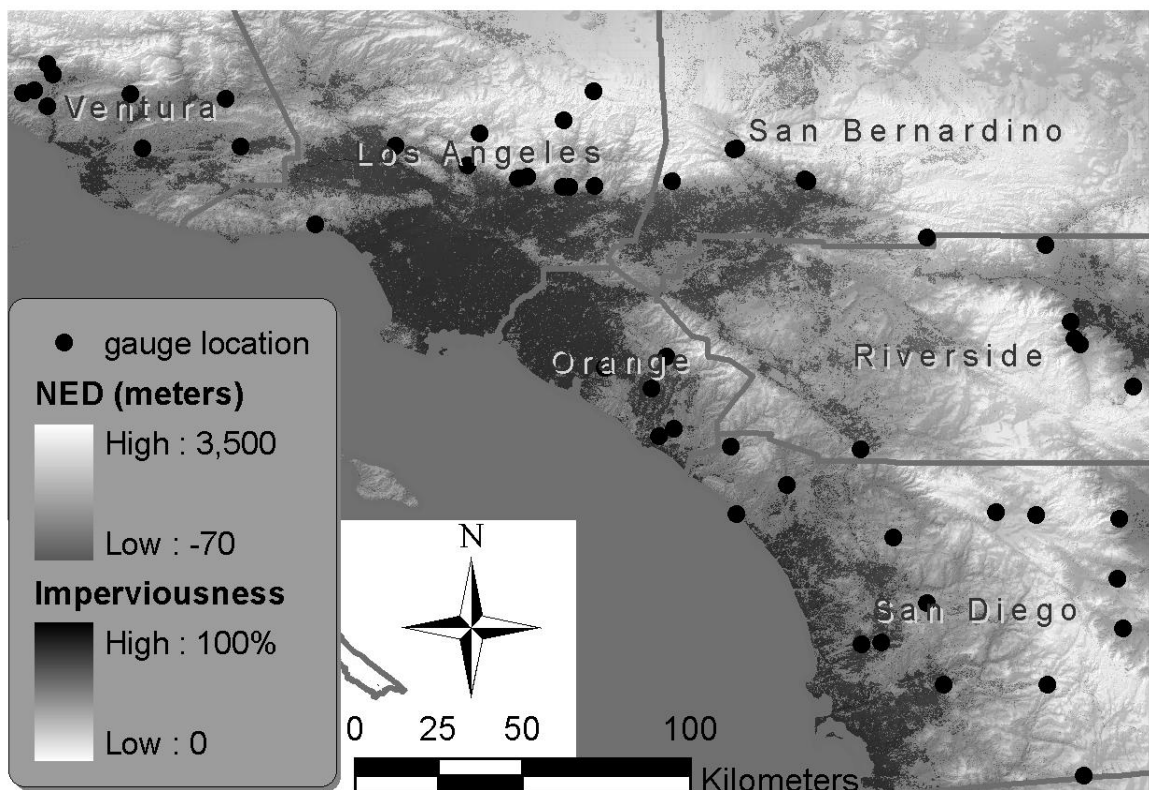


**Figure 1.1 – Locations of gauges used in equation development, overlaid by gradients of elevation and imperviousness**

**Table 1.1 – Selected gradients of the 52 USGS gauges used to develop models (i.e., model-application bounds)**

<b>Key Gradient</b>	<b>Minimum - Maximum</b>	<b>Mean</b>	<b>Units</b>
drainage area	0.5 - 105 (1.4 - 270)	30 (80)	mi <sup>2</sup> (km <sup>2</sup> )
peak record	14 - 94	45	yrs
average annual rainfall	11 - 36 (280 - 900)	23 (600)	in (mm)
drainage density	1.3 - 4.1 (0.8 - 2.6)	2.3 (1.4)	mi/mi <sup>2</sup> (km/km <sup>2</sup> )
average surface slope	5 - 52	26	%
imperviousness	0 - 26	3.6	%

Study sites generally had normal distributions of variables such as record length, precipitation, and surface slope, although drainage area and density showed a small positive skew. Imperviousness, however, had a highly positive skew of 2.5. As of 2001, only 15 gauges had watersheds with more than 1% impervious area, while only 6 were greater than 10% imperviousness. Most of the gauges are located in watersheds that remain predominantly undeveloped on the outskirts of the valleys surrounding Los Angeles and San Diego. In Los Angeles County, for example, several gauges are located northeast of the city where streams draining the Transverse Ranges meet the open valleys outside of the urban areas. The most developed gauges are generally located near the coast and distributed across Ventura, Orange, and San Diego Counties.

Another notable spatial trend is that 8 gauges located in the eastern-most portion of the domain and 1 gauge in the far southeast at the Mexican border lie in what is effectively a rain shadow. Stratified by USGS 8-digit Hydrologic Unit Codes (HUCs) of 18100200 or 18070305, the so-called ‘Dry’ gauges were subject to less mean annual

precipitation as well as different types of events (i.e., local convective thunderstorms in addition to winter frontal storms). As we shall see, such differences in climatic boundary conditions can have a significant influence on the hydrologic behavior of receiving streams.

### **1.2.2 Instantaneous peak flows**

Next, procedures were developed to populate recurrence-interval flows for the 1-, 1.5-, 2-, 5-, 10-, 25-, 50-, and 100-yr events from peak-flow data as recorded by the USGS. Their method seemed to be a hybrid of an annual-maximum and partial-duration approach, with an average of one record per calendar/water year, but cases of same-year peaks and occasional gaps during dry years. If a gauge was online during a no-flow year and a corresponding peak of 0 was not already recorded, the record was augmented for two purposes. First, it standardized the sample size at all gauges to make the Weibull plotting position a function of years of gauge record rather than years of selected peaks (i.e., an annual-maximum series). Second, it represented the annual probability of having a 0-flow year. This was required on 9 gauges and had clear implications on  $Q_1$ ; however, it had little effect on higher recurrence intervals. For example, recurrence probabilities such as  $Q_{1.5}$  and  $Q_2$  generally had several similar flows near those rankings such that a shift would still result in a flow from the same range (e.g., 349 vs. 331 cfs for  $Q_{1.5}$  and 570.5 vs. 571 cfs for  $Q_2$  at Arroyo Seco). Even less effect would be seen at the higher flows (i.e.,  $p = 1/25$  vs.  $1/24$  is effectively equivalent as representative of the 25-yr flow).

Other cases of record gaps included years with the date and/or stage of the peak but no flow. Interpolations based on USGS-rating relationships were used to estimate a

reasonable flow for that date based on equivalent gauge heights and/or daily-mean flows. This was performed at 10 gauges, representing less than 20% of the total. The interpolated flows were not used to determine a flow for a specific return interval; rather, they were simply used as placeholders in the plotting-position rankings.

Flows were proportionally ranked to determine recurrence probabilities via the Weibull plotting position (Chow, 1964; Yevjevich, 1972). Although a plenitude of stochastic models have been used to represent hydrologic processes such as annual precipitation, annual-maximum flows (Chow *et al.*, 1988), and streamflow time series (Salas and Smith, 1981), we considered three statistical distributions most closely related to the U. S. Water Resources Council Method for flood-flow frequency. Because a central component of this chapter is an updated alternative to the 1977 regional equations, it was prudent to attempt to harmonize with the standard USGS procedures wherever justified.

I began with the Log-Pearson Type III method, which is the recommended distribution by the USGS since 1967 (U. S. Water Resources Council, 1967). Because the Log-Pearson Type III method is essentially a gamma distribution weighted by the skew of the logarithmic transformations of the peak flows, it was logical to explore the applicability of the unbiased component distributions. For simplicity, the natural logarithm was fitted, as opposed to base 10. As an easily invertible function, the cumulative distribution gamma function most pragmatically took the form of an inverse gamma. In this light, the inverse gamma could be used to predict flows based on probabilities of nonoccurrence (1-probability of occurrence) rather than model recurrence probabilities based on flows. By solving for the gamma parameters that minimized

residual squares between recorded and modeled flows, proportional weight is given to the larger flows; whereas, the reverse procedure would dampen the significance of larger flows by minimizing residuals among recurrence probabilities.

Despite application in previous studies, the Log-Pearson Type III performed the poorest due to the flashy regimes and the corresponding effect on the skew factor. A skew factor is necessary because the Log-Pearson Type III distribution cannot be solved analytically when inverted. Even by following the recommended weighting scheme, which attempts to correct for the effect of extreme events and smaller samples (U. S. Water Resources Council, 1981), the large number of gauges with years of very low or no flow typically converted a highly positive skew in arithmetic space to a negative skew after the log-transformation. As discussed by Chow *et al.* (1988), this imposes an artificial upper bound on the data. Attempts to account for the low/zero flows within the confines of the Log-Pearson Type III method via the addition of correction factors both large and small either adversely affected the distribution shape ( $\text{Log}(Q + 100 \text{ cfs})$ ) or ineffectively adjusted its magnitude ( $\text{Log}(Q + 0.1 \text{ cfs})$ ). This case is exemplified in Figure 1.2.

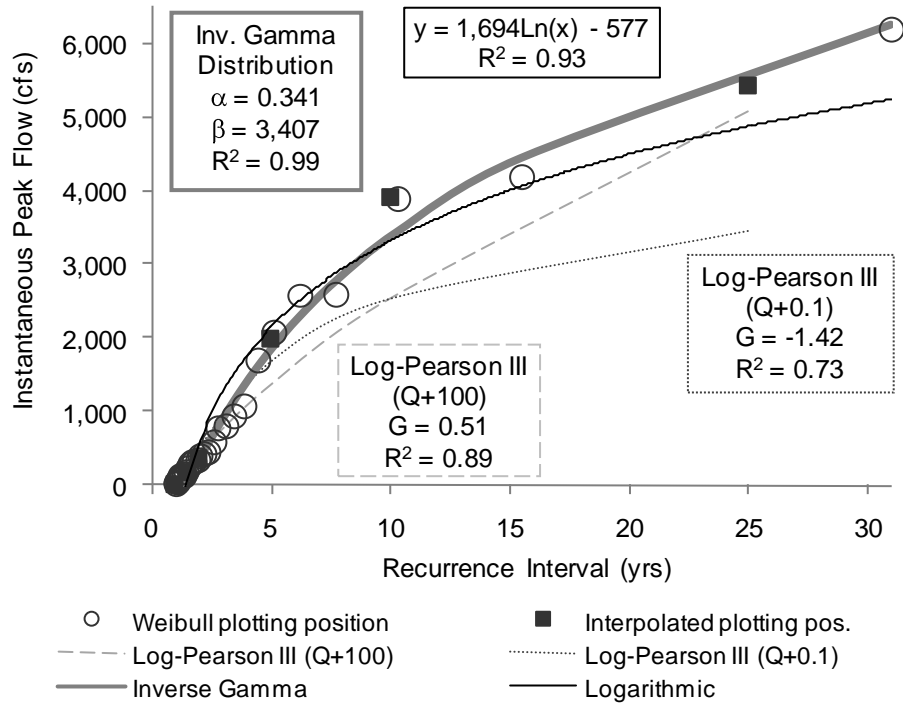


**Figure 1.2 – Flow vs. recurrence interval of 30-yr record at USGS gauge no. 11033000, WF San Luis Rey R. near Warner Springs, California, with logarithmic, Log-Pearson Type III adjusted (Q+0.1) and (Q+100), and inverse gamma distributions**

In contrast, both the logarithmic and inverse gamma distributions performed relatively well, with the inverse gamma superior in every case (mean  $R^2 = 0.95$ , with only four cases  $< 0.90$ ). Bounded by zero by definition, the gamma function is ideal for modeling skewed distributions without the need for a log transformation (Chow *et al.*, 1988), making it practically designed for the flashy ephemeral regimes of southern California. Gamma distribution flows were used for models greater than or equal to the 5-yr interval, while the Weibull plotting position was used for the 1-, 1.5-, and 2-yr events due to nominal interpolation gaps over the smaller ranges given the relatively large record lengths.

### 1.2.3 Long-term cumulative durations

Processing of daily-mean flows toward the development of cumulative-duration curves for ungauged sites was guided by the ultimate application of such models in magnitude-frequency analyses for sediment transport as a part of the broader hydromodification project. First, daily-mean flows were binned via a histogram procedure analogous to the initial steps of an effective discharge calculation after Biedenharn *et al.* (2000, 2001). Histogram bins were scaled by the maximum daily-mean flow on record ( $Q_{\max}$ ) rather than an instantaneous peak flow (e.g.,  $Q_2$  after Watson *et al.* (1997)) for several reasons. Foremost, and as we shall see,  $Q_{\max}$  could be predicted with much greater accuracies than the highly variable  $Q_2$ . Scaling with  $Q_{\max}$  also ensured consistent temporal scales for the duration analyses because daily-mean discharges were the only long-term records widely available (i.e., opposed to shorter intervals such as 1-hr or 15-min). This was unfortunate because representing flashy regimes with daily-mean data can result in substantial differences in long-term sediment-transport yields – the application for which our models are directly intended. For example, Watson *et al.* (1997) reported 50% differences between sediment yields produced from 15-min and 24-hr flows in small ( $< 1,000 \text{ km}^2$ ) flashy systems in the Yazoo River Basin of Mississippi. Even so, because of data availability I was constrained to working with daily-mean flows if I was to have any idea of flow durations.

To continue, scaling duration curves to a daily-mean flow was more judicious than an instantaneous peak flow because the two time scales were not transferable or even scalable. The ratio of peak to daily mean was not consistent across return periods, sites, or even equivalent flows at the same site. For example, two equivalent 10-yr peak

flows recorded at the same gauge could have corresponding daily-mean flows that differed by a factor of 2 in rural settings, and up to 3 in urban settings, potentially attributable to the spatial extent, intensity, or even timing of the event.

As such,  $Q_{\max}$  became a more practical upper bound when determining histogram bin size. For example, the size of arithmetically segregated bins would follow the function after Raff *et al.* (2004):

$$H_{B\text{-arth}} = (Q_{\max} - Q_{\min}) / N_B \quad \text{Eq. (1.1)}$$

where:

$H_{B\text{-arth}}$  = bin size of arithmetically-spaced histogram bins;

$Q_{\max}$  = maximum flow of record;

$Q_{\min}$  = minimum flow of record; and

$N_B$  = number of bins.

Regarding the selection of the type and number of bins for our models, their influence on sediment-distribution curves – the ultimate application in this overall project – was considered. Hey (1997) found that 25 equally-spaced arithmetic bins typically resulted in continuous distributions for determining effective discharge; however, up to 250 arithmetic bins have been necessary on streams with a large number of low flows. The truly limiting factor in bin selection is ensuring a relatively continuous flow-frequency distribution such that no bins are populated by 0 days of occurrence (Biedenharn *et al.*, 2000, 2001). Although arithmetic bins are statistically more prudent, the extreme flashiness of ephemeral streams in southern California made logarithmic bins the only practical way to represent flow frequency without discontinuities. The following equation was used to size logarithmically equivalent bins after Raff *et al.* (2004):

$$H_{B\text{-log}} = \{\ln(Q_{\max}) - \ln(Q_{\min})\} / (N_B - 1) \quad \text{Eq. (1.2)}$$

where:

$H_{B\text{-log}}$  = bin size of logarithmically-spaced histogram bins;

$Q_{\max}$  = maximum flow of record;

$Q_{\min}$  = minimum flow of record; and

$N_B$  = number of bins.

To be consistent across all gauges toward development of a regional equation, we set  $Q_{\min}$  equal to 0.01 cfs at all sites, the lowest non-zero daily-mean flow reported by any gauge. Bins 1 through  $N_B$  were then populated by the total number of days of occurrence at flow rates within the respective bins. Lower and upper bounds of each logarithmically-spaced bin were determined using the following equations after Raff *et al.* (2004):

$$B_{\text{lwr-log}} = e^{\{\ln(Q_{\min}) + (B-2) \cdot H_{B\text{-log}}\}} \quad \text{Eq. (1.3)}$$

$$B_{\text{upr-log}} = e^{\{\ln(Q_{\min}) + (B-1) \cdot H_{B\text{-log}}\}} \quad \text{Eq. (1.4)}$$

where:

$B_{\text{lwr-log}}$  = lower logarithmically-spaced bound of bin number (B);

$B_{\text{upr-log}}$  = upper logarithmically-spaced bound of bin number (B); and

B = bin number (i.e., 1 to  $N_B$ , where  $N_B$  = total number of bins).

Setting  $N_B$  equal to 25 provided a reasonable balance of resolution (small bin sizes) and continuous frequency distributions. All but three gauges, Buckhorn (6 yrs), Honda Barranca (9 yrs), and Keys C (14 yrs), had daily records long enough to sufficiently populate 25 bins. Little San Gorgonio, despite having a long enough record

(37 yrs), was skewed by an extreme flow resulting in three of the top six bins being empty with the remaining three only having 1 day of occurrence. An additional three gauges (Cucamonga, Pechanga, and Waterman) each had one bin populated with 0 days of occurrence. Due to the fact that adjacent bins were amply populated, we ‘borrowed’ 0.5 days from each adjacent bin to convert the 0-day bin into a 1-day bin. Of the original 52 gauges, this resulted in 48 that could be included in the models.

In order to represent the histograms in a concise, transferable format, the next step was to convert them into probability density functions (PDFs) by fitting power functions to the centroids of the bins representing the geomorphically effective range of flows. DDFs, as earlier defined, are *conditional* PDFs dependent on 25 logarithmically-distributed bins between 0.01 and  $Q_{\max}$ . Had the distributions been such that we could have kept the bin sizes sufficiently small to take the limit as  $H_B \rightarrow 0$  and  $N_B \rightarrow \infty$ , a function fit to the upper-bin boundary ( $B_{\text{upr}}$ ) would have been an unconditional PDF capable of predicting the probability (or days of occurrence) for any flow. With the data constricted to mean 24-hr flows, the record was too discontinuous among the high discharges to arrive at an *unconditional* PDF. Hence, the trial-and-error procedure described above was necessary to determine the most consistent boundary conditions for defining histograms without 0-day bins.

Again looking toward application, with a high likelihood of under-predicting sediment transport due to data intervals of days rather than minutes, further bias was avoided by fitting the DDFs to the arithmetic-bin centroids, as opposed to the logarithmic centroids. This positioned each centroid on a slightly higher flow than the otherwise geometric centroid (e.g., 806 cfs vs. 774 cfs for bin 21 at San Antonio, or 8,119 cfs vs.

7,793 cfs for bin 25). Given that sediment transport increases non-linearly with flow, such a scheme would better approximate the composite transport of the individual flows within the bin.

The next consideration was which bins would be important to represent for sediment transport. Their shape was such that bins 12-25, and particularly bins 16-25, were relatively continuous such that they could be well represented with simple power functions. Fortuitously, those bins that could be well-fit coincided with the same ranges that would be important for sediment transport. From preliminary analyses it was apparent that streams characterized by threshold behavior (i.e.,  $\tau_{*BF} \sim 0.03$  to  $0.06$ ) would be sufficiently represented with a 16-25 scheme, while live-bed channels (i.e.,  $\tau_{*BF} \sim 1$  to  $10+$ ) would require the broader range. Below bin 12, and as we shall see in Chapter 3, it was anticipated that cumulative sediment transport would be relatively insignificant compared to the rest of the regime.

Figure 1.3 offers an example of a typical DDF fit of bins 16-25 at the San Antonio gauge. Overlaid in the Figure 1.3 is the De Luz gauge as an example of one of the poorer fits (i.e., 13 gauges with  $R^2 < 0.95$ , 5 gauges  $< 0.90$ ). By depicting two gauges with relatively similar watersheds, Figure 1.3 also alludes to the significance of the gauge-record length. DDFs scaled nonlinearly with years of duration, primarily attributable to the extreme flashiness and inter-year variability in precipitation. Longer gauge records have higher probabilities of experiencing an extreme precipitation event, corresponding to nonlinear increases in flows and durations.

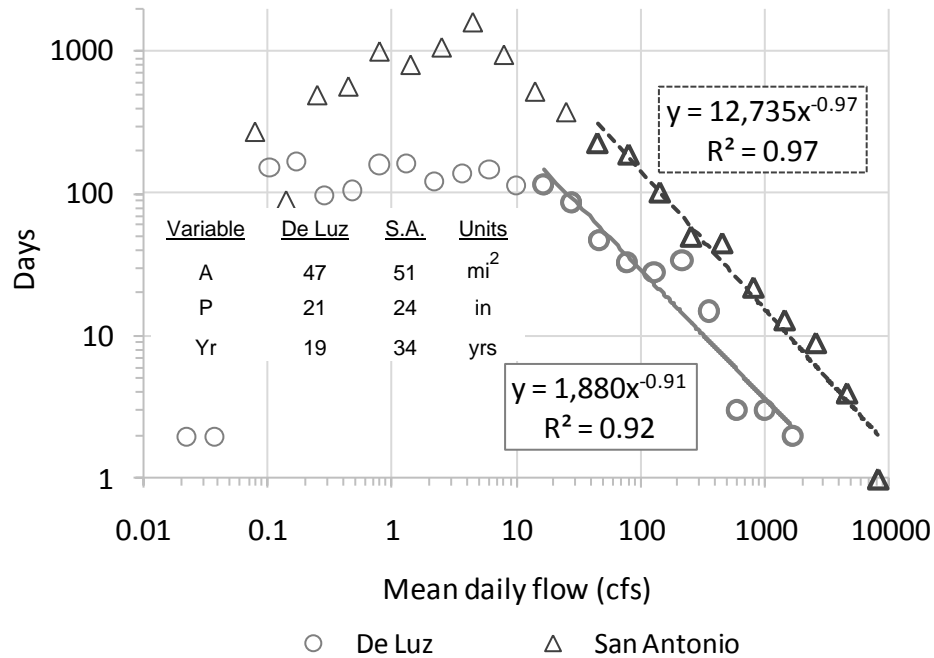


**Figure 1.3 – DDFs of gauges De Luz and San Antonio fitted to centroids of logarithmically-distributed histogram bins 16-25 with selected parameters of drainage area, average annual precipitation, and record length**

Apparent in Figure 1.3, the 16-25 scheme with the coefficient and exponent parameters termed d1 and d2, respectively, showed largely homoscedastic residuals at the risk of not capturing all sediment-transporting bins in live-bed channels (bin 16 of San Antonio = 45 cfs). The second scheme, termed day1 and day2, regressed bins 12-25 to more conservatively include all significant sediment-transporting flows (e.g., bin 12 at San Antonio = 4.5 cfs). However, as one could envision with De Luz (Figure 1.3), the disadvantage in including bins 12-15 is that it resulted in more heteroscedastic residuals at some gauges.  $R^2$  values were also slightly worse, with 8 gauges less than 0.90 and 17 gauges less than 0.95. The general form of the power functions used in the respective schemes are:

$$\text{days}_{@Q} = d1 * Q^{d2} \quad (\text{bins 16-25, i.e., } \tau_{*BF} \sim 0.03 \text{ to } 0.06) \quad \text{Eq. (1.5)}$$

$$\text{days}_{@Q} = \text{day1} * Q^{\text{day2}} \quad (\text{bins 12-25, i.e., } \tau_{*BF} \sim 1 \text{ to } 10+) \quad \text{Eq. (1.6)}$$

where:

$\text{days}_{@Q}$  = number of days of occurrence at flow rate (Q);

Q = arithmetic average of daily-mean flows corresponding to the lower- and upper-bin boundaries defined by Eqs. (1.3) and (1.4), respectively (cfs);

d1 = coefficient for power function fit to bins 16-25;

d2 = exponent for power function fit to bins 16-25;

day1 = coefficient for power function fit to bins 12-25;

day2 = exponent for power function fit to bins 12-25; and

$\tau_{*BF}$  = dimensionless shear-stress ranges at approximate 'bankfull' flow range (i.e., on the order of  $Q_{10}$ ) corresponding to threshold (0.03 to 0.06), and live-bed (1 to 10+) behavior.

With the outlined methods for processing daily-mean flows, DDFs were fit to all gauges to populate a matrix of their respective components (i.e.,  $Q_{max}$ , d1/day1, d2/day2). The data set was used to develop models of each DDF component as multivariate functions of statistically-significant physical parameters, offering an objective method for estimating flows and cumulative durations at ungauged sites. In this light, long-term simulations of flow and sediment transport may be modeled after regional data as an alternative to conventional rainfall runoff models.

#### 1.2.4 Measures of urbanization

An investigation focused on understanding the influence of urbanization on flow regimes should dedicate great care to measuring its extent. With the goal of objectively representing urbanization in both space and time, we first looked to what other researchers used to characterize it, including but not limited to:

- % impervious area (Leopold, 1968; Espey and Winslow, 1974; Sauer *et al.*, 1983; Booth, 1991, 2000; Galster *et al.*, 2006),
- % developed (Rantz, 1971; Galster *et al.*, 2006),
- % served by storm sewers (Leopold, 1968; Rantz, 1971),
- % paved (Hollis, 1975),
- road density (Konrad and Booth, 2002),
- population density (Sauer *et al.*, 1983; Konrad and Booth, 2002), and
- numerical indices, e.g., function of channel conditions, stormwater connectivity, etc. (Espey and Winslow, 1974; Sauer *et al.*, 1983).

Measures have ranged from qualitative groupings (e.g., rural vs. urban) to fully continuous variables (e.g., % impervious). One of the more widely used approaches is to employ the USGS National Urban Equations developed by Sauer *et al.* (1983). The second most significant variable in the seven-parameter approach is the Basin Development Factor (BDF), which is a subjectively-assigned composite index (0 to 12) of channel improvements, channel linings, storm drains/sewers, and curb and guttered streets. From preliminary analyses it was determined that liberally assigning BDF values improved the performance of the USGS urban equations for southern California.

Informed by these previous approaches, there were several goals regarding the quantification of urbanization in our equations. First, despite being an empirical approach, assurance of fidelity of the hydrologic process is desired. Next, measures should be readily quantifiable via publically available GIS data (i.e., no subjectivity or field investigations necessary). Third, the variable should be a continuous metric wherever possible (e.g., % impervious) rather than taking the form of a dummy variable such as high, medium, and low. Finally, because urbanization is not constant through time, we needed to be able to measure changes in spatial extent over the gauge records.

Arguably, the measure of urbanization that is most rooted in theory and most important hydrologically is imperviousness (Novotny, 2003). Impervious surfaces diminish infiltration potential, converting precipitation directly into surface runoff. This is in large contrast to natural soil surfaces that delay overland flow until infiltration capacity is exceeded by the precipitation rate (Horton, 1945). Furthermore, by eliminating the vegetative layer, impervious surfaces lack the associated interception storage of plant surfaces (Chow, 1964). Additionally, they increase flows by decreasing surface roughness relative to soil/vegetated surfaces (Chow, 1959).

Yet, it is whether an impervious surface is *connected* to the drainage network that determines if the potential effects are transferred downstream. Effective Impervious Area (EIA) is defined as impervious surfaces that are directly connected to the downstream drainage system, consequently excluding any areas draining to pervious surfaces (Booth and Jackson, 1997). Although it is more representative of process than total impervious area (TIA), EIA can be arduous to measure. The two measures have been correlated on regional scales such as for Denver, Colorado (Alley and Veenhuis, 1983) and western

Washington (Dinicola, 1989); however, large differences in stormwater regulations throughout the country both in space and time suggest that the application of such relations to other regions would be imprudent. Fortunately for this research (although unfortunately for receiving streams), stormwater in southern California has largely gone unmitigated to date at the subdivision scale. This makes TIA generally much more representative of EIA than in other regions. Additionally, TIA is readily quantifiable in GIS via the USGS national impervious raster from 2001. Meeting both criteria of being objectively quantifiable and largely representative of process, TIA was used as one measure of urbanization.

Other important physical descriptors of urbanization are alterations of the hydrologic network via storm sewers, channelization/lining, or artificial surface storage. The latter has a diminishing effect on peak flows, while the other network adjustments can amplify peaks via decreased roughness and often shorter/steeper flow paths. Unfortunately, no public domain GIS layers were available to quantify storm sewers; therefore, it was decided to measure both road density and impervious area as potential surrogates. The USGS National Hydrography Dataset (NHD) offered measures of known artificial-channel adjustments in existing stream networks (e.g., ‘artificial path’, ‘canalditch’, ‘connector’, or ‘pipeline’). Quantifications of such artificial stream-network links were included, although they did not prove to be statistically significant in preliminary models.

As such, impervious area and road density were determined as the primary measures of urbanization. State of California (CA-Atlas) road vectors from 2000 and 2007, along with a USGS impervious raster (2001), were used as digital sources of

contemporary urbanization data. The 2000 vector file was clipped to match georeferenced historical USGS topographic quadrangle maps, providing two additional snapshots of road density in time (typically ranging between the 1950s to 1980s). An example at one of the most urban gauges, Arroyo Trabuco (gauge no. 11047300), is presented in Figure 1.4, along with 2001 impervious levels. Knowing which roads were not constructed at respective points in time provided the basis for clipping-out associated impervious areas from the 2001 raster file such that changes in imperviousness through time could also be estimated. This procedure was performed for each watershed greater than 1% impervious area in 2001 (15 gauges), with the expectation that watersheds with less than 1% impervious area in 2001 would show little change in development through time. As a check to see how urban measures changed in a rural setting, the historical procedure was performed on one gauge with 0.4% impervious area in 2001 (Lone Pine, gauge no. 11063500).

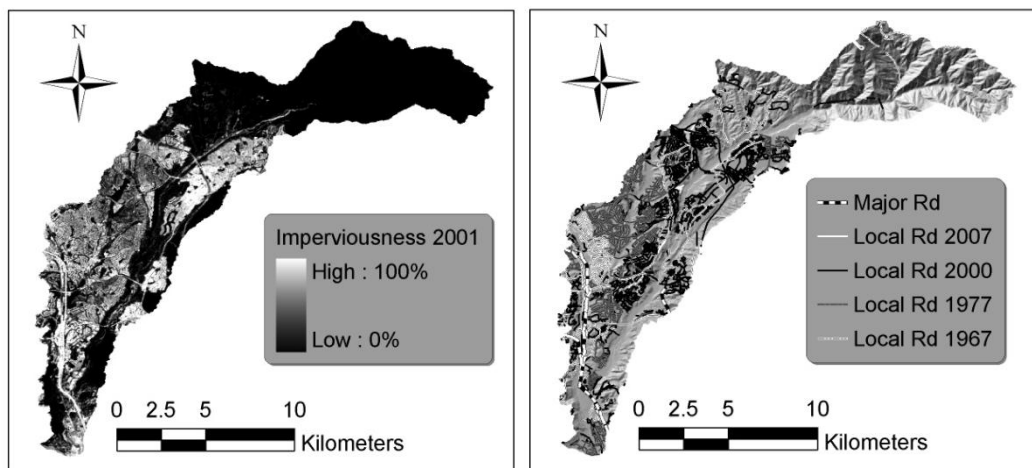


**Figure 1.4 – 2001 imperviousness and road vectors tracked through time per USGS historic quadrangle maps and current CA-Atlas shapefiles at Arroyo Trabuco (Orange County, California, near X of I-5 and I-405)**

From these measures of spatial extent in time, the trapezoidal rule was used to integrate changes in impervious area and road density over each gauge record to estimate mean values for the record. Although clearly imprecise due to the gaps between measured data, a simple linear interpolation between known measurements represents the mean estimate for all possible rates of change that could have occurred. To test the applicability of this assumption, regression lines were fit to the four known measurements to determine the global trend of the data. As seen in Figure 1.5, both imperviousness and road density proceeded quite linearly during the ‘development’ period at Arroyo Trabuco from 1967 to 2000, then leveled off during the last decade. In every case, a linear regression matched or surpassed the performance of other tested distributions such as logarithmic, power, or exponential in terms of  $R^2$  (typically  $\geq 0.95$ ). These linear correlations were also applied as quality assurance of the trapezoidal procedure via analytical integration over the gauge-record lengths.

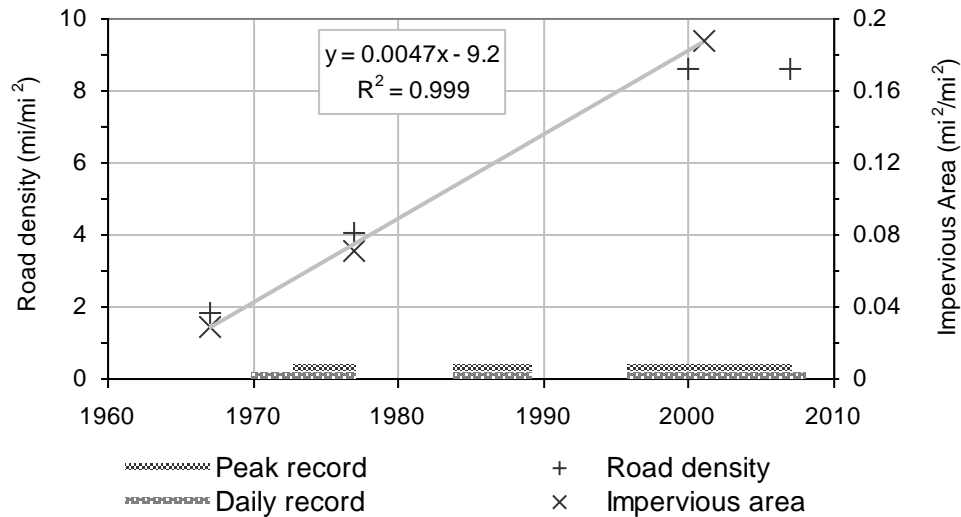


**Figure 1.5 – Imperviousness and road density through time at Arroyo Trabuco, overlaid by active gauge years and linear trendline of imperviousness (1967 - 2001)**

The gauges with the most urbanized records, those with the five highest integrated road densities (i.e.,  $> 4 \text{ mi/mi}^2$ ), were covered by measured values of road density over the entire record of flow, adding confidence to the trapezoidal integrations. However, ten of the gauges had records that extended beyond the earliest measured road-density value. Several methods were used to both bound the true value and obtain a more likely estimate as a function of the known measurements. An upper limit was determined by projecting the earliest road-density value as constant to the beginning of the gauge record, while assuming no roads were present prior to the earliest measurement served as a lower bound. More targeted estimates were determined by projecting the linear regression of the measured data to the beginning of the record. The two cases where this seemed illogical were at Aliso (gauge no. 11047500) and San Diego (gauge no. 11048500), in which the projected line intersected zero prior to the start of the gauge due to rapid development rates in the latter parts of the records that caused steep linear correlations. As it is unlikely these two drainages had a road-density value of zero during the twentieth century, it was important to consider an alternative beyond simply holding the earliest road-density value constant.

This was resolved through the understanding that the historical rate of change of road density was related to present extent of development. Watersheds with little development and corresponding road density had small degrees of change through time, compared to highly-developed watersheds. As depicted in Figure 1.6, the linear rate of change in road density going back in time becomes exponentially smaller, with a lower starting value in 2000. By measuring road density through time to a point of approximately 2 to 4 road miles per square mile ( $\text{mi/mi}^2$ ) of drainage area, it can be

reasonably assumed that the watershed had relatively little change in road density prior to that time (i.e., less than  $0.05 \text{ (mi/mi}^2\text{)/yr}$ ).

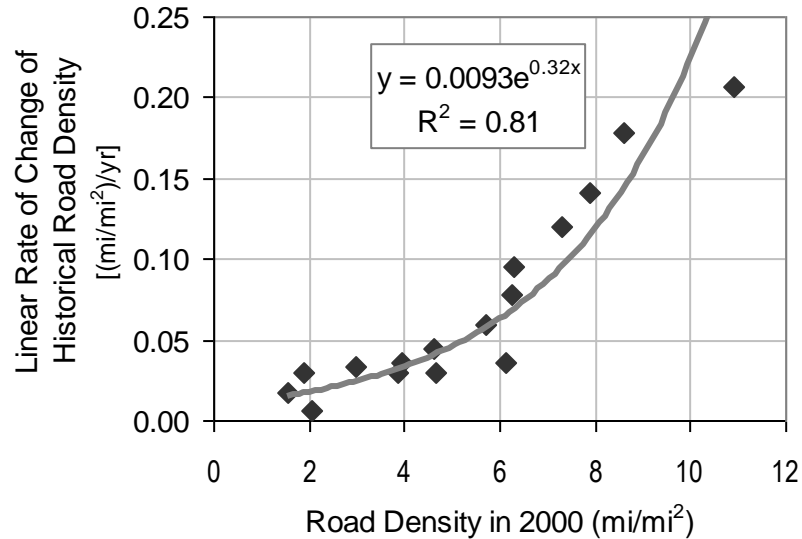


**Figure 1.6 – Average linear rate of change of measured historic road density as an exponential function of measured road density in 2000**

In every case, road density through time was tracked to a known value less than  $4 \text{ mi/mi}^2$ , justifying the use of this relation to project reasonable values of road density to the beginning of the gauge record. Even more importantly, this function could be applied to the rural watersheds where measurements were not made prior to 2000. Justified by the fact that none of the gauges with unmeasured road-density histories had values greater than  $3 \text{ mi/mi}^2$  in 2000, mean values of road density for all gauge records could be ultimately estimated. This was important because it avoided using a dummy variable to group urban and non-urban gauges, enabling a continuous variable for all gauges based on actual measurements.

A procedure analogous to the approach described above regarding road density was also performed for impervious area. After tracking the progression of urbanization

in such detail, several time-integrated measures were quantified of both road density and impervious area to test in the models. Those that proved to be most consistently significant (i.e.,  $p < 0.05$ ) in preliminary models are indicated in **bold**:

- Imperviousness (TIA)
  - **Average spatial extent** (i.e., mean spatial extent of imperviousness as tracked through time)
  - **Maximum spatial extent** (i.e., spatial extent during last year of gauge record)
  - Fraction of record  $>$  (i.e., amount of time out of total years of record greater than xx% impervious area)
    - 1.5%
    - **5%**
    - **7.5%**
    - 10%
    - 15%
- Road Density
  - Average spatial extent
  - Maximum spatial extent
  - Fraction of record  $>$ 
    - 2 mi/mi<sup>2</sup>
    - 4 mi/mi<sup>2</sup>
    - 5 mi/mi<sup>2</sup>

- 6 mi/mi<sup>2</sup>
- 8 mi/mi<sup>2</sup>

One potential explanation for the discrepancy in statistical significance between impervious area and road density is that TIA is a better surrogate for EIA than road density given such little stormwater mitigation to date. Even so, one might ask the logical question that if road density and imperviousness are linearly correlated (e.g., Figure 1.5), why was road density not significant at least as a surrogate of TIA? The answer lies in the fact that the two variables tend to be linearly correlated at individual sites; however, they are *exponentially* correlated across all sites. As evident in Figure 1.7, a relatively undeveloped gauge in a rural setting could have road densities up to 4 mi/mi<sup>2</sup> and still have minimal amounts of impervious area (i.e., ~1.5%), while a gauge in a developing watershed with just 50% higher road density could have over 7 times as much impervious area (i.e., 6 mi/mi<sup>2</sup> relative to 10% imperviousness). Furthermore, the exponential relation masks potentially critical differences in imperviousness in the early phases of development when ~2 mi/mi<sup>2</sup> could represent less than 0.1% TIA in a rural basin or greater than 2% in a developing basin. The correlation is also misrepresentative in highly urban basins (i.e., the relationship seems more linear than exponential above ~6 mi/mi<sup>2</sup>). Such a scattered-exponential-linear relationship between road density and TIA would make it difficult for a continuous model to use one measure as a surrogate for the other.

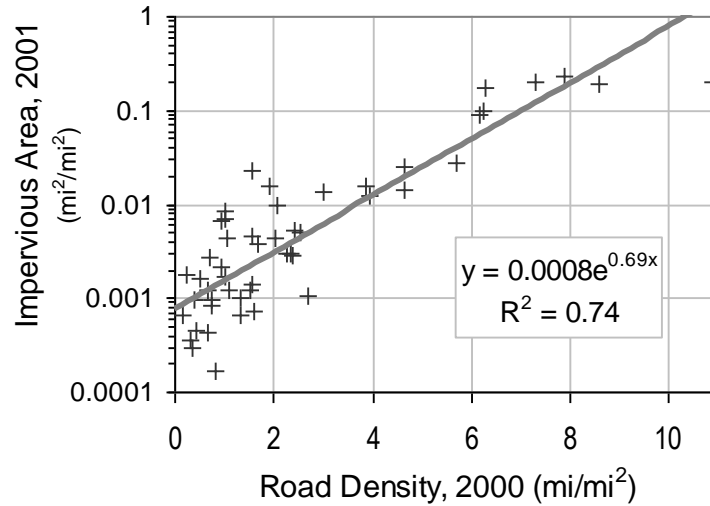


**Figure 1.7 – Exponential correlation between impervious area (2001) and road density (2000) across all sites**

### 1.2.5 Other physically-based parameters

As discussed by Schumm (1991), one way to avoid specious conclusions in empirical studies is to develop multiple competing hypotheses. It is not enough to infer causation by observing higher flows in urban settings. To be truly exhaustive, other possibilities should be offered and tested such as: are they in steeper watersheds, were they active during exceptional precipitation years, and so forth? By employing statistical software it is possible to test the influence of an expansive array of potentially competing factors. To do so, all one needs to do is measure them.

A matrix of readily quantifiable hydrogeomorphic metrics was populated across varying temporal and spatial scales, summarized earlier in Table 1.2. Beyond USGS flow records, long-term precipitation gauges in Los Angeles (LA) and San Diego (SD) were used as a relative measure of temporal variation in regional precipitation. GIS data were acquired from public-domain sources such as the USGS, U.S. Department of Agriculture (USDA), National Oceanic and Atmospheric Administration (NOAA), and

State of California geospatial clearinghouse (CAL-Atlas). Empty fields in some USDA polygons compromised the capacity to develop trends via Natural Resources Conservation Service (NRCS) soil types; however, most source data were complete. Two sources of average annual precipitation were available. The USGS layer (1900 - 1960) was slightly coarser than the NRCS (1961 - 1990) shapefile, but because the 1977 USGS equations for southern California were developed with the former both precipitation coverages were tested in the models. General resolution of these source data was such that their precision was typically on the order of 1% of the measurement (e.g., 10-m National Elevation Dataset (NED) over 1 km of channel).

ArcMap software by Environmental Systems Research Institute (ESRI), including extensions such as 'spatial analyst,' was used to optimize GIS measurements such as delineating watersheds and flow paths. Automated results from NED processing were cross-checked with existing shapefiles such as USGS Hydrologic Unit Code (HUC) boundaries and NHD flowlines.

**Table 1.2 – Summary of parameters tested in models with significance of variables**

Variable Key: primary in **bold**, secondary in *italics*, and no statistical significance is normal

	<b>Variable</b>	<b>Units</b>	<b>Definition (equation)</b>	<b>GIS Source/Scale</b>
spatial (x and y)	<b>A</b>	mi <sup>2</sup>	drainage area	HUC and NED/ 10 m
	<b>Stm</b>	mi	total stream length	NHD/ 1:24,000
	<b>DD</b>	mi/mi <sup>2</sup>	drainage density (DD = Stm/A)	
	<b>L</b>	mi	length of main channel from gauge to basin divide	
	<b>Shp</b>	mi/mi <sup>2</sup>	main-channel length divided by drainage area, i.e., shape (Shp = L/A)	
	<i>W<sub>vy</sub></i>	ft	valley width, measured from base of hillslope at gauge location	
	<i>Ord</i>	-	order – Strahler (1952) stream order	
	<i>Arf<sub>Stm</sub></i>	-	artificial fraction of total stream length, i.e., code ≠ 460	NHD
topographic (x, y, and z)	<b>Rlf</b>	ft	total relief along main channel, i.e., elevation at divide minus gauge	
	<i>Elev</i>	ft	average basin elevation, i.e., average of elevations at 10% and 85% of main-channel length measured from gauge to divide	
	<i>Gage</i>	ft	elevation at gauge	
	<b>S<sub>chn</sub></b>	ft/mi	average slope of main channel via elevations at 10% and 85% points	
	<b>Vly</b>	ft/mi	valley slope at gauge measured across geomorphically continuous valley ~10% of main-channel length or ~1,500 ft (500 m)	
	<b>Srf</b>	ft/ft	average surface slope of watershed	
precipitation	<b>P</b>	in	average annual precipitation (area-weighted)	USGS (1900 - 1960)
	<i>Pnracs</i>	in	average annual precipitation (area-weighted)	NRCS (1961 - 1990)
	<i>P224</i>	in	2-yr 24-hr precipitation volume (area-weighted)	NRCS
	<b>IP</b>	-	precipitation intensity relative to annual average (IP = P224/Pnracs)	
	<i>LAhst</i>	-	relative difference from long-term precipitation average of 15.07 in recorded at LA during gauged years	(1878 - 2006)
	<b>LAwt<sub>yr</sub></b>	-	number of exceptionally 'wet' precipitation years (50% > LA avg, i.e., > 22.6 in) during gauge record	
	<b>LAwt<sub>rt</sub></b>	-	relative number of exceptionally 'wet' precipitation years (50% > LA avg) during gauge record divided by gauge record	
	<i>SDhst</i>	-	relative difference from long-term precipitation average of 9.96 in recorded at SD during gauged years	(1850 - 2005)
	<i>SDwt<sub>yr</sub></i>	-	number of exceptionally 'wet' precipitation years (50% > SD avg, i.e., > 14.9 in) during gauge record	
<i>SDwt<sub>rt</sub></i>	-	relative number of exceptionally 'wet' precipitation years (50% > SD avg) during gauge record divided by gauge record		
hydrogeomorphic setting	<i>Cnf</i>	binary	gauge located in a process-domain of confined (i.e., step-pool/bedrock) qualitative rating via google earth aerials	
	<i>NW</i>	binary	subjectively-grouped gauges located in northwest part of domain	
	<i>lwNW</i>	binary	subjectively-grouped gauges located in lower northwest part of domain (i.e., lower elevations and broader valleys)	
	<i>N</i>	binary	subjectively-grouped gauges located in north part of domain	
	<i>NE</i>	binary	subjectively-grouped gauges located in northeast part of domain	
	<i>S</i>	binary	subjectively-grouped gauges located in south part of domain	
	<i>W</i>	binary	subjectively-grouped gauges located in west-central part of domain (i.e., near the Pacific coast)	
	<i>HUC</i>	-	objective 8-digit watershed code defined by USGS	
<b>Dry</b>	binary	subjectively-grouped gauges located in far east and south parts of domain in a rain shadow on the east slope of the mountains defined by 8-digit HUCs 18100200 or 18070305		

Figure 1.8 depicts the inter-annual, decadal, and multi-decadal trends in regional precipitation as recorded at the two long-term rain gauges. It includes the number of active gauges as well as number of gauges above specified levels of road density, suggesting that the more urban period of record (post ~1970) potentially had larger volumes of precipitation than the pre-urban period. By looking at records of individual gauges, Figure 1.9 shows some of the more urban records were active during wetter years; however, the most urban gauge (Arroyo Trabuco) was active during one of the driest composite climates on record. As such, I included the relative difference between mean annual precipitation during flow records, along with the number of exceptionally wet years ( $50\% > \text{mean}$ ), in the models.

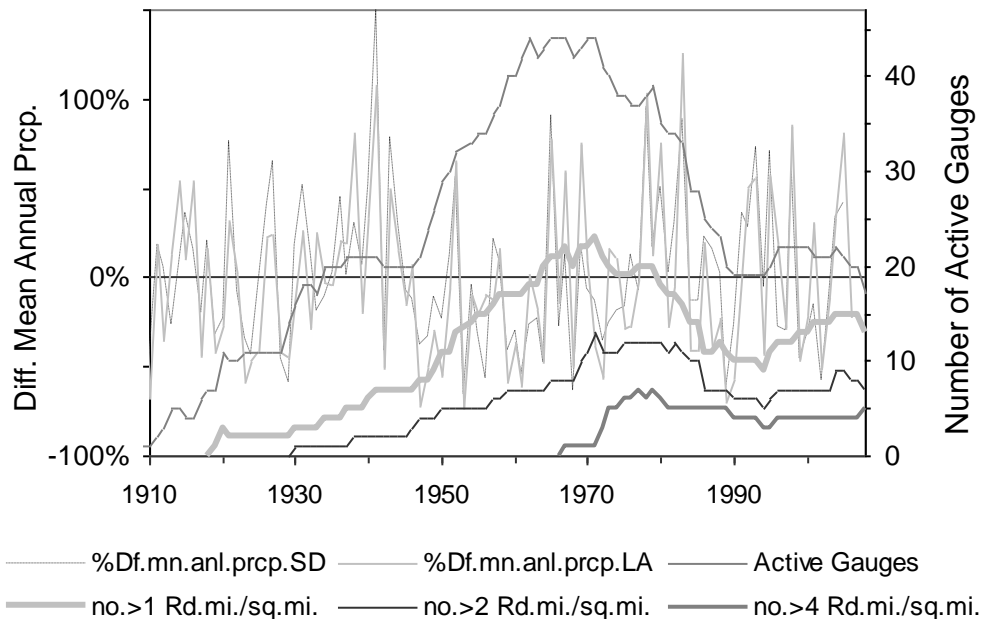


**Figure 1.8 – Inter-annual precipitation variability recorded at Los Angeles and San Diego overlaid with number of active gauges and number greater than specified road-density levels (indicating increasing urbanization)**

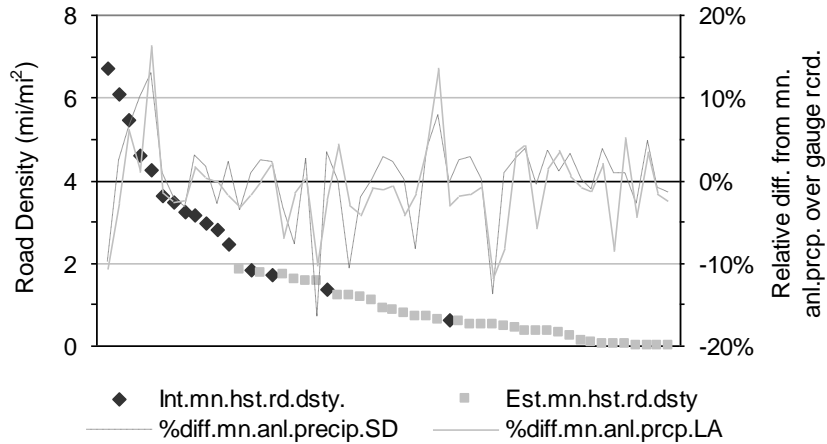


**Figure 1.9 – Integrated and estimated mean historic road density overlaid by relative difference from long-term mean in recorded precipitation at Los Angeles and San Diego during gauge records**

Although watershed shape varies throughout the study domain from linear to dendritic, sinuosity is generally low (typically < 1.1). Such regular down-valley alignment is optimal for transport of high water and sediment loads. The departure in the overall trend of main-channel length (length of longest stem from gauge traced to drainage divide) as a function of drainage area from Hack’s (1957) relationship is less important than the variance within the sample. That Figure 1.10 indicates an exponent less than the widely accepted minimum of 0.5 (Knighton, 1998) can be attributed to the large number of linearly-shaped small basins in the sample, resulting in a higher coefficient and smaller exponent over the range (i.e., Hack  $L = 1.4 A^{0.6}$  vs.  $L = 2.25 A^{0.49}$  in mi and  $mi^2$ , respectively).

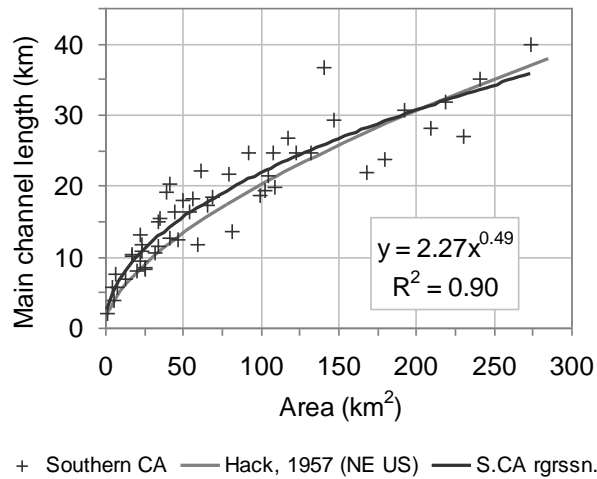


**Figure 1.10 – Main-channel length (to basin divide) vs. drainage area with southern California and Hack’s NE US relationship plotted**

The variance in the length-area relationship within the sample pointed to the importance of representing such physical differences in the models. This was particularly important because one of the most exceptionally linear watersheds (Arroyo Trabuco, 37 km to 140 km<sup>2</sup>) was also one of the most urbanized. In the event that area and main-channel length were not significant in a given model individually, the parameter ‘shape’ was added as an alternative independent variable, defined as main-channel length/area.

Drainage density showed general agreement with the pattern observed by Gregory (1976) when plotted versus mean annual precipitation. As seen in Figure 1.11, the two variables tend to be positively correlated in the semiarid regime and negatively correlated in the more humid regime. Additional parameters not explicitly accounted for in the models were vegetative cover, soil type/depth, and bedrock permeability due to incomplete spatial data. However, it is rational to assume that vegetation density is implicitly captured in a discontinuous/threshold manner via mean annual precipitation, which is the primary process-based explanation to the pattern in Figure 1.11. Other

potentially contributing, but admittedly inter-correlated, factors which exhibited similarly-shaped patterns with drainage density included the 2-yr 24-hr precipitation, average surface slope, and average basin elevation. Two additional variables that showed scattered, slightly positive correlations with drainage density were total basin relief and the 2-yr 24-hr precipitation volume standardized by the mean annual precipitation.

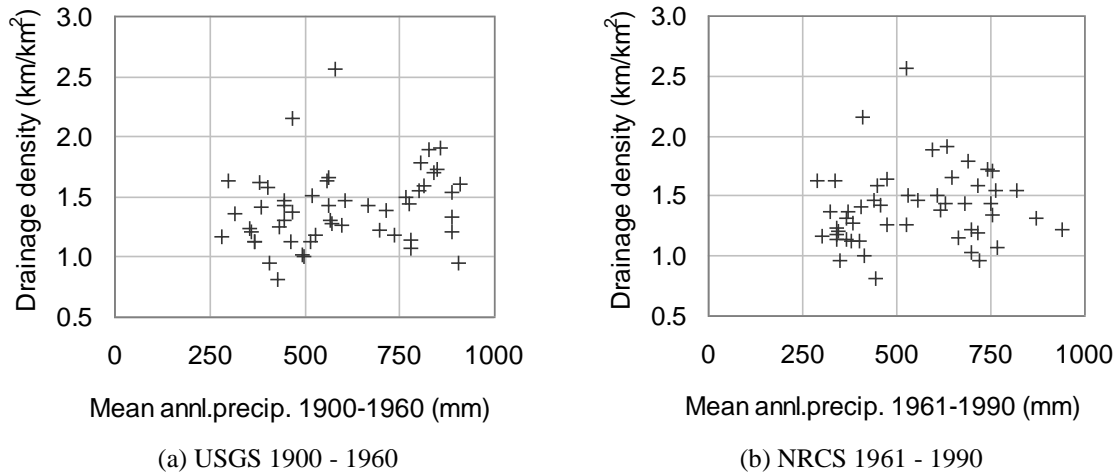


**Figure 1.11 – Drainage density vs. area-averaged mean annual precipitation**

Such a heterogeneous setting and complex interrelations among climatic, topographic, and fluvial geomorphic parameters resulted in the need to test an extensive matrix of variables in the models (i.e., Table 1.2). Beyond representing physical processes with appropriate and quantitative parameters, it was also important to guide their combination in model design to obviate potential collinearity issues.

### 1.2.6 Analytical methods and model design

Ultimately, all of these steps in this seemingly epic story informed model design. The objectives of the modeling were two-fold: first was to represent process by

determining which variables were most significant in shaping flow magnitudes and durations, and second was to determine which combinations and forms of these critical variables resulted in the most optimally-fit models for application. To guide the selection process, two sequential cross-validation schemes (e.g., 50/50 and 75/25) were performed prior to final model design.

Multivariate power functions via regression analysis have been widely used by the USGS in developing regional equations for recurrence-interval flows (Jennings *et al.*, 1994). Our analyses continue in this tradition. We used Statistical Analysis Software (SAS) as our primary computing tool. Hundreds of iterations of models were run with various withholding schemes using both forward and backward selection to determine the most consistently significant parameters and candidate models for final testing. Due to sample variance, some variables were tested in multiple forms (e.g., exponential and power) and varied units (e.g., slope in ft/ft or ft/mi), expanding the range of variables from which the models could select. For example, the exponential forms of imperviousness often returned superior or equivalent p-values to the power form.

Model forms that were congruent with hydrologic theory and had high performance in the initial 50/50 cross-validation scheme were nominated to the next phase. Performance was measured via several indicators such as a high significance of individual variables (typically  $p < 0.05$ ), high adjusted  $R^2$  and/or minimum Mallow's  $C_p$ , and homoscedastic residuals across both calibration and validation data. We assessed model performance, including standard diagnostics, in both logarithmic and arithmetic space. In general, we attempted to follow the guideline of ca. 10 observations per

predictor variable, such that models from the first calibration phase typically had only 2 to 3 independent variables (i.e., per 26 samples).

The next cross-validation step was a ~75/25 scheme, justifying up to four independent variables with 40 samples. High performing models from this phase were nominated to final model selection, at which point, in the tradition of the USGS, no gauges were withheld for cross validation. With 52 samples, 5 independent variables in each model were targeted, allowing for exceptions in cases of high performance. Informed by the results from the cross-validation steps, the basic model framework for peak-flow equations combined one parameter of each of the following process-based categories to preclude collinear variables from competing to represent the same process within the same model:

- watershed/network size: drainage area ( $A$ ) or total stream length ( $Stm$ );
- spatial efficiency: shape ( $Shp$ ) or drainage density ( $DD$ );
- precipitation: mean annual ( $P$ ), 2-yr 24-hr volume ( $P_{224}$ ), or 2-yr 24-hr relative to mean annual ( $IP$ );
- topographic efficiency: average slope of watershed surface ( $Srf$ ), average channel slope ( $S_{chn}$ ), valley slope at site ( $Vly$ ), and total relief along main channel ( $Rlf$ );
- discontinuous hydrogeomorphic setting: rain shadow HUCs 18100200 or 18070305 ( $Dry$ ); and
- imperviousness ( $TIA$ ): average imperviousness over record ( $Imp_{av}$ ), maximum imperviousness of record ( $Imp_{max}$ ), fraction of record length greater than 5%

impervious ( $Imp_5$ ), and fraction of record length greater than 7.5% impervious ( $Imp_7$ ).

Identical steps were taken in designing equations for the component parameters of the DDFs (i.e.,  $Q_{max}$ ,  $d1/day1$ ,  $d2/day2$ ). Based on overall accuracies, standard diagnostics, and theoretical agreement of models tested during the initial calibration/validation schemes described above, candidate equation/variable formats were selected for final testing. Preliminary models of  $Q_{max}$  showed that network spatial efficiency (e.g.,  $Shp$  and  $DD$ ) was not as important as other more probabilistic parameters that increased the odds of having an extremely large/long event. Years of gauge record ( $Yrs$ ) and the number of active gauge years that were exceptionally ‘wet’, that is, 50% greater than the long-term mean recorded at LA ( $LAWt_{yr}$  and  $LAWt_{rt}$ ) were metrics that increased such probability. Consequently, the basic format for  $Q_{max}$  equations combined parameters from the following categories:

- watershed/network size: drainage area ( $A$ ) or total stream length ( $Stm$ );
- precipitation: mean annual ( $P$ ), 2-yr 24-hr volume ( $P_{224}$ ), or 2-yr 24-hr relative to mean annual ( $IP$ );
- topographic efficiency: average slope of watershed surface ( $Srf$ ), average channel slope ( $S_{chn}$ ), valley slope at site ( $Vly$ ), and total relief along main channel ( $Rlf$ );
- discontinuous hydrogeomorphic setting: rain shadow HUCs 18100200 or 18070305 ( $Dry$ );
- imperviousness ( $TIA$ ): average imperviousness over record ( $Imp_{av}$ ), maximum imperviousness of record ( $Imp_{max}$ ), fraction of record length greater than 5%

impervious ( $Imp_5$ ), and fraction of record length greater than 7.5% impervious ( $Imp_7$ );

- record length: total years of gauge record (Yrs); and
- exceptionally ‘wet’ years: number of active gauge years that precipitation recorded at LA gauge was  $> 50\%$  above mean from 1878 - 2006 of 15.07 in, *i.e., number of years precipitation at LA gauge  $> 22.6$  in ( $LAwt_{yr}$ )*, or number of ‘wet’ years relative to total number of gauged years ( $LAwt_{rt}$ ), *e.g., 0.147 wet yrs/yr on average, or approximately 1 ‘wet’ year every 7 yrs.*

Regarding the magnitude of the DDFs, process-based variables corresponding to more volume should theoretically increase  $d1/day1$  (i.e., watershed size, precipitation, topographic efficiency, and record length).  $Q_{max}$  should also amplify  $d1/day1$  due to the fact that, all else being equal, a larger  $Q_{max}$  represents a larger individual storm event corresponding to longer durations of all flows over the extended rising and falling limbs. Almost counter intuitively, ‘dry’ could intensify  $d1/day1$  because the DDFs are scaled to  $Q_{max}$ , and ‘dry’ watersheds have disproportionately small daily flows of record. This results in bin distributions corresponding to much lower flows than those in typical basins (e.g., bin 16 corresponding to 3 versus 11 cfs for an average basin) and longer durations for equivalent bins (especially for the lower bins) despite much shorter durations for equivalent flows. In contrast, a network’s spatial efficiency should correspond to waning durations for equivalent watersheds due to larger concentrated peak flows and a broader range of flows over the event hydrograph. With equivalent precipitation volumes, a less efficient basin would have a narrower range of flows over the hydrograph and

consequently longer durations of those flows. In short, with the exception of spatial efficiency measures (DD or Shp),  $d1/day1$  had the same equation design as  $Q_{max}$ .

In terms of the shape of the DDFs, it was hypothesized that variables that increased the likelihood of larger flows (imperviousness, Yrs, and IP) would stretch the curves out, resulting in less negative values of  $d2/day2$ . In contrast, processes that create more volume (precipitation and topographic efficiency) without changing the scale ( $Q_{max}$ ) would tend to steepen the curve, making a more negative  $d2/day2$ . Consequently, variables that should best explain the shape of the curve are direct measures of the magnitude ( $d1/day1$ ) and scale ( $Q_{max}$ ). All else being equal, a larger DDF magnitude would correspond to a steeper (more negative) shape due to the fact that all of the DDFs tend to converge on very low durations (e.g., order of  $\sim 1$  to  $\sim 10$  days) in the most extreme part of the tail. Likewise, a smaller scale ( $Q_{max}$ ) would tend to correlate to a steeper curve, while a larger scale would correspond to a flatter curve. The most extreme examples of the prior case are ‘dry’ watersheds: disproportionately small scales with correspondingly steep curves. As such,  $d1/day1$  and  $Q_{max}$  were included in some of the  $d2/day2$  models to evaluate the performance benefits relative to the risk of compounding prediction errors on the application side. Instantaneous peak flows were also tested as a substitute for  $Q_{max}$ , with  $Q_{10}$  being the best candidate for final models due to performance in predicting  $d2/day2$ , as well as regularly having the best prediction accuracies among all  $Q_i$ 's in preliminary models.

### 1.3 Results

The presentation of results is divided into three subsections. First, the results of the two cross-validation schemes are summarized with a focus on the consistently significant variables that informed the final models. For brevity, cross-validation equations and figures are presented in Appendix B. To be sure, the reader should know that those equations passing cross-validation directly informed the final models. Second, peak-flow equations are presented with performance comparisons to the USGS equations. Lastly, the DDF component equations are summarized.

In the following sections, we present the 4 to 6 superior models for each dependent variable because different models returned similar performance using alternative surrogates of the same process. For example,  $S_{rf}$ ,  $S_{chn}$ , and  $V_{ly}$  all are attempts to represent the topographic efficiency of the watershed. Of course, none of these measures are truly representative of an entire network, but each has the potential to capture the process in a different way. By presenting all high-performing models, we reduce the risk of giving too much weight to one measure. One can envision cases where this would be important, for example a flatter watershed (low  $S_{rf}$ ) that happened to have a steeper slope at the gauge (high  $V_{ly}$ ) or moderate main-channel slope across the 10 to 85% portion of the trunk (medium  $S_{chn}$ ).

Finally, recall that the models were developed using gauges ranging in drainage area from 0.5 to 105  $mi^2$  with 0 to 26% TIA (Table 1.1); therefore, the equations should not be applied to watersheds outside of those bounds. A detailed examination of the effect of urbanization is presented in Section 1.4 (Implications).

### 1.3.1 Cross-validation summaries and individual variable performance

Cross-validation schemes are summarized below (Tables 1.3 and 1.4). The behavior of return-interval flows varied from the low to high intervals as evident by the change in predictor variables associated with the most variance and highest significance. In general, variables that accounted for the most variance across all return intervals of instantaneous peak flows were Stm, A, Shp, Vly, S<sub>chn</sub>, IP, and Dry roughly in order of decreasing significance (i.e., adjusted partial R<sup>2</sup> of 0.5 for Stm, 0.1 for Dry at the 10-yr flow). Measures of imperviousness accounted for up to one quarter of the variance of the 1-yr flow, with decreasing significance for higher flows (e.g., adjusted partial R<sup>2</sup> ~0.10 for 2-yr flows and 0.01 to 0.03 for 10-yr flows).

**Table 1.3 – Summary of the 26/26 cross-validation scheme**

Dependent Variable	Predictor Variables Tested	Models Passing Calbrated	Models Passing Validated	Urban p < 0.05 in Any Validated Models?	Consistently Significant Variables	Average Cali-brated* R <sup>2</sup>	Average Vali-dated* R <sup>2</sup>
Q1	52	2	1	✓	P, ImpMax	0.9	0.4
Q1.5		5	2	✓	IP, ImpMax, dry	0.8	0.4
Q2		5	2	✓	IP, ImpMax, dry	0.7	0.5
Q5		5	4	p = 0.06	strm, IP, dry	0.5	0.6
Q10g		5	4	p = 0.13	strm, IP, dry	0.8	0.6
Q25g		6	3		A, P, dry	0.9	0.6
Q50g		5	3		A, P, dry	0.9	0.6
Q100g		5	3		A, P, dry	0.9	0.6
Qmax	52	10	3		strm, dry	0.9	0.7
day1	53	9	4	✓	P, Yr, srf, shp, ImpAv/5/7	0.7	0.9
day2	54	17	5	p = 0.06	P, Yr, Q10, day1, ImpAv/5/7	0.9	0.8

\*R<sup>2</sup> reported from arithmetic space

**Table 1.4 – Summary of the 40/12 cross-validation scheme**

Dependent Variable	Predictor Variables Tested	Models Passing Calibrated	Models Passing Validated	Urban p < 0.05 in Any Validated Models?	Consistently Significant Variables	Average Calibrated* R <sup>2</sup>	Average Validated* R <sup>2</sup>
Q1	52	1	1	✓	srf, ImpMax, dry	0.7	0.5
Q1.5		6	1	✓	IP, rlf, shp, ImpMax, dry	0.6	0.7
Q2		5	3	✓	IP, ImpMax, dry	0.6	0.5
Q5		4	3		strm, IP, dry	0.7	0.7
Q10g		6	3		strm, IP, dry	0.8	0.8
Q25g		5	3		strm, IP, dry	0.8	0.8
Q50g		5	3		strm, dry	0.8	0.8
Q100g		5	3		strm, dry	0.8	0.8
Qmax	52	14	6		P, Yr, strm, rlf, dry	0.7	0.8
d1	53	23	4	✓	P, Yr, dd, srf, Qmax, Imp7, dry	0.7	0.6
d2	54	8	6	✓	Yr, Q10, day1, ImpAv	0.9	0.9

\*R<sup>2</sup> reported from arithmetic space

Regarding  $Q_{max}$ , urbanization was less significant than other process-based categories such as scale and hydrogeomorphic settings. As a representation of the highly variable climate, record length (Yrs) was an important predictor of  $Q_{max}$  (~0.2 adjusted partial R<sup>2</sup>). This is in agreement with basic probability theory, that the longer a gauge was active, the more likely it would experience an extreme event. Although models that included measures of network spatial efficiency (e.g., Shp and DD) were tested, they did not prove to be significant. Perhaps because the dependent variable is a daily-mean flow, spatial efficiency, which would result in flashier hydrograph due to better concentrated delivery of water, would become insignificant when the more variable instantaneous flows are averaged over 24 hrs.

After testing hundreds of models for the magnitude and shape parameters of the DDFs, we determined that variables such as  $Q_{max}$ ,  $Q_{10}$ , d1, and day1 were highly

significant in nearly every case, especially regarding predictions of  $d_2/day_2$ . This was undesirable due to the potential to compound prediction errors in model application, but it was effectively unavoidable. For example, both  $d_1$  and  $Q_{10}$  individually accounted for up to 40% of the  $d_2$  variance, with respective multivariate models approaching  $R^2$  values of 0.9. Predictions of  $d_1/day_1$  had less circularity, with Yrs accounting for up to 50% of the total variance and  $Q_{max}$  much less (adjusted partial  $R^2$  up to 0.15 for day1 and 0.02 for d1). Concerns of collinearity were dampened via the individual p-values of the potentially distressing terms, which were highly significant (i.e.,  $p \ll 0.05$ ) in every case where they appear together as predictor variables. Finally, and central to this research, measures of imperviousness were regularly significant in predicting both magnitude and shape ( $p < 0.05$  in more than half of the models).

### **1.3.2 Peak-flow equations**

Five equations are presented for all return-interval flows. By using the same equation formats for all recurrence intervals, one can see how the influence of individual terms changes over return periods. In general, there seems to be a somewhat abrupt behavior change around the 2-yr and 5-yr events, transitioning from a high influence on drainage efficiency, rainfall intensity, and imperviousness to more of a dependency on scale such as area and total stream length.

Four equations take the form discussed above, which includes combinations of drainage size, efficiency, precipitation, setting, and urbanization. The final form (Eq. (1.11)) is presented as a revision to the USGS 1977 equations that were functions of only A and P. We added an exponential term for  $Imp_{max}$  because it models the effects of

urbanization in a simple continuous form (i.e.,  $\text{Imp}_{\max} \rightarrow 0$ , urban term  $\rightarrow 1$ , equation  $\rightarrow$  rural equation). Due to its simplicity, the equation has much lower  $R^2$  values than the other forms; however, we include it to avoid giving exclusive dependence to Dry, which was significant in the balance of equations. We present each equation with the corresponding units and parameters for each return interval via a supplemental table. *In the following equations and tables, uppercase terms indicate variables and lowercase nomenclature indicates the corresponding  $\beta$  parameter from the regression. Bold font draws attention to terms with varied units:*

$$Q_i = e^{(\text{Incpt})} * \text{Stm}^{\text{stm}} * e^{(\text{shp} * \text{Shp})} * \text{IP}^{\text{ip}} * e^{(\text{dry} * \text{Dry})} * \text{Vly}^{\text{vly}} * e^{(\text{impmax} * \text{Impmax})} \quad \text{Eq. (1.7)}$$

where:

$\text{IP} = P_{224}/P_{\text{nrcs}}$ , i.e., 2-yr 24-hr volume/average annual volume (in/in);

$\text{Dry} = 1$  if HUC 18100200 or 18070305, else  $\text{Dry} = 0$ ;

$\text{Imp}_{\max}$  impervious area as **fraction** of total drainage area (**mi<sup>2</sup>/mi<sup>2</sup>**);

Table 1.2 presented variable definitions and corresponding parameters and units for Eq. (1.7) are tabulated in Table 1.5.

**Table 1.5 – Corresponding parameters and units for Eq. (1.7)**

Return Period (yrs)	Incpt (-)	stm (mi)	shp (mi/mi <sup>2</sup> )	ip (-)	dry (-)	vly (ft/mi)	imp <sub>max</sub> (-)	Adjusted R <sup>2</sup>	p-exceptions (p > 0.05)
1	2.65	0	-1.03	4.51	-3.89	1.43	26.6	0.59	shp 0.28, ip 0.14
1.5	9.58	0.216	-1.08	4.08	-2.33	0.431	9.37	0.65	stm 0.43
2	9.73	0.254	-1.02	3.41	-1.99	0.277	6.67	0.65	stm 0.30, vly 0.10
5	9.07	0.600	-0.455	2.60	-1.29	0.112	2.68	0.79	shp 0.17, vly 0.30, imp <sub>max</sub> 0.10
10	7.95	0.677	-0.428	1.83	-1.39	0.177	0	0.84	shp 0.12
25	7.14	0.745	-0.371	1.38	-1.44	0.250	0	0.81	shp 0.20
50	6.86	0.774	-0.347	1.19	-1.46	0.282	0	0.79	shp 0.26
100	6.71	0.793	-0.331	1.06	-1.48	0.304	0	0.79	shp 0.30

$$Q_i = e^{(\text{Incpt}) * A^a * DD^{dd} * e^{(\text{ip} * \text{IP})} * e^{(\text{dry} * \text{Dry})} * S_{\text{chn}}^{\text{chn}} * \text{Imp}_{\text{av}}^{\text{impav}}} \quad \text{Eq. (1.8)}$$

where:

**Imp<sub>av</sub>** expressed as **percentage** of total drainage area (**mi<sup>2</sup>/mi<sup>2</sup>**) \* **100%**;

**Imp<sub>av</sub> ≥ 1%** or else term is dropped; and

Table 1.2 presented variable definitions and corresponding parameters and units for Eq. (1.8) are tabulated in Table 1.6.

**Table 1.6 – Corresponding parameters and units for Eq. (1.8)**

Return Period (yrs)	Incpt (-)	a (mi <sup>2</sup> )	dd (mi/mi <sup>2</sup> )	ip (-)	dry (-)	chn (ft/mi)	imp <sub>av</sub> (%)	Adjusted R <sup>2</sup>	p-exceptions (p > 0.05)
1	-4.09	0	2.61	0	-3.14	0.560	1.57	0.52	dd 0.16, S <sub>chn</sub> 0.24
1.5	-4.63	0.621	0.698	21.8	-2.13	0.554	0.679	0.61	dd 0.30
2	-2.48	0.672	0.442	18.4	-1.93	0.423	0.470	0.61	dd 0.46, S <sub>chn</sub> 0.09
5	0.838	0.783	0.473	15.0	-1.28	0.159	0.152	0.78	dd 0.21, S <sub>chn</sub> 0.27, imp <sub>av</sub> 0.18
10	1.70	0.860	0.538	10.0	-1.35	0.261	0	0.83	dd 0.08
25	2.04	0.913	0.639	7.06	-1.37	0.364	0	0.81	
50	2.23	0.937	0.681	5.82	-1.38	0.410	0	0.79	
100	2.39	0.953	0.709	4.98	-1.38	0.442	0	0.77	ip 0.11

$$Q_i = e^{(\text{Incpt}) * A^a * \text{IP}^{\text{ip}} * e^{(\text{dry} * \text{Dry})} * e^{(\text{srf} * \text{Srf})} * \text{Imp}_{\text{max}}^{\text{impmax}}} \quad \text{Eq. (1.9)}$$

where:

**Srf** = average surface slope of watershed (ft/ft);

**Imp<sub>max</sub>** expressed as **percentage** of total drainage area (**mi<sup>2</sup>/mi<sup>2</sup>**) \* **100%**;

**Imp<sub>max</sub> ≥ 1%** or else term is dropped; and

Table 1.2 presented variable definitions and corresponding parameters and units for Eq. (1.9) are tabulated in Table 1.7.

**Table 1.7 – Corresponding parameters and units for Eq. (1.9)**

Return Period (yrs)	Incpt (-)	a (mi <sup>2</sup> )	ip (-)	dry (-)	srf (-)	imp <sub>max</sub> (%)	Adjusted R <sup>2</sup>	p-exceptions (p > 0.05)
1	-1.10	0	0	-3.03	5.90	1.59	0.57	
1.5	8.19	0.504	3.53	-1.89	3.16	0.584	0.60	
2	8.33	0.571	3.06	-1.74	2.12	0.397	0.61	srf 0.07
5	9.32	0.738	2.69	-1.20	0.676	0.104	0.77	srf 0.35, imp <sub>max</sub> 0.31
10	8.39	0.785	1.88	-1.22	1.27	0	0.82	
25	7.77	0.815	1.35	-1.20	1.90	0	0.80	
50	7.57	0.829	1.13	-1.19	2.18	0	0.78	
100	7.47	0.838	0.975	-1.18	2.37	0	0.77	

$$Q_i = e^{(\text{Incpt})} * \text{Stm}^{\text{stm}} * P_{224}^{\text{p224}} * e^{(\text{dry} * \text{Dry})} * \text{Rlf}^{\text{rlf}} * \text{Imp}_5^{\text{imp5}} \quad \text{Eq. (1.10)}$$

where:

$P_{224}$  = 2-yr 24-hr volume (in);

Rlf = total relief along main channel from divide to outlet (ft);

**Imp<sub>5</sub>** = **percentage** of record > 5% imperviousness (yr/yr) \* **100%**;

Imp<sub>5</sub> ≥ 1% or else term is dropped; and

Table 1.2 presented variable definitions and corresponding parameters and units for Eq. (1.10) are tabulated in Table 1.8.

**Table 1.8 – Corresponding parameters and units for Eq. (1.10)**

Return Period (yrs)	Incpt (-)	stm (mi)	p <sub>224</sub> (in.)	dry (-)	rlf (-)	imp <sub>5</sub> (%)	Adjusted R <sup>2</sup>	p-exceptions (p > 0.05)
1	-2.41	0	2.62	-2.25	0	0.970	0.55	
1.5	-3.28	0.467	0.611	-2.41	0.675	0.360	0.53	p <sub>224</sub> 0.40, rlf 0.10
2	-0.850	0.564	0.554	-2.08	0.430	0.264	0.54	p <sub>224</sub> 0.39, rlf 0.24
5	2.65	0.777	0.336	-1.41	0.133	0.100	0.70	p <sub>224</sub> 0.44, rlf 0.59, imp <sub>5</sub> 0.16
10	2.51	0.771	0.173	-1.48	0.282	0	0.79	p <sub>224</sub> 0.56, rlf 0.14
25	2.40	0.769	0.246	-1.40	0.360	0	0.80	p <sub>224</sub> 0.40
50	2.41	0.769	0.282	-1.37	0.393	0	0.79	p <sub>224</sub> 0.35
100	2.44	0.769	0.307	-1.34	0.415	0	0.77	p <sub>224</sub> 0.33

$$Q_i = e^{(\text{Incpt}) * A^a * P^p * e^{(\text{impmax} * \text{Impmax})}} \quad \text{Eq. (1.11)}$$

where:

$P$  = average annual rainfall, USGS: 1900 - 1960 (in);

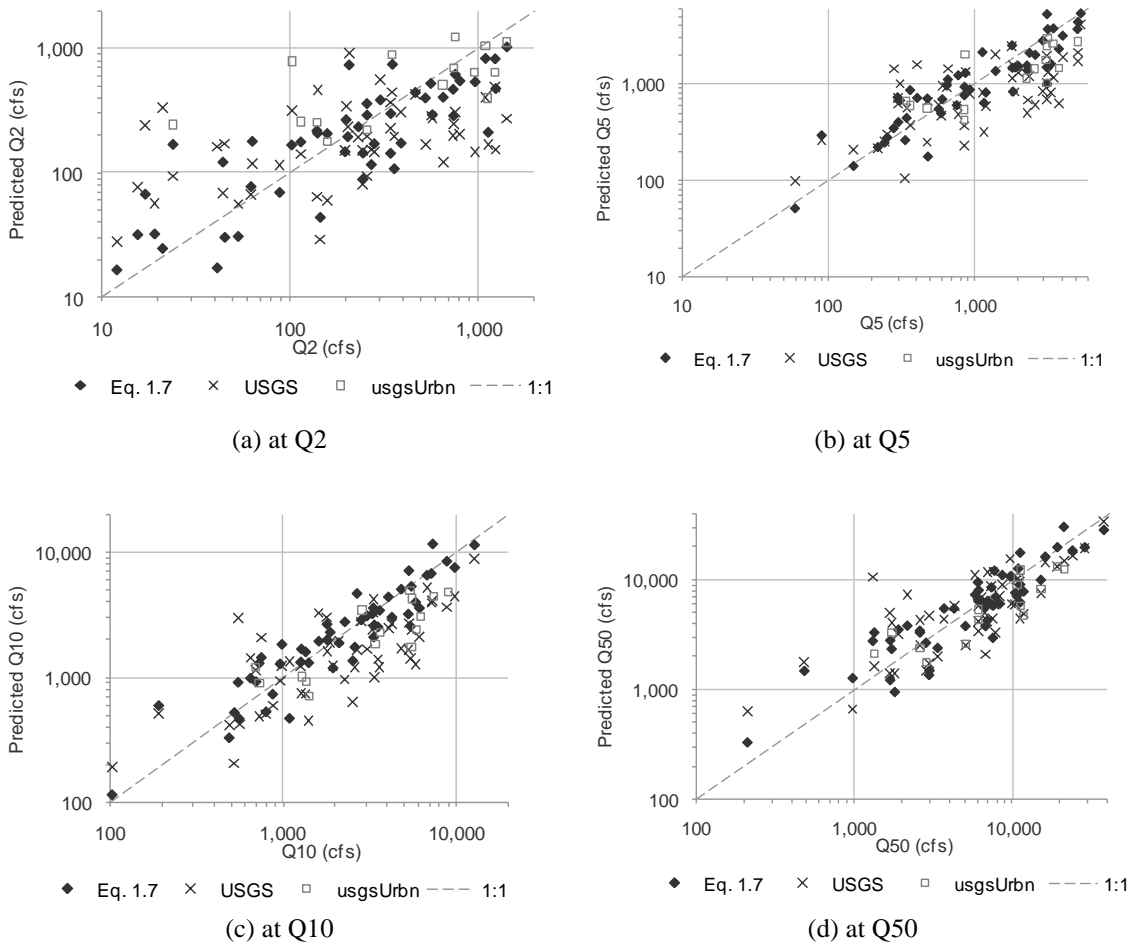
$\text{Imp}_{\text{max}}$  impervious area as **fraction** of total drainage area ( $\text{mi}^2/\text{mi}^2$ ); and

Table 1.2 presented variable definitions and corresponding parameters and units for Eq. (1.11) are tabulated in Table 1.9.

**Table 1.9 – Corresponding parameters and units for Eq. (1.11)**

Return Period (yrs)	Incpt (-)	a ( $\text{mi}^2$ )	p (in.)	$\text{imp}_{\text{max}}$ (-)	Adjusted $R^2$	p-exceptions ( $p > 0.05$ )
1	-12.5	0	4.13	33.8	0.43	
1.5	-3.92	0.435	2.18	16.7	0.30	
2	-2.42	0.525	1.88	13.3	0.32	
5	0.281	0.749	1.36	7.12	0.54	
10	0.980	0.774	1.38	4.50	0.61	
25	1.54	0.792	1.40	2.75	0.62	$\text{imp}_{\text{max}}$ 0.17
50	1.83	0.800	1.40	1.96	0.62	$\text{imp}_{\text{max}}$ 0.33
100	2.06	0.806	1.41	1.42	0.61	$\text{imp}_{\text{max}}$ 0.49

Figure 1.12 provides a graphical example of the model performance of Eq. (1.7) relative to a 1:1 line as well as the USGS rural (1977) and urban (1983) equations. The general improvement with return period is evident up to  $Q_{10}$ , with relatively consistent precision at higher return intervals. Also, the disparity between our models and the USGS models decreases with increasing return period.



**Figure 1.12 – Comparison of performance between Eq. (1.7), USGS rural (1977), and USGS urban (1983)**

For reference, a summary of  $R^2$  from arithmetic space is provided in Table 1.10 comparing our equations with the performance of the USGS rural (1977) and urban (1983) equations. By liberally assigning BDF values to the sites, it was found that the USGS urban equation performed moderately well for higher return intervals ( $Q_{25}$  to  $Q_{100}$ ,  $R^2 \sim 0.4$  to  $0.7$ ) and quite poorly for lower recurrence frequencies ( $Q_2$  to  $Q_{10}$ ,  $R^2 \sim 0.1$  to  $0.4$ ), while even more poorly with conservative BDF estimates. For example, San Diego Creek (gauge no. 11048500), located in Orange County, was the only gauge in southern

California used in the development of the equations. Using their BDF rating of 1 returned relative errors of -47 to -67% for estimates of  $Q_2$  through  $Q_{100}$ , while a BDF rating of 5 improved the range by 4% (i.e., -43% to -63%).

**Table 1.10 – Comparison of  $Q_i$  model performance with USGS rural (1977) and urban (1983) equations using  $R^2$  values from arithmetic space**

Return Period (yrs)	$R^2$ (arithmetic space)					USGS 1977	USGS 1983
	Eq. (1.7)	Eq. (1.8)	Eq. (1.9)	Eq. (1.10)	Eq. (1.11)	Rural	Urban
1.5	0.51	0.54	0.51	0.39	0.31	-	-
2	0.54	0.50	0.48	0.41	0.26	-0.20	0.31
5	0.74	0.72	0.71	0.59	0.41	0.18	0.28
10	0.82	0.83	0.80	0.78	0.58	0.37	0.27
25	0.82	0.86	0.82	0.84	0.66	0.63	0.41
50	0.80	0.85	0.81	0.83	0.68	0.72	0.53
100	0.78	0.84	0.79	0.82	0.68	0.75	0.60

Given the longer records and a focus on smaller watersheds, our models generally outperform the USGS equations. The exception is the relatively poorly performing Eq. (1.11), which we intentionally included to have one model with a consistent format to the 1977 equations. The updated  $f(A, P)$  model with an urban component still outperformed the USGS equations in approximately 2/3 of the cases.

### 1.3.3 Duration density functions

Simulation of a DDF for an ungauged location requires the estimation of its three components: scale ( $Q_{max}$ ), shape ( $d1$  and  $d2$ ), and magnitude ( $day1$  and  $day2$ ). The bin sizes of the cumulative-duration curves were designed to be scaled by  $Q_{max}$  according to Eq. (1.2). Equations for estimating  $Q_{max}$  (cfs) at an ungauged location are listed in order of decreasing adjusted  $R^2$ . Corresponding measures of accuracy are listed in Table 1.11.

**Table 1.11 – Summary of component (scale) equations for DDFs:  $Q_{\max}$  (for Eq. (1.2))**

	Equation Number	Independent Variable	Adjusted $R^2$	Mean Abs. Error Arithmetic Space (%)	p-exceptions ( $p > 0.05$ )
$Q_{\max}$ (cfs)	Eq. (1.12)	f(A, P, Dry, Rlf, LAwt <sub>yr</sub> )	0.79	31%	
	Eq. (1.13)	f(Stm, P <sub>224</sub> , Dry, S <sub>chn</sub> , Yrs, LAwt <sub>rt</sub> )	0.79	32%	S <sub>chn</sub> 0.08, LAwt <sub>rt</sub> 0.24
	Eq. (1.14)	f(A, IP, Dry, Srf, LAwt <sub>yr</sub> )	0.77	37%	IP 0.10
	Eq. (1.15)	f(Stm, IP, Dry, Vly, Yrs)	0.75	39%	IP 0.09
	Eq. (1.16)	f(Stm, P, Imp <sub>max</sub> , Yrs)	0.65	41%	Imp <sub>max</sub> 0.06

Variables in Eqs. (1.12) through (1.16) are defined in Table 1.2.

$$Q_{\max} = e^{-4.62 * A^{0.832} * P^{0.879} * e^{(-2.04 * Dry)} * Rlf^{0.756} * LAwt_{yr}^{0.457}} \quad \text{Eq. (1.12)}$$

where:

P = area-weighted mean annual precipitation, USGS 1900 - 1960 (in);

Dry = 1 if HUC 18100200 or 18070305, else Dry = 0;

Rlf = total change in elevation along main channel between drainage divide and gauge (ft); and

LAwt<sub>yr</sub> = number of years precipitation recorded at LA gauge is > 50% above long-term mean (1878 - 2006) of 15.07 in (i.e., # of years precip > 22.6 in).

$$Q_{\max} = e^{-0.417 * Stm^{0.988} * P_{224}^{0.821} * e^{(-1.89 * Dry)} * e^{(5.82 * S_{chn})} * Yrs^{0.647} * e^{(2.57 * LAwt_{rt})}} \quad \text{Eq. (1.13)}$$

where:

P<sub>224</sub> = NOAA 2-yr 24-hr precipitation (in);

S<sub>chn</sub> = average channel slope measured via 10% and 85% distances along the main channel between drainage divide and gauge (ft/ft);

Yrs = number of years of record (i.e., # of years user is simulating); and

**LAWt<sub>rt</sub>** = number of years precipitation at LA gauge is > 50% above long-term mean (1878 - 2006) of 15.07 in (i.e., # of years precipitation > 22.6 in) **relative to number of years simulating** (e.g., 0.147 wet yrs/yr on average).

$$Q_{\max} = e^{4.41} * A^{0.908} * IP^{1.13} * e^{(-1.99 * Dry)} * e^{(3.48 * Srf)} * LAWt_{yr}^{0.646} \quad \text{Eq. (1.14)}$$

where:

IP = 2-yr 24-hr precipitation, NOAA, relative to mean annual NRCS, 1960 - 1991 (in/in);

**Srf** = average watershed surface slope (ft/ft); and

LAWt<sub>yr</sub> = number of years precipitation at LA gauge is > 50% above long-term mean.

$$Q_{\max} = e^{2.42} * Stm^{0.883} * IP^{1.20} * e^{(-2.10 * Dry)} * Vly^{0.308} * Yrs^{0.674} \quad \text{Eq. (1.15)}$$

where:

**Vly** = valley slope of geomorphically continuous valley at site (up to ~1,500 ft or 10% of channel length) (ft/mi).

$$Q_{\max} = e^{-4.83} * Stm^{0.845} * P^{2.24} * e^{(4.60 * Imp_{\max})} * Yrs^{0.506} \quad \text{Eq. (1.16)}$$

where:

**Imp<sub>max</sub>** = maximum impervious extent as a fraction of total drainage area (mi<sup>2</sup>/mi<sup>2</sup>).

Figure 1.13 presents a comparison of the performance between Eqs. (1.12) and (1.13) – the best fitted of all five equations. Not only do they return reasonably accurate estimates of  $Q_{\max}$ , but more importantly, Figure 1.13 demonstrates the general trend that extreme outliers from one equation are typically improved via the application of another equation. This lends justification to why more than one equation is presented for each dependent variable, such that by applying multiple equations the influence of outliers may be dampened.

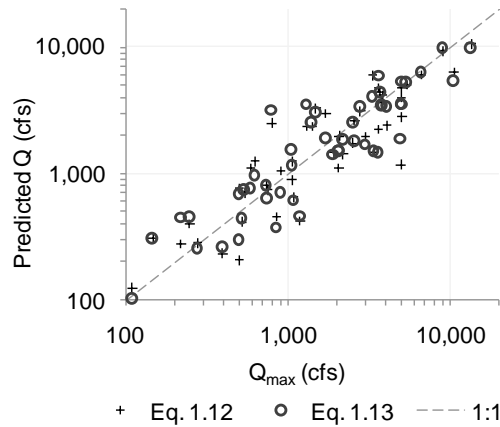


**Figure 1.13 – Model performance of Eqs. (1.12) and (1.13) (predicted  $Q_{\max}$  vs. actual) with 1:1 ‘perfect-fit’ line overlaid**

Power functions (Eqs. (1.5) and (1.6)) are used to predict durations of bin flows. Two forms of the power function cover different ranges of bins (i.e., bins 16-25 with d1 and d2 or bins 12-25 using day1 and day2). Equations for the coefficient and exponent of the respective power functions are presented below, with summaries of adjusted  $R^2$  and p-value exceptions listed in the respective tables. Corresponding measures of accuracy are listed in Table 1.12.

**Table 1.12 – Summary of component (magnitude and shape) equations for DDFs: d1 and d2 (for Eq. (1.5), bins 16-25)**

Equation Number	Independent Variable	Adjusted R <sup>2</sup>	Mean Abs. Error Arithmetic Space (%)	p-exceptions (p > 0.05)	
Eq. (1.17)	f(A, DD, P, S <sub>chn</sub> , Imp <sub>av</sub> , Yrs)	0.74	50%	Imp <sub>av</sub> 0.10	
Eq. (1.18)	f(DD, P, Dry, Imp <sub>7</sub> , Yrs, Q <sub>max</sub> )	0.75	45%		
d <sub>1</sub>	Eq. (1.19)	f(A, DD, P, S <sub>rf</sub> , Imp <sub>av</sub> , Yrs)	0.73	41%	Imp <sub>av</sub> 0.09
	Eq. (1.20)	f(A, DD, P, R <sub>lf</sub> , Imp <sub>7</sub> , Yrs)	0.73	45%	
Eq. (1.21)	f(Shp, DD, P, Dry, S <sub>chn</sub> , Imp <sub>5</sub> , Yrs, Q <sub>max</sub> )	0.76	44%	Shp 0.15, Dry 0.24, Imp <sub>5</sub> 0.10	
d <sub>2</sub>	Eq. (1.22)	f(Imp <sub>av</sub> , Yrs, Q <sub>10</sub> , d <sub>1</sub> )	0.88	6.1%	
	Eq. (1.23)	f(Dry, S <sub>chn</sub> , Imp <sub>av</sub> , Yrs, Q <sub>10</sub> , d <sub>1</sub> )	0.88	6.0%	
	Eq. (1.24)	f(P <sub>224</sub> , Dry, Imp <sub>av</sub> , Yrs, Q <sub>10</sub> , d <sub>1</sub> )	0.89	5.8%	Imp <sub>av</sub> 0.16
	Eq. (1.25)	f(Shp, IP, Dry, S <sub>chn</sub> , Imp <sub>av</sub> , Yrs, d <sub>1</sub> )	0.82	7.5%	Shp 0.14, Imp <sub>av</sub> 0.20, Yrs 0.08

Variables in Eqs. (1.17) through (1.25) are defined in Table 1.2.

$$d_1 = e^{-15.7} * A^{0.907} * DD^{-1.55} * P^{2.54} * S_{chn}^{0.966} * e^{(7.37 * impav)} * Yrs^{2.55} \quad \text{Eq. (1.17)}$$

where:

**S<sub>chn</sub>** = average channel slope measured via 10% and 85% distances along the main channel between drainage divide and gauge (**ft/mi**); and

**Imp<sub>av</sub>** = average impervious extent over record as a fraction of total drainage area (**mi<sup>2</sup>/mi<sup>2</sup>**).

$$d_1 = e^{-12.9} * DD^{-1.46} * P^{3.01} * e^{(1.68 * Dry)} * e^{(1.73 * imp7)} * Yrs^{2.32} * Q_{max}^{0.592} \quad \text{Eq. (1.18)}$$

where:

**Imp<sub>7</sub>** = fraction of record over 7.5% imperviousness (**yr/yr**).

$$d_1 = e^{-9.86} * A^{0.788} * DD^{-2.12} * P^{1.96} * e^{(6.03 * Srf)} * e^{(7.82 * impav)} * Yrs^{2.54} \quad \text{Eq. (1.19)}$$

where:

**Srf** = average surface slope of watershed (**ft/ft**); and

**Imp<sub>av</sub>** = (**mi<sup>2</sup>/mi<sup>2</sup>**).

$$d_1 = e^{-17.9 * A^{0.476} * DD^{-1.58} * P^{2.89} * Rlf^{0.964} * e^{(1.40 * imp7)} * Yrs^{2.54}} \quad \text{Eq. (1.20)}$$

where:

**Imp<sub>7</sub>** = (**yr/yr**).

$$d_1 = e^{-12.0 * Shp^{-1.25} * DD^{-1.82} * P^{2.05} * e^{(0.737 * Dry)} * S_{chn}^{0.727} * e^{(0.997 * imp5)} * Yrs^{2.29} * Q_{max}^{0.495}} \quad \text{Eq. (1.21)}$$

where:

**Imp<sub>5</sub>** = fraction of record over 5% imperviousness (**yr/yr**).

Eq. (1.22) includes the four most significant variables in predicting d2 via forward selection (d1, Q<sub>10</sub>, Yrs, and imp<sub>av</sub>), while Eqs. (1.23) and (1.24) are variations that include more variables with less significance. Eq. (1.25) is a model that excludes Q<sub>10</sub> for comparison. It is plotted with Eq. (1.22) in Figure 1.14 demonstrating the consistently superior accuracy of the latter. In this case, one could justify excluding Eq. (1.25) in practice:

$$d_2 = -2.09 + 1.24 * imp_{av} + 0.124 * \ln(Yrs) + 0.202 * \ln(Q_{10}) - 0.117 * \ln(d_1) \quad \text{Eq. (1.22)}$$

where:

**Imp<sub>av</sub>** = (**mi<sup>2</sup>/mi<sup>2</sup>**).

$$d_2 = -1.85 - 0.0537 * \text{Dry} - 0.763 * S_{\text{chn}} + 0.968 * \text{imp}_{\text{av}} + 0.114 * \ln(\text{Yrs}) + 0.174 * \ln(Q_{10}) - 0.110 * \ln(d_1) \quad \text{Eq. (1.23)}$$

where:

$$S_{\text{chn}} = (\text{ft/ft}); \text{ and}$$

$$\text{Imp}_{\text{av}} = (\text{mi}^2/\text{mi}^2).$$

$$d_2 = -1.89 - 0.119 * \ln(P_{224}) - 0.100 * \text{Dry} + 0.664 * \text{imp}_{\text{av}} + 0.121 * \ln(\text{Yrs}) + 0.190 * \ln(Q_{10}) - 0.109 * \ln(d_1) \quad \text{Eq. (1.24)}$$

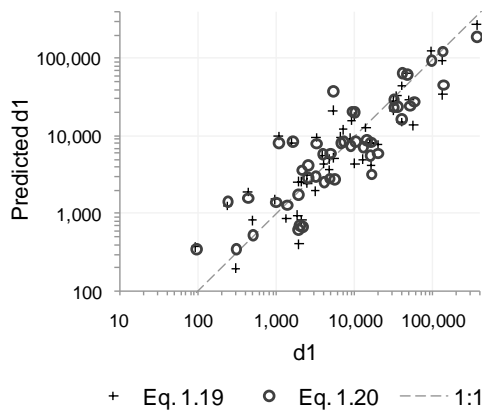
where:

$$\text{Imp}_{\text{av}} = (\text{mi}^2/\text{mi}^2).$$

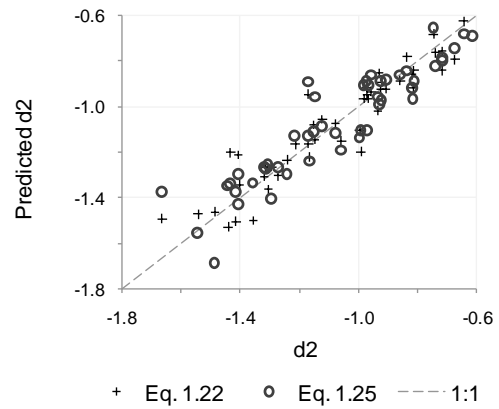
$$d_2 = -0.743 - 0.429 * \text{Shp} + 2.75 * \text{IP} - 0.233 * \text{Dry} - 0.838 * S_{\text{chn}} + 0.672 * \text{imp}_{\text{av}} + 0.106 * \ln(\text{Yrs}) - 0.103 * \ln(d_1) \quad \text{Eq. (1.25)}$$

where:

$$\text{Imp}_{\text{av}} = (\text{mi}^2/\text{mi}^2).$$



(a)  $d_1$  Eqs. (1.19) and (1.20)



(b)  $d_2$  Eqs. (1.22) and (1.25)

**Figure 1.14 – Model performance of (predicted vs. actual) with 1:1 ‘perfect-fit’ lines overlaid**

Predictions of ‘day1’ were even more accurate than those of d1. Table 1.13 summarizes the following equations.  $Imp_{av}$ ,  $Imp_7$ , and  $Imp_5$  were all highly significant ( $p \ll 0.05$ ) after Yrs,  $Q_{max}$ , and Srf. Two forms of the equation are presented for each metric of urbanization. Eqs. (1.29) through (1.31) include the five most significant predictors (DD, Srf,  $Imp_x$ , Yrs, and  $Q_{max}$ ), while Eqs. (1.26) through (1.28) add DD, P, and  $S_{chn}$ . Although a total of eight independent variables was less desirable, they offer more complete representations of the effect of urbanization. That is, imperviousness is still predicted to have an exponential effect on days of occurrence even after accounting for the wide range of other theoretically important, relatively significant variables.

**Table 1.13 – Summary of component (magnitude and shape) equations for DDFs: day1 and day2 (for Eq. (1.6), bins 12-25)**

	Equation Number	Independent Variable	Adjusted $R^2$	Mean Abs. Error Arithmetic Space (%)	p-exceptions ( $p > 0.05$ )
day <sub>1</sub>	Eq. (1.26)	f(Shp, DD, P, $S_{chn}$ , Srf, $Imp_7$ , Yrs, $Q_{max}$ )	0.87	38%	P 0.15, Schn 0.08
	Eq. (1.27)	f(Shp, DD, P, $S_{chn}$ , Srf, $Imp_5$ , Yrs, $Q_{max}$ )	0.87	38%	P 0.14, Schn 0.06
	Eq. (1.28)	f(Shp, DD, P, $S_{chn}$ , Srf, $Imp_{av}$ , Yrs, $Q_{max}$ )	0.86	38%	P 0.16, Schn 0.07
	Eq. (1.29)	f(DD, Srf, $Imp_7$ , Yrs, $Q_{max}$ )	0.84	37%	
	Eq. (1.30)	f(DD, Srf, $Imp_5$ , Yrs, $Q_{max}$ )	0.83	37%	
	Eq. (1.31)	f(DD, Srf, $Imp_{av}$ , Yrs, $Q_{max}$ )	0.82	36%	
day <sub>2</sub>	Eq. (1.32)	f(Rlf, $Imp_7$ , Yrs, $Q_{10}$ , day <sub>1</sub> )	0.82	7.4%	$Imp_7$ 0.15
	Eq. (1.33)	f( $S_{chn}$ , $Imp_5$ , Yrs, $Q_{10}$ , day <sub>1</sub> )	0.82	7.4%	$Imp_5$ 0.16
	Eq. (1.34)	f( $Imp_{av}$ , Yrs, $Q_{10}$ , day <sub>1</sub> )	0.80	7.6%	
	Eq. (1.35)	f( $P_{224}$ , Dry, Yrs, $Q_{10}$ , day <sub>1</sub> )	0.82	7.1%	

Variables in Eqs. (1.12) through (1.16) are defined in Table 1.2.

Models for ‘day2’ showed slightly less precision than those of d2; however, the sample range was also narrower (i.e., -1.4 to -0.6 vs. -1.7 to -0.6).  $Imp_{av}$ ,  $Imp_7$ , and  $Imp_5$  showed similar significance and interchangeability as the equations for ‘day1.’ For

consistency, we include one equation with each of those parameters. Precipitation terms and ‘dry’ had less significance generally. We included one equation with both terms for good measure.

$$\text{day}_1 = e^{-6.80} * e^{(-1.46 * \text{Shp})} * e^{(-0.820 * \text{DD})} * P^{0.587} * S_{\text{chn}}^{0.423} * e^{(4.84 * \text{Srf})} * e^{(1.64 * \text{imp}_7)} * \text{Yrs}^{1.98} * Q_{\text{max}}^{0.545} \quad \text{Eq. (1.26)}$$

$$\text{day}_1 = e^{-6.86} * e^{(-1.50 * \text{Shp})} * e^{(-0.815 * \text{DD})} * P^{0.605} * S_{\text{chn}}^{0.462} * e^{(4.70 * \text{Srf})} * e^{(1.42 * \text{imp}_5)} * \text{Yrs}^{1.96} * Q_{\text{max}}^{0.536} \quad \text{Eq. (1.27)}$$

$$\text{day}_1 = e^{-6.58} * e^{(-1.55 * \text{Shp})} * e^{(-0.818 * \text{DD})} * P^{0.598} * S_{\text{chn}}^{0.458} * e^{(4.87 * \text{Srf})} * e^{(11.1 * \text{imp}_{\text{av}})} * \text{Yrs}^{1.92} * Q_{\text{max}}^{0.514} \quad \text{Eq. (1.28)}$$

$$\text{day}_1 = e^{-5.08} * \text{DD}^{-1.88} * e^{(6.38 * \text{Srf})} * e^{(1.64 * \text{imp}_7)} * \text{Yrs}^{1.87} * Q_{\text{max}}^{0.706} \quad \text{Eq. (1.29)}$$

$$\text{day}_1 = e^{-4.92} * \text{DD}^{-1.87} * e^{(6.37 * \text{Srf})} * e^{(1.38 * \text{imp}_5)} * \text{Yrs}^{1.84} * Q_{\text{max}}^{0.696} \quad \text{Eq. (1.30)}$$

$$\text{day}_1 = e^{-4.69} * \text{DD}^{-1.86} * e^{(6.40 * \text{Srf})} * e^{(10.4 * \text{imp}_{\text{av}})} * \text{Yrs}^{1.80} * Q_{\text{max}}^{0.679} \quad \text{Eq. (1.31)}$$

where:

Shp (mi/mi<sup>2</sup>), DD (mi/mi<sup>2</sup>), P (in), **S<sub>chn</sub> (ft/mi)**, Srf (ft/ft), Imp<sub>5</sub> and Imp<sub>7</sub> (yr/yr),

**Imp<sub>av</sub> (mi<sup>2</sup>/mi<sup>2</sup>)**, Yrs (yr), Q<sub>max</sub> (cfs).

$$\text{day}_2 = -1.23 - 0.0679 * \ln(\text{Rlf}) + 0.0866 * \text{imp}_7 + 0.133 * \ln(\text{Yrs}) + 0.166 * \ln(Q_{10}) - 0.117 * \ln(\text{day}_1) \quad \text{Eq. (1.32)}$$

$$\text{day}_2 = -1.53 - 0.907 * S_{\text{chn}} + 0.0743 * \text{imp}_5 + 0.112 * \ln(\text{Yrs}) + 0.143 * \ln(Q_{10}) - 0.110 * \ln(\text{day}_1) \quad \text{Eq. (1.33)}$$

$$\text{day}_2 = -1.76 + 0.897 * \text{imp}_{\text{av}} + 0.143 * \ln(\text{Yrs}) + 0.169 * \ln(Q_{10}) - 0.129 * \ln(\text{day}_1) \quad \text{Eq. (1.34)}$$

$$\text{day}_2 = -1.46 - 0.155 * \ln(P_{224}) - 0.102 * \text{Dry} + 0.113 * \ln(\text{Yrs}) + 0.152 * \ln(Q_{10}) - 0.107 * \ln(\text{day}_1) \quad \text{Eq. (1.35)}$$

where:

$P_{224}$  (in),  $S_{\text{chn}}$  (ft/ft),  $S_{\text{rf}}$  (ft/ft),  $R_{\text{lf}}$  (ft),  $\text{Imp}_5$  and  $\text{Imp}_7$  (yr/yr),  $\text{Imp}_{\text{av}}$  ( $\text{mi}^2/\text{mi}^2$ ),  
 $\text{Yrs}$  (yr),  $Q_{10}$  (cfs).

Lastly, the gauges used to calibrate these models had a positively skewed range of ~20 to 95 yrs with a mean of ~45 and standard deviation of ~20. In application, we recommend simulations within one standard deviation of the mean (i.e., ~25 to 65 yrs, convenient for the typical engineering time frame of ~50 yrs).

## 1.4 Implications and Discussion

The models predict higher peak flows (especially for  $\leq Q_5$ ), and longer durations across all sediment-transporting flows in urban watersheds. As an example, I applied them to a hypothetical watershed with average conditions, controlling for everything but imperviousness. I included a ‘dry’ scenario to document hydrologic implications in those watersheds east of the Peninsular Ranges.

Beyond model application, case studies were presented of two gauges whose records spanned periods of relatively undeveloped and developed periods. With pre- and post-urban data in the same watersheds, the paired samples offer clear support to the broader statistical models, building a weight of evidence toward our overall conclusions.



the median peak/dry factors are presented as a ‘typical’ level of influence. For reference, the range of influence across all five equations is provided at the 20% impervious level.

**Table 1.14 – Influence of urbanization (maximum impervious extent of watershed) and Dry setting on peak-flow rates**

Flow	'dry' Factor* East Slope HUCs 18100200 or 18070305	Peak Factors* for Impervious Extent, Imp <sub>max</sub>					Factor Range at 20% Impervious	
		1%	5%	10%	15%	20%	Minimum	Maximum
Q <sub>1</sub> **	x 0.05	x 1	5.4	37	74	117	90	900
Q <sub>1.5</sub>	x 0.11	x 1	2.3	4.8	5.2	6.5	5.2	28
Q <sub>2</sub>	x 0.14	x 1	1.9	3.0	3.4	3.8	3.3	14
Q <sub>5</sub>	x 0.28	x 1	1.2	1.4	1.5	1.6	1.4	4.2
Q <sub>10</sub>	x 0.25	x 1	1	1	1	1	1	2.5
Q <sub>25</sub>	x 0.25	x 1	1	1	1	1	1	1.7
Q <sub>50</sub>	x 0.25	x 1	1	1	1	1	1	1.5
Q <sub>100</sub>	x 0.26	x 1	1	1	1	1	1	1.3

\* 'typical' factors (i.e., median influence factors of all five sets of Qi equations)

\*\* Q<sub>1</sub> factors should largely be ignored – many gauges had Q<sub>1</sub> = 0

The peak factors presented here are generally larger than those from previous studies. For example, Hammer (1972) and Hollis (1975) suggested that the 1.5- to 2-yr flows could double or triple at 10 to 20% imperviousness, and Bledsoe and Watson (2001) found peak factors ranging 1.5 to 4 dependent on regional setting. At those same impervious ranges and flow intervals, median peak factors from the models ranged 3 to 6.5; however, some models suggested increases by as much as 14x for Q<sub>2</sub> and 28x for Q<sub>1.5</sub> at 20% imperviousness. Though such increases may seem extreme, the flashiness of the setting combined with limited flow-control practices suggest that peak factors of southern California could be larger than in other regions.

Peak/dry factors for 1-yr flows should be tempered with the knowledge that twenty gauges recorded entire years of no flow resulting in Q<sub>1</sub> = 0 cfs. In contrast, the four most urban gauges (Imp<sub>av</sub> 9 to 14%) had significant 1-yr flows (26 to 236 cfs) with

no 0-flow years over records of 23 to 43 yrs. Although significant, such dramatic peak factors mean less in practice when they are relative to a mean of 12 cfs and median of 0.6 cfs for all 52 gauges.

$Q_{\max}$  showed less influence from urbanization mostly attributable to the overwhelming influence of Yrs and Dry. Dry, in particular, dampened the influence of precipitation, lumping all 'non-dry' into similar categorical behavior. Urbanization in the lower valleys with less rainfall had similar maximum flows to those in higher basins with more rainfall. When Dry was withheld from the model (Eq. (1.16)), the exponent of the precipitation term was more than doubled, with  $\text{Imp}_{\max}$  also significant to the  $p < 0.06$  level. However, without the Dry term, the model treated the systems on the east slope in a more continuous, precipitation-based way, rather than in the more representative discontinuous behavior recorded by the gauges. Therefore, Eq. (1.16) had poorer accuracies than the four equations that included Dry.

Regarding the DDF curves, imperviousness had an exponential effect on the magnitude of the curve ( $d1$ , i.e., # of days), with a linear effect on  $d2$  (shape). This is interpreted not only as exponentially more days of equivalent flows, but non-proportional increases in the durations of the highest flows (i.e., a less negative  $d2$ ) all else being equal (including  $d1$ , on which  $d2$  is highly dependent). Figure 1.16 depicts how Arroyo Trabuco, despite having 25% less annual rainfall and years of record is nearly overlaid with the DDF of San Antonio.

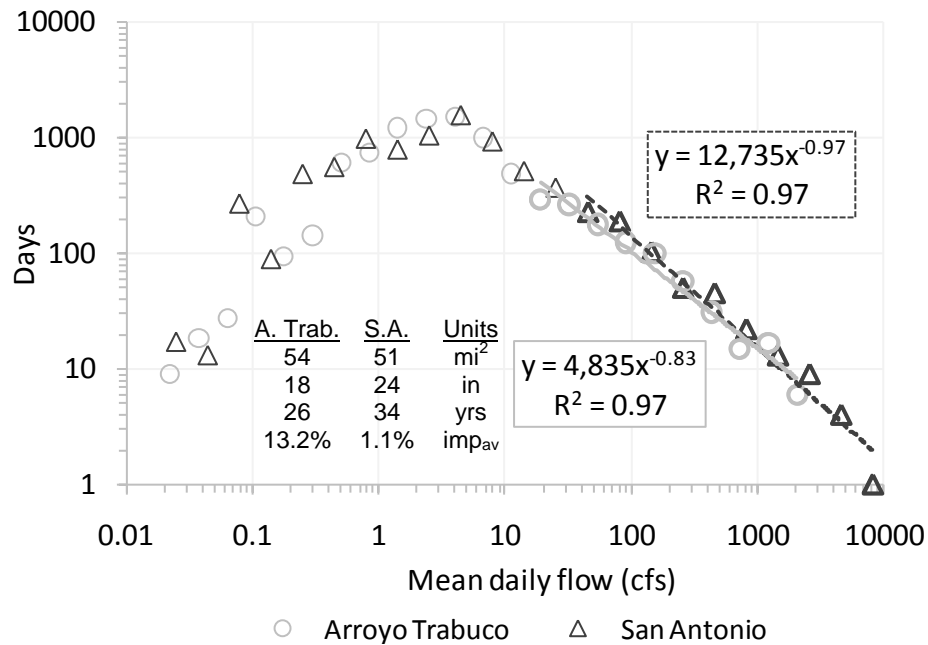


**Figure 1.16 – DDFs of gauges Arroyo Trabuco and San Antonio fitted to centroids of logarithmically-distributed histogram bins 16-25 with selected parameters of drainage area, average annual precipitation, record length, and average impervious area**

Yet, because d2 is also highly dependent on d1, and d1 is dramatically larger in urban watersheds, their combined effect is relatively consistent increases in durations of all sediment-transporting flows. Figure 1.17 presents a 25-yr simulation of an average watershed set in a lower valley (where urbanization most often occurs) under average climatic conditions (~4 ‘wet’ yrs over 25 yrs) across three scenarios: dry, rural, and urban. Differing only by levels of imperviousness (i.e., imp<sub>av</sub> 12% vs. 0.5%), the urban setting was predicted to have approximately three times as many days of equivalent sediment-transporting flows as the rural setting. In contrast, the ‘dry’ setting not only has much shorter durations of equivalent flows, but also much lower flows generally (Q<sub>max</sub> 154 cfs vs. 1,090 cfs for the rural/urban scenarios). Figure 1.17(a) presents the d1/d2 model (bins 16-25), while Figure 1.17(b) depicts the day1/day2 model (bins 12-25). The

two models have relatively good agreement when superimposed, especially among the rural and urban components. Table 1.15 summarizes some of the key input metrics and results of the simulations.

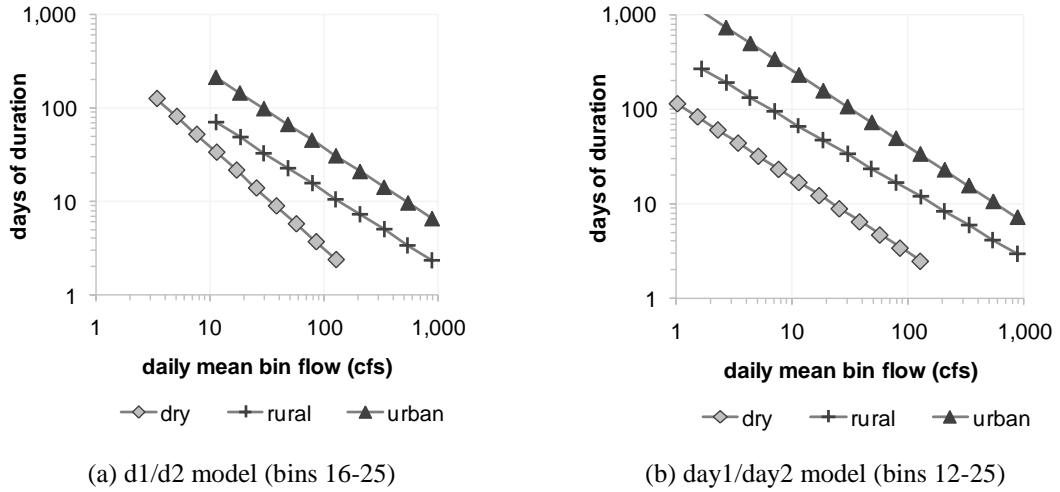


**Figure 1.17 – DDFs of 25-yr simulations of equivalent watersheds in ‘dry’, rural, and urban settings**

**Table 1.15 – Summary of 25-yr DDF simulation for ‘dry’, rural, and urban scenarios in an average\* watershed**

	Variable	‘dry’	Rural	Urban
key values for DDF model input	$Imp_{av}$	0.5%	0.5%	12%
	$Q_{max}$ (cfs)	154	1,090	1,090
	$Q_{10}$ (cfs)	719	2,690	2,810
d1/d2 model	d1	485	463	1,510
	d2	-1.10	-0.78	-0.80
	days @ ~125 cfs	2	11	31
	days @ ~350 cfs	-	5	14
	days @ ~900 cfs	-	2	7
day1/day2 model	day1	119	386	1,600
	day2	-0.80	-0.72	-0.80
	days @ ~125 cfs	3	12	34
	days @ ~350 cfs	-	6	16
	days @ ~900 cfs	-	3	7

\*‘average’ watershed (A ~30 mi<sup>2</sup>, P ~14 in, DD ~1.9 mi/mi<sup>2</sup>, Srf ~18%, 4 ‘wet’ yr)

Lastly, we should note that the equations should not be applied over combinations of ‘dry’ and ‘urban’ settings due to the lack of data in the ‘dry’ setting with more than nominal amounts of imperviousness (i.e., > 1%). The discontinuous behavior relative to their counterparts on the west slope, even for equivalent drainage areas, slopes, and rainfall, is most likely attributable to two factors. First, these areas receive less of the pseudo-regular precipitation delivered by winter frontal storms originating in the Pacific Ocean. Secondly, watersheds on the east slope are subject to local summer convective thunderstorms with high intensities but rare frequencies. Such differences in climatic boundary conditions could result in different vegetation, sediment production, and drainage-network structures, and ultimately the marked differences in hydrologic behavior recorded by the gauges. Although we could postulate that these systems too would be subject to significant flow alterations associated with urbanization, we have no empirical data in the sub-region to support this.

#### **1.4.2 At-a-station effects of urbanization**

Two gauges had sufficiently long records to span periods of both relatively undeveloped and developing/developed states. By dividing the records into equal periods, San Diego and Arroyo Simi were processed into ‘pre-urban’ and ‘post-urban’ samples. Both gauges were highly influenced by urbanization across all peaks and durations of record. For example, Arroyo Simi, depicted in Figure 1.18(a), had more than a ten-fold difference in the 2-yr flow (2,040 cfs vs. 174 cfs), while the 25-yr flow was over three times as large at 10,700 cfs relative to 3,000 cfs. Figure 1.18(b) summarizes the record at the rural gauge of Hopper Creek spanning the same time frame. By comparison, peak

flows differed by an average of only 20% across the two periods in the rural setting, and are likely attributable to the variability in the inter-period precipitation.

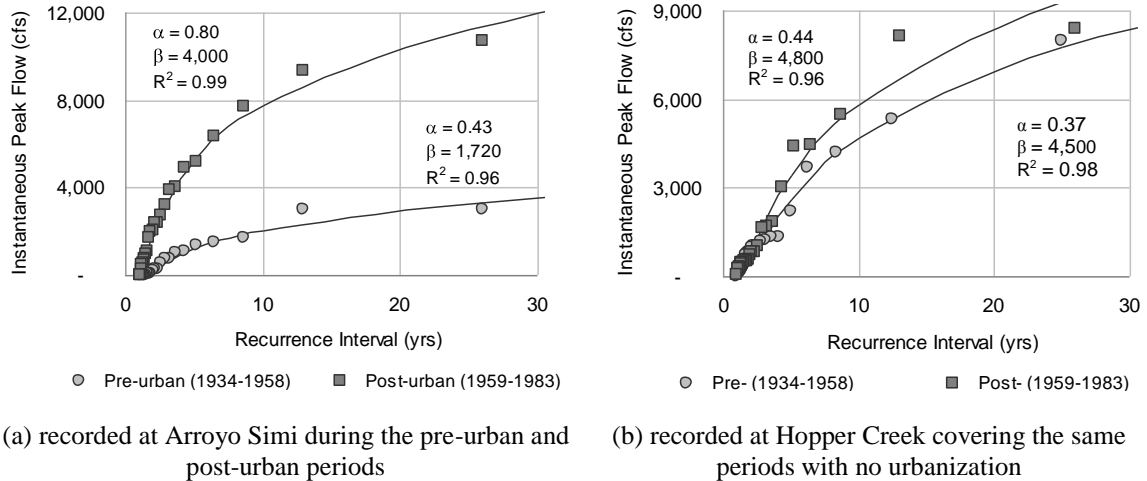


**Figure 1.18 – Instantaneous peak flow relative to recurrence interval, with fitted gamma distributions**

The long-term durations of daily-mean flows were also clearly affected by the change in land use at Arroyo Simi and San Diego. Figure 1.19(a) presents the respective DDFs of Arroyo Simi, recording both higher flows and longer durations for the urban regime. The maximum daily discharges over the 24.5-yr periods were 1,000 and 3,610 cfs, respectively, with the undeveloped regime incurring only 4 days at 500 cfs and 2 days at 800 cfs, while the post-developed regime had 21 days at 600 cfs and 8 days at 1,000 cfs. Additionally, 5 days at 1,700 cfs and 2 days at 2,900 cfs were recorded during the post-urban period, with no days of comparable flows in the pre-urban period. Presuming sediment is entrained by these higher flows, the post-developed regime had on average 4 to 5 times as many days of respective sediment-transporting flows as the pre-developed case, with an additional 7 days of flows that far exceeded the maximum flow in the undeveloped setting.

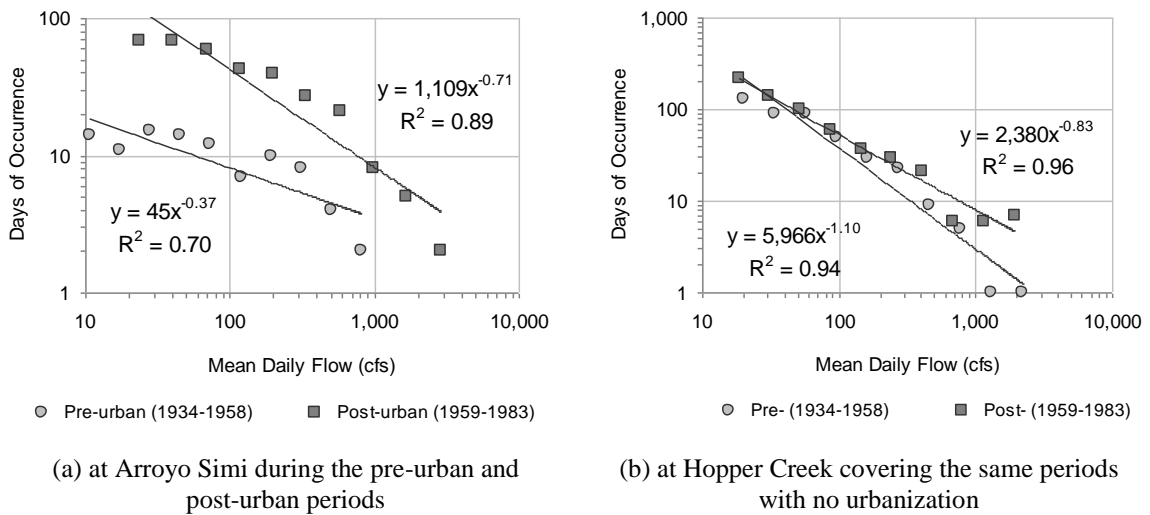


**Figure 1.19 – Cumulative-duration histogram centroids, with fitted DDFs**

In contrast, bin flows and durations during the same two periods at the undeveloped gauge were relatively similar. Figure 1.19(b) presents the nearly overlaid DDFs of Hopper Creek, with all but the two largest bins differing by an average of only 50%. The latter period experienced 6 days at 1,100 cfs and 7 days at 1,900 cfs, while the earlier period only had 1 day at each of the corresponding bins of 1,300 and 2,200 cfs. Even so, the maximum daily flow was actually largest in the ‘pre-’ period (2,770 cfs vs. 2,400 cfs).

To summarize, the rural gauge had a small vertical shift in the DDF between the two periods with slightly more days of similar flows. However, the urban gauge showed dramatic shifts in the DDF both vertically and laterally. At both San Diego and Arroyo Simi,  $Q_{\max}$  increased by a factor of 3 to 4, while durations of corresponding bin-flows increased by factors of 3 to 6 from the undeveloped to urban portions of the records.

We considered potential differences in climate as a competing hypothesis to urbanization as the primary cause of increased flows and durations between the two

periods. As seen in Figure 1.20(a), the pre-urban period of Arroyo Simi (1934 - 1958) begins with relatively wet years and trends downward, while the post-urban period (1959 - 1983) begins in a relative drought and trends upward. While the higher peak flows in the respective periods generally correspond with exceptionally wetter years, precipitation alone clearly cannot explain the somewhat flat trend in peak flows during the pre-urban period and the largely upward trend during the post-urban period. In contrast, the relative similarity among the highest peaks between the same two periods at the rural gauge of Hopper Creek (Figure 1.20(b)) and better correlation with the higher precipitation years adds support for causation between urbanization and the latter-period extreme flows recorded at Arroyo Simi.

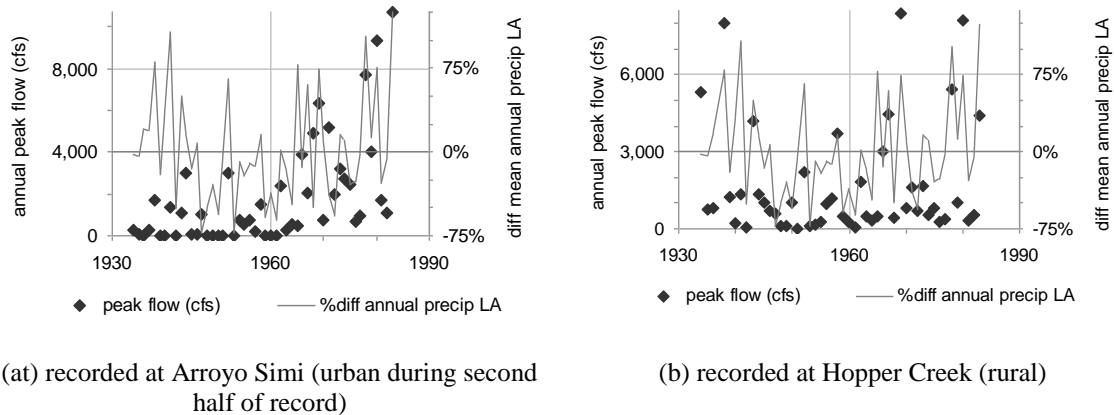


**Figure 1.20 – Annual peak flows overlaid with relative difference in mean annual precipitation at Los Angeles weather station**

By tracking urbanization through time via impervious cover, the positive trend in peak flows at Arroyo Simi is much better explained (Figure 1.21). Indeed, multivariate at-a-station regression can explain up to 60% of the variance in annual peak flows at Arroyo Simi by including imperviousness and annual precipitation as recorded at Los Angeles. Several transformations (e.g., logarithmic, square, and exponential) were

applied to the data for both backward and forward elimination, with imperviousness highly significant ( $p < 0.0001$ ) and accounting for 30 to 40% of the total variance.

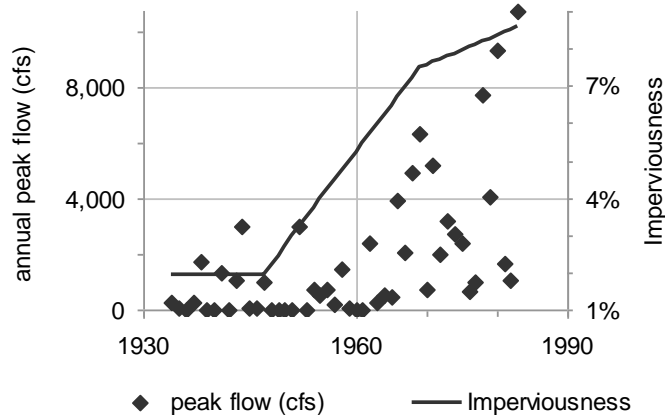


**Figure 1.21 – Annual peak flows recorded at Arroyo Simi overlaid with interpolated percentage of impervious cover in the watershed as tracked via historic USGS quadrangle maps**

Of course, rainfall data corresponding to the storms that created the individual peaks at the gauging station would probably be much more predictive than annual rainfall in Los Angeles; however, such data were not available. Even so, rainfall at the Los Angeles weather station does provide a surrogate of regional trends in climate through time. Other metrics tested from these data were the number of exceptionally wet and dry years during the gauge record, that is, precipitation years that were greater or less than the mean annual rainfall by 50%. These values are included in Table 1.16 for comparison.

**Table 1.16 – Comparison of flows, durations, climate, and imperviousness over the pre-urban and post-urban periods of Arroyo Simi and San Diego**

Variable/ Value	Arroyo Simi (Ventura County)			San Diego (Orange County)			
	Pre-urban 1934 - 1958	Post-urban 1959 - 1983	Post/ Pre	Pre-urban 1950 - 1967	Post-urban 1968 - 1985	Post/ Pre	
peak flows	<b>Return Interval</b> (yrs)	<b>Flow Pre</b> (cfs)	<b>Flow Post</b> (cfs)	<b>Ratio</b>	<b>Flow Pre</b> (cfs)	<b>Flow Post</b> (cfs)	<b>Ratio</b>
	1	-	14	∞	-	448	∞
	1.5	19	891	> 40	726	1,233	1.7
	2	174	2,040	12	907	1,937	2.1
	5	1,278	5,138	4.0	1,932	6,363	3.3
	10	2,059	7,790	3.8	2,910	8,192	2.8
	25	3,305	11,237	3.4	4,025	11,625	2.9
	50	4,301	13,877	3.2	4,866	14,237	2.9
100	5,326	16,536	3.1	5,704	16,859	3.0	
durations	<b>~ Mean Daily Flow</b> (cfs)	<b>Days Pre</b> (#)	<b>Days Post</b> (#)	<b>Ratio</b>	<b>Days Pre</b> (#)	<b>Days Post</b> (#)	<b>Ratio</b>
	100	7	42	6.0	9	37	4.1
	200	10	39	3.9	6	32	5.3
	400	8	27	3.4	8	26	3.3
	600	4	21	5.2	3	9	3.0
	800	2	8	4.0	-	10	∞
	1,700	-	5	∞	-	6	∞
	2,900	-	2	∞	-	-	∞
extreme flows and Los Angeles precipitation*	<b>Variable</b> (unit)	<b>Pre</b> (varied units)	<b>Post</b> (varied units)	<b>Ratio</b>	<b>Pre</b> (varied units)	<b>Post</b> (varied units)	<b>Ratio</b>
	mean annual precipitation (in.)	15.0	15.7	1.04	13.4	16.0	1.2
	'wet' years (#)	3	6	2	3	4	1.3
	'high' peaks (#)	2	10	5	1	6	6.0
	'dry' years (#)	4	3	0.75	4	1	0.25
	'low' peaks (#)	18	8	0.44	11	5	0.45
impervious- ness	<b>Spatial extent during period</b>	<b>TIA Pre</b> (%)	<b>TIA Post</b> (%)	<b>Ratio</b>	<b>TIA Pre</b> (%)	<b>TIA Post</b> (%)	<b>Ratio</b>
	maximum	4.7	8.6	1.8	3.2	14.9	4.5
	mean	2.6	7.2	2.8	3.2	9.7	2.9

\* 'wet' and 'high' correspond to years/events 50% greater than the respective means, while 'dry' and 'low' indicate years/events 50% lower than the mean

As indicated in Table 1.16, the urban records did correspond to periods of slightly higher precipitation in terms of the annual precipitation at the Los Angeles weather station and number of exceptionally wet and dry years. However, these climatic

differences alone cannot explain the dramatic differences in flows and durations. The most telling difference in Table 1.16 is the number of exceptionally high peaks relative to exceptionally wet years. For example, the post-urban period of Arroyo Simi experienced 10 flows that were over 50% higher than the mean, while the pre-urban period experienced only two such flows (differing by a factor of 5). However, the respective periods only differed by a factor of 2 in number of exceptionally wet years (6 vs. 3).

Another convincing difference between the two regimes appears in Figure 1.18. The post-urban period of Arroyo Simi has 9 flows larger than the largest instantaneous peak flow from the pre-urban period. In the case of San Diego, there are five flows higher than the maximum from the pre-urban regime. By comparison, the rural gauge at Hopper Creek had only two flows during the latter period that were higher than the highest peak from the first half of the record and they differed by only 5% (i.e., 8,400 and 8,120 cfs vs. 8,000 cfs). Also recall that the rural gauge recorded a higher  $Q_{\max}$  and only slightly less (50%) days of equivalent flows during the earlier period.

The differences in flows and durations between undeveloped and developed periods at the same gauges and the relative similarity during the same periods at the rural gauge add to the weight of evidence that such changes are largely attributable to urbanization. In fact, these differences observed at individual gauges were larger than what is predicted in the models, particularly in terms of  $Q_{\max}$ . The effects of urbanization captured in the models may have been dampened by the widespread variability across all sites, most of which were still relatively undeveloped. As more years of data are gathered at urban gauges, the models could be further refined to account for urbanization with a more equitable sampling of urban data.

## 1.5 Summary and Conclusions

The overarching objective of this chapter was to understand the effects of urbanization on the magnitude and duration elements of flow regimes in southern California (i.e., ‘hydromodification’). In doing so, updated alternatives to the USGS regional equations were offered for peak flows, which outperformed both rural (Waananen and Crippen, 1977) and urban (Sauer *et al.*, 1983) models in 27 out of 30 cases in terms of  $R^2$ . The difference was particularly substantial for more frequent return periods (e.g.,  $R^2 \sim 0.6$  to  $0.8$  vs.  $< 0.4$  at  $Q_{10}$ ). Beyond peak flows, I developed a method for estimating long-term cumulative durations at ungauged sites. DDFs expand on previous approaches to histogram-style duration curves in that their magnitude, shape, and scale are based on a watershed’s physical properties rather than scaling based on a nearby gauge and a single flow. Most importantly regarding hydromodification, both the peak flow and DDF models account for urbanization using measures of total impervious area, which were statistically significant ( $p < 0.05$ ), particularly for peak flows  $\leq Q_2$  and the magnitude (coefficient) component of DDFs, resulting in longer durations across all flows greater than some nominal value (e.g., 1 to 10 cfs).

Multivariate regression controlling for other potentially significant hydro-climatic variables (e.g., drainage area, mean annual rainfall, surface slope, etc.) correlated urbanization to higher peaks and longer durations of all geomorphically significant flows. These effects were also documented at individual gauges whose records spanned both pre-urban and post-urban periods. Moreover, these effects were not linear. Although several metrics, units, and equation forms were tested regarding urbanization, the form that was most significant was typically the exponential of total imperviousness as a

fraction of the drainage area. That is, flows and durations associated with identical watersheds differing only by measures of imperviousness (e.g., ~1% and ~10%) would be disproportionately larger. In terms of peaks, differences would be most substantial at the more frequent events (e.g., ~5x  $Q_{1.5}$ , ~3x  $Q_2$ , and ~1.4x  $Q_5$ ). Regarding durations of daily-mean flows, ~2 to 3 times as many days of *all* sediment-transporting flows would be predicted.

Such changes in the hydrologic regime can have far-reaching effects on receiving channels in terms of cumulative erosive energy and channel stability. Particularly for channels considered highly susceptible to hydromodification (e.g., live-bed unconfined systems), significant changes in channel form such as incision, widening, or planform shifts are anticipated if land-cover conversions from porous to impervious go unmitigated. The relatively dramatic responses in channel form that have been observed throughout the region are better explained in the context of such equally compelling changes in flow rates and durations of sediment-transporting events. The physically-based, empirically-calibrated hydrologic models presented here may become powerful tools in developing a process-based understanding of hydromodification on channel stability in southern California.

## **1.6 Future Work**

The logical next step is to apply these hydrologic models to sites where geomorphic data have been collected to evaluate whether changes in flows correspond to sediment discontinuities that in turn correlate to channel degradation. For example, can

risk-based models of channel stability be developed using these hydrologic models as a starting point? This question is addressed in Chapter 3.

Future work could also focus on the refinement of the DDF models developed in this chapter. For example, I was limited to daily-mean flow data for these analyses, but one could follow up with the USGS in a subsequent study to see if any of the gauges have 15-min or hourly data over their entire record (i.e., 20 of the 52 gauges were ‘real-time’ sites offering 15-min data for the last 60 days but only daily data over extended records). If one could acquire the finer resolution data for enough sites, they could repeat the histogram procedure in the hope of developing a scaling factor for the DDFs in this dissertation.

## **1.7 Acknowledgements**

I would like to thank organizations and individuals who contributed to this paper in terms of funding, data collection, and analysis. This research was funded in part by a State of California research grant, for which we are very grateful. Eric Stein of the Southern California Coastal Water Research Project (SCCWRP) played a primary role in acquiring research funds. Becky Schaffner of SCCWRP was extremely helpful in providing GIS assistance and training. The USGS continues to deliver spatial and hydrologic data to the public domain that are unparalleled in terms of scale and quality. I would like to extend my gratitude to all staff (past and present), and particularly to Scott Patterson of the South Poway Field Office whose time and care in answering questions provided clarity regarding individual gauges. The chapter is much improved as a result.

## 1.8 References

- Alley, W.A. and Veenhuis, J.E., 1983. Effective impervious area in urban runoff modeling. *Journal of Hydrological Engineering*, ASCE, 109(2): 313-319.
- Benda, L. and Dunne, T., 1997a. Stochastic forcing of sediment routing and storage in channel networks. *Water Resources Research*, 33(12): 2865-2880.
- Benda, L. and Dunne, T., 1997b. Stochastic forcing of sediment supply to channel networks from landsliding and debris flow. *Water Resources Research*, 33(12): 2849-2863.
- Biedenharn, D.S., Copeland, R.R., Thorne, C.R., Soar, P.J., Hey, R.D., and Watson, C.C., 2000. Effective Discharge Calculation: A Practical Guide. ERDC/CHLI TR-00-15, U.S. Army Corps of Engineers, Engineer Research and Development Center, Coastal and Hydraulics Laboratory, Vicksburg, MS.
- Biedenharn, D.S., Thorne, C.R., Soar, P.J., Hey, R.D. and Watson, C.C., 2001. Effective discharge calculation guide. *International Journal of Sediment Research*, 16(4): 445-459.
- Bledsoe, B.P. and Watson, C.C., 2001. Effects of urbanization on channel instability. *Journal of the American Water Resources Association*, 37(2): 255-270.
- Booker, F.A., Dietrich, W.E. and Collins, L.M., 1993. Runoff and erosion after the Oakland firestorm. *California Geology*, 46: 159-173.
- Booth, D.B., 1990. Stream-channel incision following drainage-basin urbanization. *Water Resources Bulletin*, 26(3): 407-417.
- Booth, D.B., 1991. Urbanization and the natural drainage system -- impacts, solutions, and prognoses. *The Northwest Environmental Journal*, 7: 93-118.

- Booth, D.B., 2000. Forest cover, impervious-surface area, and the mitigation of urbanization impacts in King County, Washington, Center for Urban Water Management, University of Washington, Seattle, WA.
- Booth, D.B. and Jackson, C.R., 1997. Urbanization of aquatic systems: degradation thresholds, stormwater detection, and the limits of mitigation. *Journal of the American Water Resources Association*, 33(5): 1077-1090.
- Bull, W.B., 1997. Discontinuous ephemeral streams. *Geomorphology*, 19(3-4): 227-276.
- California Forest and Range Experiment Station, 1951. Some aspects of watershed management in southern California. U. S. Department of Agriculture, Forest Service, California Forest and Range Experiment Station, Berkeley, CA, pp. 28.
- Chin, A., 2006. Urban transformation of river landscapes in a global context. *Geomorphology*, 79(3-4): 460-487.
- Chin, A. and Gregory, K.J., 2001. Urbanization and adjustment of ephemeral stream channels. *Annals of the Association of American Geographers*, 91(4): 595-608.
- Chow, V.T., 1959. Open Channel Hydraulics. McGraw-Hill Book Company, Inc., New York, NY, 680 pp.
- Chow, V.T., 1964. Handbook of Applied Hydrology. McGraw-Hill, Inc., New York, NY, 1467 pp.
- Chow, V.T., Maidment, D.R. and Mays, L.W., 1988. Applied Hydrology. McGraw-Hill, Inc., New York, NY, 572 pp.
- Coleman, D., MacRae, C. and Stein, E.D., 2005. Effect of increases in peak flows and imperviousness on the morphology of southern California streams. Stormwater

- Monitoring Coalition, Southern California Coastal Water Research Project, Westminister, CA.
- Dinicola, R.A., 1989. Characterization and simulation of rainfall-runoff relations for headwater basins in western King and Snohomish Counties, Washington State. Water-Resources Investigation Report 89-4052, U.S. Geological Survey.
- Durbin, T.J., 1974. Digital simulation of the effects of urbanization on runoff in the upper Santa Ana River Valley, Menlo Park, CA. U.S. Geological Survey.
- Emmett, W.W., 1975. The channels and waters of the upper Salmon River, Idaho. Professional Paper 870A. U.S. Geological Survey, Washington, DC.
- Environmental Protection Agency, 2006. Guidance specifying management measures for nonpoint pollution in coastal waters. Chapter 6: Management Measures for Hydromodification. U.S. Environmental Protection Agency.
- Espey, W.H., Jr. and Winslow, D.E., 1974. Urban flood frequency characteristics, *Proceedings, Journal Hydraulics Division*, American Society of Civil Engineers, pp. 279-293.
- Galster, J.C., Pazzaglia, F.J., Hargreaves, B.R., Morris, D.P., Stephen, C., Peters, S.C., and Weisman, R.N., 2006. Effects of urbanization of watershed hydrology: The scaling of discharge with drainage area. *Geology*, 34(9): 713-716.
- Graf, W.L., 1981. Channel instability in a braided sand-bed river. *Water Resources Research*, 17: 1087-1094.
- Graf, W.L., 1988. Fluvial Processes in Dryland Rivers. Springer-Verlag, Berlin.
- Gregory, K.J., 1976. Drainage networks and climate. In: E. Derbyshire (Editor), Geomorphology and Climate, Wiley-Interscience, Chichester, pp. 289-315.

- Hack, J.T., 1957. Studies of longitudinal stream profiles in Virginia and Maryland. Professional Paper 294-B, U. S. Geological Survey.
- Hammer, T.R., 1972. Stream channel enlargement due to urbanization. *Water Resources Research*, 8: 139-167.
- Hey, R.D., 1975. Design discharge for natural channels. In: R.D. Hey and T.D. Davies (Editors), Science, Technology and Environmental Management, Saxon House, pp. 73-88.
- Hey, R.D., 1997. Channel response and channel forming discharge: literature review and interpretation, Final Report, U.S. Army Contract Number R&D 6871-EN-01.
- Hollis, G.E., 1975. Effect of urbanization on floods of different recurrence interval. *Water Resources Research*, 11(3): 431-435.
- Horton, R.E., 1945. Erosional development of streams and their drainage basins: hydrophysical approach to quantitative morphology. *Geol. Soc. of Am. Bull.*, 56: 275-270.
- Jennings, M.E., Thomas, W.O.J. and Riggs, H.C., 1994. Nationwide summary of U.S. Geological Survey regional regression equations for estimating magnitude and frequency of floods for ungaged sites, 1993. Water-Resources Investigation Report 94-4002, U.S. Geological Survey, pp. 196.
- Knighton, A.D., 1998. Fluvial Forms and Processes: A New Perspective. John Wiley & Sons Ltd., New York, NY, 383 pp.
- Konrad, C.P. and Booth, D.B., 2002. Hydrologic trends associated with urban development for selected streams in the Puget Sound Basin, Western Washington.

- Water-Resources Investigations Report 02-4040, U.S. Geological Survey, Tacoma, WA.
- Leopold, L.B., 1968. Hydrology for urban land planning -- A guidebook on the hydrologic effects of urban land use. Circular 554, U. S. Geological Survey.
- Leopold, L.B., 1994. A View of the River. Harvard University Press, Cambridge, MA, 29 pp.
- Los Angeles County Flood Control District, 1959. Report on debris reduction studies for mountain watersheds of Los Angeles County. Los Angeles County Flood Control District, Los Angeles, CA, pp. 164.
- McPhee, J., 1989. The Control of Nature. Farrar, Straus, and Giroux, New York, NY.
- Mooney, D.M., 2007. SIAM - Sediment Impact Analysis Methods. Ph.D. Dissertation, Colorado State University, Fort Collins, CO, 375 pp.
- Novotny, V., 2003. Water Quality: Diffuse Pollution and Watershed Management. John Wiley and Sons, New York, NY.
- Pickup, G. and Warner, R.F., 1976. Effects of hydrologic regime on magnitude and frequency of dominant discharge. *Journal of Hydrology*, 29: 51-75.
- Poff, N.L., Bledsoe, B.P. and Cuhaciyan, C.O., 2006. Hydrologic variation with land use across the contiguous United States: Geomorphic and ecological consequences for stream ecosystems. *Geomorphology*, 79(3-4): 264-285.
- Raff, D.A., Bledsoe, B.P. and Flores, A.N., 2004. GeoTool User's Manual. Colorado State University, Fort Collins, CO.
- Rantz, S.E., 1971. Suggested criteria for hydrologic design of storm-drainage facilities in the San Francisco Bay region, California. U.S. Geological Survey.

- Roesner, L.A. and Bledsoe, B.P., 2002. Physical effects of wet weather flows on aquatic habitats - present knowledge and research needs. WERF Project Number 00-WSM-4, Water Environment Research Foundation.
- Salas, J.D. and Smith, R.A., 1981. Physical basis of stochastic models of annual flows. *Water Resources Research*, 17(2): 428-430.
- Santa Clara, 2004. Hydromodification Management Plan Report, Santa Clara Valley Urban Runoff Pollution Prevention Program, Sunnyvale, CA.
- Sauer, V.B., Thomas, W.O.J., Stricker, V.A. and Wilson, K.V., 1983. Flood characteristics of urban watersheds in the United States, U. S. Geological Survey.
- Schumm, S.A., 1991. To Interpret the Earth: Ten Ways to be Wrong. Cambridge University Press, 133 pp.
- Simon, A. and Downs, P.W., 1995. An interdisciplinary approach to evaluation of potential instability in alluvial channels. *Geomorphology*, 12: 215-232.
- Strahler, A.N., 1952. Hypsomic analysis of erosional topography. *Geol. Soc. of Am. Bull.*, 63: 1117-1142.
- Trimble, S.W., 1997. Contribution of stream channel erosion to sediment yield from an urbanizing watershed. *Science*, 278: 1442-1444.
- U.S. Army Corps of Engineers, 2009. HEC-RAS 4.0. Hydrologic Engineering Center - River Analysis System, Davis, CA.
- U.S. Water Resources Council, 1967. A uniform technique for determining flood flow frequencies. Bulletin 15 of the Hydrology Subcommittee, U.S. Water Resources Council, Washington, DC, pp. 15.

- U.S. Water Resources Council, 1981. Guidelines for determining flood flow frequency. Bulletin 17B of the Hydrology Subcommittee, U.S. Water Resources Council, Washington, DC, pp. 28.
- Waananen, A.O., 1969. Urban effects on water yield. In: W.L. Moore and C.W. Morgan (Editors), Water Resources Symposium, University of Texas Press, pp. 169-182.
- Waananen, A.O. and Crippen, J.R., 1977. Magnitude and frequency of floods in California. U. S. Geological Survey.
- Waters, T.F., 1995. Sediment in streams -- sources, biological effects, and control. American Fisheries Society, Monograph 7: 251.
- Watson, C.C., Dubler, D. and Abt, S.R., 1997. Demonstration erosion control project report. submitted to U.S. Army Engineer Waterways Experiment Station, Vicksburg, MS.
- Williams, G.P., 1978. Bank-full discharge of rivers. *Water Resources Research*, 14(6): 1141-1154.
- Wolman, M.G. and Gerson, R., 1978. Relative scales of time and effectiveness of climate in watershed geomorphology. *Earth Surface Processes*, 3: 189-208.
- Wolman, M.G. and Miller, J.P., 1960. Magnitude and frequency of forces in geomorphic processes. *Journal of Geology*, 68: 54-74.
- Yevjevich, V., 1972. Probability and Statistics in Hydrology. Water Resources Publications, Fort Collins, CO, 302 pp.

## 1.9 GIS Data Sources

**Cal-Atlas:** *2000 and 2007 Roadway Shapefiles*, State of California geospatial clearinghouse, [gis.ca.gov](http://gis.ca.gov).

**Google Earth:** *Present-day Aerial Photography*, [earth.google.com](http://earth.google.com).

**National Oceanic and Atmospheric Administration (NOAA):** *Precipitation Intensities for 2-year, 24-hour Storm*, <http://www.nws.noaa.gov/oh/hdsc/noaaatlas2.htm> (Atlas 2) and [hdsc.nws.noaa.gov/hdsc/pfds/pfds\\_gis.html](http://hdsc.nws.noaa.gov/hdsc/pfds/pfds_gis.html) (Atlas 14).

**United States Department of Agriculture (USDA), Natural Resources Conservation Service (NRCS):** *Soil Surveys, Average Annual Precipitation Shapefile (1961 - 1990)*, <http://datagateway.nrcs.usda.gov/>.

**United States Geological Survey (USGS):** *Historical Aerial Photography and Quadrangle Topographic Maps, National Elevation Dataset (NED), 2001 Impervious Raster, National Hydrography Dataset (NHD), Average Annual Precipitation Shapefile (1900 - 1960)*, <http://seamless.usgs.gov>.

## CHAPTER 2

# REGIONALLY-CALIBRATED PROBABILISTIC THRESHOLDS OF GEOMORPHIC STABILITY: KEY COMPONENTS OF A SCREENING TOOL FOR ASSESSING CHANNEL SUSCEPTIBILITY TO HYDROMODIFICATION IN SOUTHERN CALIFORNIA

**Abstract.** Until recently, streamflow alteration associated with urban development in southern California has typically gone unmitigated and resulted in significant channel adjustments such as incision and/or widening with far-reaching effects on adjacent land and throughout drainage networks (both upstream and downstream). A field-calibrated screening tool was developed to assess channel susceptibility to hydromodification – changes in the delivery of water and sediment via the conversion of land from undeveloped to urban. The tool, which represents a collaboration of several researchers, is structured as a decision tree with a transparent, process-based flow of logic that provides qualitative sensitivity ratings of low, medium, high, or very high through a combination of relatively simple but quantitative input parameters that are derived from both field and Geographic Information System data. The screening rating foreshadows the level of data collection, modeling, and ultimate mitigation efforts that can be expected for a particular stream-segment type and geomorphic setting. With additional revisions of the screening tool anticipated in conjunction with ongoing field-verification efforts and end-user feedback, this chapter is focused on 1) the general framework of a susceptibility

screening tool, and 2) the development of risk-based analyses of geomorphic thresholds, a central component of key decision nodes in the screening tool.

Geomorphic thresholds are real and of great concern in stream management, such that any susceptibility assessment scheme should account for the proximity to such threshold-based responses. Logistic-regression analyses of braiding, incision, and bank stability directly and probabilistically assess proximity to geomorphic thresholds, and offer a framework for assessing risk that goes beyond expert judgment. Calibrated with local data that were collected in an extensive field campaign, the logistic models were highly significant (i.e.,  $p < 0.005$  to  $p < 0.0001$ ) and correctly classified unstable states in ~90% of the cases using simple but powerful predictor variables that can be measured at the screening/reconnaissance level. A screening tool that incorporates objective probabilistic-based components is novel relative to previous and more subjective classification schemes, such that regionally-diverse agencies and staff can quantitatively assess channel susceptibility with less variable results. The regionally-calibrated thresholds suggest that channels in southern California may be more sensitive than streams in other regions of the U.S. for equivalent flows, bed-material sizes, valley slopes, and bank heights/angles. Some potential explanations include the semiarid climate (and typically little reinforcing vegetation), erodible soils, flashy-flow regime, and high-sediment loads.

## **2.1 Introduction**

Streams in semiarid settings are known to be highly dynamic (Wolman and Gerson, 1978; Graf, 1981, 1988; Bull, 1997), and those of southern California are no

exception. Furthermore, hydromodification is ubiquitous throughout the region – broadly defined by the U.S. Environmental Protection Agency (EPA) as the “alteration of the hydrologic characteristics of coastal and noncoastal waters” (EPA, 2006). More specifically, we define hydromodification in the context of the streams of southern California as changes in watershed hydrologic processes following land conversion from undeveloped to urban. Common effects of the altered flow and sediment regimes from urban areas have been described across hydrogeomorphic settings including increased sediment transport, channel incision, widening, and enlargement (Wolman, 1967; Hammer, 1972; Booth, 1990, 1991; MacRae, 1997; Pizzuto *et al.*, 2000; Bledsoe and Watson, 2001a; Chin, 2006). However, consistent with previous work in the semiarid environment (Trimble, 1997) and specific to the region (Coleman *et al.*, 2005), channel responses to urbanization in southern California were observed to be on faster and larger scales. Complex responses from incision-driven evolution analogous to the original Channel Evolution Model (CEM; Schumm *et al.* (1984)) to planform shifts such as meandering to braided have cascading effects to both adjacent land and upstream/downstream. These responses are attributable to the intersection of high-energy fine-grained systems with a vast human footprint, described in detail in the following sub-sections.

### **2.1.1 The natural and anthropogenic setting**

The hydrogeomorphic setting of southern California gives rise to channels that are arguably more dynamic than humid and/or lower relief regions. The domain is bounded by the Transverse Ranges to the north and Peninsular Ranges to the east, with a total

relief of up to 3,500 m and short-travel distances to the Pacific Ocean on the order of 50 to 100 km. Such steep slopes produce substantial sediment loads, particularly when coupled with regional climatic and lithologic settings. Sediment yields from 115 debris basins in the San Gabriel Mountains had estimated yields ranging from 100 to 7,440 m<sup>3</sup>/km<sup>2</sup>/yr with a mean of 1,600 m<sup>3</sup>/km<sup>2</sup>/yr (Lavé and Burbank, 2004). The region's largely heterogeneous lithologies can generally be described as having a limited amount of coarse material with an abundance of fines. Gradations of regional debris-dam sediments have averaged 50% by volume fine ( $d < 0.06 \text{ mm}$ ), 42% sand, and less than 7% gravels and boulders ( $d > 2 \text{ mm}$ ) (Taylor, 1981). The climate is characterized as semiarid/Mediterranean, with precipitation and vegetative cover typically increasing with elevation from average annual extremes of 200 to 1,000 mm/yr and sparse grasses/chaparral to dense coniferous stands, respectively. Climate change is predicted to increase sediment delivery in the region largely as a result of a corresponding shift from sage to grassland (Gabet and Dunne, 2002, 2003).

This leads to predominant channel forms of single-thread and braided across both sand and gravel substrates. Almost exclusively ephemeral, flow regimes are extremely flashy with short-lived instantaneous peaks that are generally much larger than the respective daily mean. For example, a 10-yr instantaneous event would ordinarily correspond to a daily-mean flow on the order of a 2- to 3-yr event, with the former approaching 20 times the latter.

In addition to seasonal patterns, the region experiences large fluctuations in inter-year precipitation, which can be subject to decadal and even multi-decadal trends. This sets the stage for an active fire regime, triggering dramatic pulses in sediment production

and runoff (Los Angeles County Flood Control District (LACFCD), 1959; Booker *et al.*, 1993; Benda and Dunne, 1997a, 1997b). With measured inter-year sediment yields varying by more than four orders of magnitude at regional debris basins (Taylor, 1981), some researchers have suggested that fire-induced sediment production is the dominant form of contemporary erosion (Lavé and Burbank, 2004). Such dynamic ambient conditions lend credence to widespread postulation that periods of substantial aggradation and degradation can be more recurrent than states of ‘equilibrium’, and that the concept itself may need to be reconsidered for the region (Wolman and Gerson, 1978; Graf, 1988; Bull, 1997).

Beyond the natural setting, southern California is home to ca. 20 million residents. From historic overgrazing to contemporary urbanization, the disturbance regime that prevailed prior to European colonization has been significantly influenced by humankind. Although our influences have changed through time – orchards have largely given way to suburban lawns – the footprint continues to expand, filling the low-lying valleys surrounding Los Angeles and San Diego and advancing upslope. Yet, in spite of the highly-dynamic setting, regulatory bodies have done little to date to mitigate hydromodification. During 6 weeks of field investigations for this study, evidence of stormwater detention/retention facilities was largely lacking. The few measures observed were inline check dams and energy dissipaters at recently constructed outfalls. As a consequence, field observations consistently indicate that it often takes no more than 5 to 10 yrs following development for channel responses to become so severe that the jurisdictional authority is forced to mitigate using structural approaches. Ensuing attenuation measures have customarily been the complete concrete/riprap lining of

trapezoidal flood-conveyance channels, resulting in little/no ecological or geomorphic function.

### **2.1.2 Hydromodification project background**

Whether for the preservation of habitat, beach-sediment recharge, or even aesthetic purposes, public opinion has shifted such that regulatory measures require improved management of hydromodification. This chapter falls under the first tier of a multifaceted collaborative project charged with developing tools for assessing and managing hydromodification in southern California. In a broad sense, three levels of project tools are designed to address the following questions:

1. Screening: which streams are most susceptible to hydromodification?
2. Modeling: what are the predicted magnitudes of responses in the most susceptible stream systems?
3. Mitigation: what are potential management measures that could be implemented to offset hydromodification effects?

Although many existing classification and mapping systems offer insights to assessing channel stability, none were developed for or would exclusively capture the totality of risk types and settings in southern California (Bledsoe *et al.*, 2008). Furthermore, existing screening systems are predominantly descriptive in nature, often relying on expert judgment and field indicators with few quantitative components. Even so, quantitative aspects of studies from other regions would likely be subject to local variability due to the unique combination of hydrogeomorphic and anthropogenic factors in southern California. A regionally-calibrated screening tool tailored to local

stakeholders and designed with their input would have clear benefits to local jurisdictions in their mandate to protect water quality from the effects of hydromodification. Hence, a broadly collaborative effort was undertaken to develop such a tool.

The specific focus of this chapter is 1) the general framework of a susceptibility screening tool, and 2) the development of risk-based analyses of geomorphic thresholds – central components of key screening-tool nodes – driven by a large sampling of regional data. With additional revisions of the screening tool anticipated in conjunction with ongoing field-verification efforts and end-user feedback, a pre-final version of the tool is presented to highlight the individual contributions of this author.

### **2.1.3 Screening-tool development, structure, and goals**

The overarching goal of the screening tool is to rapidly assess the susceptibility of a stream segment in its watershed context to hydromodification. Risk is classified by three interconnected types (*sensu* Downs and Gregory (1995)):

1. probability of response: proximity to response threshold;
2. likely severity of response: magnitude, duration, and spatial extent; and
3. likely direction of response: vertical versus lateral (or both).

Development of the screening tool was guided by a project Technical Advisory Committee (TAC), whose members included academics, consultants, and local authorities who will ultimately use the tool in their mandate to protect water quality. With their sights set on application, the TAC converged on several guiding principles. First, susceptibility should be hierarchically-assessed across watershed, valley, and channel-segment scales (*sensu* Frissell *et al.* (1986) and Montgomery and Buffington

(1998)). They also desired transparent and process-based flow of logic. These goals directed the selection of a decision tree as the tool's most logical structure.

The type, level, and precision of data collection required in the tool was informed by an expansive body of previously-published classification systems summarized by Bledsoe *et al.* (2008). The tool begins with an office component (*sensu* Thorne (2002) and Vermont Agency of Natural Resources (VTNR; 2004)) that takes advantage of the recent proliferation of Geographical Information System (GIS) and aerial photography technology. Field reconnaissance is also required (*sensu* Downs and Thorne (1996)) with a goal of completing both field and office components in less than 1 day each. These initial assessments avoid detailed channel surveys but do require a minimum amount of field measurements such as median bed particle size ( $d_{50}$ ). In this light, screening assessments can employ quantitative – albeit simplified – metrics where possible, rather than being wholly subjective. And despite the immense regional complexity, the stakeholders wanted each node to pass the test of Occam's razor. That is, the tool avoids becoming unnecessarily complex if the same screening rating can be attained through fewer procedures. One way to streamline the tool was to include early 'off ramps' for clear risk types such as fully engineered and in good condition (low), CEM Types III and IV (very high), and alluvial fans (separate management strategies). Photographs provide users with unambiguous examples throughout.

Through three decision trees including watershed context, vertical susceptibility, and lateral susceptibility, the user arrives at a composite screening rating of low, medium, high, or very high. Although clearly qualitative, the ratings are designed to have direct implications to the next phases in the review process by dictating what level of

subsequent data collection and modeling will be required. They also foreshadow the ultimate level of mitigation that could be required, although verified by modeling in most cases. For example, a rating of ‘*low*’ would correspond to a confined/bedrock channel or one that is fully reinforced and in good condition. Proposed developments affecting only low-risk systems bypass the need for more detailed analysis, ensuring the minimum mitigation level as determined by the stakeholders. A ‘*medium*’ rating corresponds to cobble/boulder systems that have modest amounts of erosive energy relative to their armoring potential. Such systems would require a detailed channel survey (*sensu* VTNR (2004)) and a level of modeling sufficient to capture threshold behavior; however, mitigation controls would likely fall somewhere between the maximum and minimum extremes for the high- and low-risk systems. For example, such projects may be required to match the pre-development hydrograph above a critical flow that entrains the given bed material but demand few controls for smaller events. In contrast, those sites rated as ‘*high*’ are likely live-bed channels or threshold channels that could conceivably respond in dramatic ways (e.g., vertically-resistant but geotechnically-unstable banks or nearing the single-thread/braiding threshold). These highly susceptible systems require the maximum level of modeling, which includes all flows and must also account for sediment supply. Finally, a ‘*very high*’ rating requires data collection and modeling rigor on par with a ‘*high*’ rating; however, it may point to different modeling tools due to the sand-dominated substrate and/or active channel adjustments such as widespread bank failure and/or active braiding.

Beyond arriving at a clear and meaningful endpoint via a transparent flow of logic, the tool is designed with the understanding that geomorphic thresholds are real

(Osman and Thorne, 1988; van den Berg, 1995; Bledsoe and Watson, 2001b) and proximity to such thresholds should be of great concern for informed stream management. Logistic-regression analyses of braiding, incision, and bank stability directly and probabilistically assess proximity to geomorphic thresholds, and offer a framework for assessing risk that goes beyond expert judgment. Such objective quantifications of risk make a screening tool more easily transferable between regionally-diverse agencies, while the probabilistic framework adds a desirable level of flexibility such that jurisdictions may stratify screening ratings via locally-acceptable levels of risk (e.g., 10% vs. 50% probability of response). With the development of such geomorphic thresholds as the centerpiece, the objectives of this chapter are the following:

- present a tentative structure to the screening tool consistent with the stakeholder goals outlined above;
- use regional data to refine probabilistic nodes for incising, braiding, and mass wasting within that structure; and
- perform preliminary validation for that structure with available data.

Additionally, the following hypotheses are added in regards to the central objective:

H<sub>0</sub>: logistic regression can be applied with reasonable success to segregate states of incising, braiding, and mass wasting from their stable/reference counterparts; and

H<sub>0</sub>: geomorphic thresholds calibrated to southern California should indicate higher susceptibilities to unstable states relative to other regions of the U.S.

## 2.2 Methods

As outlined above, the geomorphic complexity of southern California is exceptional. Although the screening tool is desirably expedient, copious amounts of data were collected and analyzed for its development. Independent reviews quality assurance/quality control (QA/QC) procedures approved by the state of California ensured that site selection, data collection, analysis, and screening-tool development were performed in defensible ways.

### 2.2.1 Site selection and channel stability

With the project designed around hydromodification, the most central gradient in site selection was urbanization. Equally important was to understand system dynamics independent of hydromodification as a reference condition. Consequently, we targeted undeveloped, developing/recently developed, and fully-developed watersheds. This resulted in an array of sites composing channel evolution stages from ‘stable’ single-thread to incising, widening, and braiding. While most channels of southern California are inherently dynamic, we define ‘stable’ for the purposes of this tool after Biedenharn *et al.* (1997): *“In summary, a stable river, from a geomorphic perspective, is one that has adjusted its width, depth, and slope such that there is no significant aggradation or degradation of the stream bed or significant planform changes (meandering to braided, etc.) within the engineering time frame (generally less than about 50 years).”*

Interpreting the definition in the context of southern California, we must think in terms of relative scales about ‘significant aggradation/degradation’. For example, consider a reach type/process-domain (Montgomery and Buffington, 1997, 1998;

Montgomery, 1999) of confined, step-pool/bedrock that temporarily aggrades with finer material (i.e., gravels and smaller) into a plane-bed form following a fire. Such a system could still warrant a 'stable' rating if, over a period of gradual flushing, it returned to the pre-fire form (as we have witnessed). There are also regional examples of braided channels that have maintained a relatively constant bandwidth for over 50 yrs. Although not traditionally considered 'stable', such special cases of braided systems could fall under a broader interpretation of the Biedenharn *et al.* (1997) definition.

Perhaps more appropriately for the context of hydromodification effects, one could think of 'stable' as a layperson might. Has the channel significantly affected adjacent land or reaches upstream/downstream through considerable headcutting, widening, or planform shifts? Empirical evidence suggests that some channels in southern California have evolved their active width and slope to absorb intrinsic pulses in flow and sediment without such complex adjustments.

With this in mind, we performed field reconnaissance at more than 50 candidate stream reaches within our targeted domains. Selection criteria included both physical and logistical parameters such as accessibility and degrees-of-freedom in potential response to urbanization. That is, we excluded fully-engineered concrete/riprap-lined channels in good condition due to their inability to adjust in either form or substrate composition. Following the initial investigations, we performed a 'gap analysis' to ensure a wide distribution of sites across regionally-important gradients such as slope, bed material, channel type/planform, evolution stage, valley setting, drainage-basin size, geopolitical setting, and of course, extent of urbanization. Ranges and means of selected variables are presented in Table 2.1.

**Table 2.1 – Summary of key gradients across 83 morphologically-distinct sub-reaches used in screening-tool development**

<b>Metric Type</b>	<b>Key Gradient</b>	<b>Minimum - Maximum</b>	<b>Mean</b>	<b>Units</b>
watershed	drainage area	0.1 - 160	17	km <sup>2</sup>
	imperviousness	0 - 26	3.6	%
	average annual rainfall	230 - 740	430	mm
	drainage density	0.2 - 3.7	1.3	km/km <sup>2</sup>
	average surface slope	5 - 52	26	%
sub-reach	channel slope	0.2 - 15	2.6	%
	top width at 2-yr flow	0.2 - 62	11	m
	median grain size	0.125 - 500	26	mm

We focused on small watersheds due to the fact that most of the region’s larger streams have been substantially altered in form (concrete/riprap lining, channelization) and/or flow (dams/diversions). For popular culture references see the automobile race/chase scenes in Grease and Terminator II filmed in the concrete-lined Los Angeles River. The spatial distribution of project stream-reaches is shown in Figure 2.1.

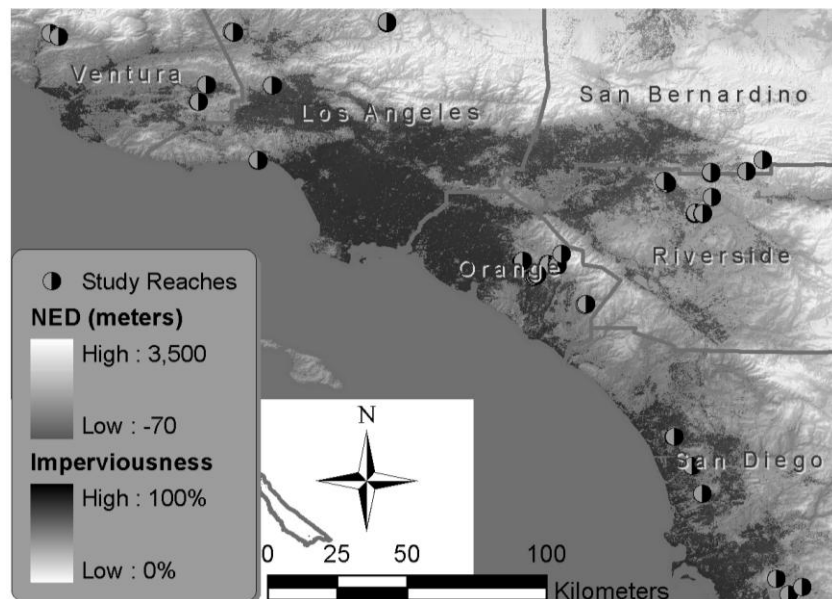


**Figure 2.1 – Overview of reaches sampled for screening-tool development**

The 52 candidates were culled through the selection-criteria analysis to 31 streams with 83 geomorphically-distinct sub-reaches or ‘sites’. Photographs and cross sections of each site are depicted in Appendix C, while watershed-, reach-, cross-section-scale metrics are summarized in Appendix D. For example, a 2-km reach may have several ‘sites’ due to significant differences in form (incised vs. widening), flow (additional tributaries), or valley setting (confined vs. alluvial valley). Admittedly interconnected, we felt the loss of independence was outweighed by the benefits gained in having such paired data to isolate differences such as valley setting or form alone (i.e., ‘stable’ vs. incising vs. widening all with the same flow and parent material). This age-old tradition of substituting space for time by capturing differing response stages along a single reach is often necessary to make inferences on projects with fixed start/stop dates such as this. Such observations should be tempered with the understanding that average rates of change decrease as time spans increase (Schumm, 1991); therefore, analyses were coupled with audits of historical aerial photography to bolster any space-for-time conclusions.

### **2.2.2 Field and GIS data collection**

Bed-material gradations were determined with a minimum of 100-particle pebble counts using a half-phi template and/or sieve samples after Bunte and Abt (2001b). Unbiased particle selection was secured through equally-spaced sampling frame transects across riffle sections after Bunte and Abt (2001a). Phi template measurements following Potyondy and Bunte (2002) are known to efficiently return more consistent readings than

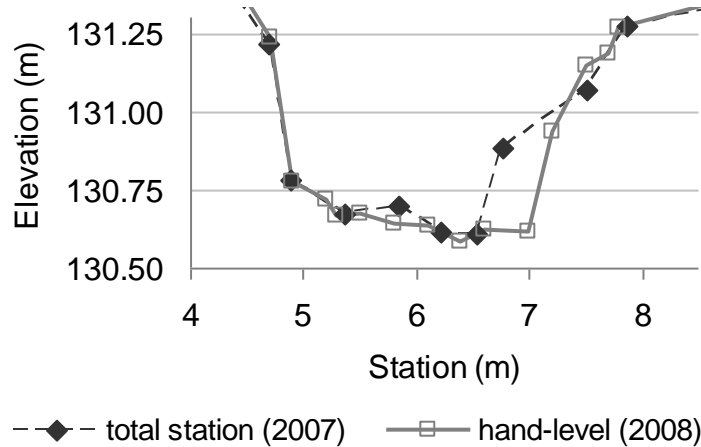
individual b-axis measurements, which is important for a tool that will be applied across diverse agencies and staff.

For sites greater than roughly 20% sand by volume, both sieving and phi-sampling were employed. Volumetric gradations (pebble counts) were composited with distributions by weight (sieve analyses) via a combination of rigid and flexible procedures designed by D. Dust and K. Bunte (Pers. Comm., 2008), and typically converged to similar median particle diameters. Rock-mass strength was measured with a Selby hammer, while penetrometer readings quantified bank strength. Unfortunately, sites varied so broadly that measurements often fell outside the calibrated range of the respective tools (both high and low). As such, segregation of sites across the said fields could only result in qualitative groupings with little analytical meaning.

Geometric data collection was primarily guided by Harrelson *et al.* (1994), with two levels of precision for cost optimization. ‘Modeling’ sites were designed for long-term monitoring via semi-permanent rebar benchmarks and detailed fluvial/sediment-transport modeling. Cross sections were spaced at short intervals ( $\leq 5$  channel widths) and surveyed with high-precision instruments. Points were translated to Global Positioning System (GPS) coordinates with lateral and vertical accuracies of 3 and 1 cm, respectively.

In contrast, ‘screening’ sites were surveyed with fewer cross sections and less precision as a tradeoff for collecting data at a larger number of reaches across a wide range of settings. A commercial-grade GPS unit located sites to within about 1 to 10 m of true position, while cross sections and profiles were shot with a 2x magnification hand-level, fiberglass tapes, and pocket rods. To attain reasonable accuracies, shots were

kept to distances less than or equal to 5 m with a fixed-height instrument stand for efficacious stabilization of the hand-level. As a check, three cross sections with modeling-level precision were resurveyed with the screening equipment at an average vertical error rate of 0.5 to 0.6 millimeters per lateral meter over 20- to 50-m transects. Figure 2.2 presents an example of the congruity between the two approaches (see unchanged top of bank locations, left bank, and bottom left portion of main channel). The repeated surveys (October 2007 vs. January 2008) also quantified enlargement due to mass wasting of the right bank following the fires of October 2007.



(a) comparison of ‘modeling’ (total station, 2007) and ‘screening’ (hand-level, 2008) surveys looking downstream



(b) photograph looking upstream capturing interim failure of right bank

**Figure 2.2 – Main channel of Cross section D at Hicks Canyon**

Finally, although equipment differed between modeling and screening sites, longitudinal profiles were surveyed in similar ways. All grade breaks along the channel thalweg were captured including heads and toes of riffles, knickpoints, and other bedform features. Important lateral transitions were also shot such as bends, thalweg crossings, etc. This kept shots to relatively short intervals, which were placed at a maximum of ~15 m with high-precision instruments and 5 m with screening equipment.

GIS data were acquired from public-domain sources such as the U.S. Geological Survey (USGS), U.S. Department of Agriculture (USDA), National Oceanic and Atmospheric Administration (NOAA), and State of California geospatial clearinghouse (CAL-Atlas). Historical and present-day aerial photography from the USGS and Google Earth were used to track changes through time, along with historical USGS quadrangle topographic maps. Unfortunately, empty fields in some USDA polygons compromised the capacity for widespread correlations in Natural Resources Conservation Service (NRCS) soil types and application of the agency's Curve Number method for estimating flow. Yet most geospatial sources were thoroughly complete. Indeed, two fields were calculated from sources spanning different time periods: roadway vectors (2000 vs. 2007) and mean annual precipitation polygons (1900 - 1960 vs. 1961 - 1990). General resolution of these source data was such that their precision was typically on the order of 1% of the measurement (e.g., 10-m National Elevation Dataset (NED) over 1 km of channel).

ArcMap software by Environmental Systems Research Institute (ESRI), including extensions such as 'spatial analyst', was used to optimize GIS measurements where possible. For tasks such as delineating watersheds and determining flow paths,

automated results from NED processing were verified with aerial photography and field investigations. They were also cross checked with existing shapefiles such as USGS Hydrologic Unit Code (HUC) boundaries and National Hydrography Dataset (NHD) flowlines. Prior to widespread use in clipping other basin-wide parameters, two separate personnel provided independent QA/QC of watershed boundaries and remedied any discrepancies.

### **2.2.3 Hydrology, hydraulics, and sediment supply**

Flows were estimated using a variety of empirical methods including the NRCS Curve Number, Rational Method, USGS regional equations, and the equations from Chapter 1 of this dissertation. The latter equations were invariably superior due to the fact that they were developed by and for small watersheds (1.4 to 270 km<sup>2</sup>) within the study domain and incorporate the effects of urbanization. Applying all five of the Chapter 1 hydrologic models provided five relatively similar estimates of individual return-interval flows; however, occasional outliers suggested the need for an averaging procedure. With the understanding that robust weighting procedures exist (e.g., information theoretic using the Akaike Information Criterion), systematically dropping the high and low estimate at each site was most effectual for excluding such outliers. The remaining three estimates generally converged to a narrow range such that a simple averaging procedure was sufficient to obtain a single-flow estimate for each return interval.

Hydraulic calculations were simplified by developing hydraulic-geometry relationships for each site. Expressing hydraulically-significant variables such as area,

hydraulic radius, and top width as functions of depth (as opposed to functions of flow) creates computational ease and facilitates the recognition of spatial patterns across reaches (Buhman *et al.*, 2002). This included power functions for area and hydraulic radius, as well as a predictor of top width that fluctuated across power, linear, logarithmic, or exponential forms. Although a theoretically correct top-width expression can be derived as a simple first-order derivative of the area function, the approach resulted in larger and more patterned residuals than direct regression of top-width data. This was attributable to channel irregularities that created small and sometimes patterned residuals in the area function, and thus compounded in the derivative.

Nearly all functions were fit to  $R^2$  values well above 0.90, with area and hydraulic radius commonly approaching 1.00 and top width often ranging between 0.97 to 0.99. Some cross sections warranted separate ‘main channel’ and ‘overbank’ functions to offset patterned residuals in the extreme tail of the curve. Interestingly, the best-fitting top width expression for braided and stable single-thread channels was regularly a power function, while the form was infrequent for incising or mass-wasting systems. Geometric discontinuities across these unstable incision-driven sequences were commonly better represented with linear, logarithmic, or exponential expressions of top width.

Normal depth for respective flows was iteratively solved via the Manning (1889) equation and hydraulic radius power function. Guided by Chow (1959), values of Manning  $n$  were estimated in the field. Compiled hydraulic results were used in development and calibration of the screening tool. Additionally, average annual sediment yields were estimated by Stillwater Sciences through a Geomorphic Landscape Unit (GLU) scheme in GIS, calibrated by regional debris-basin data.

## 2.2.4 Analytical and statistical methods

Geomorphically-important variables from published literature were computed for each site and tested for significance in segregating data into stability groupings that were consistent with theory and exploitable for the screening tool. Shear stress, dimensionless shear stress, stream power, and specific stream power all showed promise in isolating high-energy unstable systems from low-energy stable systems (Schumm, 1977; Simons and Simons, 1987; Brookes, 1988; Chang, 1988; Nanson and Croke, 1992; Rhoads, 1995), but dependence on channel slope, depth, and/or width made them impractical for a screening assessment. A more pragmatic index was a surrogate for specific stream power after van den Berg (1995), which uses valley slope in place of channel slope as a representation of the potential energy of the valley setting. Valley slope has been demonstrated as a geomorphically-significant parameter by numerous researchers, especially in semiarid environments (Patton and Schumm, 1975; Schumm *et al.*, 1980). It represents more of an inherent boundary condition over longer temporal scales than more readily adjustable channel slope.

By substituting the standard regime form of channel width, potential specific stream power is defined after van den Berg (1995) as:

$$\omega \approx \gamma/\alpha * S_v * Q_{bf}^{0.5} \quad \text{Eq. (2.1)}$$

where:

$\omega$  = function of valley slope, estimated bankfull or dominant discharge, and an assumed regime width that varies between sand- and gravel-bed rivers, i.e., width =  $\alpha * Q^{0.5}$

where:

$\alpha$  = regression coefficient computed for a particular collection of streams,  
specific (i.e., unit) stream power = total stream power/width, and total  
stream power =  $\gamma * Q * S$

where:

$\gamma$  = specific weight of the water and sediment mixture (e.g., often assumed to  
be that of water = 9810 N/m<sup>3</sup>).

Bledsoe and Watson (2001b) further simplified the approach by dropping the  
coefficients  $\gamma$  and  $\alpha$ , to eliminate dependence on variable regime constants across  
regional settings. Their ‘mobility index’ is defined as:

$$\omega_v = S_v * Q_2^{0.5} \quad \text{Eq. (2.2)}$$

where:

$\omega_v$  = function of valley slope and estimated mean-annual discharge represented  
by the 2-yr recurrence interval.

By performing logistic regression of the mobility index relative to median particle  
diameter ( $d_{50}$ ), Bledsoe and Watson (2001b) discerned states of incising, braiding, and  
stable-meandering (i.e., sinuosity  $\geq 1.3$ ) with over 80% accuracy.

Logistic regression offers utility when analyzing binomial distributions (e.g.,  
stable vs. unstable) in that rather than predicting the individual variable (i.e., 0 or 1) the  
probability of the response is modeled over a continuous range of 0 to 1 (Menard, 1995;  
Christensen, 1997; Ott and Longnecker, 2001). Such a continuous probabilistic  
framework has clear benefits for application in a screening tool; not only can response

thresholds be identified, but the *proximity* to such thresholds can be directly assessed regarding the risk of response. The logistic-regression function that models the probability of a response ( $p$ ) as a function of independent variables ( $x_i$ ) is expressed by the following equation:

$$p = \frac{\exp(\beta_0 + \beta_1 x_1 + \dots + \beta_n x_n)}{1 + \exp(\beta_0 + \beta_1 x_1 + \dots + \beta_n x_n)} \quad \text{Eq. (2.3)}$$

The S-curve represents a probability of response that increases exponentially when  $x_i$  is small, and slowly approaches the limit of 1 as  $x_i$  becomes large. Because linear combinations of independent predictor variables can vary between  $-\infty$  and  $+\infty$ , parameter interpretation is done in the context of the odds ratio (i.e.,  $p/(1 - p)$ ), which in conjunction with a logarithmic transformation results in a dependent variable that will likewise vary between  $-\infty$  and  $+\infty$ . Referred to as the logistic transformation, the log of the odds ratio ( $p'$ ) becomes a function of the standard linear-regression model:

$$p' = \ln\left(\frac{p}{1-p}\right) = \beta_0 + \beta_1 x_1 + \dots + \beta_n x_n \quad \text{Eq. (2.4)}$$

Logistic-regression models are generally fit using maximum likelihood techniques via an iterative process that optimizes parameters to maximize the probability of observing the data that were actually observed. The SAS software package (SAS Institute, 2004) was used to make the iterative procedure more efficient. Parameterization routines which used both the Fisher's scoring method and Newton-Raphson method were used and converged on identical models to  $\geq 3$  significant figures.

Model performance was assessed via the  $\chi^2$  statistic that compares the likelihood for the fitted model ( $L_1$ ) to that of the null model ( $L_0$ ) in which all  $\beta$ -parameters are zero. The  $\chi^2$  statistic was computed using three variations of the chi-squared distribution including the Likelihood Ratio (chi-squared), Score (asymptotic chi-squared), and Wald (approximate chi-squared). Associated p-values indicate the level of significance of the fitted model relative to the null. The percentage of observations correctly classified also served as a tangible measure of overall model performance.

Significance of individual predictor variables was assessed using standard errors, confidence intervals,  $\chi^2$  statistics, and associated p-values. Potential effects of collinearity were minimized by keeping the number of independent variables to a minimum. Logistic-regression diagnostics were used to assess homoscedasticity, and identify and assess the influence of outliers as a complement to overall-performance assessment. Among others, they included influence plots of Pearson and deviance residuals, the hat matrix diagonal, and observation-withholding schemes such as the standardized difference in parameters (DFBETAS) and change in deviance (DIFDEV). Although influential cases of outlying observations were identified, they do not necessarily imply problems in the model (Menard, 1995). Due to the fact that there was no physically-based reason for excluding those data, they were retained in the models to present a more realistic range of risk and a better representation of misclassification rates that can be expected in model application.

Both vertical (incising) and lateral (braiding) thresholds were developed in this manner. High-energy confined/bedrock systems, including reaches at Proctor, Topanga, San Juan, Stewart, Santiago, Siverado, and Escondido, were prominently sorted by grain

size alone and were not included in the final logistic-regression analyses due to minimum degrees-of-freedom. Due to the additional resistance provided by hardpan, Hovnanian was also excluded. ‘Stable’ sites were considered single-thread channels in unconfined alluvial valleys that were not observably incising, widening, or braiding (i.e., Dulzura, Challenger (A and C), Perris2, AltPerris (B and C), and Acton (F and G)). This included several cases of ‘recovered’ sites; that is, sub-reaches that had undergone evolutionary sequences and returned to some semblance of single-thread quasi-equilibrium (i.e., Perris1\_A, Borrego\_D, and McGonigle). Data at ‘constructed’ sites with either vertical or lateral artificial reinforcement were not used in these analyses (i.e., Santiago\_B, Hasley1\_Trib, Hicks\_A, Borrego\_A, and Oak Glenn).

Sites classified as ‘incising’ and ‘widening’ were those with significant incision (i.e., nearing or exceeding critical bank height) and/or active bank failure. Finally, ‘braided’ sites were broadly defined with the objective of segregating all laterally-dynamic systems with multiple flow paths. As such, any sub-reach taking a minimum of two actively adjusting flow paths at small to moderate flow events was included. This definition captured systems with a wide range of sediment supplies, flow types, and cases of vegetated bars, which other classification systems may have considered ‘anastomosing’; however, their high-energy settings offered little justification to treat them as being statistically different for the purposes of the screening tool.

Regarding susceptibility to lateral adjustments, bank data were used to develop regional logistic thresholds for mass wasting. Heights and angles were compiled for each bank that was not artificially reinforced. Non-planar banks were measured in four ways (summarized in detail in Appendix E) to test various schemes for representing non-planar

geometries. Heights and angles most representative for purposes of mass wasting based on failure theory presented by Osman and Thorne (1988) were used in the analyses. For detailed procedures of special cases, see Appendix C. Stability of each bank was rated via a detailed assessment of the extent of mass wasting (absent, broken, complete, and failed), fluvial bank erosion (significant and insignificant), consolidation (moderate/well, poor, and unconsolidated), confinement (hillslope, boulder/bedrock, and unconfined) dominant bank vegetation (extent and type), and artificial reinforcement (embanked, fill, graded, riprap, and none). With the objective of representing the risk of mass-wasting failure, these ratings systematically informed the global stability rating of stable/unstable geometries. For example, the height and angle of a failed bank that has slumped to the angle of repose has little utility in identifying the critical dimensions that caused the failure.

As consolidation can be particularly subjective, the intention of the rating scheme was to segregate geotechnical capacity classes for applicability to mass-wasting analyses. A summary of their ratings are as follows:

- Risk of bank failure more attributable to fluvial forces:
  - Unconsolidated – bank composed of alluvial material that until recently was the channel bed (< ~10 yrs) and shows no real consolidation, with failures evident at the angle of repose of sand (~30°).
  - Poorly consolidated – bank appears to be a weak consolidation of typically well-sorted materials, including cases of historic alluvium, but with enough settling time to show at least some consolidation.

- Bank failure can be attributable to mass wasting and/or fluvial erosion:
  - Moderately/well-consolidated – bank composed of more poorly sorted materials with consolidation much greater than that of recent/historic alluvium. Individual particles are difficult to distinguish even with close inspection of the bank.

In conclusion, the various approaches are most concisely summarized via the precautionary principle; that is, in cases of uncertainty I erred on the side of being conservative due to ultimate application as a screening-tool node.

Heights of moderately- to well-consolidated banks in unconfined channels (i.e., those banks that were not simply connected to the adjacent hillslope) were plotted versus angle, in which the stratification of stable and unstable banks clearly followed a log-log decay. The shape was analogous to the theoretical Culmann relationship of critical bank height for slab failure via the geotechnical mechanism of mass wasting:

$$H_c = \frac{4c' \sin \alpha \cos \phi'}{\gamma (-\cos (\alpha - \phi'))} \quad \text{Eq. (2.5)}$$

where:

$H_c$  = critical bank height required to generate instability with respect to slab failure via mass wasting;

$c'$  = effective cohesion of bank material (kPa);

$\alpha$  = bank angle (°);

$\phi'$  = effective friction angle of the bank material (°); and

$\gamma$  = unit weight of the soil (kN/m<sup>3</sup>).

The presence of tension cracks, which can account for up to half of the total height (Terzaghi, 1943; Thorne, 1982), can be incorporated via the following relations:

$$H_{cz} = H_c - z \quad \text{Eq. (2.6)}$$

$$z = \frac{2c'}{\gamma} \tan\left(45 + \frac{\phi'}{2}\right) \quad \text{Eq. (2.7)}$$

where:

$H_{cz}$  = critical bank height required for mass-wasting failure with a tension crack (m); and

$z$  = tension-crack depth (m).

By back-solving for the 50% logistic risk using the Culmann equation adjusted for the presence of tension cracks, regional stress parameters for mass wasting could be estimated. Specific weight was bounded by USDA soil-survey values of 1.50 to 1.81 g/cm<sup>3</sup> (i.e., 14.7 to 17.8 kN/m<sup>3</sup> or 93.6 to 113 lb/ft<sup>3</sup>). The friction angle was constrained between 12 and 28° leaving cohesion free to fluctuate 0 to 40 kPa (~800 lb/ft<sup>2</sup>) after measured/typical ranges from other regions (Lawler *et al.*, 1997; Simon *et al.*, 2000). As the presence of pore-water pressure is unknown and the values were not directly measured but fitted within the constraints of measured data, they would be more appropriately termed *operational* stress parameters (C. Thorne, 2009, Pers. Comm.).

Regarding the relative severity of lateral adjustments, it was necessary to develop an index to represent how wide a valley the channel could occupy if lateral adjustments were initiated. The valley-width index is defined as:

$$VWI = W_{\text{valley}} / W_{\text{channel}} \quad \text{Eq. (2.8)}$$

where:

VWI = function of valley bottom width relative to channel width,  $W_{\text{valley}}$  is measured between hillslope grade breaks at the valley floor, and  $W_{\text{channel}}$  is approximated by the width between the top of banks or the top width at the 10-yr flow.

## **2.3 Results**

The purpose of the screening tool is two-fold: first, to assess channel susceptibility to hydromodification, and second, to direct the next phases of the review process. As described in the introduction, both of those goals are met by arriving at a qualitative rating of low, medium, high, or very high via three decision trees. The following section describes what types of risk factors correspond to individual screening ratings, while Section 3.2 presents the decision trees.

### **2.3.1 Screening-tool risk types**

A gradient of four screening ratings offers an assessment of relative susceptibility to hydromodification. The ratings have direct implications regarding the next phases of data collection and modeling. They also foreshadow the ultimate mitigation level, although verified by modeling in most cases. The following sub-sections describe each screening rating and the corresponding risk factors. They typically include a minimum of two (sometimes interconnected) components:

1. Relative severity: given a response, how severe (e.g., magnitude, duration, etc.) could the response become?

2. Likelihood of response: how susceptible is the system to responding (i.e., proximity to a response threshold).

Some discussion is provided regarding the rationale for selected segregations between stability ratings. For brevity, logistic probabilities of various states are expressed as  $p_{\text{state}}$ .

### **2.3.1.1 Low**

A ‘low’ screening rating corresponds to the most resilient of regional-channel types. Projects affecting only reaches rated as ‘low’ will not be required to perform detailed channel surveys or modeling. Rather, they will be routed directly to the minimum mitigation level as determined by project stakeholders. Key delineations for low systems are coarse grain sizes  $d_{50} > 128$  mm or frequent grade control spaced at intervals  $\leq 5$  channel widths. The selection of 5 channel widths was informed by a general pool-riffle spacing of 5 to 7 channel widths in stable systems (Newbury, 1995), but it was primarily selected to be conservative, i.e., such spacing does not leave much room for adjustment, as evident in our data. Grain size of 128 mm was driven by the goal of segregating confined systems with frequent influence from bedrock outcroppings. There were four such sites in our data (Topanga\_A, Stewart\_A, Silverado\_A, and Escondido\_A), all of which were  $\geq 128$  mm. The rating of ‘low’ includes the following characteristics:

- Watershed Context
  - Engineered bed and bank in good condition

- Vertical Susceptibility
  - Frequent grade control (e.g., spaced at intervals  $\leq 5$  channel widths)
  - Boulder/cobble bed:  $d_{50} > 128$  mm
- Lateral Susceptibility
  - Consolidated bank with:
    - $p_{\text{mass wasting}} < 10\%$  and  $p_{\text{braiding}} < 50\%$
  - Unconsolidated bank, toe composed of cobbles/boulders  $> 64$  mm with:
    - $p_{\text{braiding}} < 50\%$

### 2.3.1.2 Medium

The ‘medium’ screening rating is intended for relatively resilient systems that clearly exhibit threshold behavior. Although they ask for a detailed channel survey, ‘medium’ systems require only a minimum level of modeling. Should modeling confirm threshold behavior, mitigation controls will likely be centered on the critical flow for entrainment rather than the full body of flows. A key measure introduced at this risk level is a  $VWI \leq 2$ . The intention was to ensure that ‘medium’ systems were relatively confined with little room to adjust laterally. Using the channel width at the 10-yr flow in the VWI equation segregated all of the systems assessed as ‘confined’ during field investigations. For reference, the 10-yr top width roughly coincided with estimates of ‘bankfull’ top width as determined by form in most cases. Risk factors attributed to a ‘medium’ susceptibility include:

- Vertical Susceptibility
  - Cobble/boulder bed:  $64 \text{ mm} > d_{50} \geq 128 \text{ mm}$  with:
    - $p_{\text{incision}} < 50\%$

- Lateral Susceptibility
  - Consolidated bank with:
    - $p_{\text{mass wasting}} < 10\%$ ,  $p_{\text{braiding}} \geq 50\%$ , and  $VWI \leq 2$
    - $p_{\text{mass wasting}} \geq 10\%$ ,  $p_{\text{braiding}} < 50\%$ , and  $VWI \leq 2$
  - Unconsolidated bank, toe composed of cobbles/boulders  $> 64$  mm with:
    - $p_{\text{braiding}} \geq 50\%$  and  $VWI \leq 2$
  - Unconsolidated bank, toe composed of fines with:
    - $p_{\text{braiding}} < 50\%$  and  $VWI \leq 2$

### 2.3.1.3 High

A ‘high’ screening rating corresponds to the types of systems that we have seen respond in dramatic ways. They typically exhibit live-bed behavior or are threshold channels that could conceivably become live bed with enough perturbation. The high rating is also applied to otherwise resilient vertical systems that are highly susceptible to lateral adjustments. Projects affecting high-risk systems demand detailed channel surveys and the highest level of modeling. The rating foreshadows a mitigation level that could encompass all flows, although ultimately determined by modeling. ‘High’ screening ratings include the following risk factors:

- Vertical Susceptibility
  - Gravel bed:  $16 \text{ mm} > d_{50} \geq 64 \text{ mm}$  with:
    - sand composition  $< 25\%$

- Lateral Susceptibility
  - Consolidated bank with:
    - $p_{\text{mass wasting}} < 10\%$ ,  $p_{\text{braiding}} \geq 50\%$ , and  $VWI > 2$
    - $p_{\text{mass wasting}} \geq 10\%$ ,  $p_{\text{braiding}} \geq 50\%$ , and  $VWI \leq 2$
    - $p_{\text{mass wasting}} \geq 10\%$  and  $VWI > 2$
  - Unconsolidated bank, toe composed of cobbles/boulders  $> 64$  mm with:
    - $p_{\text{braiding}} \geq 50\%$  and  $VWI > 2$
  - Unconsolidated bank, toe composed of fines with:
    - $p_{\text{braiding}} \geq 50\%$  and  $VWI \leq 2$
    - $VWI > 2$
  - Banks currently experiencing mass wasting, extensive fluvial erosion, or chute formation and:
    - $VWI \leq 2$

#### **2.3.1.4 Very high**

The ‘very high’ screening rating is reserved for the most-susceptible of systems. These include sand-dominated systems, braided channels, and streams already incurring significant adjustments (i.e., incision past critical bank height). Such a score comes with the same surveying and modeling requirements as the ‘high’ rating; however, there are two important differences. First, although modeling requirements are identical, ‘very high’ systems may use a different set of modeling tools due to the prevalence of sand. Second, the ‘very high’ rating defaults to the maximum mitigation requirement as determined by the stakeholders.

In some cases, a ‘very high’ rating may be evident prior to ever going into the field. For example, fundamental geology tells us that watersheds dominated by granitic materials are likely to have limited amounts of coarse material in the study area. Weathering of such parent material typically produces sand-sized sediments rather than more resistant cobbles and boulders. This has been regionally ground-verified by Dust and Bledsoe (2009). Such knowledge is beneficial for obvious reasons. For example, a developer could skip the field screening altogether, or budget time for detailed surveying in conjunction with screening reconnaissance. Several risk factors indicate a ‘very high’ susceptibility:

- Watershed Context
  - Live-bed systems without sufficient grade control (GC)
  - Unconfined channels composed of sand beds without GC
  - Channels with actively failing banks and significant widening
  - Watersheds dominated by granite after Dust and Bledsoe (2009) without GC
- Vertical Susceptibility
  - Bed composed of small gravels:  $d_{50} \leq 16$  mm without GC
  - Beds composed of  $\geq 25\%$  sand without GC
- Lateral Susceptibility
  - Banks currently experiencing mass wasting, extensive fluvial erosion, or chute formation and:
    - $VWI > 2$

### 2.3.1.5 Alternative management

Two specific cases fall outside the scope of this screening tool and warrant alternative management:

- Alluvial fans
  - Alluvial fans are clearly very high-risk settings in need of special management requirements and modeling steps. We recommend that managers discourage development in such inherently unstable settings.
- Tidal/ocean
  - Projects discharging directly to the ocean or tidal backwater warrant separate management due to the unique, generally low-risk boundary conditions.

### 2.3.2 Screening-tool decision trees and geomorphic thresholds

The following is a presentation of the three decision trees that are central to the screening tool: watershed context (Figure 2.3), vertical susceptibility (Figure 2.4), and lateral susceptibility (Figure 2.5). Supplemental figures and tables including logistic regression of incision, braiding, and mass wasting are also presented. The trees include a series of questions, with each answer represented by a node. The font/color scheme is as follows:

Non-terminal  
node

**TERMINAL  
node**

**ALTERNATIVE  
management**

Although nearly final in the present form, future revision will likely add more detailed questions involving special cases, for example, what does grade control in ‘good condition’ entail? The basic decision-tree format across three primary domain types (i.e., watershed, vertical susceptibility, and lateral susceptibility, has prevailed through several rounds of stakeholder input and is currently in the field-testing phase.

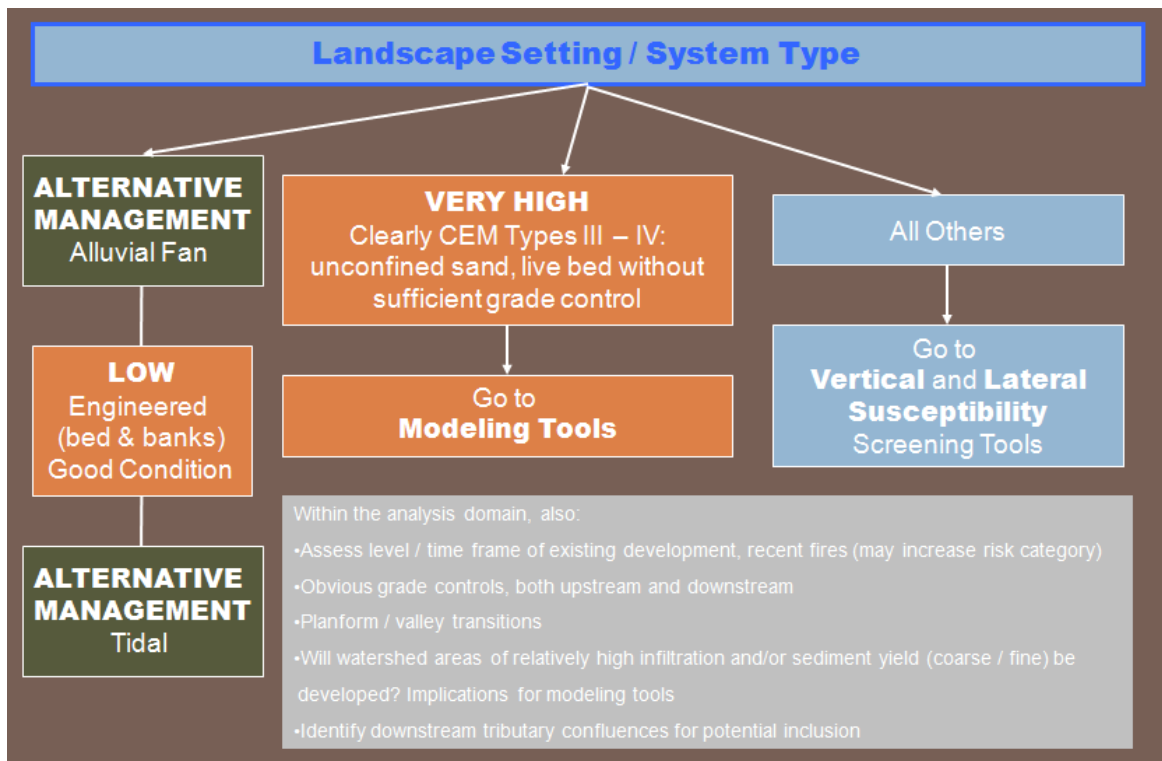


**Figure 2.3 – Watershed context**

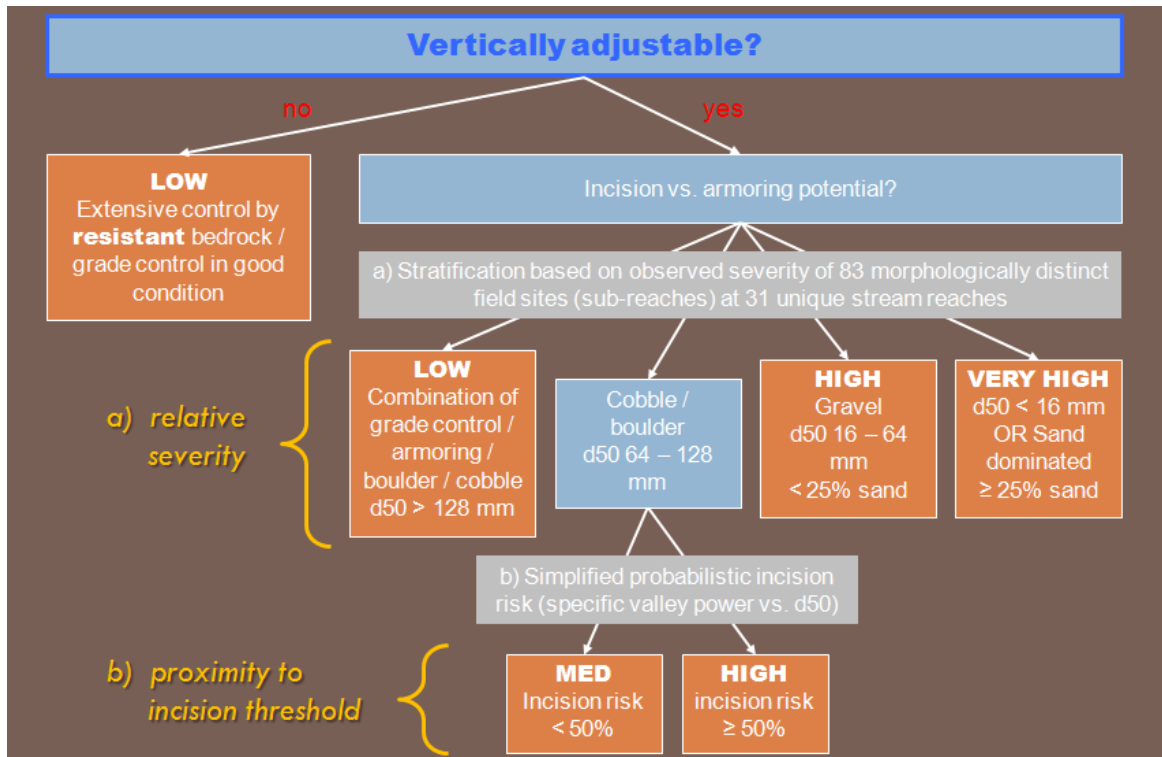


Figure 2.4 – Vertical susceptibility

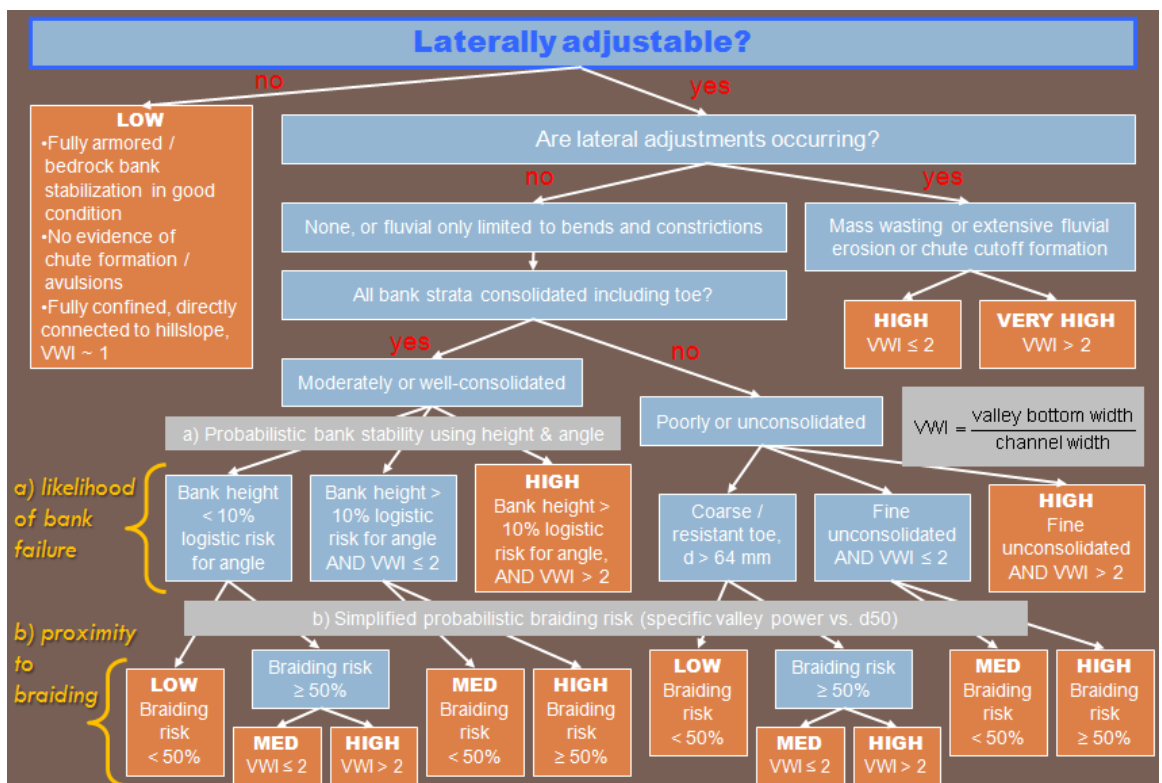
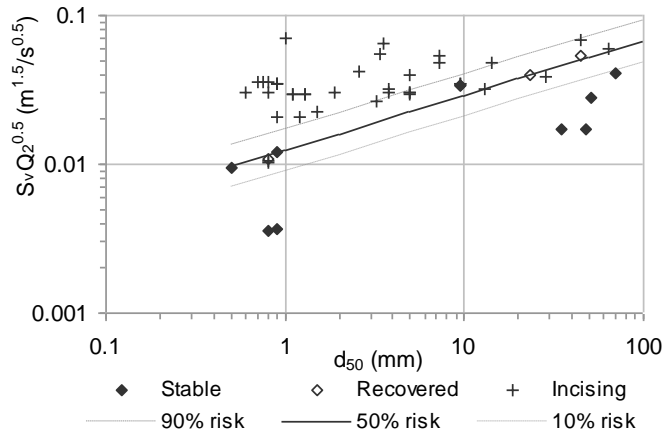


Figure 2.5 – Lateral susceptibility

Logistic-regression analyses were able to successfully segregate states of incising and braiding relative to stable unconfined single-thread settings with relatively narrow levels of overlap. Although many combinations of variables were tested for significance, using the ‘mobility’ index vs.  $d_{50}$  scheme after Bledsoe and Watson (2001b) commanded a similar assortment of stability states with efficacy comparable to that of more data-intensive indices such as dimensionless shear stress ( $\tau_* \sim 0.1$  at  $Q_2$ ) (see Figure 2.6 and Table 2.2). The southern California thresholds fell conspicuously lower than those from Bledsoe and Watson (2001b), suggesting that these systems may be more sensitive than those in other regions of the U.S. For equivalent bed-material sizes and valley slopes, the 10-yr flow in southern California aligns with the critical mobility indices of other regions. This is most likely attributable to the semiarid climate, flashy-flow regime, and high-sediment loads. It is notable that the 10-yr instantaneous flow would most regularly attenuate to a daily-mean flow equal to that of a 2- to 3-yr event. That is, it typically takes a 10-yr storm to create any sort of a meaningful duration at a 2-yr flow magnitude. Another important distinction between the Bledsoe and Watson (2001b) thresholds was that they segregated unstable forms from stable meandering systems (i.e., sinuosity  $\geq 1.3$ ), whereas most of the ‘stable’ sites were relatively straight (i.e., mean sinuosity = 1.15, with Challenger\_C, Perris1, and Perris2 meandering at sinuosities  $\geq 1.3$ ).



**Figure 2.6 – Vertical supplement: logistic regression of incising channels (CEM Types II or III) vs. single-thread stable (CEM Type I) or recovered (i.e., CEM Type IV → V) systems in unconfined valleys**

**Table 2.2 – Corresponding ‘mobility index’ values for 50% probability of incision for cobble-bed systems**

50% Risk	
$d_{50}$ (mm)	$S_v Q_2^{0.5}$ ( $m^{1.5}/s^{0.5}$ )
16	0.034
32	0.044
64	0.057
96	0.066
128	0.074

Within the context of the mobility-index scheme, several flow-recurrence intervals and grain sizes were tested in combination (i.e.,  $Q_2$ ,  $Q_{10}$  X  $d_{50}$ , and  $d_{84}$ ) to determine if a varied scheme would have superior performance over that of the 2-yr flow and  $d_{50}$ . As presented in Appendix E, alternative approaches did not significantly outperform the Bledsoe and Watson (2001b) scheme, such that departure from such widely-used metrics was not warranted. Performance measures and relative significance are summarized in Table 2.3. The worst performance was in regards to correctly classifying stable systems as stable; however, one is not necessarily alarmed with misclassifications in that direction. In the context of a screening tool, the implication would be to flag currently ‘stable’ systems in otherwise high-risk settings – one of the primary objectives of a screening assessment.

**Table 2.3 – Performance measures of logistic-regression analyses of geomorphic thresholds of incision, braiding, and mass wasting**

Model	p-values			% Correctly Classified	
	Overall Model	Individual Terms		Unstable	Stable
		D <sub>50</sub>	S <sub>v</sub> Q <sub>z</sub> <sup>0.5</sup>		
Pr(incision)	<0.0001	0.01	0.007	(35/38) 92%	(9/13) 69%
Pr(braiding)	0.005	0.03	0.01	(17/19) 89%	(7/13) 54%
		Height	Angle		
Pr(mass wasting)	<0.0001	0.01	0.02	(34/36) 94%	(121/125) 97%

As evident in Figure 2.7 and Table 2.4, results of logistic regression regarding mass-wasting failure in unconfined moderately- to well-consolidated banks had relatively high performance. Appendix E includes logistic results of thresholds for other settings (e.g., poorly/unconsolidated banks or confined hillslopes); however, they had poorer performance and offer less utility than in more consolidated banks. By back-solving the Culmann equation for the 50% risk in Figure 2.8 (Table 2.5), *operational* stress parameters for critical bank height were:  $\gamma = 1.81 \text{ g/cm}^3$  (i.e.,  $17.8 \text{ kN/m}^3$  or  $113 \text{ lb/ft}^3$ ),  $\phi = 21.1^\circ$ , and  $c = 1.72 \text{ kPa}$  ( $35.8 \text{ lb/ft}^2$ ). Although quite lower than other regions where cohesion values are typically more on the order of 10 kPa or greater (Lawler *et al.*, 1997), such negligible cohesive strength was consistent with field observations. Broadly speaking, southern California banks have little geotechnical capacity. Frequently unconsolidated, even banks that are moderately- or well-consolidated are often inappreciably cohesive. This is compounded by the semiarid climate and overall lack of durable bank vegetation. Moreover, high sediment loads can lead to central bar deposition that promotes flow deflection into banks and further weakening. These

characteristics collectively result in extremely low thresholds for mass wasting relative to other parts of the country.

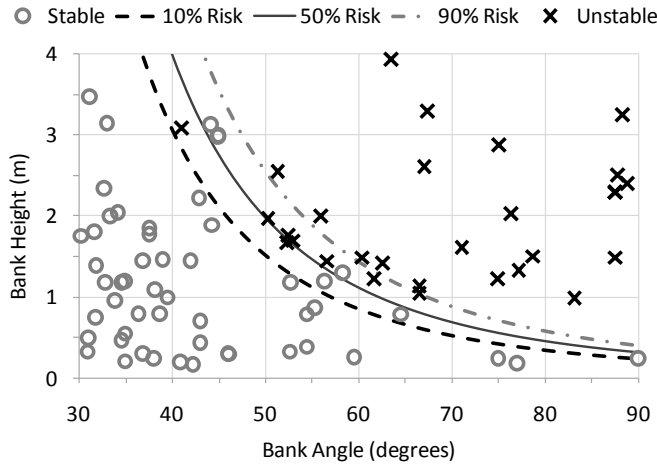


**Figure 2.7 – Lateral supplement: logistic regression of mass wasting in moderately- and well-consolidated banks vs. stable bank geometries**

**Table 2.4 – Corresponding geometries for 10% risk of mass wasting**

Angle (°)	Height (m)
30	7.6
35	4.7
40	3.7
45	2.1
50	1.5
55	1.1
60	0.85
65	0.66
70	0.52
80	0.34
90	0.24

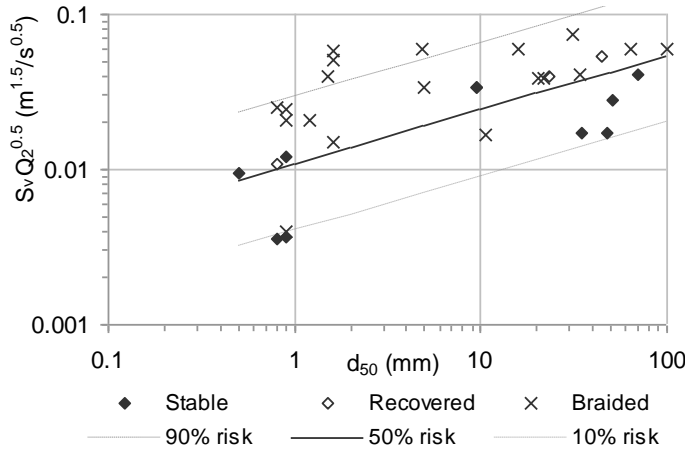


**Figure 2.8 – Lateral supplement: logistic regression of braided channels vs. single-thread stable (CEM Type I) or recovered (i.e., CEM Type IV → V) systems in unconfined valleys**

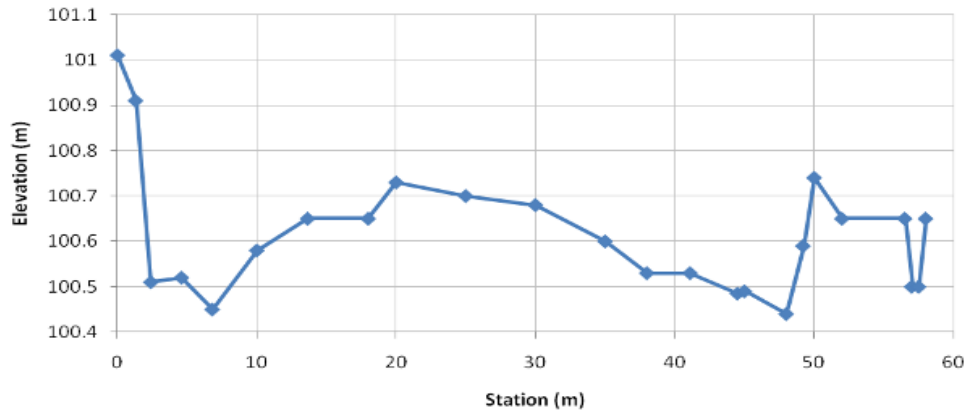
**Table 2.5 – Corresponding ‘mobility index’ values for 50% risk of braiding in gravel- and cobble-bed systems**

50% Risk	
$d_{50}$ (mm)	$S_v Q_2^{0.5}$ ( $m^{1.5}/s^{0.5}$ )
16	0.029
32	0.036
64	0.046
96	0.053
128	0.059

Inspection of Figures 2.6 through 2.8 offers a rationale as to why 10% mass-wasting risk versus 50% incision/braiding risk were selected as critical discriminators. The bank data were distributed more equitably over their entire range with little practical difference between the 10% and 50% risk lines. In contrast, the skewed and overlapping ranges for incision and, particularly, braiding resulted in a much broader risk bandwidth. The two unstable outliers in the braiding logistic (AltPerris\_A and Proctor\_A,  $d_{50} = 0.9$  mm and 10.5 mm, respectively) are special cases rather than the norm. Both have distributary flow paths but there is little alluvial bar activity, with much of the flow potentially sub-surface and/or hyporheic (Figure 2.9). The two observations may be the primary reason that the braiding threshold is slightly lower than the incision threshold; however, other factors such as sediment supply and valley expansions are likely influential.



(a) photographs looking upstream



(b) cross-section geometry looking downstream

**Figure 2.9 – Cross section A at AltPerris**

Cases of braiding in such low-energy settings are not the primary risk type the braiding logistic is intended to screen (i.e., such cases would be more appropriately identified in the observational/watershed context tree). Consequently, the 50% risk was judged a more reasonable screening index for braiding and incising, especially given that the two diagrams are used exclusively over the coarse-grain sizes where the thresholds are more apparent. However, these thresholds may be more refined through tool application and feedback. Yet even in its present form, the screening tool is designed such that jurisdictions may cater to risk levels acceptable to local stakeholders.

### 2.3.3 Defining the analysis domain

An important component to this approach is that risk must be assessed over an analysis domain that covers all of the stream reaches that could be physically affected by the proposed development. That is, one cannot exclusively consider the project outfall. Rather, the screening tool needs to be applied to the most susceptible reach within the analysis domain. Although several scaling and flow attenuation methods were evaluated, in the interest of simplicity, the following ways to define the domain extent were selected:

- Downstream – *If rating at outfall < HIGH (Vertical OR Lateral), extend reconnaissance downstream until reaching the first of the following:*
  - engineered channel (bed and bank) in good condition
  - tidal backwater influences
  - tributary confluence of equal or higher Strahler (1952) order
  - *or a distance over which applicant demonstrates flow is attenuated (magnitude and duration)*
- Upstream – *If rating at outfall < HIGH (Vertical), must look upstream until reaching the first of the following:*
  - grade control (natural or artificial) sufficient to check inadvertent headcutting
  - vertical susceptibility of LOW

### **2.3.4 Composite-screening rating**

After applying the screening tool to the most susceptible reach within the analysis domain, a straightforward integration of vertical and lateral ratings may be beneficial to stakeholders for converging on a composite rating. Such a process would require two steps in most cases. First, a composite (vert/lat) rating is determined as the higher of the vertical and lateral susceptibility scores. If the vert/lat rating falls into either a medium or high category, the second step is to consider sediment supply. Vert/lat scores that are either low or very high are considered ‘final’ screening ratings.

A screening-level estimate of sediment supply is determined via an automated GIS scheme developed for this project by Stillwater Sciences. Their Geomorphic Landscape Unit (GLU) approach combines watershed-scale geomorphic and land-use parameters into a first-order prediction of average annual sediment yield. Regional debris-basin data were used to calibrate the procedure. Quantitative estimates are segregated into qualitative ratings scaled relative to regional sediment yields of ‘low’, ‘medium’, and ‘high’.

Watersheds rated as having a ‘high’ sediment supply may be inherently more susceptible to states of instability relative to similar watersheds with lower yields. Among other reasons, gravels and cobbles are known to become more easily entrained when mixed with more than 20 to 30% sand (Wilcock, 1998). Despite the fact that transporting sediment consumes erosive energy, capacity-limited channels are more likely to become braided channels with high-sediment supplies (Montgomery and Buffington, 1997; Schumm, 1980). One process-based explanation for braiding is that

insufficient capacity to transport high sediment loads leads to a higher probability for middle-bar formation (Leopold and Wolman, 1957).

Consequently, the final step in the screening process for ‘medium’ or ‘high’ vert/lat scores that lie in watersheds rated as ‘high’ sediment supplies is to augment by one level. That is, ‘medium’ susceptibilities are increased to ‘high’, while ‘high’ scores translate to ‘very high’. This process is summarized by the schematic in Figure 2.10.

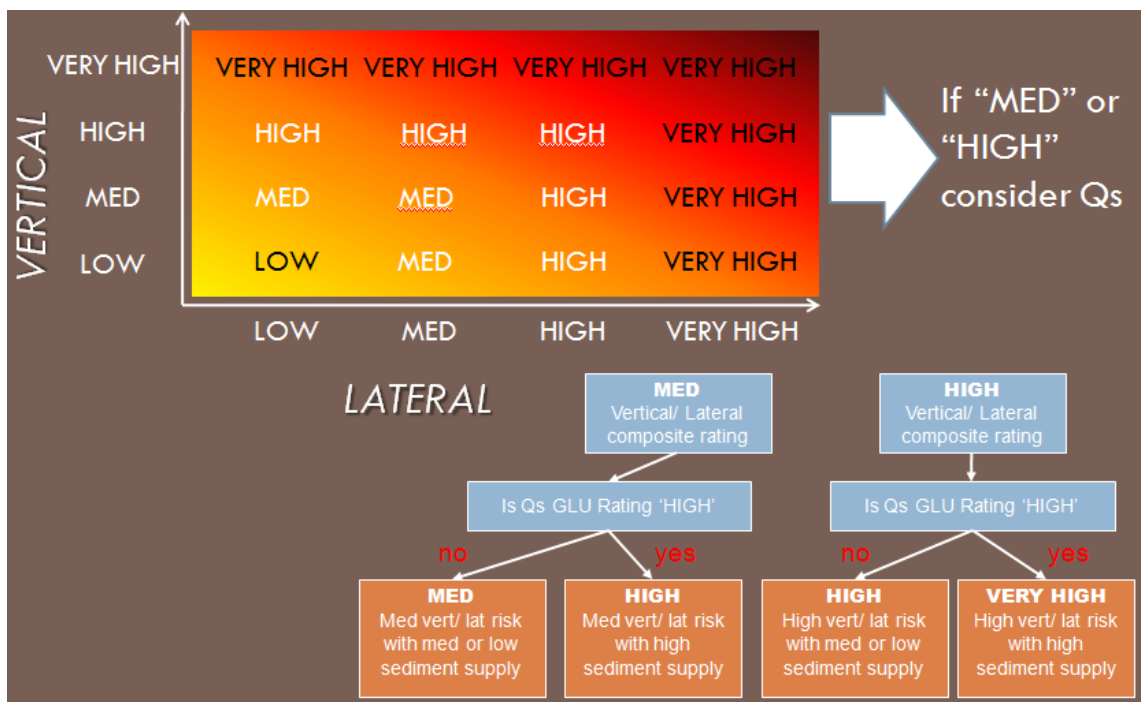


**Figure 2.10 – Integration of vertical and lateral susceptibility ratings into a composite rating, with sediment-supply augmentation**

## 2.4 Preliminary Validation

To date, the screening tool has been tested on the 83 sub-reaches that were used in its development. Admittedly circular in its infancy, the tool is intended to be refined via application and feedback. However, one way to validate the tool in its present form is to compare screening rates to relative magnitudes of adjustment. That is, how much have

these sites ‘enlarged’ in response to (and independent of) hydromodification, and do the scales of adjustment correspond with screening ratings?

For the purposes of this comparison, ‘enlargement’ was defined in a way that is more consistent with how a layperson might think of an active channel. That is, how much space does the channel (opposed to flow) occupy relative to its former size. Such a definition is measured by the cross-sectional area up to the top of bank. ‘Enlargement’ is computed as:

$$\Delta A\% = (A_{\text{post}} - A_{\text{pre}}) / A_{\text{pre}} \quad \text{Eq. (2.9)}$$

where:

$\Delta A\%$  = relative channel enlargement between the current area occupied by the channel ( $A_{\text{post}}$ ) and the historic or pre-developed channel ( $A_{\text{pre}}$ ), and cross-sectional area as measured from the top of bank (as opposed to a depth at a specific return interval).

Table 2.6 offers a gradient of examples from least susceptible to most disturbed. Although the reference cross section ( $A_{\text{pre}}$ ) had to be conservatively inferred from historic aerial photographs and field indicators, the results are telling suggestions of channel dynamics. For example, since its development in the 1990s and 2000s, sub-reaches at Acton, a fine-grained unconfined system, have enlarged at approximately 35, 120, 900, and 1,300% (Acton\_D depicted in Figure 2.11). Moreover, watershed impervious cover is only 2 to 3%, levels that might seem nearly inappreciable in other regions. This and similar cases of dramatic changes in fine-grained systems with little urbanization

reinforce the notion that these are highly susceptible systems and warrant a ‘very high’ screening rating.

**Table 2.6 – Screening rating, estimated ‘enlargement’, and key geomorphic parameters at selected study sites**

Sub-reach Name	Vertical Susceptibility	Lateral Susceptibility	Estimated Enlargement	Impervious Area	d <sub>50</sub> (mm)	Reference (yr)
Escondido_A	low	low	~0%	14%	128	1947
Topanga_B	med	very high	~0 - 50%	1.4%	100	1947 - 1989
SanAntonio_A	high	very high	~0 - 100%	0.2%	64	1947 - 1989
Borrego_B	very high	very high	~500%	14%	1.6	1952
Acton_C	very high	very high	> 1,000%	2.4%	5	~1990s



**Figure 2.11 – Photograph looking upstream at Acton\_D: d<sub>50</sub> = 9.4 mm with enlargement since development in 1990s approximated at 900%**

San Antonio Creek demonstrates the susceptibility of even a coarse-gravel/small-cobble bed systems. The incising low-flow channel is set within a braided bandwidth that is severely incised through a poorly-sorted alluvial floodplain (3.5-m bank height relative to the 65-m width). Two cross sections range in d<sub>50</sub> from 16 to 64 mm with only

0.2% watershed imperviousness. Other notable factors include upstream channelization (earlier than 1947) and a relatively high-sediment supply estimated at 3,200 t/km<sup>2</sup>/yr. Yet, even if the channel wasn't already braided with failing banks, the high sediment supply would augment an otherwise 'high' vertical rating to final grade of 'very high' with the current rating scheme.

Topanga is an interesting case study as well. Three sub-reaches range in grain size and confinement from 500 mm and confined upstream to 100 mm, unconfined, and braided in the mid-reach, and 88 mm and confined downstream. Aerial photography from 1947 through 1989 documents large pulses in sediment supply, which is predicted by the GLU scheme to have a 'medium' sediment yield of 1,800 t/km<sup>2</sup>/yr. The unconfined section incurred periods of braiding and single-thread form, hence an approximate enlargement range of 0 to 50%. The upstream confined/bedrock section ( $d_{50}$  500 mm) showed nominal effects from the sediment pulses through time, while the flatter confined section downstream ( $d_{50}$  88 mm) documented aggradational periods that occasionally caused multiple flow paths within the relatively narrow valley (i.e., VWI < 2). This reach exemplifies the importance of looking over an appropriate analysis domain at the screening level. For example, a proposed project at the upstream site (composite rating of 'low') could have undesirable effects in the unconfined braided section just 400 m downstream if mitigation controls were not designed with downstream reaches in consideration.

Finally, Escondido is bounded by bedrock in its bed and banks. The resilient system has shown no appreciable changes in form despite a highly-developed watershed at 14% imperviousness. Although the San Dieguito Reservoir has likely played a role in

mitigating flows, this and several other bedrock systems (Silverado and Santiago) are clear examples of the region's least susceptible forms. It goes without saying that no systems are completely static, which is why we recommend a minimum level of control for all projects.

## **2.5 Summary and Conclusions**

Informed by a literature review (Bledsoe *et al.*, 2008), field reconnaissance, and data collection, the structure of a process-based screening tool is proposed for hierarchically assessing channel susceptibility to hydromodification in southern California. Stakeholders converged on a decision-tree structure with a parsimonious theme. Three decision trees, watershed context, vertical susceptibility, and lateral susceptibility, combine risk factors of both severity and likelihood of response (*sensu* Downs and Gregory (1995)) to offer relative risk ratings of low, medium, high, or very high.

Three key screening nodes were calibrated using logistic regression of regional data with relatively high performance (i.e., ~90% classification accuracy of unstable states). The logistic thresholds offer a simple but quantitative method for probabilistically assessing channel susceptibility via proximity to such thresholds. Although empirical, the shape of the mass-wasting threshold showed fidelity to geotechnical stability theory. The geomorphic thresholds of incising, braiding, and mass wasting are consistent with field observations, historic analyses, and previous literature in suggesting that streams in southern California are inherently more susceptible to changes in watershed hydrologic and sediment processes associated with urbanization. Such sensitivity is directly

attributable to the hydrogeomorphic setting, most notably the flashy/seasonal flow regime, high relief, and little vegetation, with an overall lack of coarse material and an abundance of fines.

Relative magnitudes of observed channel responses also influenced tool design. This was evident in preliminary validation: sites rated with the highest risk were also the most dynamic, represented by conservative estimations of channel enlargement relative to a pre-urban or reference condition. With the precautionary principle as our overarching guide, many systems fell into ratings of ‘high’ and ‘very high’, as seen in Table 2.6. This is not to say that all ‘high’ systems are equally susceptible, but rather, they warrant a detailed level of additional analysis to ensure that mitigation controls are properly designed to minimize risk.

In this light, each rating has a purpose in guiding subsequent phases such as surveying and modeling, and even foreshadows the ultimate mitigation level that could be required. For example, a ‘low’ requires no further analysis and only the minimum mitigation level; therefore, we included a sufficient number of screening steps to reasonably ensure that systems rated as ‘low’ are indeed exceptionally resilient. The medium, high, and very high ratings demand detailed surveys but different levels of modeling and point to different modeling tools. There are additional benefits in having separate lateral and vertical ratings. For example, Topanga\_B in Table 2.6 is vertically resistant (medium) but laterally braiding (very high). Modeling the sediment supply of larger particles during high flows would likely be more important than a simulation across all flows, including those which could only transport wash load. In contrast, a

fine-grained live-bed system such as Acton\_D rated ‘very high’ both vertically and laterally should conceivably require modeling over all flows to guide mitigation.

In conclusion, we fully expect this version of the tool to be refined as stakeholders provide feedback and additional data that enhance both flexibility and defensibility. It is defensible as a process-based, first-order prediction of risk that requires a limited but important set of field and office measurements. It is flexible through its use of logistic thresholds and independent/hierarchical components. That is, jurisdictions may stratify screening ratings via locally acceptable levels of risk (e.g., 10% vs. 50% probability of response, or incision-driven vs. lateral/braiding responses). Consequently, the tool structure could be transferred to other regions experiencing hydromodification and re-calibrated with local data.

## **2.6 Acknowledgements**

I would like to thank numerous organizations and individuals who contributed to this screening tool from funding to data collection and reviews. This research was funded in part by the State of California and San Diego County for which I am grateful. Eric Stein of the Southern California Coastal Water Research Project (SCCWRP) played a primary role in acquiring research funds, project management, and provided several reviews. Fellow Colorado State University graduate student Dave Dust was instrumental in field-data collection and took most of the photographs. SCCWRP staff, including Becky Schaffner, Liesl Tiefenthaler, Greg Lyon, and Jeff Brown, played critical roles in equipment acquisition, data collection and logistics, and GIS assistance. Stillwater Sciences conducted modeling site surveys, developed the sediment-supply GIS scheme,

and provided reviews. Among others, I would like to acknowledge Derek Booth, Scott Dusterhoff, and Alexander Wong. The project's TAC provided multiple reviews and was central in guiding conceptual design. Colin Thorne (University of Nottingham) graciously offered an independent screening and the tool is much improved as a result.

## **2.7 References**

- Benda, L. and Dunne, T., 1997a. Stochastic forcing of sediment routing and storage in channel networks. *Water Resources Research*, 33(12): 2865-2880.
- Benda, L. and Dunne, T., 1997b. Stochastic forcing of sediment supply to channel networks from landsliding and debris flow. *Water Resources Research*, 33(12): 2849-2863.
- Biedenharn, D.S., Elliot, C.M. and Watson, C.C., 1997. The WES Stream Investigation and Streambank Stabilization Handbook. U. S. Army Engineer Waterways Experiment Station, Vicksburg, MS, 338 pp.
- Bledsoe, B.P., Hawley, R.J. and Stein, E.D., 2008. Stream channel classification and mapping systems: Implications for assessing susceptibility to hydromodification effects in southern California. Southern California Coastal Water Research Project (SCCWRP), Costa Mesa, CA.
- Bledsoe, B.P. and Watson, C.C., 2001a. Effects of urbanization on channel instability. *Journal of the American Water Resources Association*, 37(2): 255-270.
- Bledsoe, B.P. and Watson, C.C., 2001b. Logistic analysis of channel pattern thresholds: meandering, braiding, and incising. *Geomorphology*, 38: 281-300.

- Booker, F.A., Dietrich, W.E. and Collins, L.M., 1993. Runoff and erosion after the Oakland firestorm. *California Geology*, 46: 159-173.
- Booth, D.B., 1990. Stream-channel incision following drainage-basin urbanization. *Water Resources Bulletin*, 26(3): 407-417.
- Booth, D.B., 1991. Urbanization and the natural drainage system -- impacts, solutions, and prognoses. *The Northwest Environmental Journal*, 7: 93-118.
- Brookes, A., 1988. Channelized Rivers: Perspectives for Environmental Management. John Wiley & Sons Ltd., Chichester, UK.
- Buhman, D.L., Gates, T.K. and Watson, C.C., 2002. Stochastic variability of fluvial hydraulic geometry: Mississippi and Red Rivers. *Journal of Hydraulic Engineering*, 128(4): 426-437.
- Bull, W.B., 1997. Discontinuous ephemeral streams. *Geomorphology*, 19(3-4): 227-276.
- Bunte, K. and Abt, S.R., 2001a. Sampling frame for improving pebble count accuracy in coarse gravel-bed streams. *Journal of the American Water Resources Association*, 37(4): 1001-1014.
- Bunte, K. and Abt, S.R., 2001b. Sampling surface and subsurface particle-size distributions in wadable gravel-and cobble-bed streams for analyses in sediment transport, hydraulics, and streambed monitoring. In: F.S. U.S. Department of Agriculture (Editor). Gen. Tech. Rep. RMRS-GTR-74, Rocky Mountain Research Station Fort Collins, CO, pp. 428.
- Chang, H.H., 1988. Fluvial Processes in River Engineering. John Wiley & Sons, New York, NY.

- Chin, A., 2006. Urban transformation of river landscapes in a global context. *Geomorphology*, 79(3-4): 460-487.
- Chow, V.T., 1959. Open Channel Hydraulics. McGraw-Hill Book Company, Inc., New York, NY, 680 pp.
- Christensen, R., 1997. Log-linear Models and Logistic Regression. Springer-Verlag, New York, NY, 483 pp.
- Coleman, D., MacRae, C. and Stein, E.D., 2005. Effect of Increases in Peak Flows and Imperviousness on the Morphology of Southern California Streams. Stormwater Monitoring Coalition, Southern California Coastal Water Research Project, Westminster, CA.
- Downs, P.W. and Gregory, K.J., 1995. Approaches to river channel sensitivity. *Professional Geographer*, 47(2): 168-175.
- Downs, P.W. and Thorne, C.R., 1996. A geomorphological justification of river channel reconnaissance surveys. *Trans Inst Br Geog NS*, 21: 455-468.
- Dust, D.W. and Bledsoe, B.P., 2009. Conceptual watershed-scale process domains for three basic flood plain morphologies in southern California. In: J.A. Ramirez (Editor), Hydrology Days, American Geophysical Union, Colorado State University.
- Dust, D.D. and Bunte, K., 2008. Rigid and flexible procedures for combining volumetric pebble counts with sieve gradations by mass. Pers. Comm.
- Environmental Protection Agency, 2006. Guidance specifying management measures for nonpoint pollution in coastal waters. Chapter 6: Management Measures for Hydromodification. U.S. Environmental Protection Agency.

- Frissell, C.A., Liss, W.J., Warren, C.E. and Hurley, M.D., 1986. A hierarchical framework for stream habitat classification: viewing streams in a watershed context. *Environmental Management*, 10(2): 199-214.
- Gabet, E.J. and Dunne, T., 2002. Landslides on coastal sage-scrub and grassland hillslopes in a severe El Nino winter: the effects of vegetation conversion on sediment delivery. *Geol. Soc. of Am. Bull.*, 114(8): 983-990.
- Gabet, E.J. and Dunne, T., 2003. A stochastic sediment delivery model for a steep Mediterranean landscape. *Water Resources Research*, 39(9): 12.
- Graf, W.L., 1981. Channel instability in a braided sand-bed river. *Water Resources Research*, 17: 1087-1094.
- Graf, W.L., 1988. Fluvial Processes in Dryland Rivers. Springer-Verlag, Berlin.
- Hammer, T.R., 1972. Stream channel enlargement due to urbanization. *Water Resources Research*, 8: 139-167.
- Harrelson, C.C., Rawlins, C. L., Potyondy, J. P., 1994. Stream channel reference sites: an illustrated guide to field technique. In: F.S. U. S. Department of Agriculture, Rocky Mountain Forest and Range Experiment Station (Editor), Gen. Tech. Rep. RM-245, Fort Collins, CO, pp. 61.
- Lavé, J. and Burbank, D., 2004. Denudation processes and rates in the Transverse Ranges, southern California: erosional response of a transitional landscape to external and anthropogenic forcing. *J. Geophys. Res.*, 109.
- Lawler, D.M., Thorne, C.R. and Hooke, J.M., 1997. Bank erosion and instability. In: C.R. Thorne, R.D. Hey and M.D. Newson (Editors), Applied Fluvial Geomorphology for River Engineering and Management. Wiley, Chichester, UK, pp. 137-172.

- Leopold, L.B. and Wolman, M.G., 1957. River channel patterns -- braided, meandering, and straight. Professional Paper 282-B, U.S. Geological Survey.
- Los Angeles County Flood Control District, 1959. Report on debris reduction studies for mountain watersheds of Los Angeles County. Los Angeles County Flood Control District, Los Angeles, CA, pp. 164.
- MacRae, C.R., 1997. Experience from morphological research on Canadian streams: Is the control of the two-year frequency runoff event the best basis for stream channel protection? In: L.A. Roesner (Editor), *Effects of Watershed Development and Management of Aquatic Ecosystems*, ASCE, New York, NY, pp. 144-162.
- Manning, R., 1889. On the flow of water in open channels and pipes. *Transactions of the Institution of Civil Engineers of Ireland*, 20: 161-195.
- Menard, S.W., 1995. Applied Logistic Regression Analysis. Sage Publications, Thousand Oaks, CA.
- Montgomery, D.R., 1999. Process domains and the river continuum. *Journal of the American Water Resources Association*, 35(2): 397-410.
- Montgomery, D.R. and Buffington, J.M., 1997. Channel-reach morphology in mountain drainage basins. *Geol. Soc. of Am. Bull.*, 109(5): 596-611.
- Montgomery, D.R. and Buffington, J.M., 1998. Channel processes, classification, and response. In: R. Naiman and R. Bilby (Editors), River Ecology and Management, Springer-Verlag New York Inc., New York, NY, pp. 13-42.
- Nanson, G.C. and Croke, J.C., 1992. A genetic classification of floodplains. *Geomorphology*, 4(459-486).

- Newbury, R., 1995. Rivers and the Art of Stream Restoration, Natural and Anthropogenic Influences in Fluvial Geomorphology. Geophysical Monograph, American Geophysical Union, pp. 137-149.
- Osman, A.M. and Thorne, C.R., 1988. Riverbank stability analysis I: theory. *Journal of Hydraulic Engineering*, 114(2): 134-150.
- Ott, R.L. and Longnecker, M., 2001. An Introduction to Statistical Methods and Data Analysis. Duxbury, Pacific Grove, CA, 1152 pp.
- Patton, P.C. and Schumm, S.A., 1975. Gully erosion, northwestern, Colorado: a threshold problem. *Geology*, 3: 88-90.
- Pizzuto, J.E., Hession, W.C. and McBride, M., 2000. Comparing gravel-bed rivers in paired urban and rural catchments of southeastern Pennsylvania. *Geology*, 28(1): 79-82.
- Potyondy, J., and Bunte, K., 2002. Sampling with the US SAH-97 hand-held particle size analyzer. In: W.E.S. Federal Interagency Sedimentation Project (Editor), Federal Interagency Sedimentation Project, Waterways Experiment Station, Vicksburg, MS, pp. 6.
- Rhoads, B.L., 1995. Stream power: a unifying theme for urban fluvial geomorphology. In: E.E. Herricks (Editor), Stormwater Runoff and Receiving Systems: Impact, Monitoring, and Assessment, (Chapter 5), CRC Press, Inc., Boca Raton, FL, pp. 65-75.
- SAS Institute, 2004. SAS 9.1 companion for windows. SAS Institute, Cary, NC.
- Schumm, S.A., 1977. The Fluvial System. Wiley-Interscience, New York, NY.

- Schumm, S.A., 1980. Some applications of the concept of geomorphic thresholds. In: D.R. Coates and J.D. Vitek (Editors), Thresholds in Geomorphology, George Allen and Unwin, London, UK, pp. 473-485.
- Schumm, S.A., 1991. To Interpret the Earth: Ten Ways to be Wrong. Cambridge University Press, 133 pp.
- Schumm, S.A., Bradley, M.T. and Begin, Z.B., 1980. Application of geomorphic principles to environmental management in semiarid regions. In: U.S. Department of Transportation (Editor), Office of Water Research and Technology.
- Schumm, S.A., Harvey, M.D. and Watson, C.C., 1984. Incised Channels: Morphology, Dynamics, and Control. Water Resources Publications, Littleton, CO.
- Simon, A., Curini, A., Darby, S.E. and Langendoen, E.J., 2000. Bank and near-bank processes in an incised channel. *Geomorphology*, 35(3-4): 193-217.
- Simons, D.B. and Simons, R.K., 1987. Differences between gravel and sand-bed rivers. In: C.R. Thorne, J.C. Bathurst and R.D. Hey (Editors), Sediment Transport in Gravel-bed Rivers, John Wiley & Sons, New York, NY, pp. 3-11.
- Strahler, A.N., 1952. Hypsomic analysis of erosional topography. *Geol. Soc. of Am. Bull.*, 63: 1117-1142.
- Taylor, B.D., 1981. Sediment management for southern California mountains, coastal plains and shoreline, Part B: Inland sediment movements by natural processes. California Institute of Technology, Pasadena, CA.
- Terzaghi, K., 1943. Theoretical Soil Mechanics. Wiley, New York, NY, 510 pp.

- Thorne, C.R., 1982. Processes and mechanisms of river bank erosion. In: R.D. Hey, J.C. Bathurst and C.R. Thorne (Editors), Gravel-bed Rivers, Wiley, Chichester, UK, pp. 227-271.
- Thorne, C.R., 2002. Geomorphic analysis of large alluvial rivers. *Geomorphology*, 44: 203-220.
- Trimble, S.W., 1997. Contribution of stream channel erosion to sediment yield from an urbanizing watershed. *Science*, 278: 1442-1444.
- van den Berg, J.H., 1995. Prediction of alluvial channel pattern of perennial rivers. *Geomorphology*, 12: 259-279.
- Vermont Agency of Natural Resources, 2004. Stream Geomorphic Assessment Program, Vermont Agency of Natural Resources, Vermont Department of Environmental Conservation, Waterbury, VT.
- Wilcock, P.R., 1998. Two-fraction model of initial sediment motion in gravel-bed rivers. *Science*, 280: 410-412.
- Wolman, M.G., 1967. A cycle of sedimentation and erosion in urban river channels. *Geografiska Annaler*, 49A(385-395).
- Wolman, M.G. and Gerson, R., 1978. Relative scales of time and effectiveness of climate in watershed geomorphology. *Earth Surface Processes*, 3: 189-208.

## **2.8 GIS Data Sources**

**Cal-Atlas:** 2000 and 2007 Roadway Shapefiles, State of California geospatial clearinghouse, [gis.ca.gov](http://gis.ca.gov).

**Google Earth:** Present-day Aerial Photography, [earth.google.com](http://earth.google.com).

**National Oceanic and Atmospheric Administration (NOAA):** *Precipitation Intensities for 2-year, 24-hour Storm*, <http://www.nws.noaa.gov/oh/hdsc/noaaatlas2.htm> (Atlas 2) and [hdsc.nws.noaa.gov/hdsc/pfds/pfds\\_gis.html](http://hdsc.nws.noaa.gov/hdsc/pfds/pfds_gis.html) (Atlas 14).

**United States Department of Agriculture (USDA), Natural Resources Conservation Service (NRCS):** *Soil Surveys, Average Annual Precipitation Shapefile (1961 - 1990)*, <http://datagateway.nrcs.usda.gov/>.

**United States Geological Survey (USGS):** *Historical Aerial Photography and Quadrangle Topographic Maps, National Elevation Dataset (NED), 2001 Impervious Raster, National Hydrography Dataset (NHD), Average Annual Precipitation Shapefile (1900 - 1960)*, <http://seamless.usgs.gov>.

## CHAPTER 3

### MODELS FOR PREDICTING LONG-TERM EFFECTS OF HYDROMODIFICATION IN SOUTHERN CALIFORNIA: MAGNITUDES AND DIRECTIONS

**Abstract.** Morphologic responses of stream channels to altered hydrologic and sediment regimes associated with urbanization (hydromodification) are qualitatively described via a novel Channel Evolution Model (CEM) specific to southern California that highlights departures from the original CEM of Schumm *et al.* (1984) such as planform shifts from single-thread to braided. Relative magnitudes of equilibrium departures are explained via dimensionless stability numbers (*sensu* Watson *et al.* (1988)), and risk factors for incision versus braiding responses are presented. Cross-sectional channel enlargement relative to pre-response reference form is modeled via multivariate regression, which was highly dependent on the ratio of post- to pre-urban sediment-transport capacity over cumulative duration simulations of 25 yrs ( $L_r$ ), which explained greater than 60% of the variance. The downstream distance to a hardpoint (e.g., bedrock or artificial) was also significant. The enlargement models point to the importance of balancing the post-developed sediment transport to the pre-developed setting over an entire range of flows rather than a single flow in order to reduce the risk of adverse channel responses to hydromodification. The need for controlling a wide range of flows was underscored by logistic-regression analyses that indicated a high risk of instability in systems with  $L_r > 1$ , especially for fine-grained systems (i.e.,  $d_{50} < 16$  mm).

### 3.1 Introduction

Hydromodification is defined for the purposes of this dissertation as changes in watershed hydrologic processes following land conversion from undeveloped to urban. Consistent with research in the semiarid environment (Trimble, 1997) and work specific to the region (Coleman *et al.*, 2005), I observed channel responses to urbanization in southern California to be on faster and larger scales relative to other regions. Complex-channel responses ranging from incision-driven trajectories analogous to the original Channel Evolution Model (CEM; Schumm *et al.* (1984)) to planform shifts such as single-thread to braided have far-reaching effects on adjacent land and throughout drainage networks. Such responses are attributable to a geomorphic setting that combines geologic, hydrologic, and climatic factors such as high relief, fine-grained bed materials, little vegetation, and an extremely flashy regime. U.S. Geological Survey (USGS) gauge data have shown that urbanization increases peak flows and variability throughout the U.S. (Konrad and Booth, 2002; Galster *et al.*, 2006; Poff *et al.*, 2006), and exponentially affects both peaks and durations in southern California, making flashy systems even more variable (Chapter 1). Stream settings known for sporadic sediment movements (Graf, 1981), extended aggradation/degradation phases, lagged recovery times (Wolman and Gerson, 1978), and infrequent periods of ‘equilibrium’ (Bull, 1997) have little resilience against an unmitigated urban flow regime. Consequently, amplified flows and durations have resulted in large sediment imbalances and extensive/accelerated changes in channel form. For example, ongoing enlargement in Borrego Canyon near Irvine (Orange County) ranges up to five times circa 1950 cross-sectional area and

greater than 2 to 3x magnifications at Hasley Canyon near Valencia (Los Angeles County) relative to the 1990s.

The present study represents components of a broader project aimed at better understanding and ultimately mitigating adverse responses to hydromodification in southern California. Collaborative end products include three tiers of tools designed to address the following questions:

1. Screening: which streams are most susceptible to hydromodification?
2. Modeling: what are the predicted magnitudes of responses in the most susceptible stream systems?
3. Mitigation: what are potential management measures that could be implemented to offset hydromodification effects?

This chapter focuses on developing an improved, process-based understanding of channel-response magnitude. That is, increased flows and durations beget higher sediment-transport potential, accumulating in large sediment deficits relative to the pre-developed regime. As we shall see, such cumulative imbalances result in proportional concomitant changes in channel form. The resulting models provide managers with tools for predicting changes in channel form in urbanizing watersheds, but more importantly, will lead to informed evaluations of various mitigation strategies to minimize the risk of such undesirable sediment imbalances. Equally important is an understanding of how these systems evolve in response to hydromodification. As a preface to response magnitude, I summarize various response sequences observed throughout the region. In summary, the goals of this chapter include:

1. Understanding of response direction:
  - a. present a channel evolution model for southern California
  - b. present risk factors for incision and braiding responses
2. Understanding of response magnitude:
  - a. develop a process-based model for channel enlargement (where reasonable estimates of pre-response form can be made)
  - b. develop dimensionless measures for departure from quasi-equilibrium geometries (i.e., departures from stable bank height and regionally-representative widths)
3. Implications to mitigation:
  - a. interpret model results in terms of potential strategies to minimize risk of hydromodification-induced channel responses

### **3.1.1 The natural and anthropogenic setting**

The hydrogeomorphic setting of southern California gives rise to channels that are inherently dynamic. Steep slopes coupled with the climatic and lithologic setting produce high-sediment yields: 100 to 7,440 m<sup>3</sup>/km<sup>2</sup>/yr (mean of 1,600 m<sup>3</sup>/km<sup>2</sup>/yr) from debris basins in the San Gabriel Mountains (Lavé and Burbank, 2004). Large fluctuations in precipitation result in an active fire regime accompanied by significant pulses in sediment production and runoff (Los Angeles County Flood Control District (LACFCD), 1959; Booker *et al.*, 1993). Climate change is predicted to increase regional sediment delivery with the anticipated shift in vegetation from sage to grassland (Gabet and Dunne, 2002, 2003). The widely-varied lithologies generally produce limited

amounts of coarse material; for example, less than 7% gravel or larger ( $d > 2$  mm) by volume in regional debris dams (Taylor, 1981). The semiarid climate leads to highly flashy regimes (e.g.,  $Q_{10}/Q_2$  ranging 4 to 163, mean 17, median 9) in almost exclusively ephemeral channels. Coupled with the high/variable loads of fine sediments, predominant channel forms are single-thread and braided across both sand and gravel substrates. Such stream settings commonly experience extended periods of aggradation and degradation and comparatively infrequent states of ‘equilibrium’ (Wolman and Gerson, 1978; Graf, 1981, 1988; Bull, 1997).

Compounding the naturally dynamic setting are southern California’s approximately 20 million residents and their ever-expanding footprint. With little flow control evident at the subdivision scale, field investigations indicated that it can take only 5 to 10 yrs following development for channel responses to become so severe that instabilities must be addressed with in-stream measures to protect imperiled infrastructure. This most typically entails concrete/riprap lining of trapezoidal flood conveyance channels with little conservation of ecological or geomorphic function.

### **3.1.2 Channel evolution models**

Much research has revolved around the concept that channels often follow predictable sequences when perturbed from equilibrium (Brice, 1981; Brookes, 1988; Downs, 1995; Rosgen, 1996). Response trajectories are often dependent on the type of disturbance (e.g., channelization, deforestation, fire, and urbanization), the regional/channel setting (i.e., humid vs. arid, meandering vs. braided, coarse vs. fine), and the spatial and temporal scale/extent of the perturbation (i.e., local vs. watershed

wide, temporary vs. permanent) (Knighton, 1998). One of the most widely-cited contributions is the CEM of Schumm *et al.* (1984), referred to here as the ‘original’ CEM. The five-stage sequence of incision-driven mass-wasting in channelized streams of northern Mississippi continues to offer a conceptual framework for other regions. It includes:

1. CEM Type I – stable;
2. CEM Type II – incising (degradation);
3. CEM Type III – incision depth exceeds critical height for bank failure and widening occurs (bank failure primarily due to geotechnically-unstable banks, i.e., mass wasting);
4. CEM Type IV – aggrading to the point that bank failures begin to cease but channel has not rebuilt a floodplain; and
5. CEM Type V – quasi-equilibrium single-thread channel connected to stable floodplain formed within abandoned floodplain trench.

The general sequence of incising, widening, aggrading, and a return to quasi-equilibrium was informed by and has since been observed across many settings and disturbance types, for example, experimental drainage networks (Schumm and Parker, 1973), gullies/arroyos in Colorado and Nebraska (Begin and Schumm, 1979), and dredged/channelized rivers in western Tennessee (Simon, 1989). Bledsoe *et al.* (2002) offered process-based quantifications of response stages, noting that slope, sediment load, and specific stream power consistently decrease as channels adjust their form to accommodate excess erosive energy.

Watson *et al.* (2002) segregated evolution stages by combining two non-dimensional measures of stability into a four-quadrant sequence:  $N_g$  (bank stability) and  $N_h$  (hydraulic stability/sediment continuity).  $N_g$  is the ratio of bank height ( $h$ ) to critical bank height for the given angle ( $h_c$ ).  $N_h$  is a measure of the current slope divided by the slope required to transport the given sediment supply. As depicted in Figure 3.1, when the channel incises beyond critical height for the respective bank angle ( $N_g > 1$ ), mass wasting begins and the channel proceeds to widen (CEM Type III). Aggrading (CEM Type IV) begins when the channel becomes sufficiently wide and flat to diminish sediment-transport capacity relative to the supply ( $N_h < 1$ ). The return to equilibrium (CEM Type V) occurs once banks become geotechnically stable ( $N_g < 1$ ) and sediment transport matches the supply ( $N_h = 1$ ).

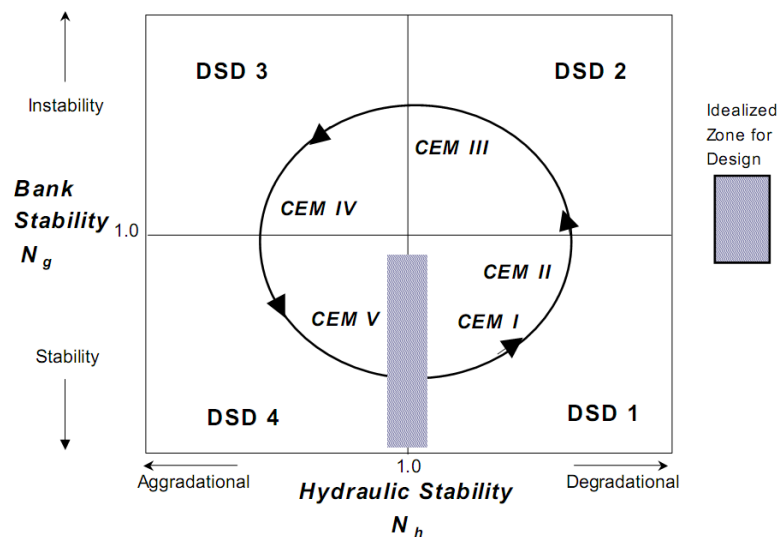


**Figure 3.1 – Dimensionless stability diagram for the CEM in incised sand-bed streams (Watson *et al.*, 2002)**

The Watson *et al.* (2002) scheme centers on the most fundamental measures of geomorphic stability. The disadvantage with the scheme is that sediment supply is often

difficult to estimate and there are limited gauge data. Furthermore, sediment supply, particularly in southern California, is not uniform in space or time. Yet, regardless of practical limitations, the framework offers a process-based representation of relative departure from equilibrium and the subsequent adjustments required for its return.

### **3.1.3 Cumulative sediment transport**

Attitudes of researchers have evolved regarding the use of single-flow analyses for assessing and managing channel stability, particularly in semiarid settings where the idea of relating a single discharge to equilibrium channel form has increasingly been brought into question (Graf, 1988; Bull, 1997). It has long been understood that all flows capable of moving sediment have the potential to affect channel form, and that it is the combination of both frequency and magnitude that leads to geomorphic *effectiveness* (Wolman and Miller, 1960). The concept has been widely applied to determine the ‘effective discharge’ (Andrews, 1980) of a given river using a variety of stochastic techniques and sediment-transport relations (Hey, 1997; Watson *et al.*, 1997; Biedenharn *et al.*, 2000, 2001; Soar, 2000). A process analogous to an effective-discharge calculation could offer greater utility in southern California by considering the cumulative sediment-transport capacity over all flows. One of the only California-based approaches to managing hydromodification to date does just this with the substitution of cumulative excess shear stress for cumulative sediment transport (Santa Clara, 2004). The so-called ‘effective work index’ is computed using binned flows from long-term rainfall runoff simulations in the Hydrologic Engineering Center - Hydrologic Modeling System (HEC-HMS) over cumulative flow durations of 50 yrs.

As an alternative to rainfall-runoff models, several researchers developed ways to scale cumulative duration curves from USGS gauges to nearby ungauged sites. Hey (1975) used a drainage-area scaling approach based on the nearest upstream/downstream gauge. A more regionalized approach was to scale using a nondimensional index such as  $Q/Q_{\text{bankfull}}$  (Emmett, 1975; Leopold, 1994) or  $Q/Q_2$  (Watson *et al.*, 1997). The disadvantage of using bankfull flow is that it is often hard to define and does not have a consistent return interval across different streams (Pickup and Warner, 1976; Williams, 1978; Biedenharn *et al.*, 2000, 2001). In either case, it may be difficult to define which gauges are similar enough to the ungauged watershed to use in the scaling procedure.

Hawley (Chapter 1) developed a regional approach as functions of multiple statistically-significant physical parameters opposed to a single flow. Duration Density Functions (DDFs) estimate cumulative durations for all geomorphically-effective flows in a logarithmically-binned histogram format. Such an approach to long-term flow durations lends itself to simple sediment-transport calculations in spreadsheet programs (e.g., Microsoft Excel<sup>®</sup>) and is also compatible with more rigorous models such as the Sediment Impact Analysis Method (SIAM) publicly available in the U.S. Army Corps of Engineers' (USACE) Hydrologic Engineering Center - River Analysis System (HEC-RAS) package (Mooney, 2007; USACE, 2009).

## **3.2 Methods**

Extensive field data were collected and analyzed for this project, guided by independent reviews and State-approved quality assurance/quality control (QA/QC) procedures. In general, the modeling approaches used and developed in this dissertation

are designed for broad application across many sites as opposed to detailed precision at fewer sites. Although process-based, the empirical models presented here are more appropriate for quantifying relative extents of change than absolute magnitudes.

In the following sub-sections, I begin by outlining the site-selection process and describe how data were collected. Next, computational methods for hydrologic, hydraulic, and sediment-transport processes are covered. To underscore method selection and process, ‘results’ that are less central to the overall conclusions are presented in some cases. The following sub-section covers how changes in channel form were both qualitatively described and quantitatively estimated. Lastly, the analytical and statistical methods are presented, describing how results from the preceding steps were used to develop final models.

### **3.2.1 Site selection and channel stability**

Undeveloped, developing/recently-developed, and fully-developed watersheds were targeted to capture a gradient of urbanization relative to the rural setting. The sites spanned channel evolution stages from ‘stable’ single-thread to incising, widening, and braiding. With the understanding that most channels of southern California are inherently dynamic, ‘stable’ is defined for the purposes of this project after Biedenharn *et al.* (1997): “*In summary, a stable river, from a geomorphic perspective, is one that has adjusted its width, depth, and slope such that there is no significant aggradation or degradation of the stream bed or significant planform changes (meandering to braided, etc.) within the engineering time frame (generally less than about 50 years).*”

It is important to consider ‘significant aggradation/degradation’ in the context of southern California. For example, a reach type/process-domain of confined, step-pool/bedrock (Montgomery and Buffington, 1997, 1998; Montgomery, 1999) that has temporarily aggraded with finer material (i.e., gravels and smaller) into a plane-bed form following a fire would not necessarily be considered ‘unstable’, because we have observed such systems return to their pre-fire form over a period of gradual flushing. Perhaps more appropriately for the context of hydromodification effects, one could think of ‘stable’ as a layperson might. Has the channel significantly affected adjacent land or reaches upstream/downstream through considerable headcutting, widening, planform shifts, and so forth? Empirical evidence suggests that some channels in southern California have evolved their active width and slope to absorb variable pulses in flow and sediment without such complex adjustments (i.e., there are even examples of braided channels that have maintained a relatively constant bandwidth for over 50 yrs; e.g., Santiago\_A).

From field reconnaissance at more than 50 candidate stream reaches, 31 streams were selected for data collection. We excluded sites that were entirely reinforced with artificial means (e.g., concrete or riprap) due to their inability to freely respond to hydromodification in terms of morphologic adjustment. The focus was also on smaller watersheds because most of the larger streams were already reinforced with flows regulated by large reservoirs. Other selection criteria included spanning representative ranges across regionally important gradients such as slope, bed material, channel type/planform, evolution stage, valley setting, drainage-basin size, geopolitical setting, and of course, extent of urbanization. Ranges and means of selected variables are

presented in Table 3.1. Locations of project stream reaches used in the analysis are denoted in Figure 3.2.

**Table 3.1 – Summary of key gradients across 84 morphologically-distinct sub-reaches/project 'sites' used in screening-tool development**

Metric Type	Key Gradient	Minimum - Maximum	Mean	Units
watershed	drainage area	0.1 - 160	17	km <sup>2</sup>
	imperviousness	0 - 26	3.6	%
	average annual rainfall	230 - 740	430	mm
	drainage density	0.2 - 3.7	1.3	km/km <sup>2</sup>
	average surface slope	5 - 52	26	%
sub-reach	channel slope	0.2 - 15	2.6	%
	top width at 2-yr flow	0.2 - 62	11	m
	median grain size	0.125 - 500	26	mm

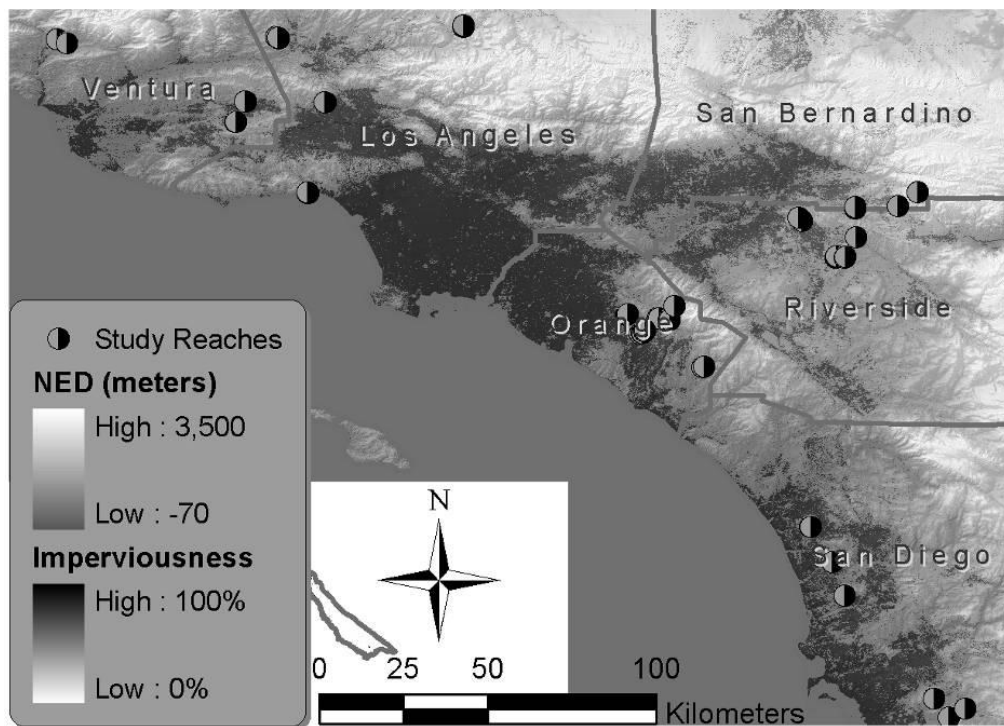


**Figure 3.2 – Overview and locations of project stream reaches used in analysis**

Across 31 streams, data were collected at 84 geomorphically-distinct sub-reaches or 'sites.' For example, a 2-km reach may have several 'sites' due to significant differences in form (incised vs. widening), flow (additional tributaries), or valley setting (confined vs. alluvial valley). The paired data were valuable in isolating differences such as valley setting or form alone (i.e., 'stable' vs. incising vs. widening, all with the same flow and parent material). Such substitutions of space for time were coupled with audits of historical aerial photography, and tempered with the understanding that average rates of change tend to decrease as time spans increase (Schumm, 1991).

### **3.2.2 Field and GIS data collection**

Bed-material samples followed Bunte and Abt (2001), with 100-particle pebble counts using a half-phi template across equally-spaced sampling frame transects at riffle sections. Sites with more than ~20% sand by volume required sieving and phi-sampling. Volumetric gradations were composited with distributions by weight using a combination of rigid and flexible procedures designed by D. Dust and K. Bunte (2008, Pers. Comm.).

Geometric survey procedures were primarily informed by Harrelson *et al.* (1994). For example, longitudinal profiles were surveyed at closely spaced points along the channel thalweg, capturing all vertical (e.g., head/toes of riffles, knickpoints, etc.) and lateral (e.g., bends, thalweg crossings, etc.) break points. The project had two levels of precision for cost optimization. 'Modeling' sites were designed for detailed fluvial/sediment-transport modeling with closely-spaced cross sections ( $\leq 5$  channel widths) and had semi-permanent rebar for long-term monitoring. Points were surveyed with high-precision instruments and translated to Global Positioning System (GPS)

coordinates with lateral and vertical accuracies of 3 and 1 cm, respectively. In contrast, ‘screening’ sites were surveyed with fewer cross sections and less precision in order to capture data at a larger number of reaches across a wide range of settings. Sites were located to within about 1 to 10 m of true position using a commercial-grade GPS unit. Geometric data were measured with a 2x magnification hand-level, fiberglass tapes, and pocket rods. Points were kept to distances less than or equal to 5 m with a fixed-height instrument stand to obtain reasonable accuracies with the hand-level. Three ‘modeling’ cross sections were resurveyed with the screening equipment to quantify average errors at the screening sites. For 20- to 50-m transects, average vertical errors were 0.5 to 0.6 millimeters per lateral meter.

All GIS data were acquired from public-domain sources including the USGS, U.S. Department of Agriculture (USDA), National Oceanic and Atmospheric Administration (NOAA), and State of California geospatial clearinghouse (CAL-Atlas). Changes through time were tracked using historical and present-day aerial photography from the USGS and Google Earth, along with historical USGS quadrangle topographic maps. Most source data were uniformly complete; however, some USDA polygons had empty fields compromising the capacity for widespread correlations in Natural Resources Conservation Service (NRCS) soil types. Precision was typically on the order of 1% of the measurement (e.g., 10-m National Elevation Dataset (NED) over 1 km of channel).

ArcMap software by Environmental Systems Research Institute (ESRI), including extensions such as ‘spatial analyst’, was used to optimize GIS measurements where possible. Automated results were cross-checked with aerial photography, field investigations, and existing shapefiles such as USGS Hydrologic Unit Code (HUC)

boundaries and National Hydrography Dataset (NHD) flowlines. Watershed boundaries were independently confirmed by two analysts.

### **3.2.3 Hydrology, hydraulics, and sediment transport**

Cumulative flow-duration curves were estimated using a regional approach developed by Hawley (Chapter 1). The DDF procedure populates long-term durations of histogram-binned flows as functions of physical parameters of the ungauged watersheds and is applicable on drainage areas larger than  $\sim 1.3 \text{ km}^2$  for simulation periods of  $\sim 25$  to 65 yrs. The disadvantage of the approach, in this case, is that it was calibrated using mean-daily flows rather than more frequent intervals (e.g., hourly or 15-min data), which can adversely affect long-term sediment yields as transport does not scale linearly with flow. For example, Watson *et al.* (1997) reported 50% lower yields using 24-hr flows relative to 15-min intervals in small ( $< 1,000 \text{ km}^2$ ) flashy systems in the Yazoo River Basin of Mississippi. Constrained by the available data, I proceeded with the known bias.

The type and number of histogram bins also affect the sediment-distribution curve (Hey, 1997; Soar, 2000; Holmquist-Johnson, 2002; Raff *et al.*, 2004). Cases have been made for various schemes; however, the limiting factor is to ensure a relatively continuous flow frequency such that no bins are populated by zero days of occurrence (Biedenharn *et al.*, 2000, 2001). Hawley (Chapter 1) found the extremely flashy regimes of southern California to best be represented by 25 logarithmically-distributed bins. As such, one small way I attempted to compensate for the likely underrepresentation of sediment transport was to fit the DDFs to the arithmetic-bin centroid rather than the

logarithmic, creating a slightly skewed bias toward the higher flows in each bin (i.e., 5.0 vs. 4.9 m<sup>3</sup>/s for bin 25 at Borrego\_B under the currently developed regime).

Like all models, DDFs are wrong; yet, they are useful to this study for many reasons. First, they are calibrated with regional data. Next, they offer an objective way to augment flows and durations for urbanization via measures of total impervious area (TIA), which in this region tend to be fairly representative of hydrologically-connected impervious area due to little flow control at the subdivision scale to date. Admittedly, this may not be the case moving forward if the recommendations in this dissertation are implemented. Third, DDF components are computed using physical parameters, which were calibrated to R<sup>2</sup> ranges of 0.7 to 0.9. Finally, it is important to note that I use the models in a relative way, comparing post-/pre-developed scenarios rather than absolute estimates of yield. That is, the inherent errors of the models are unbiased in affecting both scenarios such that results are meaningful in terms of relative imbalances.

DDF simulations of the past 25 yrs were performed for developed (actual) and undeveloped scenarios during the same time period. The idea was to compare estimates of sediment-transport potential to determine if sediment imbalances between the two regimes corresponded to observed/inferred changes in form. The USGS national impervious raster from 2001 provided an objective way to measure total imperviousness. Without other digital sources from the time frame, impervious extent in 2001 was used as the representative measure during the period for practicality. In Hawley (Chapter 1), the author did not find large departures between current and time-integrated impervious measures at gauges active during the last 25 yrs. That is, ‘developed’ watersheds had relatively high measures and ‘undeveloped’ drainages had nominal levels. The strategy

breaks down in watersheds that only recently had development (i.e., post-2001); however, those sites were few (i.e., Acton, San Timeteo, and to a small degree at Hasley). The simulation period of 1982 - 2007 had 6 yrs of exceptional precipitation, quantified as 50% greater than the long-term mean-annual precipitation at Los Angeles (i.e., > 22.6 in, 574 mm). For reference, that is well above average rates (i.e., typically 0.147 ‘wet’ years per year, ~ 1 ‘wet’ yr every 7 yrs of record). A more ‘average’ 25-yr period would have only had 3 to 4 exceptional precipitation years. I mention this because the related terms ( $LAwt_{rt}$  and  $LAwt_{yr}$ ) were significant in predicting the maximum daily flow ( $Q_{max}$ ) over the simulation period, which determines the scale of the DDFs.

Resulting DDFs of cross sections at Borrego Canyon and Escondido Creek are presented in Figure 3.3. The DDFs were developed in English units for consistency with USGS equations; however, flows were converted to SI units prior to application in sediment transport. These were two of the most urbanized watersheds, with 14% imperviousness in 2001. This translated to approximately three times as many days of equivalent sediment-transporting flows between the undeveloped and urban simulations. In contrast, sites at Acton with only 2 to 3% impervious area in 2001 were modeled to have increases in cumulative durations of ~11%, making the two DDF curves nearly overlaid.

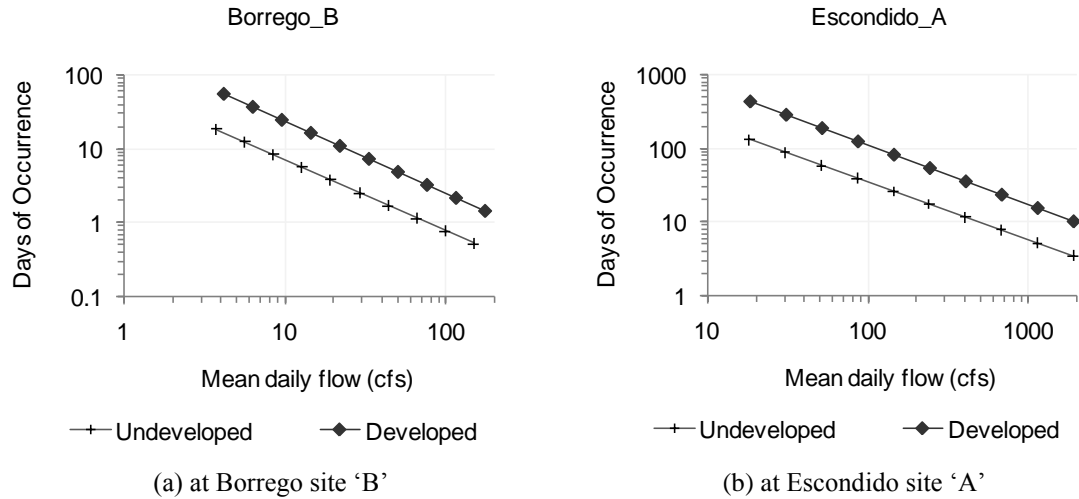


**Figure 3.3 – DDF simulations of the past 25-yr under developed (actual) and undeveloped regimes**

After pre-/post-developed DDFs were estimated, hydraulics and sediment transport were determined for bin-flow centroids. Hydraulic calculations were simplified by using hydraulic-geometry relationships developed for each site. This included power functions for area and hydraulic radius ( $R^2$  commonly approaching 1.00), and a predictor of top width that fluctuated across power, linear, logarithmic, or exponential forms ( $R^2$  typically ranging 0.97 to 0.99). The top width of both braided and stable single-thread channels was generally best fit with a power function of depth, whereas geometric discontinuities in mass-wasting systems were best represented by alternative expressions.

Normal depth at the respective flows was iteratively solved via the Manning (1889) equation and hydraulic radius power function. Following hydraulic computations for each bin flow at all 84 sites, sediment transport was estimated at each flow. Only 8 sites had median particle sizes less than gravel (i.e.,  $d_{50} < 2$  mm), making bedload equations more applicable than suspended-/total-load equations. Among the sandier sites, all but one was in the very coarse range (i.e.,  $d_{50} > 1$  mm) nearing that of gravels,

with the smallest median particle in the range of coarse sand (i.e.,  $1 \text{ mm} > d_{50} > 0.5 \text{ mm}$ ). Acknowledging that poorly-sorted materials traveling over non-rigid beds do not behave uniformly, I again elected to go the route of simplicity and used the Meyer-Peter and Müller (1948) equation. Although more recent approaches have demonstrated higher accuracies in certain applications by accounting for the range of bed material (Parker, 1990; Wilcock and Crowe, 2003) or the fraction of sand/gravel (Wilcock and Kenworthy, 2002), our pebble counts were designed for representative values of the median particle ( $d_{50}$ ) rather than the full gradation. Also recall that I am estimating long-term yields for relative comparisons at the same sites rather than attempting to predict exact transport rates.

Using Chien's (1956) format as presented by Julien (1998), and with corrected parameters from Wong and Parker (2006), the Meyer-Peter and Müller equation for volumetric unit bedload discharge becomes:

$$q_{bv} = 3.97 * (\tau_* - \tau_{*c})^{1.6} * \{(G-1)gd_s^3\}^{0.5} \quad \text{Eq. (3.1)}$$

where:

$q_{bv}$  = unit bedload discharge by volume ( $\text{m}^2/\text{s}$ );

$\tau_*$  = dimensionless shear stress, approximated for gradually-varied flow as  $\tau_* = RS_f / \{(G-1) * d_s\}$ , where R = hydraulic radius and the friction slope,  $S_f$ , may be approximated by the bed slope;

$\tau_{*c}$  = Shields parameter for incipient motion, calibrated to this equation as  $\tau_{*c} = 0.047$ ;

G = specific gravity of sediment,  $G = 2.65$ ;

$g$  = acceleration of gravity,  $g = 9.81 \text{ m/s}^2$ ; and

$d_s$  = sediment particle diameter, applied in our case for the median particle,  $d_{50}$ .

Unit bedload rates were calculated for each bin ( $q_{b\text{-bin}}$ ) and integrated across the respective channel width and over the number of flow days to estimate bin bedloads ( $L_{b\text{-bin}}$ ) during the simulation period. A more rigorous scheme that accounts for shear-stress partitioning was less requisite because even the largest bin flows tended to be contained within the main channel. Summing the bedloads from each bin provided a cumulative estimate of bedload yield for the 25-yr simulation. The procedure, analogous to an effective-discharge determination (Biedenharn *et al.*, 2000, 2001; Soar, 2000), is depicted graphically in Figure 3.4 for cross sections at San Antonio and Acton under the developed regime from 1982 to 2007. Hawley (Chapter 1) developed two forms of the DDF procedure:  $d1/d2$  for bins 16-25 with high accuracies and homoscedastic residuals and  $day1/day2$  modeling bins 12-25 with less precision and more patterned residuals in some cases. At San Antonio, for example, critical shear stress was not exceeded until bin 19 ( $2 \text{ m}^3/\text{s}$ ), making the more accurate  $d1/d2$  scheme (bins 16-25) applicable. In contrast, the fine-bed material on the steep slopes at Acton was modeled to be in motion at practically all flows. The lowest bin flow that could be modeled by the alternative  $day1/day2$  scheme was  $0.008 \text{ m}^3/\text{s}$  (bin 12). With a frequency of nearly 1,000 days, the ‘effectiveness’ of this and smaller flows precipitously dropped relative to that of larger flows due to significantly lower transport rates. The 25-yr bedload of bin 12 was estimated at  $\sim 1,000 \text{ m}^3$ , less than 1% of the total ( $\sim 170,000 \text{ m}^3$ ) over all flows. As such, I

was comfortable with the DDF model not capturing flows lower than bin 12 in such cases where the effective transport was nominal despite a shear stress larger than critical.

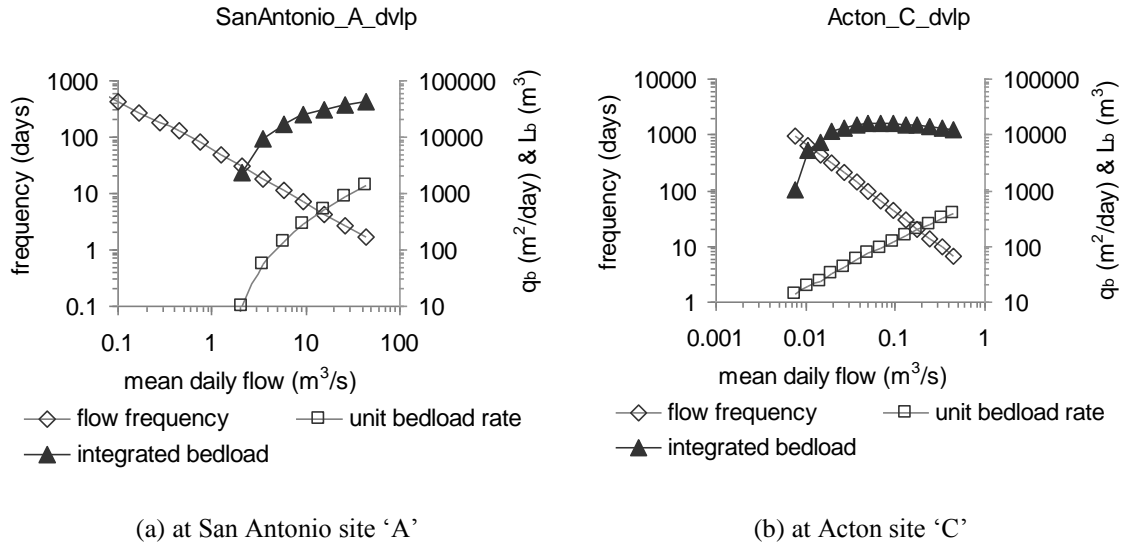


**Figure 3.4 – Cumulative flow durations, incremental sediment-transport rates, and cumulative bedloads across 25-yr DDF simulations under-developed regimes**

Different bin types/sizes would likely result in different shapes of the cumulative bedload curve, but it is worth noting that the ‘effective’ discharge in the case of SanAntonio\_A was simply the highest bin: 1.67 days at 43.5 m<sup>3</sup>/s, with a unit bedload rate of ~1,400 m<sup>2</sup>/day integrated over the channel width and frequency to a bedload yield of ~43,000 m<sup>3</sup> over 25 yrs, composing more than 25% of the total yield (165,000 m<sup>3</sup>). The effective discharge at Acton under this simulation was bin 19, with 65 days at 0.07 m<sup>3</sup>/s. Even so, the concept would appear to have little meaning in this application because bedloads from bins 15-25 (i.e., flows ranging 0.02 – 0.45 m<sup>3</sup>/s) were within 75% of that of the effective discharge (i.e., bedloads ranging ~12,000 to 16,000 relative to bin 19 at ~16,000 m<sup>3</sup>) and no bin represented more than 10% of the total yield. Such a case

exemplifies the importance of considering cumulative sediment transport rather than a single flow.

Finally, bedload estimates from the undeveloped and developed simulations were compared. Their direct ratio ( $L_r = L_{\text{developed}}/L_{\text{undeveloped}}$ ) informed the models presented in the results. Figure 3.5(a) depicts a comparison of the developed and undeveloped simulations at Borrego over the last 25 yrs using the ‘day’ scheme (bins 12-25). Durations of equivalent bins were 3.57 times larger on average in the developed simulation, which was predicted to transport 3.69 times as much bedload over 25 yrs (i.e., 146,000 m<sup>3</sup> vs. 40,000 m<sup>3</sup>). Although not equivalent by definition, average differences in bin-flow durations typically corresponded to similar differences in integrated bedload. Three modeling schemes were tested, ‘d1/d2’, ‘day1/day2’, and a combined method (bins 12-15 ‘day’, bins 16-25 ‘d’), each reporting similar load ratios between developed and undeveloped scenarios. I used the average of the three schemes ( $L_{r_{\text{avg}}}$ ) in the models.

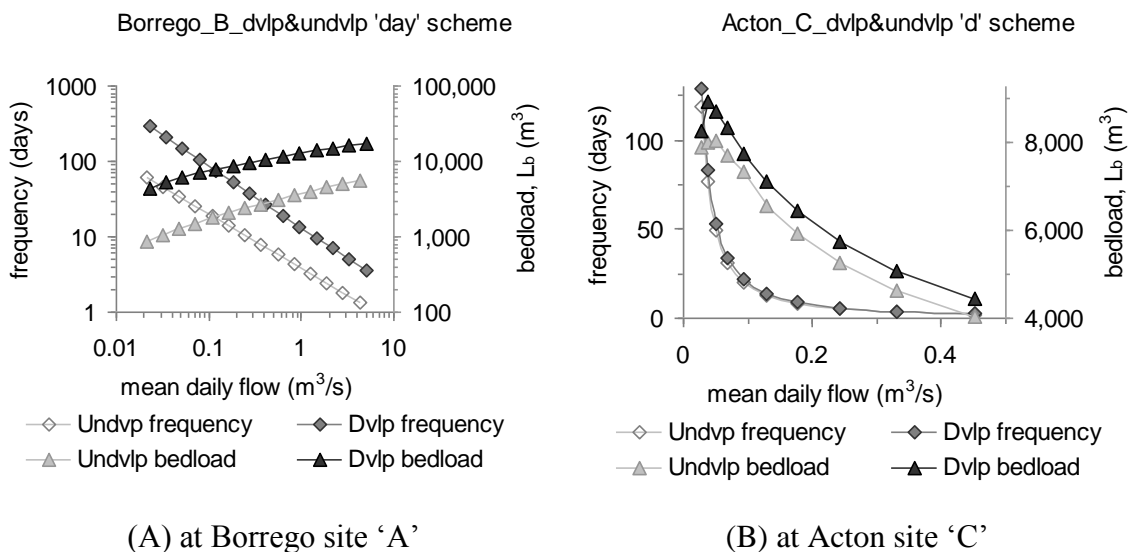


**Figure 3.5 – Cumulative flow durations and bedloads across 25-yr DDF simulations under-developed regimes and undeveloped regimes**

Figure 3.5(b) offers an example of the ‘d’ scheme (bins 16-25) applied at Acton (site C). Arithmetic scales are used because of the narrow differences between the two scenarios, a result of low (i.e., 2.4%) imperviousness in 2001. Bin frequencies increased by an average factor of 1.09 and cumulative bedload was 1.08 times larger (71,000 vs. 65,000 m<sup>3</sup>).

### **3.2.4 Channel evolution, enlargement, and representative form**

Channel-evolution sequences and planform data were compiled based on field observations during a combined 6 weeks of reconnaissance and data collection from Spring 2007 through Winter 2007/2008. Although stages not recognized in the original Schumm *et al.* (1984) CEM were apparent, initial observations were kept within its framework, including:

1. Stable: no significant channel incision or bank failure
2. Incising: significant incision at or approaching critical bank height, but no appreciable widening
3. Widening: significant bank failure with incision still possible/likely
4. Deposition: significant deposition with possible beginnings of floodplain reformation (although some bank failure/additional widening still possible)
5. Recovered: return to quasi-equilibrium

Married to these directional response phases were classifications of current planform, namely single- or multi-threaded flow paths. Due to relatively low sinuosities, single-thread channels were typically ‘straight’ rather than meandering. Multi-threaded systems generally fell into the widely-accepted definition of braided morphologies with

non-cohesive floodplains and dynamic unvegetated bars (Nanson and Croke, 1992). Although limited cases of vegetated islands were present, they were likely submerged by higher flows and were not necessarily set in low-energy/anastomosing floodplains. With the understanding that bars and islands are interrelated – bars can aggrade to islands (Knighton, 1998) and vegetation can be scoured degrading islands to bars – all multi-threaded channels were considered braided for these analyses. Furthermore, multi-thread classifications were strictly observational, independent of any quantifiable thresholds from other regions/studies; for example, a width-to-depth ratio of ~50 (Fredsoe, 1978).

Field-based inferences were then cross-checked with historic aerial photos and maps, primarily from the USGS. Aerial photos were also used in combination with historic reports, testimony of local residents, and field indicators to re-project a representation of the historic channel form. Given the uncertainties associated with such inferences, the re-projections were conservative in that they erred on the side of less departure from present-day form. Resolution and abundance of references varied such that some re-projections were most likely overly conservative, with conclusions at many sites as effectively unchanged. Consequently, only streams with noticeably large changes had meaningful estimates of enlargement. Figure 3.6 depicts overlaid cross sections at Borrego relative to a conservative re-projection of the historic cross section based on a series of aerial photographs (1947, 1952, 1967, 1974, 1982, 1986, and 1988) combined with the cross section at a present-day drop structure (Borrego\_A). Photographs in 1947, 1952, and 1967 capture a relatively narrow, single-thread channel that by 1974 has begun to widen in sections (Borrego\_B), with enlargement continuing through the present.

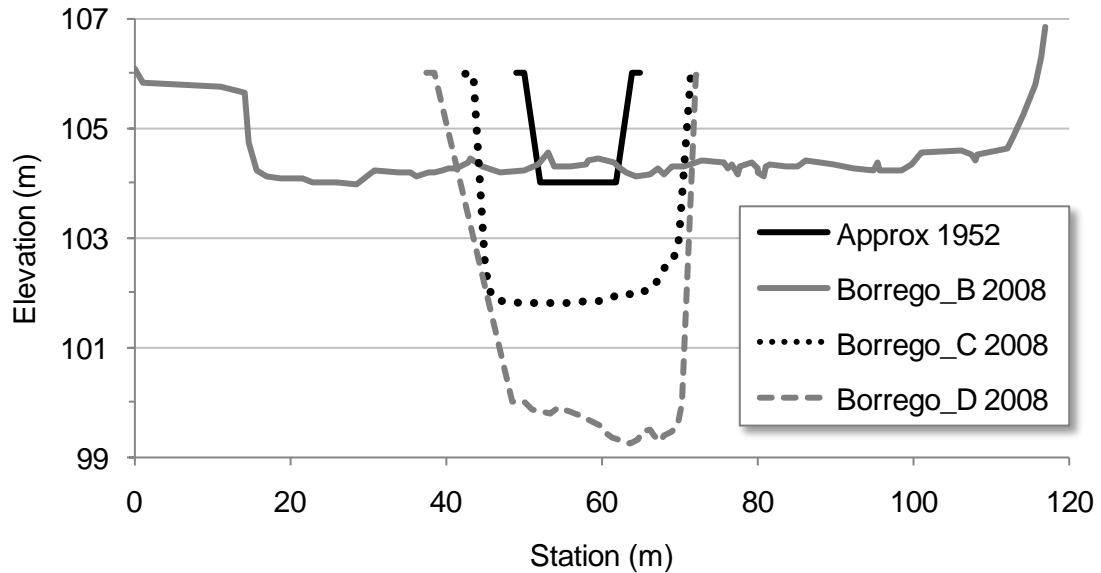


**Figure 3.6 – Surveyed cross sections at Borrego Canyon relative to projected 1952 form via aerial photograph and cross section at present-day drop structure**

Rather than use a cross-sectional area defined by a return-interval flow, I compared measures of what a layperson might quantify as the ‘active channel’ or those areas actively being affected by fluvial activity through channel flows/adjustments (as opposed to overbank/floodplain). A more explicit definition would be the cross-sectional area encompassed by the top of bank (of the lowest bank). Because differences were generally large, enlargement was quantified by relative magnitudes (ratios) rather than absolute or percent differences:

$$\Delta A_{\text{ratio}} = A_{\text{post}} / A_{\text{pre}} \quad \text{Eq. (3.2)}$$

where:

$\Delta A_{\text{ratio}}$  = enlargement expressed as the relative magnitude ( $\text{m}^2/\text{m}^2$ );

$A_{\text{pre}}$  = best estimate of historic (reference) cross-sectional area; and

$A_{\text{post}}$  = surveyed cross-sectional area to top of bank (2007/2008).

An alternative to inferring historic form from aerial photographs and field indicators is to measure the relative departure from regionally representative stable channel forms using present-day geometries. After Watson *et al.* (2002), one measure of disequilibrium is the ratio of bank height to critical bank height for mass-wasting failure at the same angle. Rather than attempting to measure individual stress parameters in the field, geometric bank data were used to calibrate a regional logistic threshold for mass wasting (Chapter 2). Plotting height versus angle in moderately- to well-consolidated banks, stable and unstable forms stratified in the shape of a log-log decay (Figure 3.7 and Table 3.2) analogous to the theoretically-derived Culmann relationship. Bank geometries and a summary of associated logistic analyses are presented in Appendices B and E.

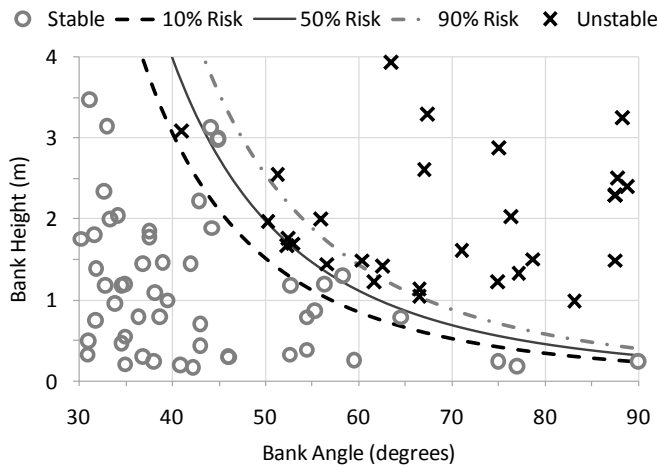


**Figure 3.7 – Logistic regression of mass wasting in moderately- and well-consolidated banks with superimposed stable and unstable bank geometries**

**Table 3.2 – Corresponding geometries for 50% risk of mass wasting**

Angle (°)	Height (m)
30	9.8
35	6.0
40	4.0
45	2.7
50	2.0
55	1.5
60	1.1
65	0.86
70	0.68
80	0.45
90	0.31

Not only is  $N_g$  a measure of bank stability (i.e.,  $N_g \leq 1$  stable,  $N_g > 1$  unstable), but departures from critical bank height provided relative measures of incision. For example,  $N_g = 2$  could broadly be interpreted as an incision-driven response (i.e., bank

height  $\sim 2x$  stable height for same angle), whereas a system characterized as ‘unstable’ with  $N_g = 0.5$  would likely be a laterally-driven response. Accordingly, a method to represent departure from lateral reference conditions was needed as a relative measure of widening and/or braiding. The simplest approach to a regional measure of ‘stable’ width is to build-off of the volumes of downstream hydraulic-geometry relations in which width tends to scale with discharge to a coefficient typically near 0.5 (Knighton, 1998). Recognizing that many factors affect channel size including bank material (Simons and Albertson, 1963; Schumm, 1971), bank vegetation (Andrews, 1984), bed material and flow regime (Osterkamp and Hedman, 1982; Yu and Wolman, 1987), regional data were used to calibrate a relation. Given that flashier and semi-arid systems tend to be wider and more variable than humid systems (Wolman and Gerson, 1978; Osterkamp, 1980), regional calibration seemed to be warranted.

Plotting the 10-yr top width versus flow for single-thread stable systems in unconfined valleys and unconstructed settings (i.e., Dulzura, Challenger (A and C), Perris2, Perris1\_A, AltPerris\_C, and Borrego\_D) resulted in a well-fit power function as a regional representation of forms sufficiently wide to dissipate energy without resulting in multiple flow paths. For reference, braided channels and incision-driven responses (CEM Types II and III) are included in Figure 3.8, and indicated nearly perfect segregation over the power function. As expected, braided systems are generally wider than the reference width for a given flow, with incising channels narrower in most cases. The only significant outlier to the pattern is the far-upstream cross section at Hicks Canyon (Hicks\_F), which is in the initial phases of incision (primarily due to headcutting from below) but still well-connected to the floodplain at the 10-yr flow. Figure 3.8(b)

shows a similar pattern at the 2-yr flow with a greater degree of overlap. The relative departure from the ‘stable’ single-thread width for a given flow offers one quantifiable measure of lateral disequilibrium in unconfined valleys. Similar to  $N_g$ ,  $N_w$  is defined as the ratio of current width to reference width for the given flow:

$$N_w = W_{10} / W_{ref} \tag{Eq. (3.3)}$$

where:

$N_w$  = relative departure from regional reference width at  $Q_{10}$ ;

$W_{10}$  = top width at 10-yr flow; and

$W_{ref}$  = regional reference width (stable single-thread) for  $Q_{10}$ .

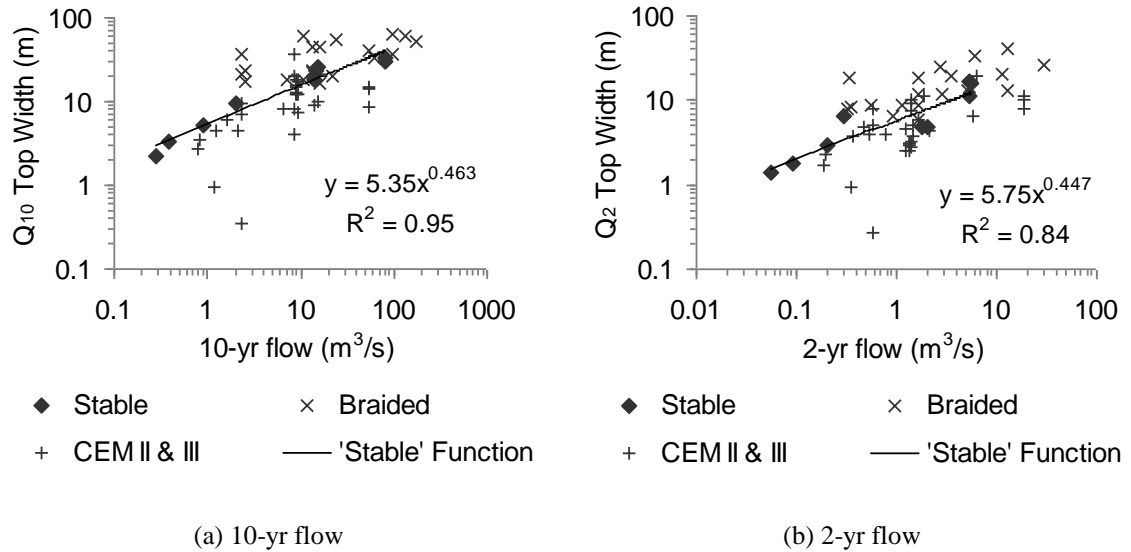


**Figure 3.8 – Top width vs. flow in unconfined, unconstructed stable, braided, and incising systems with superimposed power functions fitted to stable sites**

As relative measures of departure from regional reference forms,  $N_g$  and  $N_w$  can be used in combination to develop a dimensionless stability diagram (*sensu* Watson *et al.*

(2002)) that could guide managers in assessing channel instabilities and potential remediation alternatives.

### **3.2.5 Analytical and statistical methods**

As a process-based representation of many contributing factors (e.g., slope, width, grain size, flow and durations, etc.), I hypothesized that sediment-transport imbalances would be highly significant in explaining changes in channel form in both continuous (i.e., regression models of ‘enlargement’) and threshold models (i.e., logistic regression models of stable vs. unstable). Even so, numerous variables were tested for statistical significance to identify potential ‘risk factors’. Based on field observations and a physical understanding of process, two variables were anticipated to be significant in addition to the sediment transport ratio: downstream distance to hardpoint ( $D_{hp}$ ) and median-grain size of bed material ( $d_{50}$ ). As channels adjust their slopes to dissipate erosive energy, many of the finer-grained systems with incision-driven responses revolved around hardpoints (e.g., exposed bedrock, road crossings/culverts, or an artificial drop structure), causing responses to become larger as one walked upstream. Regarding grain size, I considered the likelihood that coarser systems were naturally less susceptible to changes in channel form, potentially irrespective of sediment-transport imbalances. This of course is despite the fact that sediment-transport capacity incorporates grain size. In contrast, I hypothesized that the opposite could be true in fine-grained systems. That is, instabilities could still occur in the finer systems despite the smallest sediment deficits predicted in our models.

Finally, total impervious area was tested as a measure of enlargement. Although several researchers have demonstrated significance in other regions (Hammer, 1972; MacRae and Rowney, 1992; MacRae, 1993, 1997) and in southern California (Coleman *et al.*, 2005), I hypothesized that imperviousness would not be a good predictor for channel response when considered independent from process and setting. Rather, I suggest that it is best to proceed via the process-based flow of logic presented here; i.e., imperviousness changes the flow regime, which may in turn affect the sediment-transport capacity (dependent on cross-sectional and bed-material setting), where prolonged imbalances could affect channel form.

### **3.3 Results**

Qualitative and analytical results are presented in three sub-sections. The first is a descriptive CEM for southern California, followed by models and risk factors of ‘enlargement’. Finally, relative measures of departures from equilibrium/reference geometries are presented, with risk factors of incising and braiding discussed.

#### **3.3.1 Response direction: a CEM for southern California**

Channels in southern California were observed to respond in ways that were analogous to and departed from the original CEM of Schumm *et al.* (1984). Some notable responses/conclusions include the following:

- Many of the response trajectories follow the original CEM of Schumm *et al.* (1984) driven by increases in flow ( $Q^+$ ), long-term decrease in basin-sediment supply ( $Q_s^-$  basin), and/or base-level drop ( $S^+$ ).

- Braided systems can also follow a sequence that is analogous to the original CEM, especially the initial stages of incision (Braided 2), widening (Braided 3), and aggrading (Braided 4). This sequence is primarily triggered by a base-level drop ( $S^+$ ) and the resulting headcutting.
- Several deviations from the original CEM were observed (Figure 3.9):
  - Phase 1-Veg: vegetated encroached low-flow channel from urban base flow. It is possible for this form to occur following other less stable stages within the CEM, such as Phase 2 or even from previously braided states. This stage was more common in San Diego County, and less prevalent in other areas.
  - Phase 2-B: widening/braided planform with little initial incision. This is likely driven by  $Q^+$ , and/or increased sediment supply from the basin ( $Q_s^+_{\text{basin}}$ ) or channel ( $Q_s^+_{\text{channel}}$ ). Relative erodibility of the bed and bank material likely plays a role, including the general cohesiveness of the floodplain.
  - Phase 4-B: widening/braided planform following significant phases of initial incision.
  - Phase 5-C: constructed channel (concrete or riprap) following any stage. This stage was generally observed as the most prevalent endpoint for streams in developments older than 5 to 10 yrs, with the exception of San Diego County where developments were typically on hilltops rather than valley bottoms.

In summary, vegetated (1-Veg) or constructed (5-C) may result from any antecedent stage across both single-thread and braided planforms. Shifts from single-thread to braided can result from both incision-driven (4-B) and incipiently lateral responses (2-B). It is also important to note that these braided states are not intended to convey static endpoints. Rather, they too could incur subsequent phases of incising, widening, and/or aggrading. It is conceivable that given enough time to flush excess sediment, braided states could return to single-thread equilibrium (Phase 5); however, most such cases would suggest that both their sediment regimes and width are so far removed from single-thread stability that the return is unlikely within the time scales of interest. This will be further discussed in Section 3.3.3.

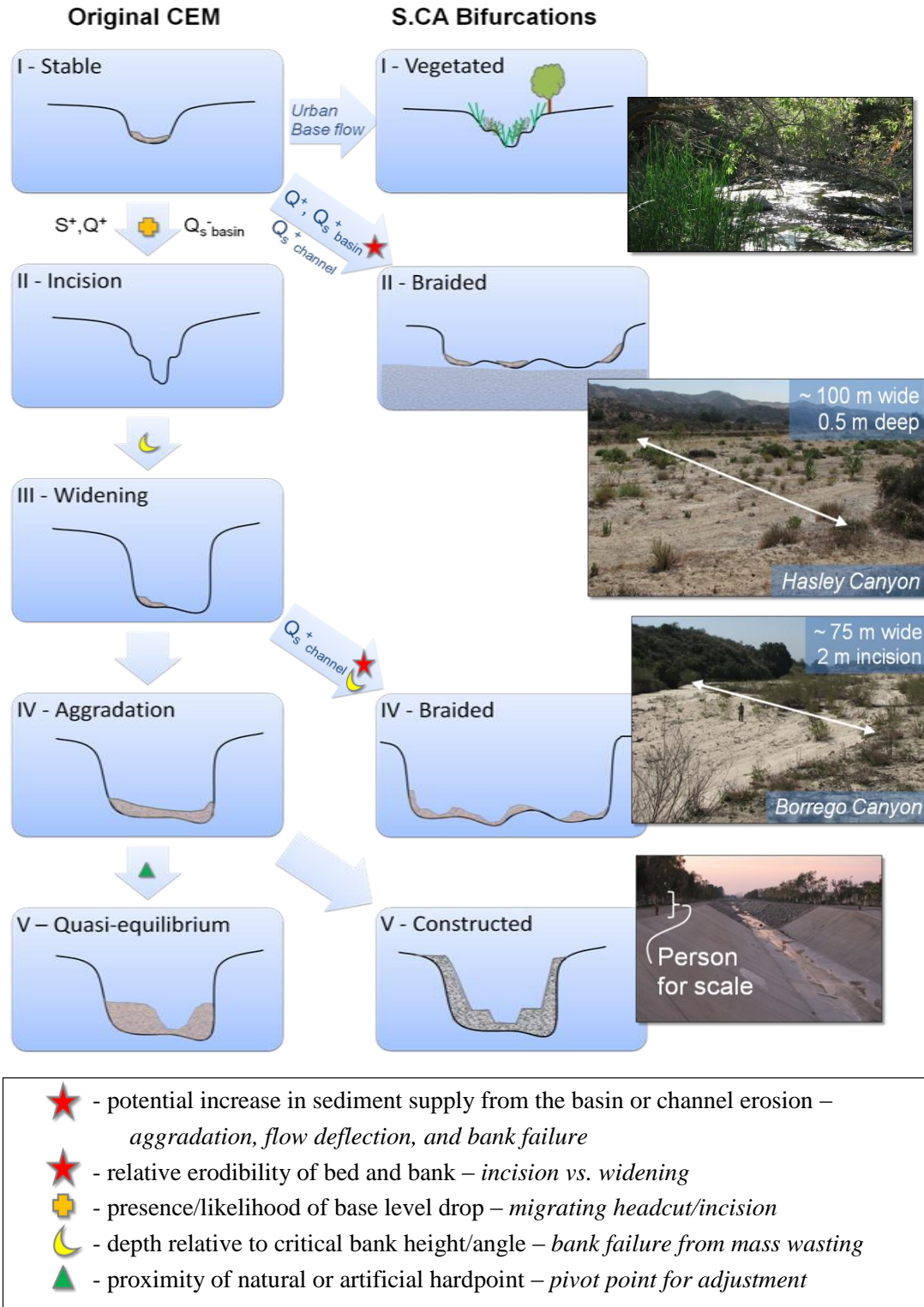


**Figure 3.9 – CEM for southern California with accompanying photographs and key mechanisms/boundary conditions**

### 3.3.2 Response magnitude: ‘enlargement’

Multivariate regression models that included all sites with the exceptions of Acton F and G (yet to respond) and San Antonio A and B (largely explained by channelization) could explain over 40% of the variance in estimations of ‘enlargement.’ Common risk factors included large hardpoint distances, sediment imbalances, wide valleys, and watersheds that were recently burned. By systematically withholding sites with poor reference conditions (Dulzura and Agua Hedionda), poor measures of current imperviousness (Acton, Dry, San Timetao, and Hasely1), watersheds with large amounts of flow control via reservoirs (Escondido), sites with less freedom to respond such as constructed banks (Hicks\_A, Borrego\_A, Santiago\_B, Yucaipa\_A, and Oak Glenn), and those primarily attributable to channelization (San Antonio), models converged on three primary variables. They were  $L_r$ ,  $d_{50}$ , and the hardpoint distance normalized by the top width at the 10-yr flow ( $D_{hp}/W_{10}$ ). Enlargement typically decreased with bed-material size and increased with hardpoint distance, as seen in Figure 3.10. A necessary caveat with the application of the hardpoint variable was that it was treated as zero in systems where headcuts were not occurring. In channels with large sediment-transport ratios, systems often pivoted their response around the nearest downstream hardpoint; however, systems in relative equilibrium would clearly not become larger as one moved upstream. This segregation was roughly quantified as a sediment-transport ratio greater than  $\sim 1.05$  in systems with a median grain size of  $> 16$  mm, and  $L_r \sim 1.01$  when  $d_{50} < 16$  mm.

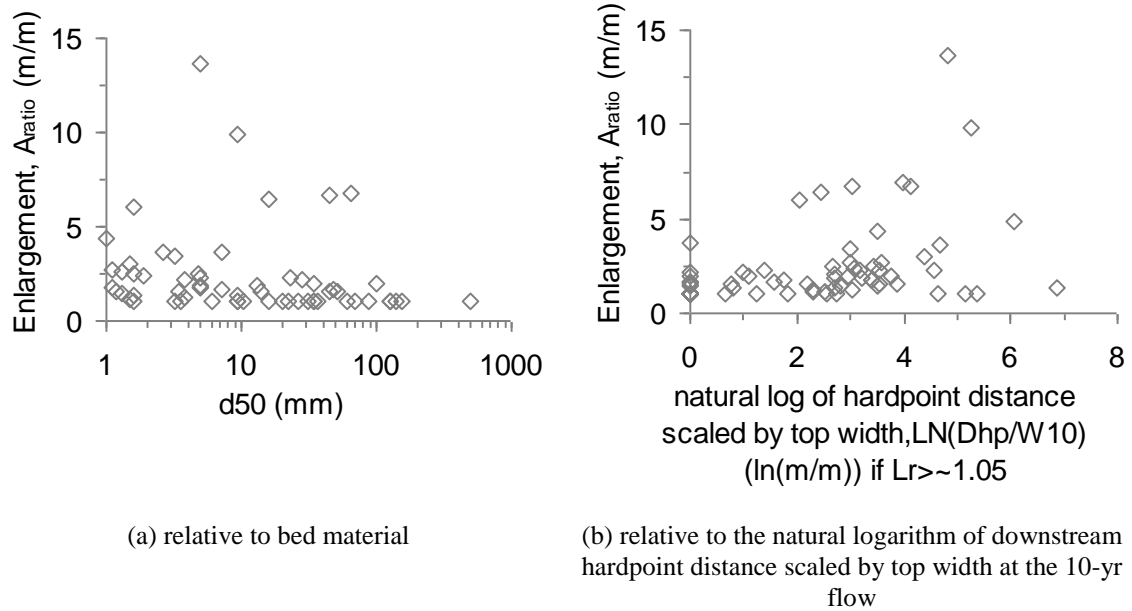


**Figure 3.10 – Enlargement ratio of all sites**

The scatter among these figures ultimately underscored the importance of including sediment-transport ratio in the models. Hydrologically duplicate sites were also removed to avoid bias toward similarly ‘enlarged’ sites that were simply in different response phases (e.g., Borrego\_C (Phase 3) vs. Borrego\_D (Phase 4 → 5) with similar flow volumes due to no tributary confluences between sites, vs. Borrego\_C → Borrego\_B with considerably more flow). By including only sites that have had several years and even decades to adjust to current development levels (Santiago\_A, Hasley2\_A, Hasley2\_Trib, Hicks\_D, Hovnanian\_B, Little Cedar\_B, Perris1\_A, Perris1\_C, Perris2\_B, Perris3\_A, AltPerris\_A, AltPerris\_C, Borrego\_B, Borrego\_C, Topanga\_A, Topanga\_C, Challenger\_A, Challenger\_C, San Juan\_A, San Juan\_B, Pigeon Pass\_A, Pigeon Pass\_C, Stewart\_A, Santiago Natural Loading Site\_B, Silverado\_A, Unnamed Tributary in Riverside County\_A, and Yucaipa\_B), model variance was predominantly explained by  $L_r$  (e.g., over 60% of the total variance).  $D_{hp}/W_{10}$  was also significant ( $p < 0.05$ );

however,  $d_{50}$  had little statistical significance, likely attributable to the fact that  $L_r$  incorporates bed-material resistance. The lack of significance may have also been caused by present-day  $d_{50}$  values that were not necessarily representative of pre-response  $d_{50}$ . That is, grain size may have coarsened if a channel has undergone substantial enlargement.  $d_{50}$  is included in one model to demonstrate its nominal influence at the  $p = 0.25$  level. When total imperviousness was substituted for  $L_r$ , models had slightly lower  $R^2$  values and grain size became even less significant. Because TIA is much easier to apply than  $L_r$ , I include the impervious-dependent models for reference; however, they are not intended to be used as predictive tools. Results of these final models are presented in Figure 3.11 and summarized in Table 3.3.

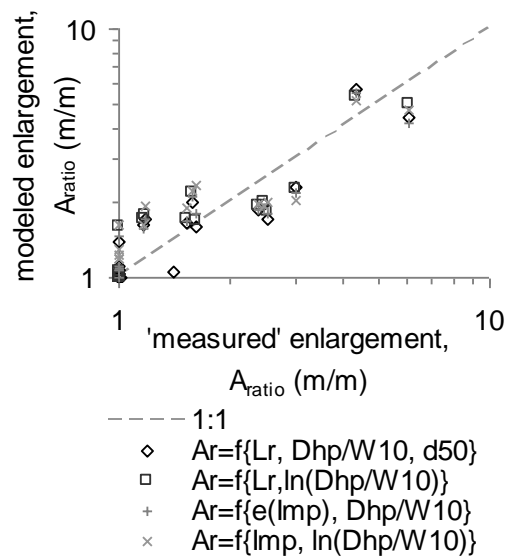


**Figure 3.11 – Modeled enlargement ratio versus estimated enlargement from best historic approximation of pre-response form of 27 most representative sites**

**Table 3.3 – Summary of best ‘enlargement’ models**

Enlargement Function	Adjusted R <sup>2</sup>	p-value Exceptions
$A_{ratio} = e^{0.062 * Lr^{0.87} * D_{hp}/W_{10}^{0.17} * d_{50}^{-0.023}}$	0.83	$d_{50} = 0.25$
$A_{ratio} = -0.36 + 1.36 * Lr + 0.28 * \ln(D_{hp}/W_{10})$	0.85	
$A_{ratio} = e^{-0.036 * e^{(7.9 * Imp)} * D_{hp}/W_{10}^{0.17}}$	0.81	
$A_{ratio} = 0.86 + 24.4 * Imp + 0.23 * \ln(D_{hp}/W_{10})$	0.80	

where:

Lr	=	$L_{developed}/L_{undeveloped}$ (average of three 25-yr DDF simulations) ( $m^3/m^3$ )
$D_{hp}/W_{10}$	=	downstream distance to nearest ‘hardpoint’ (bedrock or artificial) scaled by top width at 10-yr flow (m/m). <b>term goes to 0 if Lr ~&lt; 1.05 if <math>d_{50} &gt; 16</math> mm OR if Lr ~&lt; 1.01 if <math>d_{50} &lt; 16</math> mm</b>
$d_{50}$	=	median grain size (mm)
Imp	=	total impervious area as fraction of area ( $m^2/m^2$ )

Although well-fit, the adjusted R<sup>2</sup> values are probably overly optimistic in application. The models are more representative of “how bad an unmitigated system could become” rather than providing absolute predictions. In consequence, they should be tempered with good judgment and field indicators/local conditions. For example, San Antonio ( $d_{50}$  16 to 64 mm, depending on cross section) has experienced significant enlargement ( $A_r \sim 6$ ,  $N_g \sim 6$ ,  $N_w \sim 1.5$ ) with very little urbanization ( $L_r \sim 1$ ). This is most likely attributable to historic channelization and headcutting from below via downstream urbanization. Alternatively, Escondido has had significant urbanization ( $L_r \sim 3$ ) and no appreciable channel adjustments ( $A_r \sim 1$ ,  $N_g$ , and  $N_w < 1$ ). The apparent stability is explained by both bedrock control and coarse-bed material ( $d_{50}$  31 to 128 mm, depending on cross section).  $L_r$  is likely overestimated in this case due to probable upstream flow control from the San Dieguito Reservoir.

### 3.3.3 Response magnitude: departure from equilibrium

Models of Ng and Nw proved to be less accurate (adjusted R<sup>2</sup> 0.5 to 0.6), with more patterned residuals. This was likely due to the fact that many of our sites were still actively adjusting and the same stream/watershed parameters could have dramatically different response phases (i.e., very narrow and deep vs. very wide and moderately deep at San Timetao and Acton). Rather than predictive models, I present risk factors for whether a system is more likely to incise or braid (Table 3.4). Nearly 50% of the variance for Nw could be explained by grain size, with smaller bed material leading to a higher risk of being wider than the regional norm for stable single-thread systems. Likewise, up to 50% of the variance for Ng was explained by hardpoint distance, with more incision as one moved upstream. This was in conjunction with approximately 10% of the variance attributable to sediment imbalance (i.e., higher sediment imbalance resulted in more incision). Interestingly, by linearly combining the Ng and Nw metrics into a composite stability rating (N<sub>comp</sub>), the same terms that were significant in the enlargement functions were also significant in predicting N<sub>comp</sub> but explained less total variance.

**Table 3.4 – Risk factors for response directions**

<b>Incising Ng<sup>+</sup>Nw<sup>-</sup></b>	<b>Risk Factor</b>	<b>Braiding Nw<sup>+</sup></b>
narrow	valley width	wide
low	fraction of sand bed material	high
high	fraction of watershed burned	low
near	downstream distance to incising stream	far
<b>far</b>	<b>downstream distance to hardpoint</b> (normalized by channel width)	
<i>Common 'enlargement' risk factors: high-sediment imbalance and small d<sub>50</sub></i>		

Beyond such intuitive stability parameters, valley width, recent fires, and fraction of sand composing the bed material provided general, but not mutually exclusive, dichotomies of incising versus braiding. Because wide channels require wide valleys, Nw was positively correlated to valley width; however, this of course did not exclude incision in wider valley settings. The portion of watershed burned was more important for incising than braiding. This could be attributable to the disruption of an armor layer (i.e., by more easily mobilizing gravels), which could lead to a vertical response. It could also be caused by the infilling from fines, which, to be flushed, require corresponding incision. However, streams with a large portion of the bed-material composed of sand set in unburned watersheds had a higher probability of being braided than others. Perhaps the most obvious criticism of such a correlation is that a low proportion of sand-bed material is not necessarily a pre-response condition in an incising stream. For example, a system that is currently incising would have less sand composing the bed material due to the concentration of energy; however, that is not to say that systems with sandy beds cannot incise. A more process-based model of bank stability would involve bank materials (*sensu* Schumm (1961, 1977), Patton and Schumm (1981), and Schumm *et al.* (1984)); however, gaps in some key USDA polygons precluded correlations using soil type. Finally, and most obviously, tributaries to channels currently incising had a high risk of incision, at least initially.

Ng and Nw were ultimately better utilized as surrogates of a system's current level of departure from 'equilibrium'/reference geometries. Ng is plotted along the vertical axis and representative of the relative severity of incision, and Nw is used as a measure of lateral departure from 'reference' conditions along the horizontal axis. Nw

replaces  $N_h$  in the Watson *et al.* (1988) approach because sediment supply is both variable and difficult to estimate. The simpler scheme, presented in Figure 3.12, has utility in understanding the relative departure from equilibrium and additionally in segregating the braiding departures from the original CEM (i.e., CEM 2B and 4B).

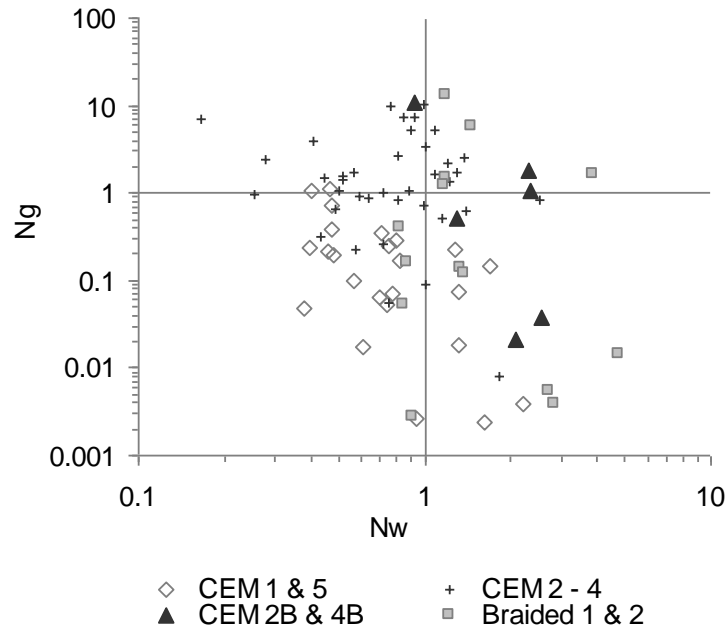


**Figure 3.12 – Dimensionless stability diagram of geotechnical bank stability ( $N_g$ ) vs. reference width ratio ( $N_w$ ) (*sensu* Watson *et al.* (1988)) with CEM stages of single-thread/incision and braided departures**

For example, once a system becomes twice as wide as the regional reference width for the given 10-yr flow ( $N_w = 2$ ), there is a high probability of braiding. Indeed, the only case of a ‘stable’ single-thread system with  $N_w > 2$  is AltPerris\_B, which is actually the transition cross section between the upstream single-thread reach and the downstream braided reach. Unless the exceptional top width is attributable to a well-connected floodplain (e.g., Challenger Park) accessed by the 10-yr flow, it is likely that the channel has become too wide to hold the flow together in one path. At the opposite

end of the abscissa is entrenchment: a high probability of incision due to the concentration of energy over too narrow of a channel. There are no 'stable' systems with top widths less than ~40% of the regional reference.

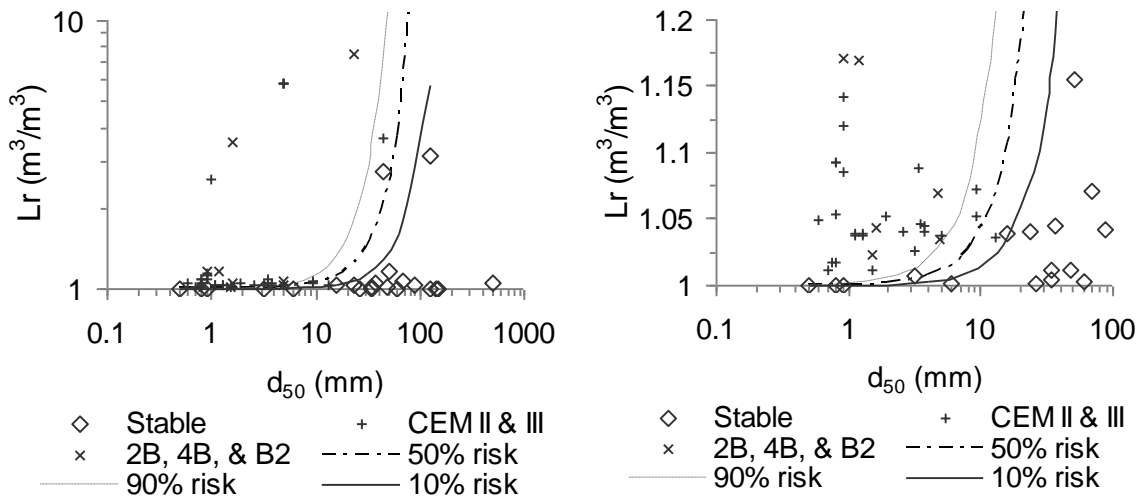
On the vertical axis, 'stable' systems (CEM 1 and 5) in both confined and unconfined valleys are generally at or well below unity ( $N_g \leq \sim 1$ ). The bulk of CEM 2 to 4 systems plot well above 1, whereas those less than 1 are most likely representative of recently failed bank dimensions or systems tending toward aggradation and floodplain reconstruction (CEM 4). Combining the two axes, braided systems that are beginning to incise or eroding into the valley wall (Braided 2) plot with unstable bank heights at widths at or well above 1. In contrast, braided channels with little/no incision occupy the lower-right quadrant with unstable widths and low banks/angles (Braided 1).

Braided systems with both stable banks and  $N_w$  near unity may be braiding primarily due to high-sediment loads. As witnessed in some of the early experimental work with channel-evolution sequences, Schumm and Parker (1973) noted that depositional phases of the CEM could result in temporary braiding with an eventual return to single-thread stability. Schumm *et al.* (1984) discussed cases of excessive deposition in Phases 4/5 that could result in braided patterns, especially at low flows. Therefore, it seems reasonable to postulate that braided channels with bandwidths that have yet to become excessively wide ( $N_w < \sim 2$ ) could eventually return to quasi-equilibrium single-thread form under the necessary sediment regime. In contrast, it is difficult to envision bandwidths greater than 3 to 4 times that of the regional reference returning to single-thread form within the time scales of interest, but data collection over larger time scales would clearly be beneficial for testing such conjectures.

### 3.4 Implications

The most basic conclusion from this study is that many/most channels in southern California are extremely sensitive to hydromodification. We found very few channels in unconfined valleys that could obtain single-thread stability without some measure of artificial control. Small degrees of development and associated sediment imbalances can create significant responses in channel form. The sediment-transport capacity ratio explained over 60% of the variance in enlargement in primarily unmitigated urban systems. It is important to recall that  $L_r$  may be underestimated due to the inherent bias in DDFs resulting from mean-daily flows rather than more frequent intervals. Yet it is possible that the lack of shear-stress partitioning may have overestimated sediment transport, potentially dampening the daily-flow bias.

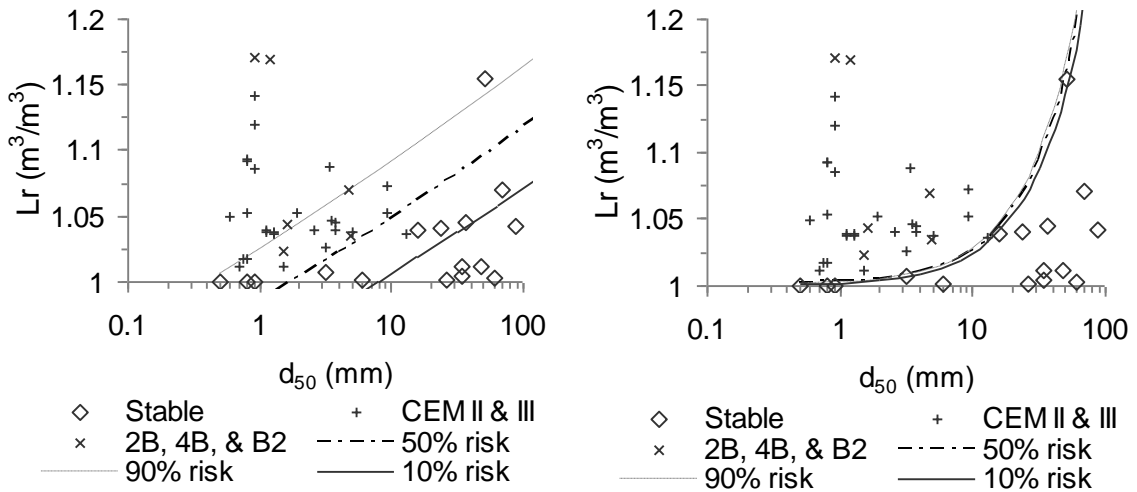
Even so, when combined with grain size,  $L_r$  provided clear stratification of channel stability using logistic-regression analysis, in which models ( $p < 0.0001$ ) and individual terms were significant ( $p < 0.05$ ). As seen in Figures 3.13 and 3.14, sand systems have essentially ‘no room’ for changes in sediment-transport capacity. Even most gravels ( $d_{50} \sim 2$  to 16 mm) appear to be extremely sensitive to seemingly nominal sediment balances (i.e.,  $L_r \sim 1.01$  to 1.05). Some capacity to absorb perturbations in erosive energy is apparent in the coarse-gravel range (i.e.,  $d_{50} \sim 16$  to 64 mm); however, true resiliency seems to require being well into the cobble range ( $d_{50} > 64$  mm) and moving toward boulders ( $d_{50} > 256$  mm). This explains the exponential logistic at the log-log scale (i.e., regressing  $\ln\{\ln(L_r)\}$  vs.  $\ln(d_{50})$ ).



(a) vertical axis log scale ranging to 10

(b) vertical axis arithmetic scale ranging to 1.2

**Figure 3.13 – Bedload ratio vs. median grain size of stable, unstable single-thread (CEM Types II and III), and unstable braided systems with superimposed logistic stability thresholds in the form  $\ln\{\ln(L_r)\}$  vs.  $\ln(d_{50})$**



(a) in the form  $\ln(L_r)$  vs.  $\ln(d_{50})$

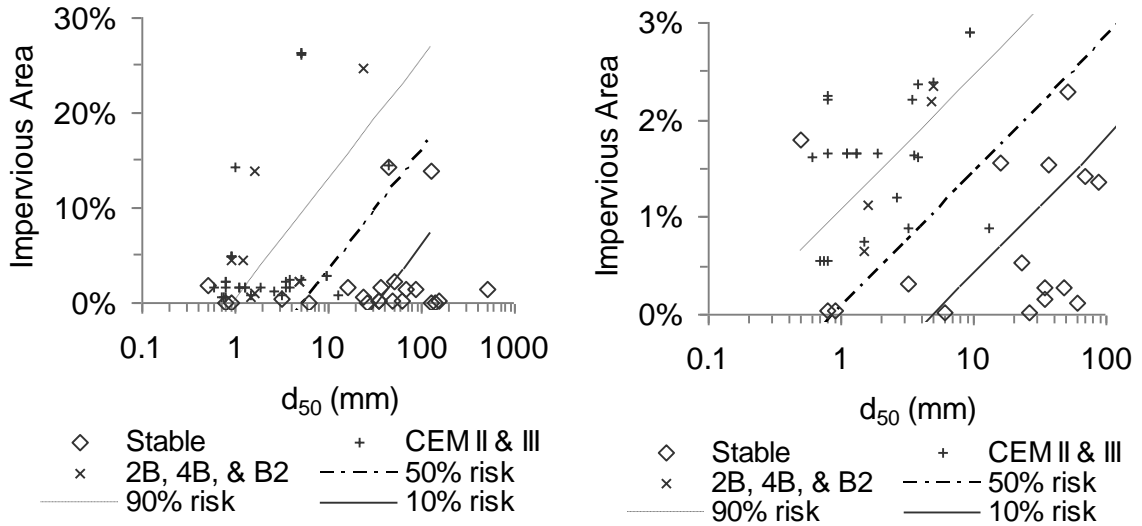
(b) in the form  $\ln\{\ln(L_r)\}$  vs.  $\ln(d_{50})$

**Figure 3.14 – Bedload ratio vs. median grain size of stable, unstable single-thread (CEM Types II and III), and unstable braided systems with superimposed logistic thresholds developed without Escondido and Borrego\_D**

Yet, with few examples of stable coarse systems in highly developed watersheds (i.e., Borrego\_D and Escondido), I tried to avoid bias by excluding those stable points with coarse beds and high Lr in an alternative model (Figure 3.14). A log-log logistic worked comparatively well in explaining the threshold at the sand/gravel range (Figure 3.14(a)). In practice, risk is probably bracketed by the two forms of the relationship (i.e., comparing identical scales of Figure 3.13(a) with Figure 3.14(a)). For example, Challenger\_A (i.e., Stable with  $L_r = 1.16$  and  $d_{50} = 51.2$  mm) was an apparent outlier in the log-log scheme (Figure 3.14(a)). Although it seemed currently stable, small levels of incision were present. Despite probable uncertainties in the hydrologic modeling of Escondido and Borrego\_D (due to large reservoir detention upstream of Escondido and at least some in-line detention at Borrego), these sites offer examples of the potential resistance of coarser materials, pointing to the value of the scheme from Figure 3.13. That is, Borrego\_D has significantly coarsened relative to downstream sections (e.g., 45 mm vs. 1 mm at Borrego\_C) and seemed to be attaining some semblance of a new equilibrium.

I also tested imperviousness in the place of the load ratio for significance in multivariate logistic regression. Although not individually significant ( $p > 0.05$ , unlike Lr), it was significant in combination with  $d_{50}$ . Figure 3.15 presents results of the same strategies (with and without Escondido and Borrego\_D), with similar stratification of stability. Consistent with Lr, minimal levels of imperviousness seem to trigger instabilities in fine-grained systems. The single outlier (Perris\_2\_B, stable at 1.8% impervious with  $d_{50} = 0.5$  mm) is both too small of a watershed for confident flow

predictions and is possibly being artificially stabilized via the remnants of a long-abandoned road embankment.



(a) with Escondido and Borrego\_D in the form impervious area vs.  $\ln(d_{50})$

(b) without Escondido and Borrego\_D in the form impervious area vs.  $\ln(d_{50})$

**Figure 3.15 – Impervious area vs. median grain size of stable, unstable single-thread (CEM Types II and III), and unstable braided systems with superimposed logistic thresholds developed**

Finally, it should be noted that these figures do not account for responses in undeveloped systems attributable to headcutting from below, channelization, or other legacy effects. That is, large responses were observed in undeveloped and even coarse systems that were not attributable to upstream urbanization (i.e., matching  $L_r$  on a new development would not ensure stability in channelized systems).

### 3.4.1 Mitigation implications

Arguably the largest implication of this study is the importance of maintaining sediment continuity in reducing the risk of adverse channel adjustments to

hydromodification. It goes without saying that the most effective way to do this is by leaving a watershed undeveloped. Conceding that urbanization will proceed, at least in some places, the logical path is to ensure that sites are designed with the goal of matching the natural-flow regime. Regarding channel stability, hydrograph matching should at least be attempted at all flows above the critical flow for entrainment of the channel-bed material ( $Q_c$ ). In many southern California systems, this is essentially all flows which clearly impose practical limitations such as minimum pipe sizes for retention/detention outfalls.

Consequently, managers could offer a range of site-specific mitigation options that are acceptable to local stakeholders and attempt to match the pre-developed cumulative sediment-transport potential. Although not intended as design guidelines, I present two alternatives using data at Borrego\_C in which total sediment bedload capacity could be matched to the undeveloped regime (Figure 3.16). The ‘detention’ scenario achieves this by providing complete detention for all events but the highest flows, which in this case would be those greater than the 5- to 10-yr event. That is, sediment transport could be matched by retaining all bin flows below a daily-mean flow of  $3.26 \text{ m}^3/\text{s}$ , allowing larger flows to pass unmitigated. All smaller events could be retained and eventually infiltrated, evaporated, used as gray-water, etc. Yet despite matching total transport capacity over the 25-yr scenario, this scheme is probably the furthest from ensuring ecological/geomorphic function and the riskiest in terms of overall stability and even flood control.

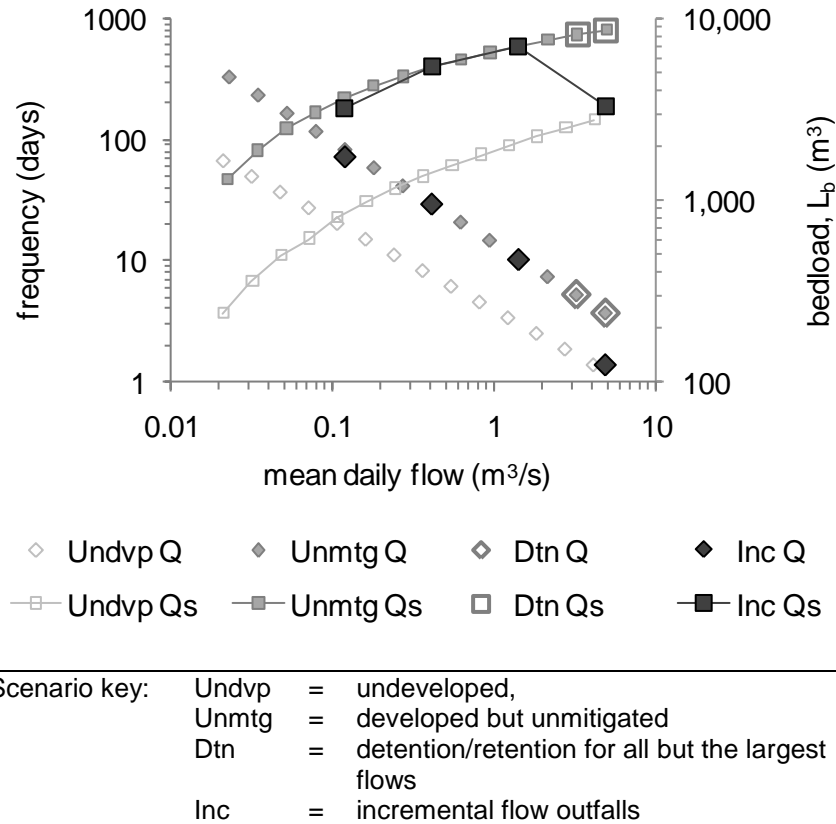


**Figure 3.16 – Hypothetical mitigation scenarios at Borrego\_C that match the cumulative sediment transport of the pre-developed regime using various detention/retention designs.**

An alternative could be a staggered detention facility (*sensu* Distributed Runoff Control (DRC); MacRae (1991, 1993, 1997)) that releases flows at incremental rates above a minimum retention/infiltration requirement (i.e., “Inc” in Figure 3.16). By designing outfalls at four flows (bins 16, 19, 22, and 25 at 0.12, 0.41, 1.4, and 4.9 m<sup>3</sup>/s), bed material is entrained more regularly and at flows that more closely resemble the undeveloped hydrograph range. Implementing such a scheme in conjunction with low impact development (LID) technologies that promote infiltration and slow runoff at the source would likely prove to be more beneficial for both stability and ecologic function.

### 3.5 Summary and Conclusions

Based on a process-based understanding of how urbanization affects flow regimes, erosive energy, and sediment transport across regional settings, the central conclusion from this dissertation is that channels in southern California generally exhibit extreme sensitivity to hydromodification in terms of morphologic response potential and overall channel stability. In Chapter 1, I demonstrated pronounced increases in magnitudes of instantaneous peak flows, especially at more frequent events (e.g.,  $\sim 5x Q_{1.5}$ ,  $\sim 3x Q_2$  and  $\sim 1.4x Q_5$  at 10% imperviousness), and substantially longer durations (e.g.,  $\sim 2$  to 3 times as many days at 10% imperviousness) of all sediment-transporting flows in urban watersheds. The DDF model that was developed to represent such changes in cumulative flow durations was novel in two ways: 1) its scale, magnitude, and shape components are predicted using a watershed's physical properties rather than scaling based on a single flow and a nearby gauge, and 2) it accounts for the effects of urbanization using direct measures of total impervious area (TIA), which was particularly significant ( $p < 0.05$  in 8 of 11 models) in describing the magnitude (i.e., coefficient). TIA proved to be an effective hydrologic surrogate for urbanization in southern California due to the overall lack of flow control at the subdivision scale to date, but (hopefully and) not necessarily the case with future development. Yet, as demonstrated in subsequent chapters, TIA was not a statistically-significant predictor of morphologic channel response when considered independent of setting and sediment transport.

Using the hydrologic models from Chapter 1, Chapter 2 focused on identifying relative susceptibilities to hydromodification across regional settings via simple measures of erosive energy and resistance. Geomorphic thresholds for incising, braiding, and mass

wasting were developed using logistic-regression analysis as a key component of a screening tool for assessing channel susceptibility to hydromodification. Beyond their high performance – correctly classifying unstable states in ~90% of the cases – using a probability-based framework to assess channel susceptibility is original in that managers can directly quantify the proximity to a given threshold, representing the relative risk of an adverse morphologic response. An added benefit to such a scheme is its flexibility: jurisdictions can screen systems based on locally acceptable levels of risk (e.g., 10% vs. 50% probability of response). The geomorphic thresholds consistently demonstrated that systems in southern California respond at much lower levels of energy and bank heights than other parts of the country, which, consistent with field observations, historic analyses, and previous literature, suggest that these systems are inherently more susceptible to hydromodification.

In this final Chapter, I presented a range of process-based response models covering relative magnitudes, directions, and stochastic risk of channel adjustments. The descriptive CEM provided empirical evidence for planform changes (such as single-thread to braided) that are significant departures from the original CEM (Schumm et al. 1984). Through dimensionless stability schemes measuring relative departures from equilibrium both vertically via bank heights ( $N_g$ ) and laterally via top widths ( $N_w$ ) (*sensu* Watson *et al.* (1988)), a manager can assess the degree of instability a channel has in its current form. Multivariate regression of these parameters identified mostly intuitive risk factors for whether a channel may incise (e.g., proximate to confluence with an incising stream, and recent fires) or braid (e.g., wide valley and bed-material composition high in sand). However, there were not enough data in either space or time to develop full

models and/or classification regression trees to offer more rigorous predictions of directional response.

There were enough data on streams with relatively sufficient time to adjust to current development levels such that several relatively well-fit ( $R^2 \geq 0.8$ ) ‘enlargement’ models were developed. Individually explaining over 60% of the variance was the process-based sediment-transport capacity ratio (Lr) that compared estimates of total bedload over 25-yr simulations of urban (actual) and undeveloped flow regimes using the DDF models derived in Chapter 1. Another significant finding was that enlargement substantially increased as one moved upstream from a hardpoint. Models that replaced Lr with total impervious area were only slightly less significant but less representative of process and less meaningful for mitigation. In general, models confirmed hypotheses that enlargement could become severe with unmitigated hydromodification (e.g., ~ 5x enlargement where  $D_{hp}/W_{10} \sim 30$  with  $Lr \sim 3.5$  and/or ~15% imperviousness, or ~2x enlargement with  $Lr \sim 1.2$  and/or ~5% imperviousness), but they should be tempered with the understanding that they are intended to estimate relative magnitudes of “how bad” an unmitigated system might become as opposed to predicting absolute channel enlargement.

The models are better used in the context of what they imply to mitigation: that the risk of adverse morphologic channel response is best reduced by minimizing increases in sediment-transport capacity on future developments. This central conclusion was further confirmed with statistically-significant ( $p < 0.0001$ ) logistic-regression models of significant ( $p < 0.05$ ) process-based variables Lr and  $d_{50}$ , which suggested that fine-grained systems, especially those less than 16 mm, have little capacity to absorb any

increases in sediment-transport potential. As such, design goals for new developments should target schemes that match pre-developed sediment-transport potential using combinations of at-the-source infiltration via LID and creative retention/detention structures. Although in-stream controls and/or complete retention/infiltration can also reduce risks, they do not ensure ecological/geomorphic function or even aesthetic benefits of free-flowing ephemeral channels.

Finally, I must reiterate that even a perfectly matched pre-developed hydrograph over all flows does not guarantee channel stability. Rather, it only *reduces the risk of increased* channel instability. As mentioned previously, most channels of southern California are inherently dynamic with natural fluxes in sediment supply and corresponding periods of aggradation, flushing, and degradation. Even the best hydrologically-matched development could disrupt the sediment supply, suggesting that overcontrol may be warranted. Furthermore, simply matching  $L_r$  does not address legacy effects such as historic channelization or overgrazing. Neither does it prevent responses from poor outfall designs or headcutting from below via downstream urbanization.

But to quote the eternal optimist Franklin Delano Roosevelt, “we must try.” The status quo only ensures continued channel instability and environmental degradation. Despite their uncertainties, the novel tools developed in this dissertation are rooted in a physical understanding and calibrated to regionally expansive hydrogeomorphic data sets. Through this improved, process-based understanding of the effects of hydromodification, the focus can now be shifted to more of an engineering-design problem; by which, through a variety of innovative mitigation schemes, adaptive management, monitoring, and feedback, the science and the profession can continue to move forward.

### **3.6 Acknowledgements**

I would like to thank numerous organizations and individuals who contributed to this research. Funding was provided in part by the State of California and San Diego County. Eric Stein of the Southern California Coastal Water Research Project (SCCWRP) played a primary role in acquiring research funds and project management. Fellow Colorado State University graduate student Dave Dust was instrumental in field-data collection and is credited with most of the site photographs. SCCWRP staff, including Becky Schaffner, Liesl Tiefenthaler, Greg Lyon, and Jeff Brown, acquired equipment, provided logistics, assisted with data collection, and graciously offered GIS assistance/training. Stillwater Sciences conducted modeling site surveys and provided reviews/guidance throughout various project phases. Among others, I would like to acknowledge Derek Booth, Scott Dusterhoff, and Alexander Wong.

### **3.7 References**

- Andrews, E.D., 1980. Effective and bankfull discharges of streams in the Yampa river basin, Colorado and Wyoming. *Journal of Hydrology*, 46: 311-330.
- Andrews, E.D., 1984. Bed-material entrainment and hydraulic geometry of gravel-bed rivers in Colorado. *Geological Society of America Bulletin*, 95: 371-378.
- Begin, Z.B. and Schumm, S.A., 1979. Instability of alluvial valley floors: A method for its assessment. *Transcripts of the American Society of Agricultural Engineering*, 22: 347-350.
- Biedenharn, D.S., Copeland, R.R., Thorne, C.R., Soar, P.J., Hey, R.D., and Watson, C.C., 2000. Effective Discharge Calculation: A Practical Guide. ERDC/CHLI TR-00-

- 15, U.S. Army Corps of Engineers, Engineer Research and Development Center, Coastal and Hydraulics Laboratory, Vicksburg, MS.
- Biedenharn, D.S., Elliot, C.M. and Watson, C.C., 1997. The WES Stream Investigation and Streambank Stabilization Handbook. U. S. Army Engineer Waterways Experiment Station, Vicksburg, Mississippi, 338 pp.
- Biedenharn, D.S., Thorne, C.R., Soar, P.J., Hey, R.D. and Watson, C.C., 2001. Effective discharge calculation guide. *International Journal of Sediment Research*, 16(4): 445-459.
- Bledsoe, B.P., Watson, C.C. and Biedenharn, D.S., 2002. Quantification of incised channel evolution and equilibrium. *Journal of the American Water Resources Association*, 38(3): 861-870.
- Booker, F.A., Dietrich, W.E. and Collins, L.M., 1993. Runoff and erosion after the Oakland firestorm. *California Geology*, 46: 159-173.
- Brice, J.C., 1981. Stability of Relocated Stream Channels. FHWA/RD-80/158, Federal Highways Administration National Technical Information Service, Washington DC.
- Brookes, A., 1988. Channelized Rivers: Perspectives for Environmental Management. John Wiley & Sons Ltd., Chichester, UK.
- Bull, W.B., 1997. Discontinuous ephemeral streams. *Geomorphology*, 19(3-4): 227-276.
- Bunte, K. and Abt, S.R., 2001. Sampling surface and subsurface particle-size distributions in wadable gravel-and cobble-bed streams for analyses in sediment transport, hydraulics, and streambed monitoring. In: F.S. U.S. Department of

- Agriculture (Editor), Gen. Tech. Rep. RMRS-GTR-74, Rocky Mountain Research Station Fort Collins, CO, pp. 428.
- Chien, N., 1956. The present status of research on sediment transport. *Transactions of the American Society of Civil Engineers*, 121: 833-868.
- Coleman, D., MacRae, C. and Stein, E.D., 2005. Effect of Increases in Peak Flows and Imperviousness on the Morphology of Southern California Streams. Stormwater Monitoring Coalition, Southern California Coastal Water Research Project, Westminster, CA.
- Downs, P., 1995. Estimating the probability of river channel adjustment. *Earth Surface Processes and Landforms*, 20: 687-705.
- Dust, D.D. and Bunte, K., 2008. Rigid and flexible procedures for combining volumetric pebble counts with sieve gradations by mass. Pers. Comm.
- Emmett, W.W., 1975. The channels and waters of the upper Salmon River, Idaho. Professional Paper 870A. U.S. Geological Survey, Washington, DC.
- Fredsøe, J., 1978. Meandering and braiding of rivers. *Journal of Fluid Mechanics*, 84: 609-624.
- Gabet, E.J. and Dunne, T., 2002. Landslides on coastal sage-scrub and grassland hillslopes in a severe El Nino winter: The effects of vegetation conversion on sediment delivery. *Geol. Soc. of Am. Bull.*, 114(8): 983-990.
- Gabet, E.J. and Dunne, T., 2003. A stochastic sediment delivery model for a steep Mediterranean landscape. *Water Resources Research*, 39(9): 12.

- Galster, J.C., Pazzaglia, F.J., Hargreaves, B.R., Morris, D.P., Stephen, C., Peters, S.C., and Weisman, R.N., 2006. Effects of urbanization of watershed hydrology: The scaling of discharge with drainage area. *Geology*, 34(9): 713-716.
- Graf, W.L., 1981. Channel instability in a braided sand-bed river. *Water Resources Research*, 17: 1087-1094.
- Graf, W.L., 1988. Fluvial Processes in Dryland Rivers. Springer-Verlag, Berlin.
- Hammer, T.R., 1972. Stream channel enlargement due to urbanization. *Water Resources Research*, 8: 139-167.
- Harrelson, C.C., Rawlins, C. L., Potyondy, J. P., 1994. Stream channel reference sites: an illustrated guide to field technique. In: F.S. U. S. Department of Agriculture, Rocky Mountain Forest and Range Experiment Station (Editor), Gen. Tech. Rep. RM-245, Fort Collins, CO, pp. 61.
- Hey, R.D., 1975. Design discharge for natural channels. In: R.D. Hey and T.D. Davies (Editors), Science, Technology and Environmental Management, Saxon House, pp. 73-88.
- Hey, R.D., 1997. Channel response and channel forming discharge: literature review and interpretation. Final Report, U.S. Army Contract Number R&D 6871-EN-01.
- Holmquist-Johnson, C.L., 2002. Computational methods for determining effective discharge in the Yazoo River Basin, Mississippi. MS Thesis, Colorado State University, Fort Collins, CO.
- Julien, P.Y., 1998. Erosion and Sedimentation. Cambridge University Press, Cambridge, 280 pp.

- Knighton, A.D., 1998. Fluvial Forms and Processes: A New Perspective. John Wiley & Sons Ltd., New York, NY, 383 pp.
- Konrad, C.P. and Booth, D.B., 2002. Hydrologic trends associated with urban development for selected streams in the Puget Sound Basin, Western Washington. Water-Resources Investigations Report 02-4040, U.S. Geological Survey, Tacoma, WA.
- Lavé, J. and Burbank, D., 2004. Denudation processes and rates in the Transverse Ranges, southern California: erosional response of a transitional landscape to external and anthropogenic forcing. *J. Geophys. Res.*, 109.
- Leopold, L.B., 1994. A View of the River. Harvard University Press, Cambridge, MA, 29 pp.
- Los Angeles County Flood Control District, 1959. Report on debris reduction studies for mountain watersheds of Los Angeles County. Los Angeles County Flood Control District, Los Angeles, CA, pp. 164.
- MacRae, C.R., 1991. A procedure for design of storage facilities for instream erosion control in urban streams. Ph.D. Thesis, University of Ottawa, Ottawa, Canada.
- MacRae, C.R., 1993. An alternate design approach for the control of instream erosion potential in urban watersheds. In: J. Marsalek and H.C. Torno (Editors), Urban Storm Drainage: Proceedings of the Sixth International Conference, IAHR/IAWQ Joint Committee on Urban Storm Drainage, Niagra Falls, Ontario, Canada, pp. 1086-1091.
- MacRae, C.R., 1997. Experience from morphological research on Canadian streams: is control of the two-year frequency runoff event the best basis for stream channel

- protection? In: L.A. Roesner (Editor), Effects of Watershed Development and Management on Aquatic Ecosystems, Proceedings of an Engineering Conference. ASCE, pp. 144-162.
- MacRae, C.R. and Rowney, A.C., 1992. The role of moderate flow events and bank structure in the determination of channel response to urbanization. In: D. Shrubsole (Editor), Resolving Conflicts and Uncertainty in Water Management, Proc. of the 45th Annual Conference of the Canadian Water Resources Association. Canadian Water Resource Association, Kingston, Ontario, Canada, pp. 12.1-12.21.
- Manning, R., 1889. On the flow of water in open channels and pipes. *Transactions of the Institution of Civil Engineers of Ireland*, 20: 161-195.
- Meyer-Peter, E. and Müller, R., 1948. Formulas for bed-load transport. Proc. 2nd Meeting International Association for Hydraulic Research, Stockholm, pp. 39-64.
- Montgomery, D.R., 1999. Process domains and the river continuum. *Journal of the American Water Resources Association*, 35(2): 397-410.
- Montgomery, D.R. and Buffington, J.M., 1997. Channel-reach morphology in mountain drainage basins. *Geol. Soc. of Am. Bull.*, 109(5): 596-611.
- Montgomery, D.R. and Buffington, J.M., 1998. Channel processes, classification, and response. In: R. Naiman and R. Bilby (Editors), River Ecology and Management, Springer-Verlag New York Inc., New York, NY, pp. 13-42.
- Mooney, D.M., 2007. SIAM - Sediment Impact Analysis Methods. Ph.D. Dissertation, Colorado State University, Fort Collins, CO, 375 pp.

- Nanson, G.C. and Croke, J.C., 1992. A genetic classification of floodplains. *Geomorphology*, 4(459-486).
- Osterkamp, W.R., 1980. Sediment-morphology relations of alluvial channels. In: Proc., Symposium on Watershed Management, pp. 188-199.
- Osterkamp, W.R. and Hedman, E.R., 1982. Perennial-stream flow characteristics related to channel geometry and sediment in Missouri River basin. United States Geological Survey Professional Paper 1242.
- Parker, G., 1990. Surface-based bedload transport relation for gravel rivers. *Journal of Hydraulic Research*, 28(4): 417-436.
- Patton, P.C. and Schumm, S.A., 1981. Ephemeral stream processes: Implications for studies of Quaternary valley fills. *Quaternary Research*, 15: 24-43.
- Pickup, G. and Warner, R.F., 1976. Effects of hydrologic regime on magnitude and frequency of dominant discharge. *Journal of Hydrology*, 29: 51-75.
- Poff, N.L., Bledsoe, B.P. and Cuhaciyan, C.O., 2006. Hydrologic variation with land use across the contiguous United States: Geomorphic and ecological consequences for stream ecosystems. *Geomorphology*, 79(3-4): 264-285.
- Raff, D.A., Bledsoe, B.P. and Flores, A.N., 2004. GeoTool User's Manual. Colorado State University, Fort Collins, CO.
- Rosgen, D., 1996. Applied River Morphology. Wildland Hydrology, Pagosa Springs, Colorado, 352 pp.
- Santa Clara, 2004. Hydromodification Management Plan Report, Santa Clara Valley Urban Runoff Pollution Prevention Program, Sunnyvale, CA.

- Schumm, S.A., 1961. The effect of sediment characteristics on erosion and deposition in ephemeral stream channels. Professional Paper 352C, U. S. Geological Survey.
- Schumm, S.A., 1971. Fluvial geomorphology: the historical perspective. In: H.W. Shen (Editor), River Mechanics, Fort Collins, CO, pp. 4-1 - 4-30.
- Schumm, S.A., 1977. The Fluvial System. Wiley - Interscience, New York, NY, 338 pp.
- Schumm, S.A., 1991. To Interpret the Earth: Ten Ways to be Wrong. Cambridge University Press, 133 pp.
- Schumm, S.A., Harvey, M.D. and Watson, C.C., 1984. Incised channels: Morphology, Dynamics, and Control. Water Resources Publications, Littleton, CO.
- Schumm, S.A. and Parker, R., 1973. Implications of complex response of drainage systems for Quaternary alluvial stratigraphy. *Nature, Physical Science*, 243: 99-100.
- Simon, A., 1989. A model of channel response in disturbed alluvial channels. *Earth Surface Processes and Landforms*, 14(1): 11-26.
- Simons, D.B. and Albertson, M.L., 1963. Uniform water conveyance channels in alluvial material. *Transactions of the American Society of Civil Engineers*, 128: 65-107.
- Soar, P.J., 2000. Channel restoration design for meandering rivers. Ph.D. Thesis, University of Nottingham, Nottingham, UK.
- Taylor, B.D., 1981. Sediment management for southern California mountains, coastal plains and shoreline, Part B: Inland sediment movements by natural processes. California Institute of Technology, Pasadena, CA.
- Trimble, S.W., 1997. Contribution of stream channel erosion to sediment yield from an urbanizing watershed. *Science*, 278: 1442-1444.

- U.S. Army Corps of Engineers, 2009. HEC-RAS 4.0. Hydrologic Engineering Center - River Analysis System, Davis, CA.
- Watson, C.C., Biedenharn, D.S. and Bledsoe, B.P., 2002. Use of incised channel evolution models in understanding rehabilitation alternatives. *Journal of the American Water Resources Association*, 38(1): 151-160.
- Watson, C.C., Dubler, D. and Abt, S.R., 1997. Demonstration erosion control project report. submitted to U.S. Army Engineer Waterways Experiment Station, Vicksburg, MS.
- Watson, C.C., Harvey, M.D., Biedenharn, D.S. and Combs, P.G., 1988. Geotechnical and hydraulic stability numbers for channel rehabilitation: Part I, the approach. In: S.R. Abt, J. Gessler and D.B. Booth (Editors), Proceedings of the ASCE 1988 National Conference on Hydraulic Engineering, Colorado Springs, CO, pp. 120-125.
- Wilcock, P.R. and Crowe, J.C., 2003. Surface-based Transport Model for Mixed-Size Sediment. *Journal of Hydraulic Engineering*, 129(2): 120-128.
- Wilcock, P.R. and Kenworthy, S.T., 2002. A two-fraction model for the transport of sand/gravel mixtures. *Water Resources Research*, 38(10).
- Williams, G.P., 1978. Bank-full discharge of rivers. *Water Resources Research*, 14(6): 1141-1154.
- Wolman, M.G. and Gerson, R., 1978. Relative scales of time and effectiveness of climate in watershed geomorphology. *Earth Surface Processes*, 3: 189-208.
- Wolman, M.G. and Miller, J.P., 1960. Magnitude and frequency of forces in geomorphic processes. *Journal of Geology*, 68: 54-74.

Wong, M. and Parker, G., 2006. Reanalysis and Correction of Bed-Load Relation of Meyer-Peter and Müller Using Their Own Database. *Journal of Hydraulic Engineering*, 132(11): 1159-1168.

Yu, B. and Wolman, M.G., 1987. Some dynamic aspects of river geometry. *Water Resources Research*, 23(3): 501-509.

### **3.8 GIS Data Sources**

**Cal-Atlas:** *2000 and 2007 Roadway Shapefiles*, State of California geospatial clearinghouse, [gis.ca.gov](http://gis.ca.gov).

**Google Earth:** *Present-day Aerial Photography*, [earth.google.com](http://earth.google.com).

**National Oceanic and Atmospheric Administration (NOAA):** *Precipitation Intensities for 2-year, 24-hour Storm*, <http://www.nws.noaa.gov/oh/hdsc/noaaatlas2.htm> (Atlas 2) and [hdsc.nws.noaa.gov/hdsc/pfds/pfds\\_gis.html](http://hdsc.nws.noaa.gov/hdsc/pfds/pfds_gis.html) (Atlas 14).

**United States Department of Agriculture (USDA), Natural Resources Conservation Service (NRCS):** *Soil Surveys, Average Annual Precipitation Shapefile (1961 - 1990)*, <http://datagateway.nrcs.usda.gov/>.

**United States Geological Survey (USGS):** *Historical Aerial Photography and Quadrangle Topographic Maps, National Elevation Dataset (NED), 2001 Impervious Raster, National Hydrography Dataset (NHD), Average Annual Precipitation Shapefile (1900 - 1960)*, <http://seamless.usgs.gov>.

**APPENDIX A**  
**GAUGE DATA**

## **A.1 Identification Numbers**

Gauges were sorted alphabetically and then assigned an abbreviated identification (ID) number. This ID number is used as the first column in all tables in this appendix for restricted space allocation. The three gauges with pre- and post-periods are tabulated as # (for entire record), #.1 (for pre-period), and #.2 (for post-period). In the following tables, these are presented in italic font.

**Table A.1 – Primary identification**

ID	USGS Gauge Name	USGS Gauge No.	Latitude	Longitude	HUC8	Dry
1	AGUACALIENTECNRWARNERSPRINGS	11031500	33.28861111	-116.6530556	18070303	0
2	ALISOCAELTORO	11047500	33.62611111	-117.6841667	18070301	0
3	ANDREASCNRPALMSPRINGS	10259000	33.76	-116.5491667	18100200	1
4	ARROYOSECNRPASADENA	11098000	34.22222222	-118.1766667	18070105	0
5	ARROYOSIMINRSIMI	11105850	34.27305556	-118.7869444	18070103	0
5.1	<i>ArroyoSimiPreUrban</i>				18070103	0
5.2	<i>ArroyoSimiPostUrban</i>				18070103	0
6	ARROYOTRABUCOASANJUANCAPISTRANO	11047300	33.49833333	-117.665	18070301	0
7	BIGROCKCNRVALYERMO	10263500	34.42083333	-117.8386111	18070106	0
8	BORREGOPALMCNRBORREGOSPRINGS	10255810	33.27888889	-116.4291667	18100200	1
9	BUCKHORNCNRVALYERMO	10263900	34.34305556	-117.9202778	18090206	0
10	CAJONCNRKEENBROOK	11063000	34.26694444	-117.4563889	18070203	0
11	CAMPOCNRCAMPO	11012500	32.59111111	-116.5247222	18070305	1
12	COYOTECREEKNEAROKVIEW	11117600	34.41666667	-119.3697222	18070101	0
13	CUCAMONGACNRUPLAND	11073470	34.17944444	-117.6280556	18070203	0
14	DEEPCNRPALMDESERT	10259200	33.63111111	-116.3913889	18100200	1
15	DELUZCNRFALLBROOK	11044900	33.36972222	-117.3216667	18070302	0
16	ETWINCNRRARROWHEADSPRINGS	11058500	34.17916667	-117.2647222	18070203	0
17	FISHCNRDUARTE	11084500	34.16583333	-117.9233333	18070106	0
18	HONDABARRANCANRSOMIS	11107000	34.26888889	-119.0488889	18070103	0
19	HOPPERCREEKNEARPIRU	11110500	34.40083333	-118.8255556	18070102	0
19.1	<i>HopperPreperiod</i>				18070102	0
19.2	<i>HopperPostperiod</i>				18070102	0
20	KEYSCTRIBAVALLEYCENTER	11040200	33.22916667	-117.0358333	18070303	0
21	LASFLORESCNROCEANSIDE	11046100	33.29222222	-117.4558333	18070301	0
22	LITTLEDALTONCNRGLENDORA	11086500	34.1675	-117.8375	18070106	0
23	LITTLESANGORGONIOCNRBEAUMONT	11056500	34.02916667	-116.9452778	18070203	0
24	LITTLESANTANITACNRSIERRAMADRE	11100500	34.18694444	-118.0430556	18070105	0
25	LITTLETUJUNGACNRSANFERNANDO	11096500	34.27444444	-118.3716667	18070105	0
26	LONEPINECNRKEENBROOK	11063500	34.26638889	-117.4630556	18070203	0
27	LOSCOCHESCNRLAKESIDE	11022200	32.83611111	-116.8994444	18070304	0
28	LOSPENASQUITOSCNRPOWAY	11023340	32.94305556	-117.1208333	18070304	0
29	LOSPENASQUITOSCNBLPOWAYCNRPOWAY	11023330	32.94916667	-117.0691667	18070304	0
30	MISSIONCNRDESERTHOTSPRINGS	10257600	34.01111111	-116.6272222	18100200	1
31	NFMATILJA	11116000	34.4925	-119.3055556	18070101	0
32	PALMCYCNRPALMSPRINGS	10258500	33.745	-116.5347222	18100200	1
33	PECHANGACNRTEMECULA	11042631	33.46416667	-117.1238889	18070302	0
34	ROGERSCNRAZUSA	11084000	34.16527778	-117.9055556	18070106	0
35	SANANTONIOCACASITASSPRINGS	11117500	34.38027778	-119.3036111	18070101	0
36	SANDIEGOCATCULVERDRNRIRVINE	11048500	33.68166667	-117.8086111	18070204	0
36.1	<i>SanDiegoPreUrban</i>				18070204	0
36.2	<i>SanDiegoPostUrban</i>				18070204	0
37	SANFELIPECNRRJULIAN	10255700	33.11861111	-116.4344444	18100200	1
38	SANJUANCNRSANJUANCAPISTRANO	11046500	33.51888889	-117.6241667	18070301	0

ID	USGS Gauge Name	USGS Gauge No.	Latitude	Longitude	HUC8	Dry
39	SANMATEOCNRSANCLEMENTE	11046300	33.47083333	-117.4722222	18070301	0
40	SANTAANACNROAKVIEW	11117800	34.42361111	-119.3402778	18070101	0
41	SANTAANITACNRSIERRAMADRE	11100000	34.19166667	-118.0163889	18070105	0
42	SANTAMARIACNRRAMONA	11028500	33.05222222	-116.9447222	18070304	0
43	SANTAPAUACNRSANTAPAUOLA	11113500	34.41333333	-119.0813889	18070102	0
44	SANTIAGOCAMODJESKA	11075800	33.71277778	-117.6441667	18070203	0
45	SWEETWATERNRDESCANSO	11015000	32.83472222	-116.6222222	18070304	0
46	TAHQUITZCNRPALMSPRINGS	10258000	33.805	-116.5583333	18100200	1
47	TOPANGACNRTOPANGABCH	11104000	34.06444444	-118.5861111	18070104	0
48	TUJUNGACBMILLCNRCOLBYRANCH	11094000	34.30916667	-118.1444444	18070105	0
49	VALLECITOCNRJULIAN	10255850	32.98611111	-116.4194444	18100200	1
50	VENTURARNRMEINERSOAKS	11116550	34.465	-119.2888889	18070101	0
51	WATERMANCANYONCREEKNRARROWHEADSPRINGS	11058600	34.18583333	-117.2722222	18070203	0
52	WFSANLUISREYRNRWARNERSPRINGS	11033000	33.29666667	-116.7588889	18070303	0

**Table A.2 – Measures of urbanization past and present**

ID	'Present Day'			During Peak Record						
	Impervious	Road Density		Fraction of Gauge Years > X% Impervious						
	2001	2000	2007	1.5%	5%	7.5%	10%	15%	Maximum	Average
	<i>Impv01</i>	<i>RdInsty00</i>	<i>RdInsty07</i>	<i>Imp1</i>	<i>Imp5</i>	<i>Imp7</i>	<i>Imp10</i>	<i>Imp15</i>	<i>ImpMax</i>	<i>ImpAv</i>
(%)	(mi/mi <sup>2</sup> )	(mi/mi <sup>2</sup> )	(yr/yr)	(yr/yr)	(yr/yr)	(yr/yr)	(yr/yr)	(%)	(%)	
1	0.08%	0.74	0.78	-	-	-	-	-	0.08%	0.08%
2	20.28%	10.90	10.94	0.23	0.11	0.02	-	-	8.05%	1.42%
3	0.00%	0.00	0.00	-	-	-	-	-	0.00%	0.00%
4	0.46%	1.55	1.59	-	-	-	-	-	0.47%	0.37%
5	10.02%	6.23	6.57	1.00	0.48	0.28	-	-	8.59%	4.92%
5.1	10.02%	6.23	6.57	1.00	-	-	-	-	4.72%	2.62%
5.2	10.02%	6.23	6.57	1.00	0.96	0.56	-	-	8.59%	7.27%
6	18.78%	8.60	8.62	1.00	1.00	0.80	0.80	0.55	18.78%	14.23%
7	0.44%	1.07	1.08	-	-	-	-	-	0.45%	0.37%
8	0.04%	0.31	0.33	-	-	-	-	-	0.04%	0.03%
9	0.18%	0.23	0.23	-	-	-	-	-	0.16%	0.16%
10	1.38%	2.99	2.99	-	-	-	-	-	1.28%	0.79%
11	0.52%	2.41	2.37	-	-	-	-	-	0.54%	0.45%
12	0.02%	0.82	0.83	-	-	-	-	-	0.02%	0.02%
13	0.03%	0.37	0.37	-	-	-	-	-	0.03%	0.03%
14	0.66%	0.93	0.93	-	-	-	-	-	0.68%	0.60%
15	0.30%	2.32	2.36	-	-	-	-	-	0.31%	0.25%
16	0.69%	1.02	1.02	-	-	-	-	-	0.72%	0.55%
17	0.07%	1.59	1.62	-	-	-	-	-	0.07%	0.06%
18	0.30%	2.25	2.27	-	-	-	-	-	0.27%	0.25%
19	0.05%	0.44	0.85	-	-	-	-	-	0.04%	0.04%
19.1	0.05%	0.44	0.85	-	-	-	-	-	0.04%	0.04%
19.2	0.05%	0.44	0.85	-	-	-	-	-	0.04%	0.04%
20	2.73%	5.70	5.97	1.00	-	-	-	-	2.67%	2.48%
21	0.84%	0.99	1.04	-	-	-	-	-	0.87%	0.72%
22	0.11%	2.70	2.59	-	-	-	-	-	0.10%	0.09%
23	0.51%	2.53	2.53	-	-	-	-	-	0.47%	0.42%
24	0.12%	0.64	1.15	-	-	-	-	-	0.11%	0.10%
25	1.00%	2.07	2.62	-	-	-	-	-	0.82%	0.67%
26	0.44%	2.04	2.04	-	-	-	-	-	0.44%	0.43%
27	9.06%	6.15	6.26	1.00	1.00	1.00	-	-	9.06%	8.86%
28	20.11%	7.30	7.57	1.00	1.00	0.87	0.78	0.48	20.11%	14.21%
29	17.17%	6.28	6.60	1.00	1.00	1.00	0.84	0.03	15.19%	12.17%
30	0.06%	0.16	0.16	-	-	-	-	-	0.07%	0.06%
31	0.10%	0.73	0.70	-	-	-	-	-	0.09%	0.09%
32	0.28%	0.71	0.72	-	-	-	-	-	0.28%	0.24%
33	1.57%	1.90	1.90	0.68	-	-	-	-	1.57%	1.41%
34	0.07%	1.31	1.31	-	-	-	-	-	0.06%	0.06%
35	1.24%	3.94	4.44	-	-	-	-	-	1.23%	1.10%

ID	'Present Day'			During Peak Record						
	Impervious	Road Density		Fraction of Gauge Years > X% Impervious						
	2001	2000	2007	1.5%	5%	7.5%	10%	15%	Maximum	Average
	<i>Impv01</i>	<i>Rdinsty00</i>	<i>Rdinsty07</i>	<i>Imp1</i>	<i>Imp5</i>	<i>Imp7</i>	<i>Imp10</i>	<i>Imp15</i>	<i>ImpMax</i>	<i>ImpAv</i>
(%)	(mi/mi <sup>2</sup> )	(mi/mi <sup>2</sup> )	(yr/yr)	(yr/yr)	(yr/yr)	(yr/yr)	(yr/yr)	(%)	(%)	
36	23.36%	7.88	7.88	1.00	0.44	0.33	0.25	-	14.89%	6.43%
36.1	23.36%	7.88	7.88	1.00	-	-	-	-	4.72%	2.62%
36.2	23.36%	7.88	7.88	1.00	0.89	0.67	0.50	-	8.59%	7.27%
37	0.38%	1.70	1.74	-	-	-	-	-	0.35%	0.33%
38	2.29%	1.55	1.56	-	-	-	-	-	0.35%	0.25%
39	0.14%	1.56	1.58	-	-	-	-	-	0.14%	0.13%
40	0.12%	1.51	1.50	-	-	-	-	-	0.12%	0.11%
41	0.12%	1.10	1.17	-	-	-	-	-	0.11%	0.10%
42	2.47%	4.63	4.70	1.00	-	-	-	-	2.47%	2.13%
43	0.10%	1.33	1.40	-	-	-	-	-	0.10%	0.09%
44	0.16%	0.50	0.62	-	-	-	-	-	0.17%	0.15%
45	0.28%	2.36	2.37	-	-	-	-	-	0.29%	0.24%
46	0.00%	0.00	0.00	-	-	-	-	-	0.00%	0.00%
47	1.44%	4.65	5.58	-	-	-	-	-	1.44%	1.14%
48	0.17%	1.01	1.03	-	-	-	-	-	0.16%	0.15%
49	0.22%	0.95	0.94	-	-	-	-	-	0.20%	0.20%
50	0.10%	0.40	0.40	-	-	-	-	-	0.09%	0.09%
51	1.53%	3.87	3.87	0.02	-	-	-	-	1.53%	1.14%
52	0.04%	0.67	0.69	-	-	-	-	-	0.04%	0.04%

**Table A.3 – Measures of precipitation past and present**

ID	Area-averaged Mean Annual Precipitation		2-yr, 24-hr Event		Historical Precipitation Recorded at LA Gauge			
	USGS	NRCS	NRCS		%Difference,	Mean Annual	'Wet' Years	
	1900 - 1960	1961 - 1990	Volume	I/PnrCS	Long-term	During Record	Of Total	Number
	<i>InchUSGS</i>	<i>InchNRCS</i>	<i>NOAA224Inch</i>	<i>NOAAtoNRCS</i>	<i>HstPrpLA</i>	<i>LInch</i>	<i>HstWetLA</i>	<i>LAWetYrs</i>
	(in.)	(in.)	(in.)	(in./in.)	(fraction)	(in.)	(fraction)	(yrs)
1	17.1	18.7	2.51	0.134	0.034	15.58	0.222	6
2	16.1	13.8	2.87	0.207	0.003	15.11	0.160	8
3	15.2	16.0	2.83	0.177	-0.017	14.82	0.207	12
4	31.6	27.1	5.14	0.190	-0.010	14.91	0.167	16
5	17.6	18.0	3.37	0.187	0.017	15.33	0.180	9
5.1	17.6	18.0	3.37	0.187	-0.005	14.99	0.120	3
5.2	17.6	18.0	3.37	0.187	0.039	15.66	0.240	6
6	18.2	15.8	3.10	0.197	-0.106	13.47	0.083	2
7	30.7	30.3	4.95	0.163	-0.018	14.79	0.167	14
8	12.5	12.7	1.88	0.148	-0.013	14.87	0.204	11
9	35.0	37.0	5.89	0.159	0.051	15.84	0.250	7
10	19.5	27.4	4.50	0.164	-0.022	14.74	0.140	8
11	16.9	17.5	2.37	0.135	0.001	15.09	0.200	14
12	28.2	24.3	5.08	0.209	-0.009	14.93	0.200	6
13	35.7	41.7	6.26	0.150	-0.044	14.40	0.128	6
14	11.1	11.8	2.26	0.191	0.043	15.71	0.244	11
15	20.8	13.4	2.35	0.175	-0.014	14.86	0.222	4
16	33.4	29.2	5.06	0.173	-0.017	14.81	0.161	14
17	33.1	29.6	5.11	0.172	-0.042	14.43	0.125	8
18	18.4	16.2	2.98	0.184	-0.102	13.53	0.167	3
19	21.9	18.7	4.32	0.230	0.020	15.37	0.170	9
19.1	21.9	18.7	4.32	0.230	-0.014	14.86	0.0612	3
19.2	21.9	18.7	4.32	0.230	0.039	15.66	0.1224	6
20	22.5	15.1	3.05	0.203	0.163	17.52	0.267	4
21	15.1	13.2	2.14	0.162	-0.015	14.84	0.179	7
22	29.0	28.1	4.77	0.170	-0.069	14.03	0.152	5
23	31.5	30.0	4.73	0.158	-0.032	14.59	0.189	7
24	34.9	29.8	5.61	0.188	-0.084	13.80	0.064	3
25	22.9	20.8	3.86	0.186	-0.042	14.43	0.133	6
26	22.4	34.3	5.34	0.156	-0.016	14.82	0.171	13
27	14.4	14.9	2.29	0.154	-0.027	14.67	0.217	5
28	13.9	13.5	2.08	0.155	0.061	15.99	0.262	11
29	14.2	13.6	2.14	0.157	0.011	15.24	0.208	5
30	20.4	20.9	3.90	0.187	0.034	15.58	0.231	9
31	32.5	23.5	4.80	0.204	0.004	15.13	0.167	9
32	11.7	11.4	2.24	0.197	0.014	15.27	0.197	14
33	17.6	14.5	2.60	0.180	0.021	15.39	0.263	5

ID	Area-averaged Mean Annual Precipitation		2-yr, 24-hr Event		Historical Precipitation Recorded at LA Gauge			
	USGS	NRCS	NRCS		%Difference,	Mean Annual	'Wet' Years	
	1900 - 1960	1961 - 1990	Volume	I/PnrCS	Long-term	During Record	Of Total	Number
	<i>InchUSGS</i>	<i>InchNRCS</i>	<i>NOAA224Inch</i>	<i>NOAAtoNRCS</i>	<i>HstPrpLA</i>	<i>LAinch</i>	<i>HstWetLA</i>	<i>LAWetYrs</i>
	(in.)	(in.)	(in.)	(in./in.)	(fraction)	(in.)	(fraction)	(yrs)
34	32.1	28.2	4.93	0.175	-0.081	13.85	0.067	3
35	23.8	21.9	4.80	0.219	-0.002	15.04	0.206	7
36	14.4	13.4	2.54	0.189	-0.024	14.70	0.194	7
36.1	14.4	13.4	2.54	0.189	-0.111	13.39	0.167	3
36.2	14.4	13.4	2.54	0.189	0.062	16.01	0.222	4
37	17.5	17.4	2.57	0.148	0.044	15.73	0.231	6
38	18.4	14.6	2.94	0.202	-0.029	14.62	0.146	6
39	20.3	14.5	2.74	0.189	-0.031	14.61	0.185	5
40	30.2	24.0	5.31	0.221	-0.009	14.93	0.200	6
41	35.0	32.3	5.62	0.174	-0.058	14.19	0.111	6
42	19.5	16.3	2.51	0.154	-0.027	14.67	0.206	14
43	30.5	24.8	5.37	0.216	-0.007	14.96	0.177	14
44	23.5	20.7	3.65	0.176	0.043	15.71	0.244	11
45	27.4	27.4	4.14	0.151	0.003	15.11	0.194	14
46	22.1	26.7	3.63	0.136	-0.025	14.69	0.203	12
47	22.2	25.5	3.84	0.151	-0.015	14.84	0.140	7
48	26.3	29.6	4.83	0.164	-0.118	13.29	0.167	4
49	15.8	17.7	2.63	0.149	0.135	17.11	0.300	6
50	33.7	25.0	5.19	0.208	-0.009	14.93	0.200	6
51	35.6	28.3	5.04	0.178	-0.020	14.77	0.145	10
52	30.7	26.1	3.88	0.148	0.036	15.61	0.212	7

**General abbreviations and symbol definitions (excluding units of measure):**

ID	identification
I/PnrCS	2-yr, 24-hr precipitation standardized by annual precipitation (i.e., NOAA224/InchNRCS)
NRCS	Natural Resources Conservation Service
USGS	U. S. Geological Survey

**Table A.4 – Spatial and topographic measures**

ID	Area		Stream Length		Drainage Density	Main Channel			Strahler Total		Elevation		Slope		Width Valley
	Total		Total	Channelized		Length	Channelized	Shape	Order	Relief	Gage	Basin	Average	Surface	
	Sqmi	StreamMi	frcnArtf	DrainDensity	PathMi	ArtfPath	Shape	Order	Rlft	ElvgageFt	ElvBsnFt	SlpChn	SlpSurf	SlpVly2	WVlyFt
	(mi <sup>2</sup> )	(mi)	(fraction)	(mi/mi <sup>2</sup> )		(fraction)	(mi/mi <sup>2</sup> )	(Strahler)	(ft)	(ft)	(ft)	(%)	(%)	(%)	(ft)
1	19.12	38.68	0.004	2.023	11.22	0.014	0.587	3	2,719	2,932	3,885	3.98%	29.9%	0.80%	820
2	8.74	13.45	0.032	1.538	8.18	0.010	0.936	2	1,352	443	855	2.18%	18.4%	1.34%	1,312
3	9.02	20.49	0.000	2.271	7.32	0.000	0.812	3	7,589	834	3,283	14.85%	51.0%	7.93%	656
4	16.09	46.34	0.004	2.881	12.68	0.000	0.788	4	4,692	1,414	2,733	4.58%	53.1%	3.34%	98
5	69.48	159.10	0.044	2.290	14.80	0.246	0.213	5	2,924	745	1,368	1.90%	22.9%	0.79%	14,108
5.1	69.48	159.10	0.044	2.290	14.80	0.246	0.213	5	2,924	745	1,368	1.90%	22.9%	0.79%	14,108
5.2	69.48	159.10	0.044	2.290	14.80	0.246	0.213	5	2,924	745	1,368	1.90%	22.9%	0.79%	14,108
6	54.31	98.54	0.066	1.814	22.79	0.025	0.420	4	4,129	82	1,171	2.13%	24.9%	0.94%	3,281
7	22.94	39.62	0.001	1.727	7.36	0.000	0.321	4	5,324	4,065	5,335	7.93%	49.8%	3.15%	98
8	21.78	47.78	0.000	2.193	11.36	0.000	0.521	4	4,912	1,138	3,423	7.45%	40.9%	12.66%	131
9	0.52	1.02	0.000	1.959	1.33	0.000	2.553	1	1,334	6,638	7,310	20.16%	31.0%	21.06%	98
10	40.48	66.68	0.083	1.647	13.38	0.271	0.331	3	4,239	2,653	3,690	3.35%	25.1%	2.27%	984
11	84.37	110.83	0.024	1.314	19.84	0.057	0.235	4	2,401	2,202	3,077	1.92%	12.5%	2.15%	246
12	13.22	29.48	0.000	2.231	7.17	0.000	0.542	3	4,160	574	1,797	7.85%	39.3%	3.85%	164
13	9.64	24.89	0.000	2.582	5.31	0.000	0.550	3	5,808	2,605	4,750	17.81%	59.1%	10.94%	98
14	30.44	57.04	0.000	1.874	13.54	0.000	0.445	3	7,322	1,373	4,387	7.76%	29.8%	12.03%	98
15	47.42	90.29	0.020	1.904	15.39	0.013	0.325	4	1,868	160	794	1.97%	25.6%	0.14%	902
16	8.72	24.28	0.000	2.783	5.86	0.000	0.672	4	4,437	1,615	3,130	11.62%	45.0%	5.20%	656
17	6.39	17.53	0.000	2.745	6.31	0.000	0.988	3	4,456	936	2,300	9.69%	51.5%	2.17%	98
18	2.36	8.16	0.010	3.462	4.75	0.018	2.014	3	1,812	354	764	3.86%	22.9%	2.36%	11,483
19	23.79	62.60	0.008	2.632	13.75	0.000	0.578	3	4,178	602	1,952	4.58%	41.8%	1.14%	4,921
19.1	23.79	62.60	0.008	2.632	13.75	0.000	0.578	3	4,178	602	1,952	4.58%	41.8%	1.14%	4,921

ID	Area		Stream Length		Drainage Density	Main Channel		Strahler Total		Elevation		Slope		Width Valley	
	Total		Total	Channelized		Length	Channelized	Shape	Order	Relief	Gage	Basin	Average		Surface
	Sqmi (mi <sup>2</sup> )	StreamMi (mi)	frcnArtf (fraction)	DrainDensity (mi/mi <sup>2</sup> )	PathMi (mi)	ArtfPath (fraction)	Shape (mi/mi <sup>2</sup> )	Order (Strahler)	Rlft (ft)	ElvgageFt (ft)	ElvBsnFt (ft)	SlpChn (%)	SlpSurf (%)	SlpVly2 (%)	WVlyFt (ft)
19.2	23.79	62.60	0.008	2.632	13.75	0.000	0.578	3	4,178	602	1,952	4.58%	41.8%	1.14%	4,921
20	7.69	15.83	0.013	2.059	4.96	0.000	0.646	3	641	1,292	1,490	1.65%	8.1%	1.41%	492
21	26.35	68.92	0.023	2.615	11.52	0.000	0.437	4	1,288	42	440	1.60%	20.0%	0.69%	3,281
22	2.73	5.22	0.000	1.912	3.59	0.000	1.314	2	2,233	1,338	2,183	10.25%	47.8%	6.04%	98
23	1.77	4.43	0.000	2.498	3.56	0.000	2.010	2	3,952	4,374	5,695	16.75%	44.7%	8.57%	591
24	1.85	3.99	0.000	2.153	2.44	0.000	1.318	3	3,240	2,191	3,217	18.57%	56.2%	11.12%	98
25	20.72	85.36	0.000	4.121	10.14	0.000	0.490	4	4,134	1,082	2,102	4.60%	35.9%	1.65%	4,921
26	15.18	31.99	0.013	2.107	11.90	0.035	0.783	2	5,720	2,623	4,452	6.55%	34.5%	4.39%	738
27	12.23	22.21	0.011	1.817	6.61	0.000	0.540	3	1,344	567	946	2.55%	17.3%	1.56%	246
28	42.03	83.35	0.010	1.983	12.27	0.013	0.292	4	2,332	270	943	2.57%	18.3%	1.25%	98
29	31.22	60.78	0.010	1.947	8.47	0.007	0.271	4	2,182	420	1,046	3.57%	18.4%	0.76%	656
30	35.44	86.02	0.053	2.427	15.28	0.231	0.431	3	6,130	2,367	4,839	7.04%	44.9%	4.41%	1,969
31	15.87	48.25	0.000	3.040	7.84	0.000	0.494	4	3,609	1,142	2,531	7.72%	44.4%	3.84%	230
32	93.15	244.14	0.007	2.621	21.74	0.000	0.233	5	5,612	686	3,058	4.20%	26.1%	2.22%	1,148
33	13.39	28.22	0.189	2.108	9.57	0.546	0.715	3	3,449	1,039	1,986	4.78%	22.1%	0.84%	820
34	6.68	17.09	0.000	2.557	6.40	0.000	0.958	4	3,536	812	1,724	6.19%	54.0%	3.60%	98
35	51.11	120.73	0.007	2.362	15.28	0.000	0.299	4	4,894	320	1,247	2.81%	30.1%	1.44%	820
36	41.59	75.92	0.122	1.825	15.37	0.024	0.370	4	1,530	72	472	1.18%	11.1%	0.66%	36,089
36.1	41.59	75.92	0.122	1.825	15.37	0.024	0.370	4	1,530	72	472	1.18%	11.1%	0.66%	36,089
36.2	41.59	75.92	0.122	1.825	15.37	0.024	0.370	4	1,530	72	472	1.18%	11.1%	0.66%	36,089
37	89.10	210.04	0.017	2.357	16.84	0.004	0.189	4	3,781	1,870	2,834	1.81%	23.5%	4.79%	131
38	105.74	233.35	0.031	2.207	24.85	0.043	0.235	4	3,049	161	1,127	1.78%	27.9%	1.40%	1,640
39	80.88	147.72	0.008	1.826	17.42	0.000	0.215	4	2,143	399	1,326	2.17%	27.6%	0.68%	98
40	9.00	21.74	0.000	2.416	6.81	0.000	0.756	3	3,955	627	1,982	9.23%	41.4%	2.95%	1,312

ID	Area		Stream Length		Drainage Density	Main Channel		Strahler Total		Elevation		Slope			Width Valley
	Total		Total	Channelized		Length	Channelized	Shape	Order	Relief	Gage	Basin	Average	Surface	
	Sqmi	StreamMi	frcnArtf	DrainDensity	PathMi	ArtfPath	Shape	Order	Rlft	ElvgageFt	ElvBsnFt	SlpChn	SlpSurf	SlpVly2	WVlyFt
	(mi <sup>2</sup> )	(mi)	(fraction)	(mi/mi <sup>2</sup> )		(fraction)	(mi/mi <sup>2</sup> )	(Strahler)	(ft)	(ft)	(ft)	(%)	(%)	(%)	(ft)
41	9.67	24.05	0.000	2.486	5.13	0.000	0.530	4	3,888	1,494	3,096	14.13%	54.3%	8.11%	98
42	56.86	91.75	0.028	1.614	18.27	0.023	0.321	4	1,954	1,304	1,884	1.51%	11.3%	0.37%	3,281
43	38.40	88.80	0.003	2.313	11.60	0.000	0.302	4	5,505	780	2,962	8.91%	40.0%	2.78%	1,886
44	13.00	26.34	0.002	2.026	9.38	0.000	0.721	3	4,285	1,213	2,242	5.12%	46.9%	1.70%	623
45	45.28	88.76	0.027	1.960	16.67	0.031	0.368	4	2,162	3,278	4,014	1.91%	20.8%	1.99%	98
46	17.02	39.26	0.004	2.307	10.24	0.010	0.602	4	9,486	755	5,128	15.05%	41.0%	6.39%	197
47	17.98	47.94	0.003	2.666	7.70	0.000	0.428	4	1,798	273	821	2.51%	29.9%	3.79%	98
48	64.86	149.69	0.000	2.308	13.58	0.000	0.209	5	3,457	2,669	4,075	4.51%	36.7%	2.44%	98
49	39.52	100.73	0.001	2.549	12.00	0.000	0.304	4	3,710	1,938	3,240	5.00%	29.9%	2.16%	98
50	74.16	227.62	0.004	3.069	19.11	0.033	0.258	5	4,685	761	2,539	4.28%	46.2%	1.09%	1,640
51	4.85	7.46	0.000	1.539	4.29	0.000	0.885	2	3,240	1,843	2,919	10.63%	45.0%	7.55%	1,148
52	25.48	47.08	0.035	1.847	10.77	0.015	0.423	4	2,889	2,798	3,818	4.27%	23.9%	1.49%	1,312

Table A.5 – Years active and return-interval flows

ID	Calendar Year		Record		% with Flow	Gamma Fit	Return-interval Flows (yrs)									
	Begin	End	Daily	Peaks			Weibull Plotting Position (#) and Gamma Distribution (#g)									
	<i>Begin</i>	<i>End</i>	<i>YrsDaily</i>	<i>YrsPeak</i>	<i>Wet</i>	<i>gammaR2</i>	1	1g	1.5	1.5g	2	2g	5	5g	10	10g
		(yrs)	(yrs)	(%)	(fraction)	Q1	gQ1	Q15	gQ15	Q2	gQ2	Q5	gQ5	Q10	gQ10	
1	1961	1987	27	27	55%	0.98	0	0.9	63	71	88	170	626	591	1,046	963
2	1930	1980	50	50	18%	0.98	0	0.3	75	93	158	231	929	852	1,404	1,412
3	1948	2008	60	59	100%	0.99	4.2	0.0	28	1	53	11	224	220	540	558
4	1910	2008	97	94	97%	0.98	12	0.0	331	103	570	348	1,710	1,809	3,155	3,305
5	1933	1983	49	50	30%	1.00	0	0.4	255	283	755	773	3,000	3,153	5,210	5,384
5.1	1933	1958	24	25	7%	0.96	0	0.7	19	105	174	289	1,278	1,200	2,100	2,059
5.2	1959	1983	24	25	55%	0.99	14	63.0	891	1,074	2,040	2,009	5,138	5,237	8,216	7,790
6	1970	2008	26	23	92%	0.91	236	8.9	1,020	441	1,420	1,021	2,912	3,447	4,680	5,565
7	1923	2008	86	84	100%	0.98	4.3	0.0	73	2	199	24	650	658	1,815	1,803
8	1950	2004	52	52	54%	0.92	0.13	0.0	8	0	16	4	115	254	537	873
9	1960	1966	6	37	14%	0.97	0	0.0	6	5	12	15	48	60	114	102
10	1920	1982	57	58	100%	0.97	22	0.0	423	91	740	423	2,639	3,100	5,822	6,204
11	1936	2008	72	71	66%	0.97	0	0.0	3	10	21	42	327	281	646	550
12	1958	1988	30	30	97%	0.96	2	5.8	399	433	736	994	4,333	3,322	5,997	5,347
13	1929	1975	47	48	100%	0.90	9.9	0.0	131	0	203	8	632	603	1,404	2,119
14	1962	2008	46	46	59%	0.93	0	0.0	69	17	244	110	1,180	1,160	1,900	2,546
15	1951	2005	19	18	25%	0.95	0	0.0	107	34	389	205	2,033	1,996	2,800	4,291
16	1919	2008	88	87	100%	0.98	14	0.0	117	34	231	142	938	929	1,884	1,806
17	1916	1979	62	62	91%	0.77	0	0.0	157	0	270	8	714	571	1,643	1,954
18	1954	1963	9	18	7%	0.98	3.3	2.7	73	55	145	114	320	337	450	523
19	1930	1983	51	49	58%	0.96	18	0.8	487	308	799	780	3,000	2,922	5,300	4,865
19.1	1933	1958	26	24	54%	0.98	18	0.5	358	168	897	537	2,200	2,618	4,640	4,700

ID	Calendar Year		Record		% with Flow	Gamma Fit	Return-interval Flows (yrs)									
	Begin	End	Daily	Peaks			Weibull Plotting Position (#) and Gamma Distribution (#g)									
	<i>Begin</i>	<i>End</i>	<i>YrsDaily</i>	<i>YrsPeak</i>	<i>Wet</i>	<i>gammaR2</i>	1	1g	1.5	1.5g	2	2g	5	5g	10	10g
		(yrs)	(yrs)	(%)	(fraction)	Q1	gQ1	Q15	gQ15	Q2	gQ2	Q5	gQ5	Q10	gQ10	
19.2	1959	1983	26	25	63%	0.96	61	2.2	494	312	691	844	4,085	3,413	6,278	5,812
20	1970	1991	14	14	83%	0.97	22	7.1	165	121	257	267	990	854	1,260	1,356
21	1951	2008	41	41	55%	0.99	0.64	0.0	15	1	63	21	802	775	2,008	2,289
22	1939	1971	32	33	42%	0.92	1.9	0.0	29	0	62	4	185	244	320	799
23	1948	1985	37	36	53%	0.85	0	0.0	11	0	19	3	205	150	306	488
24	1916	1979	47	46	89%	0.91	2.3	0.0	26	2	44	10	85	91	116	190
25	1928	1973	45	45	17%	0.95	0	0.0	144	9	256	77	1,349	1,132	2,097	2,693
26	1920	2007	77	77	100%	0.85	2.1	0.0	99	0	196	5	540	299	674	987
27	1983	2008	25	24	100%	0.97	26	3.6	98	84	139	168	474	477	693	729
28	1964	2008	44	43	100%	0.96	49	52.1	597	712	963	1,173	2,955	2,592	4,151	3,644
29	1969	1993	24	23	97%	0.97	102	29.4	453	463	651	869	2,540	2,278	3,080	3,396
30	1967	2008	41	40	64%	0.97	0	0.0	9	2	17	20	219	311	769	750
31	1928	1983	54	50	100%	0.99	0	0.2	349	195	560	554	2,691	2,369	4,064	4,098
32	1930	2008	73	73	39%	0.99	0	0.4	147	222	358	533	1,971	1,883	3,161	3,082
33	1987	2007	20	20	11%	0.94	0	0.0	8	0	24	5	397	364	739	1,281
34	1917	1962	45	45	59%	0.97	10	0.2	120	75	244	195	576	756	1,374	1,272
35	1949	1983	34	34	67%	0.98	0	0.6	668	366	1,093	1,106	6,510	5,068	7,959	8,944
36	1949	1985	36	36	63%	0.98	0	8.6	905	568	1,239	1,218	3,319	3,755	6,397	5,896
36.1	1950	1967	18	18	28%	0.98	0	84.0	726	553	907	920	1,932	2,060	2,550	2,910
36.2	1968	1985	18	18	98%	0.98	448	141.0	1,233	1,286	1,937	2,293	6,363	5,621	7,720	8,192
37	1958	1983	25	25	61%	0.84	0.38	0.0	6	0	10	3	125	407	519	1,617
38	1928	1969	41	41	82%	0.98	1.8	0.0	129	24	350	213	3,570	3,118	7,705	7,406
39	1952	2008	30	30	56%	0.97	0.65	0.3	253	233	463	778	5,009	3,991	8,400	7,266
40	1958	1988	30	30	65%	0.98	1	8.9	341	369	524	769	2,553	2,293	3,688	3,562

ID	Calendar Year		Record		% with Flow	Gamma Fit	Return-interval Flows (yrs)									
	Begin	End	Daily	Peaks			Weibull Plotting Position (#) and Gamma Distribution (#g)									
	<i>Begin</i>	<i>End</i>	<i>YrsDaily</i>	<i>YrsPeak</i>	<i>Wet</i>	<i>gammaR2</i>	1	1g	1.5	1.5g	2	2g	5	5g	10	10g
		(yrs)	(yrs)	(%)	(fraction)	Q1	gQ1	Q15	gQ15	Q2	gQ2	Q5	gQ5	Q10	gQ10	
41	1916	1970	54	54	100%	0.94	17	0.0	145	1	343	19	710	647	1,546	1,882
42	1912	2008	70	68	48%	0.96	0	0.0	24	0	102	15	1,376	867	2,670	2,851
43	1927	2007	78	72	97%	0.99	7.9	0.0	660	162	1,230	718	5,414	5,027	10,000	9,941
44	1961	2007	46	46	59%	0.95	1.7	0.0	172	17	280	113	1,387	1,194	1,961	2,618
45	1905	2008	74	73	76%	0.97	0.6	0.0	43	10	140	90	1,408	1,392	2,957	3,352
46	1947	2008	59	59	75%	0.97	0	0.0	18	5	41	40	353	481	1,294	1,092
47	1930	1979	49	49	85%	0.98	21	0.2	582	229	1,130	687	3,020	3,117	5,070	5,484
48	1948	1971	24	24	84%	0.95	7	0.0	95	0	302	16	1,770	1,802	4,600	6,860
49	1963	1983	20	20	99%	0.99	0.11	0.0	7	5	45	31	322	303	547	649
50	1959	1988	27	27	63%	0.98	0	0.0	98	33	206	321	5,694	5,297	11,414	12,943
51	1921	1985	70	65	95%	0.94	0	0.0	73	9	114	45	292	345	669	699
52	1913	1986	32	30	85%	0.98	0.2	0.1	171	99	342	343	1,976	1,828	3,900	3,365

**General abbreviations and symbol definitions (excluding units of measure):**

# ID for the entire record  
 #g ID for gamma distribution  
 ID identification

**Table A.6 – Return-interval flows and DDF parameters**

ID	Return-interval Flows (yrs)																DDF Terms														
	Weibull Plotting Position (#) and Gamma Distribution (#g)																Peaks			Daily			Daily			Bins 16- 25			Bins 12-25		
	25	25g	50	50g	100	100g	Skew	St Dev	Mean	Coef Dev	Skew	St Dev	Mean	Coef Dev	Min	Max	Coef	Exp	Fit	Coef	Exp	Fit									
	Q25	gQ25	Q50	gQ50	Q100	gQ100	SkPk	SDPk	MnPk	CvPk	SkDly	SDDly	MnDly	CVDly	Qmin	Qmax	d1	d2	dR2	day1	day2	dayR2									
	(cfs)	(cfs)	(cfs)	(cfs)	(cfs)	(cfs)					(cfs)	(cfs)	(cfs)	(cfs)	(cfs)	(cfs)															
1	1,440	1,490	-	1,905	-	2,329	1.5	401.7	316.8	1.3	17.5	16.9	2.7	6.4	-	624	2,126	-0.991	0.97	901	-0.806	0.95									
2	2,450	2,211	2,500	2,843	-	3,491	1.8	640.0	474.5	1.3	28.2	11.3	0.9	12.5	-	521	437	-0.717	0.95	268	-0.608	0.96									
3	1,105	1,160	1,710	1,689	-	2,261	3.6	335.0	178.4	1.9	20.7	7.5	2.9	2.6	-	395	19,850	-1.543	0.99	10,872	-1.396	0.98									
4	5,682	5,549	8,540	7,371	8,620	9,264	2.7	1,661.5	1,145.9	1.5	28.8	56.3	9.9	5.7	-	3,690	94,878	-1.241	0.98	27,145	-1.037	0.97									
5	9,310	8,617	10,700	11,194	-	13,848	2.0	2,478.0	1,813.5	1.4	31.8	54.4	4.7	11.6	-	3,610	1,588	-0.745	0.88	1,401	-0.733	0.88									
5.1	3,000	3,305	-	4,301	-	5,326	1.7	887.7	623.2	1.4	28.2	20.3	1.3	16.2	-	1,000	45	-0.370	0.70	29	-0.284	0.74									
5.2	10,700	11,237	-	13,877	-	16,536	1.3	2,974.3	2,932.4	1.0	24.5	74.1	8.1	9.1	-	3,610	1,109	-0.710	0.89	1,209	-0.733	0.88									
6	10,000	8,546	-	10,886	-	13,276	2.7	2,125.6	2,079.9	1.0	15.3	86.6	15.3	5.7	-	2,560	4,835	-0.835	0.97	4,041	-0.804	0.98									
7	3,585	3,920	5,125	5,813	8,300	7,873	4.1	1,213.0	613.5	2.0	22.8	54.7	17.8	3.1	0.70	3,300	362,896	-1.441	0.98	61,230	-1.142	0.93									
8	2,640	2,160	2,990	3,369	-	4,713	3.3	660.6	244.6	2.7	22.3	4.9	1.0	5.0	-	277	4,049	-1.406	0.96	2,027	-1.229	0.96									
9	168	163	169	212	-	262	1.9	45.5	33.2	1.4	17.4	1.7	0.2	7.5	-	45	-	-	-	-	-	-									
10	11,922	11,079	13,951	15,131	-	19,392	2.6	3,215.4	1,956.5	1.6	26.7	77.0	10.9	7.0	0.50	3,800	9,132	-0.922	0.97	18,335	-1.034	0.98									
11	880	967	1,161	1,311	1,580	1,672	2.5	295.7	164.8	1.8	18.2	15.7	3.4	4.6	-	745	31,444	-1.356	0.98	3,630	-0.903	0.84									
12	7,450	8,192	-	10,424	-	12,702	1.5	2,244.4	1,819.4	1.2	25.1	70.4	7.8	9.1	-	2,980	2,515	-0.817	0.96	1,963	-0.776	0.98									
13	4,500	5,315	10,300	8,335	-	11,698	5.2	1,596.6	657.0	2.4	61.0	44.0	8.0	5.5	0.30	4,050	50,296	-1.404	0.96	33,267	-1.335	0.98									
14	5,700	4,827	7,100	6,765	-	8,825	3.3	1,371.5	786.1	1.7	23.7	17.8	2.1	8.3	-	850	2,494	-0.970	0.97	1,409	-0.852	0.97									
15	7,500	8,031	-	11,194	-	14,547	2.8	1,830.6	1,134.9	1.6	25.8	44.0	5.0	8.7	-	2,060	1,880	-0.906	0.92	495	-0.668	0.87									
16	2,969	3,164	3,710	4,285	6,000	5,459	3.2	949.6	604.6	1.6	17.7	18.1	5.2	3.5	0.10	795	40,335	-1.314	0.98	17,202	-1.135	0.97									
17	2,157	4,827	8,563	7,525	-	10,522	6.6	1,691.1	677.5	2.5	55.5	33.8	4.6	7.3	-	3,370	31,295	-1.294	1.00	12,314	-1.140	0.99									
18	770	780	-	979	-	1,180	1.7	196.0	184.0	1.1	35.9	2.3	0.1	17.5	-	110	-	-	-	-	-	-									
19	8,120	7,646	8,400	9,848	-	12,107	1.9	2,190.5	1,677.8	1.3	26.7	54.9	6.2	8.8	-	2,770	6,622	-0.925	0.98	2,859	-0.783	0.97									
19.1	8,000	7,796	-	10,299	-	12,894	1.7	887.7	623.2	1.4	28.2	20.3	1.3	16.2	-	2,770	5,966	-1.101	0.94	1,622	-0.882	0.93									

ID	Return-interval Flows (yrs)																DDF Terms														
	Weibull Plotting Position (#) and Gamma Distribution (#g)																Peaks			Daily			Daily			Bins 16- 25			Bins 12-25		
	25	25g	50	50g	100	100g	Skew	St Dev	Mean	Coef Dev	Skew	St Dev	Mean	Coef Dev	Min	Max	Coef	Exp	Fit	Coef	Exp	Fit									
	Q25 (cfs)	gQ25 (cfs)	Q50 (cfs)	gQ50 (cfs)	Q100 (cfs)	gQ100 (cfs)	SkPkS	SDPkS	MnPkS	CvPkS	SkDly	SDDly	MnDly	CVDly	Qmin (cfs)	Qmax (cfs)	d1	d2	dR2	day1	day2	dayR2									
19.2	8,400	9,282	-	12,048	-	14,894	1.3	2,974.3	2,932.4	1.0	24.5	74.1	8.1	9.1	-	2,400	2,380	-0.825	0.96	1,337	-0.725	0.96									
20	1,680	2,057	-	2,604	-	3,162	1.5	486.0	454.4	1.1	19.4	15.7	2.1	7.4	-	500	-	0.000	-	-	0.000	-									
21	4,200	5,201	7,300	7,850	-	10,753	3.4	1,422.2	646.8	2.2	26.3	23.3	1.9	12.5	-	1,050	501	-0.673	0.98	277	-0.555	0.95									
22	2,124	1,926	-	2,975	-	4,135	4.0	520.2	212.5	2.4	17.8	3.3	0.7	4.7	-	147	1,903	-1.433	0.97	660	-1.126	0.94									
23	976	1,171	1,990	1,806	-	2,509	5.1	338.9	124.7	2.7	98.8	10.8	0.7	16.2	-	1,180	-	-	-	-	-	-									
24	338	350	536	485	-	627	3.5	95.8	66.3	1.4	25.9	4.4	1.0	4.6	-	220	3,234	-1.415	0.95	1,472	-1.206	0.96									
25	4,220	5,374	8,500	7,695	-	10,185	3.6	1,488.3	847.6	1.8	29.2	24.5	2.5	9.8	-	1,300	3,184	-0.967	0.98	806	-0.704	0.90									
26	1,900	2,391	3,646	3,699	6,180	5,148	5.9	783.8	386.6	2.0	65.8	13.5	2.0	6.8	-	1,480	5,352	-1.214	0.97	7,974	-1.285	0.98									
27	1,090	1,074	-	1,340	-	1,610	1.5	277.8	269.4	1.0	13.4	7.6	1.9	3.9	0.04	248	1,972	-1.147	0.94	1,121	-1.003	0.96									
28	4,750	5,023	4,760	6,060	-	7,093	1.1	1,404.7	1,548.7	0.9	12.9	55.5	11.0	5.1	-	1,400	3,912	-0.738	0.96	4,721	-0.775	0.98									
29	4,990	4,905	-	6,062	-	7,227	1.5	1,269.6	1,294.8	1.0	14.2	43.1	6.9	6.2	-	1,060	1,361	-0.716	0.96	793	-0.613	0.96									
30	1,680	1,509	1,750	2,169	-	2,877	2.7	420.8	201.4	2.1	23.4	13.3	3.0	4.5	-	540	8,802	-1.305	0.91	3,774	-1.112	0.92									
31	5,780	6,619	9,440	8,638	-	10,720	2.3	1,871.7	1,380.4	1.4	35.5	75.2	10.9	6.9	0.10	4,980	39,922	-1.169	0.98	16,655	-1.033	0.98									
32	4,400	4,782	5,670	6,121	7,000	7,492	1.9	1,427.8	1,067.4	1.3	22.8	37.5	5.0	7.4	-	2,040	16,131	-1.078	0.93	4,518	-0.851	0.92									
33	3,120	3,218	-	5,048	-	7,087	3.7	704.8	299.1	2.4	54.5	12.7	0.7	18.5	-	900	306	-0.955	0.87	136	-0.790	0.90									
34	2,070	2,013	2,400	2,601	-	3,205	2.1	563.5	437.7	1.3	21.6	15.6	2.8	5.5	-	738	7,212	-1.165	0.98	2,629	-0.954	0.96									
35	14,886	14,654	-	19,248	-	24,000	2.0	3,972.7	2,855.2	1.4	38.7	146.9	14.9	9.9	-	10,400	12,735	-0.972	0.97	6,841	-0.885	0.98									
36	8,662	8,867	10,400	11,180	-	13,532	2.0	2,362.8	2,204.1	1.1	20.8	53.3	6.5	8.2	-	2,170	975	-0.643	0.92	2,302	-0.792	0.95									
36.1	4,040	4,025	-	4,866	-	5,704	1.5	996.5	1,207.7	0.8	19.6	22.9	2.1	10.8	-	815	105	-0.480	0.82	85	-0.441	0.86									
36.2	10,400	11,625	-	14,237	-	16,859	1.2	2,898.1	3,200.4	0.9	16.4	71.5	10.9	6.5	-	2,170	588	-0.591	0.91	2,034	-0.807	0.94									
37	6,150	4,341	-	6,982	-	9,956	4.8	1,231.0	329.4	3.7	29.2	9.0	1.0	9.2	-	500	238	-0.811	0.73	227	-0.805	0.87									
38	14,790	14,764	22,400	21,135	-	27,965	3.3	4,316.4	2,081.9	2.1	30.6	120.2	14.0	8.6	-	6,600	15,685	-0.982	0.96	5,565	-0.827	0.96									
39	11,207	12,168	12,500	16,144	-	20,276	1.8	3,304.8	2,142.0	1.5	20.8	96.7	12.5	7.8	-	3,740	5,465	-0.858	0.99	2,269	-0.715	0.97									
40	5,098	5,314	-	6,674	-	8,053	1.4	1,443.3	1,273.1	1.1	22.3	48.2	5.9	8.2	-	1,900	2,102	-0.815	0.99	1,527	-0.756	0.98									

ID	Return-interval Flows (yrs)						DDF Terms															
	Weibull Plotting Position (#) and Gamma Distribution (#g)						Peaks			Daily			Daily			Bins 16- 25			Bins 12-25			
	25	25g	50	50g	100	100g	Skew	St Dev	Mean	Coef Dev	Skew	St Dev	Mean	Coef Dev	Min	Max	Coef	Exp	Fit	Coef	Exp	Fit
	Q25	gQ25	Q50	gQ50	Q100	gQ100	SkPkS	SDPkS	MnPkS	CvPkS	SkDly	SDDly	MnDly	CVDly	Qmin	Qmax	d1	d2	dR2	day1	day2	dayR2
(cfs)	(cfs)	(cfs)	(cfs)	(cfs)	(cfs)									(cfs)	(cfs)							
41	5,200	4,237	7,000	6,372	-	8,707	3.9	1,204.5	669.6	1.8	34.3	36.2	6.7	5.4	-	2,500	34,558	-1.270	0.98	14,127	-1.116	0.98
42	5,270	6,889	10,761	10,650	15,200	14,814	4.6	2,226.2	952.4	2.3	32.7	72.2	6.6	10.9	-	4,960	9,967	-0.933	0.95	2,349	-0.706	0.90
43	16,274	17,615	23,404	23,973	27,500	30,648	2.6	5,139.9	3,384.7	1.5	28.9	135.7	23.5	5.8	-	8,900	131,671	-1.150	0.98	42,867	-0.986	0.97
44	6,220	4,961	6,520	6,953	-	9,070	3.1	1,389.6	812.0	1.7	33.2	64.4	7.4	8.7	-	3,590	14,098	-1.058	0.97	4,296	-0.862	0.95
45	8,600	6,741	10,337	9,684	11,200	12,845	3.2	2,189.2	1,067.3	2.1	30.3	66.1	10.9	6.1	-	5,000	134,106	-1.318	0.96	16,805	-0.993	0.92
46	2,186	2,116	2,900	2,992	-	3,928	2.8	633.2	318.4	2.0	23.1	19.1	5.1	3.7	-	1,080	56,915	-1.486	0.93	10,203	-1.148	0.91
47	10,130	8,966	12,200	11,766	-	14,661	2.4	2,547.3	1,995.7	1.3	36.7	67.2	5.9	11.3	-	4,920	4,745	-0.929	0.93	1,788	-0.777	0.94
48	20,700	17,987	-	28,678	-	40,669	4.1	4,308.4	1,742.3	2.5	35.7	94.0	12.1	7.8	-	5,320	16,205	-1.123	0.96	5,394	-0.951	0.95
49	1,160	1,213	-	1,690	-	2,195	2.6	284.0	169.8	1.7	34.4	1.4	0.2	7.2	-	77	94	-1.168	0.86	38	-0.862	0.82
50	28,000	26,256	-	37,858	-	50,335	2.8	6,684.1	3,152.7	2.1	28.3	295.0	23.8	12.4	-	13,300	1,082	-0.613	0.79	4,038	-0.792	0.91
51	989	1,259	1,773	1,725	-	2,217	3.6	365.6	239.1	1.5	26.7	9.1	2.9	3.1	-	590	45,815	-1.665	0.96	13,564	-1.399	0.95
52	5,426	5,677	-	7,558	-	9,514	2.1	1,494.0	1,024.5	1.5	15.5	49.9	10.0	5.0	-	1,700	10,125	-0.995	0.96	2,362	-0.727	0.89

**General abbreviations and symbol definitions (excluding units of measure):**

#	ID for the entire record
#g	ID for gamma distribution
#.1	ID for pre-period record
#.2	ID for post-period record
Coef	Coefficient
Coef Dev	Coefficient of Deviation
Exp	Exponent
ID	identification
Max	Maximum
Min	Minimum
St Dev	Standard Deviation

## **APPENDIX B**

### **CROSS-VALIDATION EQUATIONS AND FIGURES**

## B.1 Superior Qi Models from Cross-validation

r<sup>2</sup> Clb/vld

$$0.6/0.5 \quad Q1 \quad Q_1 = e^{-0.72} \cdot e^{\left\langle 1.5 \cdot sf \right\rangle} \cdot e^{\left\langle 3.2 \cdot dry \right\rangle} \cdot e^{\left\langle 3.5 \cdot imp_{max} \right\rangle} \quad (\text{B.1})$$

$$0.6/0.7 \quad Q1.5 \quad Q_{1.5} = e^{-3.7} \cdot e^{\left\langle 22.2 \cdot ip \right\rangle} \cdot rlf^{0.61} \cdot e^{\left\langle 0.78 \cdot shp \right\rangle} \cdot e^{\left\langle 2.4 \cdot dry \right\rangle} \cdot e^{\left\langle 0.2 \cdot imp_{max} \right\rangle} \quad (\text{B.2})$$

$$0.6/0.6 \quad Q2 \quad Q_2 = e^{2.6} \cdot e^{\left\langle 19.8 \cdot ip \right\rangle} \cdot e^{\left\langle 1.1 \cdot shp \right\rangle} \cdot e^{\left\langle 1.9 \cdot dry \right\rangle} \cdot e^{\left\langle 6.4 \cdot imp_{max} \right\rangle} \quad (\text{B.3})$$

$$0.8/0.7 \quad Q5 \quad Q_5 = e^{3.1} \cdot strm^{0.39} \cdot e^{\left\langle 16.8 \cdot ip \right\rangle} \cdot e^{\left\langle 0.71 \cdot shp \right\rangle} \cdot e^{\left\langle 1.7 \cdot dry \right\rangle} \quad (\text{B.4})$$

$$0.8/0.9 \quad Q10 \quad Q_{10} = e^{4.0} \cdot strm^{0.57} \cdot e^{\left\langle 11.5 \cdot ip \right\rangle} \cdot e^{\left\langle 0.60 \cdot shp \right\rangle} \cdot e^{\left\langle 5 \cdot vly \right\rangle} \cdot e^{\left\langle 1.5 \cdot dry \right\rangle} \quad (\text{B.5})$$

$$0.8/0.8 \quad Q25 \quad Q_{25} = e^{4.4} \cdot A^{0.77} \cdot e^{\left\langle 6.6 \cdot ip \right\rangle} \cdot e^{\left\langle 2 \cdot sf \right\rangle} \cdot e^{\left\langle 1.3 \cdot dry \right\rangle} \quad (\text{B.6})$$

$$0.8/0.7 \quad Q50 \quad Q_{50} = e^{5.2} \cdot A^{0.89} \cdot e^{\left\langle 6.1 \cdot sf \right\rangle} \cdot e^{\left\langle 1.4 \cdot dry \right\rangle} \quad (\text{B.7})$$

$$0.8/0.7 \quad Q100 \quad Q_{100} = e^{5.3} \cdot A^{0.91} \cdot e^{\left\langle 6.3 \cdot sf \right\rangle} \cdot e^{\left\langle 1.3 \cdot dry \right\rangle} \quad (\text{B.8})$$

## B.2 Superior DDF Models from Cross-validation

r<sup>2</sup> Clb/vld

$$0.7/0.8 \quad Qmax \quad Q_{max} = e^{-3.6} \cdot strm^{0.75} \cdot P^{0.78} \cdot rlf^{0.50} \cdot yr^{0.53} \cdot e^{\left\langle 2.0 \cdot dry \right\rangle} \quad (\text{B.9})$$

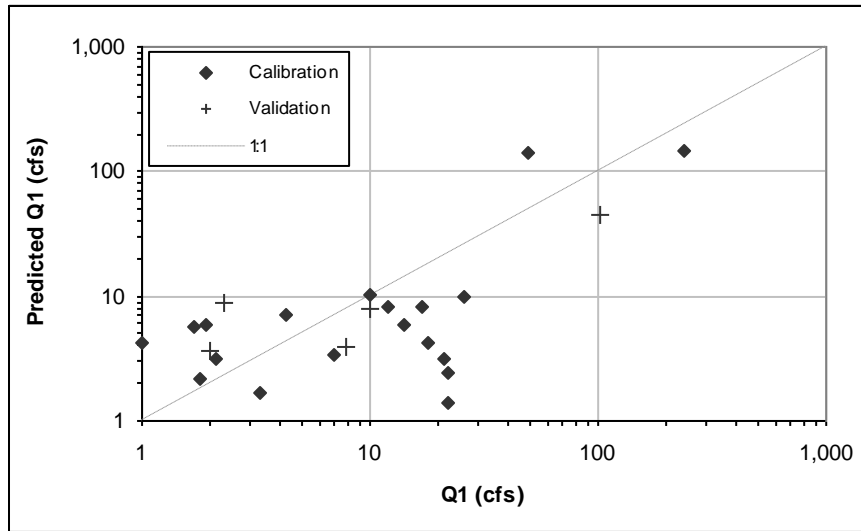
$$0.7/0.7 \quad d1 \quad d_1 = e^{-12.9} \cdot P^{3.5} \cdot yr^{2.4} \cdot dd^{-2.3} \cdot Q_{max}^{0.47} \cdot e^{\left\langle 5 \cdot dry \right\rangle} \cdot e^{\left\langle 7 \cdot imp_{7.5} \right\rangle} \quad (\text{B.10})$$

$$0.9/0.9 \quad d2 \quad d_2 = -1.9 + 0.093 \cdot \ln \left\langle r \right\rangle + 0.20 \cdot \ln \left\langle Q_{10} \right\rangle + 0.11 \cdot \ln \left\langle \mathbb{1}_1 \right\rangle + 0.94 \cdot imp_{avg} \quad (\text{B.11})$$

$$0.8/0.8 \quad day1 \quad day_1 = e^{-3.9} \cdot yr^{1.8} \cdot dd^{-2.4} \cdot e^{\left\langle 0 \cdot sf \right\rangle} \cdot Q_{max}^{0.62} \cdot e^{\left\langle 1.0 \cdot imp_{avg} \right\rangle} \quad (\text{B.12})$$

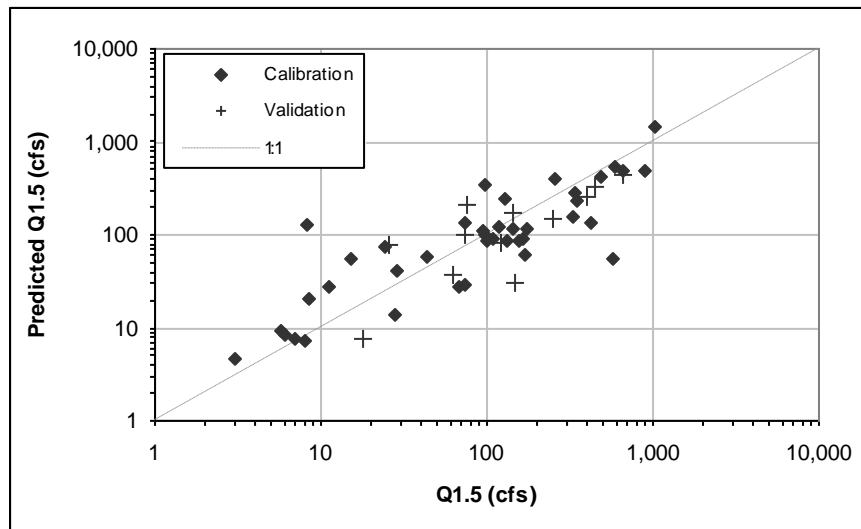
$$0.9/0.8 \quad day2 \quad day_2 = -1.9 + 0.096 \cdot \ln \left\langle \mathbb{1} \right\rangle + 0.17 \cdot \ln \left\langle r \right\rangle + 0.18 \cdot \ln \left\langle Q_{10} \right\rangle + 0.16 \cdot \ln \left\langle \mathbb{1}_{ay1} \right\rangle + 0.99 \cdot imp_{avg} \quad (\text{B.13})$$

### B.3 Cross-validation Performance Figures



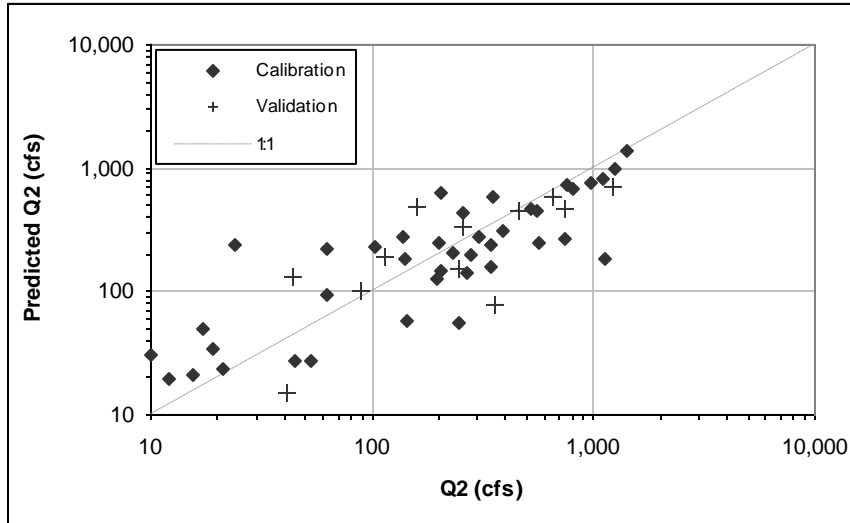
$$Q_1 = e^{-0.72} \cdot e^{(1.5rf)} \cdot e^{(3.2dry)} \cdot e^{(3.5imp_{max})}$$

Figure B.1 – Cross-validation for Q1: 40/12 scheme,  $R^2$  clb/vld = 0.6/0.5



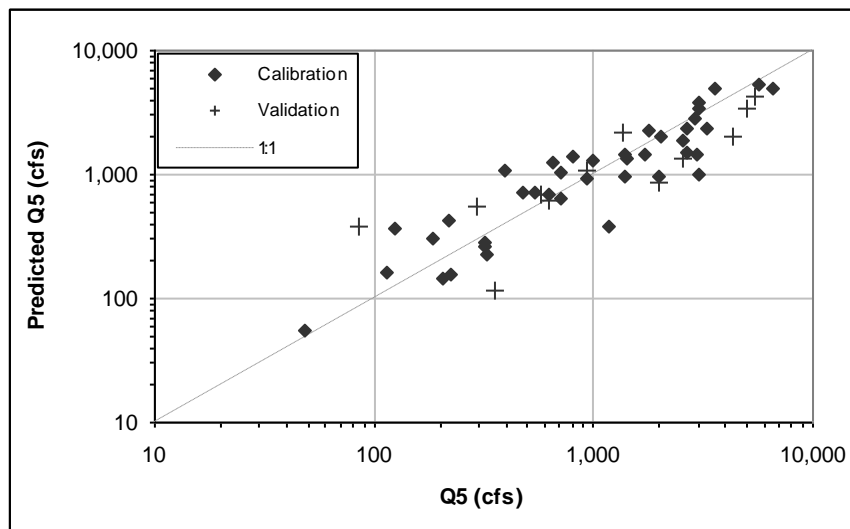
$$Q_{1.5} = e^{-3.7} \cdot e^{(22.2ip)} \cdot rlf^{0.61} \cdot e^{(0.78shp)} \cdot e^{(2.4dry)} \cdot e^{(0.2imp_{max})}$$

Figure B.2 – Cross-validation for Q1.5: 40/12 scheme,  $R^2$  clb/vld = 0.6/0.7



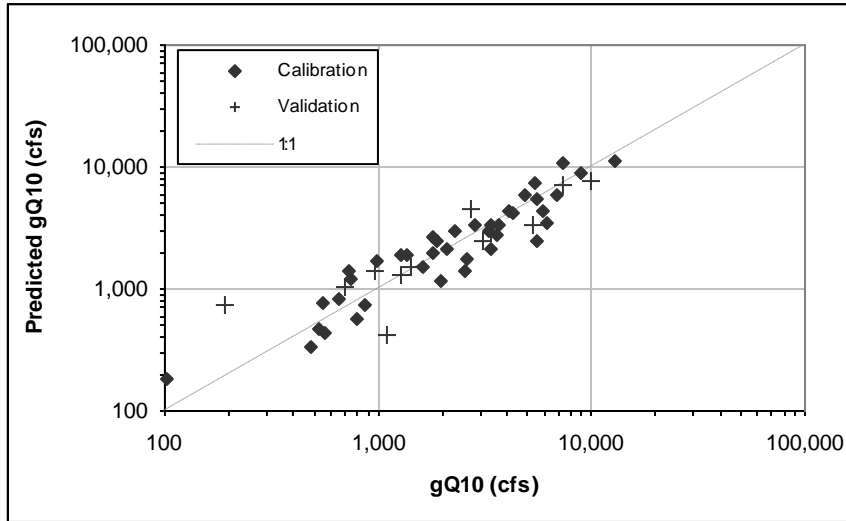
$$Q_2 = e^{2.6} \cdot e^{(19.8 \cdot ip)} \cdot e^{(1.1 \cdot shp)} \cdot e^{(1.9 \cdot dry)} \cdot e^{(0.4 \cdot imp_{max})}$$

Figure B.3 – Cross-validation for Q2: 40/12 scheme,  $R^2$  clb/vld = 0.6/0.6



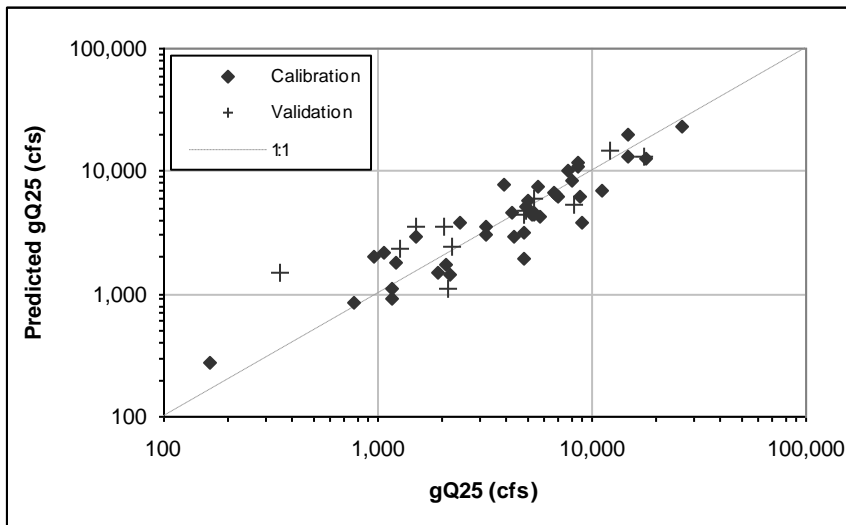
$$Q_5 = e^{3.1} \cdot strm^{0.39} \cdot e^{(16.8 \cdot ip)} \cdot e^{(0.71 \cdot shp)} \cdot e^{(1.7 \cdot dry)}$$

Figure B.4 – Cross-validation for Q5: 40/12 scheme,  $R^2$  clb/vld = 0.8/0.7



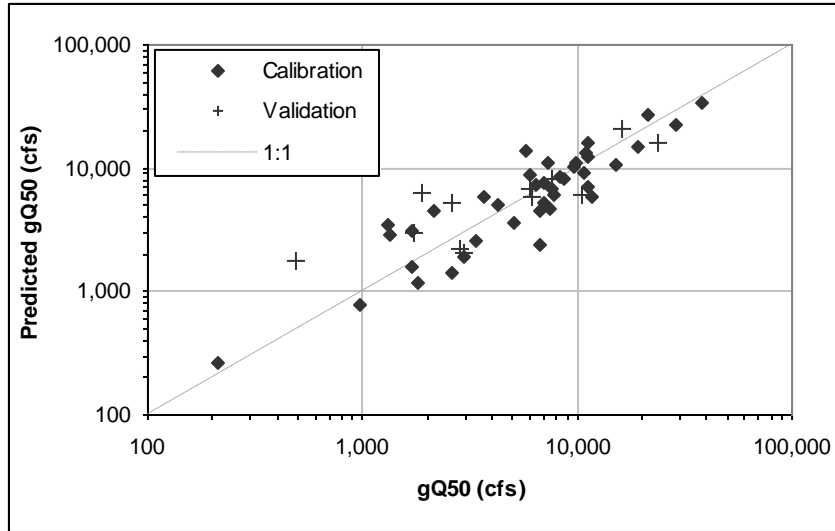
$$Q_{10} = e^{4.0} \cdot strm^{0.57} \cdot e^{(11.5 \cdot ip)} \cdot e^{(-0.60 \cdot shp)} \cdot e^{(-1.5 \cdot vly)} \cdot e^{(-1.5 \cdot dry)}$$

Figure B.5 – Cross-validation for Q10: 40/12 scheme,  $R^2$  clb/vld = 0.8/0.9



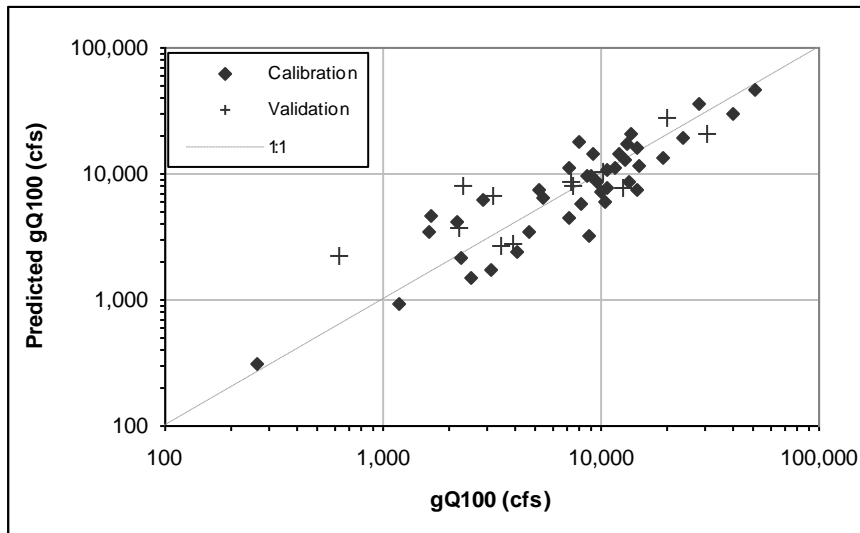
$$Q_{25} = e^{4.4} \cdot A^{0.77} \cdot e^{(6.6 \cdot ip)} \cdot e^{(-2 \cdot stf)} \cdot e^{(-1.3 \cdot dry)}$$

Figure B.6 – Cross-validation for Q25: 40/12 scheme,  $R^2$  clb/vld = 0.8/0.8



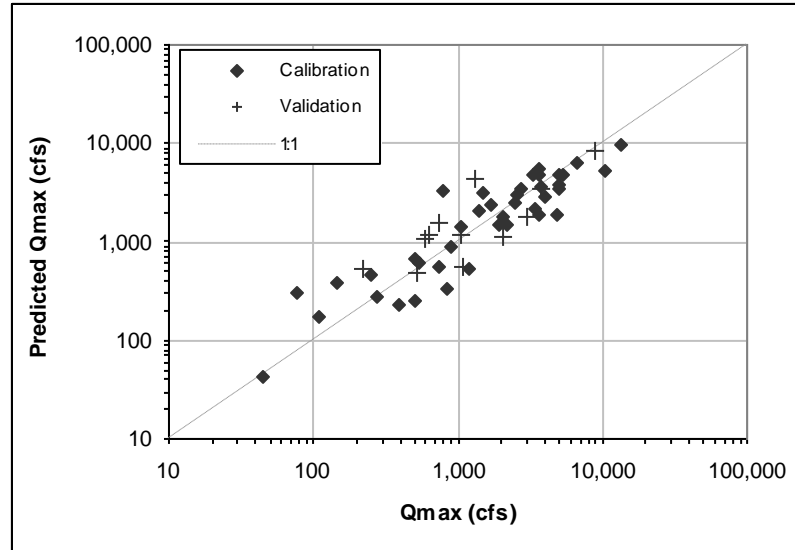
$$Q_{50} = e^{5.2} \cdot A^{0.89} \cdot e^{6.1 \cdot sf} \cdot e^{1.4 \cdot dry}$$

Figure B.7 – Cross-validation for Q50: 40/12 scheme,  $R^2$  clb/vld = 0.8/0.7



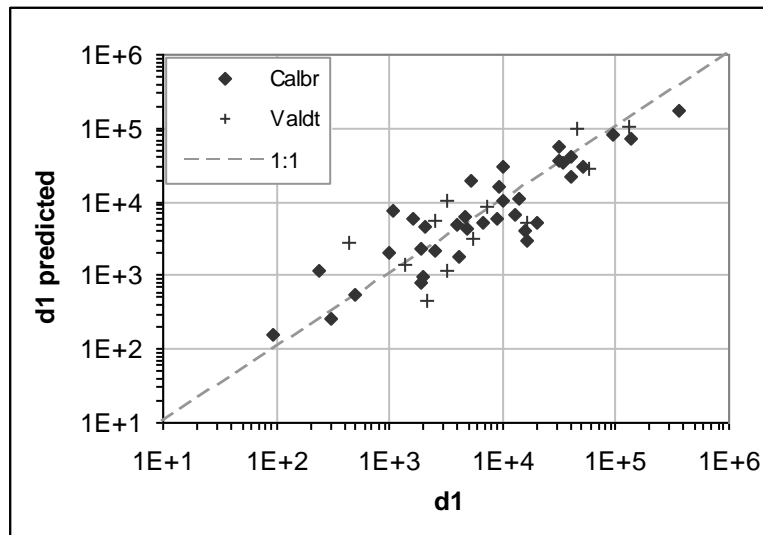
$$Q_{100} = e^{5.3} \cdot A^{0.91} \cdot e^{6.3 \cdot sf} \cdot e^{1.3 \cdot dry}$$

Figure B.8 – Cross-validation for Q100: 40/12 scheme,  $R^2$  clb/vld = 0.8/0.7



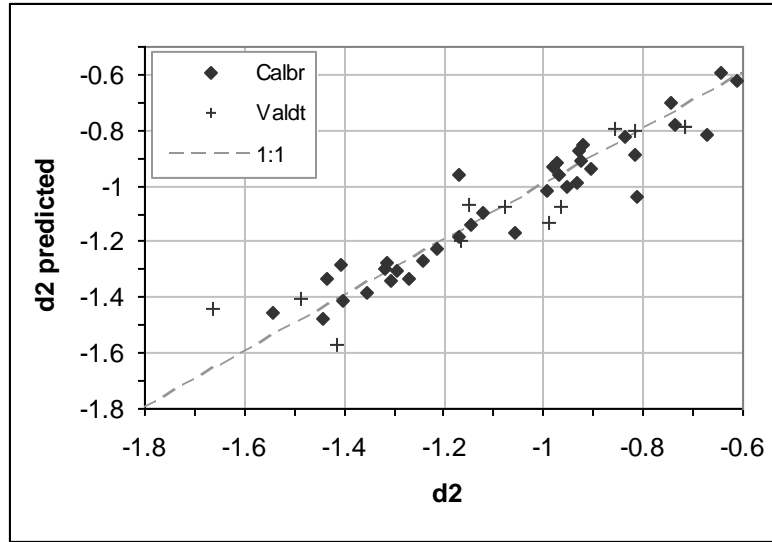
$$Q_{\max} = e^{-3.6} \cdot strm^{0.75} \cdot P^{0.78} \cdot rlf^{0.50} \cdot yr^{0.53} \cdot e^{(-2.0 \cdot dry)}$$

Figure B.9 – Cross-validation for Qmax: 40/12 scheme, R<sup>2</sup> clb/vld = 0.7/0.8



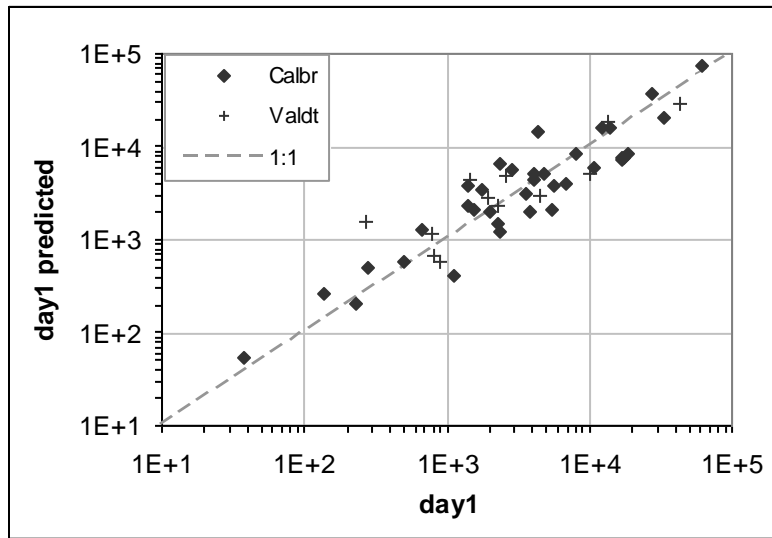
$$d_1 = e^{-12.9} \cdot P^{3.5} \cdot yr^{2.4} \cdot dd^{-2.3} \cdot Q_{\max}^{0.47} \cdot e^{(5 \cdot dry)} \cdot e^{(7 \cdot imp_{7.5})}$$

Figure B.10 – Cross-validation for d1: 36/12 scheme, R<sup>2</sup> clb/vld = 0.7/0.7



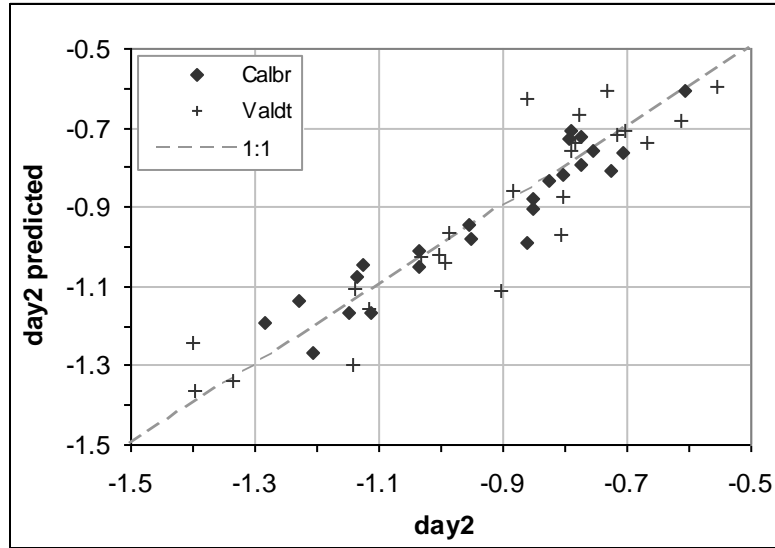
$$d_2 = -1.9 + 0.093 \cdot \ln \left( \frac{r}{r_0} \right) + 0.20 \cdot \ln \left( \frac{Q_{10}}{Q_{10,0}} \right) - 0.11 \cdot \ln \left( \frac{C_1}{C_{1,0}} \right) + 0.94 \cdot imp_{avg}$$

Figure B.11 – Cross-validation for d2: 36/12 scheme,  $R^2$  clb/vld = 0.9/0.9



$$day_1 = e^{-3.9} \cdot yr^{1.8} \cdot dd^{-2.4} \cdot e^{(0.57f)} \cdot Q_{max}^{0.62} \cdot e^{(1.0 \cdot imp_{avg})}$$

Figure B.12 – Cross-validation for day1: 36/12 scheme,  $R^2$  clb/vld = 0.8/0.8



$$day_2 = -1.9 + 0.096 \cdot \ln(P) + 0.17 \cdot \ln(r) + 0.18 \cdot \ln(Q_{10}) - 0.16 \cdot \ln(day_1) + 0.99 \cdot imp_{avg}$$

**Figure B.13 – Cross-validation for day2: 24/23 scheme,  $R^2$  clb/vld = 0.9/0.8**

**APPENDIX C**

**HYDROMODIFICATION SITE CROSS-SECTIONS, BANKS, AND  
PHOTOGRAPHS**

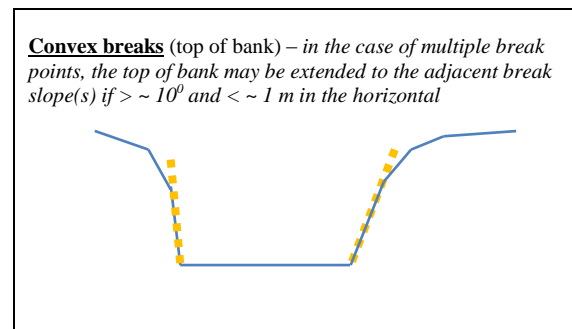
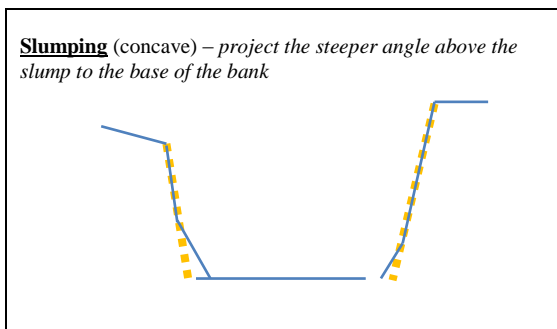
## C.1 PURPOSE AND MEASUREMENT PROTOCOL

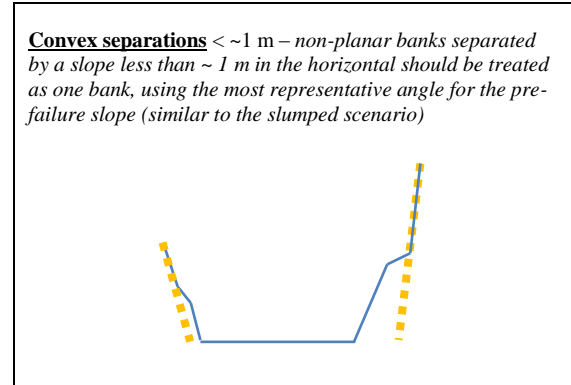
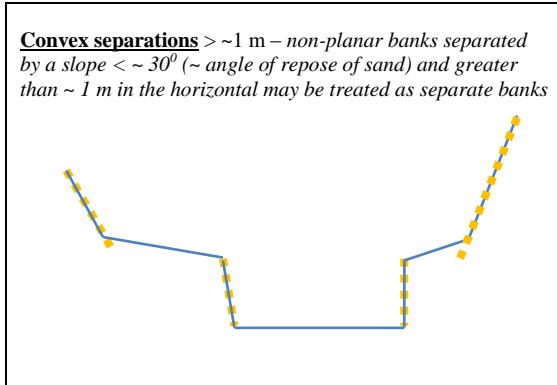
These data were used in the development of a “screening tool” which estimates a first-order risk classification of a channel’s susceptibility to adversely responding to the effects of hydromodification in southern California. In particular, these data were used to develop the section of the screening tool focused on assessing bank stability at the time of the field assessment based on measurements.

Since the screening tool is intended to err on the side of overestimating risk, the precautionary principles were used where field indicators were unclear. That is:

- where the stability of a bank was uncertain, we erred on the side of classifying as unstable;
- where an unstable angle was uncertain, the smaller angle was used; and
- where an unstable height was uncertain, the smaller height was used.

Banks were measured in vein of capturing the angle and height most representative for purposes of mass wasting based on failure theory presented by Osman and Thorne (1988). Special cases are outlined below.





The 1-m horizontal discriminator was selected based on the fact that observable failure blocks (i.e., still relatively intact) were typically well less than 1 m.

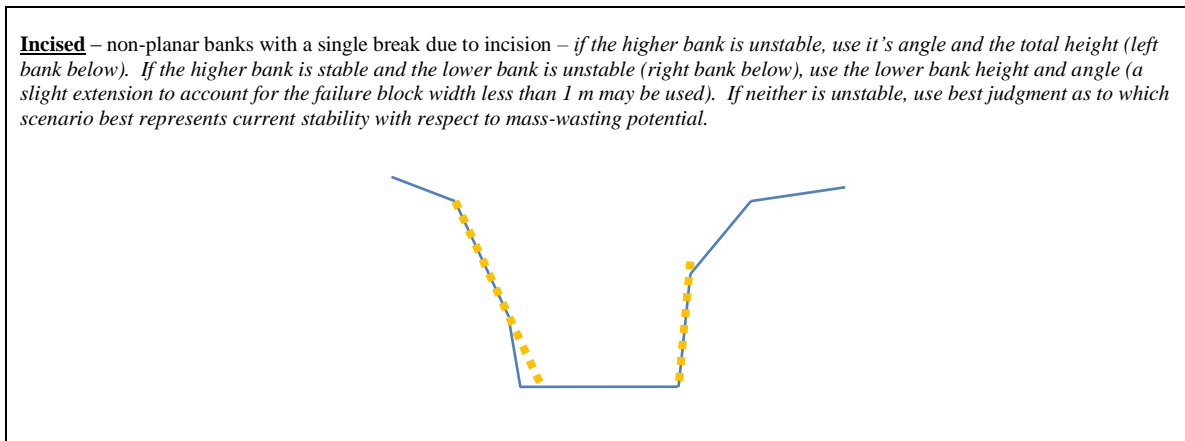


Table C.1 presents the layout key and Table C.2 presents the bank-stability key for the cross sections, banks, and photographs of surveyed hydromodification sites.

**Table C.1 – Layout key**

**Unique ID (Stream\_Cross Section)**

**Surveyed by (Organization), Month-Year**

**Note(s)/Site History:**

**Left Bank (LB)**      Stability rating

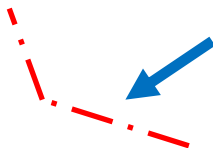
**Right Bank (RB)**      Stability rating

**Photograph(s)**

*Close-up view with object for scale if available*

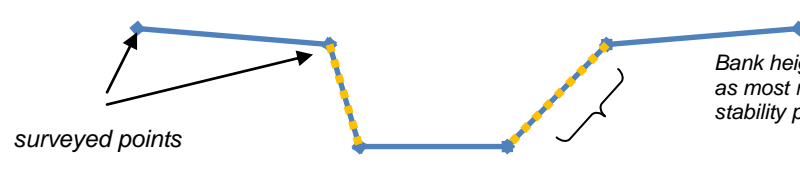
**Photograph(s)**

*Dashed-dot red line represents approximate location of cross section, bent at bank location. Solid blue arrow indicates flow direction*



**Surveyed Cross Section** (looking downstream)

*Grid provided for individual horizontal to vertical scale*



*Bank height and projected angle used as most representative for mass wasting stability purposes*

*surveyed points*

**Table C.2 – Bank-stability key**

<b>STABLE</b>	no visible bank failure
<b>U-MW-C</b>	unstable, mass wasting, in moderately or well-consolidated banks
<b>U-MW-PC</b>	unstable, mass wasting, in poorly-consolidated banks
<b>U-FLUVIAL</b>	failure primarily due to fluvial forces (e.g., submerged shear stress, bend erosion, etc.)
<b>U-MW-UC</b>	mass wasting evident but in unconsolidated banks (e.g., old bed of braided channel)
<b>U-FAILED</b>	geometry post-mass failure (i.e., nearing angle of repose for unconsolidated material)
<b>S-CONSTR</b>	stable banks, but constructed/ graded and should not be included in analyses
<b>S-CONFND</b>	stable banks, but confined by hillslope

Note(s):

LB U-MW-C

RB S-CONSTR



Near Santiago\_A looking downstream

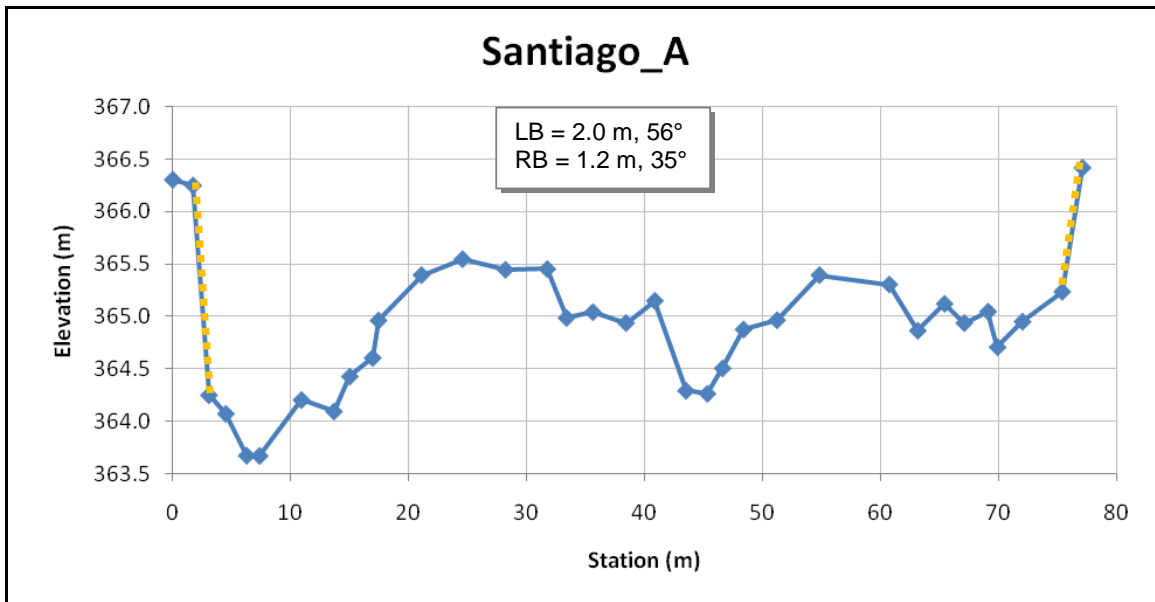


Figure C.1 – Santiago\_A

Note(s): Flood control embankment constructed on right bank (date unknown)

LB S-CONFND

RB S-CONSTR (upper) and U-MW-UC (lower)

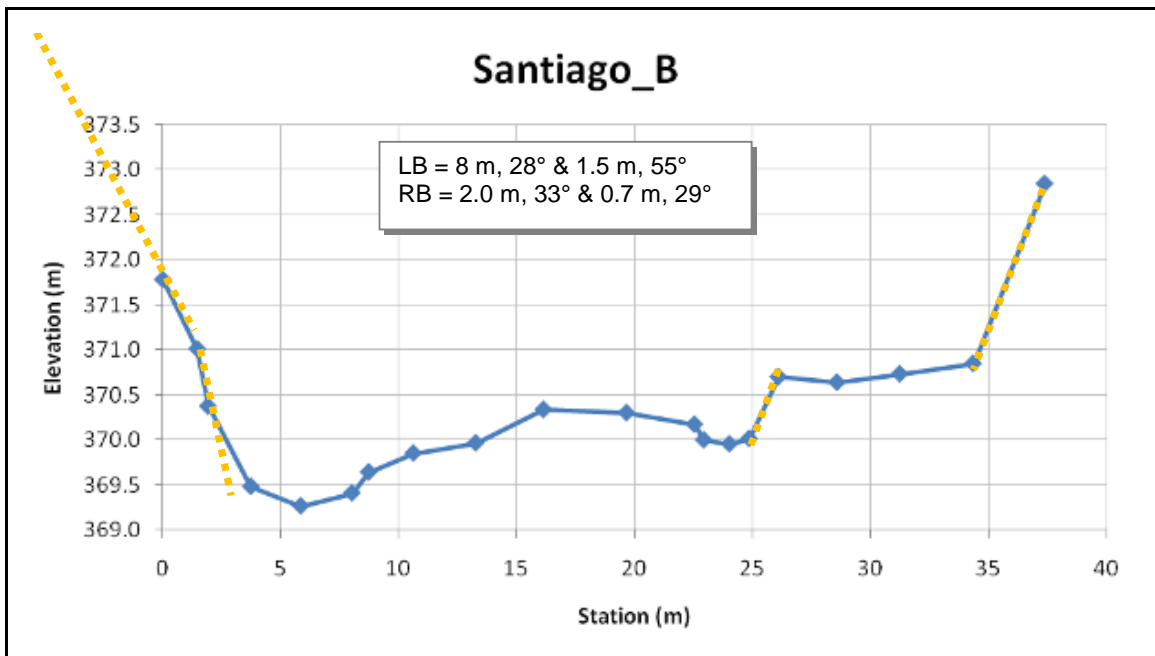
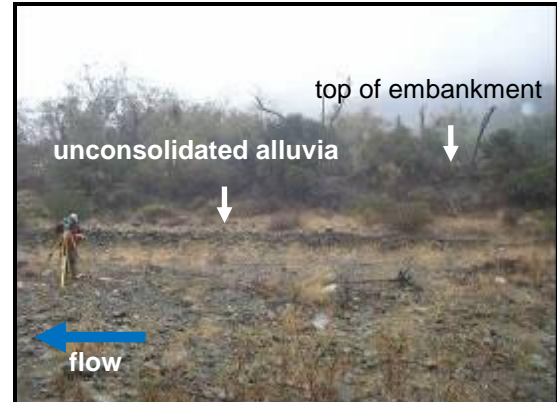


Figure C.2 – Santiago\_B

Note(s): Site was graded and realigned/partially channelized during development circa 2002.

LB U-MW-PC

RB U-MW-PC



Near Hasley1\_A looking upstream



Near Hasley1\_A looking downstream

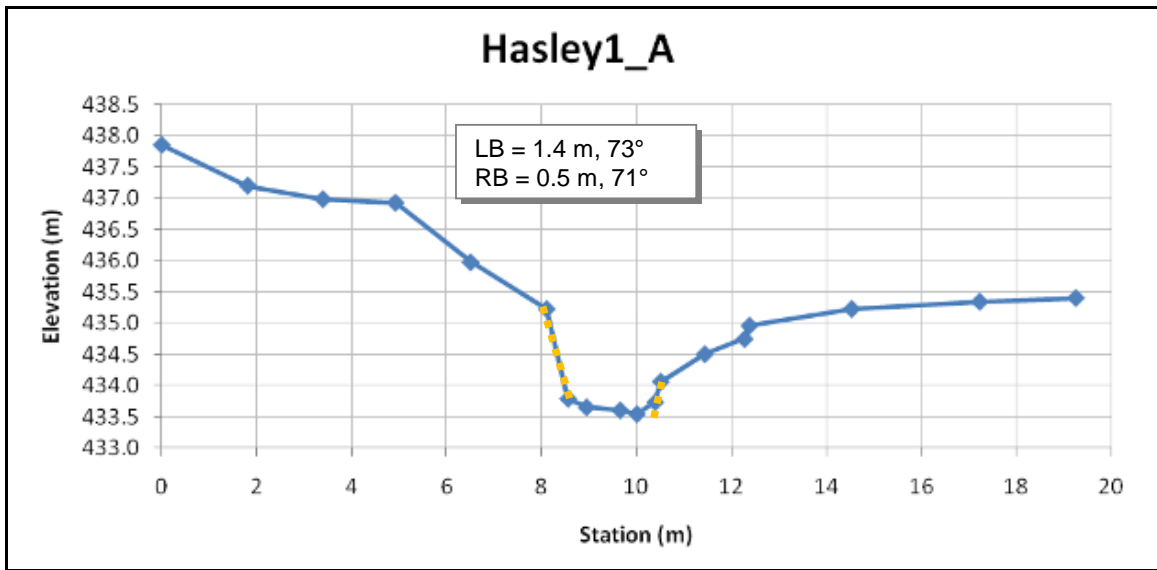


Figure C.3 – Hasley1\_A

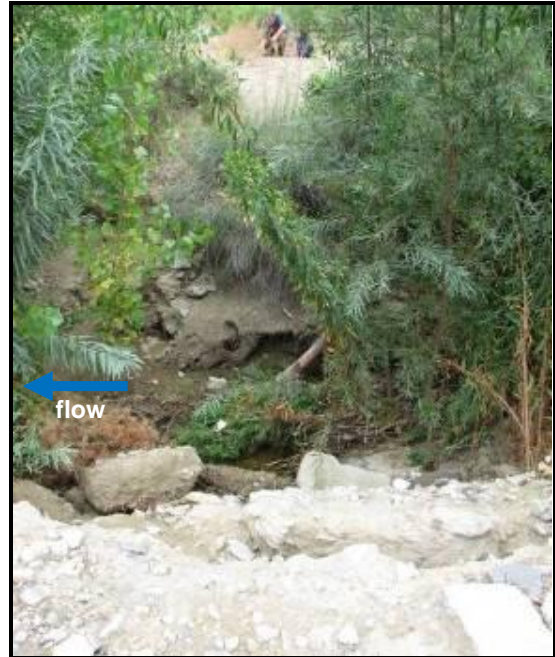
Note(s): Site was graded and realigned/partially channelized during development circa 2002.

LB U-MW-PC

RB U-MW-PC



Near Hasley1\_B



Near Hasley1\_B

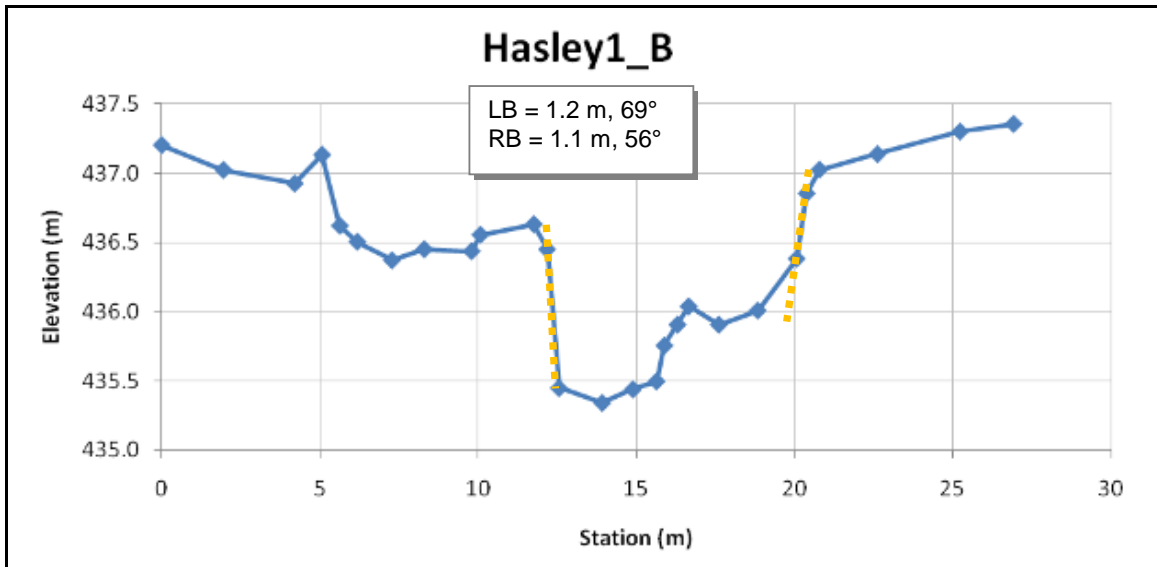


Figure C.4 – Hasley1\_B

Note(s): *Right bank is unconsolidated fill (i.e., built up higher than original floodplain for lot creation)*

LB STABLE

RB S-CONSTR

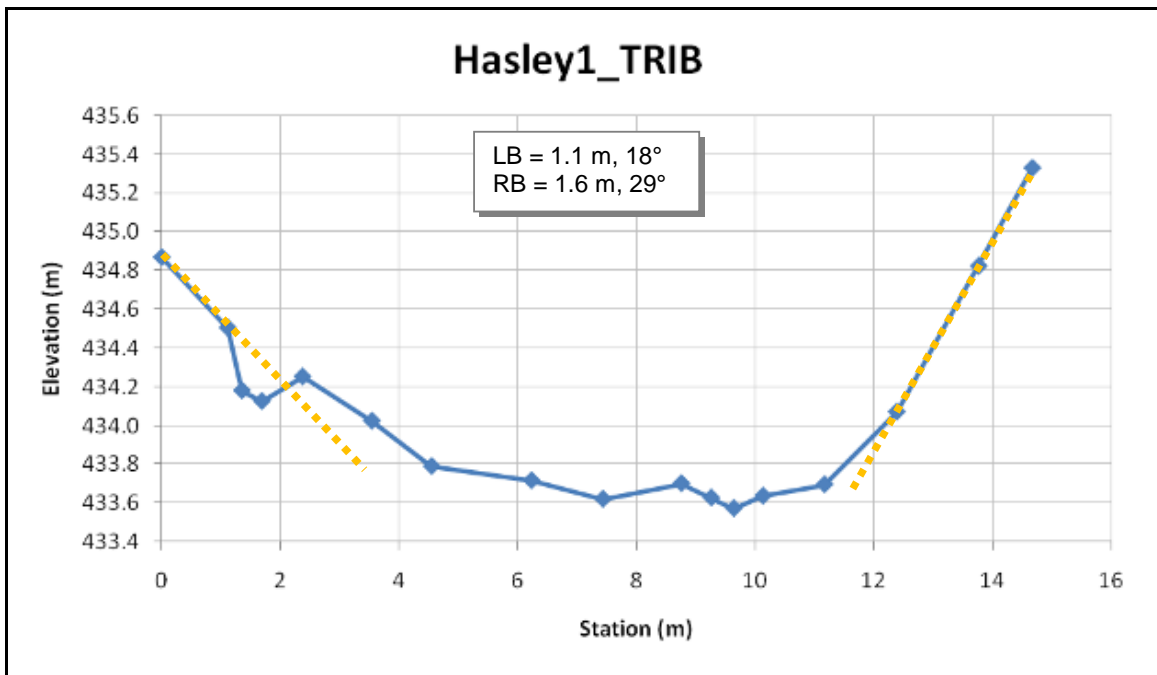


Figure C.5 – Hasley1\_TRIB

Note(s):

LB U-FAILED

RB U-MW-PC



Near Hasley2\_A (survey captured geometry of a recently failed bank (<math><30^{\circ}</math> vs. pictured >math>>75^{\circ}</math>))

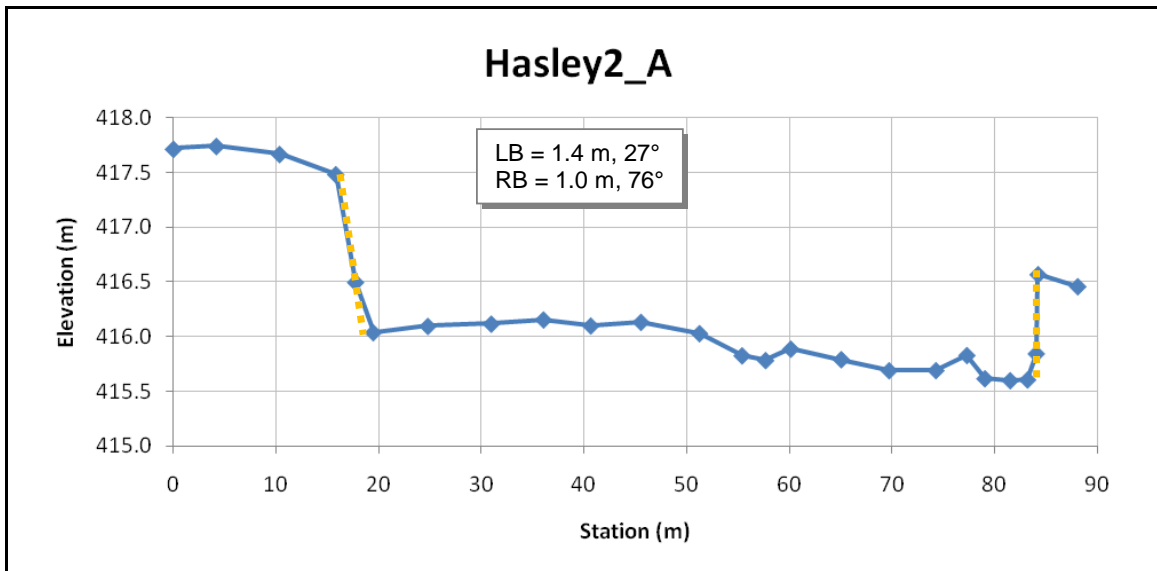


Figure C.6 – Hasley2\_A

Note(s):

LB U-MW-C

RB STABLE-PC



*Rilling evident, but no mass wasting, possibly graded*

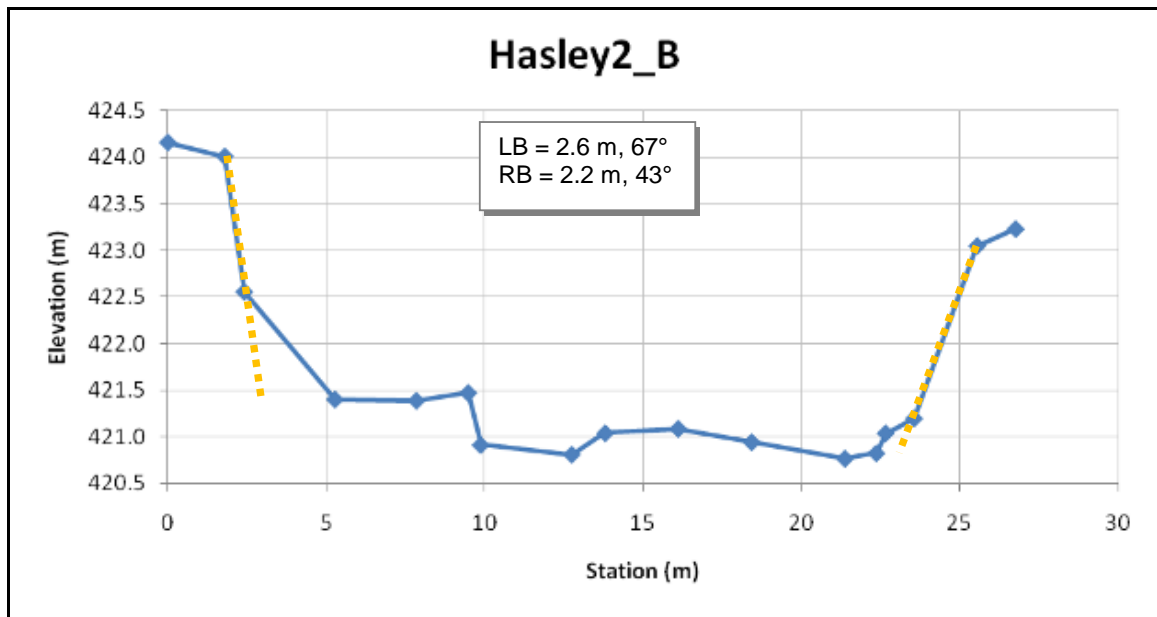


**Figure C.7 – Hasley2\_B**

Note(s):

LB U-MW-PC

RB U-MW-PC



Near Hasley2\_TRIB, 6-in ruler for scale (just downstream, ~1.5x taller, similar composition)



IMG0984

Near Hasley2\_TRIB (just downstream, ~2x taller similar composition)



Zoomed out at cross section

flow



top of bank

top of bank at cross section

flow

Downstream photograph

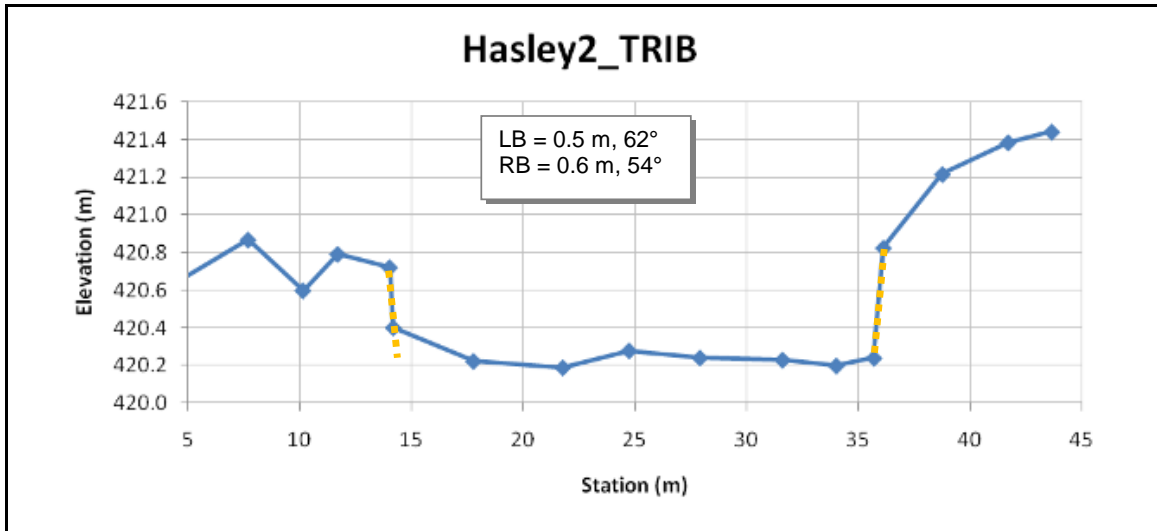


Figure C.8 – Hasley2\_TRIB

Note(s):

LB STABLE-PC (upper) U-MW-UC (lower) RB STABLE-PC (upper) STABLE-UC (lower)



*Unconsolidated bed of pre-incised channel*

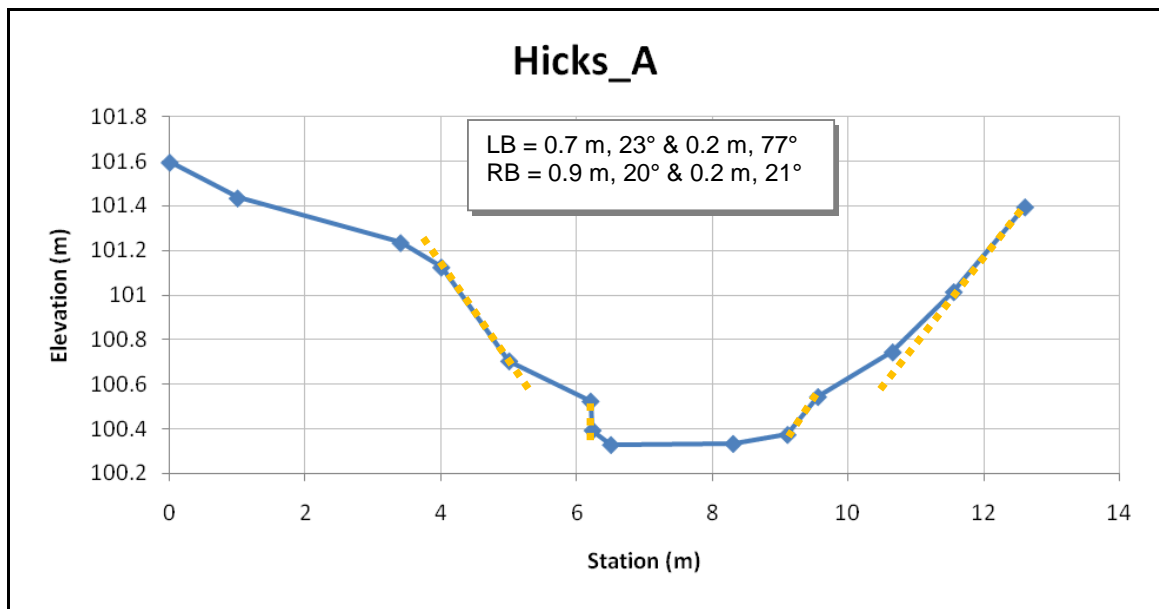
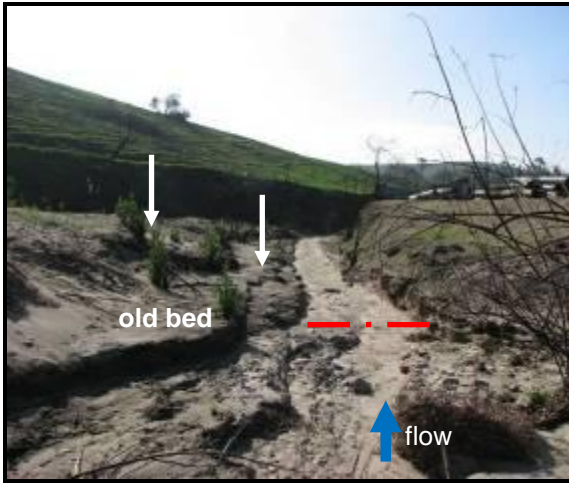


**Figure C.9 – Hicks\_A**

Note(s):

LB U-FAILED (upper) and U-FAILED (lower)

RB U-MW-PC



Fluvial activity across failed surfaces makes it difficult to re-project pre-failure geometry

Historic MW (dotted arrows) converges with recent MW (solid arrows) just downstream of survey. Just upstream of cross section, MW through pre-incised bed

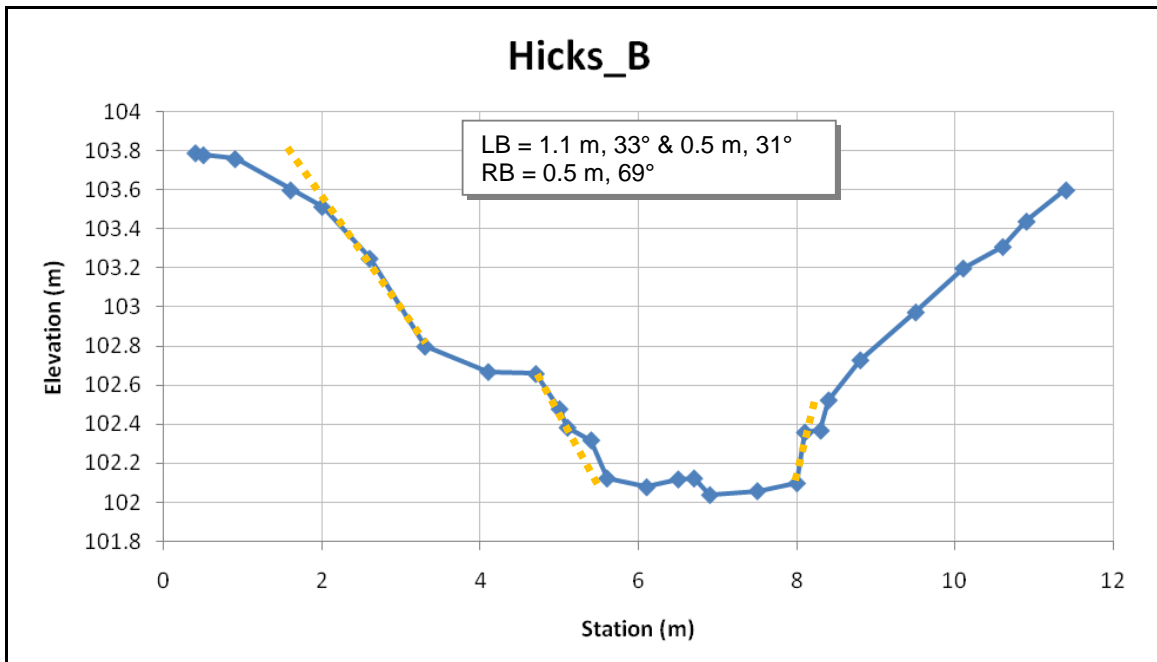


Figure C.10 – Hicks\_B

Note(s):

LB U-MW-PC (upper) and U-MW-PC (lower)

RB STABLE-UC



Looking upstream



Looking upstream

Fluvial erosion is significant (bend), but mass wasting is ubiquitous

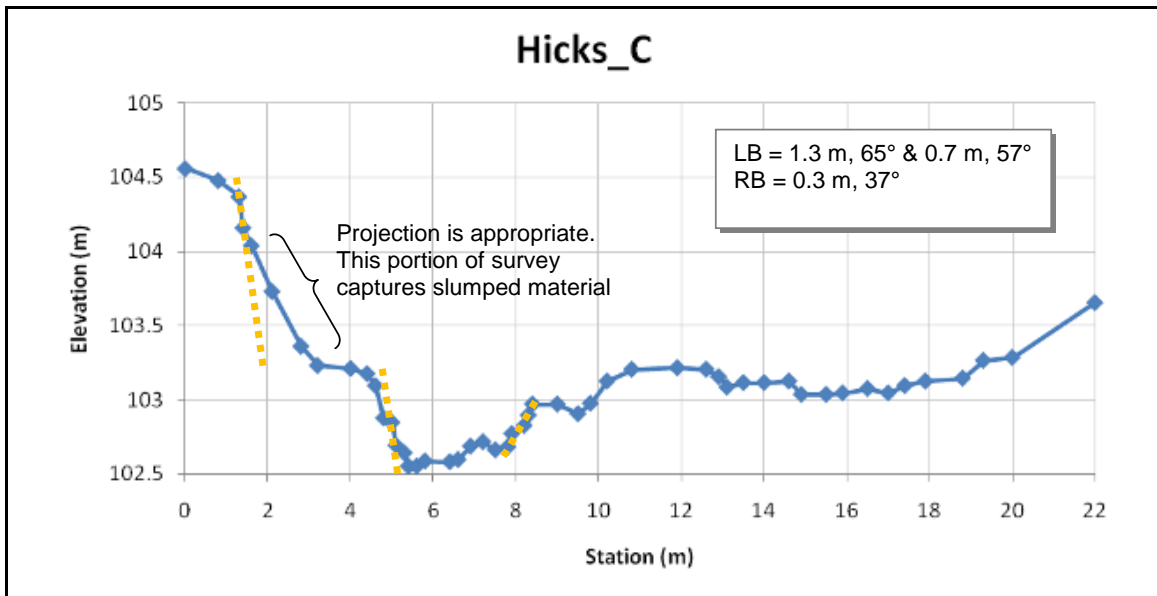
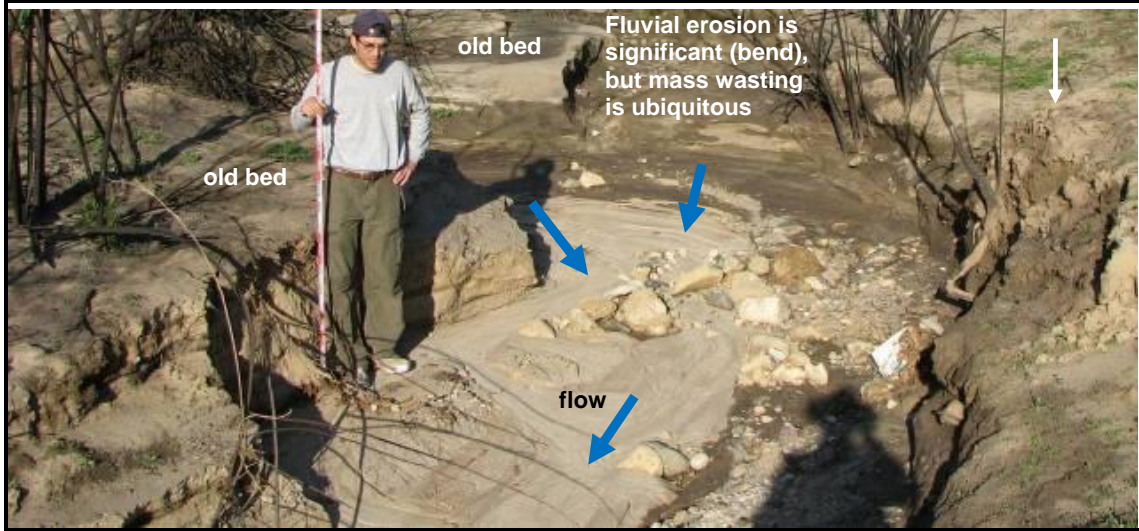


Figure C.11 – Hicks\_C

Note(s):

LB U-MW-PC

RB U-MW-PC



Looking upstream

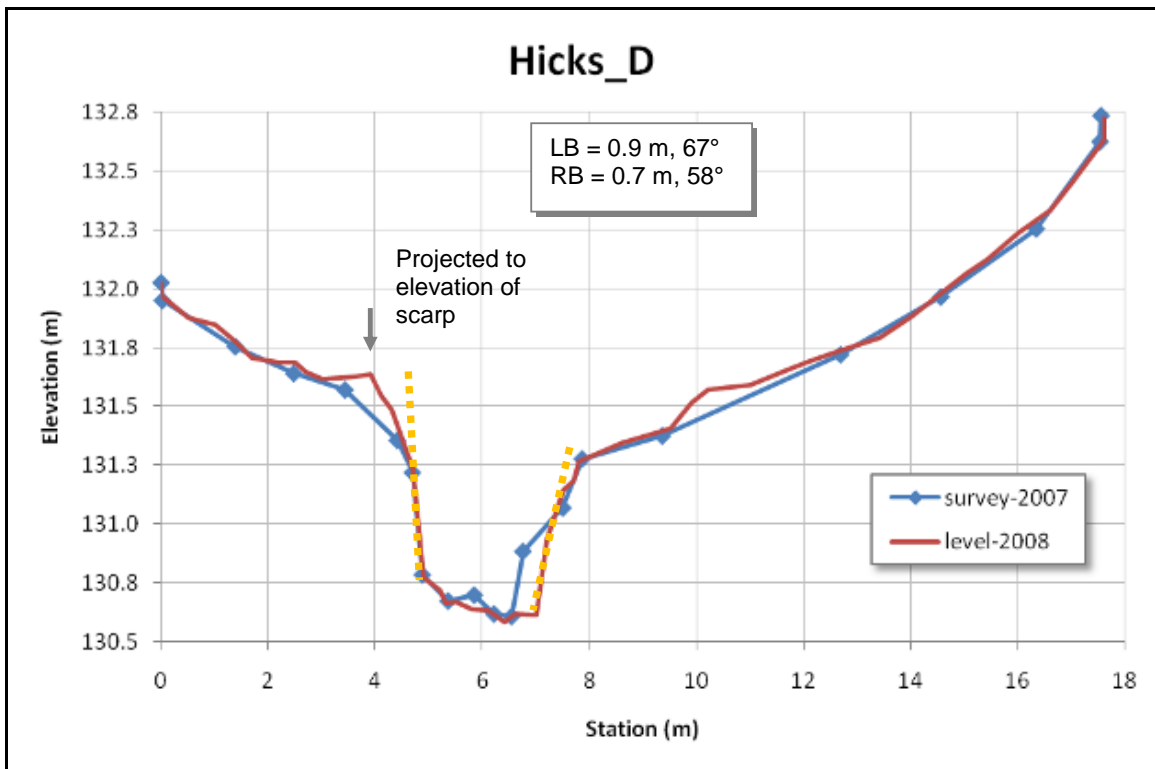


Figure C.12 – Hicks\_D

Note(s):

LB U-MW-PC

RB U-MW-PC



Looking upstream

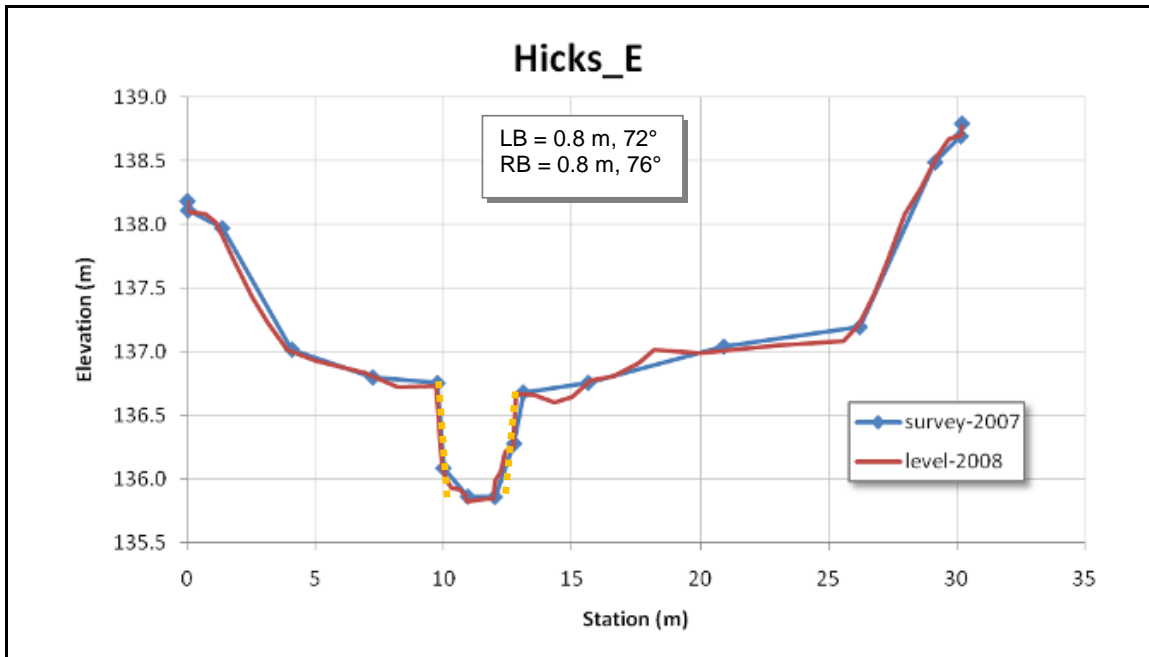
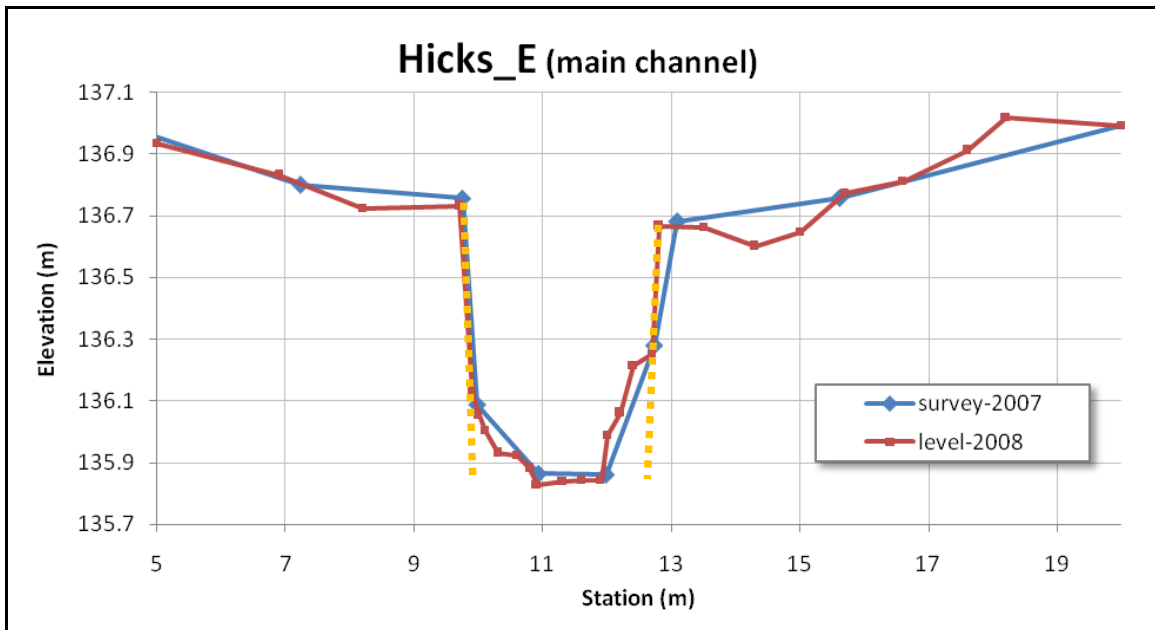


Figure C.13 – Hicks\_E



The purpose of presenting this detailed figure is to exemplify the differences between surveys. The CSU/SCCWRP 2008 level survey had many more shots, resulting in more precise geometry. In cases, bank angles were significantly different ( $76^\circ$  vs.  $48^\circ$  for the right bank of Hicks\_E), despite a relatively constant cross section between survey dates.

To Stillwater's credit, they were surveying many cross sections through dense shapparal (pre-fire). The CSU/SCCWRP surveys were post-fire, which made their collection much easier despite having less precise equipment.

The scarp in the pre-fire (2007) photograph of the right bank below is consistent with the post-fire (2008) photograph on the previous page.



**Figure C.13 (continued) – Hicks\_E**

Note(s):

LB U-MW-PC

RB U-MW-PC



Looking downstream

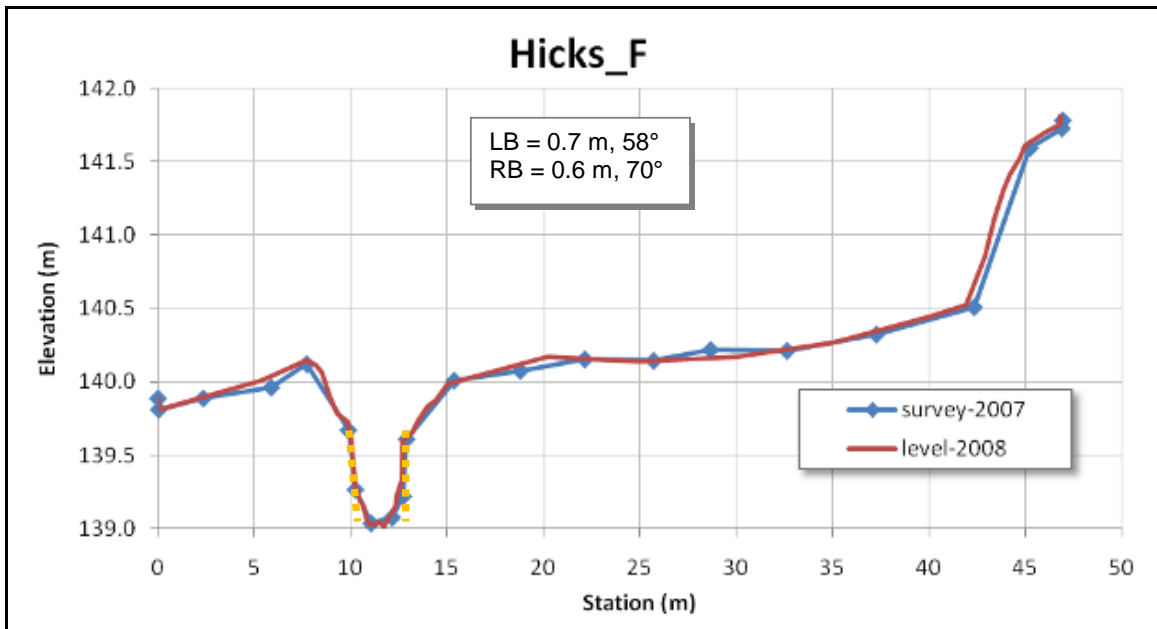


Figure C.14 – Hicks\_F

Note(s):

LB STABLE

RB U-MW-C



Looking upstream

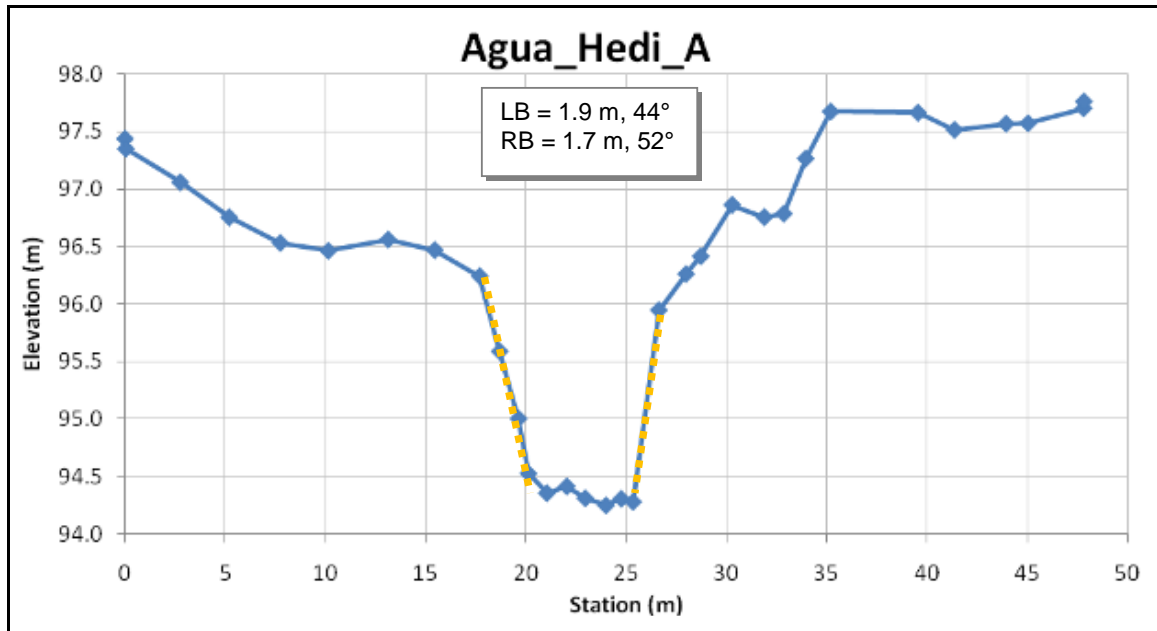


Figure C.15 – Agua\_Hedi\_A

Note(s):

LB U-MW-C

RB U-MW-C (upper) U-FLUVIAL (lower)



Upper portion



Lower portion

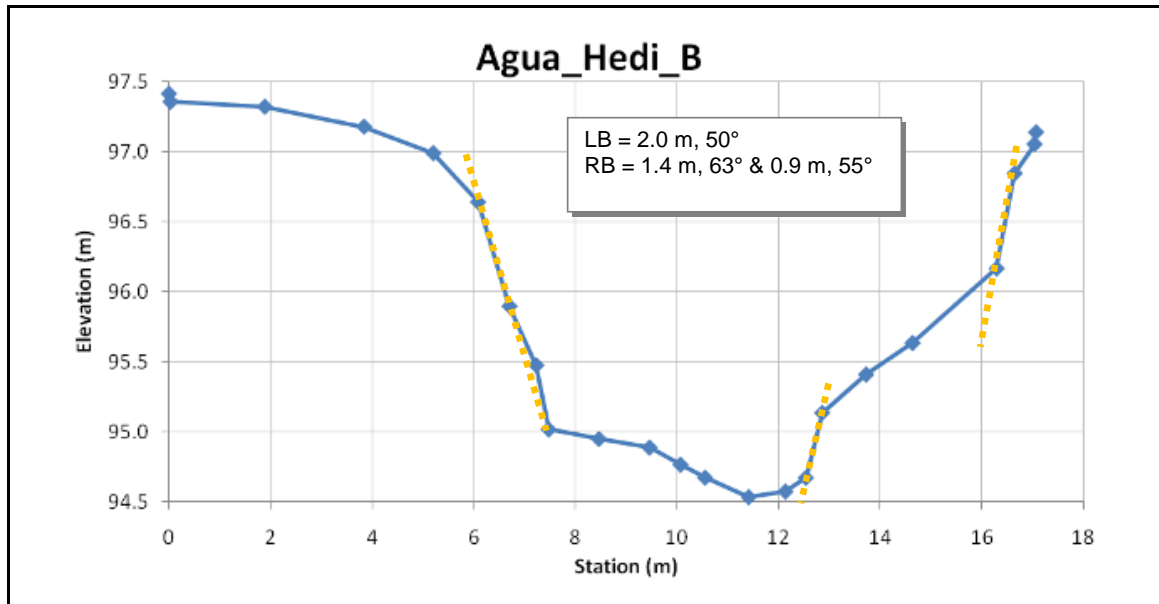


Figure C.16 – Agua\_Hedi\_B

Note(s):

LB U-MW-C

RB U-MW-C (upper) and U-MW-C (lower)



Looking downstream



Looking upstream

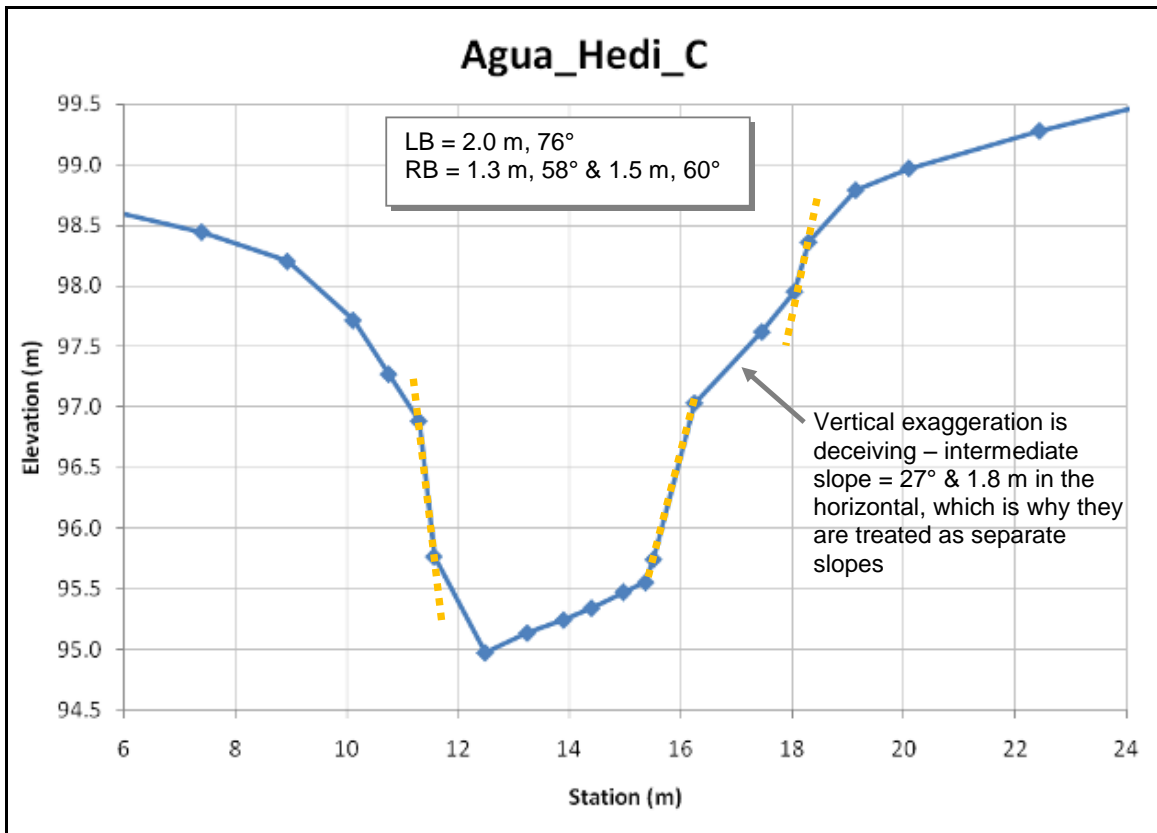


Figure C.17 – Agua\_Hedi\_C

Note(s):

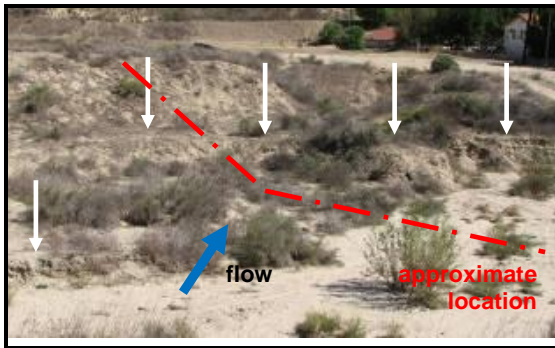
LB STABLE (upper) and U-FAILED (lower) RB U-MW-C (upper) and U-MW-C (lower)



Looking downstream



Looking upstream



Looking downstream



Looking upstream

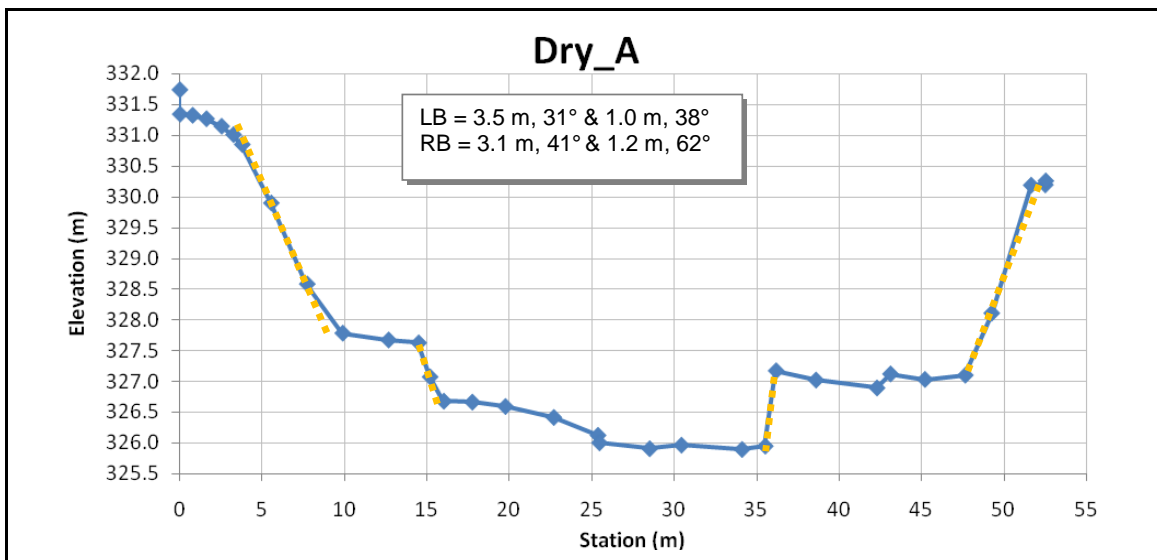


Figure C.18 – Dry\_A

Dry\_B

Stillwater Sciences, Oct-2007

Note(s):

LB STABLE (upper) and U-FAILED (lower)

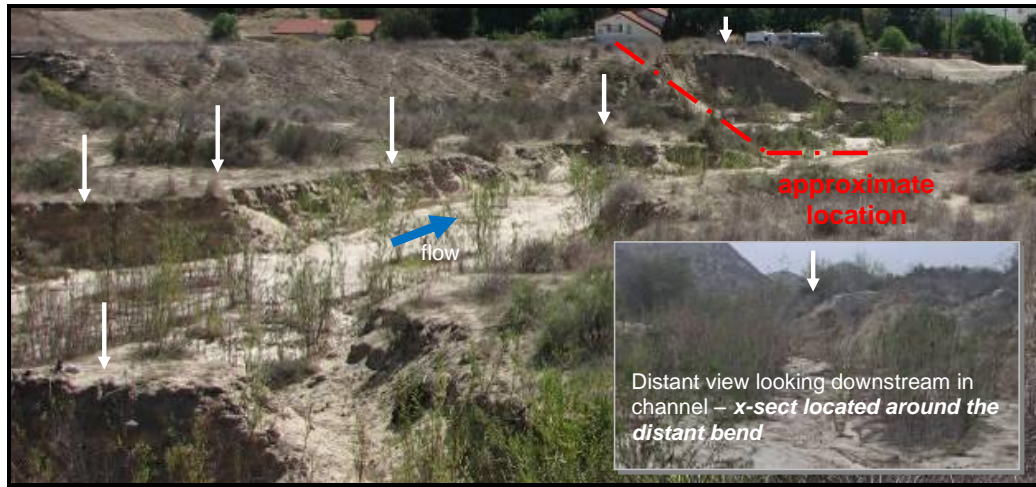
RB STABLE (upper) and U-MW-C (lower)



Looking downstream



Looking upstream



Distant view looking downstream

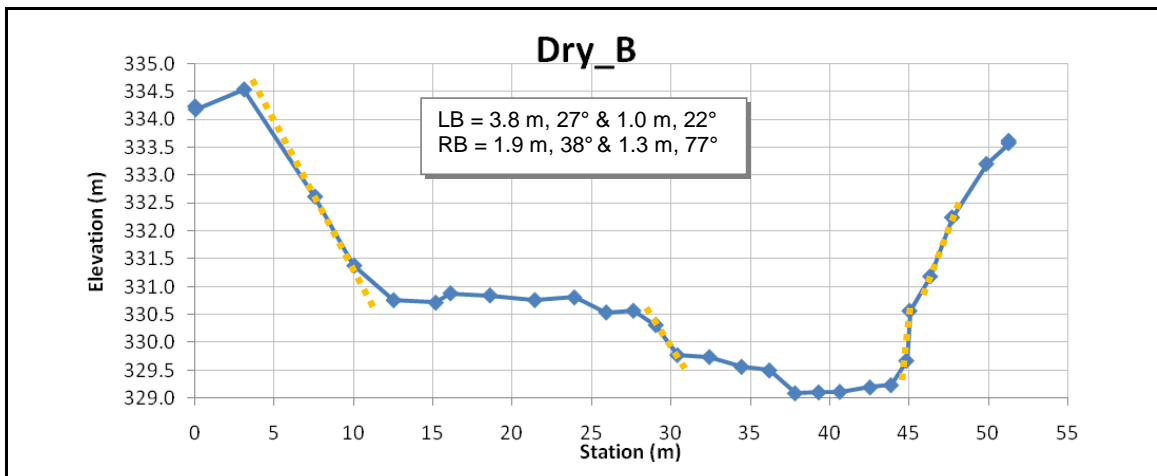
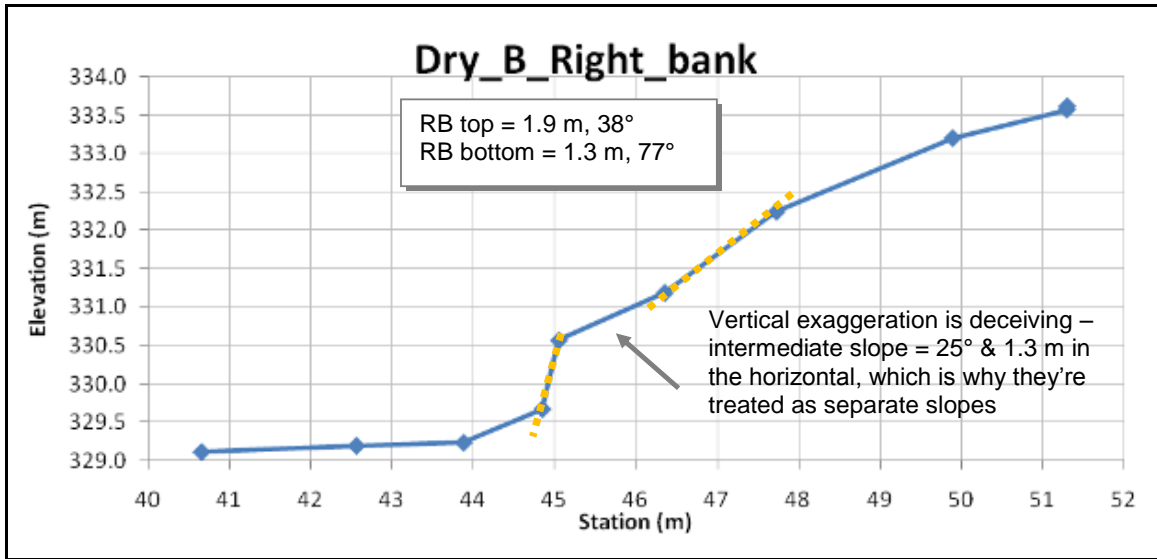


Figure C.19 – Dry\_B



*With such a wide cross-section, this view is intended to more easily delineate the various bank slopes and break points.*

**Figure C.19 (continued) – Dry\_B**

Dry\_C

Stillwater Sciences, Oct-2007

Note(s):

LB STABLE

RB U-MW-C



Looking downstream



Looking upstream

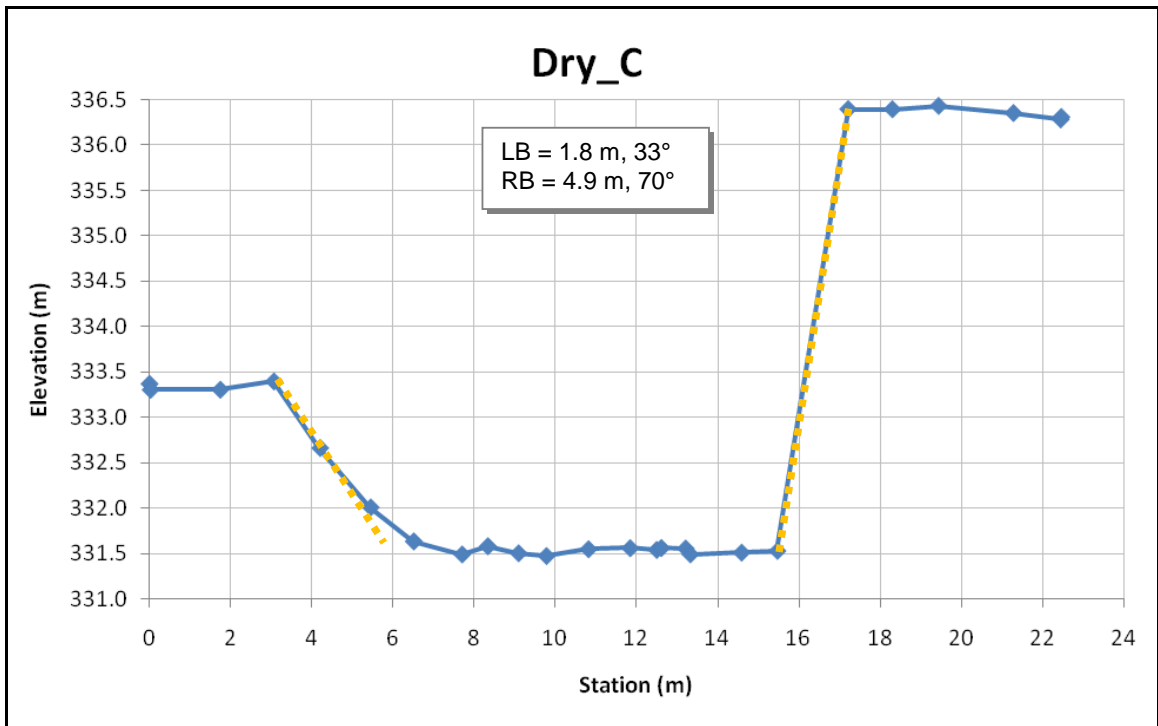
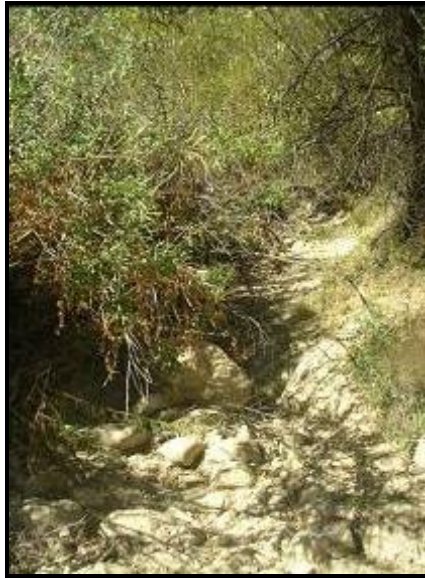


Figure C.20 – Dry\_C

Note(s):

LB STABLE

RB STABLE



Looking upstream



Looking downstream

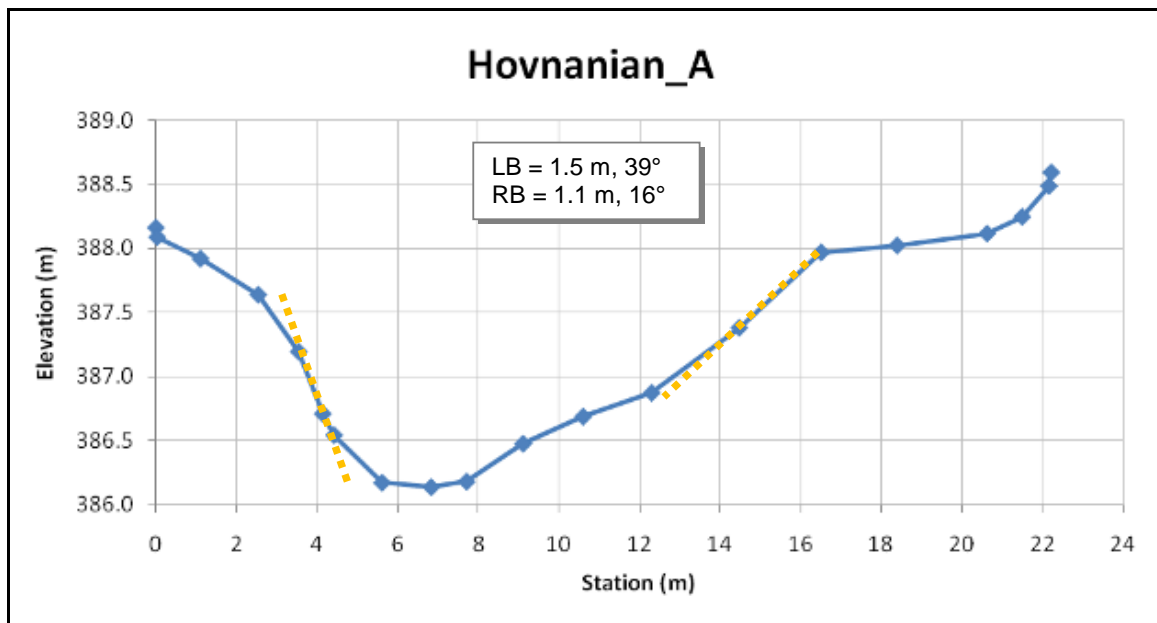


Figure C.21 – Hovnanian\_A

Note(s):

LB STABLE

RB STABLE



Looking upstream



Looking downstream

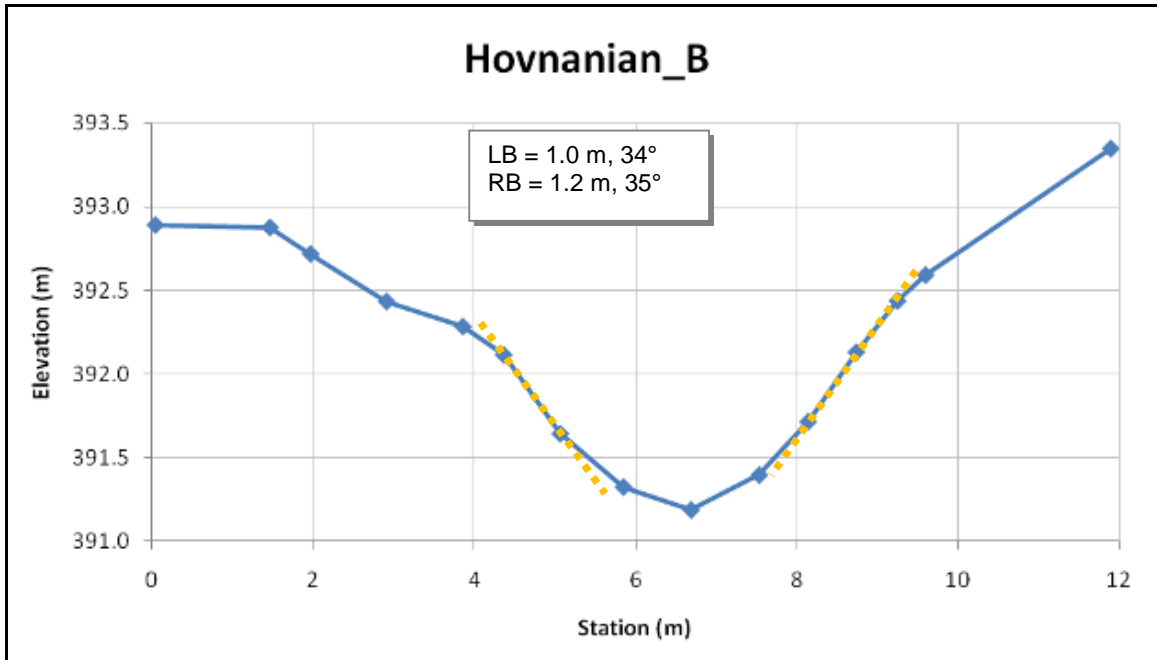


Figure C.22 – Hovnanian\_B

Note(s):

LB U-MW-C

RB U-MW-C (upper) and U-MW-C (lower)



Looking upstream



Looking downstream

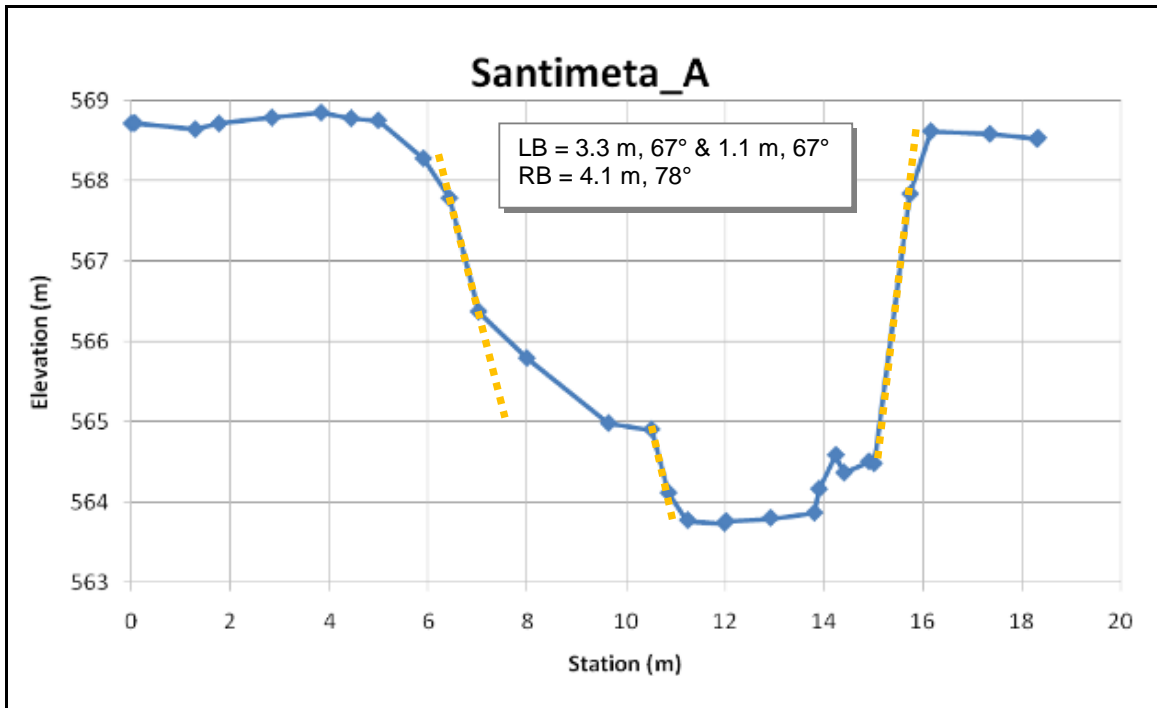


Figure C.23 – Santimeta\_A (San Timetao)

Note(s):

LB U-MW-C

RB U-MW-C



Looking upstream



Looking downstream

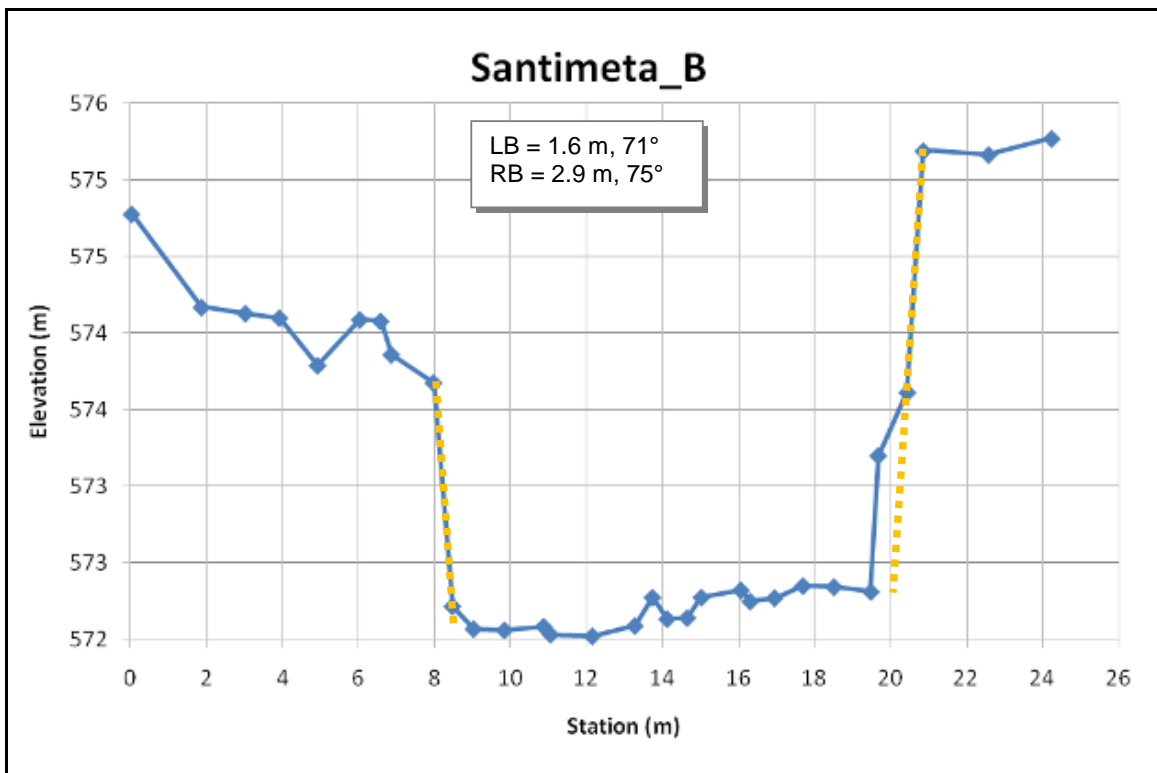


Figure C.24 – Santimeta\_B (San Timetao)

Note(s):

LB U-MW-C

RB U-MW-C



Looking upstream



Looking downstream



View of left bank

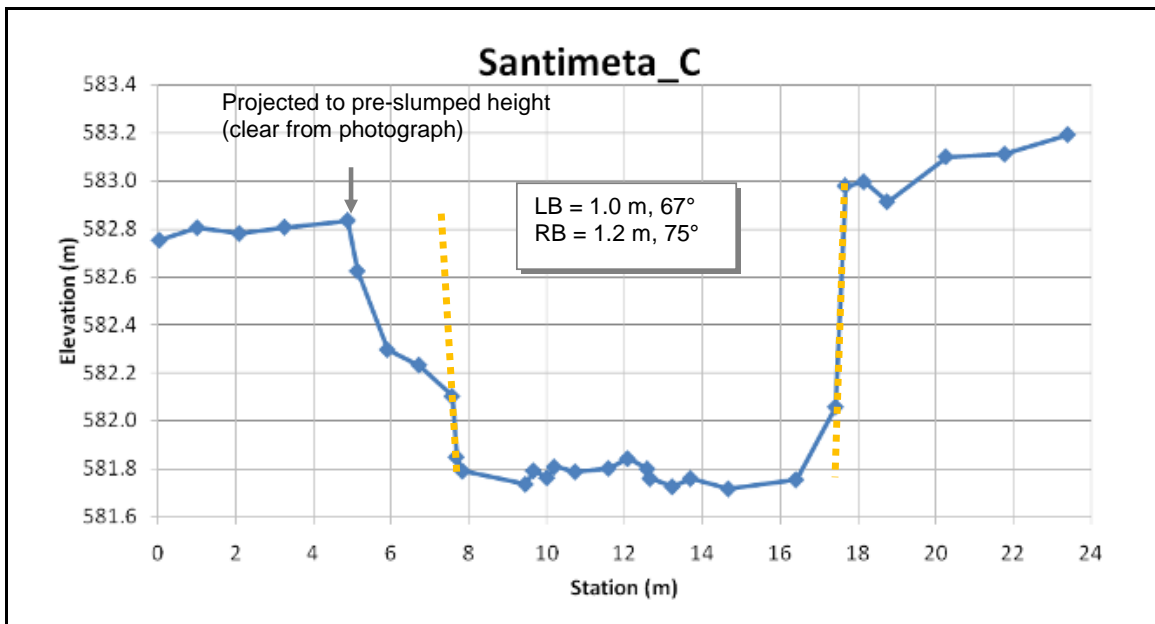


Figure C.25 – Santimeta\_C (San Timetao)

Note(s):

LB U-MW-PC

RB U-MW-PC



Looking upstream



Looking downstream

*Incising through poorly consolidated alluvia downstream of bridge (forced confinement)*

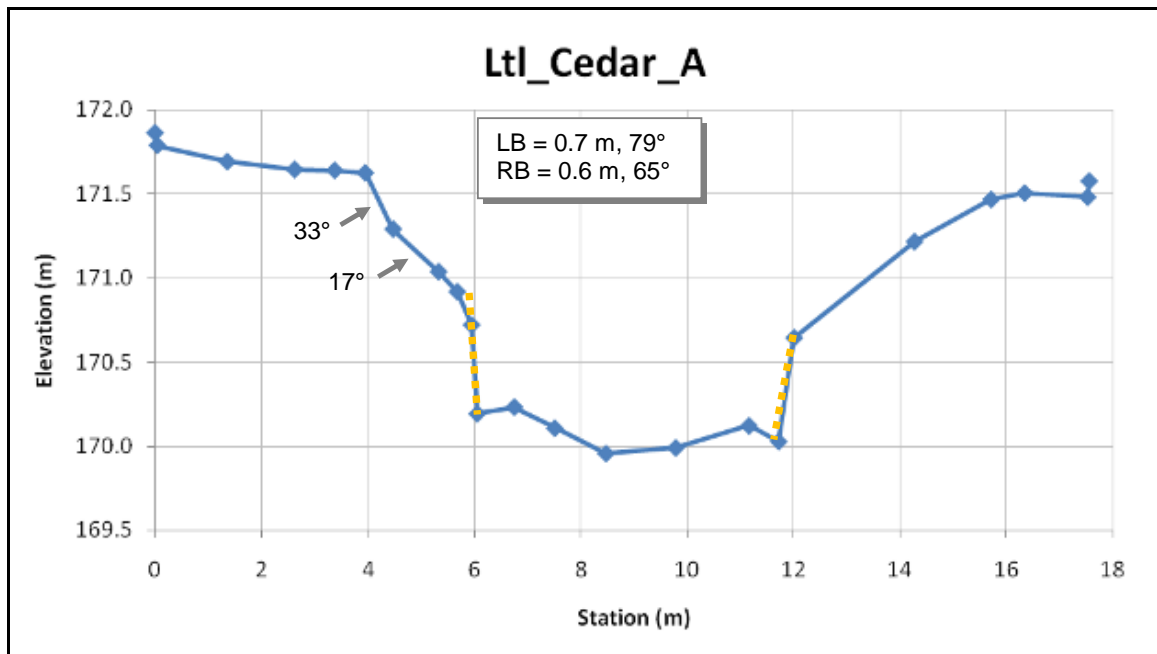


Figure C.26 – Ltl\_Cedar\_A (Little Cedar)

Note(s):

LB STABLE-UC

RB U-FAILED (lower) and STABLE (upper)



Looking downstream, w/ distant view of downstream left bank and near view of right bank

Looking upstream

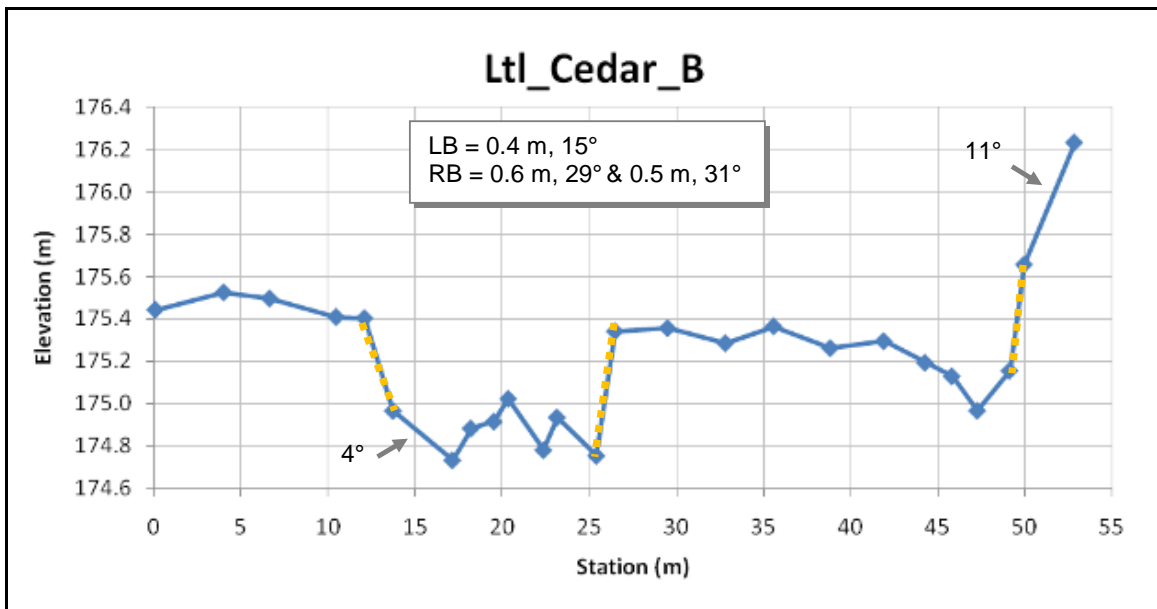


Figure C.27 – Ltl\_Cedar\_B (Little Cedar)

Proctor\_A

Stillwater Sciences, Oct-2007

Note(s):

LB U-FAILED

RB U-MW-UC (lower) and STABLE (upper)



Looking upstream



Looking downstream



View from downstream section looking upstream toward Proctor\_A

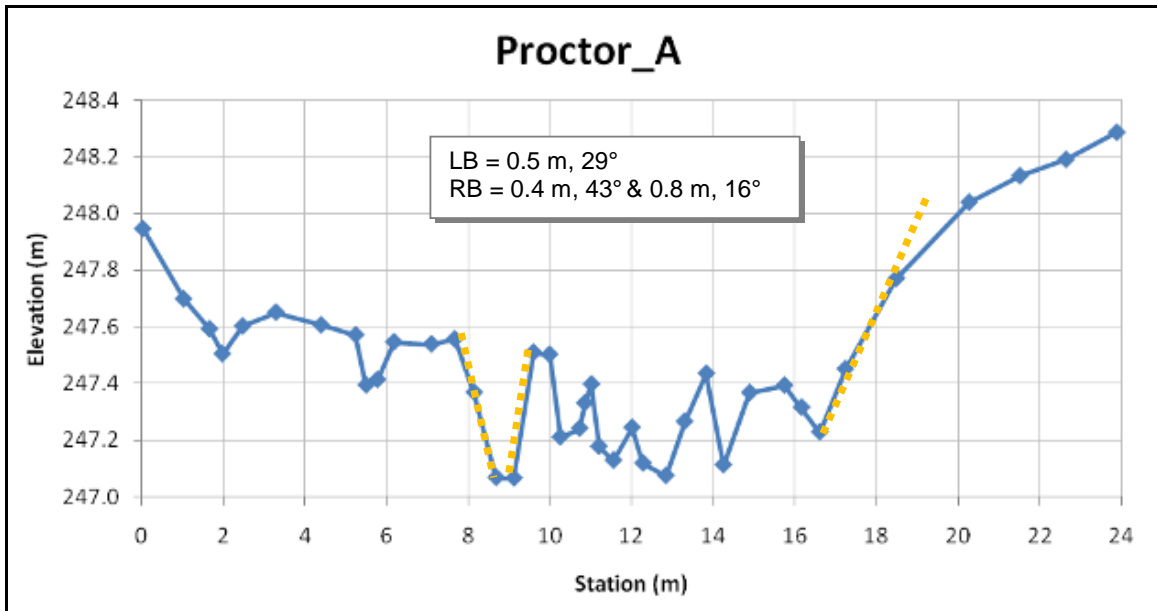


Figure C.28 – Proctor\_A

Note(s):

LB STABLE (upper) and U-MW-UC (lower) RB STABLE (upper) and U-MW-UC (lower)



Looking upstream



Looking downstream

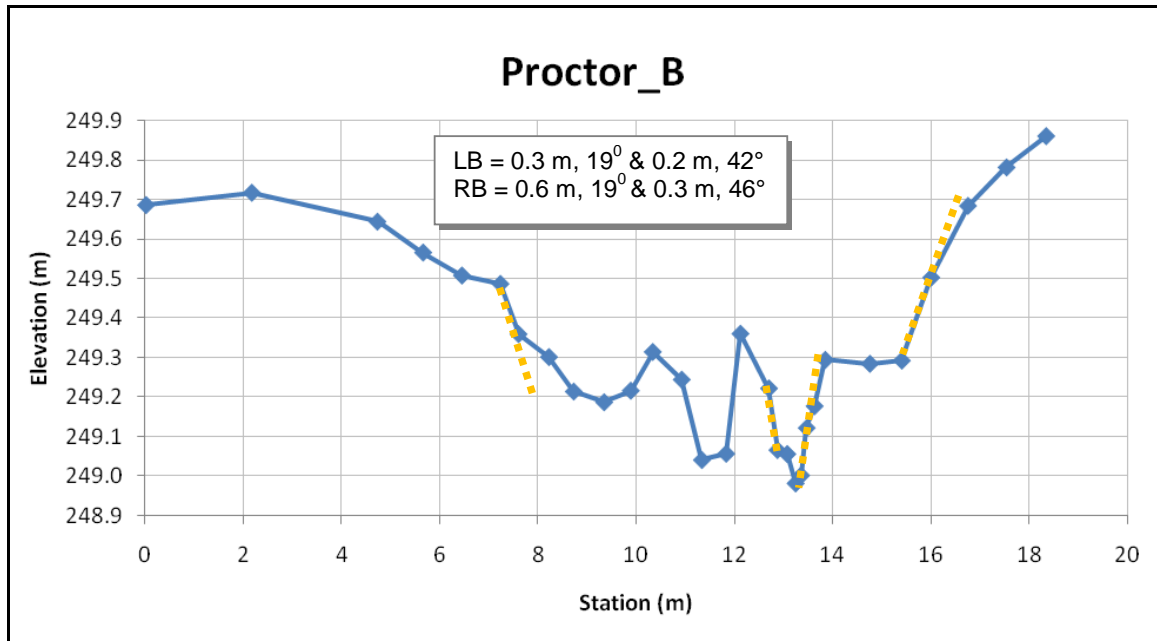


Figure C.29 – Proctor\_B

Note(s):

LB STABLE (upper) and U-FAILED (lower) RB STABLE (upper) and U-FAILED (lower)



Looking upstream



Looking downstream

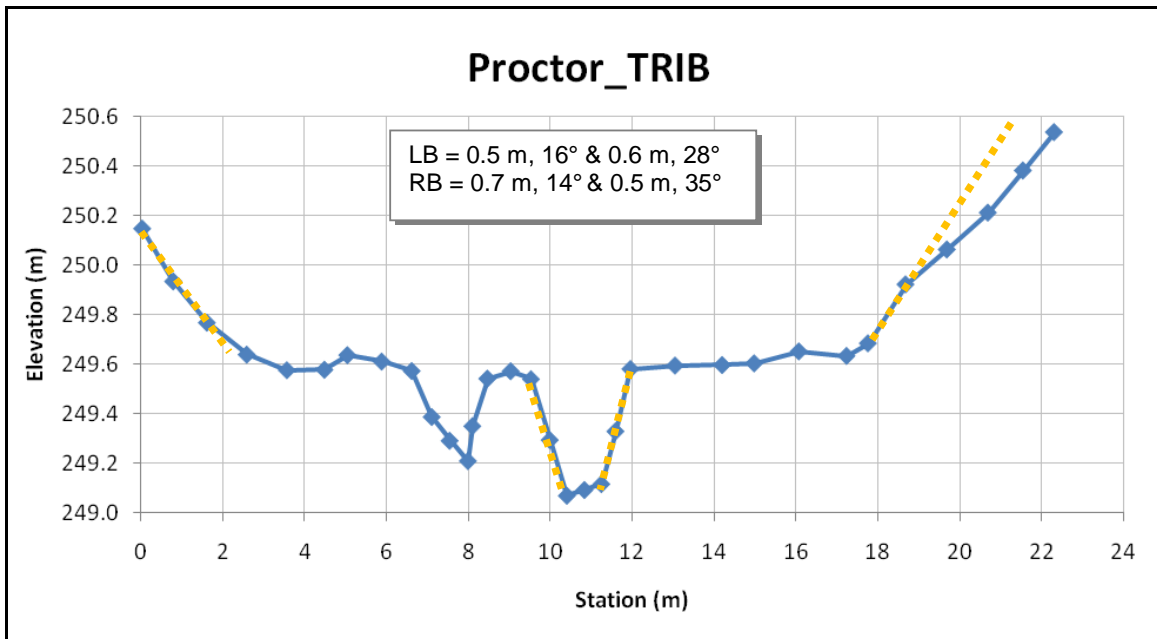


Figure C.30 – Proctor\_TRIB

Perris\_1\_A

Riverside County, Oct-2007

Note(s):

LB STABLE-PC

RB STABLE-PC



Looking upstream near location of Perris\_1\_A

This portion of Perris\_1 was graded (date unknown) to redirect flow to a single culvert at the bottom of the reach

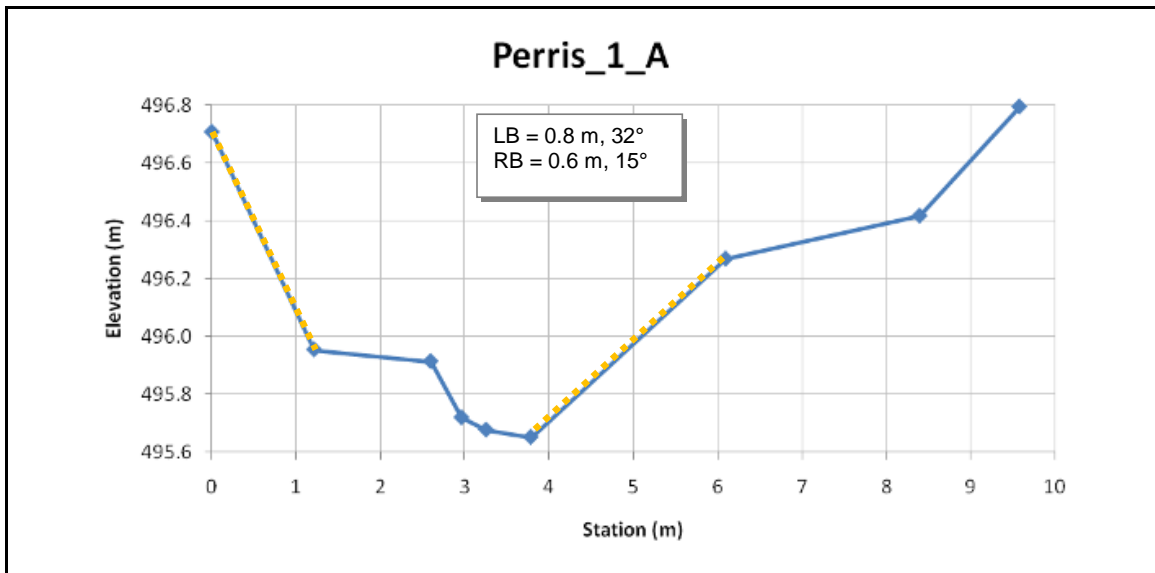


Figure C.31 – Perris\_1\_A

Note(s):

LB STABLE-PC

RB U-MW-PC



Looking upstream near location of Perris\_1\_B

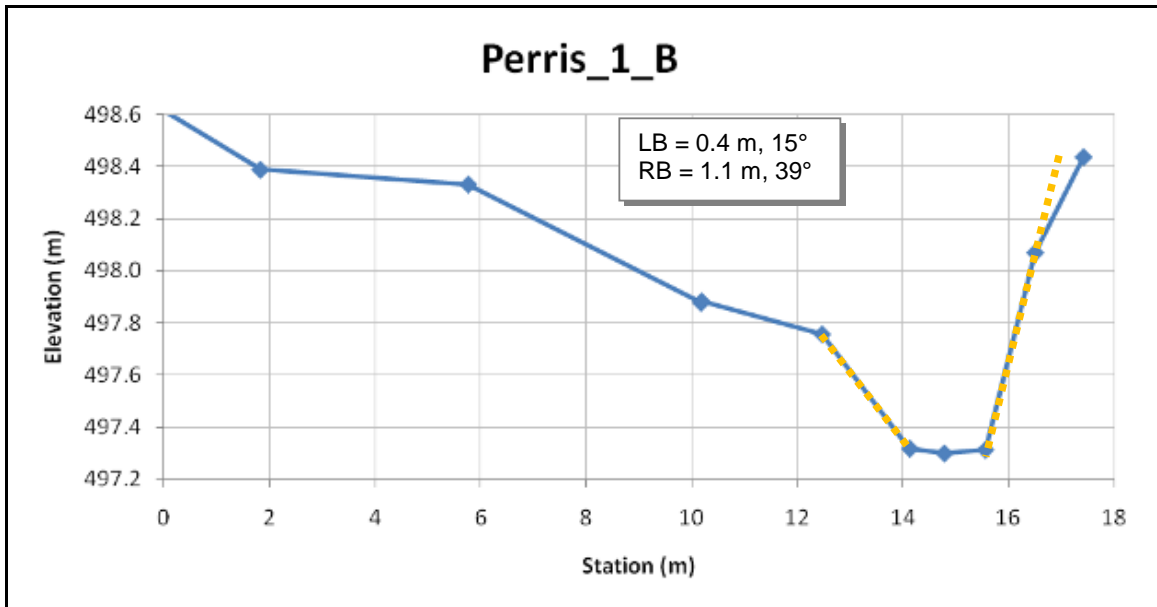


Figure C.32 – Perris\_1\_B

Perris\_1\_C

Riverside County, Oct-2007

Note(s):

LB U-MW-PC (upper) and U-MW-PC (lower)

RB U-MW-PC



Looking upstream near location of Perris\_1\_C

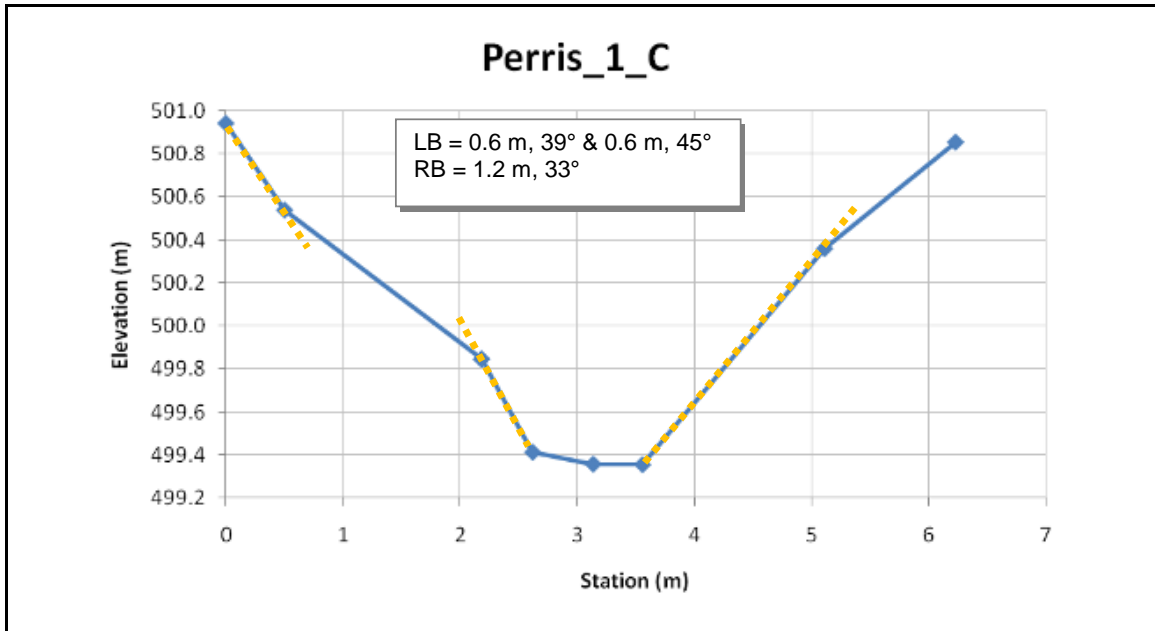


Figure C.33 – Perris\_1\_C

Perris\_2\_A

Riverside County, Oct-2007

Note(s):

LB STABLE-PC

RB STABLE-PC



Looking upstream near location of Perris\_2\_A

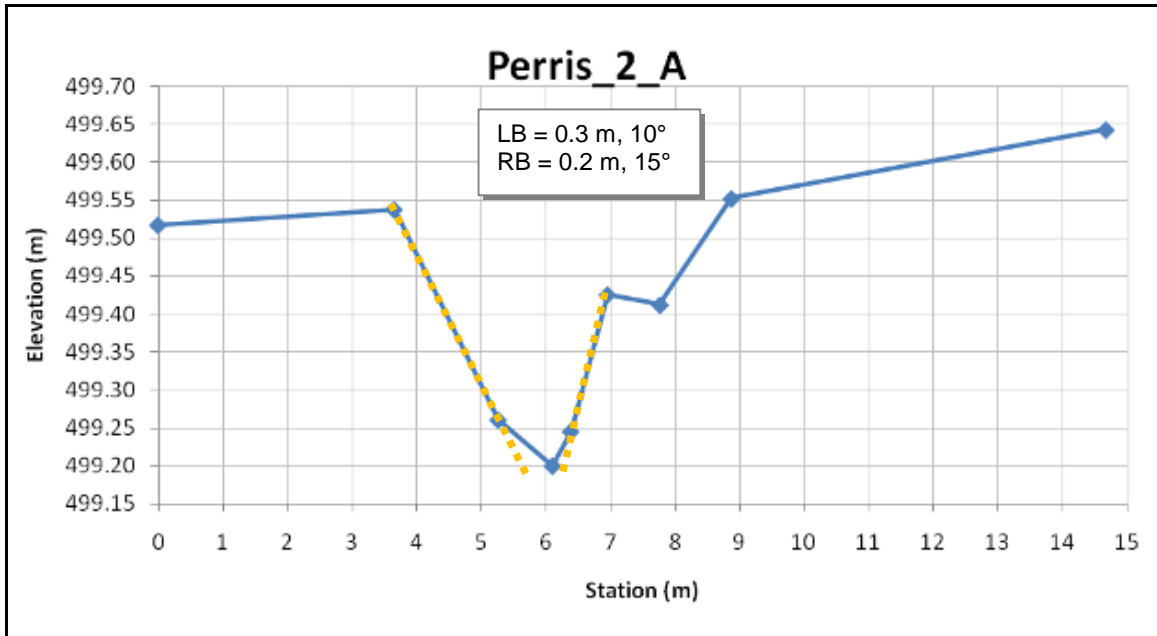


Figure C.34 – Perris\_2\_A

Perris\_2\_B

Riverside County, Oct-2007

Note(s):

LB STABLE-PC

RB U-MW-PC



Looking upstream near location of Perris\_2\_B



View of right bank near location of Perris\_1\_C

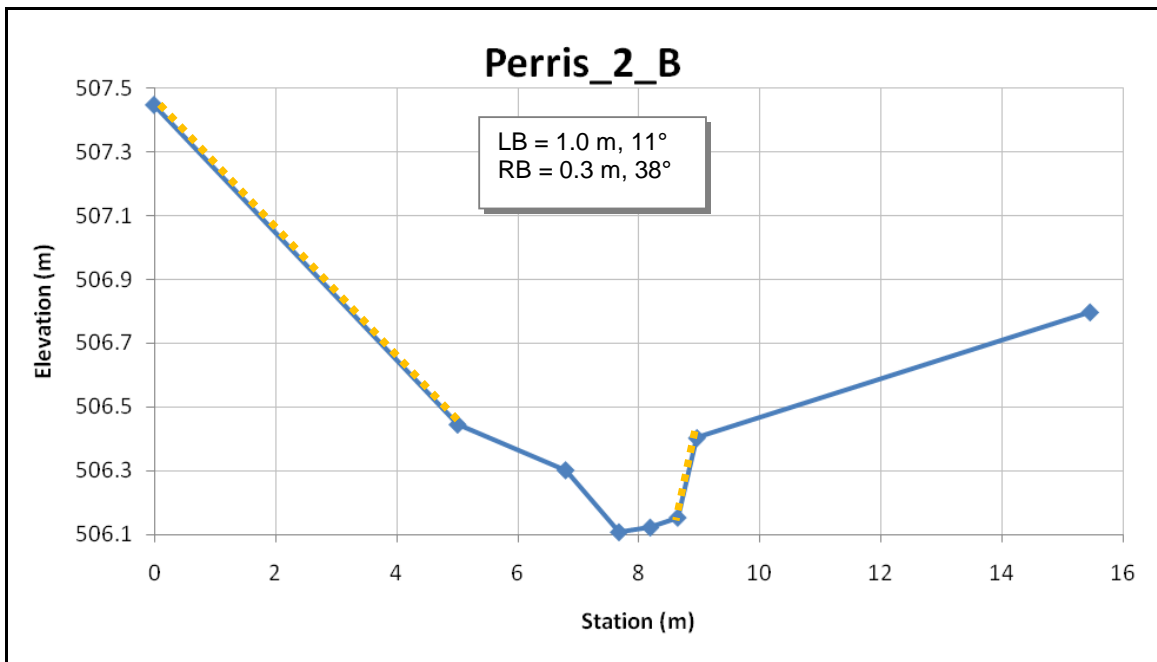


Figure C.35 – Perris\_2\_B

Perris\_3\_A

Riverside County, Oct-2007

Note(s):

LB STABLE-UC

RB STABLE-PC



Looking upstream near location of Perris\_3\_A

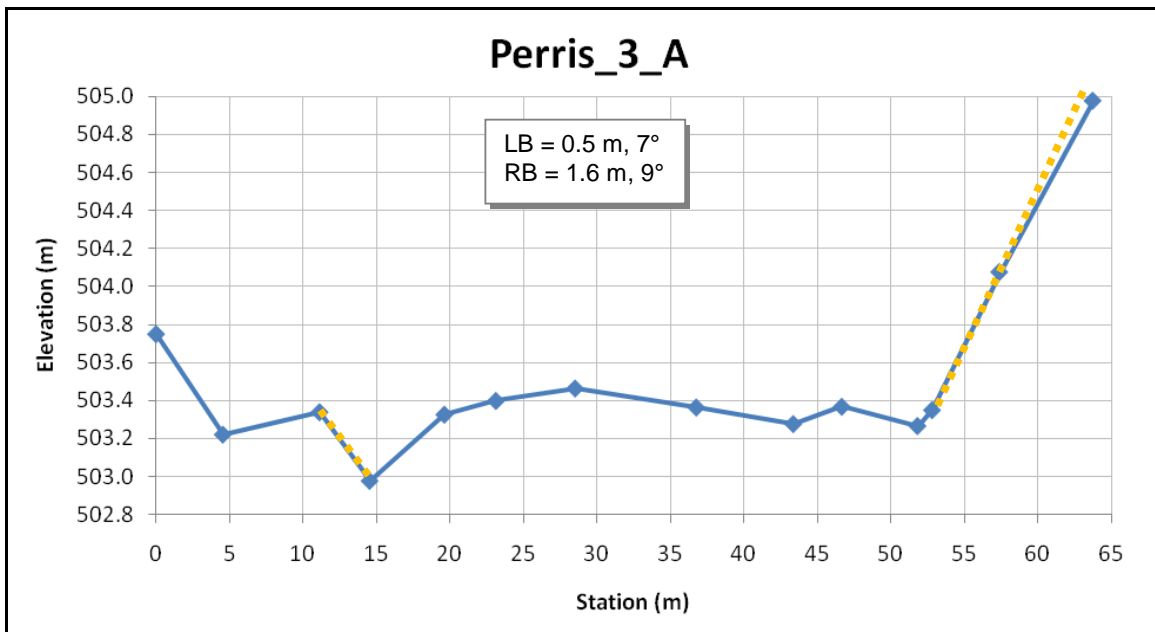


Figure C.36 – Perris\_3\_A

Perris\_3\_B

Riverside County, Oct-2007

Note(s):

LB STABLE-UC

RB STABLE-UC (lower) and STABLE-PC (upper)



Looking upstream near location of Perris\_3\_B

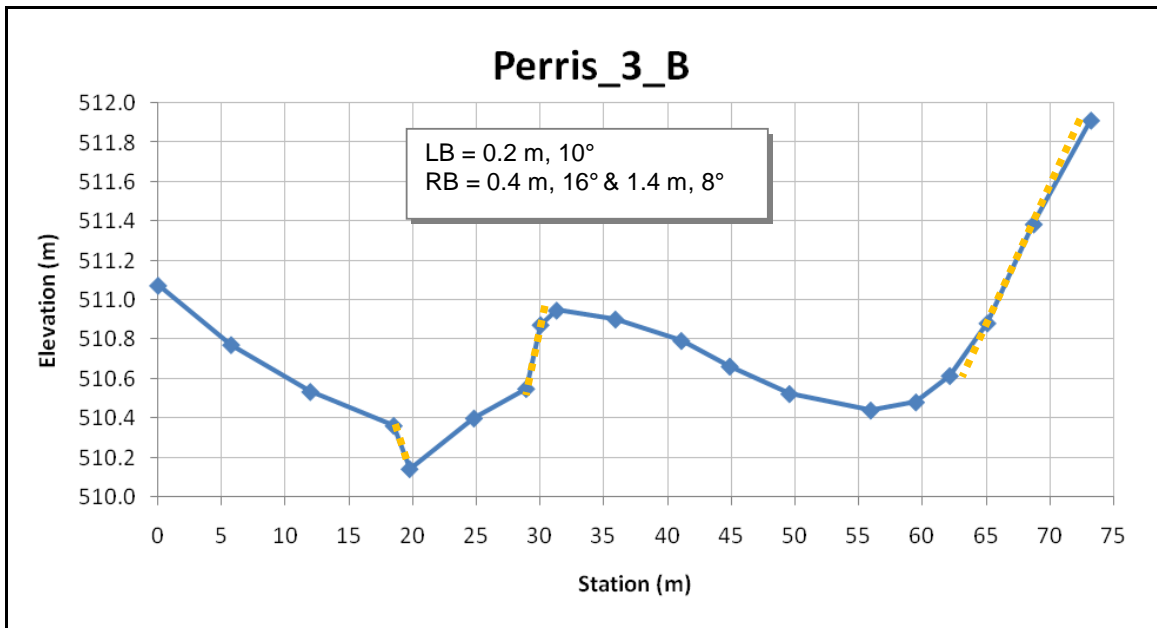


Figure C.37 – Perris\_3\_B

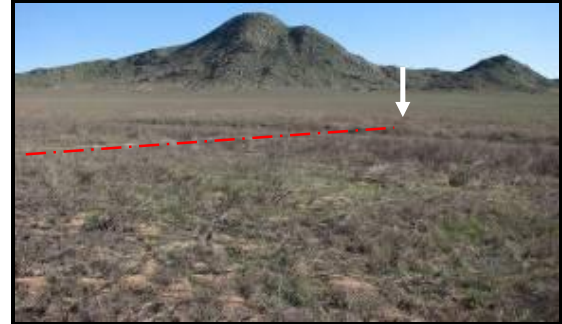
Note(s):

LB STABLE-PC

RB STABLE-PC



Looking upstream (including right bank) of AltPerris\_A



Looking upstream (including left bank) of AltPerris\_A

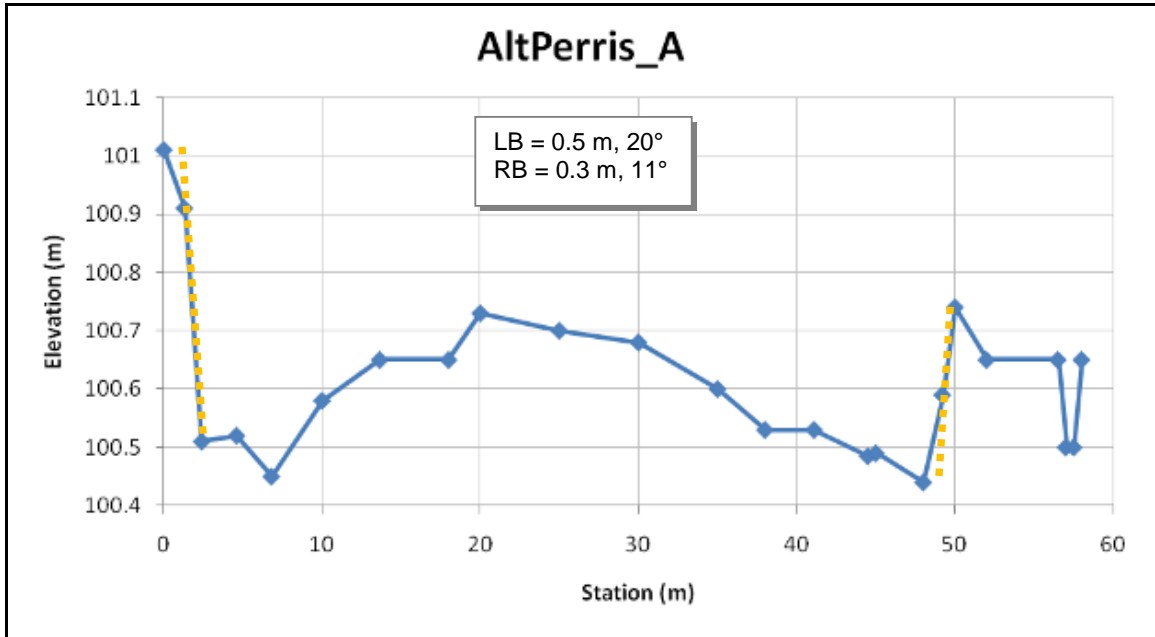


Figure C.38 – AltPerris\_A

Note(s):

LB STABLE-PC

RB STABLE-PC



Looking downstream at AltPerris\_B

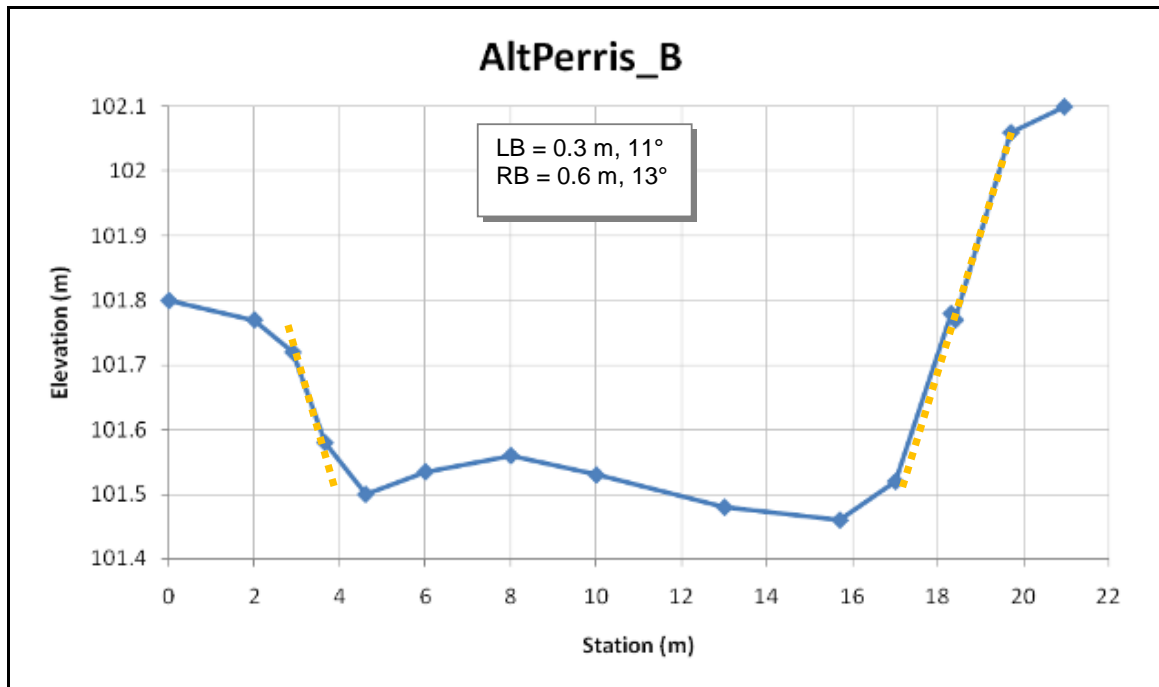


Figure C.39 – AltPerris\_B

AltPerris\_C

CSU, Jan-2008

Note(s):

LB STABLE-PC

RB STABLE-PC



Looking upstream at AltPerris\_C

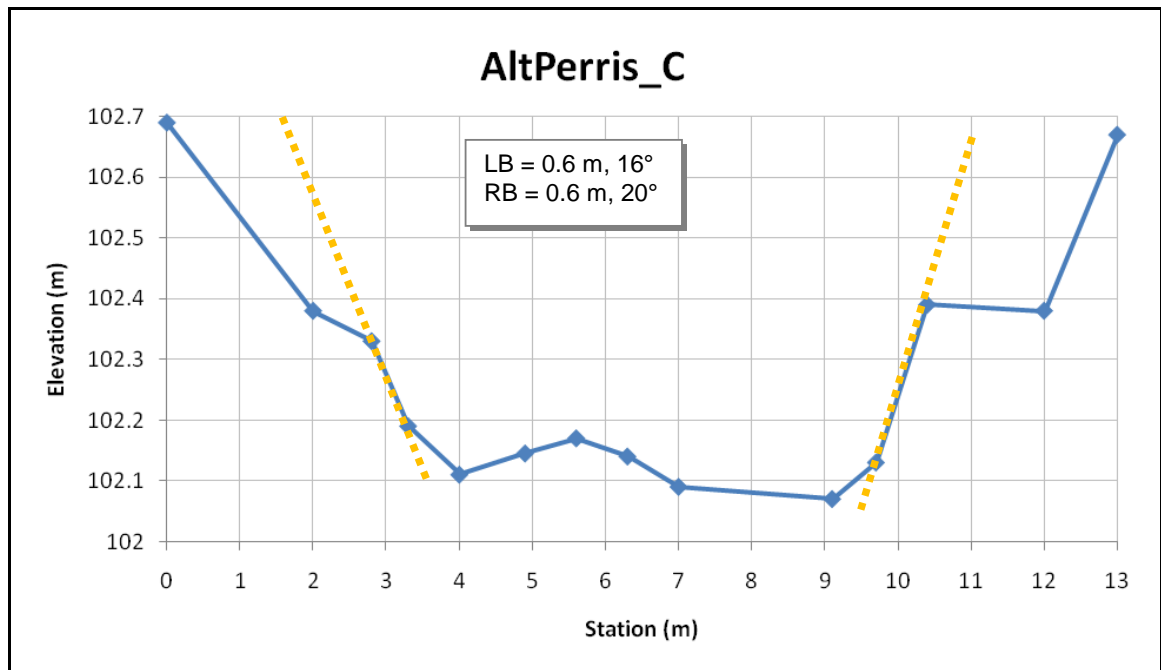


Figure C.40 – AltPerris\_C

Dulzura\_A

CSU, Jan-2008

Note(s):

LB STABLE-PC

RB STABLE-UC (lower) and STABLE-PC (upper)



Looking upstream at Dulzura\_A

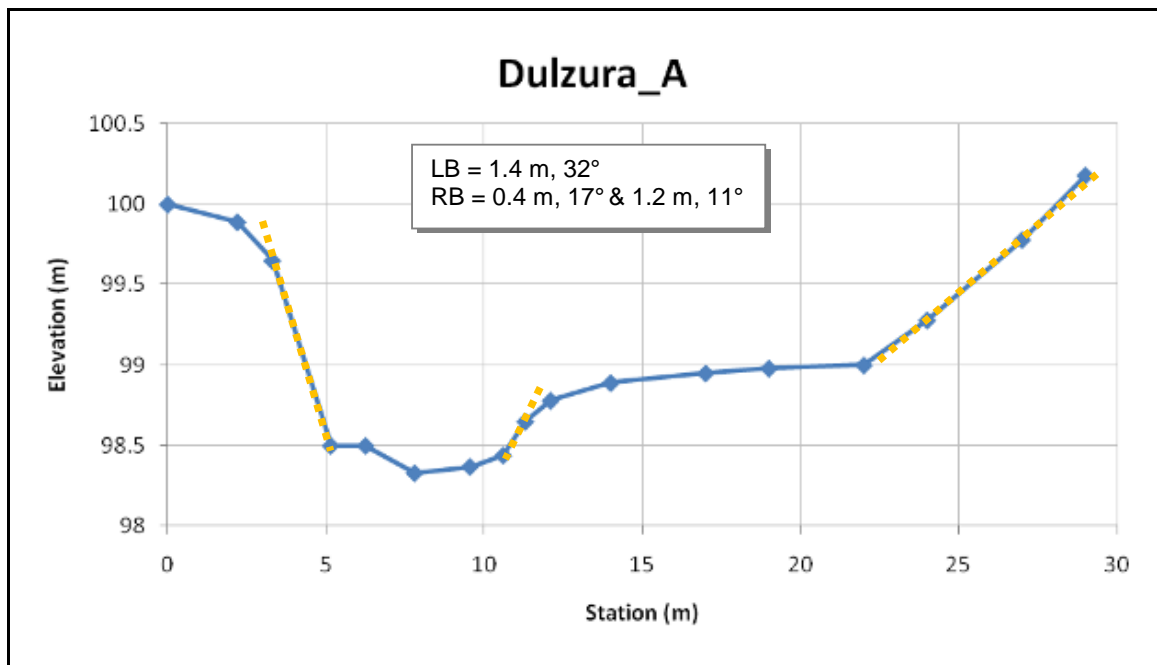


Figure C.41 – Dulzura\_A

Dulzura\_B

CSU, Jan-2008

Note(s):

LB U-FAILED

RB U-MW-PC



Looking downstream at left bank of Dulzura\_B



Looking downstream at right bank of Dulzura\_B

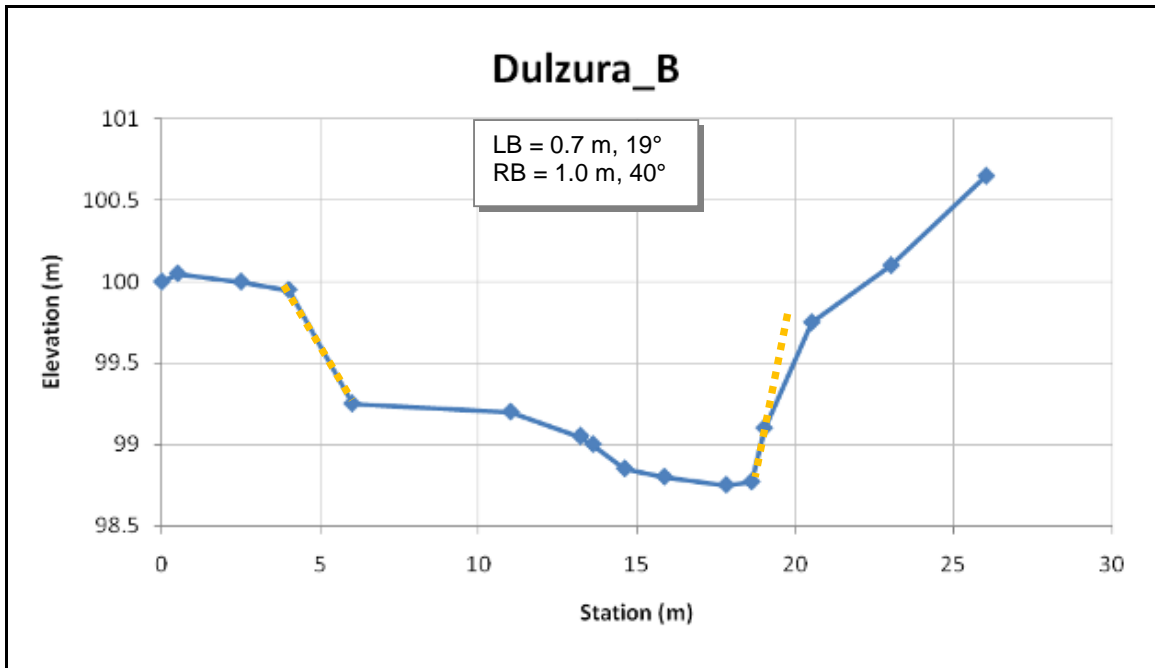


Figure C.42 – Dulzura\_B

Acton\_A

CSU/SCCWRP, Jan-2008

Note(s):

LB STABLE-PC

RB STABLE-PC



Looking downstream at Acton\_A

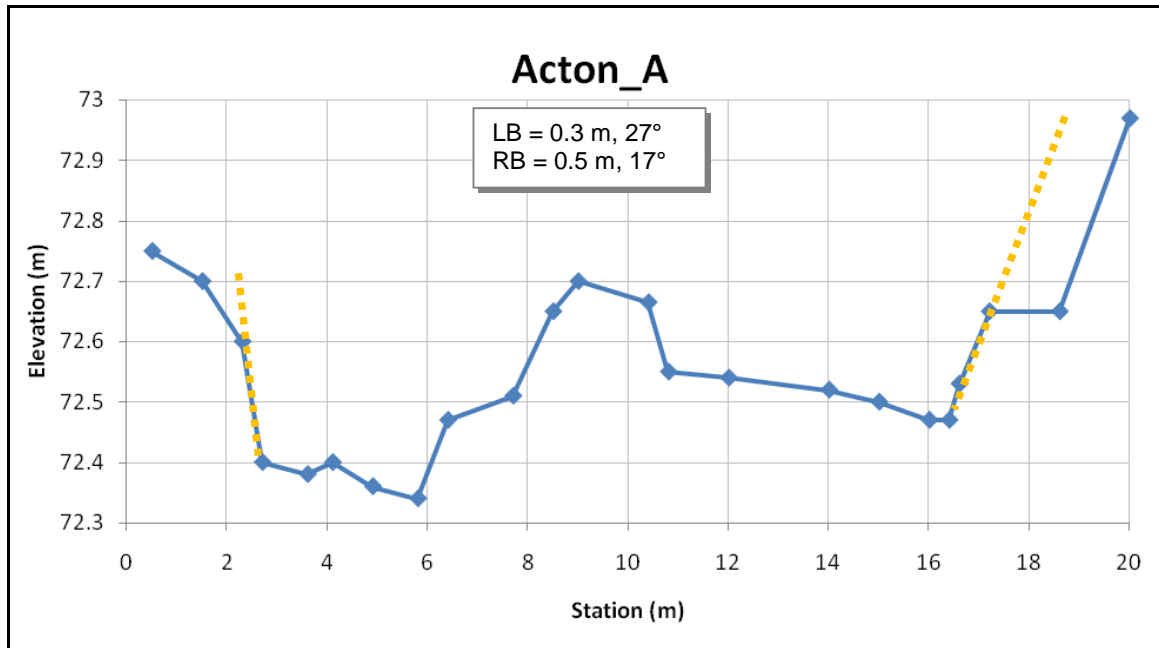


Figure C.43 – Acton\_A

Acton\_B

CSU/SCCWRP, Jan-2008

Note(s):

LB U-MW-PC

RB U-MW-PC



Looking upstream at Acton\_B

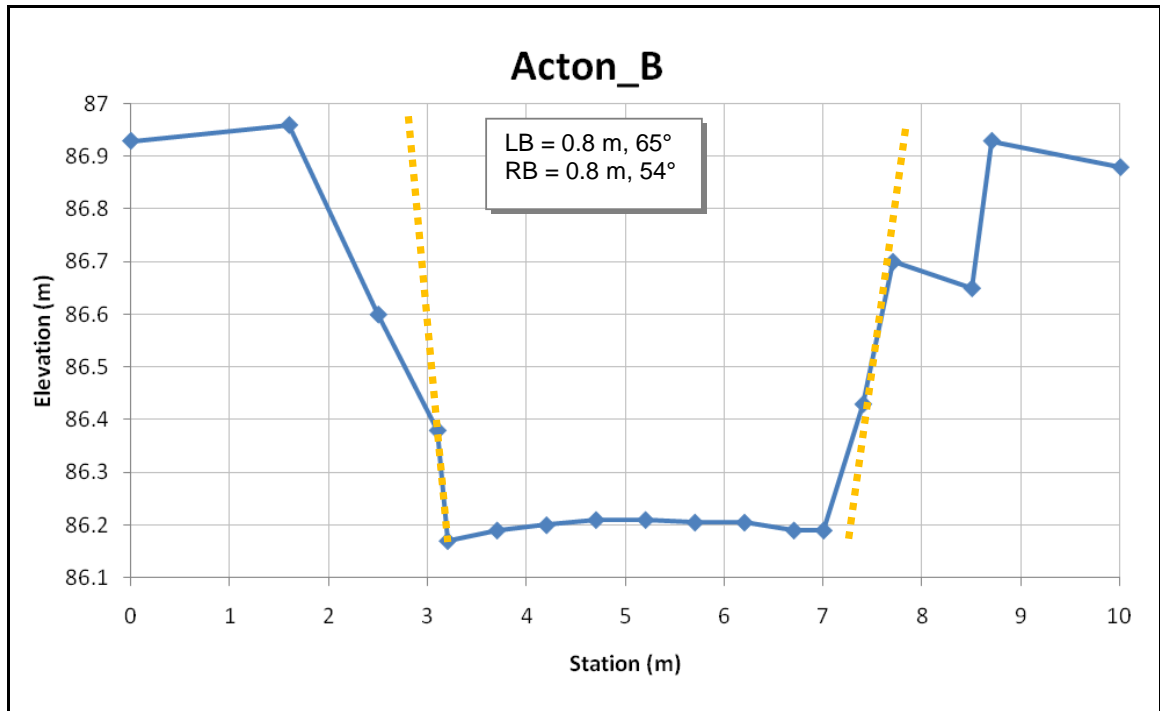


Figure C.44 – Acton\_B

Note(s):

LB U-MW-C (upper) and U-MW-PC (lower) RB U-MW-C



Looking downstream at Acton\_C

Lower left bank appears to be at edge of old channel bank and bed. It's not fully unconsolidated, but not nearly as consolidated as the outer banks.

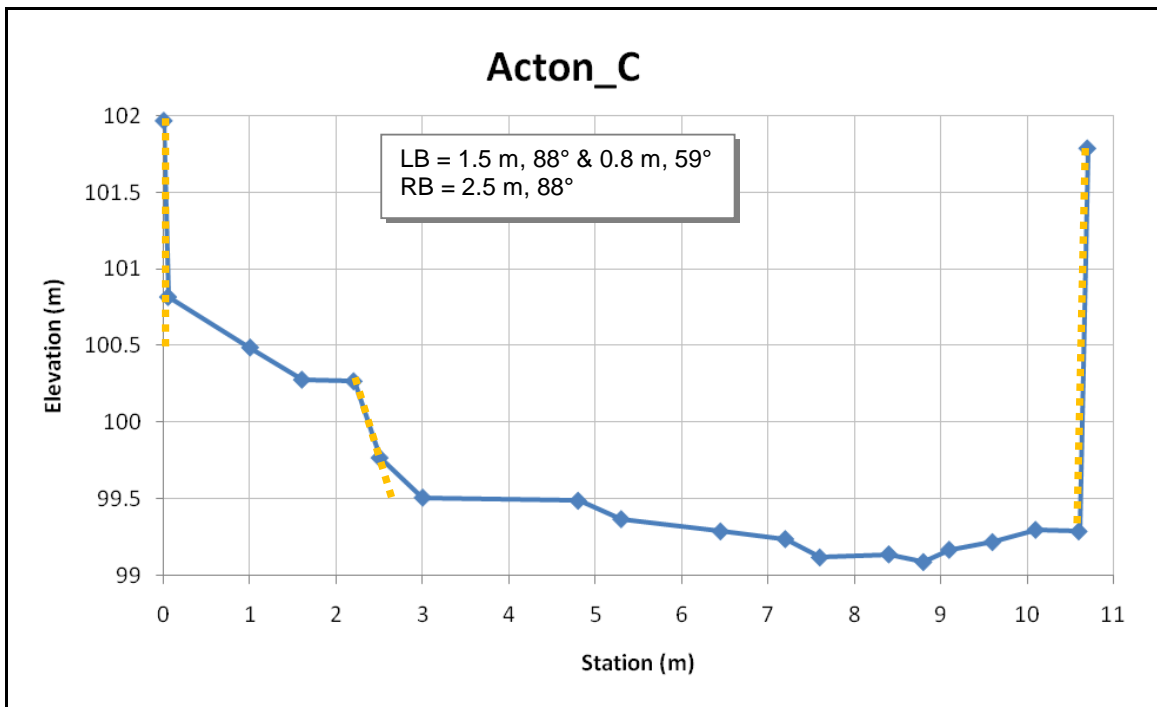


Figure C.45 – Acton\_C

Acton\_D

CSU/SCCWRP, Jan-2008

Note(s):

LB U-MW-C

RB U-MW-C



Looking upstream at Acton\_D

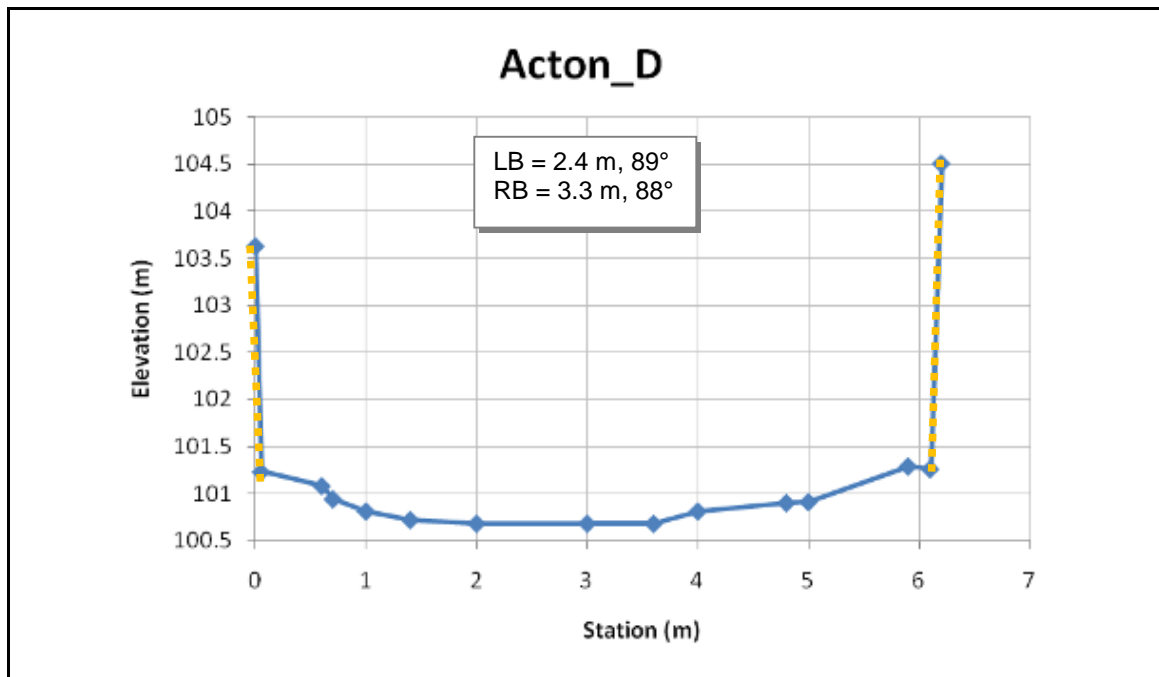


Figure C.46 – Acton\_D

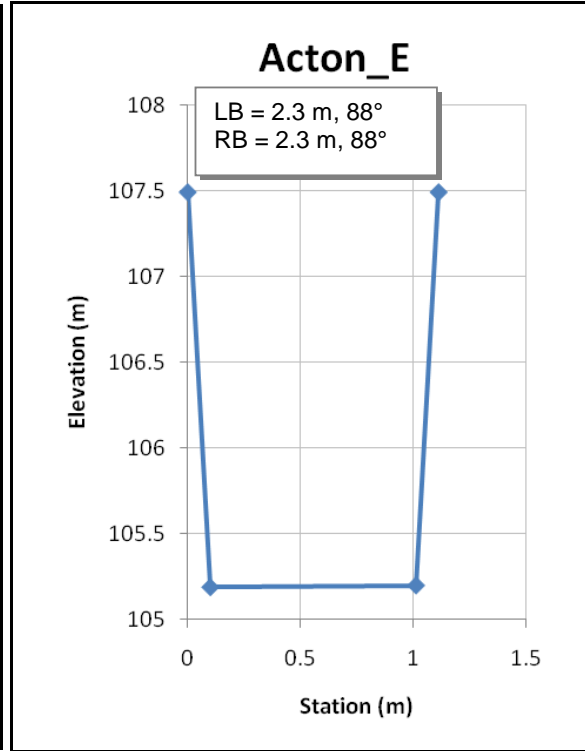
Acton\_E

CSU/SCCWRP, Jan-2008

Note(s):

LB U-MW-C

RB U-MW-C



Looking upstream and down into Acton\_E

Cross-section was taped, not surveyed due to hazard risk

**Figure C.47 – Acton\_E**

Note(s):

LB S-CONSTR

RB S-CONSTR



Looking downstream near Borrego\_A

Cross section was drawn from aerials and photographs – not surveyed

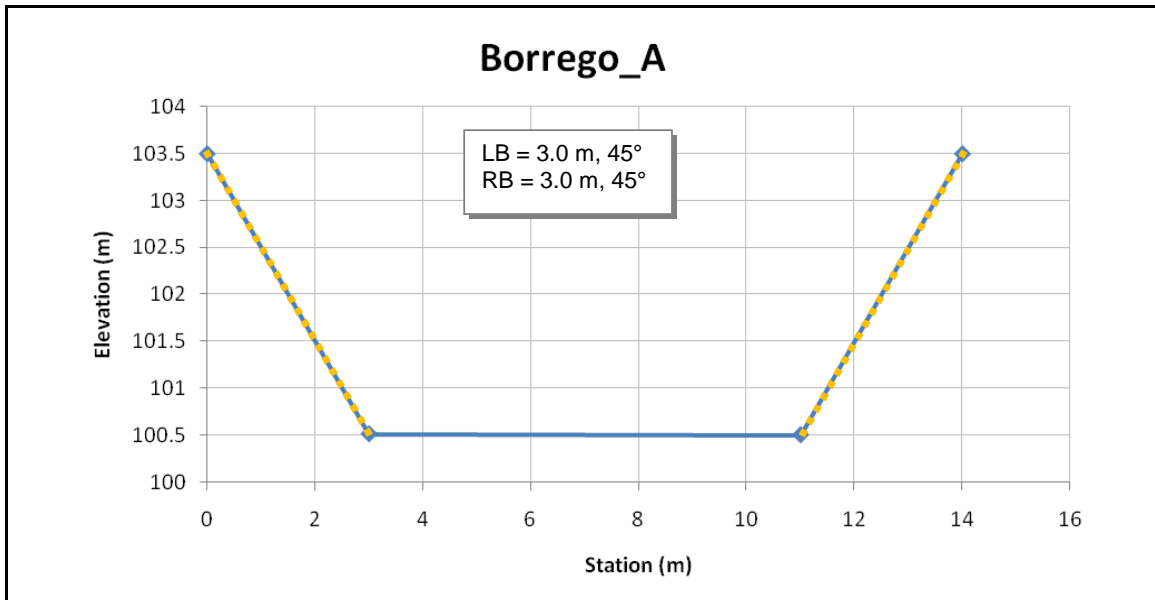


Figure C.48 – Borrego\_A

Note(s):

LB U-MW-C

RB U-MW-C



Left bank of Borrego\_B



Looking upstream at right bank of Borrego\_B



Looking from left to right bank of Borrego\_B

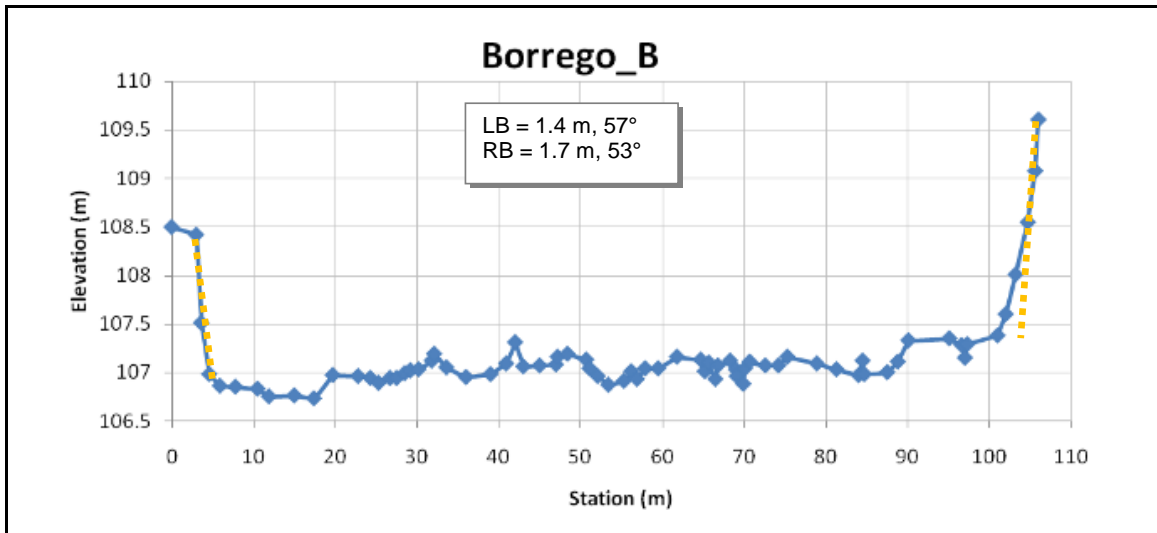


Figure C.49 – Borrego\_B

Note(s):

LB U-MW-C

RB U-MW-C



Looking downstream at left bank of Borrego\_C



Looking downstream at right bank of Borrego\_C



Looking downstream at Borrego\_C

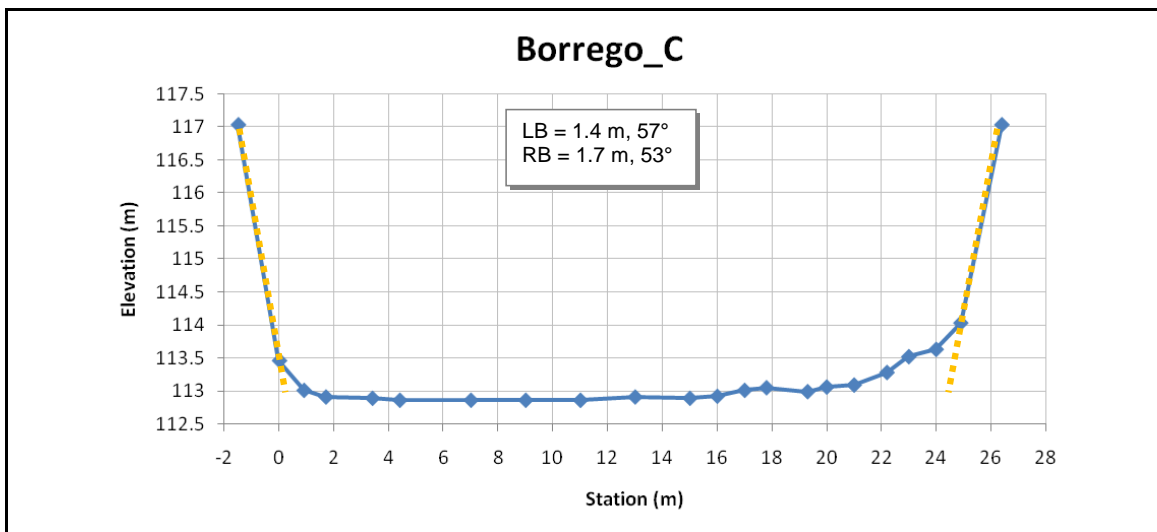


Figure C.50 – Borrego\_C

Note(s):

LB U-MW-C

RB U-MW-C



Looking downstream at Borrego\_D

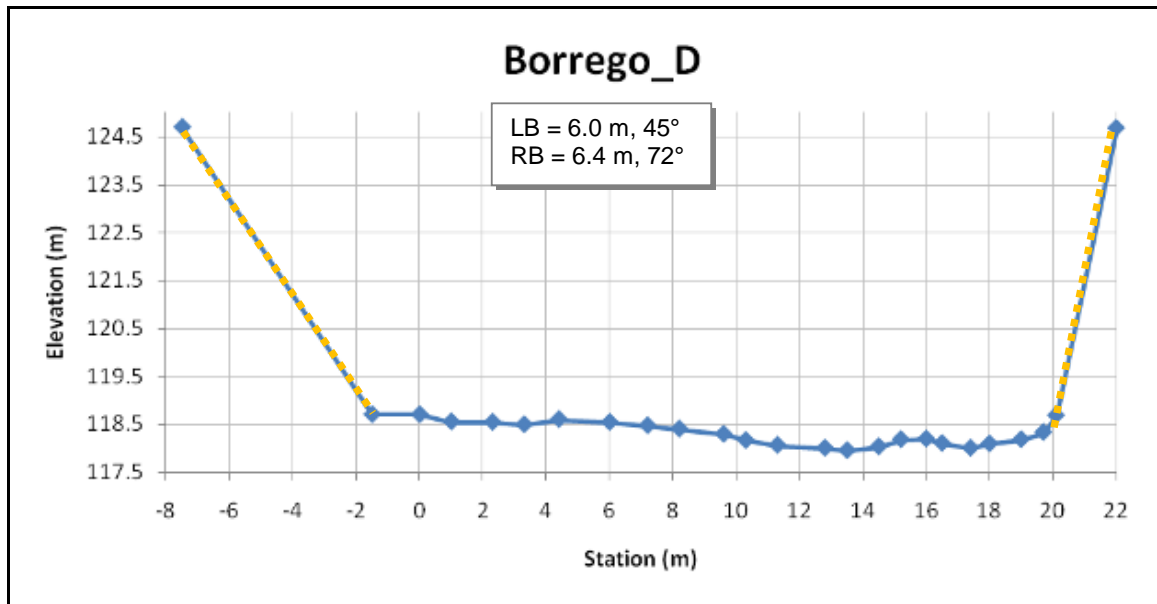


Figure C.51 – Borrego\_D

Note(s):

LB U-MW-C (upper) and U-MW-PC (lower) RB U-FAILED (upper) and U-MW-PC (lower)

*Incised section is classified as PC (poorly consolidated) instead of UC (unconsolidated) because, although they are a part of a historic bed, tree locations indicate that the tops of these banks have been at that elevation for 20+ yrs, which is considerably different from the way we've been applying the UC rating.*



Looking upstream at Borrego\_E



Looking downstream at Borrego\_E

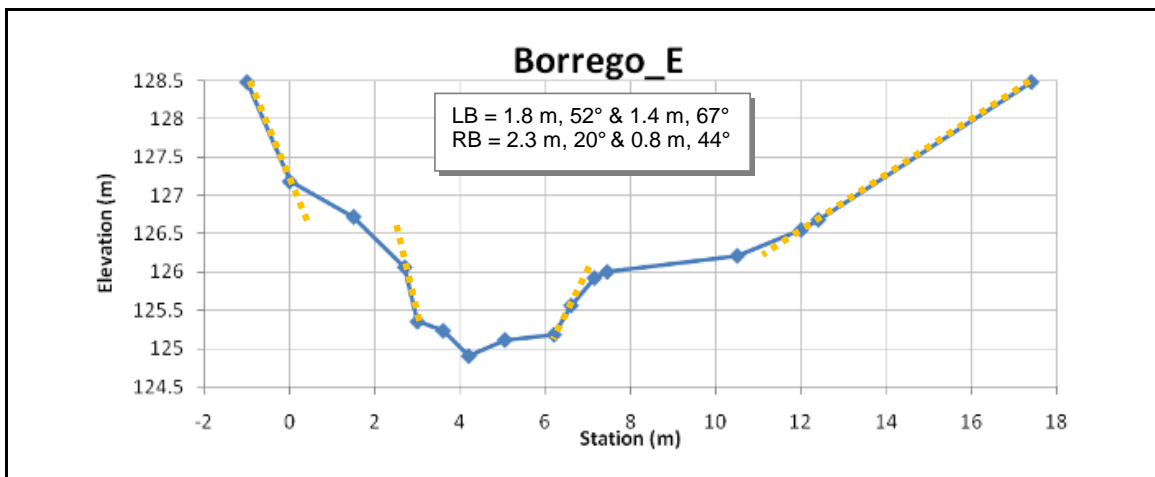
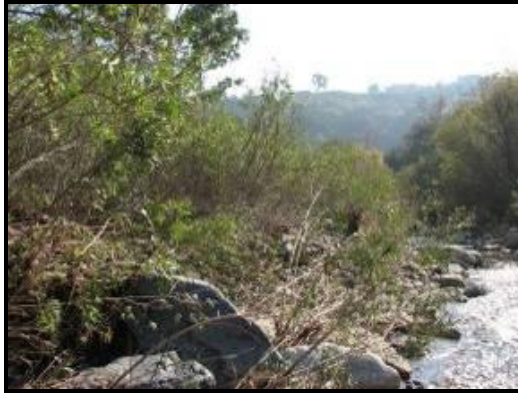


Figure C.52 – Borrego\_E

Note(s):

LB U-MW-UC (left) and STABLE-UC (right)

RB U-MW-UC (left) and STABLE-UC (right)



Looking downstream at left bank of right main channel of Topanga\_A



Looking upstream the right main channel toward Topanga\_A (left main channel hidden by vegetated island)

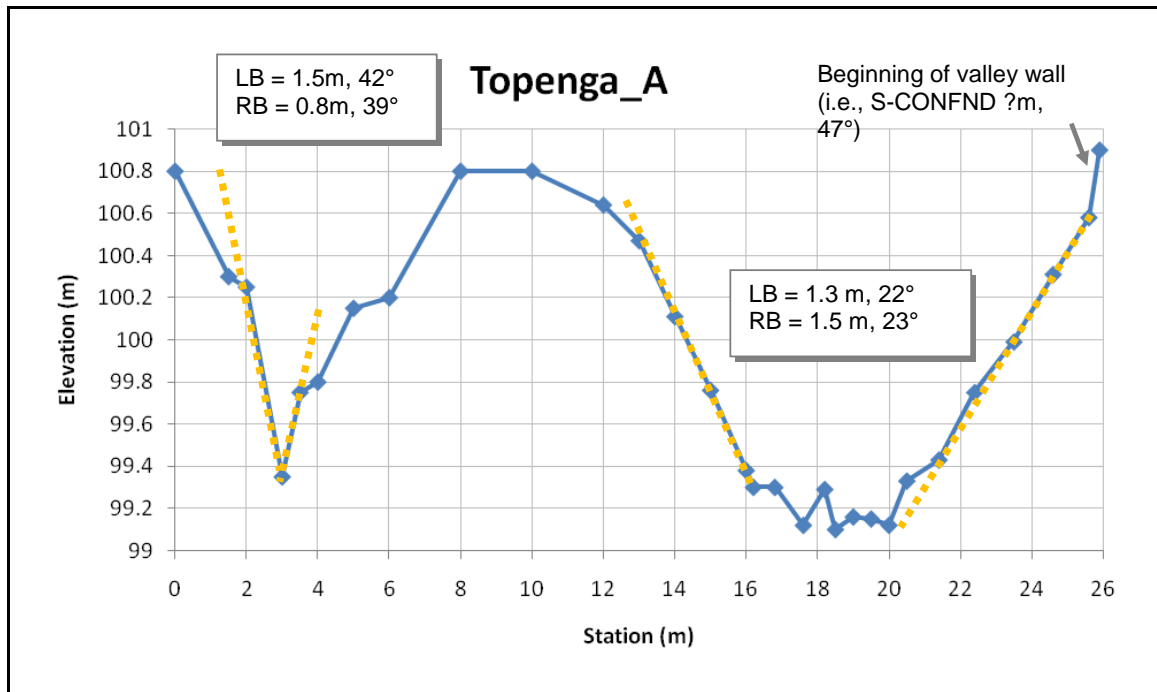


Figure C.53 – Topanga\_A

Note(s):

LB U-CONFND

RB STABLE-UC



Looking upstream at base of left bank of Topanga\_B



Looking upstream toward Topanga\_B with view of right bank

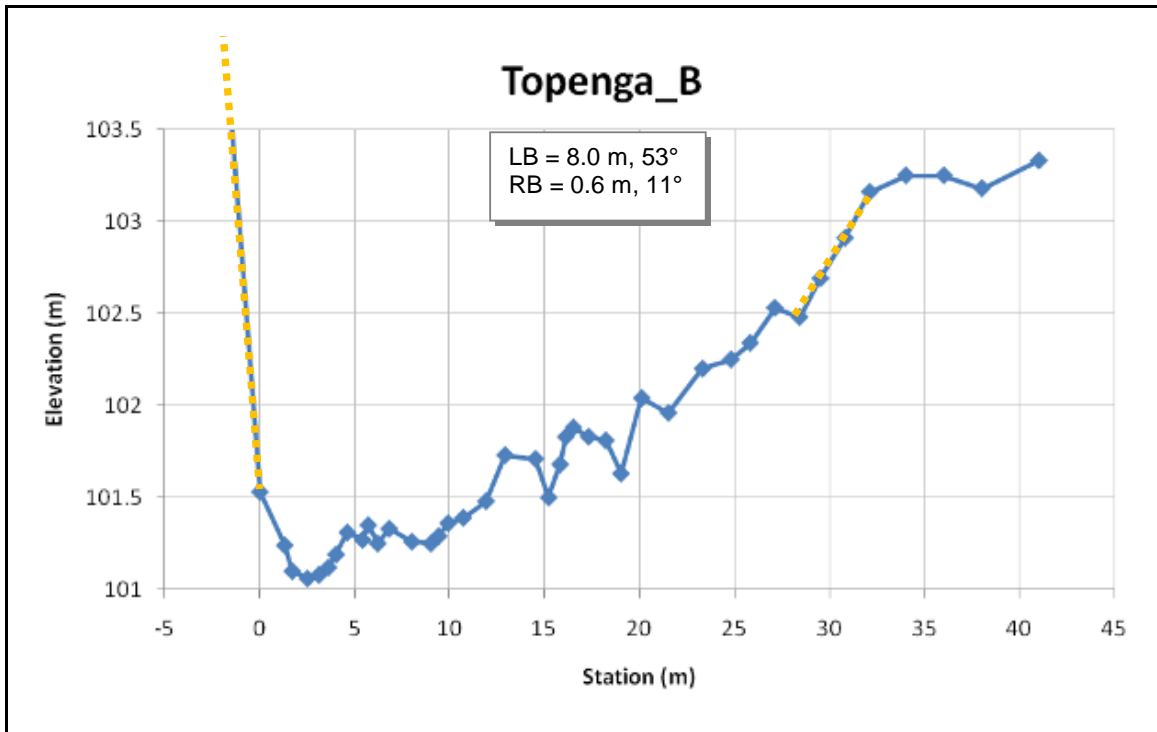
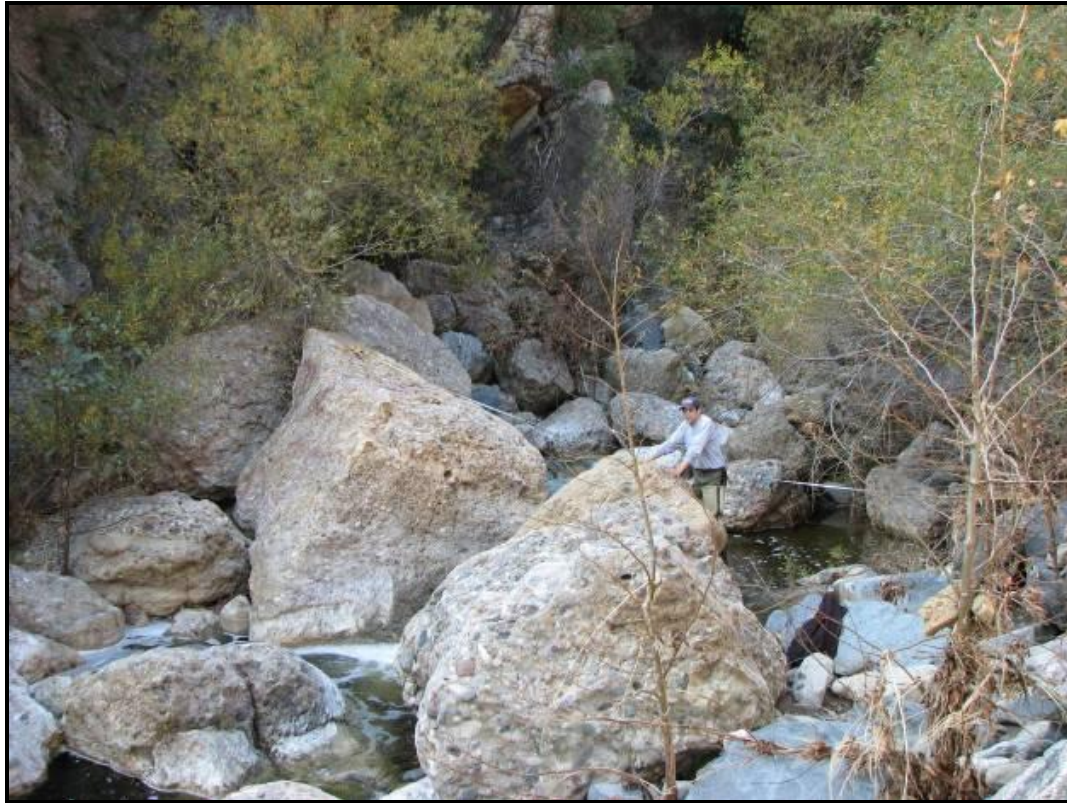


Figure C.54 – Topanga\_B

Note(s):

LB U-CONFND

RB U-CONFND



Looking from left to right bank of Topanga\_C

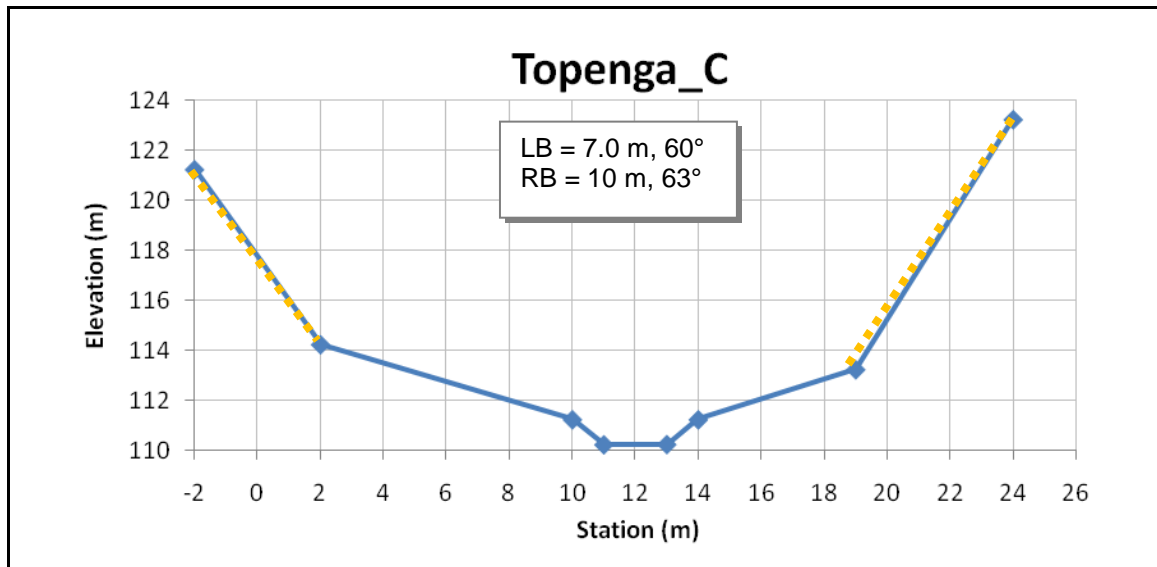


Figure C.55 – Topanga\_C

Note(s):

LB U-MW-C

RB STABLE



Looking downstream at Challengr\_A with view of left bank



Looking upstream toward Challengr\_A with view of right bank



Close up of left bank

Although fluvial is a factor (downstream of a bend, along with scouring at tree), MW is extensive upstream and to a small extent downstream

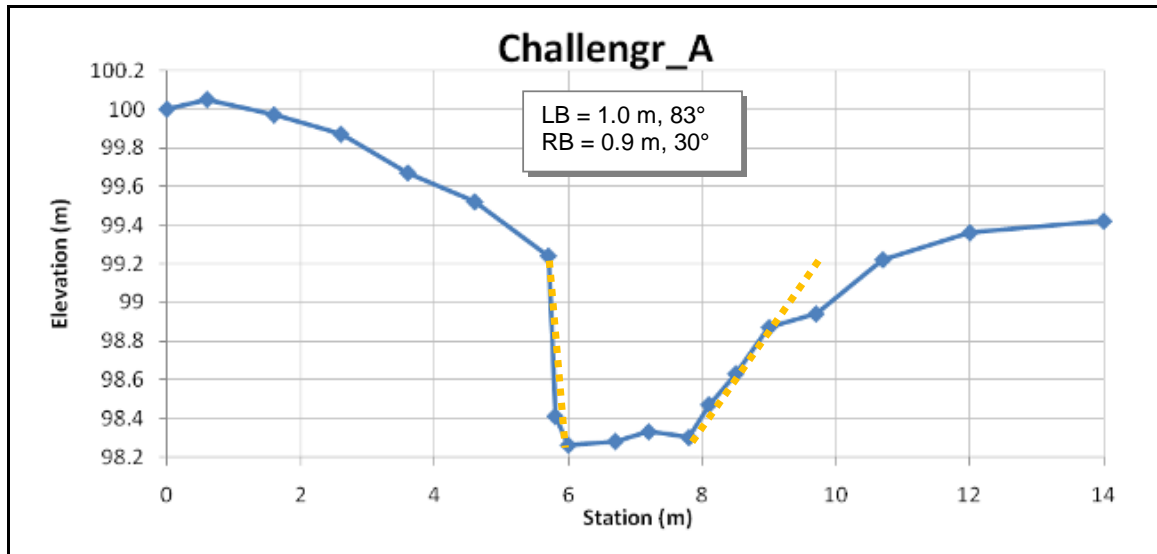


Figure C.56 – Challengr\_A (Challenger Park)

Note(s):

LB U-MW-UC

RB U-MW-UC



Looking upstream at Challengr\_B – incision w/ MW through poorly consolidated alluvia (old bed), with beginnings of MW of original left bank (white arrows)

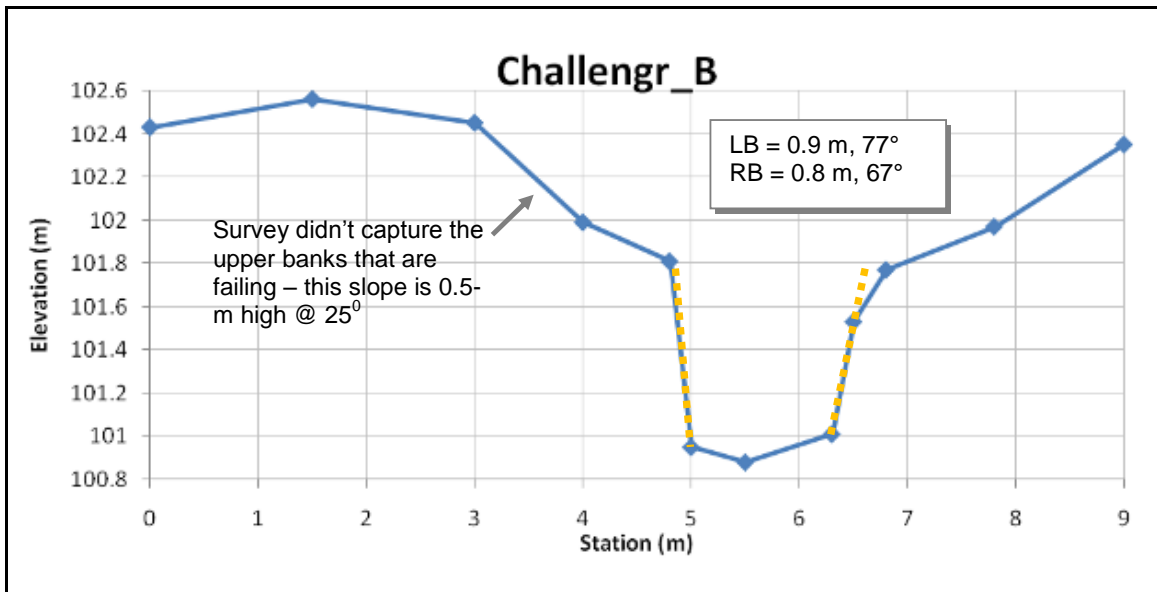


Figure C.57 – Challengr\_B (Challenger Park)

Note(s):

LB STABLE

RB STABLE



Looking upstream at Challengr\_C with view of left bank



Looking downstream at Challengr\_C with view of right bank – MW evident just upstream



View of right bank of Challengr\_C – slight MW upstream, but not at surveyed section

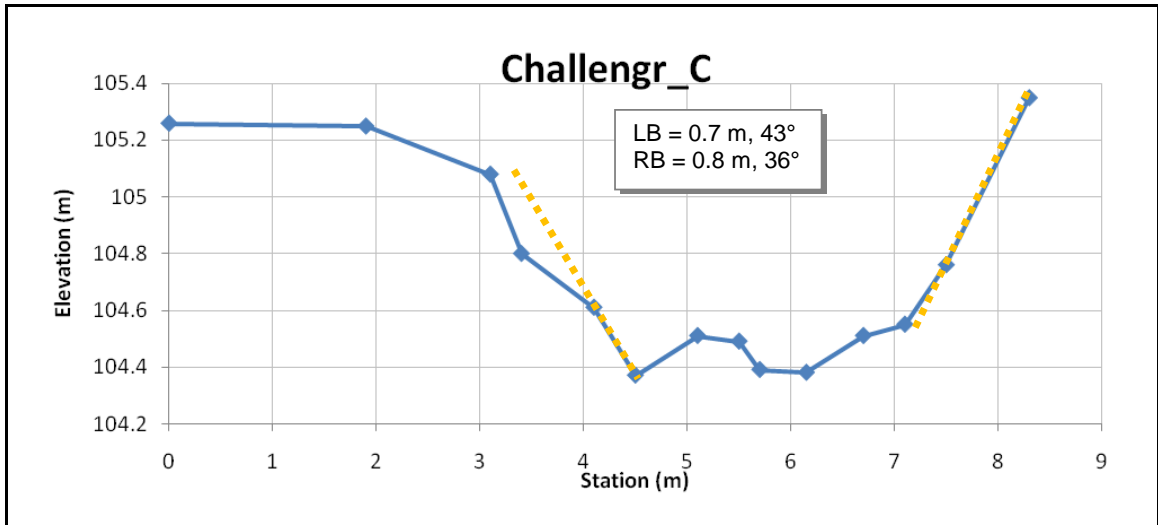


Figure C.58 – Challengr\_C (Challenger Park)

Note(s):

LB STABLE-UC

RB STABLE-UC



Looking downstream at McGonigle\_A (main channel) MW through unconsolidated alluvia

No photograph looking far left – thick vegetation (hydrophilic trees and shrubs) through the 'island', after which the valley floor is poorly maintained as a grassed access road



Looking toward far right bank of McGonigle\_A

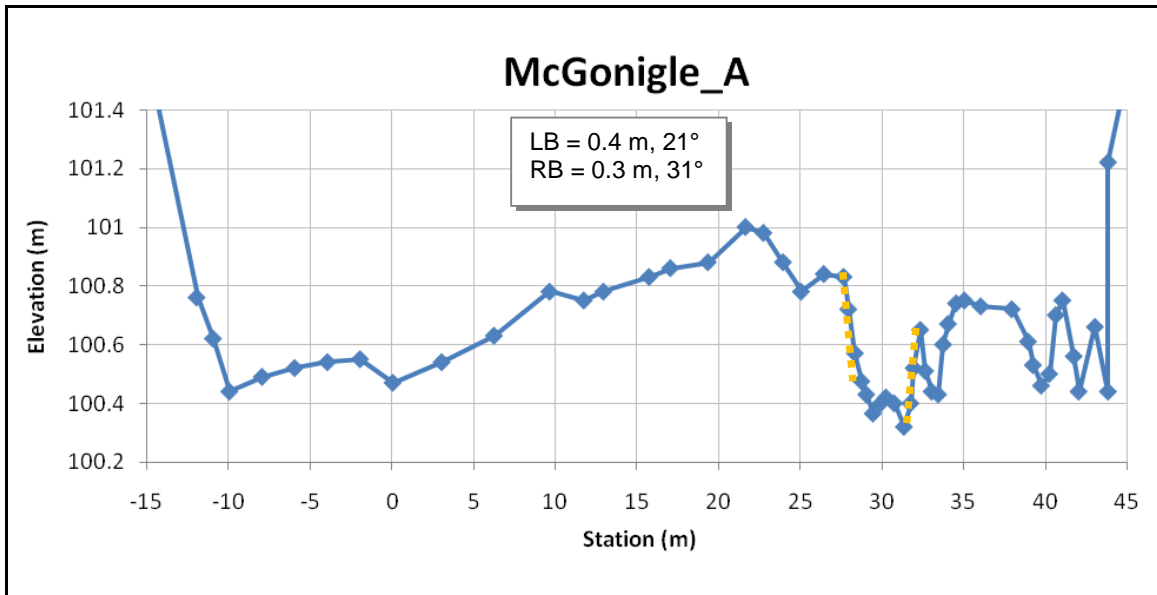


Figure C.59 – McGonigle\_A

Note(s):

LB U-MW-UC

RB U-MW-C



Representative of left bank of main channel of SanJuan\_A – MW of unconsolidated alluvia



Looking downstream at SanJuan\_A with view of far right bank



View of far left valley wall – not captured by the survey

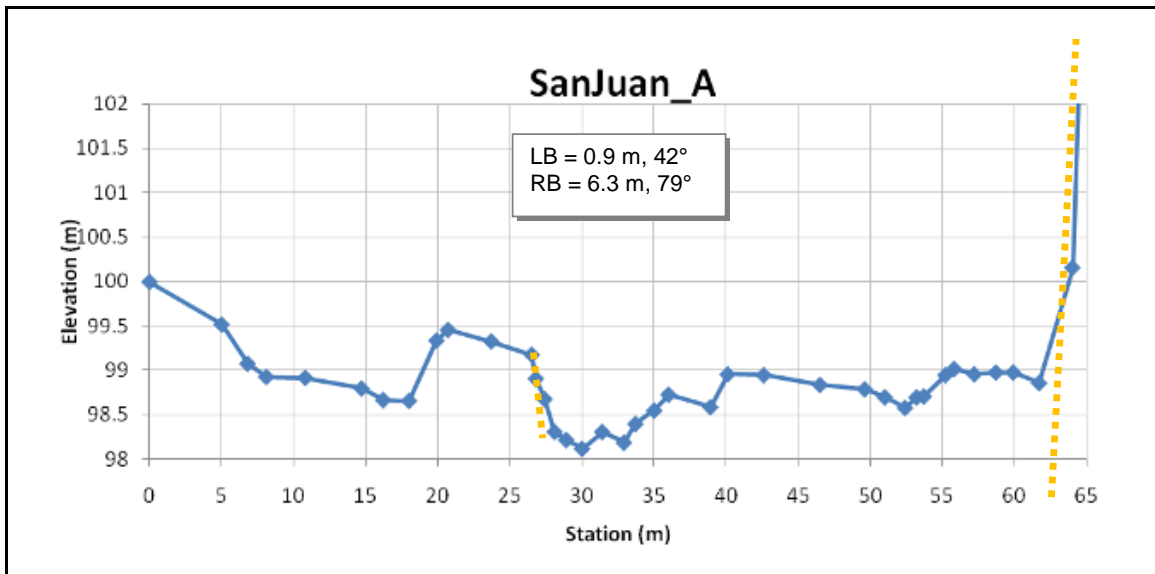


Figure C.60 – SanJuan\_A

Note(s):

LB STABLE-UC

RB S-CONFND



Looking upstream at left bank of SanJuan\_B



Looking downstream at right bank of SanJuan\_B



Although slight MW is evident in the photo of the left bank (left), it is just downstream of the surveyed cross-section, and not representative of the shot geometry. Similarly, the right bank photo (above) shows slight MW through unconsolidated alluvia upstream of the surveyed cross-section, which is itself stable.

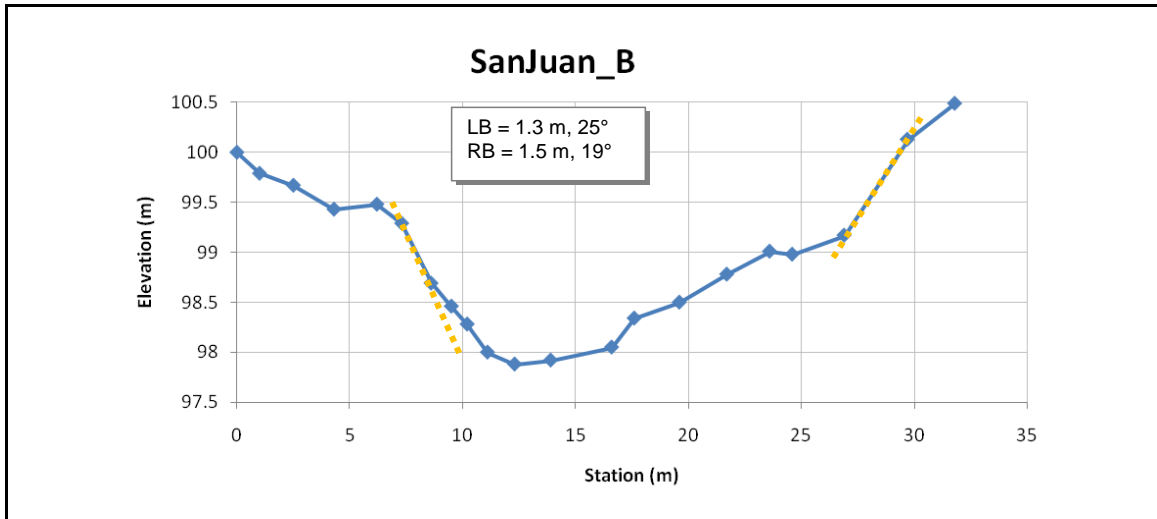


Figure C.61 – SanJuan\_B

Note(s):

LB U-MW-PC

RB U-MW-UC



Looking upstream at Pigeon\_A – site was graded during development in the 1980's. Left bank does not appear to be fill (inset) – seems poorly to moderately consolidated. Right bank composed of more alluvial material (unconsolidated)

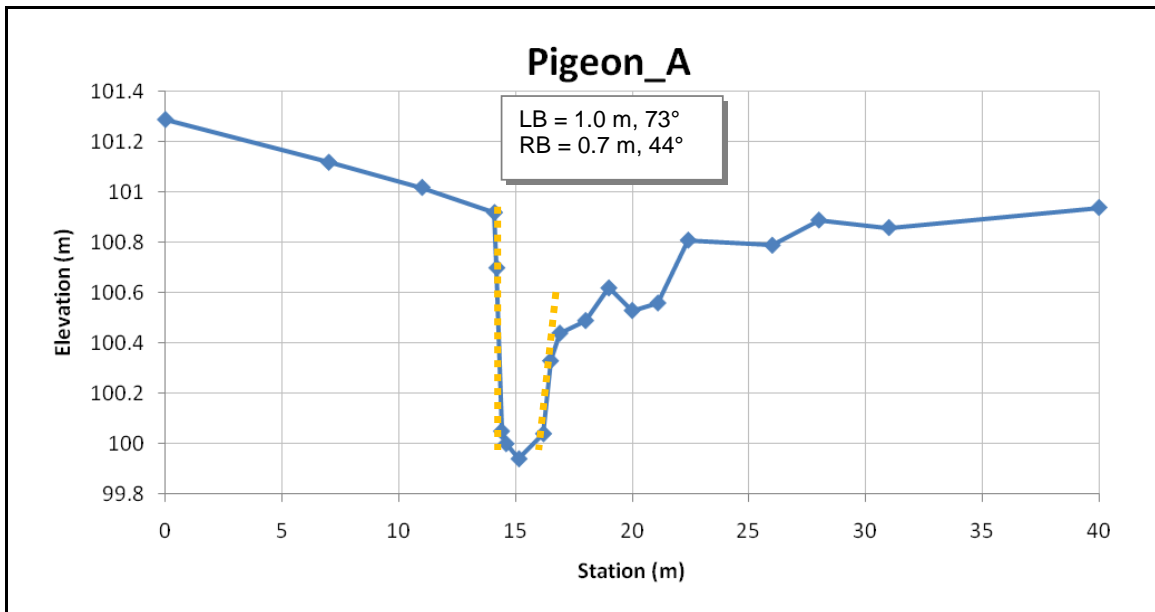


Figure C.62 – Pigeon\_A (Pigeon Pass)

Note(s):

LB U-MW-PC

RB STABLE-UC



Looking from right to left bank of Pigeon\_B

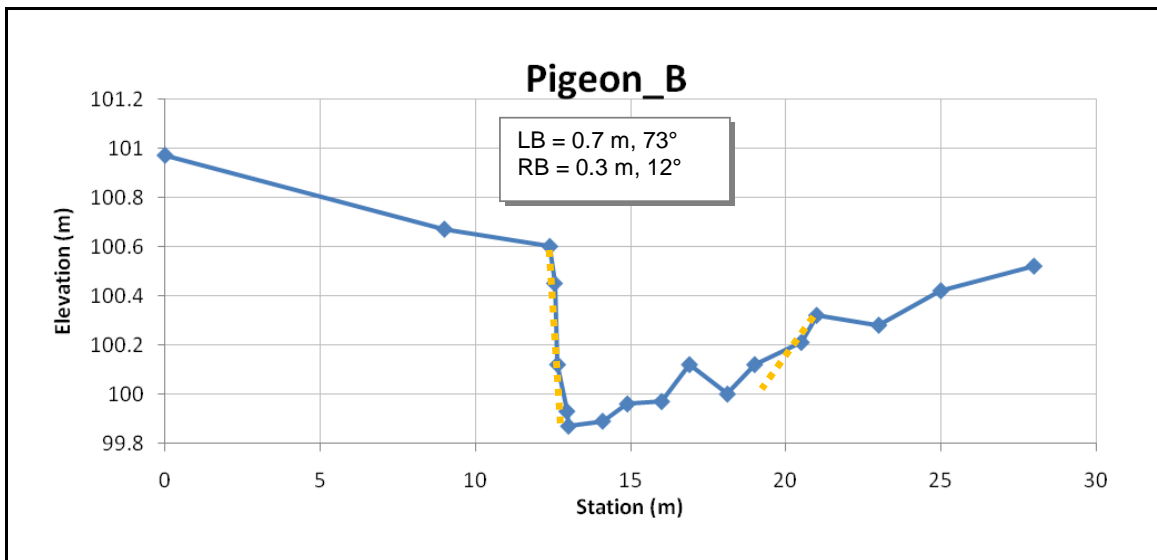


Figure C.63 – Pigeon\_B (Pigeon Pass)

Note(s):

LB U-MW-PC

RB U-MW-PC



View of left bank of Pigeon\_C



Just downstream of Pigeon\_C – MW evident both banks

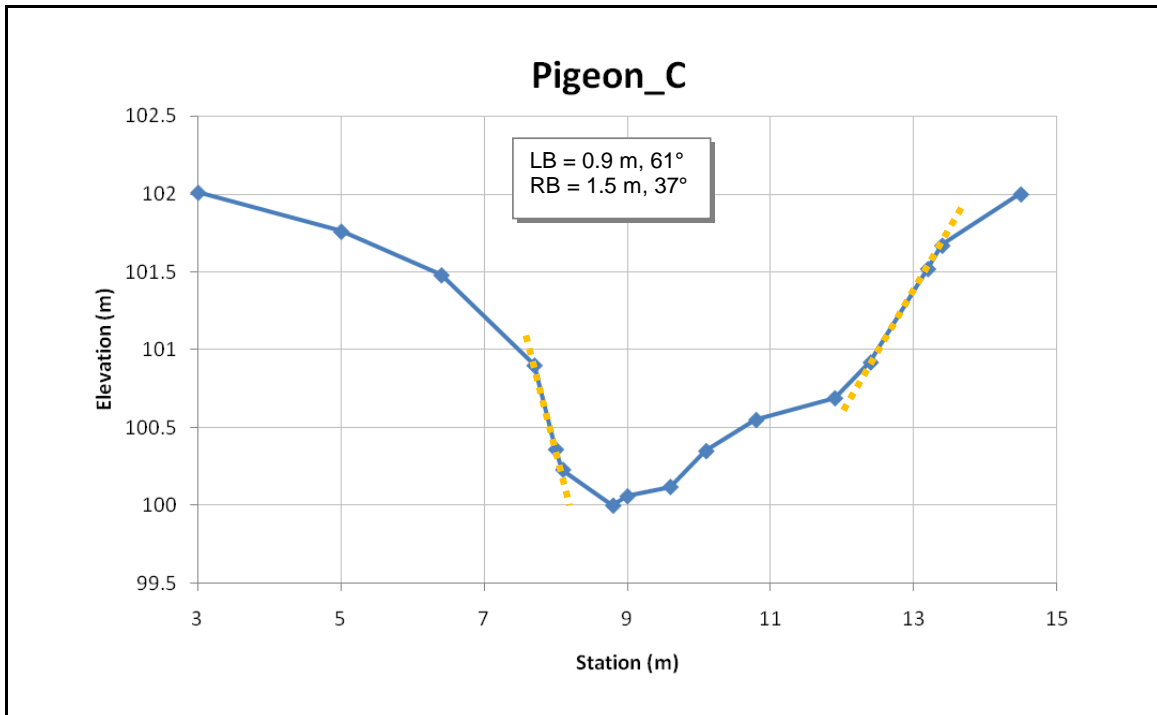


Figure C.64 – Pigeon\_C (Pigeon Pass)

Note(s):

LB STABLE-UC

RB S-CONFND and S-CONFND



Looking downstream with view of left bank of Stewart\_A



Looking downstream with view of right bank of Stewart\_A – survey captured geometry of boulder embedded in bank (rather than unconsolidated MW just up and downstream)



MW in unconsolidated right bank (left) just upstream from cross-section. ~ 2 m @ 70°

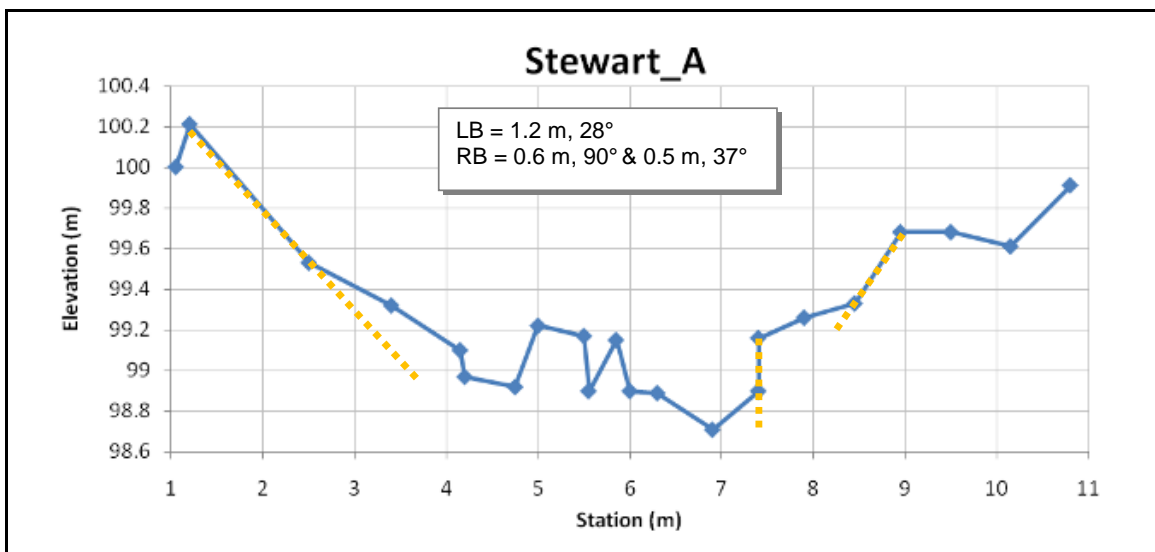


Figure C.65 – Stewart\_A

Santiagbd\_A (Santiago at Tucker Bird Sanctuary)

CSU, Jan-2008

Note(s):

LB U-CONFND (upper) and U-MW-UC (lower)

RB STABLE (upper) and U-MW-UC (lower)



Looking upstream with view of left bank (valley wall) of Santiagbd\_A

Right bank of Santiagbd\_A

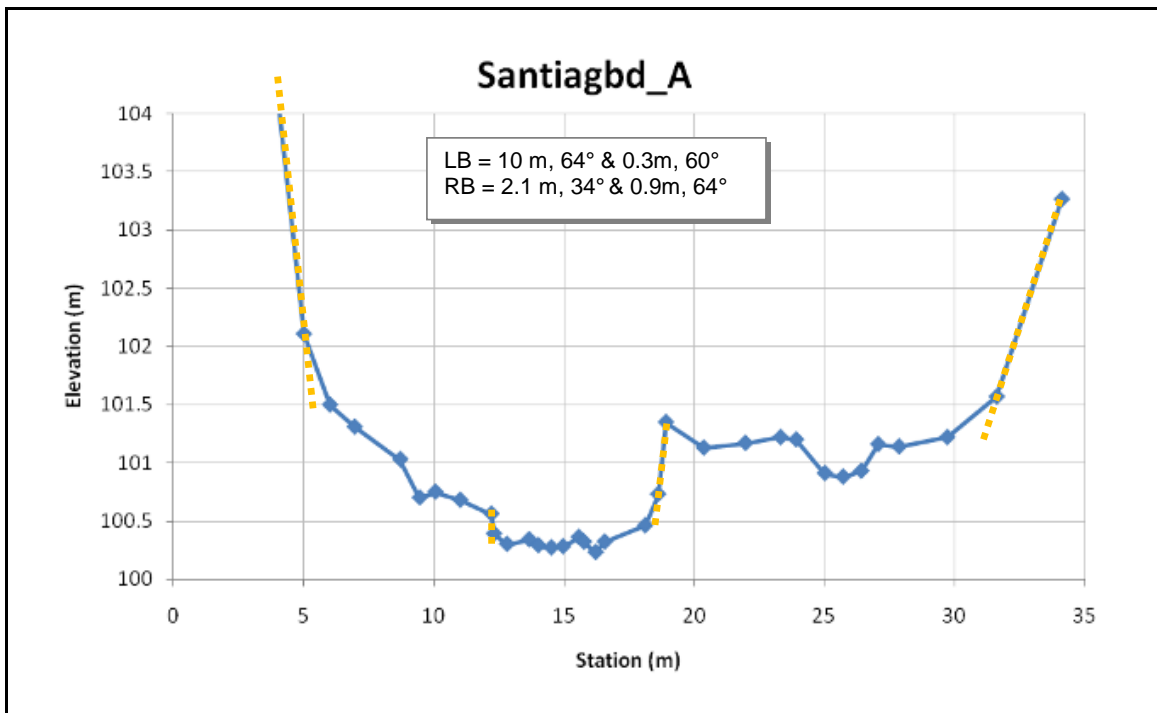


Figure C.66 – Santiagbd\_A (Santiago at Tucker Bird Sanctuary)

Santiagbd\_B (Santiago at Tucker Bird Sanctuary)

CSU, Jan-2008

Note(s):

LB U-CONFND (upper) and STABLE-UC (lower)

RB STABLE (upper) and U-MW-UC (lower)



Looking downstream with view of the left bank (valley wall) of Santiagbd\_B



Looking downstream with view of right bank of Santiagbd\_B



Looking upstream with view of the right bank of Santiagbd\_B

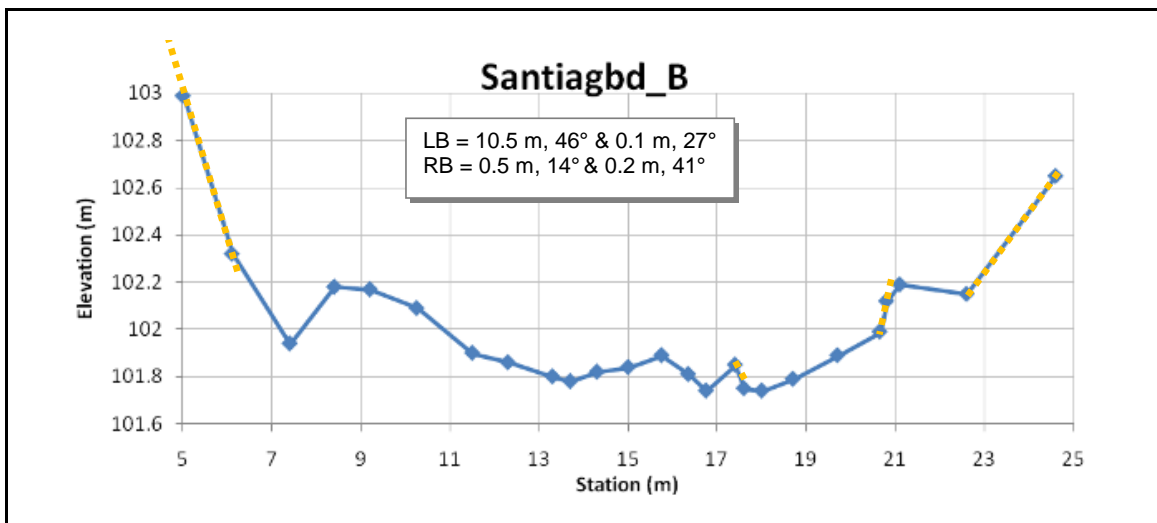
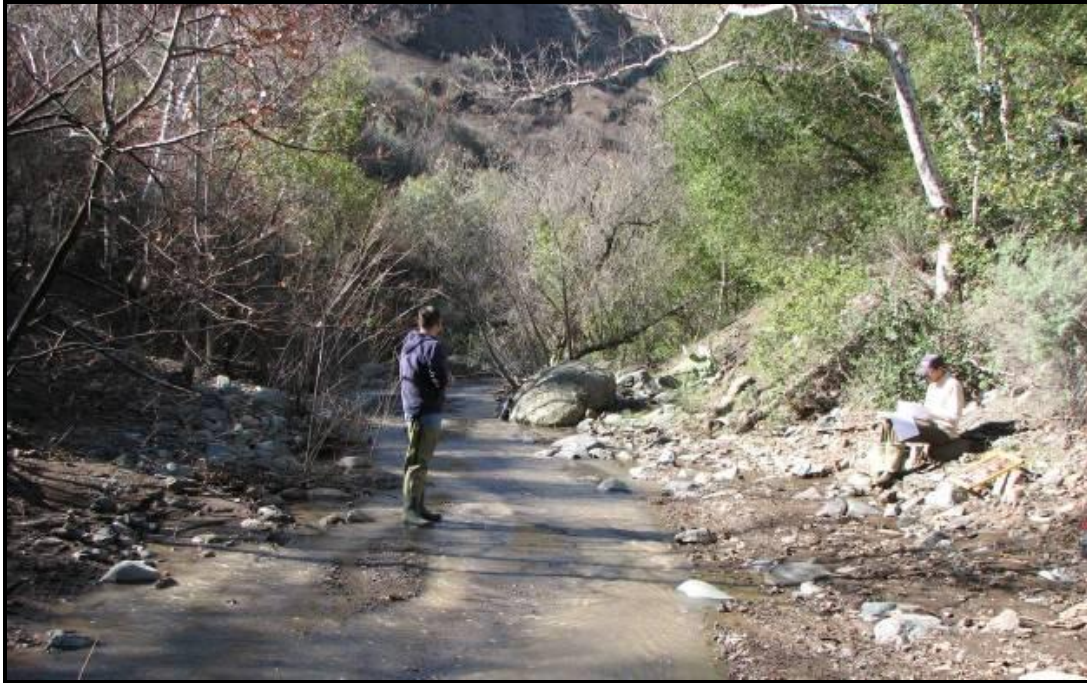


Figure C.67 – Santiagbd\_B (Santiago at Tucker Bird Sanctuary)

Note(s):

LB U-CONFND (upper) and U-MW-UC RB STABLE  
(lower)



Looking downstream at Santiagnl\_A

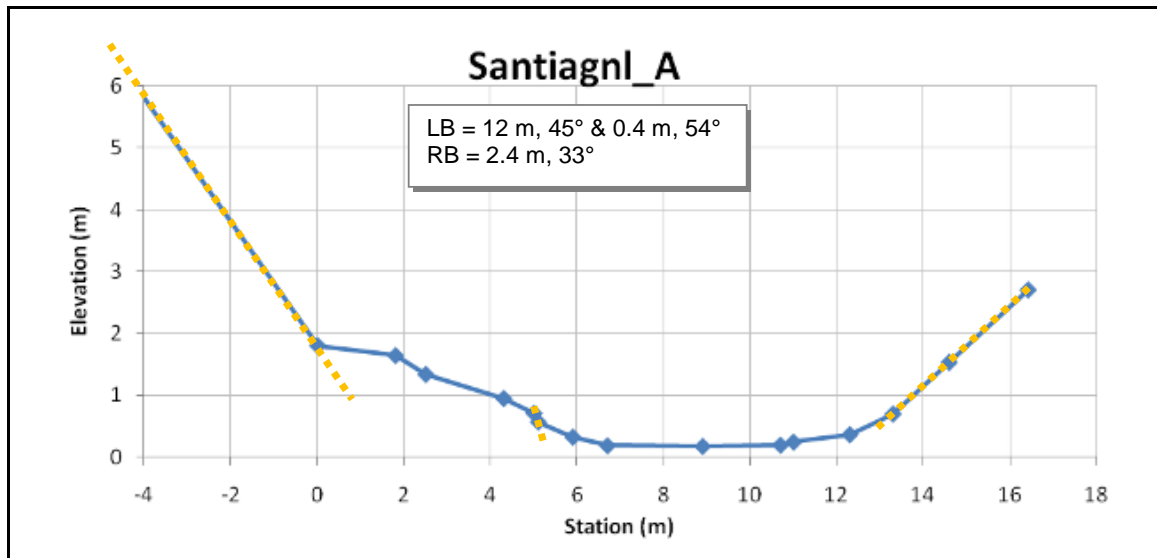


Figure C.68 – Santiagnl\_A (Santiago at Natural-loading site)

Santiagnl\_B (Santiago at natural-loading site)

CSU/SCCWRP, Jan-2008

Note(s):

LB U-MW-UC

RB STABLE (upper) and STABLE (lower)



Looking downstream at Santiagnl\_B with view of left bank

Looking upstream at Santiagnl\_B



Although not at one of the cross-sections, the purpose of the close-up bank photo (left) is to show how unstable the unconsolidated alluvia are

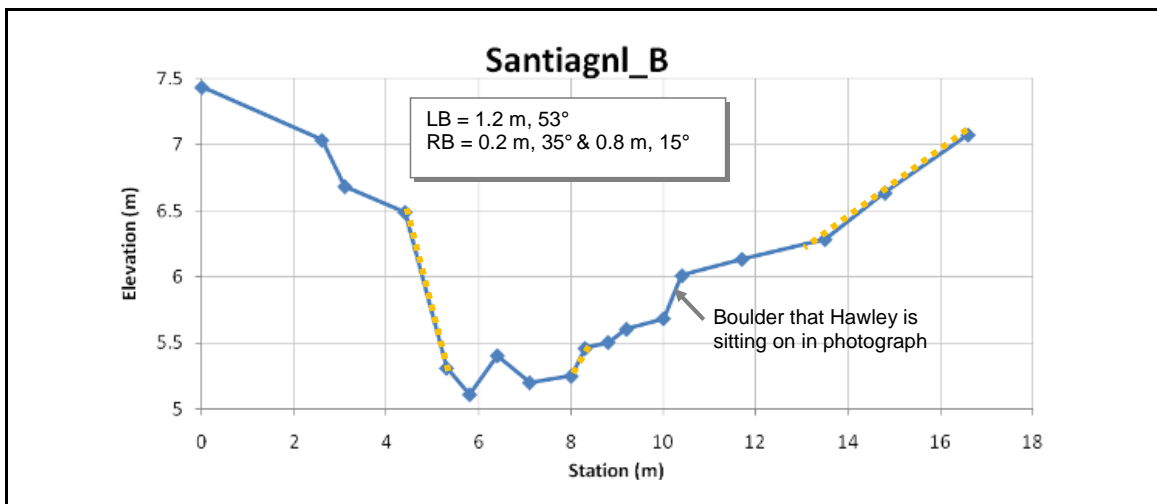


Figure C.69 – Santiagnl\_B (Santiago at natural-loading site)

Note(s):

LB STABLE

RB STABLE



Looking upstream at Silverado\_A with view of left bank



Looking at right bank of Silverado\_A

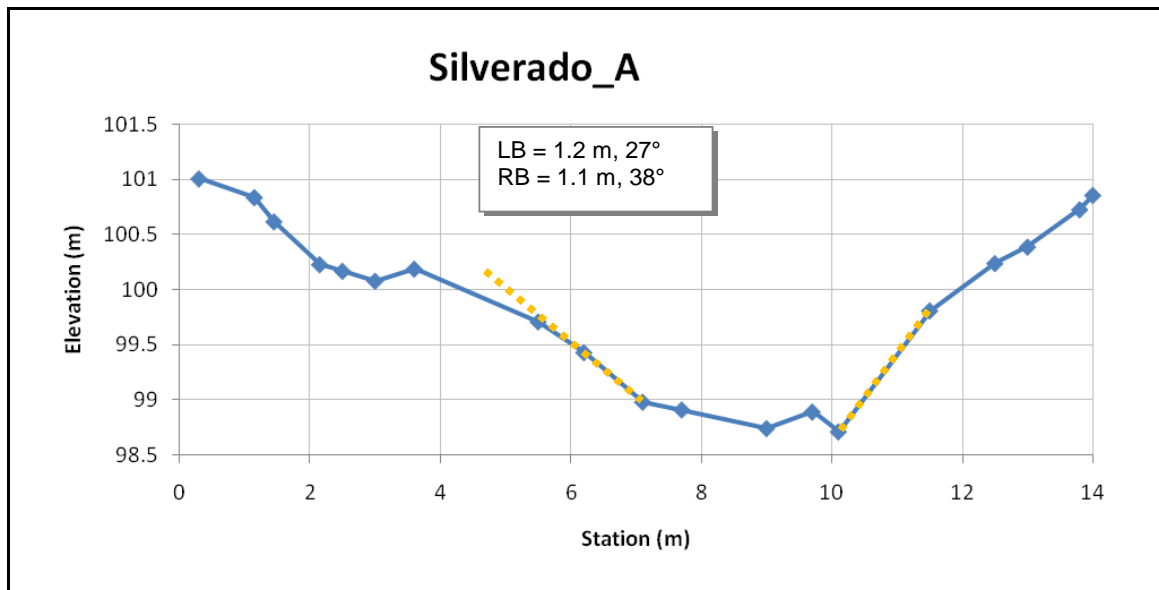


Figure C.70 – Silverado\_A

Note(s):

LB S-CONFND (upper) and STABLE (lower)

RB S-CONFND



Looking from right to left bank (valley wall) of Silverado\_B



Looking upstream at Silverado\_B



Looking downstream at Silverado\_B

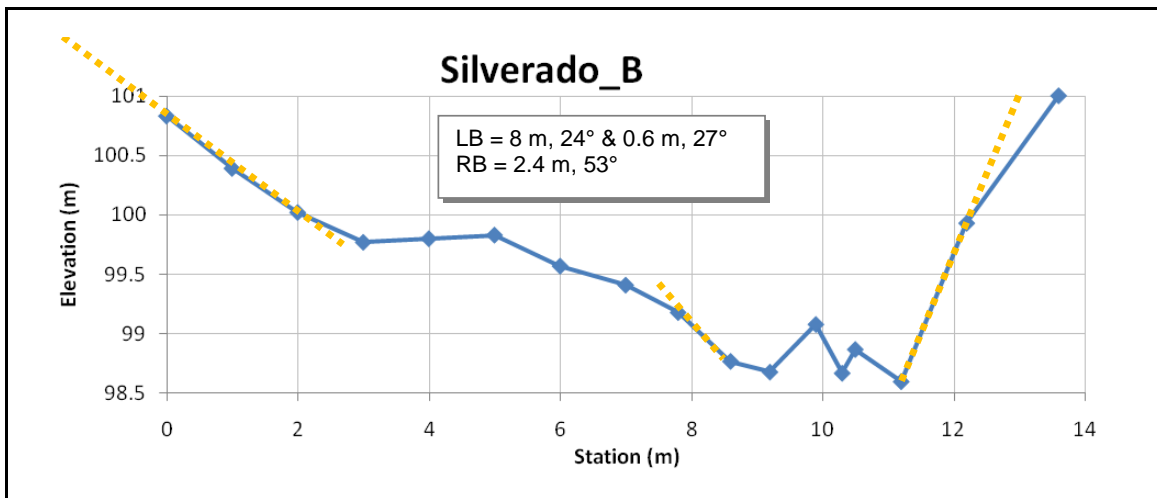


Figure C.71 – Silverado\_B

Note(s):

LB S-CONFND (upper) and STABLE-UC (lower)

RB S-CONFND (upper) and S-CONFND (lower)



Looking downstream at Escondido\_A

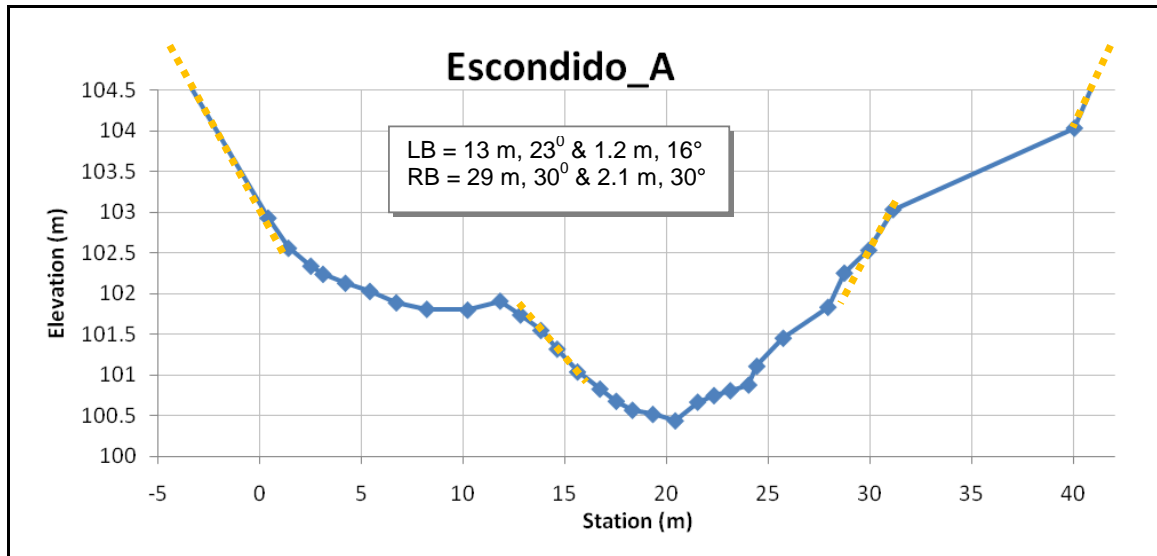


Figure C.72 – Escondido\_A

Note(s):

LB S-CONFND (upper) and U-MW-UC (lower)

RB S-CONFND (upper) and STABLE-UC (lower)



Looking upstream at left bank of Escondido\_B



Looking downstream right channel of Escondido\_B



Looking from left bank upstream toward middle island of Escondido\_B

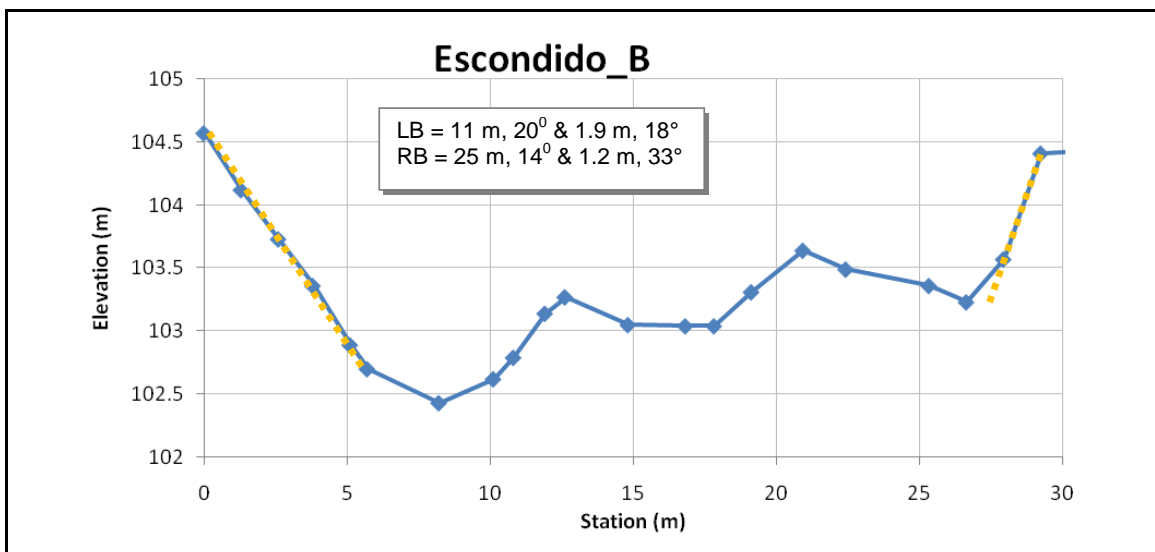


Figure C.73 – Escondido\_B

Note(s):

LB U-MW-UC

RB STABLE-UC



Looking from right bank of SanAntoni\_A at knickpoint just upstream from SanAntoni\_B



Looking upstream from near SanAntoni\_A, toward left bank of SanAntoni\_B

These sites are literally less than 30-m apart. Therefore, the outer banks are only counted once (see SanAntoni\_B next page). Only the within the additional incision within the main channel are counted for SanAntoni\_A.

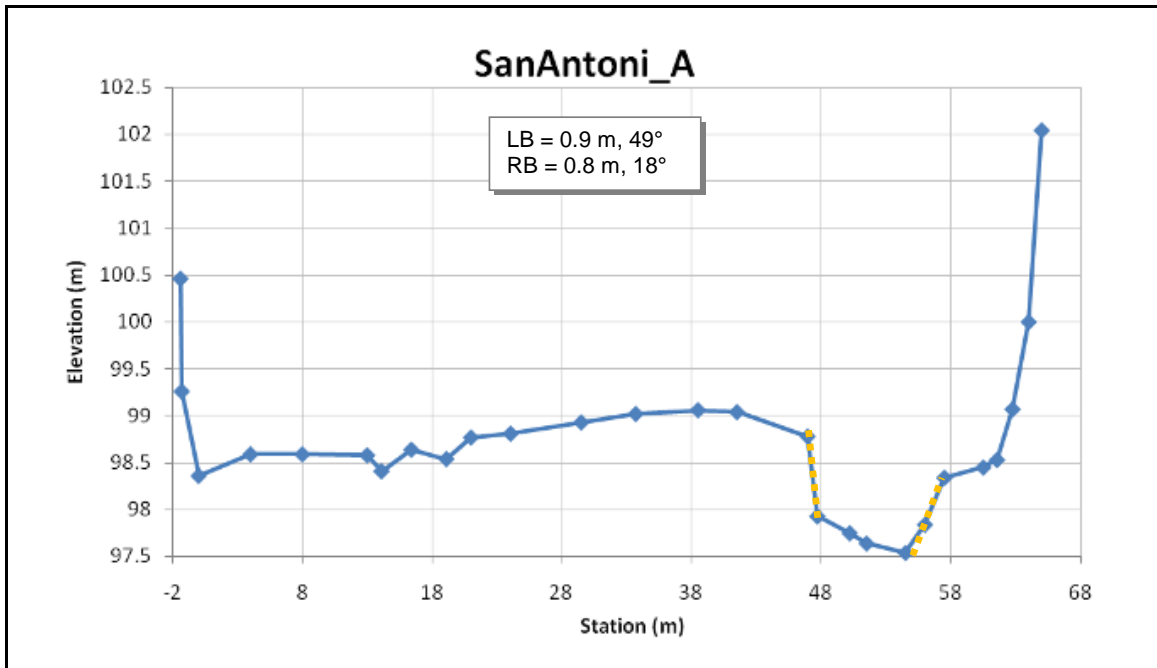


Figure C.74 – SanAntoni\_A (San Antonio)

Note(s):

LB U-MW-PC (upper) and STABLE-UC (lower)

RB U-MW-PC (upper) and STABLE-UC (lower)



Looking at left bank of SanAntoni\_B



Looking downstream of SanAntoni\_B

Although banks are composed of mixed alluvia, they seem to have at least a small degree of consolidation (i.e., poorly consolidated). They stand at angles well over the angle of repose. Furthermore, their height and location indicate that they were formed from deposition quite some time ago (i.e., 50+yrs). I've been using the UC (unconsolidated) label on material that literally just a few years ago was deposited/ a part of the channel bed.

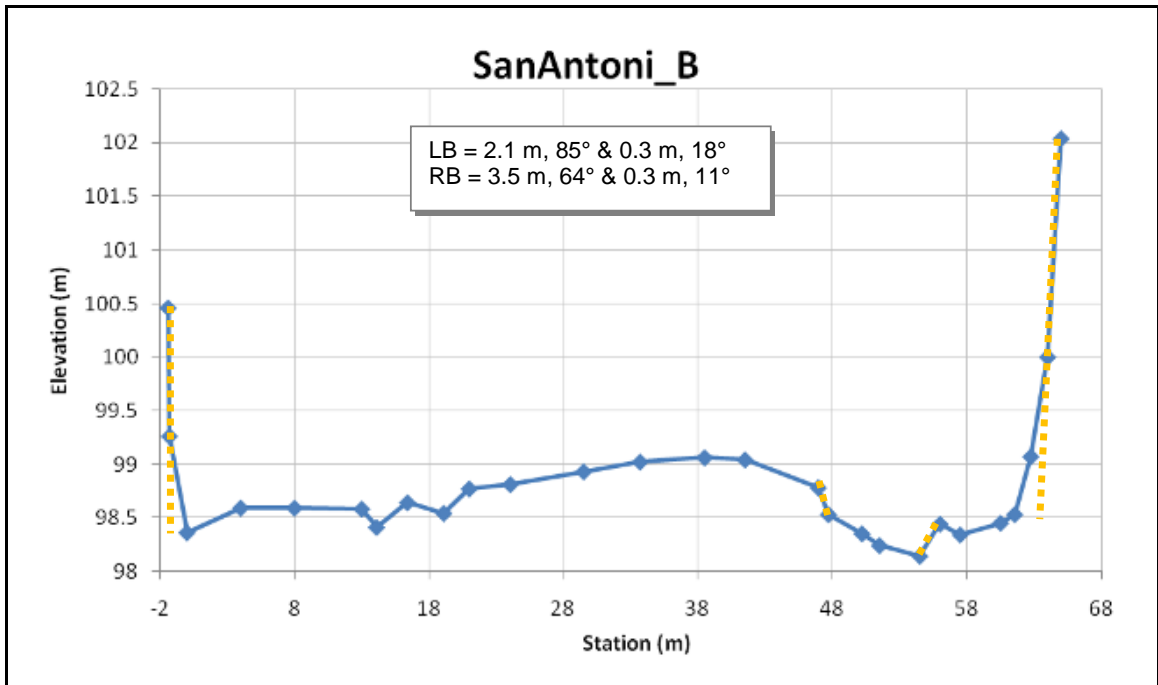


Figure C.75 – SanAntoni\_B (San Antonio)

Alt\_RC2\_A (unnamed headwater in Riverside County)

CSU, Jan-2008

Note(s):

LB STABLE

RB STABLE



Looking upstream at Alt\_RC2\_A

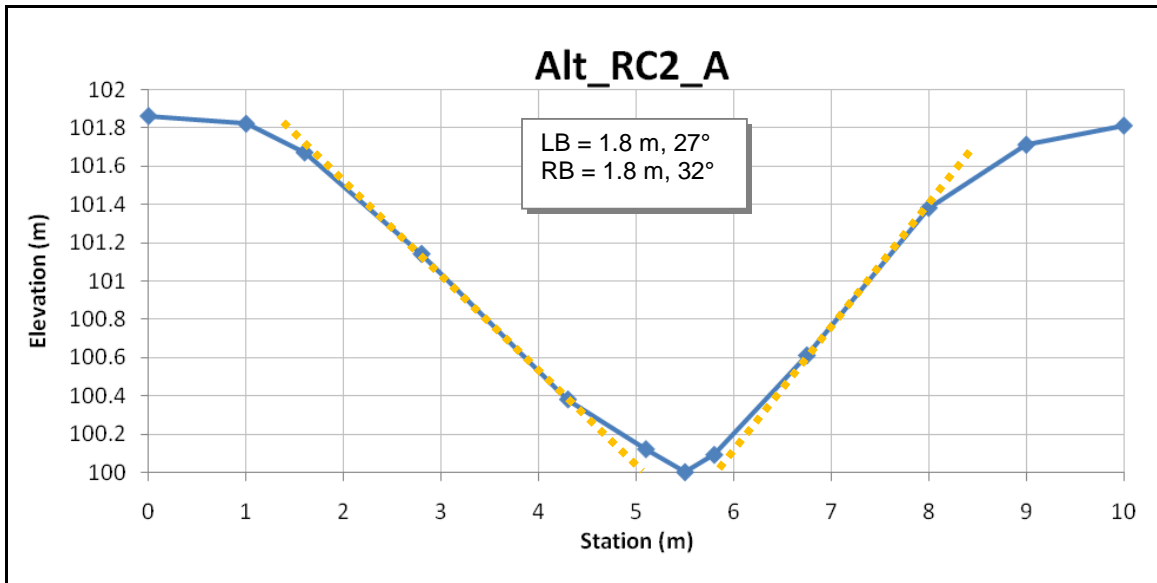


Figure C.76 – Alt\_RC2\_A (unnamed headwater in Riverside County)

Note(s):

LB U-MW-C

RB S-CONSTR



Looking at left bank of Yucaipa\_A



Looking upstream at right bank of Yucaipa\_A



Looking upstream at Yucaipa\_A

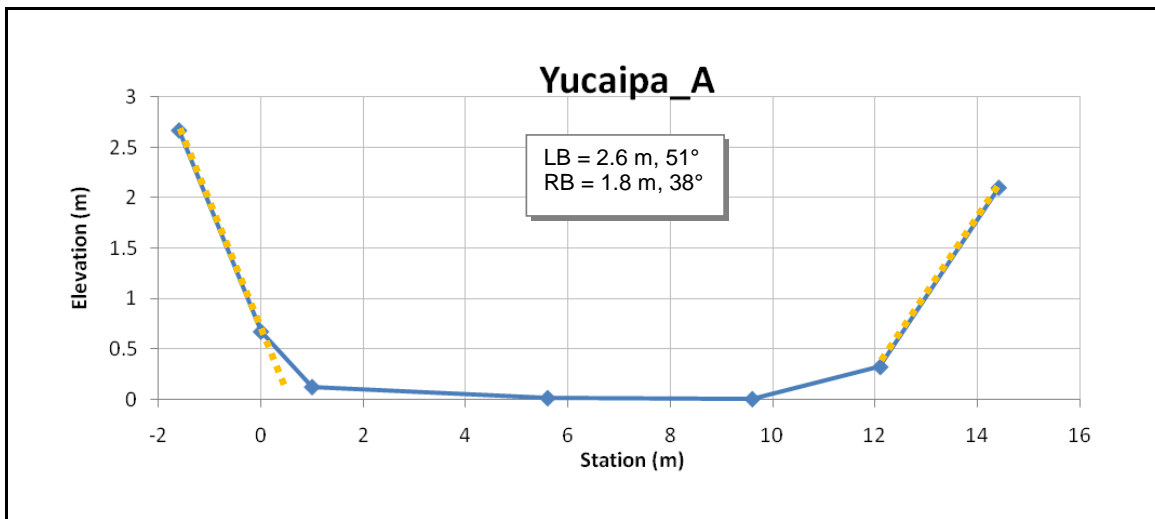


Figure C.77 – Yucaipa\_A

Note(s):

LB U-MW-C

RB U-MW-C



Looking upstream at left bank of Yucaipa\_B



Looking at upstream toward right bank of Yucaipa\_B



Looking downstream at Yucaipa\_B

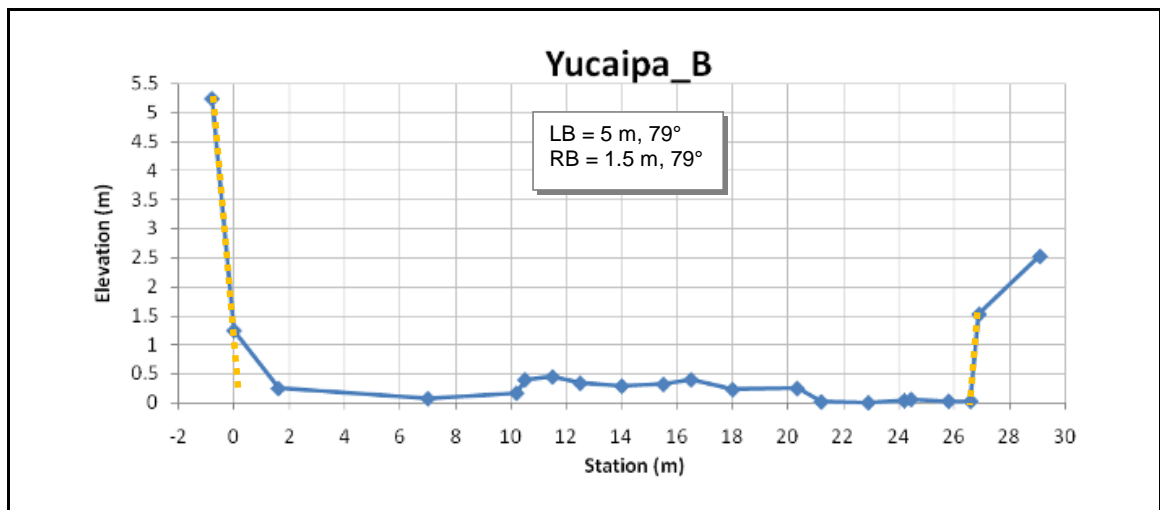


Figure C.78 – Yucaipa\_B

Note(s):

LB U-MW-C

RB U-MW-C



Looking upstream at OakGlenn\_A



Looking downstream at OakGlenn\_A

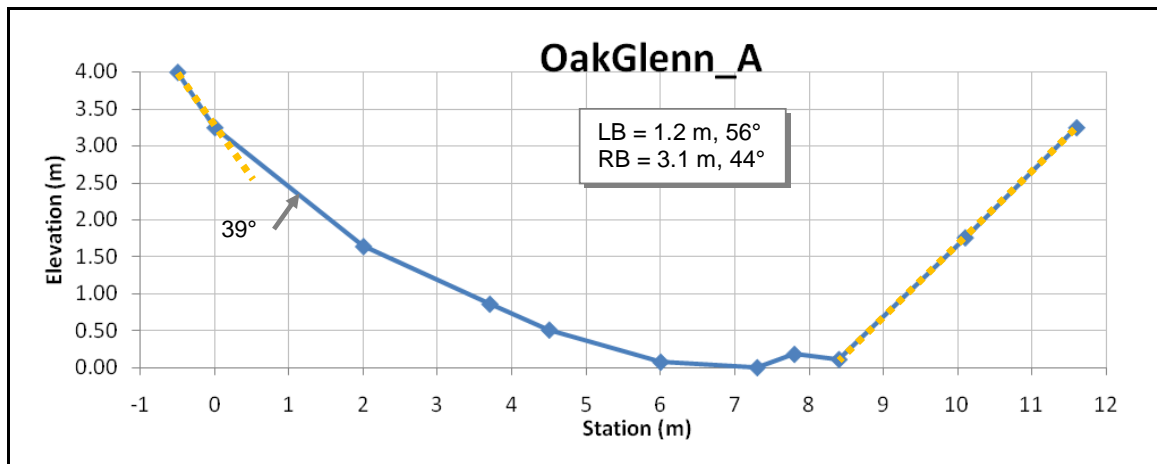


Figure C.79 – OakGlenn\_A

**APPENDIX D**  
**HYDROMODIFICATION SITE DATA**

**Table D.1 – Location and watershed metrics**

Unique ID	Sub-site Description	County	Latitude (decimal °)	Longitude (decimal °)	Total Drainage Area	Watershed Area-Average Annual Precipitation USGS (1900 - 1960)	Watershed Area-Average Annual Precipitation NRCS (1961 - 1990)	8-digit HUC = 18100200	Total Stream Length	%Channelized or Artificial	Drainage Density (stream length/drainage area)	Strahler Stream Order at Site	NOAA 2-yr, 24-hr Volume
					<i>Drn_Area_km</i> (km <sup>2</sup> )	<i>Prcp_USGS_mm</i> (mm)	<i>Prcp_NRCS_mm</i> (mm)	<i>HUCdry</i> (binary)	<i>Stream_km</i> (km)	<i>frac_Chnlzd</i> (fraction)	<i>Drain_Density</i> (km/km <sup>2</sup> )	<i>Order</i> (Strahler)	<i>Prcp24hr_V</i> (mm)
Santiago_A	DS-braided	OR	33.7153	-117.6468	35.09	594	524	0	42.92	0%	1.223	3.0	93
Santiago_B	US-pool-riffle	OR	33.7127	-117.6447	33.67	596	526	0	42.39	0%	1.259	3.0	93
Hasley_1_A	DS-incised, CEM2	LA	34.4672	-118.6648	3.98	368	432	0	4.87	0%	1.224	2.0	81
Hasley_1_B	US-wide, CEM3	LA	34.4672	-118.6655	3.98	369	432	0	4.81	0%	1.208	2.0	81
Hasley_1_TRIB	TRIB-stable	LA	34.4668	-118.6653	0.42	356	432	0	0.07	0%	0.169	1.0	81
Hasley_2_A	DS-braided	LA	34.4631	-118.6588	11.69	383	432	0	20.89	0%	1.787	3.0	81
Hasley_2_B	US-incised	LA	34.4647	-118.6606	6.41	379	432	0	9.94	0%	1.551	3.0	81
Hasley_2_TRIB	TRIB-braided	LA	34.4641	-118.6594	5.05	391	432	0	10.63	0%	2.105	2.0	81
Hicks_A_08	stable @ road	OR	33.7206	-117.7304	3.87	422	372	0	5.73	0%	1.480	2.0	69
Hicks_B_08	incised	OR	33.7213	-117.7296	3.87	422	372	0	5.72	0%	1.478	2.0	69
Hicks_C_08	wide	OR	33.7216	-117.7296	3.87	422	372	0	5.71	0%	1.476	2.0	69
Hicks_D_08	wide_LVL	OR	33.7223	-117.7291	3.73	425	374	0	5.49	0%	1.473	2.0	69
Hicks_D_07	wide_SRVY	OR	33.7223	-117.7291	3.73	425	374	0	5.49	0%	1.473	2.0	69
Hicks_E_08	wide_LVL	OR	33.7237	-117.7276	3.58	429	376	0	5.27	0%	1.472	2.0	69
Hicks_E_07	wide_SRVY	OR	33.7237	-117.7276	3.58	429	376	0	5.27	0%	1.472	2.0	69
Hicks_F_08	incise_LVL	OR	33.7246	-117.7270	3.51	429	376	0	5.12	0%	1.458	2.0	69
Hicks_F_07	incise_SRVY	OR	33.7246	-117.7270	3.51	429	376	0	5.12	0%	1.458	2.0	69
Agua_Hedi_A	DS, CEM 2, almost beginning to widen	SD	33.1543	-117.2412	27.12	341	330	0	32.08	3%	1.183	3.0	62
Agua_Hedi_B	mid, CEM 3	SD	33.1540	-117.2397	26.97	341	330	0	31.93	3%	1.184	3.0	62
Agua_Hedi_C	US, CEM 2-3	SD	33.1547	-117.2377	26.84	341	330	0	31.72	3%	1.182	3.0	62
Dry_A	DS, CEM 2-3	VT	34.2928	-118.7468	3.16	384	432	0	5.60	0%	1.775	2.0	87

Unique ID	Sub-site Description	County	Latitude (decimal °)	Longitude (decimal °)	Total Drainage Area	Watershed Area- Average Annual Precipitation USGS (1900 - 1960)	Watershed Area- Average Annual Precipitation NRCS (1961 - 1990)	8-digit HUC = 18100200	Total Stream Length	%Channelized or Artificial	Drainage Density (stream length/ drainage area)	Strahler Stream Order at Site	NOAA 2-yr, 24-hr Volume
					<i>Drn_Area_km</i>	<i>Prcp_USGS_mmm</i>	<i>Prcp_NRCS_mmm</i>	<i>HUCCode</i>	<i>Stream_km</i>	<i>frac_Chnlzd</i>	<i>Drain_Density</i>	<i>Order</i>	<i>Prcp2)24h_V</i>
					(km <sup>2</sup> )	(mm)	(mm)	(binary)	(km)	(fraction)	(km/km <sup>2</sup> )	(Strahler)	(mm)
Dry_B	mid, CEM 3-4?	VT	34.2938	-118.7474	3.09	384	432	0	5.48	0%	1.775	2.0	87
Dry_C	US, CEM 3	VT	34.2946	-118.7479	2.98	384	432	0	5.37	0%	1.802	2.0	87
Hovnanian_A	DS-stable	LA	34.2909	-118.5343	3.76	560	509	0	4.09	1%	1.089	1.0	100
Hovnanian_B	US-stable	LA	34.2919	-118.5348	3.74	560	509	0	3.97	1%	1.062	1.0	100
Santimeta_A	DS, CEM 3	SB	34.0073	-117.1197	1.45	356	381	0	0.77	0%	0.532	0.0	64
Santimeta_B	mid, CEM 3, 4-B? (starting)	SB	34.0085	-117.1197	1.45	356	381	0	0.62	0%	0.431	0.0	64
Santimeta_C	US, CEM 3	SB	34.0100	-117.1199	1.45	356	381	0	0.42	0%	0.290	0.0	64
Ltl_Cedar_A	DS, forced single	SD	32.6437	-116.8708	7.21	413	392	0	14.67	0%	2.034	3.0	60
Ltl_Cedar_B	US, braided	SD	32.6431	-116.8692	7.21	413	392	0	14.67	0%	2.034	3.0	60
Proctor_A	DS	SD	32.6945	-116.9096	11.23	345	381	0	18.39	2%	1.638	3.0	56
Proctor_B	US	SD	32.6954	-116.9092	5.81	346	381	0	8.47	0%	1.457	3.0	56
Proctor_TRIB	TRIB	SD	32.6946	-116.9089	3.48	351	381	0	5.56	7%	1.599	2.0	55
Perris_1_A	DS, CEM 2, responded?	RS	33.8744	-117.1714	0.45	356	330	0	0.52	0%	1.158	0.0	55
Perris_1_B	mid, CEM2, 3?, responding	RS	33.8749	-117.1719	0.45	356	330	0	0.44	0%	0.977	0.0	55
Perris_1_C	US, CEM2, US of conc. Outfall, responded?	RS	33.8757	-117.1720	0.43	356	330	0	0.33	0%	0.769	0.0	55
Perris_2_A	DS, CEM1	RS	33.8760	-117.1696	0.14	356	330	0	0.24	0%	1.656	0.0	55
Perris_2_B	US, CEM1	RS	33.8776	-117.1707	0.11	356	330	0	0.03	0%	0.283	0.0	55
Perris_3_A	DS, braided, stable	RS	33.8775	-117.1685	1.46	356	330	0	1.64	0%	1.123	1.0	55
Perris_3_B	US, braided, stable	RS	33.8799	-117.1695	1.39	356	330	0	1.33	0%	0.956	1.0	55
AltPerris_A	DS-braided	RS	33.8752	-117.1478	1.64	356	330	0	1.36	0%	0.826	1.0	55
AltPerris_B	mid-reach single-thread	RS	33.8759	-117.1473	1.25	356	330	0	1.26	0%	1.006	1.0	55
AltPerris_C	US-possibly slight incision	RS	33.8767	-117.1469	1.24	356	330	0	1.16	0%	0.933	1.0	55
Dulzura_A	DS-incised or stable?	SD	32.6683	-116.8267	70.24	490	413	0	108.83	2%	1.550	4.0	65

Unique ID	Sub-site Description	County	Latitude (decimal °)	Longitude (decimal °)	Total Drainage Area	Watershed Area- Average Annual Precipitation USGS (1900 - 1960)	Watershed Area- Average Annual Precipitation NRCS (1961 - 1990)	8-digit HUC = 18100200	Total Stream Length	%Channelized or Artificial	Drainage Density (stream length/ drainage area)	Strahler Stream Order at Site	NOAA 2-yr, 24-hr Volume
					<i>Drn_Area_km</i>	<i>Prcp_USGS_mmm</i>	<i>Prcp_NRCS_mmm</i>	<i>HUCCode</i>	<i>Stream_km</i>	<i>Frac_Chnlzd</i>	<i>Drain_Density</i>	<i>Order</i>	<i>Prcp2/24hr_V</i>
					(km <sup>2</sup> )	(mm)	(mm)	(binary)	(km)	(fraction)	(km/km <sup>2</sup> )	(Strahler)	(mm)
Dulzura_B	US-incised or stable?	SD	32.6685	-116.8254	70.24	490	413	0	108.83	2%	1.550	4.0	65
Acton_A	DS braided	LA	34.4923	-118.1662	2.02	229	279	0	1.10	0%	0.544	1.0	51
Acton_B	transition	LA	34.4948	-118.1660	1.95	229	279	0	0.78	0%	0.401	1.0	51
Acton_C	widening	LA	34.4978	-118.1662	1.87	229	279	0	0.46	0%	0.248	1.0	51
Acton_D	incised/wide	LA	34.4983	-118.1659	1.42	229	279	0	0.37	0%	0.258	1.0	51
Acton_E	US incised	LA	34.4984	-118.1655	1.42	229	279	0	0.32	0%	0.223	1.0	51
Acton_F	US starting to incise	LA	34.4985	-118.1652	1.42	229	279	0	0.29	0%	0.204	1.0	51
Acton_G	US 'stable'	LA	34.4985	-118.1651	1.42	229	279	0	0.28	0%	0.200	1.0	51
Borrego_A	DS constrict (I-C)	OR	33.6707	-117.6934	7.06	440	368	0	11.05	0%	1.565	2.0	73
Borrego_B	braided (IV-B)	OR	33.6725	-117.6906	6.99	440	368	0	10.74	0%	1.538	2.0	73
Borrego_C	widening	OR	33.6737	-117.6873	6.84	443	369	0	10.19	0%	1.490	2.0	73
Borrego_D	incised/wide	OR	33.6781	-117.6838	5.76	454	376	0	8.09	0%	1.405	2.0	73
Borrego_E	US incised	OR	33.6794	-117.6819	5.68	454	376	0	7.86	0%	1.383	2.0	73
Topanga_A	DS incised/braided	LA	34.0474	-118.5798	49.80	561	638	0	83.61	0%	1.679	4.0	97
Topanga_B	braided	LA	34.0482	-118.5807	49.80	559	632	0	83.61	0%	1.679	4.0	97
Topanga_C	US steppool	LA	34.0504	-118.5815	48.92	559	632	0	81.11	0%	1.658	4.0	97
Challengr_A	DS-stable	VT	34.2400	-118.7754	7.43	457	487	0	12.37	0%	1.666	2.0	80
Challengr_B	mid-incised	VT	34.2397	-118.7727	7.32	457	489	0	12.09	0%	1.651	2.0	80
Challengr_C	US-stable	VT	34.2388	-118.7717	7.06	457	489	0	11.93	0%	1.691	2.0	80
Mcgonigle_A	vegetated	SD	32.9698	-117.1478	5.12	330	330	0	7.40	0%	1.445	2.0	48
Sanjuan_A	DS-braided	OR	33.5809	-117.5267	105.24	533	402	0	122.29	0%	1.162	4.0	80
Sanjuan_B	US-steppool	OR	33.5828	-117.5236	103.67	533	402	0	119.17	0%	1.149	4.0	80
Pigeon_A	DS-incised/braided	RS	33.9741	-117.2631	6.47	356	381	0	8.24	1%	1.274	2.0	61

Unique ID	Sub-site Description	County	Latitude (decimal °)	Longitude (decimal °)	Total Drainage Area	Watershed Area- Average Annual Precipitation USGS (1900 - 1960)	Watershed Area- Average Annual Precipitation NRCS (1961 - 1990)	8-digit HUC = 18100200	Total Stream Length	%Channelized or Artificial	Drainage Density (stream length/ drainage area)	Strahler Stream Order at Site	NOAA 2-yr, 24-hr Volume
					<i>Drn_Area_km</i>	<i>Prcp_USGS_mmm</i>	<i>Prcp_NRCS_mmm</i>	<i>HUCCode</i>	<i>Stream_km</i>	<i>frac_Chnlzd</i>	<i>Drain_Density</i>	<i>Order</i>	<i>Prcp2/24h_V</i>
					(km <sup>2</sup> )	(mm)	(mm)	(binary)	(km)	(fraction)	(km/km <sup>2</sup> )	(Strahler)	(mm)
Pigeon_B	mid-braided	RS	33.9742	-117.2632	6.47	356	381	0	8.24	1%	1.274	2.0	61
Pigeon_C	US-pool riffle	RS	33.9822	-117.2699	3.53	356	381	0	4.63	0%	1.312	2.0	60
Stewart_A	cascade	VT	34.4607	-119.2511	4.73	665	533	0	7.88	0%	1.666	2.0	122
Santiagbd_A	DS-incised	OR	33.7096	-117.6183	17.84	607	557	0	23.90	0%	1.339	3.0	95
Santiagbd_B	US-planebed	OR	33.7092	-117.6175	17.84	607	557	0	23.90	0%	1.339	3.0	95
Santiagnl_A	DS-planebed	OR	33.7084	-117.6150	17.07	610	562	0	23.55	0%	1.380	3.0	95
Santiagnl_B	US steppool	OR	33.7092	-117.6142	16.99	610	562	0	23.55	0%	1.386	3.0	95
Silverado_A	DS-steppool	OR	33.7458	-117.6018	21.75	686	510	0	27.07	1%	1.245	3.0	96
Silverado_B	US-steppool	OR	33.7458	-117.6009	21.75	686	510	0	27.07	1%	1.245	3.0	96
Escondido_A	DS-steppool	SD	33.0609	-117.1814	156.73	443	355	0	142.81	14%	0.911	4.0	67
Escondido_B	US-braided-veg	SD	33.0604	-117.1803	156.73	443	355	0	142.81	14%	0.911	4.0	67
Sanantoni_A	DS-braided/incised	VT	34.4496	-119.2247	31.14	711	576	0	56.66	1%	1.820	3.0	134
Sanantoni_B	US-braided, about to incise	VT	34.4496	-119.2247	31.14	711	576	0	56.66	1%	1.820	3.0	134
Alt_RC2_A	incised	RC	33.9292	-117.1173	0.16	356	361	0	0.57	0%	3.654	0.0	62
Yucaipa_A	DS-incised/widening	SB	34.0141	-117.0061	16.70	566	602	0	22.70	0%	1.359	3.0	100
Yucaipa_B	US-braided/incised	SB	34.0142	-117.0051	11.48	565	603	0	17.56	0%	1.529	3.0	101
Oakglenn_A	steppool	SB	34.0506	-116.9529	1.77	744	763	0	2.50	0%	1.413	1.0	119

**General abbreviations and symbol definitions (excluding units of measure):**

conc.	concrete	OR	Orange
constrct	constructed	RC	Riverside County
CEM	Channel Evolution Model	RS	Riverside
DS	downstream	SB	San Bernardino
HUC	Hydrologic Unit Codes	SD	San Diego
ID	identification	TRIB	Tributary
LA	Los Angeles	US	upstream
mid	middle	USDA	U.S. Department of Agriculture
NOAA	National Oceanic and Atmospheric Administration	VT	Ventura
NRCS	Natural Resources Conservation Service		

**Table D.2 – USGS (1977) rural flows and Hawley-Bledsoe rural and urban flows**

Unique ID	USGS 1977 Regional Equations (rural flows)						Averaged Hawley-Bledsoe Flows (average of middle three flows, dropping the low and high) for Rural (_rl) and Developed (_urbn) Settings													
	Q2_USGS_m3s	Q5_USGS_m3s	Q10_USGS_m3s	Q25_USGS_m3s	Q50_USGS_m3s	Q100_USGS_m3s	Q1.5_HB_rl	Q1.5_HB_urbn	Q2_HB_rl	Q2_HB_urbn	Q5_HB_rl	Q5_HB_urbn	Q10_HB_rl	Q10_HB_urbn	Q25_HB_rl	Q25_HB_urbn	Q50_HB_rl	Q50_HB_urbn	Q100_HB_rl	Q100_HB_urbn
Santiago_A	4.27	17.35	34.77	77.28	122.70	174.38	2.55	2.55	5.27	5.27	23.72	23.72	53.82	53.82	97.91	97.91	134.29	134.29	172.51	172.51
Santiago_B	4.18	16.91	33.89	75.27	119.48	169.74	2.53	2.53	5.20	5.20	23.29	23.29	53.03	53.03	96.80	96.80	132.94	132.94	170.74	170.74
Hasley_1_A	0.41	1.44	2.69	5.57	8.49	11.70	0.62	0.62	1.24	1.24	4.68	4.68	8.70	8.70	13.68	13.68	17.60	17.60	21.61	21.61
Hasley_1_B	0.41	1.45	2.71	5.61	8.55	11.77	0.62	0.62	1.24	1.24	4.65	4.65	8.59	8.59	13.63	13.63	17.54	17.54	21.54	21.54
Hasley_1_TRIB	0.08	0.24	0.43	0.85	1.26	1.70	0.06	0.06	0.12	0.12	0.29	0.30	0.49	0.72	0.74	1.25	0.95	1.68	1.16	2.13
Hasley_2_A	0.95	3.55	6.78	14.35	22.15	30.86	1.28	1.36	2.67	2.77	12.58	12.71	24.30	24.30	40.05	40.05	52.62	52.62	65.56	65.56
Hasley_2_B	0.61	2.19	4.13	8.63	13.23	18.32	0.87	0.95	1.77	1.88	7.51	7.64	14.06	14.06	22.62	22.62	29.40	29.40	36.37	36.37
Hasley_2_TRIB	0.54	1.92	3.61	7.53	11.53	15.94	0.78	0.78	1.63	1.63	7.07	7.07	13.24	13.24	21.46	21.46	27.97	27.97	34.67	34.67
Hicks_A_08	0.50	1.79	3.36	7.00	10.72	14.80	0.63	0.75	1.25	1.41	4.84	5.01	9.37	9.37	15.34	15.34	20.09	20.09	24.97	24.97
Hicks_B_08	0.50	1.79	3.36	7.00	10.72	14.80	0.64	0.76	1.27	1.43	4.87	5.04	9.42	9.42	15.40	15.40	20.16	20.16	25.06	25.06
Hicks_C_08	0.50	1.79	3.36	7.00	10.72	14.80	0.64	0.76	1.28	1.43	4.87	5.04	9.43	9.43	15.41	15.41	20.17	20.17	25.07	25.07
Hicks_D_08	0.49	1.75	3.29	6.86	10.51	14.51	0.62	0.74	1.23	1.39	4.68	4.85	9.08	9.08	14.86	14.86	19.46	19.46	24.18	24.18
Hicks_D_07	0.49	1.75	3.29	6.86	10.51	14.51	0.62	0.74	1.23	1.39	4.68	4.85	9.08	9.08	14.86	14.86	19.46	19.46	24.18	24.18
Hicks_E_08	0.49	1.73	3.24	6.76	10.35	14.28	0.60	0.72	1.20	1.35	4.50	4.67	8.75	8.75	14.34	14.34	18.79	18.79	23.36	23.36
Hicks_E_07	0.49	1.73	3.24	6.76	10.35	14.28	0.60	0.72	1.20	1.35	4.50	4.67	8.75	8.75	14.34	14.34	18.79	18.79	23.36	23.36
Hicks_F_08	0.48	1.70	3.20	6.65	10.19	14.05	0.60	0.72	1.19	1.35	4.44	4.60	8.61	8.61	14.10	14.10	18.46	18.46	22.94	22.94
Hicks_F_07	0.48	1.70	3.20	6.65	10.19	14.05	0.60	0.72	1.19	1.35	4.44	4.60	8.61	8.61	14.10	14.10	18.46	18.46	22.94	22.94
Agua_Hedi_A	1.44	5.56	10.73	22.94	35.53	49.81	1.31	15.73	3.21	19.09	18.57	35.73	36.49	54.80	57.90	65.41	74.81	74.81	92.15	92.15
Agua_Hedi_B	1.44	5.54	10.68	22.84	35.37	49.58	1.31	15.66	3.20	19.03	18.52	35.60	36.31	54.34	57.59	64.97	74.40	74.40	91.64	91.64
Agua_Hedi_C	1.43	5.52	10.64	22.75	35.24	49.39	1.30	15.61	3.19	18.98	18.46	35.47	36.13	53.90	57.29	64.55	74.00	74.00	91.13	91.13
Dry_A	0.37	1.30	2.41	4.98	7.58	10.42	0.74	0.74	1.41	1.41	5.28	5.28	9.27	9.27	14.41	14.41	18.46	18.46	22.61	22.61
Dry_B	0.37	1.28	2.38	4.90	7.46	10.26	0.74	0.74	1.40	1.40	5.21	5.21	9.10	9.10	14.12	14.12	18.08	18.08	22.14	22.14

Unique ID	USGS 1977 Regional Equations (rural flows)						Averaged Hawley-Bledsoe Flows (average of middle three flows, dropping the low and high) for Rural (_rl) and Developed (_urbn) Settings													
	Q2_USGS_m3s	Q5_USGS_m3s	Q10_USGS_m3s	Q25_USGS_m3s	Q50_USGS_m3s	Q100_USGS_m3s	Q1.5_HB_rl	Q1.5_HB_urbn	Q2_HB_rl	Q2_HB_urbn	Q5_HB_rl	Q5_HB_urbn	Q10_HB_rl	Q10_HB_urbn	Q25_HB_rl	Q25_HB_urbn	Q50_HB_rl	Q50_HB_urbn	Q100_HB_rl	Q100_HB_urbn
Dry_C	0.36	1.25	2.31	4.77	7.26	9.98	0.73	0.73	1.39	1.39	5.11	5.11	8.92	8.92	13.84	13.84	17.73	17.73	21.71	21.71
Hovnanian_A	0.78	2.81	5.37	11.37	17.61	24.44	0.84	1.06	1.49	1.76	4.68	4.96	8.77	8.77	14.64	14.64	19.41	19.41	24.35	24.35
Hovnanian_B	0.77	2.80	5.34	11.32	17.53	24.33	0.84	1.07	1.50	1.77	4.62	4.93	8.67	8.67	14.49	14.49	19.20	19.20	24.07	24.07
Santimeta_A	0.19	0.63	1.14	2.31	3.48	4.74	0.16	0.35	0.33	0.58	1.01	1.28	1.87	2.29	3.03	3.78	3.96	4.96	4.92	6.17
Santimeta_B	0.19	0.63	1.14	2.31	3.48	4.74	0.16	0.35	0.33	0.59	0.96	1.22	1.77	2.29	2.84	3.78	3.70	4.96	4.59	6.17
Santimeta_C	0.19	0.63	1.14	2.31	3.48	4.74	0.15	0.34	0.33	0.57	0.85	1.09	1.56	2.29	2.47	3.78	3.20	4.96	3.96	6.17
Ltl_Cedar_A	0.76	2.77	5.27	11.09	17.09	23.73	0.82	0.82	1.65	1.65	6.54	6.54	15.64	15.64	30.54	30.54	42.03	42.03	54.02	54.02
Ltl_Cedar_B	0.76	2.77	5.27	11.09	17.09	23.73	0.83	0.83	1.68	1.68	6.59	6.59	15.78	15.78	30.67	30.67	42.18	42.18	54.21	54.21
Proctor_A	0.78	2.88	5.45	11.47	17.62	24.48	0.38	0.49	0.99	1.13	6.54	6.75	13.20	13.20	21.71	21.71	28.49	28.49	35.47	35.47
Proctor_B	0.49	1.74	3.26	6.76	10.31	14.24	0.25	0.45	0.62	0.91	3.71	4.04	7.23	7.23	11.50	11.50	14.86	14.86	18.63	18.63
Proctor_TRIB	0.35	1.21	2.24	4.60	6.98	9.59	0.26	0.26	0.58	0.58	2.56	2.56	5.71	5.71	10.14	10.14	13.47	13.47	16.90	16.90
Perris_1_A	0.08	0.25	0.45	0.89	1.33	1.79	0.08	0.11	0.16	0.20	0.49	0.54	0.90	0.90	1.40	1.40	1.79	1.84	2.19	2.30
Perris_1_B	0.08	0.25	0.45	0.89	1.33	1.79	0.08	0.11	0.15	0.20	0.46	0.51	0.84	0.84	1.31	1.38	1.69	1.84	2.07	2.30
Perris_1_C	0.08	0.25	0.44	0.86	1.28	1.73	0.07	0.10	0.14	0.18	0.40	0.45	0.73	0.79	1.13	1.34	1.45	1.78	1.78	2.23
Perris_2_A	0.04	0.11	0.19	0.36	0.53	0.70	0.04	0.05	0.08	0.09	0.24	0.24	0.39	0.39	0.57	0.57	0.71	0.73	0.86	0.92
Perris_2_B	0.03	0.09	0.15	0.29	0.43	0.57	0.02	0.03	0.04	0.06	0.10	0.11	0.16	0.28	0.24	0.46	0.31	0.61	0.37	0.76
Perris_3_A	0.19	0.63	1.15	2.32	3.50	4.76	0.16	0.17	0.35	0.35	1.33	1.33	2.60	2.60	4.21	4.21	5.44	5.44	6.71	6.71
Perris_3_B	0.18	0.61	1.10	2.23	3.36	4.57	0.15	0.16	0.32	0.33	1.20	1.20	2.30	2.30	3.71	3.71	4.82	4.82	5.96	5.96
AltPerris_A	0.21	0.69	1.26	2.56	3.86	5.26	0.16	0.16	0.33	0.33	1.25	1.25	2.31	2.31	3.73	3.73	4.85	4.99	6.01	6.37
AltPerris_B	0.17	0.56	1.02	2.05	3.08	4.19	0.15	0.15	0.31	0.31	1.08	1.08	2.07	2.07	3.34	3.34	4.35	4.35	5.39	5.39
AltPerris_C	0.17	0.56	1.01	2.04	3.06	4.17	0.14	0.14	0.30	0.30	1.04	1.04	1.99	1.99	3.21	3.21	4.18	4.18	5.17	5.17
Dulzura_A	10.22	44.42	90.96	206.51	330.76	476.01	2.09	2.09	5.25	5.25	32.62	32.62	79.66	79.66	147.99	147.99	201.99	201.99	258.27	258.27
Dulzura_B	10.22	44.42	90.96	206.51	330.76	476.01	2.09	2.09	5.26	5.26	32.65	32.65	79.75	79.75	148.03	148.03	202.05	202.05	258.33	258.33
Acton_A	0.12	0.38	0.68	1.36	2.02	2.73	0.22	0.31	0.44	0.57	1.39	1.51	2.59	2.59	4.03	4.03	5.17	5.17	6.34	6.34

Unique ID	USGS 1977 Regional Equations (rural flows)						Averaged Hawley-Bledsoe Flows (average of middle three flows, dropping the low and high) for Rural (_rl) and Developed (_urbn) Settings													
	Q2_USGS_m3s	Q5_USGS_m3s	Q10_USGS_m3s	Q25_USGS_m3s	Q50_USGS_m3s	Q100_USGS_m3s	Q1.5_HB_rl	Q1.5_HB_urbn	Q2_HB_rl	Q2_HB_urbn	Q5_HB_rl	Q5_HB_urbn	Q10_HB_rl	Q10_HB_urbn	Q25_HB_rl	Q25_HB_urbn	Q50_HB_rl	Q50_HB_urbn	Q100_HB_rl	Q100_HB_urbn
Acton_B	0.11	0.37	0.67	1.32	1.96	2.66	0.21	0.29	0.41	0.53	1.18	1.28	2.14	2.14	3.25	3.25	4.14	4.14	5.04	5.04
Acton_C	0.11	0.36	0.64	1.28	1.89	2.56	0.19	0.26	0.37	0.47	0.93	1.05	1.62	1.62	2.47	2.47	3.15	3.15	3.86	3.92
Acton_D	0.09	0.29	0.52	1.02	1.51	2.04	0.13	0.20	0.26	0.37	0.72	0.83	1.24	1.24	1.90	1.90	2.42	2.53	2.96	3.17
Acton_E	0.09	0.29	0.52	1.02	1.51	2.04	0.12	0.19	0.25	0.36	0.68	0.79	1.17	1.17	1.78	1.90	2.27	2.53	2.78	3.17
Acton_F	0.09	0.29	0.52	1.02	1.51	2.04	0.12	0.18	0.25	0.35	0.66	0.77	1.13	1.13	1.72	1.90	2.19	2.53	2.67	3.17
Acton_G	0.09	0.29	0.52	1.02	1.51	2.04	0.12	0.18	0.24	0.35	0.65	0.76	1.13	1.13	1.70	1.90	2.17	2.53	2.65	3.17
Borrego_A	0.83	3.04	5.80	12.25	18.92	26.30	0.94	4.56	1.93	5.93	8.56	12.39	15.83	15.83	25.00	25.00	32.06	32.06	39.31	39.31
Borrego_B	0.82	3.02	5.75	12.15	18.75	26.07	0.98	4.78	1.98	6.15	8.54	12.51	15.77	15.77	24.54	24.54	31.45	31.45	38.54	38.54
Borrego_C	0.82	3.00	5.71	12.07	18.64	25.90	0.97	5.09	1.97	6.42	8.34	12.52	15.27	15.71	23.78	23.78	30.49	30.49	37.37	37.37
Borrego_D	0.75	2.73	5.20	10.97	16.93	23.50	0.80	4.41	1.60	5.52	6.67	10.45	12.35	14.20	19.75	20.48	25.62	25.62	31.65	31.65
Borrego_E	0.74	2.71	5.15	10.85	16.73	23.22	0.84	4.64	1.65	5.73	6.66	10.54	12.36	14.15	19.82	20.35	25.49	25.49	31.29	31.29
Topanga_A	5.02	20.64	41.53	92.64	147.27	209.79	1.85	2.21	4.32	4.92	24.63	26.14	61.24	61.24	118.31	118.31	163.96	163.96	211.89	211.89
Topanga_B	4.98	20.49	41.21	91.88	146.04	208.02	1.91	2.25	4.43	5.04	25.01	26.53	62.46	62.46	118.98	118.98	164.73	164.73	212.74	212.74
Topanga_C	4.92	20.21	40.63	90.56	143.91	204.95	1.95	2.21	4.65	5.09	26.06	27.63	62.38	62.38	115.88	115.88	160.31	160.31	206.92	206.92
Challengr_A	0.91	3.37	6.45	13.68	21.16	29.46	0.80	1.07	1.67	2.06	7.03	7.54	14.99	14.99	26.45	26.45	35.77	35.77	45.44	45.44
Challengr_B	0.91	3.34	6.38	13.53	20.92	29.12	0.81	1.19	1.65	2.12	6.92	7.41	14.79	14.79	26.15	26.15	35.41	35.41	45.02	45.02
Challengr_C	0.88	3.24	6.19	13.12	20.29	28.23	0.81	0.96	1.65	1.83	6.82	7.02	14.61	14.61	25.94	25.94	35.17	35.17	44.78	44.78
Mcgonigle_A	0.41	1.46	2.72	5.62	8.55	11.77	0.32	3.01	0.76	3.57	3.50	6.38	7.87	13.46	13.62	16.02	18.16	18.16	22.85	22.85
Sanjuan_A	7.90	33.63	68.48	154.55	247.02	354.16	5.00	5.00	11.28	11.28	62.42	62.42	133.91	133.91	233.69	233.69	315.01	315.01	399.52	399.52
Sanjuan_B	7.82	33.25	67.67	152.69	244.00	349.78	4.97	4.97	11.19	11.19	61.45	61.45	131.67	131.67	229.58	229.58	309.36	309.36	392.27	392.27
Pigeon_A	0.55	1.98	3.73	7.76	11.87	16.42	0.50	0.88	1.12	1.67	5.01	5.61	10.55	10.55	17.52	17.52	23.06	23.06	28.77	28.77
Pigeon_B	0.55	1.98	3.73	7.76	11.87	16.42	0.50	0.88	1.12	1.67	5.01	5.61	10.55	10.55	17.52	17.52	23.06	23.06	28.77	28.77
Pigeon_C	0.36	1.24	2.31	4.75	7.22	9.93	0.36	0.36	0.79	0.79	3.17	3.17	6.53	6.53	10.88	10.88	14.34	14.34	17.90	17.90
Stewart_A	1.21	4.48	8.69	18.68	29.21	40.77	2.60	2.60	3.85	3.85	10.75	10.75	20.11	20.11	34.33	34.33	45.91	45.91	57.96	57.96

Unique ID	USGS 1977 Regional Equations (rural flows)						Averaged Hawley-Bledsoe Flows (average of middle three flows, dropping the low and high) for Rural (_rl) and Developed (_urbn) Settings													
	Q2_USGS_m3s	Q5_USGS_m3s	Q10_USGS_m3s	Q25_USGS_m3s	Q50_USGS_m3s	Q100_USGS_m3s	Q1.5_HB_rl	Q1.5_HB_urbn	Q2_HB_rl	Q2_HB_urbn	Q5_HB_rl	Q5_HB_urbn	Q10_HB_rl	Q10_HB_urbn	Q25_HB_rl	Q25_HB_urbn	Q50_HB_rl	Q50_HB_urbn	Q100_HB_rl	Q100_HB_urbn
Santiagbd_A	2.72	10.69	21.17	46.47	73.34	103.57	1.77	1.77	3.45	3.45	14.13	14.13	32.35	32.35	59.78	59.78	82.50	82.50	106.31	106.31
Santiagbd_B	2.72	10.69	21.17	46.47	73.34	103.57	1.77	1.77	3.45	3.45	14.13	14.13	32.34	32.34	59.76	59.76	82.47	82.47	106.26	106.26
Santiagnl_A	2.66	10.43	20.64	45.28	71.45	100.87	1.75	1.75	3.39	3.39	13.72	13.72	31.73	31.73	59.18	59.18	81.92	81.92	105.77	105.77
Santiagnl_B	2.65	10.39	20.57	45.13	71.21	100.52	1.75	1.75	3.38	3.38	13.69	13.69	31.66	31.66	59.11	59.11	81.82	81.82	105.64	105.64
Silverado_A	3.83	15.32	30.69	68.15	108.31	153.64	2.92	2.92	5.37	5.37	20.44	20.44	44.70	44.70	81.87	81.87	112.73	112.73	145.08	145.08
Silverado_B	3.83	15.32	30.69	68.15	108.31	153.64	2.91	2.91	5.37	5.37	20.44	20.44	44.75	44.75	81.94	81.94	112.82	112.82	145.19	145.19
Escondido_A	7.79	33.39	67.76	152.46	242.84	348.26	3.17	17.50	8.72	29.27	60.06	99.38	129.98	173.73	222.93	267.81	298.42	341.15	379.54	415.75
Escondido_B	7.79	33.39	67.76	152.46	242.84	348.26	3.17	17.50	8.72	29.29	60.07	99.40	130.01	173.73	222.97	267.81	298.47	341.15	379.54	415.75
Sanantoni_A	5.25	21.45	43.36	97.18	155.23	221.13	7.23	7.23	12.88	12.88	49.09	49.09	94.91	94.91	162.05	162.05	217.10	217.10	274.52	274.52
Sanantoni_B	5.25	21.45	43.36	97.18	155.23	221.13	7.23	7.23	12.88	12.88	49.09	49.09	94.91	94.91	162.05	162.05	217.10	217.10	274.52	274.52
Alt_RC2_A	0.04	0.11	0.20	0.38	0.56	0.75	0.06	0.06	0.12	0.12	0.36	0.36	0.62	0.62	0.93	0.93	1.18	1.18	1.43	1.43
Yucaipa_A	2.32	9.02	17.77	38.80	61.03	86.00	1.37	1.67	2.88	3.31	12.81	13.34	28.22	28.22	51.06	51.06	69.84	69.84	89.44	89.44
Yucaipa_B	1.76	6.74	13.16	28.52	44.69	62.75	1.13	1.47	2.31	2.83	9.83	10.72	21.66	21.66	39.37	39.37	53.95	53.95	69.17	69.17
Oakglenn_A	0.72	2.54	4.87	10.33	16.06	22.25	0.69	0.72	1.07	1.08	2.50	2.50	5.72	6.08	11.14	11.14	15.67	15.67	20.37	20.37

**General abbreviations and symbol definitions (excluding units of measure):**  
 ID identification  
 USGS U. S. Geological Survey

**Table D.3 – Topographic, urbanization, and soils**

	Total Basin Relief	Elevation at Outlet (at site)	Average Basin Elevation (from 10 and 85% pts)	Travel Distance to Outfall of Furthest Flow Path	Average Slope along Flow Path (from 10 and 85% pts)	Average Surface Slope in Watershed	Valley Slope (GIS) 2nd Option (valley slope dictated by configuration of watershed-confluences, consistent valley widths, etc.)	Valley Width (GIS) using 'Slope' Surface of Watershed	Total Road Length in Watershed 2000	Total Road Length in Watershed 2007	NRCS Type A Soil (sand, loamy sand, or sandy loam)	NRCS Type B Soil (silt loam or loam)	NRCS Type C Soil (sandy clay loam)	NRCS Type D Soil (clay loam, silty clay loam, sandy clay, silty clay, or clay)	Percent Impervious Area	Impervious Area Note
	Relief	Elev_Site	Av_Basin_Elev	Dist_flow_path	Av_Chnl_Slope	Av_Surf_Slope	S_Valley_GIS_2	W_Valley_GIS	Roads_2000_m	Roads_2007_m	NRCS_A	NRCS_B	NRCS_C	NRCS_D	Prcnt_Imprv	
Unique ID	(m)	(m)	(m)	(m)	(m/m)	(m/m)	(m/m)	(m)	(m)	(m)	(fraction)	(fraction)	(fraction)	(fraction)	(%)	
Santiago_A	1,312	364	675	15,615	0.049	0.46	0.017	230	18,510	18,510	0.01	0.01	0.24	0.74	0.25%	
Santiago_B	1,306	370	683	15,088	0.051	0.47	0.017	190	10,488	13,057	0.01	0.00	0.24	0.75	0.16%	
Hasley_1_A	278	436	520	3,847	0.051	0.22	0.029	125	10,233	15,674	0.00	0.18	0.82	0.00	0.88%	more since 01
Hasley_1_B	276	439	520	3,752	0.052	0.22	0.024	125	10,233	15,674	0.00	0.18	0.82	0.00	0.88%	more since 01
Hasley_1_TRIB	121	436	478	1,062	0.095	0.18	0.044	125	516	1,136	0.00	0.99	0.01	0.00	0.31%	more since 01
Hasley_2_A	316	416	524	5,451	0.045	0.22	0.030	180	31,081	40,764	0.00	0.67	0.33	0.00	1.12%	more since 01
Hasley_2_B	292	422	511	4,274	0.046	0.23	0.030	180	16,601	25,467	0.00	0.40	0.60	0.00	1.19%	more since 01
Hasley_2_TRIB	312	420	528	5,285	0.047	0.21	0.031	180	11,989	13,216	0.00	1.00	0.01	0.00	0.65%	more since 01
Hicks_A_08**	409	129	259	4,420	0.072	0.27	0.026	85	6,519	6,519	0.03	0.09	0.40	0.48	1.62%	
Hicks_B_08**	406	132	261	4,311	0.074	0.27	0.026	60	6,180	6,180	0.03	0.09	0.40	0.48	1.62%	
Hicks_C_08**	405	133	261	4,286	0.074	0.27	0.026	60	6,180	6,180	0.03	0.09	0.40	0.48	1.62%	
Hicks_D_08**	403	136	263	4,189	0.075	0.27	0.026	85	6,083	6,083	0.02	0.10	0.41	0.47	1.65%	
Hicks_D_07**	403	136	263	4,189	0.075	0.27	0.026	85	6,083	6,083	0.02	0.10	0.41	0.47	1.65%	
Hicks_E_08**	398	140	268	3,967	0.079	0.27	0.026	85	5,869	5,869	0.02	0.09	0.43	0.47	1.65%	
Hicks_E_07**	398	140	268	3,967	0.079	0.27	0.026	85	5,869	5,869	0.02	0.09	0.43	0.47	1.65%	
Hicks_F_08**	395	143	269	3,851	0.081	0.28	0.026	85	5,736	5,736	0.01	0.09	0.43	0.47	1.65%	
Hicks_F_07**	395	143	269	3,851	0.081	0.28	0.026	85	5,736	5,736	0.01	0.09	0.43	0.47	1.65%	
Agua_Hedi_A	408	97	204	11,289	0.022	0.13	0.007	72	154,976	160,336	0.01	0.21	0.32	0.47	26.36%	
Agua_Hedi_B	404	101	204	11,129	0.022	0.13	0.007	95	154,004	159,364	0.01	0.21	0.32	0.47	26.27%	
Agua_Hedi_C	402	103	204	10,924	0.022	0.13	0.007	72	153,717	159,077	0.01	0.21	0.32	0.47	26.17%	
Dry_A	323	329	394	3,750	0.038	0.27	0.030	190	-	1,249	0.08	0.25	0.07	0.61	0.55%	more since 01
Dry_B	319	334	397	3,629	0.038	0.27	0.030	130	-	1,249	0.07	0.25	0.06	0.61	0.55%	more since 01
Dry_C	316	336	397	3,521	0.039	0.27	0.030	130	-	1,249	0.07	0.26	0.06	0.62	0.56%	more since 01

Unique ID	Total Basin Relief	Elevation at Outlet (at site)	Average Basin Elevation (from 10 and 85% pts)	Travel Distance to Outfall of Furthest Flow Path	Average Slope along Flow Path (from 10 and 85% pts)	Average Surface Slope in Watershed	Valley Slope (GIS) 2nd Option (valley slope dictated by configuration of watershed-confluences, consistent valley widths, etc.)	Valley Width (GIS) using 'Slope' Surface of Watershed	Total Road Length in Watershed 2000	Total Road Length in Watershed 2007	NRCS Type A Soil (sand, loamy sand, or sandy loam)	NRCS Type B Soil (silt loam or loam)	NRCS Type C Soil (sandy clay loam)	NRCS Type D Soil (clay loam, silty clay loam, sandy clay, or silty clay)	Percent Impervious Area	Impervious Area Note
	Relief	Elev_site	Av_Basin_Elev	Dist_flow_path	Av_Chnl_Slope	Av_Surf_Slope	S_Valley_GIS_2	W_Valley_GIS	Roads_2000_m	Roads_2007_m	NRCS_A	NRCS_B	NRCS_C	NRCS_D	Prnt_Imprv	
	(m)	(m)	(m)	(m)	(m/m)	(m/m)	(m/m)	(m)	(m)	(m)	(fraction)	(fraction)	(fraction)	(fraction)	(%)	
Hovnanian_A*	496	388	545	4,433	0.085	0.40	0.041	100	4,412	4,412	0.00	0.42	0.09	0.49	1.54%	
Hovnanian_B*	492	393	547	4,312	0.086	0.40	0.041	45	4,412	4,412	0.00	0.42	0.09	0.49	1.55%	
Santimeta_A	113	571	620	2,158	0.050	0.12	0.046	325	3,950	3,950	0.00	0.89	0.11	0.00	4.90%	
Santimeta_B	110	574	624	2,018	0.054	0.12	0.046	115	3,950	3,950	0.00	0.89	0.11	0.00	4.90%	
Santimeta_C	101	583	629	1,828	0.052	0.12	0.046	100	3,950	3,950	0.00	0.89	0.11	0.00	4.90%	
Ltl_Cedar_A	865	172	465	6,198	0.119	0.36	0.030	130	68	68	0.00	0.00	0.00	1.00	0.08%	
Ltl_Cedar_B	861	176	474	6,035	0.124	0.36	0.030	120	68	68	0.00	0.00	0.00	1.00	0.08%	
Proctor_A	92	251	280	3,995	0.016	0.19	0.016	50	14,241	15,604	0.00	0.12	0.15	0.73	1.49%	
Proctor_B	92	251	280	3,921	0.016	0.14	0.016	95	13,334	13,334	0.00	0.23	0.28	0.48	2.73%	
Proctor_TRIB	252	251	323	3,889	0.042	0.20	0.031	35	907	907	0.00	0.00	0.00	1.00	0.02%	
Perris_1_A	103	497	531	1,640	0.050	0.08	0.024	250	2,021	2,021	0.08	0.20	0.72	0.00	2.21%	
Perris_1_B	102	498	535	1,559	0.058	0.08	0.02	250	2,021	2,021	0.08	0.20	0.72	0.00	2.21%	
Perris_1_C	99	500	538	1,453	0.057	0.08	0.02	250	1,872	1,872	0.08	0.20	0.72	0.00	2.26%	
Perris_2_A	50	500	520	978	0.048	0.05	0.040	180	551	551	0.00	0.14	0.30	0.55	1.41%	
Perris_2_B	42	508	525	770	0.049	0.05	0.040	180	357	357	0.00	0.14	0.30	0.55	1.80%	
Perris_3_A	262	497	560	2,798	0.047	0.09	0.043	400	2,310	2,310	0.09	0.32	0.41	0.18	0.36%	
Perris_3_B	246	512	568	2,487	0.049	0.09	0.043	400	1,903	1,903	0.09	0.32	0.41	0.18	0.35%	
AltPerris_A	237	490	525	2,280	0.039	0.11	0.007	1,450	-	-	0.00	0.99	0.01	0.00	0.03%	
AltPerris_B	237	490	530	2,187	0.046	0.10	0.007	1,450	-	-	0.00	0.99	0.01	0.00	0.03%	
AltPerris_C	236	491	531	2,088	0.048	0.10	0.007	1,450	-	-	0.00	0.99	0.01	0.00	0.03%	
Dulzura_A	774	216	485	15,277	0.045	0.24	0.0075496	455	90,954	93,390	0.00	0.18	0.35	0.47	0.28%	
Dulzura_B	774	216	485	15,148	0.045	0.24	0.0075496	385	90,954	93,390	0.00	0.18	0.35	0.47	0.28%	
Acton_A	357	926	1,019	3,273	0.065	0.18	0.044	160	4,883	6,085	0.00	0.22	0.59	0.19	2.34%	more since 01
Acton_B	344	938	1,028	2,959	0.071	0.18	0.044	160	4,603	5,781	0.00	0.20	0.60	0.20	2.37%	more since 01
Acton_C	332	950	1,040	2,638	0.072	0.19	0.058	130	4,286	5,491	0.00	0.18	0.61	0.21	2.39%	more since 01

Unique ID	Total Basin Relief	Elevation at Outlet (at site)	Average Basin Elevation (from 10 and 85% pts)	Travel Distance to Outfall of Furthest Flow Path	Average Slope along Flow Path (from 10 and 85% pts)	Average Surface Slope in Watershed	Valley Slope (GIS) 2nd Option (valley slope dictated by configuration of watershed-confluences, consistent valley widths, etc.)	Valley Width (GIS) using 'Slope' Surface of Watershed	Total Road Length in Watershed 2000	Total Road Length in Watershed 2007	NRCS Type A Soil (sand, loamy sand, or sandy loam)	NRCS Type B Soil (silt loam or loam)	NRCS Type C Soil (sandy clay loam)	NRCS Type D Soil (clay loam, silty clay loam, sandy clay, or silty clay)	Percent Impervious Area	Impervious Area Note
	Relief	Elev_site	Av_Basin_Elev	Dist_flow_path	Av_Chnl_Slope	Av_Surf_Slope	S_Valley_GIS_2	W_Valley_GIS	Roads_2000_m	Roads_2007_m	NRCS_A	NRCS_B	NRCS_C	NRCS_D	Prcnt_Imprv	
	(m)	(m)	(m)	(m)	(m/m)	(m/m)	(m/m)	(m)	(m)	(m)	(fraction)	(fraction)	(fraction)	(fraction)	(%)	
Acton_D	332	950	1,046	2,541	0.078	0.19	0.058	50	4,160	5,311	0.00	0.20	0.69	0.11	2.90%	more since 01
Acton_E	326	956	1,047	2,491	0.078	0.19	0.058	50	4,160	5,311	0.00	0.20	0.69	0.11	2.90%	more since 01
Acton_F	324	959	1,048	2,464	0.078	0.19	0.058	90	4,160	5,311	0.00	0.20	0.69	0.11	2.90%	more since 01
Acton_G	324	959	1,048	2,458	0.078	0.19	0.058	90	4,160	5,311	0.00	0.20	0.69	0.11	2.90%	more since 01
Borrego_A*	350	169	267	7,369	0.031	0.23	0.020	270	18,073	18,316	0.07	0.12	0.54	0.28	13.83%	
Borrego_B*	345	173	272	7,050	0.031	0.23	0.023	240	18,074	18,317	0.07	0.11	0.54	0.28	13.97%	
Borrego_C*	337	181	280	6,673	0.031	0.24	0.028	300	18,075	18,318	0.07	0.11	0.55	0.28	14.27%	
Borrego_D*	322	196	288	6,095	0.034	0.26	0.023	230	17,611	17,611	0.06	0.10	0.60	0.24	14.23%	
Borrego_E*	317	201	291	5,860	0.034	0.26	0.029	220	17,612	17,612	0.06	0.11	0.60	0.23	14.40%	
Topanga_A*	620	12	207	14,577	0.025	0.31	0.025	55	139,475	167,335	0.00	0.00	0.63	0.37	1.37%	
Topanga_B*	619	13	207	14,577	0.025	0.31	0.027	100	139,338	167,198	0.00	0.00	0.63	0.37	1.37%	
Topanga_C*	599	33	212	14,179	0.025	0.31	0.098	20	138,777	166,637	0.00	0.00	0.63	0.37	1.38%	
Challengr_A*	391	291	402	5,310	0.049	0.36	0.020	60	10,269	10,269	0.00	0.13	0.23	0.64	2.28%	
Challengr_B*	386	296	410	5,027	0.053	0.36	0.038	25	10,091	10,091	0.00	0.13	0.21	0.66	2.22%	
Challengr_C*	382	300	416	4,870	0.056	0.37	0.030	25	8,227	8,227	0.00	0.13	0.21	0.66	1.41%	
Mcgonigle_A	268	93	193	4,598	0.053	0.19	0.021	55	34,811	34,811	0.00	0.012	0.015	0.974	24.80%	
Sanjuan_A*	800	178	539	23,577	0.037	0.33	0.012	350	75,526	75,526	0.0150	0.0350	0.4560	0.4940	0.13%	
Sanjuan_B*	795	183	539	23,000	0.037	0.33	0.013	40	74,592	74,592	0.0150	0.0350	0.4530	0.4970	0.13%	
Pigeon_A*	313	536	652	4,501	0.066	0.18	0.016	160	18,155	18,155	0.00	0.52	0.42	0.06	4.57%	
Pigeon_B*	313	536	652	4,501	0.066	0.18	0.016	160	18,155	18,155	0.00	0.52	0.42	0.06	4.57%	
Pigeon_C*	293	556	675	3,302	0.090	0.19	0.025	100	6,378	6,378	0.00	0.51	0.39	0.10	0.75%	
Stewart_A	1,004	300	680	5,187	0.169	0.46	0.10	650	3,666	3,666	0.00	0.20	0.00	0.80	0.12%	
Santiagbd_A	1,257	419	747	12,261	0.063	0.48	0.026	50	3,549	3,549	0.01	0.00	0.12	0.87	0.03%	
Santiagbd_B	1,254	422	747	12,261	0.063	0.48	0.026	50	3,549	3,549	0.01	0.00	0.12	0.87	0.03%	
Santiagnl_A	1,243	433	761	11,916	0.067	0.48	0.029	40	2,792	2,792	0.01	0.00	0.12	0.87	0.02%	

Unique ID	Relief (m)	Elev_site (m)	Av_Basin_Elev (m)	Dist_flow_path (m)	Av_Chnl_Slope (m/m)	Av_Surf_Slope (m/m)	S_Valley_GIS_2 (m/m)	W_Valley_GIS (m)	Reads_2000_m (m)	Reads_2007_m (m)	NRCS_A (fraction)	NRCS_B (fraction)	NRCS_C (fraction)	NRCS_D (fraction)	Prant Imprv (%)	Impervious Area Note
Santiagnl_B	1,240	436	761	11,916	0.067	0.48	0.029	40	2,792	2,792	0.01	0.00	0.12	0.87	0.02%	
Silverado_A**	907	486	766	8,643	0.076	0.50	0.055	30	17,164	17,164	0.03	0.00	0.06	0.92	0.00%	
Silverado_B**	904	489	766	8,558	0.076	0.50	0.055	30	17,164	17,164	0.03	0.00	0.06	0.92	0.00%	
Escondido_A	629	75	295	33,519	0.014	0.17	0.014	40	641,329	672,276	0.0004	0.3371	0.4138	0.2487	13.81%	
Escondido_B	629	75	295	33,402	0.014	0.17	0.014	50	641,329	672,276	0.0004	0.3371	0.4138	0.2487	13.81%	
Sanantoni_A	1,388	237	653	10,913	0.098	0.44	0.017	2,500	32,570	32,570	0.00	0.29	0.02	0.69	0.19%	
Sanantoni_B	1,388	237	653	10,913	0.098	0.44	0.017	2,500	32,570	32,570	0.00	0.29	0.02	0.69	0.19%	
Alt_RC2_A**	89	512	534	659	0.067	0.17	0.063	90	-	-	0.09	0.07	0.10	0.74	0.00%	
Yucaipa_A	711	891	1,133	8,642	0.062	0.28	0.036	200	35,643	35,643	0.082	0.556	0.096	0.268	1.63%	
Yucaipa_B	703	899	1,133	8,549	0.062	0.29	0.036	200	28,660	28,660	0.064	0.485	0.137	0.315	2.18%	
Oakglenn_A	1,052	1,412	1,828	3,125	0.325	0.52	0.11	240	3,254	3,833	0.00	0.18	0.29	0.53	0.53%	

**Notes:** \* incomplete soil data over relatively small portions of watershed (NRCS soil-type values less suspect)  
 \*\* incomplete soil data over large portions of watershed (NRCS soil-type values highly suspect)

**General abbreviations and symbol definitions (excluding units of measure):**  
 ID identification  
 GIS geographic information system  
 NRCS Natural Resources Conservation Service  
 pts points (i.e., the locations at 10% and 85% of the length of the main channel as measured from the outfall to drainage divide)

**Table D.4 – Rational and NRCS CN methods, valley, reach, and cross-section metrics**

Composite NRCS Curve Number	Undeveloped NRCS Curve Number (i.e., no impervious area)	Composite C (Rational Method)	Undeveloped C (Rational Method), No Impervious Area	Rational 2-yr, 24-hr Flow (Rational Method), Undeveloped-metric	Rational 2-yr, 24-hr Flow (Rational Method), Developed-metric	NRCS 2-yr, 24-hr Flow (CN Method), Undeveloped-metric	NRCS 2-yr, 24-hr Flow (CN Method), Developed-metric	Percent Burned within Last 5 yrs	Valley Slope	Valley Width	Sinuosity at Reach (stream length / valley dist)	Width of Active Floodplain	Connected to Hillslope?	Valley Wall Bedrock?	Channel Slope	Bankfull Top Width	Top Width Prior to Braiding/ Incising	Bankfull Depth Prior to Braiding/ Incising	Slope Prior to Incising/ Braiding	Maximum Depth within Banks	
NRCS_CN_comp	NRCS_CN_undhp	Rainl_C_comp	Rainl_C_undhp	Q2un_Rt_24m	Q2_Rtnl_24m	Q2un_NR_24m	Q2_NRCS_24m	Prnt_Burn	Slope_Valley	Width_Valley	Sinuosity	Width_Fldpln	Hillslp_cnct	Hillslp_Bdrck	Slope_Chnnl	Width_Top	Width_Top_pre	Depth_BF_pre	Slope_Chn_pre	Depth_BF	
Unique ID				(m <sup>3</sup> /s)	(m <sup>3</sup> /s)	(m <sup>3</sup> /s)	(m <sup>3</sup> /s)	2007, unless noted (0-25%, 25-50%, 50-75%, 75-100%)	(m/m)	(m)	(m/m)	(m)	(1 = yes, 0 = no)	(1 = yes, 0.5 = riprap or sandbag, 0 = no)	(m/m)	(m)	(m)	(m)	(m/m)	(m)	
Santiago_A	86.95	86.93	0.62	0.62	23.164	23.194	23.801	23.826	0%	0.0215	265	1.06	75.4	1	1	0.0174	75.4	75.4	2.18	0.0203	2.58
Santiago_B	87.00	86.98	0.62	0.62	22.269	22.288	22.887	22.902	0%	0.0162	250	1.02	32.9	1	0.5	0.015	32.9	32.9	2.14	0.0159	2.52
Hasley_1_A	83.70	83.58	0.54	0.53	1.979	1.993	1.937	1.948	0%	0.0354	140	1.073	13	1	0	0.0267	4.27	12.74	0.9	0.0306	1.41
Hasley_1_B	83.70	83.58	0.54	0.53	1.979	1.993	1.937	1.948	0%	0.0354	90	1.073	16	0	0	0.0343	8.3	15.71	1.12	0.0306	1.29
Hasley_1_TRIB	77.14	77.07	0.45	0.45	0.177	0.178	0.151	0.151	0%	0.0333	100	1.096	15	0	0	0.0263	11.39	NA	NA	NA	0.68
Hasley_2_A	79.88	79.67	0.49	0.48	5.281	5.338	4.757	4.803	0%	0.0271	200	1.03	68	0	0	0.0192	68.42	68.42	0.88	0.0265	0.97
Hasley_2_B	82.00	81.81	0.52	0.51	3.055	3.086	2.880	2.905	0%	0.0271	160	1.03	24	0	0	0.0149	23.74	23.74	1.15	0.0265	2.28
Hasley_2_TRIB	77.18	77.04	0.45	0.45	2.126	2.141	1.808	1.820	0%	0.0366	95	1.06	40	0	0	0.0348	24.43	28.44	0.32	NA/?	0.53
Hicks_A_08	85.32	85.12	0.59	0.58	1.797	1.816	1.561	1.577	100%	0.02	90	1.21	10	1	0	0.0132	8.15	8.15	0.71	0.0185	0.19
Hicks_B_08	85.32	85.12	0.59	0.58	1.797	1.816	1.561	1.577	100%	0.02	90	1.21	10	1	0	0.0139	3.7	3.7	0.34	0.0185	0.62
Hicks_C_08	85.32	85.12	0.59	0.58	1.797	1.816	1.561	1.577	100%	0.02	90	1.23	15	0	0	0.0214	6.4	14.9	0.3	0.0185	0.66
Hicks_D_08	85.37	85.16	0.59	0.58	1.729	1.747	1.506	1.522	100%	0.0253	80	1.23	15	0	0	0.0259	6	6.3	0.4	0.0185	1.05
Hicks_D_07	85.37	85.16	0.59	0.58	1.729	1.747	1.506	1.522	0%	0.0253	80	1.21	15	0	0	0.027	5.92	5.92	0.5	0.0185	0.96
Hicks_E_08	85.58	85.37	0.59	0.59	1.666	1.683	1.461	1.476	100%	0.0276	90	1.63	24	0	0	0.0197	3.1	14.3	0.41	0.0185	0.84
Hicks_E_07	85.58	85.37	0.59	0.59	1.666	1.683	1.461	1.476	0%	0.0276	90	1.63	24	0	0	0.0192	3.35	16.82	0.34	0.0185	0.89
Hicks_F_08	85.63	85.43	0.59	0.59	1.634	1.651	1.436	1.451	100%	0.0276	90	1.63	40	0	0	0.0163	7.3	12.5	0.56	0.0185	1.14
Hicks_F_07	85.63	85.43	0.59	0.59	1.634	1.651	1.436	1.451	0%	0.0276	90	1.63	40	0	0	0.0146	11.08	12.5	0.56	0.0185	1.09
Agua_Hedi_A	88.16	84.64	0.67	0.58	11.130	13.042	8.882	10.746	0%	0.007	40	1.1	35	0	0.5	0.0042	15.58	25.07	0.91	0.0064	2.31

Unique ID	Composite NRCS Curve Number	Undeveloped NRCS Curve Number (i.e., no impervious area)	Composite C (Rational Method)	Undeveloped C (Rational Method), No Impervious Area	Rational 2-yr, 24-hr Flow (Rational Method), Undeveloped-metric (m <sup>3</sup> /s)	Rational 2-yr, 24-hr Flow (Rational Method), Developed-metric (m <sup>3</sup> /s)	NRCS 2-yr, 24-hr Flow (CN Method), Undeveloped-metric (m <sup>3</sup> /s)	NRCS 2-yr, 24-hr Flow (CN Method), Developed-metric (m <sup>3</sup> /s)	Percent Burned within Last 5 yrs	Valley Slope	Valley Width	Sinuosity at Reach (stream length / valley dist)	Width of Active Floodplain	Connected to Hillslope?	Valley Wall Bedrock?	Channel Slope	Bankfull Top Width	Top Width Prior to Braiding/Incising	Bankfull Depth Prior to Braiding/Incising	Slope Prior to Incising/Braiding	Maximum Depth within Banks
	NRCS_CN_comp	NRCS_CN_undvp	Rainl_C_comp	Rainl_C_undvp	Q2un_Rt_24m	Q2_Rtnl_24m	Q2un_NR_24m	Q2_NRCS_24m	Prctnt_Burn	Slope_Valley	Width_Valley	Sinuosity	Width_Flcpn	Hillslp_cnct	Hillslp_Bdrck	Slope_Chnnl	Width_Top	Width_Top_pre	Depth_BF_pre	Slope_Chn_pre	Depth_BF
					(m <sup>3</sup> /s)	(m <sup>3</sup> /s)	(m <sup>3</sup> /s)	(m <sup>3</sup> /s)	2007, unless noted (0-25%, 25-50%, 50-75%, 75-100%)	(m/m)	(m)	(m/m)	(m)	(1 = yes, 0 = no)	(1 = yes, 0.5 = riprap or sandbag, 0 = no)	(m/m)	(m)	(m)	(m)	(m/m)	(m)
Agua_Hedi_B	88.15	84.64	0.67	0.58	11.070	12.965	8.834	10.681	0%	0.007	50	1.1	12	0	0	0.0028	11.82	11.82	0.89	0.0064	2.52
Agua_Hedi_C	88.13	84.64	0.67	0.58	11.018	12.897	8.792	10.623	0%	0.007	60	1.1	20	0	0	0.0021	14.85	14.85	1.65	0.0064	3.71
Dry_A	83.25	83.17	0.57	0.57	1.796	1.802	1.673	1.678	100%	0.0254	140	1.15	40	0	0	0.0227	27.93	34.76	1	0.0221	1.28
Dry_B	83.32	83.24	0.57	0.57	1.760	1.766	1.642	1.648	100%	0.0254	160	1.15	35	0	0	0.0205	21.14	21.14	1.31	0.0221	1.72
Dry_C	83.40	83.31	0.57	0.57	1.702	1.708	1.590	1.595	100%	0.0254	120	1.15	20	0	0	0.0239	14.14	21.14	1.31	0.0221	1.93
Hovnanian_A	83.36	83.13	0.56	0.56	2.402	2.428	2.473	2.494	0%	0.0415	50	1.35	25	0	0	0.0314	16.46	NA	NA	NA	1.83
Hovnanian_B	83.36	83.13	0.56	0.56	2.389	2.415	2.460	2.481	0%	0.0415	50	1.35	20	0	0	0.0314	8.13	NA	NA	NA	1.69
Santimeta_A	78.85	77.86	0.48	0.46	0.492	0.518	0.341	0.362	0%	0.0443	200	1.14	11.17	0	0	0.0732	4.5	11.17	0.83	0.0505	1.17
Santimeta_B	78.85	77.86	0.48	0.46	0.492	0.518	0.341	0.362	0%	0.0443	100	1.14	20.82	0	0	0.0507	13.9	20.82	1.1	0.0505	2.06
Santimeta_C	78.85	77.86	0.48	0.46	0.492	0.518	0.341	0.362	0%	0.0443	86	1.14	12.8	0	0	0.0513	12.8	23.37	0.44	0.0505	1.12
Ltl_Cedar_A	87.97	87.96	0.65	0.65	3.248	3.249	2.705	2.706	0%	0.0258	100	1.03	20	0	0	0.02	12.38	45.97	0.71	0.0266	1.55
Ltl_Cedar_B	87.97	87.96	0.65	0.65	3.248	3.249	2.705	2.706	0%	0.0258	100	1.03	50	0	0	0.0259	45.97	45.97	0.64	0.0266	0.79
Proctor_A	86.42	86.25	0.62	0.61	4.424	4.461	3.388	3.423	50%	0.0142	85	1.07	18.44	0	0	0.0127	18.44	NA	NA	NA	0.88
Proctor_B	84.98	84.61	0.59	0.58	2.155	2.193	1.589	1.625	50%	0.0142	120	1.07	14.58	0	0	0.014	14.58	NA	NA	NA	0.73
Proctor_TRIB	88.00	88.00	0.65	0.65	1.420	1.420	1.115	1.115	100%	0.0232	18	1	20.65	0	0	0.021	20.65	NA	NA	NA	0.57
Perris_1_A	81.96	81.59	0.52	0.51	0.144	0.147	0.097	0.099	0%	0.0281	45	1.413	9.58	0	0	0.006	4.88	9.58	0.79	0.0165	0.62
Perris_1_B	81.96	81.59	0.52	0.51	0.144	0.147	0.097	0.099	0%	0.0281	40	1.413	11.66	0	0	0.0138	11.66	11.66	0.57	0.0171	1.03
Perris_1_C	81.96	81.59	0.52	0.51	0.139	0.142	0.093	0.095	0%	0.0281	40	1.413	6.23	0	0	0.0072	6.23	6.23	1.01	0.0141	1.5
Perris_2_A	85.70	85.53	0.60	0.59	0.054	0.054	0.040	0.041	0%	0.0388	60	1.32	5.22	0	0	0.0251	5.22	NA	NA	NA	0.34
Perris_2_B	85.75	85.53	0.60	0.59	0.042	0.043	0.031	0.032	0%	0.0388	100	1.32	10.45	0	0	0.0346	3.95	NA	NA	NA	0.3

Unique ID	Composite NRCS Curve Number	Undeveloped NRCS Curve Number (i.e., no impervious area)	Composite C (Rational Method)	Undeveloped C (Rational Method), No Impervious Area	Rational 2-yr, 24-hr Flow (Rational Method), Undeveloped-metric	Rational 2-yr, 24-hr Flow (Rational Method), Developed-metric	NRCS 2-yr, 24-hr Flow (CN Method), Undeveloped-metric	NRCS 2-yr, 24-hr Flow (CN Method), Developed-metric	Percent Burned within Last 5 yrs	Valley Slope	Valley Width	Sinuosity at Reach (stream length / valley dist)	Width of Active Floodplain	Connected to Hillslope?	Valley Wall Bedrock?	Channel Slope	Bankfull Top Width	Top Width Prior to Braiding/ Incising	Bankfull Depth Prior to Braiding/ Incising	Slope Prior to Incising/ Braiding	Maximum Depth within Banks
	NRCS_CN_comp	NRCS_CN_undvdp	Rainl_C_comp	Rainl_C_undvdp	Q2in_Rt_24m	Q2_Rtnl_24m	Q2in_NR_24m	Q2_NRCS_24m	Prnct_Burn	Slope_Valley	Width_Valley	Sinuosity	Width_Fldpln	Hillslp_cnct	Hillslp_Bdrck	Slope_Chnnl	Width_Top	Width_Top_pre	Depth_BF_pre	Slope_Chm_pre	Depth_BF
					(m <sup>3</sup> /s)	(m <sup>3</sup> /s)	(m <sup>3</sup> /s)	(m <sup>3</sup> /s)	2007, unless noted (0-25%, 25-50%, 50-75%, 75-100%)	(m/m)	(m)	(m/m)	(m)	(1 = yes, 0 = no)	(1 = yes, 0.5 = riprap or sandbag, 0 = no)	(m/m)	(m)	(m)	(m)	(m/m)	(m)
Perris_3_A	80.94	80.88	0.52	0.52	0.477	0.479	0.305	0.307	0%	0.0254	110	1.15	57	0	0	0.0142	57.37	NA	NA	NA	0.77
Perris_3_B	80.94	80.88	0.52	0.52	0.454	0.456	0.291	0.292	0%	0.0254	100	1.15	65	0	0	0.0168	65.08	NA	NA	NA	0.93
AltPerris_A	77.09	77.08	0.45	0.45	0.469	0.469	0.264	0.264	0%	0.0099	1000	1.07	60	0	0	0.0102	48.7	NA	NA	NA	0.3
AltPerris_B	77.09	77.08	0.45	0.45	0.356	0.357	0.200	0.200	0%	0.0099	900	1	30	0	0	0.0072	16.3	NA	NA	NA	0.31
AltPerris_C	77.09	77.08	0.45	0.45	0.354	0.354	0.199	0.199	0%	0.0099	700	1	20	0	0	0.0049	13	13	0.36	0.0072	0.6
Dulzura_A	84.89	84.86	0.58	0.58	30.476	30.531	25.407	25.457	100%	0.0064	140	1.07	18.7	0	0	0.006	6.95	26.8	1	0.006	0.45
Dulzura_B	84.89	84.86	0.58	0.58	30.476	30.531	25.407	25.457	100%	0.0064	140	1.07	20	0	0	0.006	5.8	20	1.05	0.006	0.84
Acton_A	84.15	83.81	0.56	0.55	0.641	0.652	0.432	0.441	0%	0.036	90	1.07	31	0	0	0.0373	18.1	12	0.32	0.0335	0.41
Acton_B	84.36	84.03	0.56	0.55	0.624	0.635	0.424	0.434	0%	0.036	55	1.04	25	0	0	0.0377	7.1	7.1	0.28	0.0347	0.79
Acton_C	84.50	84.17	0.56	0.55	0.600	0.610	0.410	0.419	0%	0.036	22	1.07	10.65	0	0	0.0509	8.5	10.5	0.32	0.0336	1.18
Acton_D	84.14	83.73	0.55	0.54	0.446	0.456	0.302	0.311	0%	0.036	15	1.08	6.2	0	0	0.0328	6.2	6	0.25	0.0333	2.95
Acton_E	84.14	83.73	0.55	0.54	0.446	0.456	0.302	0.311	0%	0.036	25	1.08	1.11	0	0	0.1517	1.11	8	0.25	0.0333	2.3
Acton_F	84.14	83.73	0.55	0.54	0.446	0.456	0.302	0.311	0%	0.036	40	1.08	10	0	0	0.0156	8	8	0.25	0.0333	0.41
Acton_G	84.14	83.73	0.55	0.54	0.446	0.456	0.302	0.311	0%	0.036	40	1.08	10	0	0	0.0105	8	NA	NA	NA	0.25
Borrogo_A	85.36	83.33	0.61	0.55	3.283	3.611	2.866	3.159	75%	0.0229	400	1.05	14	0	0.5	0.0201	14	14	3	0.0199	3
Borrogo_B	85.43	83.38	0.61	0.55	3.252	3.579	2.844	3.137	75%	0.0229	395	1.05	101.7	1	1	0.0178	101.7	47	1	0.0199	1.69
Borrogo_C	85.53	83.46	0.61	0.55	3.186	3.512	2.792	3.084	75%	0.0229	530	1.05	27.9	0	0	0.0144	27.9	47	1	0.0199	4.17
Borrogo_D	85.56	83.50	0.61	0.55	2.674	2.949	2.357	2.602	75%	0.0229	420	1.04	29.48	1	1	0.0306	29.5	47	1	0.0199	6.73
Borrogo_E	85.68	83.61	0.61	0.55	2.639	2.914	2.337	2.580	75%	0.0229	330	1.04	18.4	1	1	0.0276	18.4	18.4	2.56	0.0199	3.58
Topanga_A	86.23	86.07	0.59	0.59	32.641	32.918	35.182	35.392	0%	0.0182	60	1.03	27	1	1	0.0278	23.9	23.9	1.7	NA	1.7

Unique ID	Composite NRCS Curve Number	Undeveloped NRCS Curve Number (i.e., no impervious area)	Composite C (Rational Method)	Undeveloped C (Rational Method), No Impervious Area	Rational 2-yr, 24-hr Flow (Rational Method), Undeveloped-metric (m <sup>3</sup> /s)	Rational 2-yr, 24-hr Flow (Rational Method), Developed-metric (m <sup>3</sup> /s)	NRCS 2-yr, 24-hr Flow (CN Method), Undeveloped-metric (m <sup>3</sup> /s)	NRCS 2-yr, 24-hr Flow (CN Method), Developed-metric (m <sup>3</sup> /s)	Percent Burned within Last 5 yrs	Valley Slope	Valley Width	Sinuosity at Reach (stream length / valley dist)	Width of Active Floodplain	Connected to Hillslope?	Valley Wall Bedrock?	Channel Slope	Bankfull Top Width	Top Width Prior to Braiding/Incising	Bankfull Depth Prior to Braiding/Incising	Slope Prior to Incising/Braiding	Maximum Depth within Banks
	NRCS_CN_comp	NRCS_CN_undvp	Rainl_C_comp	Rainl_C_undvp	Q2in_Rt_24m	Q2_Rtnl_24m	Q2in_NR_24m	Q2_NRCS_24m	Prctnt_Burn	Slope_Valley	Width_Valley	Sinuosity	Width_Fldpln	Hillslp_cnct	Hillslp_Bdrck	Slope_Chnnl	Width_Top	Width_Top_pre	Depth_BF_pre	Slope_Chn_pre	Depth_BF
					(m <sup>3</sup> /s)	(m <sup>3</sup> /s)	(m <sup>3</sup> /s)	(m <sup>3</sup> /s)	2007, unless noted (0-25%, 25-50%, 50-75%, 75-100%)	(m/m)	(m)	(m/m)	(m)	(1 = yes, 0 = no)	(1 = yes, 0.5 = riprap or sandbag, 0 = no)	(m/m)	(m)	(m)	(m)	(m/m)	(m)
Topanga_B	86.23	86.07	0.59	0.59	32.641	32.918	35.182	35.392	0%	0.0182	100	1.03	47	1	1	0.0175	42.3	32.1	1.69	0.0192	2.19
Topanga_C	86.23	86.07	0.59	0.59	32.061	32.335	34.557	34.764	0%	0.1	15	1	15	1	1	0.1	17.5	17.2	4	NA	4
Challengr_A	86.14	85.87	0.61	0.60	4.105	4.160	3.899	3.946	0%	0.0196	70	1.03	25	0	0	0.0094	3.3	6.3	0.49	0.0159	0.98
Challengr_B	86.19	85.93	0.61	0.60	4.060	4.112	3.855	3.900	0%	0.0228	40	1.32	20	0	0	0.0061	2	6	0.64	0.0159	0.89
Challengr_C	86.12	85.95	0.61	0.60	3.914	3.946	3.717	3.745	0%	0.0268	25	1.32	15	0	0	0.0244	5.2	NA	NA	NA	0.71
Mcgonigle_A	90.35	87.83	0.72	0.65	1.821	2.033	1.303	1.538	0%	0.0203	53.8	1.19	53.8	1	0	0.0103	16.2	21.6	0.34	0.017	0.51
Sanjuan_A	85.89	85.87	0.59	0.59	57.051	57.095	54.755	54.792	0%	0.0144	260	1.13	160	1	0	0.0177	41.5	NA	NA	NA	0.84
Sanjuan_B	85.90	85.88	0.59	0.59	56.231	56.274	53.962	53.998	0%	0.0150	40	1.05	31.8	1	1	0.0075	20.7	NA	NA	NA	1.6
Pigeon_A	81.78	81.01	0.52	0.50	2.267	2.359	1.641	1.719	25%	0.0104	50	1	50	1	0.5	0.0153	8.3	13.9	0.48	0.0229	0.98
Pigeon_B	81.78	81.01	0.52	0.50	2.267	2.359	1.641	1.719	25%	0.0104	50	1	50	1	0.5	0.0214	15.6	15.6	0.56	0.0229	0.65
Pigeon_C	81.35	81.23	0.51	0.51	1.239	1.247	0.892	0.898	25%	0.0272	110	1.06	25	0	0	0.0074	11.5	NA	NA	NA	2
Stewart_A	85.82	85.81	0.61	0.61	4.047	4.050	4.551	4.553	0%	0.1007	30	1	30	1	1	0.1007	6.45	NA	NA	NA	0.97
Santiagbd_A	87.47	87.47	0.64	0.64	12.380	12.381	12.818	12.820	75%	0.0266	65	1.03	30	1	1	0.0197	12.9	28.1	0.75	0.0182	1.12
Santiagbd_B	87.47	87.47	0.64	0.64	12.380	12.381	12.818	12.820	75%	0.0266	65	1.03	30	1	1	0.0182	19.6	NA	NA	NA	0.91
Santiagnl_A	87.47	87.47	0.64	0.64	11.842	11.843	12.259	12.260	75%	0.0343	20	1.07	20	1	1	0.0242	17.3	NA	NA	NA	1.47
Santiagnl_B	87.47	87.47	0.64	0.64	11.792	11.793	12.207	12.208	75%	0.0343	15	1.07	15	1	1	0.0322	6	NA	NA	NA	1.38
Silverado_A	87.20	87.20	0.64	0.64	15.222	15.222	15.635	15.635	20%	0.0543	25	1.04	15	1	1	0.0382	8.9	NA	NA	NA	1.48
Silverado_B	87.20	87.20	0.64	0.64	15.222	15.222	15.635	15.635	20%	0.0543	25	1.04	15	1	1	0.0455	7.2	NA	NA	NA	1.23
Escondido_A	85.11	83.04	0.60	0.54	65.002	71.787	53.297	59.399	25%	0.0507	35	1.07	40	1	1	0.0397	16.9	NA	NA	NA	1.47
Escondido_B	85.11	83.04	0.60	0.54	65.002	71.787	53.297	59.399	25%	0.0151	50	1.07	45	1	1	0.0111	29.2	NA	NA	NA	1.98

Composite NRCS Curve Number	Undeveloped NRCS Curve Number (i.e., no impervious area)	Composite C (Rational Method)	Undeveloped C (Rational Method), No Impervious Area	Rational 2-yr, 24-hr Flow (Rational Method), Undeveloped-metric	Rational 2-yr, 24-hr Flow (Rational Method), Developed-metric	NRCS 2-yr, 24-hr Flow (CN Method), Undeveloped-metric	NRCS 2-yr, 24-hr Flow (CN Method), Developed-metric	Percent Burned within Last 5 yrs	Valley Slope	Valley Width	Sinuosity at Reach (stream length / valley dist)	Width of Active Floodplain	Connected to Hillslope?	Valley Wall Bedrock?	Channel Slope	Bankfull Top Width	Top Width Prior to Braiding/ Incising	Bankfull Depth Prior to Braiding/ Incising	Slope Prior to Incising/ Braiding	Maximum Depth within Banks	
NRCS_CN_comp	NRCS_CN_undvp	Rainl_C_comp	Rainl_C_undvp	Q2un_Rt_24m	Q2_Rtnl_24m	Q2un_NR_24m	Q2_NRCS_24m	Prcnt_Burn	Slope_Valley	Width_Valley	Sinuosity	Width_Flpph	Hillslp_cnct	Hillslp_Bdrck	Slope_Chnnl	Width_Top	Width_Top_pre	Depth_BF_pre	Slope_Chm_pre	Depth_BF	
<b>Unique ID</b>				(m <sup>3</sup> /s)	(m <sup>3</sup> /s)	(m <sup>3</sup> /s)	(m <sup>3</sup> /s)	2007, unless noted (0-25%, 25-50%, 50-75%, 75-100%)	(m/m)	(m)	(m/m)	(m)	(1 = yes, 0 = no)	(1 = yes, 0.5 = riprap or sandbag, 0 = no)	(m/m)	(m)	(m)	(m)	(m/m)	(m)	
Sanantoni_A	84.81	84.78	0.59	0.59	28.260	28.293	32.943	32.967	0%	0.0222	1000	1.04	65	0	0	0.0249	21.25	65.4	2.92	0.0124	1.5
Sanantoni_B	84.81	84.78	0.59	0.59	28.260	28.293	32.943	32.967	0%	0.0222	1000	1.04	65	0	0	0.0124	65.4	65.4	2.1	0.0124	2.32
Alt_RC2_A	84.69	84.69	0.60	0.60	0.067	0.067	0.052	0.052	0%	0.042	65	1.08	10	0	0	0.0359	8	NA	NA	NA	1.71
Yucaipa_A	79.87	79.57	0.51	0.50	9.668	9.807	9.586	9.700	0%	0.045387	260	1.02	15	1	0.5	0.0371	15.5	?	?	?	2.1
Yucaipa_B	81.03	80.66	0.53	0.52	6.899	7.024	6.962	7.064	0%	0.045387	230	1.02	30	1	0.5	0.0371	29.6	?	?	?	2.625
Oakglenn_A	85.19	85.12	0.59	0.58	1.406	1.411	1.597	1.600	0%	0.0825	100	1.00	15	1	0	0.0734	11.6	12	3.64		3.25

**General abbreviations and symbol definition (excluding units of measure):**  
 C constant (i.e., for Rational Method)  
 CN Curve Number  
 ID identification  
 NRCS Natural Resources Conservation Service

**Table D.5 – Hydraulic geometry forms and parameters: A, R, and W, as f(d)**

Unique ID	Depth Functions (applicable to this depth)	Area Function Type (area = function (depth))	Area Parameter #1	Area Parameter #2	Hydraulic Radius Function Type (R = function (depth))	Hydraulic Radius Parameter #1	Hydraulic Radius Parameter #2	Top Width Function Type (Area = function (depth))	Top Width Function Form	Top Width Parameter #1	Top Width Parameter #2	Alternative Depth Functions (applicable above this depth)	Alternative Depth Functions (applicable below this depth)	Alternative Area Function Type (area = function (depth))	Alternative Area Parameter #1	Alternative Area Parameter #2	Alternative Hydraulic Radius Function Type (R = function (depth))	Alternative Hydraulic Radius Parameter #1	Alternative Hydraulic Radius Parameter #2	Alternative Top Width Function Type (area = function (depth))	Alternative Top Width Function Form	Alternative Top Width Parameter #1	Alternative Top Width Parameter #2
	Depth_App	Area_Funcn	a1	a2	R_Funcn	r1	r2	TW_Funcn	TW_Funcn_Form	t1	t2	Alt_Depth_Min	Alt_Depth_Max	Alt_A_Funcn	Alt_a1	Alt_a2	Alt_R_Funcn	Alt_r1	Alt_r2	Alt_TW_Funcn	Alt_TW_Form	Alt_t1	Alt_t2
Santiago_A	2.58	Power	10.77	1.884	Power	0.458	0.807	Power	$T = t1 * Depth^t2$	22.99	1.07	2.58											
Santiago_B	2.51	Power	8.848	1.875	Power	0.527	0.992	Power	$T = t1 * Depth^t2$	16.39	0.874	2.51											
Hasley_1_A	1.5	Power	2.324	1.687	Power	0.507	1.002	Power	$T = t1 * Depth^t2$	3.606	0.595	1.5											
Hasley_1_B	1.75	Power	5.074	1.667	Power	0.537	0.97	Power	$T = t1 * Depth^t2$	8.578	0.664	1.75											
Hasley_1_TR_IB	1.29	Power	10.63	1.98	Power	0.661	1.144	Log-linear	$T = t1 + \{ \ln(Depth) \}^t2$	12.52	4.102	1.29											
Hasley_2_A	0.97	Power	42.66	1.888	Power	0.528	0.964	Power	$T = t1 * Depth^t2$	80.04	0.92	0.97											
Hasley_2_B	2.29	Power	13.63	1.784	Power	0.645	1.137	Power	$T = t1 * Depth^t2$	20.35	0.632	2.29											
Hasley_2_TR_IB	0.53	Power	35.71	1.627	Power	1.073	1.259	Log-linear	$T = t1 + \{ \ln(Depth) \}^t2$	26.99	4.765	0.53											
Hicks_A_08	1.065	Power	5.421	1.341	Power	0.599	0.867	Linear	$T = t1 + Depth^t2$	2.11	7.879	N/A											
Hicks_B_08	1.56	Power	4.057	1.534	Power	0.57	0.95	Linear	$T = t1 + Depth^t2$	1.326	5.338	N/A											
Hicks_C_08	0.6	Power	4.851	1.687	Power	0.601	1.025	Linear	$T = t1 + Depth^t2$	0.784	8.523	0.6	1.105	Power	9.189	2.751	Power	0.445	0.942	Linear	$T = t1 + Depth^t2$	-5.463	24.7
Hicks_D_08	0.7	Power	3.257	1.587	Power	0.704	1.114	Log-linear	$T = t1 + \{ \ln(Depth) \}^t2$	3.353	0.77	0.7	1.39	Power	3.401	2.26	Power	0.418	0.228	Log-linear	$T = t1 + \{ \ln(Depth) \}^t2$	8.567	16.78
Hicks_D_07	0.7	Power	2.968	1.648	Power	0.544	0.977	Log-linear	$T = t1 + \{ \ln(Depth) \}^t2$	3.662	1.071	0.7	1.342	Power	3.536	2.425	Power	0.394	0.502	Log-linear	$T = t1 + \{ \ln(Depth) \}^t2$	9.277	16.43
Hicks_E_08	0.75	Power	2.71	1.394	Power	0.612	0.947	Log-linear	$T = t1 + \{ \ln(Depth) \}^t2$	3.3	0.752	0.75	2.27	Power	3.71	2.691	Power	0.431	0.872	Log-linear	$T = t1 + \{ \ln(Depth) \}^t2$	10.57	23.71
Hicks_E_07	0.75	Power	2.729	1.302	Power	0.625	0.904	Log-linear	$T = t1 + \{ \ln(Depth) \}^t2$	3.431	0.732	0.75	2.25	Power	3.873	2.654	Power	0.433	0.872	Log-linear	$T = t1 + \{ \ln(Depth) \}^t2$	11.09	23.41
Hicks_F_08	0.65	Power	2.878	1.511	Power	0.661	1.039	Power	$T = t1 * Depth^t2$	3.799	0.421	0.65	1.135	Power	3.252	2.033	Power	0.378	-0.02	Exponential	$T = t1 * e^{\{ \ln(Depth) \}^t2}$	0.597	2.572
Hicks_F_07	0.65	Power	3.155	1.455	Power	0.691	1.039	Power	$T = t1 * Depth^t2$	3.599	0.798	0.65	1.08	Power	3.6	1.988	Power	0.368	-0.21	Log-linear	$T = t1 + \{ \ln(Depth) \}^t2$	9.683	16.47
Agua_Hedi_A	1.75	Power	5.718	1.528	Power	0.696	1.114	Log-linear	$T = t1 + \{ \ln(Depth) \}^t2$	7.236	1.733	1.75											
Agua_Hedi_B	2.5	Power	4.285	1.656	Power	0.566	0.983	Power	$T = t1 * Depth^t2$	6.929	0.639	2.5											



Unique ID	Depth Functions (applicable to this depth)	Area Function Type (area = function (depth))	Area Parameter #1	Area Parameter #2	Hydraulic Radius Function Type (R = function (depth))	Hydraulic Radius Parameter #1	Hydraulic Radius Parameter #2	Top Width Function Type (Area = function (depth))	Top Width Function Form	Top Width Parameter #1	Top Width Parameter #2	Alternative Depth Functions (applicable above this depth)	Alternative Depth Functions (applicable below this depth)	Alternative Area Function Type (area = function (depth))	Alternative Area Parameter #1	Alternative Area Parameter #2	Alternative Hydraulic Radius Function Type (R = function (depth))	Alternative Hydraulic Radius Parameter #1	Alternative Hydraulic Radius Parameter #2	Alternative Top Width Function Type (area = function (depth))	Alternative Top Width Function Form	Alternative Top Width Parameter #1	Alternative Top Width Parameter #2
	Depth_App	Area_Functn	a1	a2	R_Functn	r1	r2	TW_Functn	TW_Func_Frm	t1	t2	Alt_Depth_Min	Alt_Depth_Max	Alt_A_Functn	Alt_a1	Alt_a2	Alt_R_Functn	Alt_r1	Alt_r2	Alt_TW_Functn	Alt_TW_Frm	Alt_t1	Alt_t2
	(m)	(power, linear, loglinear)			(power, linear, loglinear)			(power, linear, loglinear)				(m)	(m)	(power, linear, loglinear)			(power, linear, loglinear)			(power, linear, loglinear)			
AltPerris_A	0.3	Power	100.9	2.19	Power	0.59	1.128	Power	T = t1*Depth*t2	170.5	1.061	0.3											
AltPerris_B	0.34	Power	28.44	1.681	Power	0.899	1.195	Log-linear	T=t1+(ln(Depth))*t2	23.41	5.331	0.34											
AltPerris_C	0.6	Power	11.67	1.546	Power	0.702	1.046	Power	T = t1*Depth*t2	16.38	0.495	0.6											
Dulzura_A	0.5	Power	8.846	1.626	Power	0.693	1.072	Power	T = t1*Depth*t2	12.49	0.546	0.5	1.67	Power	10.34	1.908	Power	0.539	0.965	Log-linear	T=t1+(ln(Depth))*t2	20.37	15.43
Dulzura_B	0.75	Power	5.68	1.614	Power	0.765	1.136	Power	T = t1*Depth*t2	7.057	0.458	0.75	1.82	Power	6.083	2.245	Power	0.579	0.68	Log-linear	T=t1+(ln(Depth))*t2	12.03	18.95
Acton_A	0.41	Power	23.58	2.053	Power	0.415	0.886	Power	T = t1*Depth*t2	56.23	1.165	0.41											
Acton_B	0.76	Power	5.668	1.359	Power	0.804	1.112	Linear	T = t1+Depth*t2	3.32	4.724	0.76											
Acton_C	2.7	Power	5.895	1.758	Power	0.592	1.063	Log-linear	T=t1+(ln(Depth))*t2	8.701	2.81	2.7											
Acton_D	2.95	Power	4.608	1.285	Power	0.643	0.902	Log-linear	T=t1+(ln(Depth))*t2	5.668	1.089	2.95											
Acton_E	2.3	Power	0.959	1.047	Power	0.308	0.591	Linear	T = t1+Depth*t2	0.909	0.087	2.3											
Acton_F	0.41	Power	24.16	2.78	Power	0.448	1.013	Power	T = t1*Depth*t2	54.48	1.79	0.41											
Acton_G	0.75	Power	12.254	1.3181	Power	0.5678	0.8052	Exponential	$T=t1*e^{(Depth * t2)}$	5.2022	2.1854	0.75											
Borrego_A	3	Power	9.246	1.09	Power	0.801	0.925	Linear	T = t1+Depth*t2	7.99	2.003	3											
Borrego_B	1.77	Power	55.01	1.968	Power	0.655	1.074	Power	T=t1*Depth*t2	83.22	0.89	1.77											
Borrego_C	4.17	Power	19.56	1.222	Power	0.801	1.007	Log-linear	T=t1+(ln(Depth))*t2	23.5	3.562	4.17											
Borrego_D	6.73	Power	9.0881	1.7383	Power	0.6113	1.0829	Log-linear	T=t1+(ln(Depth))*t2	18.146	6.2589	6.73											
Borrego_E	3.58	Power	3.052	1.981	Power	0.474	1.009	Linear	T = t1+Depth*t2	0.435	5.249	3.58											
Topanga_A	1.7	Power	7.524	1.848	Power	0.529	1.007	Linear	T = t1+Depth*t2	0.751	12.89	1.7	3.7	Power	8.1139	1.7036	Power	0.3688	1.3963	Log-linear	T=t1+(ln(Depth))*t2	22.413	4.1282
Topanga_B	2.27	Power	11.379	1.8627	Power	0.5562	0.9539	Linear	T = t1+Depth*t2	1.9373	17.511	2.27											
Topanga_C	4	Power	4.0298	1.3468	Power	0.5715	0.8137	Exponential	$T=t1*e^{(Depth * t2)}$	2.2435	0.5945	4											
Challengr_A	1.16	Power	3.348	1.464	Power	0.515	0.875	Exponential	$T=t1*e^{(Depth * t2)}$	1.529	1.428	1.16	1.79	Power	2.7174	3.0883	Power	0.3556	0.7803	Log-linear	T=t1+(ln(Depth))*t2	4.2141	38.573



Unique ID	Depth Functions (applicable to this depth)	Area Function Type (area = function (depth))	Area Parameter #1	Area Parameter #2	Hydraulic Radius Function Type (R = function (depth))	Hydraulic Radius Parameter #1	Hydraulic Radius Parameter #2	Top Width Function Type (Area = function (depth))	Top Width Function Form	Top Width Parameter #1	Top Width Parameter #2	Alternative Depth Functions (applicable above this depth)	Alternative Depth Functions (applicable below this depth)	Alternative Area Function Type (area = function (depth))	Alternative Area Parameter #1	Alternative Area Parameter #2	Alternative Hydraulic Radius Function Type (R = function (depth))	Alternative Hydraulic Radius Parameter #1	Alternative Hydraulic Radius Parameter #2	Alternative Top Width Function Type (area = function (depth))	Alternative Top Width Function Form	Alternative Top Width Parameter #1	Alternative Top Width Parameter #2
	(m)	(power, linear, loglinear)			(power, linear, loglinear)			(power, linear, loglinear)				(m)	(m)	(power, linear, loglinear)			(power, linear, loglinear)			(power, linear, loglinear)			
Yucaipa_B	2.625	Power	18.156	0.7166	Power	0.7166	1.1132	Log-linear	$T=t1+(\ln(\text{Depth}))^*t2$	24.9	6.4789	2.625											
Oakglenn_A	3.25	Power	3.9051	1.6125	Power	0.5786	1.014	Power	$T=t1*\text{Depth}^*t2$	6.0921	0.5588	3.25											

**General abbreviations and symbol definitions (excluding units of measure):**  
# number  
ID identification  
R hydraulic radius

Table D.6 – Cross-section metrics, bed material, and critical metrics for sediment transport

Bankfull Area	Bankfull Hydraulic Radius	Bankfull Flow Rate	Bankfull Stream Power	Bankfull Specific Stream Power	Bank Height	Bank Hardness Penetrometer	Bank Hardness Rock Hammer	Bank Cohesion	Bank Stratification	Bank Angle	Bank Vegetation	Bed Vegetation	Bar Activity	Median Bed Material	16th Percentile Bed Material	64th Percentile Bed Material	Range of Bed Material (d84/d16)	Percent Sand	Distance to DS Hardpoint	Dhp (ONLY IF Lravg>1.05 for d50>16 mm, or Lravg<1.01 for d50 < 16 mm) else = 0	Dhp/WQ10	Distance to DS Incising Stream (base-level drop) if >1,000 or NA, =1,000	Hydraulic Radius for Sediment Transport	Depth for Sediment Transport	Area for Sediment Transport	Critical Flow for Sediment Transport	
Area_BF	Hyd_Radius_BF	Flow_BF	Pwr_BF	Sp_Pwr_BF	Bank_ht_max	Bank_Pentrom	Bank_Hmmr	Bank_cohesn	Bank_strat	Bank_angl	Bank_veg	Bed_veg	Bar_actvty	d50	d16	d84	d84_to_d16	Pcrlt_Sand	Dist_Hrdpnt	Dhp_Important	Dhp/WQ10	Dist_BsdDp	R_Crit	Depth_Crit	Area_Crit	Flow_Crit	
(m <sup>2</sup> )	(m)	(m <sup>3</sup> /s)	(Watt/m)	(Watt/m <sup>2</sup> )	(m)	(tons/ft <sup>2</sup> )	(10-100)			(°)				(mm)	(mm)	(mm)	(mm/mm)	(%)	(m)	(m)	(m/m)	(m)	(m)	(m)	(m <sup>2</sup> )	(m <sup>3</sup> /s)	
Santiago_A	64.23	0.98	149.7	25,549	339	2.57	N/A	13	yes	yes	55.94	low	low	mod central bars not very vegetated	22	2	70.8	35	18%	9,600	-	-	1000	0.098	0.148	0.295	0.148
Santiago_B	50.06	1.31	131.3	19,317	587	2	N/A	N/A	no	no	33.45	low	low	alternating point bars	34	6.4	127.4	20	9%	10,127	-	-	1000	0.176	0.331	1.111	0.762
Hasley_1_A	4.15	0.72	12.1	3,157	739	1.44	0.75	N/A	no	yes	72.56	low	none	alternating point bars	13	2.1	92.6	44	15%	100	100	25	1000	0.038	0.075	0.029	0.012
Hasley_1_B	7.76	0.69	18.7	6,276	756	1.18	N/A	N/A	no	no	56.14	low	low	alternating point bars	3.2	0.5	25.7	51	44%	164	164	20	1000	0.007	0.012	0.003	0.000
Hasley_1_TRIB	4.95	0.43	6.1	1,563	137	1.64	N/A	N/A	no	no	28.9	mod	mod	none	3.2	0.5	25.7	51	44%	100	100	13	1000	0.009	0.024	0.007	0.001
Hasley_2_A	40.28	0.51	65.0	12,243	179	0.96	3	N/A	yes	yes	76.01	low	low	high/central bars	1.6	0.5	11.6	23	56%	1,700	-	-	1000	0.006	0.010	0.008	0.001
Hasley_2_B	59.30	1.65	171.1	25,004	1,053	2.61	4.5	N/A	yes	yes	67	low	none	high but not major bars	2.6	0.6	28.9	48	46%	1,950	-	-	1000	0.014	0.033	0.032	0.004
Hasley_2_TRIB	12.71	0.48	24.3	8,299	340	0.63	N/A	N/A	no	no	54.33	low	none	high/central bars	1.5	0.5	40	80	58%	1,850	-	-	1000	0.003	0.010	0.021	0.001
Hicks_A_08	0.58	0.14	0.9	118	15	1.02	N/A	N/A	no	no	19.9	low	none	none	0.6	0.3	1.3	4	93%	25	25	3	1000	0.004	0.003	0.002	0.000
Hicks_B_08	1.95	0.36	2.6	354	96	0.425	N/A	N/A	no	yes	57.17	low	none	none	0.6	0.3	1.3	4	93%	150	150	20	1000	0.003	0.004	0.001	0.000
Hicks_C_08	2.05	0.36	2.3	486	76	0.625	N/A	N/A	no	yes	47.73	low	low	mod alt pt bars and overbank braids	3.8	0.5	31.2	62	44%	175	175	10	1000	0.014	0.025	0.010	0.001
Hicks_D_08	3.80	0.40	5.1	1,286	214	0.65	N/A	N/A	no	yes	34.99	low	none	mod alt pt bars	1.9	0.6	72.4	121	51%	283	283	22	1000	0.006	0.013	0.003	0.000
Hicks_D_07	3.20	0.36	3.1	830	140	0.67	N/A	N/A	no	yes	29.9	low	none	mod alt pt bars	0.8	0.3	11.3	38	71%	283	283	19	1000	0.002	0.004	0.000	0.000
Hicks_E_08	2.32	0.47	2.8	541	174	0.825	3	N/A	no	yes	76.45	low	none	mod alt pt bars	1.3	0.4	53.7	134	58%	534	534	34	1000	0.005	0.006	0.002	0.000
Hicks_E_07	2.84	0.48	2.7	507	151	0.89	3	N/A	no	yes	70.89	low	none	mod alt pt bars	1.1	0.4	36.3	91	64%	534	534	30	1000	0.004	0.004	0.002	0.000
Hicks_F_08	4.24	0.35	4.1	663	91	0.58	3	N/A	no	yes	69.68	low	none	mod alt pt bars	1.3	0.4	53.7	134	58%	722	722	20	1000	0.006	0.011	0.003	0.000
Hicks_F_07	4.27	0.33	2.9	414	37	0.53	3	N/A	no	yes	65.16	low	none	mod alt pt bars	1.1	0.4	36.3	91	0.6393	722	722	36	1000	0.006	0.010	0.004	0.000
Agua_Hedi_A	16.98	1.05	32.4	1,335	86	1.7	N/A	N/A	no	no	52.28	high	low	mod alt pt bars	5	2.2	15.5	7	13%	50	50	6	1000	0.092	0.163	0.358	0.135
Agua_Hedi_B	19.54	1.39	25.8	709	60	2.1	N/A	N/A	yes	no	50.26	high	low	mod alt pt bars	5	2.2	15.5	7	13%	225	225	15	1000	0.138	0.239	0.400	0.113
Agua_Hedi_C	24.43	1.65	28.4	585	39	1.91	N/A	N/A	yes	no	76.34	high	low	mod alt pt bars	5	2.2	15.5	7	13%	416	416	30	1000	0.185	0.401	0.411	0.111

Bankfull Area	Bankfull Hydraulic Radius	Bankfull Flow Rate	Bankfull Stream Power	Bankfull Specific Stream Power	Bank Height	Bank Hardness Penetrometer	Bank Hardness Rock Hammer	Bank Cohesion	Bank Stratification	Bank Angle	Bank Vegetation	Bed Vegetation	Bar Activity	Median Bed Material	16th Percentile Bed Material	84th Percentile Bed Material	Range of Bed Material (d84/d16)	Percent Sand	Distance to DS Hardpoint	Dhp (ONLY IF Lavg>1.05 for d50-16 mm, or Lavg>1.01 for d50 < 16 mm) else = 0	Dhp/WG10	Distance to DS Incising Stream (base-level drop) if >1,000 or NA, =1,000	Radius for Hydraulic Sediment Transport	Depth for Sediment Transport	Area for Sediment Transport	Critical Flow for Sediment Transport	
Area_BF	Hyd_Radius_BF	Flow_BF	Pwr_BF	Sp_Pwr_BF	Bank_ht_max	Bank_Penitrom	Bank_Hinmr	Bank_cohesn	Bank_strat	Bank_angl	Bank_veg	Bed_veg	Bar_actvty	d50	d16	d84	d84_to_d16	Prcnt_Sand	Dist_Hrdpnt	Dhp_important	Dhp/WG10	Dist_BSDrp	R_Crit	Depth_Crit	Area_Crit	Flow_Crit	
Unique ID	(m <sup>2</sup> )	(m)	(m <sup>3</sup> /s)	(Watt/m)	(Watt/m <sup>2</sup> )	(m)	(tons/ft <sup>2</sup> )	(10-100)		(°)				(mm)	(mm)	(mm)	(mm/mm)	(%)	(m)	(m)	(m/m)	(m)	(m)	(m)	(m <sup>2</sup> )	(m <sup>3</sup> /s)	
Dry_A	21.17	0.92	121.0	26,944	965	1.22	N/A	N/A	no	yes	61.65	low	low	mod alt pt bars	0.7	0.4	1.3	3	94%	33	33	3	1000	0.002	0.004	0.004	0.000
Dry_B	22.53	1.10	57.3	11,518	545	1.33	N/A	N/A	no	no	77.18	low	low	mod alt pt bars	0.75	0.4	4.35	11	86%	180	180	15	1000	0.003	0.004	0.003	0.000
Dry_C	25.03	1.65	77.2	18,102	1,280	4.87	N/A	N/A	no	no	70.34	low	low	mod alt pt bars	0.8	0.4	7.4	19	78%	293	293	24	1000	0.003	0.007	0.009	0.000
Hovnanian_A	14.76	1.02	29.8	9,166	557	1.47	N/A	N/A	no	yes	39.01	high	mod	alt bars	36.7	2	157.1	78.6	24%	1,100	-	-	1000	0.091	0.135	0.274	0.110
Hovnanian_B	7.70	0.90	14.2	4,385	539	1.2	N/A	N/A	yes	yes	33.09	high	mod	alt bars	16	2	173.3	86.7	38%	1,100	-	-	1000	0.040	0.076	0.032	0.007
Santimeta_A	4.40	0.63	19.5	14,010	3,113	4.13	4.5	N/A	yes	yes	77.71	low	none	high	0.9	0.3	6	20.0	72%	4,400	4,400	12,502	153.5	0.001	0.001	0.000	0.000
Santimeta_B	26.60	1.34	132.4	65,836	4,736	2.06	4.5	N/A	yes	yes	71.06	low	none	high	0.9	0.35	4.65	13.3	74%	4,547	4,547	648	300	0.001	0.002	0.001	0.000
Santimeta_C	13.05	0.92	55.8	28,086	2,194	1.22	4.5	N/A	yes	yes	74.86	low	none	high	0.9	0.4	3.3	8.3	77%	4,751	4,751	500	504	0.001	0.003	0.004	0.000
Lit_Cedar_A	11.47	0.96	21.4	4,194	339	0.62	N/A	N/A	no	no	64.68	mod	low	mod?	28.5	16	83.7	5.2	2%	165	165	17	46	0.111	0.178	0.423	0.186
Lit_Cedar_B	15.30	0.33	18.4	4,687	102	1.26	N/A	N/A	no	no	31.04	mod	mod	mod?	20.3	7.8	62.8	8.1	7%	329	329	20	210	0.061	0.132	0.312	0.121
Proctor_A	34.04	0.73	62.2	7,755	421	0.81	N/A	N/A	no	no	19.6	mod	mod	vegetated	10.5	1.6	70.6	44.1	19%	4,000	-	-	1000	0.064	0.126	0.195	0.070
Proctor_B	4.82	0.30	5.1	702	48	0.57	N/A	N/A	no	no	19.3	mod	mod	vegetated	1.6	0.3	17.7	59.0	55%	4,000	-	-	1000	0.009	0.018	0.001	0.000
Proctor_TRIB	1.91	0.16	1.6	336	16	0.47	N/A	N/A	no	no	28.25	mod	mod	vegetated	6.05	0.95	44.15	46.5	37%	4,000	-	-	1000	0.022	0.037	0.015	0.003
Perris_1_A	1.91	0.32	1.3	74	15	0.75	N/A	N/A	yes	no	31.8	low	low	none	0.8	0.3	2.5	8.3	79%	47	47	9	1000	0.010	0.015	0.003	0.000
Perris_1_B	4.12	0.49	5.0	680	58	1.12	4.5	N/A	no	no	38.78	low	low	none	0.8	0.3	2.6	8.7	79%	53	53	15	1000	0.004	0.003	0.001	0.000
Perris_1_C	4.19	0.73	5.2	370	59	0.43	4.5	N/A	no	no	44.79	low	low	none	0.8	0.3	2.7	9.0	78%	28	28	10	1000	0.009	0.008	0.002	0.000
Perris_2_A	0.81	0.17	0.9	215	41	0.23	N/A	N/A	no	no	17.65	low	low	none	0.9	0.3	2.2	7.3	82%	215	-	-	1000	0.003	0.004	0.000	0.000
Perris_2_B	0.61	0.15	0.7	246	62	0.25	N/A	N/A	no	no	38.06	low	low	none	0.5	0.25	1.6	6.4	90%	447	-	-	1000	0.001	0.001	0.000	0.000
Perris_3_A	17.49	0.28	16.2	2,258	39	1.71	N/A	N/A	no	no	9.02	low	low	moderately vegetated bars	0.8	0.3	2.3	7.7	82%	71	-	-	1000	0.004	0.006	0.000	0.000
Perris_3_B	27.10	0.34	31.2	5,137	79	1.43	N/A	N/A	no	no	7.87	low	low	moderately vegetated bars	0.9	0.3	2.9	9.7	75%	400	-	-	1000	0.004	0.007	0.000	0.000
AltPerris_A	7.22	0.15	4.5	451	9	0.5	0.8	N/A	no	no	19.98	mod	mod	vegetated	0.9	0.4	1.9	4.8	86%	200	200	5	1000	0.007	0.019	0.018	0.001
AltPerris_B	3.97	0.22	2.7	190	12	0.6	0.8	N/A	no	no	12.58	mod	mod	vegetated	0.9	0.4	1.8	4.5	90%	300	300	18	1000	0.010	0.023	0.049	0.004
AltPerris_C	5.30	0.41	6.8	329	25	0.32	0.8	N/A	no	no	20.38	mod	mod	vegetated	0.8	0.3	1.7	5.7	90%	400	400	41	1000	0.013	0.022	0.031	0.004
Dulzura_A	2.41	0.29	1.5	88	13	1.39	N/A	N/A	no	no	31.9	mod	none	alternate point bars	34.6	3.2	81.3	25.4	14%	3,400	-	-	1000	0.447	0.665	4.552	3.705
Dulzura_B	4.11	0.51	3.7	216	37	1.43	N/A	N/A	no	no	42.8	mod	none	alternate point bars	47.7	2	129.4	64.7	20%	3,400	-	-	1000	0.617	0.827	4.180	4.215
Acton_A	3.78	0.19	3.5	1,291	71	0.35	0.75	N/A	no	no	26.6	low	none		4.9	2.3	12.1	5.3	10%	70	70	4	1000	0.010	0.015	0.004	0.001
Acton_B	3.90	0.59	22.3	8,240	1,161	0.51	0.75	N/A	no	no	42	low	none		3.8	2	8.8	4.4	20%	425	425	95	1000	0.008	0.016	0.020	0.006
Acton_C	7.89	0.71	22.4	11,179	1,315	2.5	0.75	N/A	no	no	87.8	low	none		5	2.1	16.9	8.0	15%	779	779	126	1000	0.008	0.017	0.004	0.001

Bankfull Area	Bankfull Hydraulic Radius	Bankfull Flow Rate	Bankfull Stream Power	Bankfull Specific Stream Power	Bank Height	Bank Hardness Penetrometer	Bank Hardness Rock Hammer	Bank Cohesion	Bank Stratification	Bank Angle	Bank Vegetation	Bed Vegetation	Bar Activity	Median Bed Material	16th Percentile Bed Material	84th Percentile Bed Material	Range of Bed Material (d84/d16)	Percent Sand	Distance to DS Hardpoint	Dhp (ONLY IF Lravg>1.05 for d50>16 mm, or Lravg>1.01 for d50 < 16 mm) else = 0	Dhp/WG10	Distance to DS Incising Stream (base-level drop) if >1,000 or NA, =1,000	Hydraulic Radius for Sediment Transport	Depth for Sediment Transport	Area for Sediment Transport	Critical Flow for Sediment Transport	
Area_BF	Hyd_Radius_BF	Flow_BF	Pwr_BF	Sp_Pwr_BF	Bank_ht_max	Bank_Penitrom	Bank_Hinmr	Bank_cohesn	Bank_strat	Bank_angl	Bank_veg	Bed_veg	Bar_activy	d50	d16	d84	d84_to_d16	Prcnt_Sand	Dist_Hrdpnt	Dhp_important	Dhp/WG10	Dist_BSDrp	R_Crit	Depth_Crit	Area_Crit	Flow_Crit	
Unique ID	(m <sup>2</sup> )	(m)	(m <sup>3</sup> /s)	(Watt/m)	(Watt/m <sup>2</sup> )	(m)	(tons/ft <sup>2</sup> )	(10-100)		(°)				(mm)	(mm)	(mm)	(mm/mm)	(%)	(m)	(m)	(m/m)	(m)	(m)	(m)	(m <sup>2</sup> )	(m <sup>3</sup> /s)	
Acton_D	18.50	1.71	75.9	24,436	3,941	3.25	0.75	N/A	no	no	88.2	low	none	9.4	2.7	33.1	12.3	10%	866	866	194	1000	0.022	0.024	0.038	0.009	
Acton_E	2.29	0.50	9.0	13,363	12,039	2.3	0.75	N/A	no	no	87.5	low	none	9.4	2.7	33.1	12.3	10%	916	916	956	1000	0.005	0.001	0.001	0.000	
Acton_F	2.03	0.18	1.3	197	25	0.41	N/A	N/A	no	no	14	med	med	9.4	2.7	33.1	12.3	10%	943	-	-	1000	0.047	0.107	0.049	0.013	
Acton_G	1.97	0.19	1.0	108	13	0.25	N/A	N/A	no	no	14	med	med	9.4	2.7	33.1	12.3	10%	949	-	-	1000	0.069	0.074	0.393	0.108	
Borrogo_A	30.62	2.21	368.6	72,682	5,192	3	N/A	N/A	no	no	45	none	none	1.6	0.8	11.2	14.0	64%	20	20	2	1000	0.006	0.005	0.030	0.007	
Borrogo_B	154.50	1.15	419.2	73,196	720	2.23	N/A	N/A	no	no	53	low	low	moderately	1.6	0.8	11.2	14.0	64%	340	340	8	1000	0.007	0.015	0.013	0.001
Borrogo_C	111.99	3.37	1,007.6	142,344	5,102	4.04	N/A	N/A	no	no	63.4	low	none	high	1	0.4	24.2	60.5	71%	685	685	33	1000	0.005	0.007	0.045	0.006
Borrogo_D	160.77	4.394	898.7	269,769	9,151	6.68	N/A	N/A	no	no	72.4	med	low	low	45	2.3	105.2	45.7	16%	1,121	1,121	61	1000	0.114	0.212	0.614	0.301
Borrogo_E	38.18	1.72	108.3	29,327	1,594	3.13	N/A	N/A	no	no	52.4	med	low	low	45	2.3	105.2	45.7	16%	20	20	2	1000	0.126	0.270	0.228	0.114
Topanga_A	20.06	0.90	45.9	12,528	524	1.78	N/A	N/A	no	no	17.7	high	none	mid bar (low)	87.8	24.7	240.1	9.7	0%	20	20	1	1000	0.245	0.465	1.831	1.758
Topanga_B	50.5	1.156	108.3	18,590	439	1.66	N/A	N/A	no	no	10.9	high	low	moderate activity/vegetated	100	14.6	331.7	22.7	4%	100	100	3	1000	0.443	0.788	7.301	8.256
Topanga_C	37.2	1.874	203.4	199,523	11,401	7	N/A	30	no	no	74.1	high	none	none	499.5	270.6	1591.2	5.9	0%	2	2	0	1000	0.387	0.620	2.117	4.043
Challengr_A	3.25	0.51	3.0	277	84	0.98	N/A	N/A	no	no	83.13	high	low	poorly developed point bars	51.2	16.6	112.7	6.8	4%	885	885	34	1000	0.422	0.797	2.403	1.966
Challengr_B	1.55	0.41	0.9	55	28	0.86	N/A	N/A	no	no	76.9	high	low	none	3.4	2	7.5	3.8	4%	1,169	1,169	48	1000	0.043	0.069	0.034	0.005
Challengr_C	2.56	0.43	3.2	759	146	0.97	N/A	N/A	no	no	36.41	high	low	alternating point bars	69.7	3.4	151.8	44.6	13%	146	146	6	1000	0.222	0.376	0.885	0.698
Mcgonigle_A	3.54	0.26	1.5	154	10	0.465	N/A	N/A	no	no	20.1	high	low	alternating point bars	23.4	11.7	41.9	3.6	1%	1,600	-	-	1000	0.176	0.347	1.420	0.475
Sanjuan_A	8.82	0.42	12.4	2,151	52	1.06	4.5	N/A	no	no	42	low	low	Mid bars (high)	34.4	2	104.8	52.4	21%	1,700	-	-	1000	0.151	0.302	1.026	0.729
Sanjuan_B	19.92	0.95	24.6	1,810	87	1.48	N/A	?	no	no	24.8	low	none	none	61.2	3.2	252.4	78.9	13%	2,277	-	-	1000	0.633	1.062	10.178	9.555
Pigeon_A	3.92	0.35	4.7	703	85	0.98	0.75	N/A	no	no	72.9	low	med	high	1.2	0.4	2.7	6.8	75%	300	300	5	1000	0.006	0.006	0.001	0.000
Pigeon_B	4.60	0.33	6.4	1,342	86	0.73	0.75	N/A	no	no	73.1	low	med	high	0.9	0.4	2.4	6.0	80%	310	310	17	1000	0.003	0.004	0.001	0.000
Pigeon_C	11.01	0.99	11.7	846	74	1.42	1	N/A	no	no	60.9	med	low	alternating point bars	1.5	0.6	3.3	5.5	62%	100	100	12	1000	0.016	0.032	0.004	0.000
Stewart_A	3.27	0.43	5.8	5,691	882	1.11	N/A	N/A	no	no	27.6	med	none	none	151.8	6.8	724	106.5	2%	200	-	-	1000	0.117	0.257	0.206	0.153
Santiagbd_A	13.09	0.74	29.4	5,677	440	1.12	N/A	N/A	no	no	64.2	low	none	alternating point bars	14.1	3.6	98.3	27.3	10%	12,954	-	-	1000	0.056	0.111	0.100	0.040
Santiagbd_B	13.77	0.58	25.3	4,510	230	11.14	N/A	N/A	no	no	46.3	low	none	none	7.2	2	21.1	10.6	17%	12,954	-	-	1000	0.031	0.056	0.066	0.017
Santiagnl_A	30.4	1.631	136.4	32,375	1,869	1.29	N/A	30	no	no	32.7	low	none	none	7.2	2	21.1	10.6	17%	13,299	-	-	1000	0.023	0.027	0.079	0.021
Santiagnl_B	8.23	0.68	17.3	5,459	910	1.38	N/A	38	no	no	52.7	low	none	none	26.2	4.9	298.6	60.9	9%	13,299	-	-	1000	0.063	0.153	0.082	0.035
Silverado_A	8.42	0.79	17.0	6,376	716	1.1	N/A	44	no	no	38.2	high	low	none	141.5	35.9	353.7	9.9	7%	3,000	-	-	1000	0.287	0.590	1.466	1.503

Bankfull Area	Bankfull Hydraulic Radius	Bankfull Flow Rate	Bankfull Stream Power	Bankfull Specific Stream Power	Bank Height	Bank Hardness Penetrometer	Bank Hardness Rock Hammer	Bank Cohesion	Bank Stratification	Bank Angle	Bank Vegetation	Bed Vegetation	Bar Activity	Median Bed Material	16th Percentile Bed Material	84th Percentile Bed Material	Range of Bed Material (d84/d16)	Percent Sand	Distance to DS Hardpoint	Dhp (ONLY IF Lravg>1.05 for d50>16 mm, or Lravg>1.01 for d50 < 16 mm) else = 0	Dhp/WQ10	Distance to DS Incising Stream (base-level drop) if >1,000 or NA, =1,000	Hydraulic Radius for Sediment Transport	Depth for Sediment Transport	Area for Sediment Transport	Critical Flow for Sediment Transport	
Area_BF	Hyd_Radius_BF	Flow_BF	Pwr_BF	Sp_Pwr_BF	Bank_ht_max	Bank_Penitrom	Bank_Himnr	Bank_cohesn	Bank_strat	Bank_angl	Bank_veg	Bed_veg	Bar_activy	d50	d16	d84	d84_to_d16	Prcnt_Sand	Dist_Hrdprt	Dhp_important	Dhp/WQ10	Dist_BSDrp	R_Crit	Depth_Crit	Area_Crit	Flow_Crit	
Unique ID	(m <sup>2</sup> )	(m)	(m <sup>3</sup> /s)	(Watt/m)	(Watt/m <sup>2</sup> )	(m)	(tons/ft <sup>2</sup> )	(10-100)		(°)				(mm)	(mm)	(mm)	(mm/mm)	(%)	(m)	(m)	(m/m)	(m)	(m)	(m)	(m <sup>2</sup> )	(m <sup>3</sup> /s)	
Silverado_B	5.18	0.56	10.3	4,589	637	1.33	N/A	45	no	no	53.1	high	low	none	124.3	16.8	384	22.9	11%	3,085	-	-	1000	0.212	0.512	0.820	0.852
Escondido_A	15.21	0.80	28.1	10,955	648	2.155	N/A	50	no	no	16.9	high	none	none	128	35.9	370.5	10.3	0%	10	-	-	1000	0.250	0.472	1.803	1.533
Escondido_B	31.85	1.05	39.4	4,289	147	1.87	N/A	N/A	no	no	18.2	high	med	vegetated midbars (low)	31.2	9.6	123.1	12.8	3%	100	-	-	1000	0.218	0.420	1.556	0.675
Sanantoni_A	17.93	0.90	49.8	12,171	573	3.51	N/A	N/A	no	no	63.9	low	low	none	64	16	180	11.3	8%	750	750	21	1000	0.199	0.350	1.481	1.504
Sanantoni_B	115.40	1.70	345.5	42,028	643	2.1	N/A	N/A	no	no	85.2	low	low	high (mid bars and alternating point bars)	16	3.1	70.2	22.6	11%	750	750	12	1000	0.100	0.204	0.773	0.350
Alt_RC2_A	6.61	0.83	27.7	9,770	1,221	1.71	N/A	N/A	yes	no	31.6	mod	mod	none	0.125	0.125	0.6	4.8	96%	200	-	-	1000	0.001	0.003	0.000	0.000
Yucaipa_A	27.0	1.591	208.6	75,906	4,886	2.55	N/A	N/A	no	no	90	mod	none	alternating point bars	3.5	2.1	8.4	4.0	12%	200	200	15	1000	0.007	0.011	0.035	0.008
Yucaipa_B	66.1	2.026	415.8	151,330	5,113	3	N/A	N/A	no	no	90	mod	none	high (mid bars)	4.8	2	18.6	9.3	17%	300	300	15	1000	0.010	0.022	1.163	0.213
Oakglenn_A	24.2	1.752	179.6	129,307	11,147	3.65	N/A	45	no	no	46.5	low	none	none	23.4	3	84.1	28.0	9%	20	20	4	1000	0.025	0.045	0.026	0.011

**General abbreviations and symbol definitions (excluding units of measure):**

alt	alternating	DS	downstream	pt	point
d16	grain size that 16 percent of the particles are finer than	ID	identification	veg	vegetated
d50	grain size that 50 percent of the particles are finer than	LRavg	average sediment-transport capacity ratio	WQ10	top width at the 10-yr flow
d84	grain size that 84 percent of the particles are finer than	mod	moderately		
Dhp	downstream distance to hardpoint	NA	not applicable		

**Table D.7 – 10-yr hydraulic metrics, load ratio, enlargement, bank stability, and reference width**

	10-yr Flow Depth	10-yr Area	10-yr Hydraulic Radius	10-yr Top Width	Q10 Overbank?	10-yr Stream Power	10-yr Specific Stream Power	10-yr Dimensionless Specific Stream Power	10-yr Shear Stress	10-yr Dimensionless Shear Stress	Average Load Ratio ( $\omega_{vp}/\omega_{ndvp}$ )	Reference BF Area	Reference Source	Enlargement Ratio ( $A_{post}/A_{pre}$ )	Representative Geotechnical Stability (max Ng of both banks, dependent on 50% MW risk in moderate-/ well-consolidated banks)	Reference Bankfull Top Width (regional Q10- dependent)	Relative Lateral Departure from Wref (regional)
	Depth_10yr	Area_10yr	HydRad_10yr	TopWidth_10yr		$Q_{10}$	$\omega_{10}$	$\omega_{10}^*$	$\tau_{10}$	$\tau_{10}^*$	Lratio	$A_{pre}$	Ref_source	$A_{Aratio}$	Max_Ng	Wref	Nw
Unique ID	(m)	(m <sup>2</sup> )	(m)	(m)	(blank or OVRBNK)	(Watt/m)	(Watt/m <sup>2</sup> )		(N/m <sup>2</sup> )		(m <sup>2</sup> /m <sup>3</sup> )	(m <sup>2</sup> )		(m <sup>2</sup> /m <sup>2</sup> )	(m/m)	(m)	(>1 tend braided, <1 tend incision)
Santiago_A	1.69	28.98	0.70	40.34		9186.19	227.73	0.67	119.47	0.34	1.01	64.23	AP: 1947, 1982	1.00	1.452	33.888	1.190
Santiago_B	1.76	25.56	0.92	26.88		7804.09	290.37	0.44	135.94	0.25	1.00	50.06	AP: 1947, 1982	1.00	0.286	33.659	0.798
Hasley_1_A	1.23	3.28	0.62	4.07		2277.62	559.06	3.61	163.09	0.78	1.04	2.25	FI: 2002 (grading)	1.84	2.371	14.567	0.280
Hasley_1_B	0.92	4.44	0.50	8.13		2889.51	355.35	18.77	167.12	3.23	1.03	2.25	FI: 2002 (grading)	3.45	1.689	14.483	0.561
Hasley_1_TRIB	0.31	1.06	0.17	7.74		184.48	23.82	1.26	45.02	0.87	1.01	4.95	FI: 2002 (grading)	1.00	0.149	4.579	1.691
Hasley_2_A	0.66	19.33	0.35	54.42		4576.06	84.09	12.56	66.38	2.56	1.04	16.33	AP: 1994	2.47	1.830	23.446	2.321
Hasley_2_B	0.85	10.26	0.54	18.40		2054.72	111.64	8.05	78.69	1.87	1.04	16.33	AP: 1994	3.63	3.344	18.197	1.011
Hasley_2_TRIB	0.41	8.51	0.35	22.79		4520.97	198.37	32.65	120.79	4.97	1.02	4.24	AP: 1989	3.00	0.509	17.701	1.288
Hicks_A_08	0.64	2.97	0.41	7.15	OVRBNK	1213.74	169.86	110.50	52.62	5.42	1.06	1.21	FI & AP:1982	1.00	0.377	15.082	0.474
Hicks_B_08	1.12	4.86	0.64	7.33	OVRBNK	1284.80	175.32	114.06	86.89	8.95	1.05	1.60	FI & AP:1982	1.22	0.652	15.119	0.485
Hicks_C_08	0.93	7.52	0.42	17.50	OVRBNK	1979.56	113.09	4.62	87.23	1.42	1.05	1.60	FI & AP:1982	1.28	0.513	15.124	1.157
Hicks_D_08	1.31	6.29	0.44	13.14	OVRBNK	2307.04	175.61	20.27	113.01	3.67	1.05	1.60	FI & AP:1982	2.37	1.076	14.862	0.884
Hicks_D_07	1.39	7.83	0.46	14.66	OVRBNK	2405.02	164.01	69.30	123.03	9.50	1.05	1.60	FI & AP:1982	2.00	0.724	14.862	0.987
Hicks_E_08	1.25	6.73	0.52	15.81	OVRBNK	1691.79	106.98	21.82	101.01	4.80	1.04	1.60	FI & AP:1982	1.45	1.601	14.612	1.082
Hicks_E_07	1.34	8.39	0.56	17.91	OVRBNK	1648.85	92.09	24.13	105.13	5.90	1.04	1.60	FI & AP:1982	1.78	1.362	14.612	1.225
Hicks_F_08	1.60	8.44	0.37	36.45	OVRBNK	1377.35	37.79	7.71	59.88	2.85	1.04	1.60	FI & AP:1982	2.65	0.841	14.503	2.513
Hicks_F_07	1.90	12.91	0.32	20.26	OVRBNK	1233.70	60.88	15.96	46.06	2.59	1.04	1.60	FI & AP:1982	2.67	0.622	14.503	1.397
Agua_Hedi_A	2.29	20.34	1.76	8.68		2257.67	260.25	7.04	72.32	0.89	5.82	9.44	FI	1.80	0.980	34.172	0.254
Agua_Hedi_B	3.45	33.33	1.91	15.29	OVRBNK	1492.74	97.62	2.64	52.54	0.65	5.84	10.44	FI	1.87	1.463	34.042	0.449
Agua_Hedi_C	4.78	39.18	2.12	13.90	OVRBNK	1110.34	79.88	2.16	43.70	0.54	5.83	14.04	FI	1.74	3.922	33.912	0.410
Dry_A	0.40	3.67	0.27	12.13		2064.99	170.28	87.91	60.46	5.34	1.01	9.66	FI	2.19	0.841	15.007	0.808
Dry_B	0.73	6.30	0.47	12.01		1829.75	152.35	70.92	94.78	7.81	1.02	10.80	FI	2.09	2.660	14.876	0.807
Dry_C	0.72	6.17	0.53	12.43		2090.57	168.18	71.07	124.18	9.59	1.02	10.80	FI	2.32	7.272	14.737	0.843
Hovnanian_A	1.04	6.19	0.60	10.27		2701.50	263.11	0.36	185.08	0.31	1.04	14.76	AP: 1982	1.00	0.343	14.625	0.702
Hovnanian_B	1.37	5.37	0.73	7.03		2669.91	379.64	1.79	224.78	0.87	1.04	7.70	AP: 1982	1.00	0.197	14.545	0.484
Santimeta_A	0.42	0.98	0.24	0.35		1644.83	4673.45	1654.94	173.04	11.88	1.14	7.10	AP: 1982	4.91	8.440	7.853	0.045

Unique ID	10-yr Flow Depth	10-yr Area	10-yr Hydraulic Radius	10-yr Top Width	Q10 Overbank?	10-yr Stream Power	10-yr Specific Stream Power	10-yr Dimensionless Specific Stream Power	10-yr Shear Stress	10-yr Dimensionless Shear Stress	Average Load Ratio (dvp/undv/lb)	Reference BF Area	Reference Source	Enlargement Ratio (Apost/Agre)	Representative Geotechnical Stability (max Ng of both banks, dependent on 50% MW risk in moderate-/well-consolidated banks)	Reference Bankfull Top Width (regional Q10-dependent)	Relative Lateral Departure from Wref (regional)
	Depth_10yr	Area_10yr	Hyd-Rad_10yr	TopWidth_10yr		Q_10yr	w_10yr	w*_10yr	tau_10yr	tau*_10yr	Lratio	Agre	Ref_source	DeltaAratio	Max_Ng	Wref	Nlw
	(m)	(m <sup>2</sup> )	(m)	(m)	(blank or OVRBNK)	(Watt/m)	(Watt/m <sup>2</sup> )		(N/m <sup>2</sup> )		(m <sup>3</sup> /m <sup>3</sup> )	(m <sup>2</sup> )		(m <sup>2</sup> /m <sup>2</sup> )	(m/m)	(m)	(>1 tend braided, <1 tend incision)
Santimeta_B	0.32	1.57	0.21	7.02		1139.25	162.26	57.46	105.89	7.27	1.09	13.83	AP: 1982	1.92	5.274	7.853	0.894
Santimeta_C	0.25	1.63	0.17	9.50		1152.73	121.39	42.99	87.07	5.98	1.12	1.89	AP: 1982	6.89	2.216	7.853	1.209
Ltl_Cedar_A	1.34	9.23	0.83	9.86		3067.72	311.20	0.62	163.76	0.35	1.00	5.22	FI & AP: 1982	2.20	1.546	19.116	0.516
Ltl_Cedar_B	0.69	10.64	0.45	16.20		4008.28	247.46	0.82	115.03	0.35	1.00	15.09	FI & AP: 1983	1.01	0.052	19.195	0.844
Proctor_A	0.94	10.46	0.42	23.46	OVRBNK	1644.52	70.09	0.62	52.20	0.31	1.06	34.04	FI	1.00	0.140	17.674	1.328
Proctor_B	0.82	6.35	0.33	18.31	OVRBNK	993.55	54.26	8.11	45.84	1.77	1.12	4.82	FI	1.00	0.122	13.377	1.369
Proctor_TRIB	0.76	4.45	0.29	15.81	OVRBNK	1176.49	74.41	1.51	60.64	0.62	1.00	1.91	FI	1.00	0.075	11.989	1.319
Perris_1_A	0.54	1.49	0.28	5.15		52.70	10.23	4.32	16.49	1.27	1.07	3.53	FI	1.51	0.092	5.082	1.014
Perris_1_B	0.40	1.10	0.24	3.52		113.73	32.28	13.64	32.31	2.49	1.09	3.99	FI	1.33	0.259	4.934	0.714
Perris_1_C	0.59	1.08	0.33	2.76		56.04	20.30	8.58	23.27	1.80	1.09	4.18	FI	1.18	0.227	4.806	0.574
Perris_2_A	0.24	0.44	0.12	3.25		96.20	29.63	10.49	30.47	2.09	1.05	0.81	FI	1.00	0.003	3.461	0.938
Perris_2_B	0.19	0.29	0.11	2.19		93.94	42.96	36.74	36.41	4.50	0.94	0.61	FI	1.00	0.054	2.950	0.741
Perris_3_A	0.42	3.97	0.17	23.80		361.56	15.19	6.42	23.14	1.79	1.00	17.49	FI	1.00	0.004	8.321	2.861
Perris_3_B	0.39	3.35	0.16	21.23		379.31	17.87	6.33	25.94	1.78	1.01	27.10	FI	1.00	0.006	7.870	2.698
AltPerris_A	0.24	4.39	0.12	37.34		231.31	6.19	2.19	11.75	0.81	1.00	7.22	FI	1.00	0.014	7.886	4.735
AltPerris_B	0.28	3.32	0.20	16.60		145.87	8.79	3.11	13.81	0.95	0.99	3.97	FI	1.00	0.004	7.485	2.218
AltPerris_C	0.35	2.26	0.23	9.68		95.45	9.86	4.17	11.11	0.86	0.99	3.78	FI	1.40	0.018	7.350	1.317
Dulzura_A	2.30	50.59	1.20	33.21	OVRBNK	4688.55	141.18	0.21	70.82	0.13	1.01	13.52	FI & AP: 1971	1.97	0.172	40.638	0.817
Dulzura_B	2.63	53.23	1.12	30.34	OVRBNK	4694.38	154.73	0.14	65.74	0.09	1.01	13.52	FI & AP: 1972	1.65	0.243	40.661	0.746
Acton_A	0.36	2.97	0.17	17.36		946.53	54.54	1.52	62.11	0.78	1.03	1.71	FI (graded Acton G ~1990s)	2.24	0.021	8.308	2.089
Acton_B	0.25	0.86	0.17	4.50		789.78	175.67	7.17	63.33	1.03	1.04	1.71	FI (graded Acton G ~1990s)	2.23	0.900	7.602	0.591
Acton_C	0.41	1.21	0.23	6.18		808.72	130.94	3.54	113.73	1.41	1.04	1.71	FI (graded Acton G ~1990s)	13.68	7.479	6.688	0.923
Acton_D	0.33	1.12	0.24	4.47		399.52	89.38	0.94	76.68	0.50	1.07	1.71	FI (graded Acton G ~1990s)	9.85	9.909	5.913	0.756
Acton_E	0.56	0.52	0.22	0.96		1747.19	1824.24	19.14	325.53	2.14	1.05	1.71	FI (graded Acton G ~1990s)	1.35	6.831	5.762	0.166
Acton_F	0.40	1.83	0.17	10.34		173.66	16.79	0.18	26.77	0.18	1.03	1.71	FI (graded Acton G ~1990s)	1.07	0.008	5.672	1.824
Acton_G	0.26	2.08	0.19	9.18	OVRBNK	115.99	12.63	0.13	19.77	0.13	1.07	1.71	FI (graded Acton G ~1990s)	1.00	0.002	5.652	1.625
Borrego_A	0.47	4.10	0.40	8.94		3121.16	349.12	52.16	79.23	3.06	3.52	23.94	AP: 1952	1.38	1.098	19.225	0.465
Borrego_B	0.50	13.94	0.31	44.74		2753.44	61.55	9.19	54.08	2.09	3.53	23.94	AP: 1952	6.04	1.085	19.191	2.331
Borrego_C	0.46	7.64	0.37	20.76		2219.51	106.92	32.33	52.12	3.22	3.50	23.94	AP: 1952	4.38	5.201	19.159	1.083

	10-yr Flow Depth	10-yr Area	10-yr Hydraulic Radius	10-yr Top Width	Q10 Overbank?	10-yr Stream Power	10-yr Specific Stream Power	10-yr Dimensionless Specific Stream Power	10-yr Shear Stress	10-yr Dimensionless Shear Stress	Average Load Ratio (dyv/undv/lb)	Reference BF Area	Reference Source	Enlargement Ratio (Apost/Agre)	Representative Geotechnical Stability (max Ng of both banks, dependent on 50% MW risk in moderate-/ well-consolidated banks)	Reference Bankfull Top Width (regional Q10- dependent)	Relative Lateral Departure from Wref (regional)
	Depth_10yr	Area_10yr	Hydr-Rad_10yr	TopWidth_10yr		Q_10yr	w_10yr	w*_10yr	tau_10yr	tau*_10yr	Lratio	Agre	Ref_source	DeltaAratio	Max_Ng	Wref	Nlw (>1 tend braided, <1 tend incision)
Unique ID	(m)	(m <sup>2</sup> )	(m)	(m)	(blank or OVRBNK)	(Watt/m)	(Watt/m <sup>2</sup> )		(N/m <sup>2</sup> )		(m <sup>3</sup> /m <sup>3</sup> )	(m <sup>2</sup> )		(m <sup>2</sup> /m <sup>2</sup> )	(m/m)	(m)	
Borrogo_D	1.02	9.35	0.62	18.25		4261.31	233.52	0.23	186.77	0.26	3.76	23.94	AP: 1952	6.72	10.397	18.280	0.998
Borrogo_E	1.66	8.35	0.79	9.16		3830.96	418.15	0.42	214.35	0.29	3.63	23.94	AP: 1952	1.51	1.042	18.252	0.502
Topanga_A	1.97	25.81	0.95	25.22	OVRBNK	16700.99	662.30	0.24	259.64	0.18	1.04	20.06	AP: 1989	1.00	0.063	35.978	0.701
Topanga_B	1.77	33.01	0.96	32.95		10723.64	325.41	0.10	164.73	0.10	1.04	25.11	FI & AP: 1989	2.01	0.003	36.310	0.908
Topanga_C	2.64	14.89	1.26	10.77		61193.67	5680.81	0.15	1234.86	0.15	1.04	37.24	AP: 1989	1.00	0.000	36.287	0.297
Challengr_A	1.75	15.35	0.55	25.84	OVRBNK	1382.49	53.50	0.04	50.79	0.06	1.16	2.06	FI & AP: 1982, 1989	1.58	2.476	18.748	1.378
Challengr_B	2.20	17.35	0.70	24.22	OVRBNK	884.90	36.53	1.76	42.05	0.76	1.09	2.37	FI & AP: 1982, 1990	1.55	1.701	18.629	1.300
Challengr_C	1.29	11.21	0.47	23.77	OVRBNK	3497.00	147.14	0.08	112.44	0.10	1.07	2.56	FI & AP: 1982, 1991	1.00	0.226	18.525	1.283
Mcgonigle_A	0.86	20.65	0.48	45.87	OVRBNK	1359.73	29.64	0.08	48.49	0.13	7.51	1.55	FI & AP: 1966, 1980, 1982, 1985, 1989	2.28	0.037	17.833	2.572
Sanjuan_A	1.71	56.70	0.91	61.29	OVRBNK	23251.16	379.38	0.57	158.46	0.28	1.00	8.82	AP 1982	1.00	13.392	51.692	1.186
Sanjuan_B	3.18	68.94	1.84	39.53	OVRBNK	9687.30	245.07	0.15	135.10	0.14	1.00	19.92	AP 1982	1.00	0.072	51.289	0.771
Pigeon_A	1.42	7.28	0.47	61.56	OVRBNK	1584.04	25.73	5.92	70.91	3.65	1.17	2.69	FI & AP: 1966, 1980, 1989	1.61	1.638	15.934	3.863
Pigeon_B	0.80	6.69	0.40	18.53	OVRBNK	2215.58	119.54	42.33	83.13	5.71	1.17	3.44	FI & AP: 1966, 1980, 1990	1.45	1.233	15.934	1.163
Pigeon_C	1.60	7.17	0.79	8.17		474.21	58.07	9.56	57.10	2.35	1.01	4.99	FI & AP: 1966, 1980, 1991	1.16	0.856	12.759	0.640
Stewart_A	1.53	8.48	0.67	12.09	OVRBNK	19864.20	1642.85	0.27	657.44	0.27	1.00	3.27	FI & AP: 1963	1.00	0.097	21.479	0.563
Santiagbd_A	1.32	14.13	0.76	19.26	OVRBNK	6252.07	324.69	1.85	146.59	0.64	1.00	8.23	FI - pre-2007 fire (i.e., filling)	1.59	0.996	26.771	0.719
Santiagbd_B	1.00	16.50	0.64	20.12	OVRBNK	5774.37	286.93	4.49	113.91	0.98	1.00	8.23	FI - pre-2007 fire (i.e., filling)	1.67	0.054	26.768	0.752
Santiagnl_A	1.25	10.62	0.89	11.57		7533.15	651.15	10.19	210.12	1.80	1.00	8.23	FI - pre-2007 fire (i.e., filling)	3.69	0.315	26.533	0.436
Santiagnl_B	1.71	12.91	0.86	12.47	OVRBNK	10000.69	801.81	1.81	271.64	0.64	1.00	8.23	FI - pre-2007 fire (i.e., filling)	1.00	0.709	26.505	0.471
Silverado_A	2.13	16.90	1.19	12.36	OVRBNK	16752.25	1355.14	0.24	446.30	0.19	1.00	8.42	FI	1.00	0.239	31.098	0.398
Silverado_B	2.06	15.39	0.99	11.83	OVRBNK	19974.77	1688.95	0.37	443.23	0.22	1.00	5.18	FI	1.00	0.048	31.113	0.380
Escondido_A	3.02	58.79	1.62	35.44	OVRBNK	67659.06	1909.11	0.40	630.91	0.30	3.13	15.21	FI	1.00	0.017	58.317	0.608
Escondido_B	3.34	96.42	1.85	50.93	OVRBNK	18917.27	371.42	0.64	201.05	0.40	3.15	31.85	FI	1.00	0.161	58.317	0.873
Sanantoni_A	1.81	33.99	0.91	36.33	OVRBNK	23184.34	638.11	0.38	221.88	0.21	1.00	17.93	AP: 1947, 1967, 1979, 1982, 1985, 1989	6.75	0.396	44.074	0.824
Sanantoni_B	1.40	52.53	0.80	64.65		11545.62	178.58	0.84	97.00	0.37	1.00	17.93	AP: 1947, 1967, 1979, 1982, 1985, 1990	6.44	5.742	44.074	1.467
Alt_RC2_A	0.3812	0.4002	0.1880	1.9746		219.0999	110.9585	759.1091	66.2221	32.7296	0.9968	6.61	FI	1.0000	0.218	4.294	0.460
Yucaipa_A	0.71	7.38	0.56	12.91		10270.57	795.69	36.74	202.03	3.57	1.05	26.23	AP: 1952, 1966, 1969, 1975, 1982, 1983, 1989	1.03	1.411	25.130	0.514

	10-yr Flow Depth	10-yr Area	10-yr Hydraulic Radius	10-yr Top Width	Q10 Overbank?	10-yr Stream Power	10-yr Specific Stream Power	10-yr Dimensionless Specific Stream Power	10-yr Shear Stress	10-yr Dimensionless Shear Stress	Average Load Ratio (dvp/undvp)	Reference BF Area	Reference Source	Enlargement Ratio (Apost/Apre)	Representative Geotechnical Stability (max Ng of both banks, dependent on 50% MW risk in moderate-/ well-consolidated banks)	Reference Bankfull Top Width (regional Q10- dependent)	Relative Lateral Departure from Wref (regional)
	Depth_10yr	Area_10yr	Hyd-Rad_10yr	TopWidth_10yr		Q_10yr	w_10yr	w*_10yr	tau_10yr	tau*_10yr	Lratio	Apre	Ref_source	DeltaAratio	Max_Ng	Wref	Nw
Unique ID	(m)	(m <sup>2</sup> )	(m)	(m)	(blank or OVRBANK)	(Watt/m)	(Watt/m <sup>2</sup> )		(N/m <sup>2</sup> )		(m <sup>3</sup> /m <sup>3</sup> )	(m <sup>2</sup> )		(m <sup>2</sup> /m <sup>2</sup> )	(m/m)	(m)	(>1 tend braided, <1 tend incision)
Yucaipa_B	0.51	11.27	0.34	20.59		7883.68	382.87	11.01	124.39	1.60	1.07	26.23	AP: 1952, 1966, 1969, 1975, 1982, 1983, 1990	2.52	10.629	22.232	0.926
Oakglenn_A	0.70	2.19	0.40	4.98		4380.55	879.14	2.35	289.29	0.76	1.04	7.32	AP: 1952, 1982, 1983	3.30	1.081	12.346	0.404

**General abbreviations and symbol definitions (excluding units of measure):**

Apost	surveyed cross-sectional area to top of bank (2007/2008)	FI	Field Indicator (and year)	OVRBANK	overbank
Apre	best estimate of historic (reference) cross-sectional area	ID	identification	Q10	flow with 10-yr return interval
AP	Aerial Photograph (and year)	max	maximum	undvp	undeveloped
BF	Bankfull (i.e., cross-sectional channel area to top of bank of active channel)	MW	mass wasting	Wref	regional reference width (unconfined stable single-thread) for Q10
dvp	developed	Ng	bank stability		

**Table D.8 – Stability, planform, and channel evolution model (CEM) stage**

Unique ID	Current Planform	Current Bedform	Manning n (main channel)	Current CEM Phase	CEM for Plotting	Vertical Stability Rating (stable, unstable, or NA)
	<i>Planform</i>	<i>Bedform</i>	<i>Manning_n</i>	<i>CEM</i>		
	(S, B, T, M)	(C, SP, PB, PR, DR)				
Santiago_A	B	PR	0.056	B1	Braiding_Valley	U
Santiago_B	S	PR	0.056	1C	Constructed	NA
Hasley_1_A	S	PB	0.045	2	Incising	U
Hasley_1_B	S	PB	0.06	3	3	U
Hasley_1_TRIB	S	PB	0.075	1C	Constructed	NA
Hasley_2_A	B	PB	0.055	2B	Braided_Widening_Sed	U
Hasley_2_B	S	PB	0.059	2	Incising	U
Hasley_2_TRIB	B	PB	0.06	2B	Braided_Widening_Sed?	U
Hicks_A_08	S	PB	0.02	1C	Constructed	NA
Hicks_B_08	S	PB	0.045	2	Incised	U
Hicks_C_08	S	PB	0.065	3	3	U
Hicks_D_08	S	PB	0.065	3	3	U
Hicks_D_07	S	PB	0.085	3	3	U
Hicks_E_08	M	PB	0.07	2	Incising	U
Hicks_E_07	M	PB	0.09	2	Incising	U
Hicks_F_08	M	PB	0.065	2	Incising	U
Hicks_F_07	M	PB	0.085	2	Incising	U
Agua_Hedi_A	S	PR	0.035	2	Incising	U
Agua_Hedi_B	S	PR	0.05	3	3	U
Agua_Hedi_C	S	PR	0.055	2	Incising	U
Dry_A	S	PB	0.025	3	3	U
Dry_B	S	PB	0.06	3	3	U
Dry_C	S	PB	0.07	3	3	U
Hovnanian_A	M	PR	0.089	1	Confined and Hardpan	NA
Hovnanian_B	M	PR	0.089	1	Confined and Hardpan	NA
Santimeta_A	S	PB	0.045	3	3	U
Santimeta_B	S	PB	0.055	3	3	U
Santimeta_C	S	PB	0.05	3	3	U
Ltl_Cedar_A	S	PB	0.074	2	Incising	U
Ltl_Cedar_B	B	PB	0.064	B1	Braiding_Valley	U
Proctor_A	B	PB	0.05	B1	Braiding_nonalluvial	U-NF
Proctor_B	B	PB	0.05	B1	Braiding_nonalluvial	U-NF
Proctor_TRIB	B	PB	0.05	1	Confined	NA
Perris_1_A	M	PB	0.055	1.5	Incised	R?
Perris_1_B	M	PB	0.06	2	Incising	U

Unique ID	Current Planform	Current Bedform	Manning n (main channel)	Current CEM Phase	CEM for Plotting	Vertical Stability Rating (stable, unstable, or NA)
	Planform (S, B, T, M)	Bedform (C, SP, PB, PR, DR)	Manning_n	CEM		
Perris_1_C	M	PB	0.055	2	Incised	U
Perris_2_A	M	PB	0.045	1	1	S
Perris_2_B	M	PB	0.045	1	1	S
Perris_3_A	B	PB	0.055	B1	Braiding_Valley&Sed	U
Perris_3_B	B	PB	0.055	B1	Braiding_Valley&Sed	U
AltPerris_A	B	PB	0.046	B1	Braiding_Tribsed?nonalluvial	U-NF
AltPerris_B	T	PR	0.046	1	Transition	S
AltPerris_C	M	PR	0.03	1	1	S
Dulzura_A	M	PR	0.056	5	1	S
Dulzura_B	M	PR	0.056	5	1	S
Acton_A	B	PB	0.068	2B	Braiding_Valley&Sed	U
Acton_B	S	PB	0.024	2	Transition	U
Acton_C	M	PR	0.063	3	3	U
Acton_D	S	PB	0.063	3	3	U
Acton_E	S	PB	0.063	2	Incising	U
Acton_F	S	PB	0.063	1.5	1	S
Acton_G	S	PB	0.063	1	1	S
Borrego_A	S	PB	0.02	1C	Constructed	NA
Borrego_B	B	PB	0.054	4B	Braided_Sed	U
Borrego_C	S	PB	0.03	3	Braiding_Sed	U
Borrego_D	S	PR	0.08395	4	4	R?
Borrego_E	S	PR	0.08395	2	Incising	U
Topanga_A	S	SP	0.068	1	Confined	NA
Topanga_B	B	PR	0.068	B1	Braiding_Valley	U
Topanga_C	S	SP	0.088	1	Confined	NA
Challengr_A	M	PR	0.0667	1.5	Incised	S?
Challengr_B	M	PR	0.07245	2	Incising	U
Challengr_C	M	PR	0.07245	1	1	S
Mcgonigle_A	M	PR	0.09545	1V	Vegetated	S?
Sanjuan_A	B	PR	0.053	B1	Braiding_Valley	U
Sanjuan_B	S	SP	0.068	1	Confined	NA
Pigeon_A	B	PB	0.05175	B2	Incising	U
Pigeon_B	B	PB	0.05	B2	Incising	U
Pigeon_C	M	PR	0.0805	2	Incising	U
Stewart_A	S	C	0.102	1	Confined	NA
Santiagbd_A	S	PB	0.051	3	Confined_Incising-Wide_Temp	U

Unique ID	Current Planform	Current Bedform	Manning n (main channel)	Current CEM Phase	CEM for Plotting	Vertical Stability Rating (stable, unstable, or NA)
	Planform (S, B, T, M)	Bedform (C, SP, PB, PR, DR)	Manning_n	CEM		
Santiagbd_B	S	PB	0.051	2	Confined_Incising_Temp	U
Santiagnl_A	S	PB	0.048	2	Confined_Incising_Temp	U
Santiagnl_B	S	SP	0.06615	1	Confined	NA
Silverado_A	S	SP	0.083	1	Confined	NA
Silverado_B	S	SP	0.073	1	Confined	NA
Escondido_A	S	SP	0.093	1	Constricting_Confined	NA
Escondido_B	B	PR	0.088	B1	Braiding_Valley	U
Sanantoni_A	S	SP	0.053	B2	Incising	U
Sanantoni_B	B	PR	0.053	B1	Braided	U
Alt_RC2_A	M	PR	0.04	1	1	NA-NF
Yucaipa_A	S	PB	0.034	3	Constructed_Widening	U
Yucaipa_B	S	PB	0.049	4B	Constructed_Braided_Valley&Wide&Sed	U
Oakglenn_A	S	SP	0.053	1C	Constructed	NA

**General abbreviations and symbol definitions (excluding units of measure):**

CEM Channel Evolution Model  
 ID identification  
 n Manning's roughness

**Current planform:**

B braided  
 M meandering  
 S straight  
 T transition (e.g., single-thread to braided)

**Current bedform:**

C cascade  
 DR dune riffle  
 PB plane bed  
 PR pool riffle  
 SP step pool

**Vertical stability:**

NA	not applicable	constructed, confined, or other stable due to outside boundary conditions
S	stable	no significant channel adjustments such as incision nearing critical bank height, widening, braiding, etc.
U	unstable	active channel adjustments such as significant incision, widening, braiding, etc.
R?	recovered?	possibly nearing or at a return to quasi-equilibrium following an obvious period of adjustment
U-NF	unstable-nonfluvial	braided planform/distributary flow; however, limited alluvium or evident fluvial activity – the channel itself is hard to locate

**CEM phases:**

1	stable	no significant channel incision or bank failure
1.5	beginnings of incision	incision but not past critical bank height
2	incising	nearing, at, or beyond critical bank height, but no significant widening
3	widening	significant widening (~> 10% channel width) – incision still possible/likely
4	deposition	bank failure and widening still possible, but clear evidence of significant deposition (with possible beginnings of floodplain reformation, alternating bars, etc.)
5	recovered	return to single-thread equilibrium

**Other CEM phases:**

1C	constructed	stable but constructed via bed and/or bank protection
1V	vegetated	stable, vegetated encroached low-flow channel
B1	braided	braided but relatively stable active belt width
B2	braided-incising	incision near, at, or beyond critical bank height within a braided channel
2B	wide-to-braided	evidence that a single-thread channel transitioned to braided planform with little intermediate incision (i.e., not far beyond critical bank height, but change in width >>2x)
4B	incised-wide-braided	evidence that a single-thread channel first incised well past critical bank height before widening to the current braided form

**Other CEM Notes:**

_Confined	valley confinement from adjacent hillslopes
_Transition	cross section located at transition between single-thread and braided planform
_Constricting	cross section located at transition between braided and single-thread planform due to downstream valley confinement
_Braided_Valley	braiding primarily due to valley expansion
_Braided_Sed	braiding primarily due to sediment-load increase (not associated with valley expansion)
_Braided_Widening	braiding primarily due to excess channel widening
Braided_nonalluvial	channel has multiple flow paths, but very little alluvial material note: could have a combination of any/all factors (e.g., Braided_Valley&Sed)

## **APPENDIX E**

### **LOGISTIC-REGRESSION SUPPLEMENT: DATA, PARAMETER ESTIMATES, AND ADDITIONAL RESULTS**

**Table E.1 – Summary of significant incising and braiding models**

Model Type	Independent Variable (1)				Independent Variable (2)				Model Performance												
	$\beta_0$	Grain Size (mm)	$\beta_1^*$	p	Mobility Index ( $m^{1.5}/s^{0.5}$ )	$\beta_2^*$	p	p	% Correctly Classified												
Unstable											Stable										
Models do not include data from confined/bedrock systems																					
Incising	29.7	$d_{50}$	-2.48	0.012	$S_v * Q_2^{0.5}$	6.76	0.007	<0.0001	92%	69%											
	17.9	$d_{84}$	-1.12	0.020	$S_v * Q_2^{0.5}$	3.73	0.004	<0.0001													
	43.5	$d_{50}$	-4.44	0.049	$S_v * Q_{10}^{0.5}$	11.9	0.048	<0.0001													
	31.0	$d_{84}$	-2.70	0.021	$S_v * Q_{10}^{0.5}$	7.60	0.015	<0.0001													
Braiding	10.0	$d_{50}$	-0.771	0.033	$S_v * Q_2^{0.5}$	2.22	0.012	0.005	89%	54%											
	8.98	$d_{84}$	-0.544	0.11	$S_v * Q_2^{0.5}$	1.88	0.018	0.023													
	16.4	$d_{50}$	-1.70	0.013	$S_v * Q_{10}^{0.5}$	4.60	0.007	<0.0001													
	14.7	$d_{84}$	-1.31	0.021	$S_v * Q_{10}^{0.5}$	3.72	0.005	0.0004													
Models include data from confined/bedrock systems																					
Incising	18.5	$d_{50}$	-2.29	0.0007	$S_v * Q_2^{0.5}$	4.00	0.005	<0.0001													
	13.7	$d_{84}$	-1.45	0.0009	$S_v * Q_2^{0.5}$	2.44	0.003	<0.0001													
	11.0	$d_{50}$	-1.85	0.0002	$S_v * Q_{10}^{0.5}$	2.73	0.002	<0.0001													
	12.4	$d_{84}$	-1.60	0.001	$S_v * Q_{10}^{0.5}$	2.51	0.005	<0.0001													

**General abbreviations and symbol definitions (excluding units of measure):**

$\beta$ -parameters correspond to log-transformed variables (i.e.,  $\beta_1 \ln(d_{50})$ ,  $\beta_2 \ln(S_v * Q_2^{0.5})$ )  
 $d_{50}$  grain size that 50 percent of the particles are finer than  
 $d_{84}$  grain size that 84 percent of the particles are finer than  
p probability value  
 $Q_2$  flow with 2-yr return interval  
 $Q_{10}$  flow with 10-yr return interval  
 $S_v$  valley slope

**Table E.2 – Summary of bank stability models**

Bank Data	Independent Variables						Model Performance	
	$\beta_0$	Height (m)		Angle (°)		p	% Correctly Classified	
		$\beta_1$	p	$\beta_2$	p		Unstable	Stable
moderate/well-consolidated	110	-8.46	0.012	-26.6	0.015	<0.0001	94%	97%
poor/moderate/well-consolidated	28.4	-1.27	0.002	-7.28	<0.0001	<0.0001		
confined hillslope	46.6	-3.39	0.08	-10.2	0.07	<0.0001		

**General abbreviations and symbol definitions (excluding units of measure):**

$\beta$ -parameters correspond to log-transformed variables (i.e.,  $\beta_1 \ln(\text{height})$ ,  $\beta_2 \ln(\text{angle})$ )  
p probability value

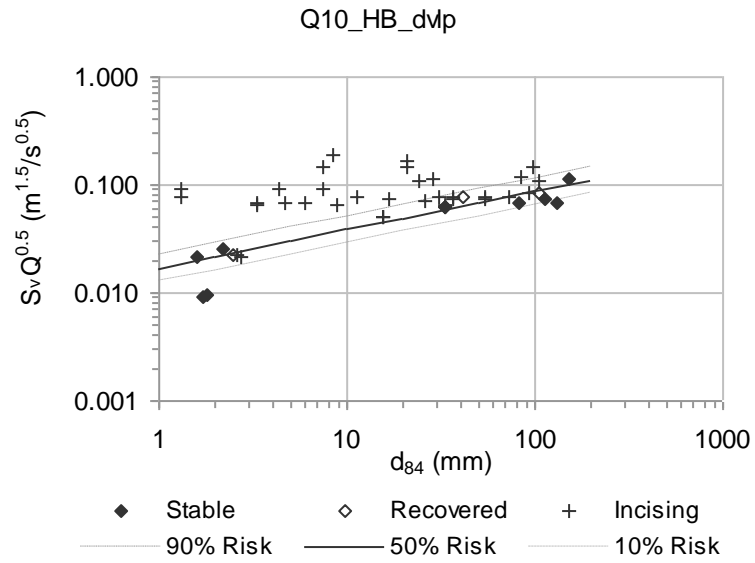


**Figure E.1 – Incision logistic MI10 vs. d84**

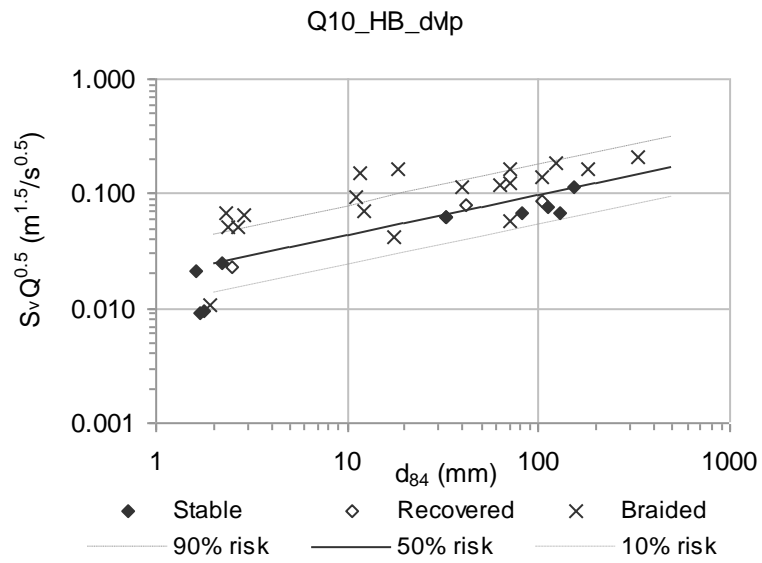


**Figure E.2 – Braiding logistic MI10 vs. d84**

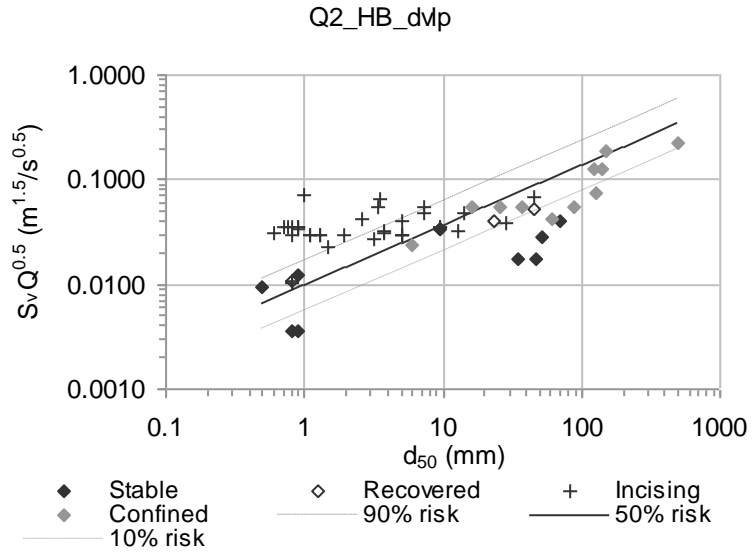


Figure E.3 – Incision logistic MI2 vs.  $d_{50}$  (including confined/bedrock systems)

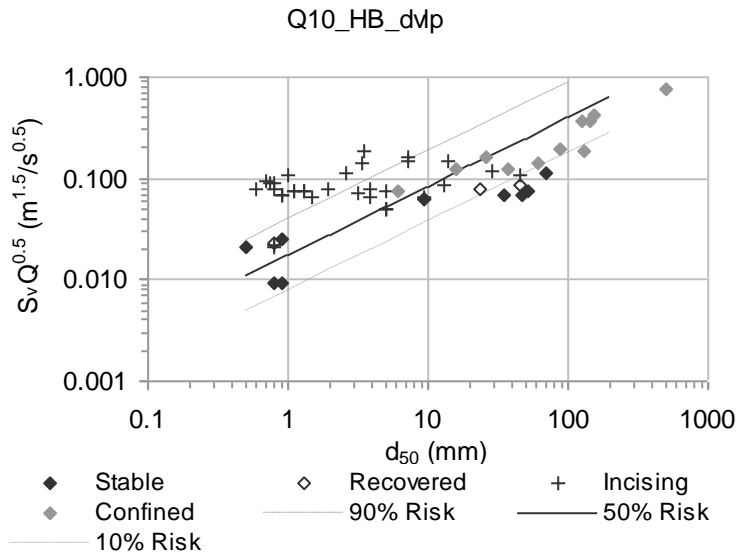
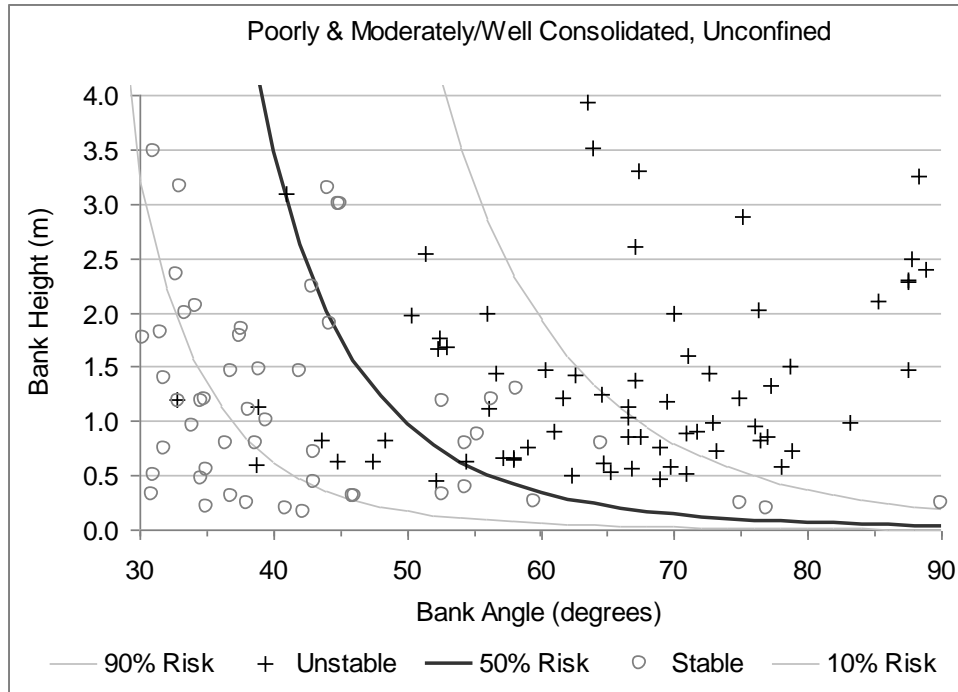
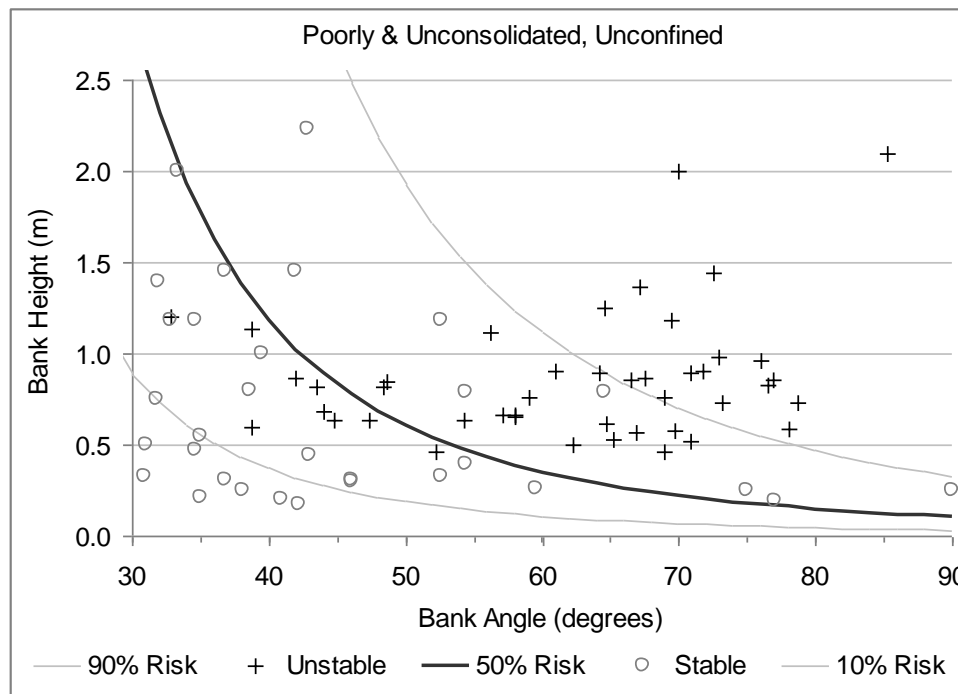


Figure E.4 – Incision logistic MI10 vs.  $d_{50}$  (including confined/bedrock systems)



**Figure E.5 – Risk of bank failure in poorly and moderately/well-consolidated materials**



**Figure E.6 – Risk of bank failure in poorly and unconsolidated materials**

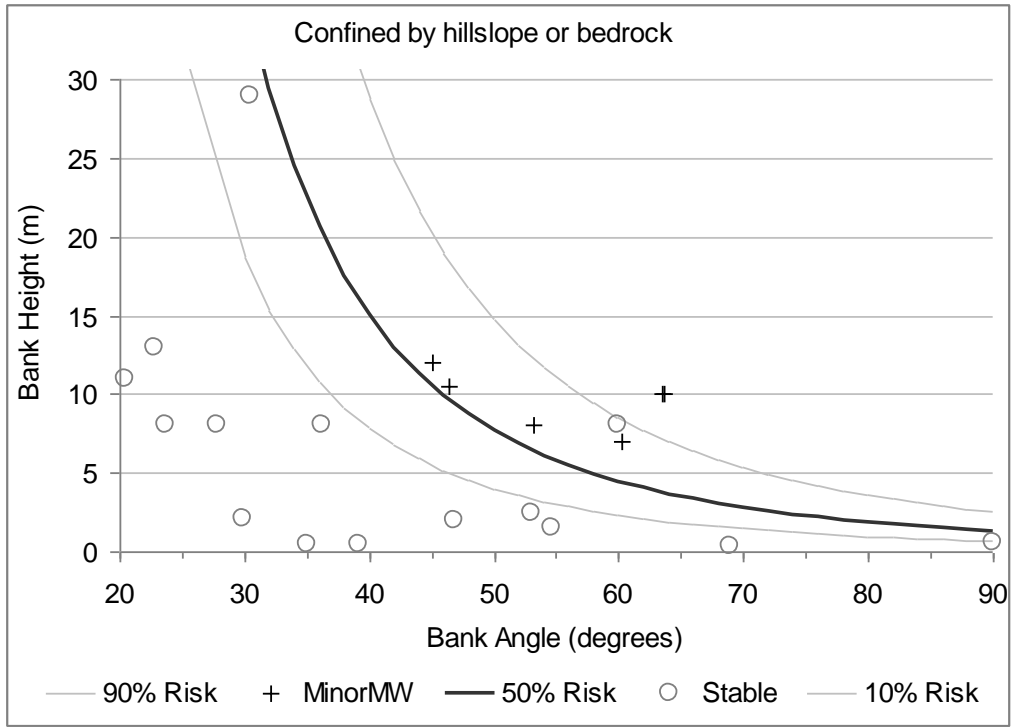


**Figure E.7 – Risk of minor mass wasting in hillslope if channel directly connected to hillslope (i.e., confined)**

**Table E.3 – Incising and braiding data**

Unique ID	2-yr Flow Metrics							10-yr Flow Metrics							Bed-material Metrics					Response for SAS	CEM Description	Vertical Stability Rating		
	Total Drainage Area	Avg_Dvlp Hawley-Bledsoe 2-yr Flow	2-yr Specific Stream Power	2-yr Dimensionless Specific Stream Power	2-yr Shear Stress	2-yr Dimensionless Shear Stress	2-yr Width to Depth Ratio	2-yr Mobility Index	Avg_Dvlp Hawley-Bledsoe 10-yr Flow	10-yr Specific Stream Power	10-yr Dimensionless Specific Stream Power	10-yr Shear Stress	10-yr Dimensionless Shear Stress	10-yr Width to Depth Ratio	10-yr Mobility Index	Median Bed Material	16th Percentile Bed Material	84th Percentile Bed Material	Percent Sand				Current CEM Phase	Screening Logistics
	<i>Drn_Area_km</i>	<i>Q2_HB_urbn</i>	<i>ω_2yr</i>	<i>ω_2yr</i>	<i>τ_2yr</i>	<i>τ_2yr</i>	<i>W/D_2yr</i>	<i>Q<sup>2.5</sup>Sv</i>	<i>Q10_HB_urbn</i>	<i>ω_10yr</i>	<i>ω_10yr</i>	<i>τ_10yr</i>	<i>τ_10yr</i>	<i>W/D_10yr</i>	<i>Q10<sup>2.5</sup>Sv</i>	<i>d50</i>	<i>d16</i>	<i>d84</i>	<i>Prcnt_Sand</i>	<i>CEM</i>				
	(km <sup>2</sup> )	(m <sup>3</sup> /s)	(Watt/m <sup>2</sup> )	(N/m <sup>2</sup> )	(N/m <sup>2</sup> )	(N/m <sup>2</sup> )		(m <sup>1.5</sup> /s <sup>0.5</sup> )	(m <sup>3</sup> /s)	(Watt/m <sup>2</sup> )	(N/m <sup>2</sup> )	(N/m <sup>2</sup> )	(N/m <sup>2</sup> )		(m <sup>1.5</sup> /s <sup>0.5</sup> )	(mm)	(mm)	(mm)	(%)					(Stable, Unstable, or NA)
Santiago_B	33.67	5.20	63.36	0.10	54.81	0.10	17.13	0.0387	53.03	290.37	0.44	135.94	0.25	15.26	0.124	34	6.4	127.4	9%	1C	1C	Cnst	Constructed	NA
Hasley_1_TRIB	0.42	0.12	6.14	0.32	21.65	0.42	31.10	0.0154	0.72	23.82	1.26	45.02	0.87	24.81	0.037	3.2	0.5	25.7	44%	1C	1C	Cnst	Constructed	NA
Hicks_A_08	3.87	1.41	40.70	26.48	22.34	2.30	16.75	0.0304	9.37	169.86	110.50	52.62	5.42	11.18	0.079	0.6	0.3	1.3	93%	1C	1C	Cnst	Constructed	NA
Borrego_A	7.06	5.93	44.66	6.67	46.55	1.80	31.94	0.0476	15.83	349.12	52.16	79.23	3.06	18.85	0.078	1.6	0.8	11.2	64%	1C	1C	Cnst	Constructed	NA
Oakglenn_A	1.77	1.08	235.08	0.63	134.72	0.36	9.96	0.1157	6.08	879.14	2.35	289.29	0.76	7.14	0.274	23.4	3	84.1	9%	1C	1C	Cnst	Constructed	NA
Hasley_2_A	11.69	2.77	20.36	3.04	29.05	1.12	88.65	0.0506	24.30	84.09	12.56	66.38	2.56	82.77	0.150	1.6	0.5	11.6	56%	2B	2B	B	Braided_Widening_Sed	U
Hasley_2_TRIB	5.05	1.63	29.65	4.88	41.44	1.71	105.82	0.0401	13.24	198.37	32.65	120.79	4.97	55.01	0.115	1.5	0.5	40	58%	2B	2B	B	Braided_Widening_Sed?	U
Acton_A	2.02	0.57	18.21	0.51	37.37	0.47	43.31	0.0334	2.59	54.54	1.52	62.11	0.78	47.61	0.071	4.9	2.3	12.1	10%	2B	2B	B	Braiding_Valley&Sed	U
Borrego_B	6.99	6.15	10.55	1.58	37.10	1.43	93.39	0.0575	15.77	61.55	9.19	54.08	2.09	89.86	0.092	1.6	0.8	11.2	64%	4B	4B	B	Braided_Sed	U
Yucaipa_B	11.48	2.83	72.81	2.09	26.34	0.34	90.63	0.0601	21.66	382.87	11.01	124.39	1.60	40.04	0.166	4.8	2	18.6	17%	4B	4B	B	Constructed_Braided_Valley&Wide&Sed	U
Santiago_A	35.09	5.27	62.23	0.18	55.08	0.15	22.30	0.0385	53.82	227.73	0.67	119.47	0.34	23.85	0.123	22	2	70.8	18%	B1	B1	B	Braiding_Valley	U
Lit_Cedar_B	7.21	1.68	35.92	0.12	45.64	0.14	36.81	0.0387	15.78	247.46	0.82	115.03	0.35	23.53	0.119	20.3	7.8	62.8	7%	B1	B1	B	Braiding_Valley	U
Proctor_A	11.23	1.13	14.23	0.13	21.59	0.13	23.66	0.0166	13.20	70.09	0.62	52.20	0.31	24.88	0.057	10.5	1.6	70.6	19%	B1	B1	B	Braiding_nonalluvial	U-NF
Proctor_B	5.81	0.91	12.83	1.92	24.09	0.93	15.96	0.0149	7.23	54.26	8.11	45.84	1.77	22.38	0.042	1.6	0.3	17.7	55%	B1	B1	B	Braiding_nonalluvial	U-NF
Perris_3_A	1.46	0.35	5.81	2.46	13.09	1.01	37.67	0.0252	2.60	15.19	6.42	23.14	1.79	56.23	0.069	0.8	0.3	2.3	82%	B1	B1	B	Braiding_Valley&Sed	U
Perris_3_B	1.39	0.33	6.74	2.39	14.55	1.00	38.10	0.0244	2.30	17.87	6.33	25.94	1.78	53.79	0.065	0.9	0.3	2.9	75%	B1	B1	B	Braiding_Valley&Sed	U
AltPerris_A	1.64	0.33	1.78	0.63	5.57	0.38	150.07	0.0040	2.31	6.19	2.19	11.75	0.81	156.24	0.011	0.9	0.4	1.9	86%	B1	B1	B	Braiding_Tribsed?nonalluvial	U-NF

Unique ID	2-yr Flow Metrics							10-yr Flow Metrics							Bed-material Metrics					Response for SAS	CEM Description	Vertical Stability Rating		
	Total Drainage Area	Avg Dvlp Hawley-Bledsoe 2-yr Flow	2-yr Specific Stream Power	2-yr Dimensionless Specific Stream Power	2-yr Shear Stress	2-yr Dimensionless Shear Stress	2-yr Width to Depth Ratio	2-yr Mobility Index	Avg Dvlp Hawley-Bledsoe 10-yr Flow	10-yr Specific Stream Power	10-yr Dimensionless Specific Stream Power	10-yr Shear Stress	10-yr Dimensionless Shear Stress	10-yr Width to Depth Ratio	10-yr Mobility Index	Median Bed Material	16th Percentile Bed Material	84th Percentile Bed Material	Percent Sand				Current CEM Phase	Screening Logistics
	$Dm\_Area\_km$	$Q2\_HB\_urbn$	$\omega\_2yr$	$\omega\_2yr$	$\tau\_2yr$	$\tau\_2yr$	$W/D\_2yr$	$Q2^{*}5^{*}Sv$	$Q10\_HB\_urbn$	$\omega\_10yr$	$\omega\_10yr$	$\tau\_10yr$	$\tau\_10yr$	$W/D\_10yr$	$Q10^{*}5^{*}Sv$	$d50$	$d16$	$d84$	$Prcnt\_Sand$				$CEM$	
(km <sup>2</sup> )	(m <sup>3</sup> /s)	(Watt/m <sup>2</sup> )	(N/m <sup>2</sup> )	(N/m <sup>2</sup> )	(N/m <sup>2</sup> )	(N/m <sup>2</sup> )	(m <sup>1.5</sup> /s <sup>0.5</sup> )	(m <sup>3</sup> /s)	(Watt/m <sup>2</sup> )	(N/m <sup>2</sup> )	(N/m <sup>2</sup> )	(N/m <sup>2</sup> )	(N/m <sup>2</sup> )	(N/m <sup>2</sup> )	(m <sup>1.5</sup> /s <sup>0.5</sup> )	(mm)	(mm)	(mm)	(%)			(Stable, Unstable, or NA)		
Topanga_B	49.80	5.04	57.33	0.02	63.00	0.04	20.51	0.0601	62.46	325.41	0.10	164.73	0.10	18.60	0.212	100	14.6	331.7	4%	B1	B1	B	Braiding_Valley	U
Sanjuan_A	105.24	11.28	98.11	0.15	70.25	0.13	24.59	0.0408	133.91	379.38	0.57	158.46	0.28	35.76	0.141	34.4	2	104.8	21%	B1	B1	B	Braiding_Valley	U
Escondido_B	156.73	29.29	35.55	0.06	101.92	0.20	15.11	0.0751	173.73	371.42	0.64	201.05	0.40	15.23	0.183	31.2	9.6	123.1	3%	B1	B1	B	Braiding_Valley	U
Sanantoni_B	31.14	12.88	39.12	0.18	39.24	0.15	54.22	0.0601	94.91	178.58	0.84	97.00	0.37	46.12	0.163	16	3.1	70.2	11%	B1	B1	B	Braided	U
Pigeon_A	6.47	1.67	28.46	6.55	36.64	1.89	9.64	0.0206	10.55	25.73	5.92	70.91	3.65	43.49	0.052	1.2	0.4	2.7	75%	B2	B2	B	Incising	U
Pigeon_B	6.47	1.67	27.22	9.64	41.14	2.82	23.17	0.0206	10.55	119.54	42.33	83.13	5.71	23.19	0.052	0.9	0.4	2.4	80%	B2	B2	B	Incising	U
Sanantoni_A	31.14	12.88	236.85	0.14	122.92	0.12	15.54	0.0601	94.91	638.11	0.38	221.88	0.21	20.06	0.163	64	16	180	8%	B2	B2	B	Incising	U
Hasley_1_A	3.98	1.24	130.42	0.84	71.20	0.34	4.64	0.0318	8.70	559.06	3.61	163.09	0.78	3.32	0.084	13	2.1	92.6	15%	2	2	I	Incising	U
Hasley_2_B	6.41	1.88	23.22	1.67	32.02	0.76	28.86	0.0417	14.06	111.64	8.05	78.69	1.87	21.58	0.114	2.6	0.6	28.9	46%	2	2	I	Incising	U
Hicks_B_08	3.87	1.43	45.13	29.36	38.00	3.91	8.15	0.0306	9.42	175.32	114.06	86.89	8.95	6.52	0.079	0.6	0.3	1.3	93%	2	2	I	Incised	U
Hicks_E_08	3.58	1.35	79.67	16.25	71.88	3.42	4.91	0.0298	8.75	106.98	21.82	101.01	4.80	12.68	0.076	1.3	0.4	53.7	58%	2	2	I	Incising	U
Hicks_E_07	3.58	1.35	72.40	18.97	79.70	4.48	4.80	0.0298	8.75	92.09	24.13	105.13	5.90	13.38	0.076	1.1	0.4	36.3	64%	2	2	I	Incising	U
Hicks_F_08	3.51	1.35	62.64	12.78	61.19	2.91	5.15	0.0297	8.61	37.79	7.71	59.88	2.85	22.80	0.075	1.3	0.4	53.7	58%	2	2	I	Incising	U
Hicks_F_07	3.51	1.35	67.74	17.75	62.28	3.50	3.94	0.0297	8.61	60.88	15.96	46.06	2.59	10.66	0.075	1.1	0.4	36.3	64%	2	2	I	Incising	U
Agua_Hedi_A	27.12	19.09	16.83	0.46	43.11	0.53	5.46	0.0300	54.80	260.25	7.04	72.32	0.89	3.78	0.051	5	2.2	15.5	13%	2	2	I	Incising	U
Agua_Hedi_C	26.84	18.98	6.59	0.18	28.95	0.36	3.17	0.0299	53.90	79.88	2.16	43.70	0.54	2.91	0.050	5	2.2	15.5	13%	2	2	I	Incising	U
Ltl_Cedar_A	7.21	1.65	54.09	0.11	58.77	0.13	12.47	0.0385	15.64	311.20	0.62	163.76	0.35	7.38	0.118	28.5	16	83.7	2%	2	2	I	Incising	U

Unique ID	2-yr Flow Metrics							10-yr Flow Metrics							Bed-material Metrics					Response for SAS	CEM Description	Vertical Stability Rating		
	Total Drainage Area	Avg Dvlp Hawley-2-yr Flow	2-yr Specific Stream Power	2-yr Dimensionless Specific Stream Power	2-yr Shear Stress	2-yr Dimensionless Shear Stress	2-yr Width to Depth Ratio	2-yr Mobility Index	Avg Dvlp Hawley-10-yr Flow	10-yr Specific Stream Power	10-yr Dimensionless Specific Stream Power	10-yr Shear Stress	10-yr Dimensionless Shear Stress	10-yr Width to Depth Ratio	10-yr Mobility Index	Median Bed Material	16th Percentile Bed Material	84th Percentile Bed Material	Percent Sand				Current CEM Phase	Screening Logistics
	$Dm\_Area\_km$	$Q2\_HB\_urbn$	$\omega\_2yr$	$\omega\_2yr$	$\tau\_2yr$	$\tau\_2yr$	$W/D\_2yr$	$Q2^{0.5}Sv$	$Q10\_HB\_urbn$	$\omega\_10yr$	$\omega\_10yr$	$\tau\_10yr$	$\tau\_10yr$	$W/D\_10yr$	$Q10^{0.5}Sv$	$d50$	$d16$	$d84$	$Prcnt\_Sand$	$CEM$				
	(km <sup>2</sup> )	(m <sup>3</sup> /s)	(Watt/m <sup>2</sup> )	(N/m <sup>2</sup> )	(N/m <sup>2</sup> )	(N/m <sup>2</sup> )	(m <sup>1.5</sup> /s <sup>0.5</sup> )	(m <sup>3</sup> /s)	(Watt/m <sup>2</sup> )	(N/m <sup>2</sup> )	(N/m <sup>2</sup> )	(N/m <sup>2</sup> )	(N/m <sup>2</sup> )	(m <sup>1.5</sup> /s <sup>0.5</sup> )	(mm)	(mm)	(mm)	(%)					(Stable, Unstable, or NA)	
Perris_1_B	0.45	0.20	9.09	3.84	18.11	1.40	11.70	0.0106	0.84	32.28	13.64	32.31	2.49	8.72	0.022	0.8	0.3	2.6	79%	2	2	I	Incising	U
Perris_1_C	0.43	0.18	5.88	2.49	12.57	0.97	5.81	0.0103	0.79	20.30	8.58	23.27	1.80	4.67	0.021	0.8	0.3	2.7	78%	2	2	I	Incised	U
Acton_B	1.95	0.53	38.92	1.59	30.30	0.49	30.61	0.0323	2.14	175.67	7.17	63.33	1.03	18.06	0.065	3.8	2	8.8	20%	2	2	I	Transition	U
Acton_E	1.42	0.36	403.95	4.24	199.66	1.31	3.80	0.0346	1.17	1824.24	19.14	325.53	2.14	1.71	0.063	9.4	2.7	33.1	10%	2	2	I	Incising	U
Borrego_E	5.68	5.73	67.22	0.07	152.00	0.21	5.62	0.0683	14.15	418.15	0.42	214.35	0.29	5.51	0.107	45	2.3	105.2	16%	2	2	I	Incising	U
Challengr_B	7.32	2.12	22.27	1.07	35.12	0.64	3.34	0.0547	14.79	36.53	1.76	42.05	0.76	10.99	0.144	3.4	2	7.5	4%	2	2	I	Incising	U
Pigeon_C	3.53	0.79	14.42	2.37	25.05	1.03	5.68	0.0225	6.53	58.07	9.56	57.10	2.35	5.11	0.065	1.5	0.6	3.3	62%	2	2	I	Incising	U
Santiagbd_B	17.84	3.45	43.35	0.68	46.34	0.40	33.42	0.0487	32.34	286.93	4.49	113.91	0.98	20.12	0.149	7.2	2	21.1	17%	2	2	I	Confined_Incising_Temp	U
SantiagnI_A	17.07	3.39	100.43	1.57	69.14	0.59	20.64	0.0538	31.73	651.15	10.19	210.12	1.80	9.28	0.165	7.2	2	21.1	17%	2	2	I	Confined_Incising_Temp	U
Hasley_1_B	3.98	1.24	89.39	4.72	74.23	1.43	11.67	0.0267	8.59	355.35	18.77	167.12	3.23	8.81	0.070	3.2	0.5	25.7	44%	3	3	I	3	U
Hicks_C_08	3.87	1.43	53.97	2.20	60.73	0.99	10.12	0.0307	9.43	113.09	4.62	87.23	1.42	18.82	0.079	3.8	0.5	31.2	44%	3	3	I	3	U
Hicks_D_08	3.73	1.39	109.72	12.67	86.23	2.80	5.48	0.0302	9.08	175.61	20.27	113.01	3.67	10.01	0.077	1.9	0.6	72.4	51%	3	3	I	3	U
Hicks_D_07	3.73	1.39	102.15	43.16	93.67	7.23	4.96	0.0302	9.08	164.01	69.30	123.03	9.50	10.56	0.077	0.8	0.3	11.3	71%	3	3	I	3	U
Agua_Hedi_B	26.97	19.03	7.69	0.21	33.62	0.42	5.22	0.0300	54.34	97.62	2.64	52.54	0.65	4.43	0.051	5	2.2	15.5	13%	3	3	I	3	U
Dry_A	3.16	1.41	33.97	17.54	24.65	2.18	54.61	0.0360	9.27	170.28	87.91	60.46	5.34	30.57	0.092	0.7	0.4	1.3	94%	3	3	I	3	U
Dry_B	3.09	1.40	36.49	16.99	40.07	3.30	25.32	0.0359	9.10	152.35	70.92	94.78	7.81	16.51	0.091	0.75	0.4	4.35	86%	3	3	I	3	U
Dry_C	2.98	1.39	32.66	13.80	46.61	3.60	32.52	0.0357	8.92	168.18	71.07	124.18	9.59	17.35	0.091	0.8	0.4	7.4	78%	3	3	I	3	U

Unique ID	2-yr Flow Metrics							10-yr Flow Metrics							Bed-material Metrics					Response for SAS	CEM Description	Vertical Stability Rating		
	Total Drainage Area	Avg Dvlp Hawley-2yr Flow	2-yr Specific Stream Power	2-yr Dimensionless Specific Stream Power	2-yr Shear Stress	2-yr Dimensionless Shear Stress	2-yr Width to Depth Ratio	2-yr Mobility Index	Avg Dvlp Hawley-10yr Flow	10-yr Specific Stream Power	10-yr Dimensionless Specific Stream Power	10-yr Shear Stress	10-yr Dimensionless Shear Stress	10-yr Width to Depth Ratio	10-yr Mobility Index	Median Bed Material	16th Percentile Bed Material	84th Percentile Bed Material	Percent Sand				Current CEM Phase	Screening Logistics
	$Dm\_Area\_km$	$Q2\_HB\_urbn$	$\omega\_2yr$	$\omega\_2yr$	$\tau\_2yr$	$\tau\_2yr$	$WID\_2yr$	$Q2^{0.5}Sv$	$Q10\_HB\_urbn$	$\omega\_10yr$	$\omega\_10yr$	$\tau\_10yr$	$\tau\_10yr$	$WID\_10yr$	$Q10^{0.5}Sv$	$d50$	$d16$	$d84$	$Prcnt\_Sand$	$CEM$				
	(km <sup>2</sup> )	(m <sup>3</sup> /s)	(Watt/m <sup>2</sup> )	(N/m <sup>2</sup> )	(N/m <sup>2</sup> )	(N/m <sup>2</sup> )		(m <sup>1.5</sup> /s <sup>0.5</sup> )	(m <sup>3</sup> /s)	(Watt/m <sup>2</sup> )	(N/m <sup>2</sup> )	(N/m <sup>2</sup> )	(N/m <sup>2</sup> )	(N/m <sup>2</sup> )	(m <sup>1.5</sup> /s <sup>0.5</sup> )	(mm)	(mm)	(mm)	(%)				(Stable, Unstable, or NA)	
Santimeta_A	1.45	0.58	874.08	309.52	93.50	6.42	1.23	0.0349	2.29	4673.45	1654.94	173.04	11.88	0.84	0.069	0.9	0.3	6	72%	3	3	I	3	U
Santimeta_B	1.45	0.59	31.90	11.29	57.18	3.93	30.69	0.0350	2.29	162.26	57.46	105.89	7.27	22.19	0.069	0.9	0.35	4.65	74%	3	3	I	3	U
Santimeta_C	1.45	0.57	20.59	7.29	42.11	2.89	60.65	0.0344	2.29	121.39	42.99	87.07	5.98	37.86	0.069	0.9	0.4	3.3	77%	3	3	I	3	U
Acton_C	1.87	0.47	38.67	1.05	66.81	0.83	19.32	0.0398	1.62	130.94	3.54	113.73	1.41	15.17	0.074	5	2.1	16.9	15%	3	3	I	3	U
Acton_D	1.42	0.37	22.48	0.24	42.90	0.28	21.56	0.0351	1.24	89.38	0.94	76.68	0.50	13.43	0.065	9.4	2.7	33.1	10%	3	3	I	3	U
Borrego_C	6.84	6.42	14.61	4.42	32.38	2.00	66.07	0.0705	15.71	106.92	32.33	52.12	3.22	44.82	0.110	1	0.4	24.2	71%	3	3	I	Braiding_Sed	U
Santiagbd_A	17.84	3.45	76.21	0.44	61.49	0.27	16.57	0.0487	32.35	324.69	1.85	146.59	0.64	14.61	0.149	14.1	3.6	98.3	10%	3	3	I	Confined_Incising-Wide_Temp	U
Yucaipa_A	16.70	3.31	100.94	4.66	65.46	1.16	43.72	0.0650	28.22	795.69	36.74	202.03	3.57	18.22	0.190	3.5	2.1	8.4	12%	3	3	I	Constructed_Widening	U
Perris_2_A	0.14	0.09	11.23	3.98	17.51	1.20	13.04	0.0121	0.39	29.63	10.49	30.47	2.09	13.40	0.025	0.9	0.3	2.2	82%	1	1	S	1	S
Perris_2_B	0.11	0.06	10.57	9.04	20.02	2.47	15.46	0.0094	0.28	42.96	36.74	36.41	4.50	11.45	0.021	0.5	0.25	1.6	90%	1	1	S	1	S
AltPerris_B	1.25	0.31	1.74	0.62	5.52	0.38	96.60	0.0037	2.07	8.79	3.11	13.81	0.95	59.53	0.009	0.9	0.4	1.8	90%	1	1	S	Transition	S
AltPerris_C	1.24	0.30	2.26	0.96	4.61	0.36	42.82	0.0036	1.99	9.86	4.17	11.11	0.86	28.01	0.009	0.8	0.3	1.7	90%	1	1	S	1	S
Acton_F	1.42	0.35	6.70	0.07	18.96	0.12	19.99	0.0343	1.13	16.79	0.18	26.77	0.18	26.17	0.062	9.4	2.7	33.1	10%	1.5	1	S	1	S
Acton_G	1.42	0.35	3.58	0.04	11.89	0.08	50.89	0.0342	1.13	12.63	0.13	19.77	0.13	35.32	0.061	9.4	2.7	33.1	10%	1	1	S	1	S
Challengr_A	7.43	2.06	31.43	0.03	39.69	0.05	6.01	0.0280	14.99	53.50	0.04	50.79	0.06	14.75	0.076	51.2	16.6	112.7	4%	1.5	1	S	Incised	S?
Challengr_C	7.06	1.83	83.68	0.04	81.47	0.07	8.36	0.0408	14.61	147.14	0.08	112.44	0.10	18.42	0.115	69.7	3.4	151.8	13%	1	1	S	1	S
Dulzura_A	70.24	5.25	18.43	0.03	25.31	0.05	21.18	0.0173	79.66	141.18	0.21	70.82	0.13	14.45	0.067	34.6	3.2	81.3	14%	5	5	S	1	S

Unique ID	2-yr Flow Metrics							10-yr Flow Metrics							Bed-material Metrics					Response for SAS	CEM Description	Vertical Stability Rating		
	Total Drainage Area	Avg Dvlp Hawley-2yr Flow	2-yr Specific Stream Power	2-yr Dimensionless Specific Stream Power	2-yr Shear Stress	2-yr Dimensionless Shear Stress	2-yr Width to Depth Ratio	2-yr Mobility Index	Avg Dvlp Hawley-10yr Flow	10-yr Specific Stream Power	10-yr Dimensionless Specific Stream Power	10-yr Shear Stress	10-yr Dimensionless Shear Stress	10-yr Width to Depth Ratio	10-yr Mobility Index	Median Bed Material	16th Percentile Bed Material	84th Percentile Bed Material	Percent Sand				Current CEM Phase	Screening Logistics
	$Dm\_Area\_km$	$Q2\_HB\_urbn$	$\omega\_2yr$	$\omega\_2yr$	$\tau\_2yr$	$\tau\_2yr$	$W/D\_2yr$	$Q2^{0.5}Sv$	$Q10\_HB\_urbn$	$\omega\_10yr$	$\omega\_10yr$	$\tau\_10yr$	$\tau\_10yr$	$W/D\_10yr$	$Q10^{0.5}Sv$	$d50$	$d16$	$d84$	$Prcnt\_Sand$				$CEM$	
(km <sup>2</sup> )	(m <sup>3</sup> /s)	(Watt/m <sup>2</sup> )	(N/m <sup>2</sup> )	(N/m <sup>2</sup> )	(N/m <sup>2</sup> )	(m <sup>1.5</sup> /s <sup>0.5</sup> )	(m <sup>1.5</sup> /s <sup>0.5</sup> )	(m <sup>3</sup> /s)	(Watt/m <sup>2</sup> )	(N/m <sup>2</sup> )	(N/m <sup>2</sup> )	(N/m <sup>2</sup> )	(N/m <sup>2</sup> )	(m <sup>1.5</sup> /s <sup>0.5</sup> )	(mm)	(mm)	(mm)	(%)						
Dulzura_B	70.24	5.26	27.53	0.03	33.13	0.04	11.72	0.0173	79.75	154.73	0.14	65.74	0.09	11.55	0.067	47.7	2	129.4	20%	5	5	S	1	S
Mcgonigle_A	5.12	3.57	3.97	0.01	34.41	0.09	28.68	0.0402	13.46	29.64	0.08	48.49	0.13	53.45	0.078	23.4	11.7	41.9	1%	1V	1.5	S	Vegetated	S?
Perris_1_A	0.45	0.20	3.21	1.36	9.23	0.71	10.13	0.0108	0.90	10.23	4.32	16.49	1.27	9.57	0.023	0.8	0.3	2.5	79%	1.5	1.5	S	Incised	R?
Borrego_D	5.76	5.52	30.33	0.03	123.25	0.17	22.88	0.0530	14.20	233.52	0.23	186.77	0.26	17.95	0.085	45	2.3	105.2	16%	4	1.5	S	4	R?
Hovnanian_A	3.76	1.76	79.63	0.11	92.41	0.16	11.77	0.0545	8.77	263.11	0.36	185.08	0.31	9.90	0.122	36.7	2	157.1	24%	1	1Cf	S	Confined and Hardpan	NA
Hovnanian_B	3.74	1.77	116.30	0.55	116.74	0.45	5.54	0.0547	8.67	379.64	1.79	224.78	0.87	5.13	0.121	16	2	173.3	38%	1	1Cf	S	Confined and Hardpan	NA
Proctor_TRIB	3.48	0.58	37.34	0.76	38.63	0.39	8.86	0.0234	5.71	74.41	1.51	60.64	0.62	20.69	0.073	6.05	0.95	44.15	37%	1	1Cf	S	Confined	NA
Topanga_A	49.80	4.92	120.50	0.04	100.78	0.07	13.96	0.0547	61.24	662.30	0.24	259.64	0.18	12.79	0.193	87.8	24.7	240.1	0%	1	1Cf	S	Confined	NA
Topanga_C	48.92	5.09	1340.46	0.04	419.61	0.05	4.86	0.2208	62.38	5680.81	0.15	1234.86	0.15	4.08	0.773	499.5	270.6	1591.2	0%	1	1Cf	S	Confined	NA
Sanjuan_B	103.67	11.19	51.18	0.03	49.87	0.05	14.15	0.0418	131.67	245.07	0.15	135.10	0.14	12.43	0.144	61.2	3.2	252.4	13%	1	1Cf	S	Confined	NA
Stewart_A	4.73	3.85	621.82	0.10	364.51	0.15	7.30	0.1885	20.11	1642.85	0.27	657.44	0.27	7.88	0.431	151.8	6.8	724	2%	1	1Cf	S	Confined	NA
Santiagni_B	16.99	3.38	182.03	0.41	115.07	0.27	7.59	0.0537	31.66	801.81	1.81	271.64	0.64	7.29	0.164	26.2	4.9	298.6	9%	1	1Cf	S	Confined	NA
Silverado_A	21.75	5.37	321.89	0.06	183.60	0.08	6.54	0.1284	44.70	1355.14	0.24	446.30	0.19	5.79	0.370	141.5	35.9	353.7	7%	1	1Cf	S	Confined	NA
Silverado_B	21.75	5.37	400.22	0.09	193.88	0.10	6.12	0.1284	44.75	1688.95	0.37	443.23	0.22	5.73	0.371	124.3	16.8	384	11%	1	1Cf	S	Confined	NA
Escondido_A	156.73	29.27	180.04	0.04	317.42	0.15	12.64	0.0750	173.73	1909.11	0.40	630.91	0.30	11.72	0.183	128	35.9	370.5	0%	1	1Cf	S	Constricting_Confined	NA
Alt_RC2_A	0.16	0.12	37.84	258.86	35.00	17.30	5.69	0.0222	0.62	110.96	759.11	66.22	32.73	5.18	0.050	0.125	0.125	0.6	96%	1	1	NA	1	NA - only one point this fine

Note: gray shading indicates columns used in the final models

**General abbreviations and symbol definitions (excluding units of measure):**

CEM Channel Evolution Model  
ID identification  
SAS Statistical Analysis Software

**SAS responses:**

B braided  
Cnst constructed  
I incising  
NA not applicable  
S stable

**CEM phases:**

1	stable	no significant channel incision or bank failure
1.5	beginnings of incision	incision but not past critical bank height
2	incising	nearing, at, or beyond critical bank height, but no significant widening
3	widening	significant widening ( $\rightarrow$ 10% channel width) – incision still possible/likely
4	deposition	bank failure and widening still possible, but clear evidence of significant deposition (with possible beginnings of floodplain reformation, alternating bars, etc.)
5	recovered	return to single-thread equilibrium
1C	constructed	stable but constructed via bed and/or bank protection
1V	vegetated	stable, vegetated encroached low-flow channel
B1	braided	braided but relatively stable active belt width
B2	braided-incising	incision near, at, or beyond critical bank height within a braided channel
2B	wide-to-braided	evidence that a single-thread channel transitioned to braided planform with little intermediate incision (i.e., not far beyond critical bank height, but change in width $\gg 2x$ )
4B	incised-wide-braided	evidence that a single-thread channel first incised well past critical bank height before widening to the current braided form

**Table E.4(a) – Bank data: left banks**

369

		Left Bank (looking downstream)														Geotechnical Stability of Left Bank via log-logistic of Un-confined, Moderately-/Well-consolidated	
Unique ID	Site Description	Bank Height Total	Bank Height above Break	Bank Height below Break	Bank Angle above Break	Bank Angle below Break	Aver-age Bank Angle	Repre-sentative Bank Height for MW	Repre-sentative Bank Angle for MW	Global Stability	Mass Wasting	Fluvial Signi-ficant	Consoli-dation	Confine-ment	Vegetation	Artifi-cial	LB_Ng
		<i>LBank_h_tot</i>	<i>LBank_h_top</i>	<i>LBank_h_btm</i>	<i>LBank_a_top</i>	<i>LBank_a_btm</i>	<i>LBank_a_avg</i>	<i>LBank_ht</i>	<i>LBank_angl</i>	(S/U)	(A/B/C/F)	(FF/NF)	(MC/PC/UC)	(HC/BC/UC)	(A/B/F/T +C/T/H)	(E/F/G/R/N)	
Santiago_A	DS-braided	2.00	N/A	N/A	55.9	55.9	55.9	2.0	55.9	U	C	NF	MC	UC	FT	N	1.45
Santiago_B	US-pool-riffle	1.529	0.637	0.892	54.67	26.05	33.89	1.529	54.67	S	A	NF	MC	HC	TT	N	Confined
Hasley_1_A	DS-incised, CEM 2	3.138	1.7	1.44	28.1	72.56	40.79	1.44	72.56	U	C	NF	PC	UC	AC	N	2.37
Hasley_1_B	US-wide, CEM 3	1.18	0.18	1	23.49	69.4	56.14	1.18	69.4	U	C	NF	PC	UC	AC	N	1.69
Hasley_1_TRIB	TRIB-stable	1.08	N/A	N/A	18.14	N/A	13.36	1.08	18.14	S	A	NF	MC	UC	TT	N	0.02
Hasley_2_A	DS-braided	1.444	0.9885	0.459	27.04	14.93	21.58	1.444	27.04	U	F	NF	PC	UC	AC	N	0.11
Hasley_2_B	US-incised	2.609	1.454	1.155	67.01	21.99	36.88	2.609	67.01	U	C	NF	MC	UC	FC	N	3.34
Hasley_2_TRIB	TRIB-braided	0.5	N/A	N/A	N/A	N/A	62.29	0.5	62.29	U	C	NF	PC	UC	FC	N	0.51
Hicks_A_08	stable @ road	0.91	0.71	0.19	22.78	77.01	17.64	0.19	77.01	S	B	FF	UC	UC	BC	E?	0.38
Hicks_B_08	incised	0.535	0.34	0.195	30.96	44.27	30.73	0.535	30.96	U	F	FF	UC	UC	BC	N	0.06
Hicks_C_08	wide	0.66	0.33	0.295	47.73	57.17	32.01	0.66	57.17	U	C	FF	PC	UC	BC	N	0.51
Hicks_D_08	wide_LVL	0.86	0.4	0.46	32.01	66.5	49.8	0.86	66.5	U	C	FF	PC	UC	BC	N	1.08
Hicks_D_07	wide_SRVY	0.57	0.14	0.43	26.01	66.82	50.75	0.57	66.82	U	C	FF	PC	UC	TC	N	0.72
Hicks_E_08	wide_LVL	0.905	0.605	0.3	71.71	25.99	53.13	0.905	71.71	U	C	FF	PC	UC	BC	N	1.44
Hicks_E_07	wide_SRVY	0.89	0.67	0.22	70.89	13.21	36.96	0.89	70.89	U	C	FF	PC	UC	TC	N	1.36
Hicks_F_08	incise_LVL	0.665	0.43	0.235	57.99	21.39	33.62	0.665	57.99	U	C	NF	PC	UC	BC	N	0.54
Hicks_F_07	incise_SRVY	0.635	0.406	0.229	47.37	15.76	28.18	0.635	47.37	U	C	NF	PC	UC	TC	N	0.27
Agua_Hedi_A	DS, CEM 2, almost beginning to widen	1.89	1.24	0.48	32.56	44.28	35.24	1.89	44.28	S	A	NF	MC	UC	TT	N	0.66
Agua_Hedi_B	mid, CEM 3	1.97	1.51	0.46	50.26	61.85	49.45	1.97	50.26	U	C	NF	MC	UC	TT	N	1.02

		Left Bank (looking downstream)														Geotechnical Stability of Left Bank via log-logistic of Un-confined, Moderately-/Well-consolidated	
Unique ID	Site Description	Bank Height Total	Bank Height above Break	Bank Height below Break	Bank Angle above Break	Bank Angle below Break	Average Bank Angle	Representative Bank Height for MW	Representative Bank Angle for MW	Global Stability	Mass Wasting	Fluvial Significant	Consolidation	Confinement	Vegetation	Artificial	LB_Ng
		<i>LBank_h_tot</i>	<i>LBank_h_top</i>	<i>LBank_h_btm</i>	<i>LBank_a_top</i>	<i>LBank_a_btm</i>	<i>LBank_a_avg</i>	<i>LBank_ht</i>	<i>LBank_angl</i>	(S/U)	(A/B/C/F)	(FF/NF)	(MC/PC/UC)	(HC/BC/UC)	(A/B/F/T/C/T/H)	(E/F/G/R/N)	
Agua_Hedi_C	US, CEM 2-3	2.03	1.12	0.79	76.34	40.79	58.08	2.03	76.34	U	C	NF	MC	UC	TT	N	3.92
Dry_A	DS, CEM 2-3	N/A	3.48	0.95	31.12	38.43	N/A	3.48	31.12	S	A	NF	MC	UC	SC	N	0.40
Dry_B	mid, CEM 3-4?	N/A	3.78	1.01	26.56	21.64	N/A	3.78	26.56	S	A	NF	MC	UC	SC	N	0.26
Dry_C	US, CEM 3	1.76	0.73	1.03	32.83	27.71	30.22	1.76	30.22	S	A	NF	MC	UC	TH	N	0.18
Hovnanian_A	DS-stable	1.47	0.44	1.02	23.92	39.01	30.23	1.47	39.01	S	A	NF	MC	UC	TT	N	0.34
Hovnanian_B	US-stable	0.96	0.17	0.79	18.49	33.91	25.73	0.96	33.91	S	A	NF	MC	UC	TT	N	0.14
Santimeta_A	DS, CEM 3	N/A	3.3	1.13	67.34	66.53	N/A	3.3	67.34	U	C	NF	MC	UC	ST	N	4.30
Santimeta_B	mid, CEM 3	1.61	N/A	N/A	N/A	N/A	71.06	1.61	71.06	U	C	NF	MC	UC	SC	N	2.48
Santimeta_C	US, CEM 3	1.04	0.54	0.31	40.02	66.5	19.43	1.04	66.5	U	C	NF	MC	UC	SC	N	1.30
Ltl_Cedar_A	DS, forced single	1.433	0.707	0.726	32.51	78.74	34.3	0.726	78.74	U	C	NF	PC	UC	TH	N	1.55
Ltl_Cedar_B	US, braided	0.67	0.437	0.233	15.01	3.91	7.58	0.437	15.01	S	A	NF	UC	UC	SC	N	0.01
Proctor_A	DS	0.49	0.19	0.3	21.34	29.29	25.66	0.49	29.29	S	F	NF	UC	UC	TC	N	0.05
Proctor_B	US	N/A	0.27	0.17	18.93	42.25	N/A	0.17	42.25	S	B	NF	UC	UC	TC	N	0.05
Proctor_TRIB	TRIB	N/A	0.51	0.57	15.73	28.28	N/A	0.47	28.28	S	F	NF	UC	UC	TC	N	0.04
Perris_1_A	DS, CEM 2, responded?	0.98	0.75	0.19	31.8	28.03	N/A	0.75	31.8	S	A	NF	PC	UC	SC	N	0.09
Perris_1_B	mid, CEM2, 3?, responding	N/A	N/A	0.44	N/A	14.8	N/A	0.44	14.8	S	A	NF	PC	UC	SC	N	0.00
Perris_1_C	US, CEM2, US of conc. Outfall, responded?	1.52	0.4	0.43	38.71	44.79	N/A	0.63	44.79	U	B	NF	PC	UC	SC	N	0.23
Perris_2_A	DS, CEM1	0.34	0.28	0.06	9.79	4.11	7.86	0.34	9.79	S	A	NF	PC	UC	SC	N	0.00
Perris_2_B	US, CEM1	N/A	1	0.19	11.31	12.45	N/A	1	11.31	S	A	NF	PC	UC	SC	N	0.00

Left Bank (looking downstream)

Unique ID	Site Description	Bank Height Total	Bank Height above Break	Bank Height below Break	Bank Angle above Break	Bank Angle below Break	Aver-age Bank Angle	Repre-sentative Bank Height for MW	Repre-sentative Bank Angle for MW	Global Stability	Mass Wasting	Fluvial Signi-ficant	Consoli-dation	Confine-ment	Vegetation	Artifi-cial	Geotechnical Stability of Left Bank via log-logistic of Un-confined, Moderately-/Well-consolidated
		<i>LBank_h_tot</i>	<i>LBank_h_top</i>	<i>LBank_h_btm</i>	<i>LBank_a_top</i>	<i>LBank_a_btm</i>	<i>LBank_a_avg</i>	<i>LBank_ht</i>	<i>LBank_angl</i>	(S/U)	(A/B/C/F)	(FF/NF)	(MC/PC/UC)	(HC/BC/UC)	(A/B/F/T +C/T/H)	(E/F/G/R/N)	<i>LB_Ng</i>
Perris_3_A	DS, braided, stable	N/A	0.53	0.36	6.65	6.06	N/A	0.53	6.65	S	A	NF	UC	UC	SC	N	0.00
Perris_3_B	US, braided, stable	N/A	0.71	0.22	3.01	9.96	N/A	0.22	9.96	S	A	NF	PC	UC	SC	N	0.00
AltPerris_A	DS-braided	0.5	0.1	0.4	4.4	19.98	11.77	0.5	19.98	S	A	NF	PC	UC	SC	N	0.01
AltPerris_B	mid-reach single thread	0.27	0.19	0.08	10.57	4.81	7.37	0.27	10.57	S	A	NF	PC	UC	SC	N	0.00
AltPerris_C	US-possibly slight incision	0.58	0.36	0.22	8.81	15.64	8.25	0.58	15.64	S	A	NF	PC	UC	SC	N	0.01
Dulzura_A	DS-incised or stable?	1.39	0.24	1.15	12.31	31.87	25.23	1.39	31.87	S	A	NF	PC	UC	ST	N	0.17
Dulzura_B	US-incised or stable?	N/A	0.7	0.25	19.29	8.53	N/A	0.7	19.29	S	F	NF	PC	UC	ST	N	0.02
Acton_A	DS brd	0.3	0.1	0.2	7.13	26.57	14.04	0.3	26.57	S	A	NF	PC	UC	SC	N	0.02
Acton_B	transition	0.79	0.58	0.21	21.8	64.54	26.28	0.79	64.54	S	B	NF	PC	UC	SC	N	0.90
Acton_C	widening	N/A	1.48	0.76	87.51	59.04	N/A	1.48	87.51	U	C	FF	MC	UC	SC	N	4.40
Acton_D	incised/wide	N/A	2.4	N/A	88.81	N/A	N/A	2.4	88.81	U	C	NF	MC	UC	SC	N	7.47
Acton_E	US incised	N/A	2.3	N/A	87.51	N/A	N/A	2.3	87.51	U	C	NF	MC	UC	SC	N	6.83
Acton_F	US starting to incise	N/A	0.25	0.16	14.04	17.74	N/A	0.16	17.74	S	A	NF	PC	UC	SC	G	0.00
Acton_G	US 'stable'	N/A	0.25	N/A	14.04	N/A	N/A	0.25	14.04	S	A	NF	PC	UC	SC	G	0.00
Borrego_A	DS constrct (I-C)	N/A	2.99	N/A	44.9	N/A	N/A	2.99	44.9	S	A	NF	MC	UC	SC	R	1.09
Borrego_B	braided (IV-B)	1.44	0.91	0.53	56.6	27.92	41.99	1.44	56.6	U	C	NF	MC	UC	TT	N	1.08
Borrego_C	widening	4.02	3.57	0.45	67.21	26.57	59.16	4.02	67.21	U	C	NF	MC	UC	TT	N	5.20
Borrego_D	incised/wide	N/A	6	N/A	45	N/A	N/A	6	45	U	C	NF	MC	UC	TT	N	2.20
Borrego_E	US incised	3.13	1.76	1.37	52.43	67.09	38.04	1.76	52.43	U	C	NF	MC	UC	TT	N	1.04
Topanga_A	DS incised/braided	N/A	1.45	1.34	41.99	21.8	N/A	1.34	21.8	S	A	NF	UC	UC	TH	N	0.05

Left Bank (looking downstream)

Unique ID	Site Description	Bank Height Total	Bank Height above Break	Bank Height below Break	Bank Angle above Break	Bank Angle below Break	Average Bank Angle	Representative Bank Height for MW	Representative Bank Angle for MW	Global Stability	Mass Wasting	Fluvial Significant	Consolidation	Confinement	Vegetation	Artificial	Geotechnical Stability of Left Bank via log-logistic of Un-confined, Moderately-/Well-consolidated
		<i>LBank_h_tot</i>	<i>LBank_h_top</i>	<i>LBank_h_btm</i>	<i>LBank_a_top</i>	<i>LBank_a_btm</i>	<i>LBank_a_avg</i>	<i>LBank_ht</i>	<i>LBank_angl</i>	(S/U)	(A/B/C/F)	(FF/NF)	(MC/PC/UC)	(HC/BC/UC)	(A/B/F/T/+C/T/H)	(E/F/G/R/N)	<i>LB_Ng</i>
Topanga_B	braided	8.43	8	0.43	53.13	19.29	77.75	8	53.13	S	B	NF	MC	HC	TT	N	Confined
Topanga_C	US steppool	N/A	7	3	60.26	20.56	N/A	7	60.26	S	B	NF	MC	HC	TT	N	Confined
Challengr_A	DS-stable	0.98	0.83	0.15	83.13	36.87	72.98	0.98	83.13	U	C	FF	MC	UC	TT	N	2.48
Challengr_B	mid-incised	1.5	0.64	0.86	24.7	76.91	36.87	0.86	76.91	U	C	NF	PC	UC	TT	N	1.70
Challengr_C	US-stable	0.71	0.28	0.43	43.03	30.96	26.89	0.71	43.03	S	A	NF	MC	UC	TT	N	0.23
Mcgonigle_A	vegetated	N/A	0.4	0.21	20.56	25.02	NA	0.4	20.56	S	A	NF	UC	UC	TH	N	0.01
Sanjuan_A	DS-braided	0.87	0.27	0.6	41.99	27.89	28.54	0.87	41.99	U	C	NF	UC	UC	SC	N	0.26
Sanjuan_B	US-steppool	1.29	0.6	0.69	24.78	17.28	18.75	1.29	24.78	S	A	NF	UC	UC	SC	N	0.07
Pigeon_A	DS-incised/braided	0.98	0.22	0.76	65.56	72.9	70.97	0.98	72.9	U	C	NF	PC	UC	AT	N	1.64
Pigeon_B	mid-braided	0.73	0.48	0.25	73.14	50.19	50.58	0.73	73.14	U	C	NF	PC	UC	AT	N	1.23
Pigeon_C	US-pool riffle	1.48	0.58	0.9	24.04	60.95	36.33	0.9	60.95	U	B	NF	PC	UC	TT	N	0.86
Stewart_A	cascade	1.24	0.68	0.56	27.61	16.35	22.46	1.24	27.61	S	A	NF	UC	UC	TT	N	0.10
Santiagbd_A	DS-incised	N/A	10	0.26	63.64	59.53	N/A	10	63.64	S	B	NF	MC	HC	BT	N	Confined
Santiagbd_B	US - planebed	N/A	10.47	0.1	46.32	26.57	N/A	10.47	46.32	S	B	NF	MC	HC	BT	N	Confined
Santiagnl_A	DS - planebed	N/A	12	0.39	45	54.46	N/A	12	45	S	B	NF	MC	HC	BT	N	Confined
Santiagnl_B	US steppool	1.73	0.55	1.18	34.99	52.67	16.85	1.18	52.67	S	C	NF	UC	UC	TT	N	0.71
Silverado_A	DS-steppool	N/A	8	1.21	36.25	26.57	N/A	1.21	26.57	S	A	NF	MC	UC	TT	N	0.08
Silverado_B	US-steppool	N/A	8	0.64	23.75	27.14	N/A	0.64	27.14	S	A	NF	MC	UC	TT	N	0.05
Escondido_A	DS-steppool	N/A	13	1.23	22.85	16.04	N/A	1.23	16.04	S	A	NF	UC	UC	TT	N	0.02
Escondido_B	US-braided-veg	1.87	0.84	1.03	19.09	19.88	18.16	1.87	18.16	S	A	NF	UC	UC	TT	N	0.04
Sanantoni_A	DS-braided/incised	N/A	0.85		48.58			0.85	48.58	U	C	NF	UC	UC	SH	N	0.40

		Left Bank (looking downstream)														Geotechnical Stability of Left Bank via log-logistic of Un-confined, Moderately-/Well-consolidated	
Unique ID	Site Description	Bank Height Total	Bank Height above Break	Bank Height below Break	Bank Angle above Break	Bank Angle below Break	Aver-age Bank Angle	Representative Bank Height for MW	Representative Bank Angle for MW	Global Stability	Mass Wasting	Fluvial Significant	Consolidation	Confinement	Vegetation	Artificial	LB_Ng
		<i>LBank_h_tot</i>	<i>LBank_h_top</i>	<i>LBank_h_btm</i>	<i>LBank_a_top</i>	<i>LBank_a_btm</i>	<i>LBank_a_avg</i>	<i>LBank_ht</i>	<i>LBank_angl</i>								
		(m)	(m)	(m)	(°)	(°)	(°)			(S/U)	(A/B/C/F)	(FF/NF)	(MC/PC/UC)	(HC/BC/UC)	(A/B/F/T+ C/T/H)	(E/F/G/R/N)	
Sanantoni_B	US_braided, about to incise	N/A	2.1	0.25	85.24	18.43	N/A	2.1	85.24	U	C	NF	PC	UC	ST	N	5.74
Alt_RC2_A	incised	1.82	0.68	1.14	23.83	26.87	22.02	1.82	26.87	S	A	NF	MC	UC	ST	N	0.13
Yucaipa_A	DS-incised/widening right at threshold - veg is holding MW back at x-sec, but MW extensive up and downstream	2.55	2	0.55	51.32	28.84	44.44	2.55	51.32	U	B	NF	MC	UC	TT	N	1.41
Yucaipa_B	US-braided/incised	5	4	1	78.69	32.02	64.37	5	78.69	U	C	NF	MC	UC	TT	N	10.63
Oakglenn_A	steppool	3.49	0.75	2.74	56.31	38.83	34.92	1.2	56.31	S	B	NF	MC	UC	TT	N	0.89

**General abbreviations and symbol definitions (excluding units of measure):**

CEM	Channel Evolution Model
conc	concrete
construct	constructed
DS	downstream
ID	identification
mid	middle
MW	mass wasting
N/A	not applicable
TRIB	tributary
US	upstream
veg	vegetated
x-sec	cross-section

**Global stability:**

- S stable although MW may be present (such as through unconsolidated media or sections of bank), x-section is generally not actively widening, particularly not widening beyond the original banks. MW may be occurring in sections but banks seem relatively stable - that is their height and angle may be near stable/unstable threshold such that any current failure should result in slopes and heights even closer or equal to that of stable. Vegetation or confinement may also be playing a significant role in the global stability.
- U unstable MW seems more complete and the channel seems to be more actively widening. Furthermore, failure in a bank typically results in a form that remains critically unstable. That is, these banks are so far past the stability threshold that failure does not move them significantly closer to stable form.

**Mass wasting:**

- A absent MW is absent from cross-section and adjacent reach in general
- B broken MW is broken (fractured/incomplete), occurring in thin slumps across only parts of the bank (vertically and/or longitudinally). MW seems to be such that it is a local phenomenon of temporary state rather than global and more perpetual.
- C complete MW is complete, occurring in large failure blocks, such that the post-failure geometry remains in a critically unstable state. Provided the stream does not 'fill' the channel back in and reach a new equilibrium, the banks seem destined to remain perpetually unstable
- F failed MW has recently occurred such that the geometry of the survey reflects that of the failed state rather than critically unstable.

**Fluvial significant:**

- FF fluvial factor direct fluvial bank erosion is a significant factor in the cause of instability.
- NF no fluvial fluvial erosion is not a significant factor (although it may be present)

**Consolidation:**

- MC moderately or well consolidated bank appears moderately to well consolidated
- PC poorly consolidated bank seems poorly consolidated. This includes banks that may be composed of historic channel beds; however, they show at least some consolidation (that is, they typically have had a chance to begin to consolidate such that they don't fail at the angle of repose of sand)
- UC unconsolidated material that until recently (<10yrs) was the channel bed. Although in the form of a bank, it shows no real consolidation and fails at angles of the angle of repose of sand ~ 30°.

**Confinement:**

- HC hillslope confined the measured height and angle is that of a hillslope which confines the channel and restricts its overall ability to significantly widen
- BC boulder or bedrock confined the measured height and angle is that of a boulder or exposed bedrock which is confining the channel and restricting its overall ability to widen
- UC unconfined the measured bank height and angle being rated is not directly confined by hillslope, boulder, or bedrock

**Dominant vegetation (extent + type):**

- extent:
- A absent vegetation at cross-section is absent from both the tops and slopes of banks
- B burned vegetation was recently burned and has not recovered to pre-fire state
- F fragmented vegetation is present but fragmented at cross section
- T thick vegetation is thick and likely playing a significant role in slope stability
- dominant type:
- C chaparral stereotypical Chaparral of southern California – generally dry and shrubby
- T temperate trees and grasses temperate species such as grasses and trees
- H hydrophilic hydrophilic species that occur only in regularly moist soils
- Artificial
- E embanked embanked (although not riprap, typically more intended or permanent than fill soil)
- (term that best describes artificial
- F fill fill (fill soil with little compaction or consolidation)
- measures affecting current bank
- G graded graded but appears to be cut into original floodplain rather than fill
- stability)
- R riprap riprap
- N none no artificial material affecting current bank stability

**Table E.4(b) – Bank data: right banks**

375

Unique ID	Site Description	Right Bank (looking downstream)															Geotechnical Stability of Right Bank via log-logistic of Unconfined, Moderately-/ Well-consolidated	Representative Geotechnical Stability of Cross Section (max Ng)
		Bank Height Total	Bank Height above Break	Bank Height below Break	Bank Angle above Break	Bank Angle below Break	Average Bank Angle	Representative Bank Height for MW	Representative Bank Angle for MW	Global Stability	Mass Wasting	Fluvial Significant	Consolidation	Confinement	Vegetation	Artificial		
		<i>RBank_h_tot</i>	<i>RBank_h_top</i>	<i>RBank_h_btm</i>	<i>RBank_a_top</i>	<i>RBank_a_btm</i>	<i>RBank_a_avg</i>	<i>RBank_ht</i>	<i>RBank_angl</i>									
		(m)	(m)	(m)	(°)	(°)	(°)			(S/U)	(A/B/C/F)	(FF/NF)	(MC/PC/UC)	(HC/BC/UC)	(A/B/F/T+ C/T/H)	(E/F/G/R/N)		
Santiago_A	DS-braided	1.18	N/A	N/A	34.6	34.6	34.6	1.2	34.6	S	A	NF	PC	UC	FC	E	0.19	1.45
Santiago_B	US-pool-riffle	2.00	N/A	N/A	33.4	33.4	33.4	2.0	33.4	S	A	NF	PC	UC	TT	E	0.29	0.29
Hasley_1_A	DS-incised, CEM2	1.225	0.895	0.519	25.36	70.82	31.69	0.519	70.82	U	C	NF	PC	UC	AC	G	0.79	2.37
Hasley_1_B	US-wide, CEM3	1.117	0.641	0.476	56.15	16.91	41.7	1.117	56.15	U	C	NF	PC	UC	FH	G	0.82	1.69
Hasley_1_TRIB	TRIB-stable	1.64	N/A	N/A	28.9	N/A	N/A	1.64	28.9	S	A	NF	PC	UC	AH	F	0.15	0.15
Hasley_2_A	DS-braided	0.96	0.72	0.24	76.01	15.74	43.19	0.96	76.01	U	C	NF	PC	UC	FC	N	1.83	1.83
Hasley_2_B	US-incised	2.23	N/A	N/A	N/A	N/A	42.91	2.23	42.91	S	A	NF	PC	UC	FC	G?	0.70	3.34
Hasley_2_TRIB	TRIB-braided	1.245	0.62	0.63	8.43	54.33	17.69	0.63	54.33	U	C	NF	PC	UC	FC	N	0.42	0.51
Hicks_A_08	stable @road	1.02	0.85	0.17	19.9	20.7	16.25	0.17	20.7	S	A	NF	UC	UC	BC	E?	0.01	0.38
Hicks_B_08	incised	1.54	1.075	0.465	27.14	68.96	23.81	0.465	68.96	U	B	NF	PC	UC	BC	E?	0.65	0.65
Hicks_C_08	wide	N/A	0.51	0.31	10.48	36.87	N/A	0.31	36.87	S	A	NF	UC	UC	BC	N	0.06	0.51
Hicks_D_08	wide_LVL	0.65	0.33	0.32	34.99	57.99	46.67	0.65	57.99	U	C	FF	PC	UC	BC	N	0.53	1.08
Hicks_D_07	wide_SRVY	0.67	0.21	0.46	29.92	52.18	26.87	0.46	52.18	U	C	FF	PC	UC	TC	N	0.27	0.72
Hicks_E_08	wide_LVL	0.825	0.415	0.41	76.45	36.5	42.51	0.825	76.45	U	C	NF	PC	UC	BC	N	1.60	1.60
Hicks_E_07	wide_SRVY	0.821	0.402	0.419	48.37	29.13	36.51	0.821	48.37	U	C	NF	PC	UC	TC	N	0.38	1.36
Hicks_F_08	incise_LVL	0.58	0.27	0.31	69.68	19.01	30.11	0.58	69.68	U	C	NF	PC	UC	BC	N	0.84	0.84
Hicks_F_07	incise_SRVY	0.53	0.39	0.14	65.16	14.38	35.74	0.53	65.16	U	C	NF	PC	UC	TC	N	0.62	0.62

Unique ID	Site Description	Right Bank (looking downstream)															Geotechnical Stability of Right Bank via log-logistic of Unconfined, Moderately-/ Well-consolidated	Representative Geotechnical Stability of Cross Section (max Ng)	
		Bank Height Total	Bank Height above Break	Bank Height below Break	Bank Angle above Break	Bank Angle below Break	Average Bank Angle	Representative Bank Height for MW	Representative Bank Angle for MW	Global Stability	Mass Wasting	Fluvial Significant	Consolidation	Confinement	Vegetation	Artificial			
		<i>RBank_h_tot</i>	<i>RBank_h_top</i>	<i>RBank_h_btm</i>	<i>RBank_a_top</i>	<i>RBank_a_btm</i>	<i>RBank_a_avg</i>	<i>RBank_ht</i>	<i>RBank_angl</i>										
		(m)	(m)	(m)	(°)	(°)	(°)			(S/U)	(A/B/C/F)	(FF/NF)	(MC/PC/UC)	(HC/BC/UC)	(A/B/F/T+/C/T/H)	(E/F/G/R/N)			
Agua_Hedi_A	DS, CEM 2, almost beginning to widen	2.58	0.91	1.67	15.89	52.28	27.54	1.67	52.28	U	C	NF	MC	UC	TT	N	0.98	0.98	
Agua_Hedi_B	mid, CEM 3	2.271	0.972	0.875	62.54	55.31	27.88	1.419	62.54	U	C	NF	MC	UC	TT	N	1.46	1.46	
Agua_Hedi_C	US, CEM 2-3	3.24	1.3	1.48	58.25	60.34	43.83	1.48	60.34	U	C	NF	MC	UC	TT	N	1.36	3.92	
Dry_A	DS, CEM 2-3	N/A	3.09	1.22	40.96	61.65	N/A	3.09	40.96	U	C	NF	MC	UC	SC	N	0.84	0.84	
Dry_B	mid, CEM 3-4?	3.01	1.85	1.33	37.59	77.18	41.74	1.33	77.18	U	C	NF	MC	UC	SC	N	2.66	2.66	
Dry_C	US, CEM 3	4.87	N/A	N/A	N/A	N/A	70.34	4.87	70.34	U	C	NF	MC	UC	SC	N	7.27	7.27	
Hovnanian_A	DS-stable	N/A	1.1	N/A	16.16	N/A	N/A	1.1	16.16	S	A	NF	MC	UC	TT	N	0.02	0.34	
Hovnanian_B	US-stable	1.2	0.15	1.04	24.02	34.9	30.12	1.2	34.9	S	A	NF	MC	UC	TT	N	0.20	0.20	
Santimeta_A	DS, CEM 3	4.13	0.78	3.36	61.77	77.71	74.47	4.13	77.71	U	C	NF	MC	UC	ST	N	8.44	8.44	
Santimeta_B	mid, CEM 3	2.88	1.991	0.889	75.05	77.71	64.38	2.88	75.05	U	C	NF	MC	UC	SC	N	5.27	5.27	
Santimeta_C	US, CEM 3	1.22	0.92	0.3	74.86	16.55	43.93	1.22	74.86	U	C	NF	MC	UC	SC	N	2.22	2.22	
Ltl_Cedar_A	DS, forced single	1.44	0.82	0.62	14.22	64.68	19.85	0.62	64.68	U	C	NF	PC	UC	TH	N	0.71	1.55	
Ltl_Cedar_B	US, braided	N/A	0.501	0.59	31.04	28.62	N/A	0.59	28.62	S	F	NF	UC	UC	SC	N	0.05	0.05	
Proctor_A	DS	N/A	0.81	0.44	16.13	43.04	N/A	0.44	43.04	S	B	NF	UC	UC	TC	N	0.14	0.14	
Proctor_B	US	N/A	0.57	0.31	19.3	46	N/A	0.31	46	S	B	NF	UC	UC	TC	N	0.12	0.12	
Proctor_TRIB	TRIB	N/A	0.73	0.47	14.53	34.61	N/A	0.47	34.61	S	F	NF	UC	UC	TC	N	0.08	0.08	
Perris_1_A	DS, CEM 2, responded?	1.15	0.38	0.62	17.71	14.93	N/A	0.62	14.93	S	A	NF	PC	UC	SC	N	0.01	0.09	

Unique ID	Site Description	Right Bank (looking downstream)															Geotechnical Stability of Right Bank via log-logistic of Unconfined, Moderately-/ Well-consolidated	Representative Geotechnical Stability of Cross Section (max Ng)	
		Bank Height Total	Bank Height above Break	Bank Height below Break	Bank Angle above Break	Bank Angle below Break	Average Bank Angle	Representative Bank Height for MW	Representative Bank Angle for MW	Global Stability	Mass Wasting	Fluvial Significant	Consolidation	Confinement	Vegetation	Artificial			
		<i>RBank_h_tot</i>	<i>RBank_h_top</i>	<i>RBank_h_btm</i>	<i>RBank_a_top</i>	<i>RBank_a_btm</i>	<i>RBank_a_avg</i>	<i>RBank_ht</i>	<i>RBank_angl</i>										
		(m)	(m)	(m)	(°)	(°)	(°)			(S/U)	(A/B/C/F)	(FF/NF)	(MC/PC/UC)	(HC/BC/UC)	(A/B/F/T+/C/T/H)	(E/F/G/R/N)			<i>LB_Ng</i>
Perris_1_B	mid, CEM2, 3?, responding	1.13	0.37	0.76	21.78	38.78	31.13	1.13	38.78	U	C	FF	PC	UC	SC	N	0.26	0.26	
Perris_1_C	US, CEM2, US of conc. Outfall, responded?	1.49	0.49	1	23.84	32.82	29.25	1.2	32.82	U	B	FF	PC	UC	SC	N	0.16	0.23	
Perris_2_A	DS, CEM1	0.23	0.18	0.05	17.65	9.07	14.87	0.23	14.87	S	A	NF	PC	UC	SC	N	0.00	0.00	
Perris_2_B	US, CEM1	0.64	0.25	0.39	3.48	38.06	N/A	0.25	38.06	S	B	NF	PC	UC	SC	N	0.05	0.05	
Perris_3_A	DS, braided, stable	1.63	0.9	0.73	8.08	9.02	8.27	1.63	9.02	S	A	NF	PC	UC	SC	N	0.00	0.00	
Perris_3_B	US, braided, stable	N/A	1.43	0.39	7.87	16.01	N/A	0.39	16.01	S	A	NF	UC	UC	SC	N	0.01	0.01	
AltPerris_A	DS-braided	0.3	0.15	0.15	10.62	7.13	8.53	0.3	10.62	S	A	NF	PC	UC	SC	N	0.00	0.01	
AltPerris_B	mid-reach single thread	0.6	0.29	0.26	12.58	11.31	7.37	0.6	12.58	S	A	NF	PC	UC	SC	N	0.00	0.00	
AltPerris_C	US-possibly slight incision	0.6	0.29	0.32	16.17	20.38	8.75	0.6	20.38	S	A	NF	PC	UC	SC	N	0.02	0.02	
Dulzura_A	DS-incised or stable?	N/A	1.18	0.41	11.31	16.7	N/A	0.41	16.7	S	A	NF	UC	UC	ST	N	0.01	0.17	
Dulzura_B	US-incised or stable?	1	0.65	0.35	23.43	39.52	27.28	1	39.52	S	B	NF	PC	UC	ST	N	0.24	0.24	
Acton_A	DS brd	0.5	0.32	0.18	12.88	16.7	7.91	0.5	16.7	S	A	NF	PC	UC	SC	N	0.01	0.02	
Acton_B	transition	0.79	0.28	0.51	54.46	41.99	23.52	0.79	54.46	S	B	NF	PC	UC	SC	N	0.53	0.90	
Acton_C	widening	N/A	2.5	N/A	87.71	N/A	N/A	2.5	87.71	U	C	FF	MC	UC	SC	N	7.48	7.48	
Acton_D	incised/wide	N/A	3.25	N/A	88.24	N/A	N/A	3.25	88.24	U	C	NF	MC	UC	SC	N	9.91	9.91	
Acton_E	US incised	N/A	2.29	N/A	87.5	N/A	N/A	2.29	87.5	U	C	NF	MC	UC	SC	N	6.80	6.83	

Unique ID	Site Description	Right Bank (looking downstream)															Geotechnical Stability of Right Bank via log-logistic of Unconfined, Moderately-/ Well-consolidated	Representative Geotechnical Stability of Cross Section (max Ng)	
		Bank Height Total	Bank Height above Break	Bank Height below Break	Bank Angle above Break	Bank Angle below Break	Average Bank Angle	Representative Bank Height for MW	Representative Bank Angle for MW	Global Stability	Mass Wasting	Fluvial Significant	Consolidation	Confinement	Vegetation	Artificial			
		<i>RBank_h_tot</i>	<i>RBank_h_top</i>	<i>RBank_h_btm</i>	<i>RBank_a_top</i>	<i>RBank_a_btm</i>	<i>RBank_a_avg</i>	<i>RBank_ht</i>	<i>RBank_angl</i>										
		(m)	(m)	(m)	(°)	(°)	(°)			(S/U)	(A/B/C/F)	(FF/NF)	(MC/PC/UC)	(HC/BC/UC)	(A/B/F/T+/C/T/H)	(E/F/G/R/N)			<i>LB_Ng</i>
Acton_F	US starting to incise	0.41	0.25	0.16	14.04	17.74	15.29	0.41	17.74	S	A	NF	PC	UC	SC	G	0.01	0.01	
Acton_G	US 'stable'	N/A	0.24	N/A	13.5	N/A	N/A	0.24	13.5	S	A	NF	PC	UC	SC	G	0.00	0.00	
Borrego_A	DS constrct (I-C)	N/A	3	N/A	45	N/A	N/A	3	45	S	A	NF	MC	UC	SC	R	1.10	1.10	
Borrego_B	braided (IV-B)	1.69	0.53	1.16	52.96	30.49	24.04	1.69	52.96	U	C	NF	MC	UC	SC	N	1.03	1.08	
Borrego_C	widening	3.94	3	0.94	63.43	23.96	54.78	3.94	63.43	U	C	NF	MC	UC	TT	N	4.25	5.20	
Borrego_D	incised/wide	6.35	6	0.35	72.43	41.16	70.09	6.35	72.43	U	C	NF	MC	UC	SC	N	10.40	10.40	
Borrego_E	US incised	N/A	2.27	0.82	19.8	43.53	N/A	2.27	19.8	S	F	NF	MC	UC	TT	N	0.06	1.04	
Topanga_A	DS incised/brd	N/A	0.8	1.46	38.66	22.78	N/A	1.46	22.78	S	A	NF	UC	UC	TH	N	0.06	0.06	
Topanga_B	braided	0.68	0.25	0.43	10.89	10.81	10.16	0.68	10.81	S	A	NF	UC	UC	TH	N	0.00	0.00	
Topanga_C	US steppool	N/A	10	2	63.43	21.8	N/A	10	63.43	S	B	NF	MC	HC	TT	N	Confined	0.00	
Challengr_A	DS-stable	0.94	0.35	0.59	15.65	29.54	17.6	0.94	29.54	S	A	NF	MC	UC	TT	N	0.09	2.48	
Challengr_B	mid-incised	1.34	0.58	0.76	17.57	68.96	26.4	0.76	68.96	U	C	NF	PC	UC	TT	N	1.07	1.70	
Challengr_C	US-stable	0.8	0.59	0.21	36.41	27.7	33.69	0.8	36.41	S	A	NF	MC	UC	TT	N	0.15	0.23	
Mcgonigle_A	vegetated	N/A	0.33	0.31	30.96	29.54	N/A	0.33	30.96	S	A	NF	UC	UC	TH	N	0.04	0.04	
Sanjuan_A	DS-braided	6.3	5	1.3	78.69	29.48	62.35	6.3	78.69	U	C	NF	MC	UC	TT	N	13.39	13.39	
Sanjuan_B	US-steppool	N/A	1.51	0.29	18.92	16.17	N/A	1.51	18.92	S	A	NF	MC	BC	SC	N	Confined	0.07	
Pigeon_A	DS-incised/brd	0.68	0.29	0.39	15.38	44.03	29.74	0.68	44.03	U	C	NF	UC	UC	SH	N	0.23	1.64	
Pigeon_B	mid-braided	0.32	0.11	0.21	12.41	7.77	6.34	0.32	12.41	S	A	NF	UC	UC	SH	N	0.00	1.23	
Pigeon_C	US-pool riffle	N/A	1.45	0.49	36.87	24.7	N/A	1.45	36.87	S	B	NF	PC	UC	TT	N	0.28	0.86	

Unique ID	Site Description	Right Bank (looking downstream)															Geotechnical Stability of Right Bank via log-logistic of Unconfined, Moderately-/ Well-consolidated	Representative Geotechnical Stability of Cross Section (max Ng)	
		Bank Height Total	Bank Height above Break	Bank Height below Break	Bank Angle above Break	Bank Angle below Break	Average Bank Angle	Representative Bank Height for MW	Representative Bank Angle for MW	Global Stability	Mass Wasting	Fluvial Significant	Consolidation	Confinement	Vegetation	Artificial			
		<i>RBank_h_tot</i>	<i>RBank_h_top</i>	<i>RBank_h_btm</i>	<i>RBank_a_top</i>	<i>RBank_a_btm</i>	<i>RBank_a_avg</i>	<i>RBank_ht</i>	<i>RBank_angl</i>										
		(m)	(m)	(m)	(°)	(°)	(°)			(S/U)	(A/B/C/F)	(FF/NF)	(MC/PC/UC)	(HC/BC/UC)	(A/B/F/T+/C/T/H)	(E/F/G/R/N)			<i>LB_Ng</i>
Stewart_A	cascade	N/A	0.52	0.55	34.99	90	N/A	0.55	90	S	A	NF	MC	BC	TT	N	Confined	0.10	
Santiagbd_A	DS-incised	N/A	2.05	0.89	34.22	64.18	N/A	0.89	64.18	U	C	NF	UC	UC	SC	N	1.00	1.00	
Santiagbd_B	US-planebed	N/A	0.5	0.2	14.04	40.91	N/A	0.2	40.91	S	B	NF	UC	UC	SC	N	0.05	0.05	
SantiagnI_A	DS-planebed	2.35	2.01	0.34	32.71	18.52	29.59	2.35	32.71	S	A	NF	MC	UC	TT	N	0.31	0.31	
SantiagnI_B	US-steppool	N/A	0.79	0.21	15.07	34.99	N/A	0.21	34.99	S	A	NF	UC	UC	SH	N	0.03	0.71	
Silverado_A	DS-steppool	3.15	2.05	1.1	33.02	38.16	N/A	1.1	38.16	S	A	NF	MC	UC	TT	N	0.24	0.24	
Silverado_B	US-steppool	2.4	1.07	1.33	37.39	53.06	45	2.4	53.06	S	A	NF	MC	BC	TT	N	Confined	0.05	
Escondido_A	DS-steppool	N/A	29	2.15	30.4	29.9	N/A	2.15	29.9	S	A	NF	MC	BC	ST	N	Confined	0.02	
Escondido_B	US-braided-veg	1.18	0.84	0.34	32.87	14.66	24.41	1.18	32.87	S	B	NF	UC	UC	TT	N	0.16	0.16	
Sanantoni_A	DS-braided/incised	0.8	0.5	0.3	18.43	11.31	14.93	0.8	18.43	S	A	NF	UC	UC	SH	N	0.02	0.40	
Sanantoni_B	US_braided, about to incise	N/A	3.51	0.3	63.89	11.31	N/A	3.51	63.89	U	C	NF	PC	UC	ST	N	3.87	5.74	
Alt_RC2_A	incised	1.81	0.43	1.38	18.26	31.63	26.04	1.81	31.63	S	A	NF	MC	UC	ST	N	0.22	0.22	
Yucaipa_A	DS-incised/widening right at threshold - veg is holding MW back at x-sec, but MW extensive up and downstream	2.1	1.78	0.32	37.57	7.29	N/A	1.78	37.57	S	A	NF	MC	UC	AT	R	0.37	1.41	

Unique ID	Site Description	Right Bank (looking downstream)															Geotechnical Stability of Right Bank via log-logistic of Unconfined, Moderately-/ Well-consolidated	Representative Geotechnical Stability of Cross Section (max Ng)
		Bank Height Total	Bank Height above Break	Bank Height below Break	Bank Angle above Break	Bank Angle below Break	Average Bank Angle	Representative Bank Height for MW	Representative Bank Angle for MW	Global Stability	Mass Wasting	Fluvial Significant	Consolidation	Confinement	Vegetation	Artificial		
		<i>RBank_h_tot</i>	<i>RBank_h_top</i>	<i>RBank_h_btm</i>	<i>RBank_a_top</i>	<i>RBank_a_btm</i>	<i>RBank_a_avg</i>	<i>RBank_ht</i>	<i>RBank_angl</i>									
		(m)	(m)	(m)	(°)	(°)	(°)			(S/U)	(A/B/C/F)	(FF/NF)	(MC/PC/UC)	(HC/BC/UC)	(A/B/F/T+/C/T/H)	(E/F/G/R/N)		
Yucaipa_B	US-braided/incised	2.5	1	1.5	24.44	78.69	45	1.5	78.69	U	C	NF	MC	UC	AT	N	3.19	10.63
Oakglenn_A	steppool	3.14	1.49	1.65	44.81	44.14	44.46	3.14	44.14	S	B	NF	MC	UC	ST	N	1.08	1.08

**General abbreviations and symbol definitions (excluding units of measure):**

- CEM Channel Evolution Model
- conc concrete
- constrct constructed
- DS downstream
- ID identification
- max maximum
- mid middle
- MW mass wasting
- N/A not applicable
- Ng bank stability
- TRIB tributary
- US upstream
- veg vegetated
- x-sec cross-section

**Global stability:**

- S stable although MW may be present (such as through unconsolidated media or sections of bank), x-section is generally not actively widening, particularly not widening beyond the original banks. MW may be occurring in sections but banks seem relatively stable - that is their height and angle may be near stable/unstable threshold such that any current failure should result in slopes and heights even closer or equal to that of stable. Vegetation or confinement may also be playing a significant role in the global stability.
- U unstable MW seems more complete and the channel seems to be more actively widening. Furthermore, failure in a bank typically results in a form that remains critically unstable. That is, these banks are so far past the stability threshold that failure does not move them significantly closer to stable form.

**Mass wasting:**

- A absent MW is absent from cross-section and adjacent reach in general
- B broken MW is broken (fractured/incomplete), occurring in thin slumps across only parts of the bank (vertically and/or longitudinally). MW seems to be such that it is a local phenomenon of temporary state rather than global and more perpetual.
- C complete MW is complete, occurring in large failure blocks, such that the post-failure geometry remains in a critically unstable state. Provided the stream does not 'fill' the channel back in and reach a new equilibrium, the banks seem destined to remain perpetually unstable
- F failed MW has recently occurred such that the geometry of the survey reflects that of the failed state rather than critically unstable.

**Fluvial significant:**

- FF fluvial factor direct fluvial bank erosion is a significant factor in the cause of instability.
- NF no fluvial fluvial erosion is not a significant factor (although it may be present)

**Consolidation:**

- MC moderately or well consolidated bank appears moderately to well consolidated
- PC poorly consolidated bank seems poorly consolidated. This includes banks that may be composed of historic channel beds; however, they show at least some consolidation (that is, they typically have had a chance to begin to consolidate such that they don't fail at the angle of repose of sand)
- UC unconsolidated material that until recently (<10yrs) was the channel bed. Although in the form of a bank, it shows no real consolidation and fails at angles of the angle of repose of sand ~ 30°.

**Confinement:**

- HC hillslope confined the measured height and angle is that of a hillslope which confines the channel and restricts its overall ability to significantly widen
- BC boulder or bedrock confined the measured height and angle is that of a boulder or exposed bedrock which is confining the channel and restricting its overall ability to widen
- UC unconfined the measured bank height and angle being rated is not directly confined by hillslope, boulder, or bedrock

**Dominant vegetation (extent + type):**

- extent:
- A absent vegetation at cross-section is absent from both the tops and slopes of banks
- B burned vegetation was recently burned and has not recovered to pre-fire state
- F fragmented vegetation is present but fragmented at cross section
- T thick vegetation is thick and likely playing a significant role in slope stability
- dominant type:
- C chaparral stereotypical Chaparral of southern California – generally dry and shrubby
- T temperate trees and grasses temperate species such as grasses and trees
- H hydrophilic hydrophilic species that occur only in regularly moist soils
- Artificial embanked embanked (although not riprap, typically more intended or permanent than fill soil)
- (term that best describes artificial measures affecting current bank stability)
- F fill fill (fill soil with little compaction or consolidation)
- G graded graded but appears to be cut into original floodplain rather than fill
- R riprap riprap
- N none no artificial material affecting current bank stability

**Table E.4(c) – Left bank data: rationale for description of second bank height and angle**

		Left Bank (looking downstream)															
Unique ID	Site Description	Bank Height Total	Bank Height above Break	Bank Height below Break	Bank Angle above Break	Bank Angle below Break	Average Bank Angle	Representative Bank Height for MW	Representative Bank Angle for MW	Global Stability	Mass Wasting	Fluvial Significant	Consolidation	Confinement	Vegetation	Artificial	Geo-technical Stability of Left Bank via log-logistic of Unconfined, Moderately/ Well Consolidated
		<i>LBank_h_tot</i>	<i>LBank_h_top</i>	<i>LBank_h_botm</i>	<i>LBank_a_top</i>	<i>LBank_a_botm</i>	<i>LBank_a_avg</i>	<i>LBank_ht</i>	<i>LBank_angl</i>								
		(m)	(m)	(m)	(°)	(°)	(°)			(S/U)	(A/B/C/F)	(FF/NF)	(MC/PC/UC)	(HC/BC/UC)	(A/B/F/T+C/T/H)	(E/F/G/R/N)	
Santiago_B_2	LB_total valley wall height and RB of incised section							8	27.83	S	A	NF	MC	HC	TT	N	Confined
Hasley_2_A_DS	to account for the fact that the LB of Hasley_2A was geometry for a recently failed bank, rather than pre/during MW (geometry from next cross section DS (x-sec 1))							0.59	78.06	U	C	NF	PC	UC	AC	N	1.22
Hicks_A_2	upper banks (stable)							0.71	22.78	S	A	NF	PC	UC	AC	E?	0.03
Hicks_B_2	upper right bank historic MW (failed, but not separated from current incision height and angle)							1.09	32.74	U	F	FF	PC	UC	BC	N	0.15
Hicks_C_2	upper left bank (true bank material - more consolidated)	1.25	0.32	0.93	64.54	27.32	30.96	1.25	64.54	U	C	FF	PC	UC	BC	N	1.42
Hicks_F_2	upper (original, pre-incised, stable banks)							0.415	23.03	S	A	NF	PC	UC	BC	N	0.02
Agua_Hedi_B_2	right, incised cut-bank																
Agua_Hedi_C_2	upper portions of banks																

		Left Bank (looking downstream)															Geo-technical Stability of Left Bank via log-logistic of Unconfined, Moderately/ Well Consolidated	
Unique ID	Site Description	Bank Height Total	Bank Height above Break	Bank Height below Break	Bank Angle above Break	Bank Angle below Break	Average Bank Angle	Representative Bank Height for MW	Representative Bank Angle for MW	Global Stability	Mass Wasting	Fluvial Significant	Consolidation	Confinement	Vegetation	Artificial		
		<i>LBank_h_tot</i>	<i>LBank_h_top</i>	<i>LBank_h_btm</i>	<i>LBank_a_top</i>	<i>LBank_a_btm</i>	<i>LBank_a_avg</i>	<i>LBank_ht</i>	<i>LBank_angl</i>									
		(m)	(m)	(m)	(°)	(°)	(°)			(S/U)	(A/B/C/F)	(FF/NF)	(MC/PC/UC)	(HC/BC/UC)	(A/B/F/T+C/T/H)	(E/F/G/R/N)		<i>LB_Ng</i>
Dry_A_2	banks within incised section also representative							0.95	38.43	U	F	NF	MC	UC	SC	N	0.21	
Dry_B_2	right upper bank also warrants inclusion (separated from incised bank by a 25° slope), additional left bank within channel not necessary, but included for balance							1.01	21.64	U	F	NF	MC	UC	SC	N	0.04	
Santimeta_A_2	LB of incised section separate and failing							1.13	66.53	U	C	NF	MC	UC	ST	N	1.42	
Ltl_Cedar_B_2	far right bank (upper) warrants inclusion																	
Proctor_A_2	far right bank (upper) warrants inclusion																	
Proctor_B_2	outer banks							0.27	18.93	S	A	NF	PC	UC	TC	N	0.01	
Proctor_B_3	left incised channel							0.2	26.24	S	F	NF	UC	UC	TC	N	0.01	
Proctor_Trib_2	outer banks							0.73	14.53	S	A	NF	PC	UC	TC	N	0.01	
Proctor_Trib_3	left incised channel							0.36	20.82	S	F	NF	UC	UC	TC	N	0.01	
Perris_1_C_2	left upper bank							0.6	38.71	U	C	NF	PC	UC	SC	N	0.14	
Perris_3_B_2	upper right bank																	
Dulzura_A	upper right bank																	
Acton_C_2	left, lower (incised) bank – PC (edge of old bank and old channel bed, but not UC)							0.76	59.04	U	C	FF	PC	UC	SC	N	0.65	

		Left Bank (looking downstream)															
Unique ID	Site Description	Bank Height Total	Bank Height above Break	Bank Height below Break	Bank Angle above Break	Bank Angle below Break	Average Bank Angle	Representative Bank Height for MW	Representative Bank Angle for MW	Global Stability	Mass Wasting	Fluvial Significant	Consolidation	Confinement	Vegetation	Artificial	Geotechnical Stability of Left Bank via log-logistic of Unconfined, Moderately/ Well Consolidated
		LBank_h_tot	LBank_h_top	LBank_h_btm	LBank_a_top	LBank_a_btm	LBank_a_avg	LBank_ht	LBank_angl								LB_Ng
		(m)	(m)	(m)	(°)	(°)	(°)			(S/U)	(A/B/C/F)	(FF/NF)	(MC/PC/UC)	(HC/BC/UC)	(A/B/F/T+C/T/H)	(E/F/G/R/N)	
Borrego_E_2	incised banks (although not unconsolidated - trees 20+yrs - composed of alluvia - very old bed)							1.37	67.09	U	C	NF	PC	UC	TT	N	1.76
Topanga_A_2	left main channel	N/A	1.45	1.34	41.99	21.8	N/A	1.45	41.99	S	C	NF	UC	UC	TH	N	0.43
Topanga_A_3	upper bank of right channel (consolidated)																
Topanga_B_2	lower left bank							0.43	19.29	S	A	NF	UC	UC	TH	N	0.01
Topanga_C_2	collapsed material							3	20.56	S	A	NF	UC	UC	TH	N	0.09
McGonigle_A_2	right channel (just next to main channel)	N/A		0.21		25.02	N/A	0.21	25.02	S	F	NF	UC	UC	TH	N	0.01
McGonigle_A_3	valley walls							13	14.91	S	A	NF	MC	HC	ST	N	Confined
Stewart_A_2	more confined (bedrock) heights and angles @ x-sec							0.35	68.96	S	A	NF	MC	BC	TT	N	Confined
Stewart_A_3	just upstream – unconsolidated MW right bank							2	70	U	C	NF	PC	UC	TT	N	2.94
Santiagbd_A_2	left incised and right outer bank	N/A	10	0.26	63.64	59.53	N/A	0.26	59.53	S	B	NF	UC	UC	BT	N	0.23
Santiagbd_B_2		N/A	10.47	0.1	46.32	26.57	N/A	0.1	26.57	S	A	NF	UC	UC	SC	N	0.01
Santiagnl_A_2	two unconsolidated left banks							0.39	54.46	S	C	NF	UC	UC	AH	N	0.26
Santiagnl_B_2	US steppool	1.73	0.55	1.18	34.99	52.67	16.85	0.55	34.99	S	B	NF	UC	UC	TT	N	0.09
Santiagnl_B_3	boulder on right and UC bank between x-sec (pictured)							0.25	75	S	C	NF	UC	UC	SH	N	0.46

		Left Bank (looking downstream)															Geo-technical Stability of Left Bank via log-logistic of Unconfined, Moderately/ Well Consolidated
Unique ID	Site Description	Bank Height Total	Bank Height above Break	Bank Height below Break	Bank Angle above Break	Bank Angle below Break	Average Bank Angle	Representative Bank Height for MW	Representative Bank Angle for MW	Global Stability	Mass Wasting	Fluvial Significant	Consolidation	Confinement	Vegetation	Artificial	LB_Ng
		LBank_h_tot	LBank_h_top	LBank_h_btm	LBank_a_top	LBank_a_btm	LBank_a_avg	LBank_ht	LBank_angl				(MC/PC/UC)	(HC/BC/UC)	(A/B/F/T+C/T/H)	(E/F/G/R/N)	
		(m)	(m)	(m)	(°)	(°)	(°)			(S/U)	(A/B/C/F)	(FF/NF)					
Silverado_A_2	left valley wall (8 m @ 30 all I can see in photo), right bank to road	N/A	8	1.21	36.25	26.57	N/A	8	36.25	S	A	NF	MC	HC	TT	N	Confined
Silverado_B_2	bottom of left valley wall at x-sec (topsoil, not rock) and bedrock between A and B (photo 1268)	N/A	8	0.64	23.75	27.14	N/A	8	23.75	S	A	NF	MC	HC	TT	N	Confined
Escondido_A_2	valley walls	N/A	13	1.23	22.85	16.04	N/A	13	22.85	S	A	NF	MC	HC	TT	N	Confined
Escondido_B_2	valley walls							11	20.42	S	A	NF	MC	HC	TT	N	Confined
Escondido_B_3	banks of island							0.65	17.65	S	A	NF	UC	UC	TT	N	0.01
Sanantoni_B	inner banks (unconsolidated but stable)	N/A	2.1	0.25	85.24	18.43	N/A	0.25	18.43	S	A	NF	UC	UC	SH	N	0.01

**General abbreviations and symbol definitions (excluding units of measure):**

DS	downstream
ID	identification
LB	left bank
MW	mass wasting
N/A	not applicable
RB	right bank
US	upstream
x-sec	cross-section

**Global stability:**

- S stable although MW may be present (such as through unconsolidated media or sections of bank), x-section is generally not actively widening, particularly not widening beyond the original banks. MW may be occurring in sections but banks seem relatively stable - that is their height and angle may be near stable/unstable threshold such that any current failure should result in slopes and heights even closer or equal to that of stable. Vegetation or confinement may also be playing a significant role in the global stability.
- U unstable MW seems more complete and the channel seems to be more actively widening. Furthermore, failure in a bank typically results in a form that remains critically unstable. That is, these banks are so far past the stability threshold that failure does not move them significantly closer to stable form.

**Mass wasting:**

- A absent MW is absent from cross-section and adjacent reach in general
- B broken MW is broken (fractured/incomplete), occurring in thin slumps across only parts of the bank (vertically and/or longitudinally). MW seems to be such that it is a local phenomenon of temporary state rather than global and more perpetual.
- C complete MW is complete, occurring in large failure blocks, such that the post-failure geometry remains in a critically unstable state. Provided the stream does not 'fill' the channel back in and reach a new equilibrium, the banks seem destined to remain perpetually unstable
- F failed MW has recently occurred such that the geometry of the survey reflects that of the failed state rather than critically unstable.

**Fluvial significant:**

- FF fluvial factor direct fluvial bank erosion is a significant factor in the cause of instability.
- NF no fluvial fluvial erosion is not a significant factor (although it may be present)

**Consolidation:**

- MC moderately or well consolidated bank appears moderately to well consolidated
- PC poorly consolidated bank seems poorly consolidated. This includes banks that may be composed of historic channel beds; however, they show at least some consolidation (that is, they typically have had a chance to begin to consolidate such that they don't fail at the angle of repose of sand)
- UC unconsolidated material that until recently (<10yrs) was the channel bed. Although in the form of a bank, it shows no real consolidation and fails at angles of the angle of repose of sand ~ 30°.

**Confinement:**

- HC hillslope confined the measured height and angle is that of a hillslope which confines the channel and restricts its overall ability to significantly widen
- BC boulder or bedrock confined the measured height and angle is that of a boulder or exposed bedrock which is confining the channel and restricting its overall ability to widen
- UC unconfined the measured bank height and angle being rated is not directly confined by hillslope, boulder, or bedrock

**Dominant vegetation (extent + type):**

- extent:
- A absent vegetation at cross-section is absent from both the tops and slopes of banks
- B burned vegetation was recently burned and has not recovered to pre-fire state
- F fragmented vegetation is present but fragmented at cross section
- T thick vegetation is thick and likely playing a significant role in slope stability
- dominant type:
- C chaparral stereotypical Chaparral of southern California – generally dry and shrubby
- T temperate trees and grasses temperate species such as grasses and trees
- H hydrophilic hydrophilic species that occur only in regularly moist soils
- Artificial
- E embanked embanked (although not riprap, typically more intended or permanent than fill soil)
- (term that best describes artificial
- F fill fill (fill soil with little compaction or consolidation)
- measures affecting current bank
- G graded graded but appears to be cut into original floodplain rather than fill
- stability)
- R riprap riprap
- N none no artificial material affecting current bank stability

**Table E.4(d) – Right bank data: rationale for description of second bank height and angle**

		Right Bank (looking downstream)														Geo-technical Stability of Right Bank via log-logistic of Unconfined, Moderately-/Well-Consolidated	Representative Geo-technical Stability of Cross Section (max Ng)		
Unique ID	Site Description	Bank Height Total	Bank Height above Break	Bank Height below Break	Bank Angle above Break	Bank Angle below Break	Average Bank Angle	Representative Bank Height for MW	Representative Bank Angle for MW	Global Stability	Mass Wasting	Fluvial Significant	Consolidation	Confinement	Vegetation	Artificial			
		<i>RBank_h_tot</i>	<i>RBank_h_top</i>	<i>RBank_h_btm</i>	<i>RBank_a_top</i>	<i>RBank_a_btm</i>	<i>RBank_a_avg</i>	<i>RBank_h_t</i>	<i>RBank_a_ngl</i>									<i>LB_Ng</i>	<i>Max_Ng</i>
		(m)	(m)	(m)	(°)	(°)	(°)			(S/U)	(A/B/C/F)	(FF/NF)	(MC/PC/UC)	(HC/BC/UC)	(A/B/ F/T +C/T/H)	(E/F/G/ R/N)			
Santiago_B_2	LB_total valley wall height and RB of incised section							0.74	28.88	U	C	NF	UC	UC	AH	N		0.07	
Hasley_2_A_DS	to account for the fact that the LB of Hasley_2A was geometry for a recently failed bank, rather than pre/during MW (geometry from next cross section DS (x-sec 1)							0.861	67.51439	U	C	NF	PC	UC	FC	N		1.13	
Hicks_A_2	upper banks (stable)							0.85	19.9	S	A	NF	PC	UC	BC	E?		0.02	
Hicks_B_2	upper right bank historic MW (failed, but not separated from current incision height and angle)																		
Hicks_C_2	upper left bank (true bank material – more consolidated)																		
Hicks_F_2	upper (original, pre-incised, stable banks)							0.395	15.82	S	A	NF	PC	UC	BC	N		0.01	
Agua_Hedi_B_2	right, incised cut-bank							0.875	55.31	S	B	FF	MC	UC	TT	N		0.61	
Agua_Hedi_C_2	upper portions of banks							1.3	58.25	S	B	NF	MC	UC	TT	N		1.07	
Dry_A_2	banks within incised section also representative							1.22	61.65	U	C	NF	MC	UC	SC	N		1.20	



Unique ID	Site Description	Right Bank (looking downstream)														Geo-technical Stability of Right Bank via log-logistic of Unconfined, Moderately-/ Well-Consolidated	Representative Geo-technical Stability of Cross Section (max Ng)	
		Bank Height Total	Bank Height above Break	Bank Height below Break	Bank Angle above Break	Bank Angle below Break	Average Bank Angle	Representative Bank Height for MW	Representative Bank Angle for MW	Global Stability	Mass Wasting	Fluvial Significant	Consolidation	Confinement	Vegetation	Artificial		
		<i>RBank_h_tot</i>	<i>RBank_h_top</i>	<i>RBank_h_btm</i>	<i>RBank_a_top</i>	<i>RBank_a_btm</i>	<i>RBank_a_avg</i>	<i>RBank_h_t</i>	<i>RBank_a_rgl</i>	(S/U)	(A/B/C/F)	(FF/NF)	(MC/PC/UC)	(HC/BC/UC)	(A/B/F/T +C/T/H)	(E/F/G/R/N)		<i>LB_Ng</i>
Borrego_E_2	incised banks (although not unconsolidated - trees 20+yrs - composed of alluvia - very old bed)						0.82	43.53	U	C	NF	PC	UC	TT	N		0.27	
Topanga_A_2	left main channel	N/A	0.8	1.46	38.66	22.78	N/A	0.8	38.66	S	C	NF	UC	UC	TH	N		0.18
Topanga_A_3	upper bank of right channel (consolidated)							2	46.85	S	A	NF	MC	HC	TT	N		Confined
Topanga_B_2	lower left bank																	
Topanga_C_2	collapsed material							2	21.8	S	A	NF	UC	UC	TH	N		0.07
McGonigle_A_2	right channel (just next to main channel)	N/A		0.31		29.54	N/A	0.33	29.54	S	F	NF	UC	UC	TH	N		0.03
McGonigle_A_3	valley walls							13	14.57	S	A	NF	MC	HC	TT	N		Confined
Stewart_A_2	more confined (bedrock) heights and angles @ x-sec							0.52	34.99	S	A	NF	MC	BC	TT	N		Confined
Stewart_A_3	just upstream - unconsolidated MW right bank							0.25	90	S	C	NF	UC	UC	TT	N		0.81
Santiagbd_A_2	left incised and right outer bank	N/A	2.05	0.89	34.22	64.18	N/A	2.05	34.22	S	A	NF	MC	UC	TC	N		0.32
Santiagbd_B_2		N/A	0.5	0.2	14.04	40.91	N/A	0.5	14.04	S	A	NF	UC	UC	SC	N		0.00
Santiagnl_A_2	two unconsolidated left banks							0.7	23.54	S	A	NF	UC	UC	AH	N		0.03
Santiagnl_B_2	US steppool	N/A	0.79	0.21	15.07	34.99	N/A	0.79	15.07	S	A	NF	UC	UC	AT	N		0.01

		Right Bank (looking downstream)															Geo-technical Stability of Right Bank via log-logistic of Unconfined, Moderately-/ Well-Consolidated	Representative Geo-technical Stability of Cross Section (max Ng)
Unique ID	Site Description	Bank Height Total	Bank Height above Break	Bank Height below Break	Bank Angle above Break	Bank Angle below Break	Average Bank Angle	Representative Bank Height for MW	Representative Bank Angle for MW	Global Stability	Mass Wasting	Fluvial Significant	Consolidation	Confinement	Vegetation	Artificial	LB_Ng	Max_Ng
		<i>RBank_h_tot</i>	<i>RBank_h_top</i>	<i>RBank_h_bot</i>	<i>RBank_a_top</i>	<i>RBank_a_bot</i>	<i>RBank_a_avg</i>	<i>RBank_h_t</i>	<i>RBank_a_rgl</i>	(S/U)	(A/B/C/F)	(FF/NF)	(MC/PC/UC)	(HC/BC/UC)	(A/B/ F/T +C/T/H)	(E/F/G/ R/N)		
SantiagnI_B_3	boulder on right and UC bank between x-sec (pictured)							0.41	39.09	S	A	NF	MC	BC	SH	N	Confined	
Silverado_A_2	left valley wall (8 m @ 30 all I can see in photo), right bank to road	3.15	2.05	1.1	33.02	38.16	N/A	3.15	33.02	S	A	NF	MC	UC	TT	N	0.43	
Silverado_B_2	bottom of left valley wall at x-sec (topsoil, not rock) and bedrock btwn A and B (photo 1268)							8	60	S	A	NF	MC	BC	TT	N	Confined	
Escondido_A_2	valley walls	N/A	29	2.15	30.4	29.9	N/A	29	30.4	S	A	NF	MC	HC	TT	N	Confined	
Escondido_B_2	valley walls							25	14.25	S	A	NF	MC	HC	TT	N	Confined	
Escondido_B_3	banks of island							0.6	11.73	S	A	NF	UC	UC	TT	N	0.00	
Sanantoni_B	inner banks (unconsolidated but stable)	N/A	3.51	0.3	63.89	11.31	N/A	0.3	11.31	S	A	NF	UC	UC	SH	N	0.00	

**General abbreviations and symbol definitions (excluding units of measure):**

DS	downstream
ID	identification
LB	left bank
max	maximum
MW	mass wasting
N/A	not applicable
Ng	bank stability
RB	right bank
US	upstream
x-sec	cross-section

**Global stability:**

S	stable	although MW may be present (such as through unconsolidated media or sections of bank), x-section is generally not actively widening, particularly not widening beyond the original banks. MW may be occurring in sections but banks seem relatively stable - that is their height and angle may be near stable/unstable threshold such that any current failure should result in slopes and heights even closer or equal to that of stable. Vegetation or confinement may also be playing a significant role in the global stability.
U	unstable	MW seems more complete and the channel seems to be more actively widening. Furthermore, failure in a bank typically results in a form that remains critically unstable. That is, these banks are so far past the stability threshold that failure does not move them significantly closer to stable form.

**Mass wasting:**

A	absent	MW is absent from cross-section and adjacent reach in general
B	broken	MW is broken (fractured/incomplete), occurring in thin slumps across only parts of the bank (vertically and/or longitudinally). MW seems to be such that it is a local phenomenon of temporary state rather than global and more perpetual.
C	complete	MW is complete, occurring in large failure blocks, such that the post-failure geometry remains in a critically unstable state. Provided the stream does not 'fill' the channel back in and reach a new equilibrium, the banks seem destined to remain perpetually unstable
F	failed	MW has recently occurred such that the geometry of the survey reflects that of the failed state rather than critically unstable.

**Fluvial significant:**

FF	fluvial factor	direct fluvial bank erosion is a significant factor in the cause of instability.
NF	no fluvial	fluvial erosion is not a significant factor (although it may be present)

**Consolidation:**

MC	moderately or well consolidated	bank appears moderately to well consolidated
PC	poorly consolidated	bank seems poorly consolidated. This includes banks that may be composed of historic channel beds; however, they show at least some consolidation (that is, they typically have had a chance to begin to consolidate such that they don't fail at the angle of repose of sand)
UC	unconsolidated	material that until recently (<10yrs) was the channel bed. Although in the form of a bank, it shows no real consolidation and fails at angles of the angle of repose of sand ~ 30°.

**Confinement:**

HC	hillslope confined	the measured height and angle is that of a hillslope which confines the channel and restricts its overall ability to significantly widen
BC	boulder or bedrock confined	the measured height and angle is that of a boulder or exposed bedrock which is confining the channel and restricting its overall ability to widen
UC	unconfined	the measured bank height and angle being rated is not directly confined by hillslope, boulder, or bedrock

**Dominant vegetation (extent + type):**

extent:	A	absent	vegetation at cross-section is absent from both the tops and slopes of banks
	B	burned	vegetation was recently burned and has not recovered to pre-fire state
	F	fragmented	vegetation is present but fragmented at cross section
	T	thick	vegetation is thick and likely playing a significant role in slope stability
dominant type:	C	chaparral	stereotypical Chaparral of southern California – generally dry and shrubby
	T	temperate trees and grasses	temperate species such as grasses and trees
Artificial (term that best describes artificial measures affecting current bank stability)	H	hydrophilic	hydrophilic species that occur only in regularly moist soils
	E	embanked	embanked (although not riprap, typically more intended or permanent than fill soil)
	F	fill	fill (fill soil with little compaction or consolidation)
	G	graded	graded but appears to be cut into original floodplain rather than fill
	R	riprap	riprap
	N	none	no artificial material affecting current bank stability